







UNIVERSITÉ LIBRE DE BRUXELLES

UNIVERSITÉ D'EUROPE

**Institut de Pharmacie**

**Laboratoire de Pharmacie Galénique et de Biopharmacie**

**Professeur Karim AMIGHI**

**DEVELOPMENT, CHARACTERIZATION AND EVALUATION OF CRYSTALLINE  
NANOPARTICLES FOR ENHANCING THE SOLUBILITY, THE DISSOLUTION RATE AND THE  
ORAL BIOAVAILABILITY OF POORLY WATER-SOLUBLE DRUGS**

**Jerome Hecq**

**Pharmacien**

**Thèse présentée en vue de l'obtention du grade de  
Docteur en Sciences Pharmaceutiques**

**Bruxelles, Septembre 2006**



## Acknowledgments

Au terme de ce travail, je tiens à adresser mes plus sincères remerciements à Monsieur le Professeur Karim AMIGHI, Directeur du Laboratoire de Pharmacie Galénique et de Biopharmacie, pour la confiance qu'il m'a témoignée en m'accueillant dans son service en tant que doctorant mais également en tant qu'assistant. Je lui témoigne ici toute ma reconnaissance pour sa constante disponibilité ainsi que pour son soutien et ses nombreux conseils et encouragements au cours de ces cinq dernières années. Je le remercie également de m'avoir fait partager son expérience et ses compétences scientifiques lors de nos nombreuses discussions. Je lui suis infiniment reconnaissant d'avoir mis à ma disposition tous les moyens nécessaires pour réaliser et finir cette thèse dans les meilleures des conditions.

Je tiens également à exprimer mes très sincères remerciements à UCB S.A. pour le soutien financier de ce travail. Je tiens tout particulièrement à remercier les Docteurs Michel DELEERS, Domenico FANARA et Henri VRANCKX pour leur soutien et leurs encouragements ainsi que pour les nombreux échanges scientifiques que nous avons eus lors de nos multiples réunions. Je leur suis très reconnaissant pour leur supervision de ce travail.

Je tiens également à remercier les Professeurs Jacques DUBOIS et Jean-Michel KAUFFMAN pour leur contribution à la supervision de ce travail.

Je tiens à exprimer ma reconnaissance au Professeur Guy DANDRIFOSSE et au Docteur Olivier PEULEN, du Département de Biochimie et de Physiologie Générale (Study Group of Digestive Tract (DiGESD)) de L'Université de Liège, pour m'avoir accueilli au sein de leur laboratoire pour les manipulations sur cultures cellulaires. Je tiens plus particulièrement à exprimer mes très sincères remerciements à Madame Géraldine NOLLEVAUX, doctorante, pour les manipulations que nous avons pu réaliser ensemble et pour m'avoir permis de profiter de ses compétences. Je la remercie également pour sa disponibilité et sa gentillesse. Ce fut un réel plaisir de travailler en sa compagnie.

Je tiens également à exprimer ma reconnaissance au Professeur Jeannine FONTAINE, Directrice du Laboratoire de Physiologie et Pharmacologie de l'Université Libre de Bruxelles, pour m'avoir accueilli au sein de son laboratoire pour la réalisation d'une partie des analyses pharmacocinétiques reprises dans ce travail et pour l'étude d'efficacité sur rats hypertendus. Je tiens plus particulièrement à remercier le Docteur David FONTAINE pour son aide précieuse dans la mise en place et dans la réalisation de ces études. Je le remercie de m'avoir fait

profiter de ses connaissances. Je tiens également à remercier Mademoiselle Julie HULIN pour son aide au cours de la réalisation de ces études.

Je tiens à remercier, au sein d'UCB S.A., toutes les personnes avec qui j'ai eu l'occasion de travailler au cours de notre collaboration. Parmi ces nombreuses personnes je tiens particulièrement à remercier Mesdames Monique BERWAER, Anne BOUQUELLE, Sarah MARQUETTE et Vanessa BISCOTTI pour leur grande aide dans le travail sur les molécules UCB-A et UCB-B. Je remercie également tout particulièrement les Docteurs Sven DEFERME et Jean-Marie NICOLAS et Mesdames Catherine VROONEN, Nathalie ALEXANDER, Silvia ROCCO et Alexandra DECLERCQ pour les études pharmacocinétiques sur la nifedipine et les Docteurs Sophie LE LAMER et Pierre BOULANGER pour les études pharmacocinétiques sur la substance ucb-35440-3. Je remercie également Madame Laurence VROYE et Monsieur Bruno MARTIN pour avoir mis à ma disposition des chaînes HPLC pour mes analyses ainsi que pour leurs nombreux conseils.

Je remercie vivement Madame Tiriana SEGATO et Monsieur Patrizio MADAU, du Laboratoire de Chimie Industrielle de L'Université Libre de Bruxelles, pour leur collaboration très précieuse concernant les études de diffraction aux rayons X et pour les analyses de microscopie électronique à balayage ainsi que pour leur grande disponibilité et leur gentillesse.

Je tiens également à remercier et témoigner ma grande reconnaissance au Professeur Marc VAN DAMME, Directeur du Service de Toxicologie de l'Université Libre de Bruxelles, pour l'accueil qu'il m'a réservé au sein de son laboratoire dans le cadre de mes tâches d'enseignement. Je lui suis très reconnaissant de l'attention qu'il a eue à mon égard au cours de ces cinq années. Je tiens à le remercier également de m'avoir permis de participer, à plusieurs reprises, à des missions d'enseignement dans le cadre d'un projet de coopération avec la République de Guinée. Je tiens également à remercier le Docteur Caroline HAYOT avec qui j'ai pris beaucoup de plaisir à donner les séminaires de spectroscopie.

Je tiens également à remercier le Docteur Christine DECAESTECKER, du Service de Toxicologie de l'Université Libre de Bruxelles, pour son aide précieuse concernant le choix et la réalisation des études statistiques pour les données des études de perméabilité.

Des remerciements tout particuliers sont à adresser à l'ensemble de mes collègues du Service de Pharmacie Galénique et de Biopharmacie pour la part qu'ils ont prise dans l'élaboration de ce travail. Sans l'ensemble de

ces derniers, ce travail aurait difficilement pu être mené à bien. Je tiens premièrement à remercier mes anciens collègues, et amis, avec qui j'ai débuté ce travail. Je remercierai particulièrement le Docteur Frédéric EECKMAN pour toute l'aide qu'il m'a apportée lors de mes débuts ainsi que pour son amitié. Je tiens également à remercier tout particulièrement le Docteur Jamila HAMDANI pour son aide et son soutien au cours de ces années ainsi que pour tous les moments passés ensemble aux Travaux Pratiques de Pharmacie Galénique. Ce fut un réel plaisir de travailler en sa compagnie. Je la remercie pour son amitié. Je tiens à remercier l'ensemble des autres doctorants toujours en service pour leur aide et leurs encouragements et plus particulièrement Monsieur Jonathan GOOLE pour sa grande gentillesse, sa très grande disponibilité et son amitié. Des remerciements tout particuliers sont adressés à Monsieur Philippe DELEUZE pour m'avoir encadré tout au long de ce travail ainsi que pour son soutien et ses conseils dans des moments plus difficiles. Je tiens également à remercier Madame Nancy VAN AELST pour son aide et pour tous les moments passés ensemble aux Travaux Pratiques de Pharmacie Galénique. Je la remercie également pour son amitié.

Je remercierai également tous mes collègues (Assistants, personnel technique, secrétariat) de l'Institut de Pharmacie avec qui j'ai pu partager de bons moments.

Un remerciement particulier est adressé au Docteur Marianne OTH, Eli Lilly Development Center Mont Saint-Guibert, pour ses conseils et pour m'avoir inspiré à démarrer ce travail.

De manière plus personnelle, je tiens à remercier l'ensemble de mes proches qui par leur amour, leur confiance et leur soutien m'ont permis de mener à bien ce travail. Je tiens à remercier à cet égard plus particulièrement mes parents, Robert, Renaud et mon grand-père qui ont toujours été d'un immense soutien et envers qui je suis énormément reconnaissant. Je tiens également à remercier la famille de Pascale et, de manière plus particulière Anne, pour m'avoir accepté si chaleureusement et pour l'immense soutien qu'elles m'apportent. Je remercie tous mes amis proches qui se reconnaîtront et tout particulièrement Serge pour l'amitié qui nous lie depuis de longues années. Sans toutes ces personnes, ce travail n'aurait jamais vu le jour.

Enfin, mes remerciements, chargés d'amour et d'émotions, vont à Pascale et Thomas, les deux êtres les plus merveilleux de ma vie. Pascale, je te remercie pour tout l'amour, le soutien, et le bonheur que tu m'apportes depuis notre rencontre ainsi que pour ton aide et tes encouragements à l'égard de ce travail. Je t'en suis infiniment reconnaissant.





---

**Abbreviations**

Å	Angstrom
ABC	ATP binding cassette
AG	Acaciae gum
AI	Absorption index
ATP	Adenosine triphosphate
C	Cycle
°C	Degrees Celsius
ca	<i>circa</i> (about)
CDER	Center for Drug Evaluation and Research
CMC	Critical micelle concentration
Cu	Copper
DCM	Dichloromethane
DI	Deionized
DMA	N,N'-dimethylacetamide
DSC	Differential Scanning Calorimetry
e.g.	<i>exempli gratia</i>
EPAS	Evaporative Precipitation into Aqueous Solutions
EtOH	Ethanol
FaSSiF	Fasted state simulated intestinal fluid
FD	Freeze-dried
FDA	Food and Drug Administration
FeSSiF	Fed state simulated intestinal fluid
flw	Following
FR	Flow rate
GAS	Gas anti-solvent precipitation
GIT	Gastrointestinal tract
GRT	Gastric residence time
H <sub>2</sub> O	Water
Hac 1% v/v	Glacial acetic acid 1% v/v solution
HPC	Hydroxypropylcellulose
HPH	High Pressure Homogenization
HPLC	High Performance Liquid Chromatography
HPMC	Hydroxypropylmethylcellulose
HPMCP	Hydroxypropylmethylcellulose Phtalate
HSM	Hot Stage Microscopy
IBD	Inflammatory bowel disease
ICH	International Conference on Harmonisation (of technical requirements for registration of pharmaceuticals for human use)
i.e.	<i>id est</i>
IMS	Intercontinental Marketing Services
IR	Immediate Release

---

IRDF	Immediate Release Dosage Form
ISO	International Organization for Standardization
IVIVC	In Vitro-In Vivo Correlation
IUVs	Intermediate-sized unilamellar vesicles
J	Joules
LD	Laser Diffraction
5-LO	5-Lipoxygenase
LMW	Low molecular weight
LUVs	Large unilamellar vesicles
M	Molar
MDR	Multidrug Resistance protein
MLVs	Multilamellar vesicles
mp	Melting point
MRPs	Multidrug Resistance related Proteins
MS	Multiple Sclerosis
MW	Molecular weight
N	Normal
NA	Not assayed
NCE	New chemical entity
ND	Not detected
Ni	Nickel
NIC	Nicardipine
NIF	Nifedipine
NP	Nanoparticle
%	Percent
PA	Polyvinyl alcohol
PCS	Photon Correlation Spectroscopy
PEG	Polyethylene Glycol
P-gp	P-glycoprotein
PK	Pharmacokinetic
PM	Pre-milling
PMC	Pre-milling cycles
PSI	Pounds per square inch (14.5 PSI = 1 bar)
PVA	Polyvinyl alcohol
PVP	Polyvinyl pyrrolidone
PXRD	Powder X-Ray Diffraction
RA	Rheumatoid Arthritis
RESS	Rapid Expansion from Supercritical Fluids
RESAS	Rapid Expansion from Supercritical to Aqueous Solutions
RH	Relative humidity
RI	Refractive index
rpm	Rotation per minutes
RT	Retention time

---

s	Second
SAS	Supercritical anti-solvent precipitation
SAS-EM	Supercritical anti-solvent-Enhanced mass transfer
SBP	Systolic Blood Pressure
SCFs	Supercritical Fluids
SD	Spray-dried / Standard deviation
SDS	Sodium Dodecyl Sulfate
SEDDS	Self-emulsifying drug delivery systems
sem	Standard Error Mean
SEM	Scanning Electron Microscopy
SEM-EDS	Scanning Electron Microscopy - Energy Dispersive Spectroscopy
SGF	Simulated gastric fluid
SHR	Spontaneously Hypertensive Rats
SIF	Simulated intestinal fluid
SIP	Steam In Place
SLN	Solid Lipid Nanoparticles
SMEDDS	Self-microemulsifying drug delivery systems
SSA	Specific surface area
SUVs	Small unilamellar vesicles
TEER	Transepithelial Electrical Resistance
THF	Tetrahydrofurane
$\theta$	Theta
UHMWPE	Ultra High Molecular Weight Polyethylene
USP	United States Pharmacopeia
UWL	Unstirred Water Layer
VCAM-1	Vascular adhesion molecule-1
vs.	Versus
WBC	White Blood Cells
w/v	weight/volume
w/w	weight/weight
v/v	volume/volume
mmol	Millimolar
h	Hour
g	Gram
mg	Milligram
ml	Milliliter
$\mu$ l	Microliter
cm	Centimeter
mm	Millimeter
$\mu$ m	Micrometer
nm	Nanometer
min	Minute



<b>I. Summary</b>	<b>3</b>
<b>II. Introduction</b>	<b>9</b>
<b>II.1. Oral drug delivery</b>	<b>11</b>
II.1.1. Physiological and anatomical considerations	11
II.1.2. Drug absorption from the gastrointestinal tract	15
II.1.2.1. Biopharmaceutical Classification System (BCS)	17
<b>II.2. Solubility / Dissolution rate theory</b>	<b>19</b>
II.2.1. Solubility	19
II.2.1.1. Theoretical background	20
II.2.1.2. Factors influencing solubility	23
II.2.1.2.1. Drug characteristics	23
II.2.1.2.2. Temperature and pressure	24
II.2.1.2.3. pKa and GIT pH profile	25
II.2.1.2.4. Crystalline state - polymorphism	27
II.2.1.2.5. Surfactants	30
II.2.1.2.6. Particle size	31
II.2.2. Dissolution	34
II.2.2.1. Theoretical background	34
II.2.2.2. Factors influencing dissolution rate	35
II.2.2.2.1. Particle size - Specific surface area (SSA)	36
II.2.2.2.2. Diffusion coefficient and the thickness of the diffusion boundary layer	37
II.2.2.2.3. Wettability	38
<b>II.3. Dissolution rate/solubility enhancement technologies</b>	<b>39</b>
II.3.1. Drug modification	40
II.3.1.1. Pharmaceutical salts	40
II.3.1.2. Prodrugs	41
II.3.2. Solubilization	42
II.3.2.1. Solubilization using a cosolvent – solvent mixture	42
II.3.2.2. Micellization	43
II.3.2.3. Emulsions – microemulsions – SEDDS/SMEDDS	44
II.3.2.4. Liposomes	45
II.3.3. Specific and non specific complexation	47
II.3.3.1. Solid dispersions or solutions in polymers	47
II.3.3.2. Inclusion complexation (cyclodextrins)	49
II.3.4. Particle size reduction	51
II.3.4.1. Controlled production from solutions	54
II.3.4.1.1. Supercritical fluid-based technologies	54
II.3.4.1.1.1. Rapid Expansion of Supercritical Solutions (RESS)	55
II.3.4.1.1.2. Gas anti-solvent (GAS) and Supercritical anti-solvent (SAS) precipitation method	56

II.3.4.1.2. Spray-drying .....	57
II.3.4.1.2. Aerosol Flow reactor method.....	57
II.3.4.1.3. Controlled precipitation process .....	58
II.3.4.1.4. Evaporative precipitation into aqueous solutions (EPAS) .....	58
II.3.4.1.5. Cryogenic Spray Process - Spray-freezing into liquids (SFL) .....	59
II.3.4.1.6. Microemulsion template methodology.....	60
II.3.4.2. Mechanical micronization (“nanoisation”) processes.....	61
II.3.4.2.1. Media milling.....	62
II.3.4.2.2. High Pressure (piston-gap) Homogenization (HPH).....	64
II.3.4.2.2.1. Principle behind particle size reduction.....	65
<b>III. Aim of the work...</b> .....	71
<b>IV. Experimental Part</b> .....	75
<b>IV.1. Model drugs</b> .....	75
IV.1.1. Nifedipine.....	75
IV.1.2. ucb-35440-3 .....	79
IV.1.3. UCB-A and UCB-B.....	81
<b>IV.2. Particle size reduction using high pressure homogenization - nanoparticle preparation</b> .....	87
IV.2.1. Introduction.....	87
IV.2.2. Materials and Methods.....	90
IV.2.2.1. Materials used for nanosuspension preparation.....	90
IV.2.2.1.1. Stabilizers/Surfactants - carriers .....	90
IV.2.2.1.2. Water.....	91
IV.2.2.2. Nanoparticle preparation.....	91
IV.2.2.2.1. Drug suspension preparation .....	91
IV.2.2.2.2. High speed stirrer-homogenizer .....	92
IV.2.2.2.3. High Pressure Homogenizer .....	93
IV.2.2.2.3.1. Apparatus - Technical characteristics .....	93
IV.2.2.2.3.2. Homogenizing protocol.....	95
IV.2.2.3. Water-removal from the nanosuspensions .....	97
IV.2.2.3.1. Freeze-drying .....	97
IV.2.2.3.1. Spray-drying .....	97
IV.2.2.4. Nanoparticle size/morphology characterization.....	97
IV.2.2.4.1. Laser diffraction .....	97
IV.2.2.4.2. Scanning Electron Microscopy (SEM) - SEM-EDS.....	102
IV.2.2.5. Chemical stability - HPLC method UCB M1 .....	103
IV.2.3. Results and discussion.....	105
IV.2.3.1. Surfactant screening - influence of the type of surfactant .....	105
IV.2.3.2. Influence of pre-milling operations.....	110
IV.2.3.3. Influence of high pressure homogenizing cycles .....	113

IV.2.3.3.1. Influence of the number of homogenizing cycles .....	113
IV.2.3.3.2. Influence of additional cycles at higher homogenizing pressure .....	118
IV.2.3.4. Influence of temperature .....	119
IV.2.3.5. Redispersion analysis - influence of carriers .....	123
IV.2.3.6. Chemical stability .....	135
IV.2.4. Conclusion .....	139
<b>IV.3. Crystalline state evaluation .....</b>	<b>141</b>
IV.3.1. Introduction .....	141
IV.3.2. Materials and Methods .....	141
IV.3.2.1. Differential Scanning Calorimetry (DSC) .....	141
IV.3.2.2. Powder X-Ray Diffraction (PXRD) .....	143
IV.3.2.3. Polarized-light optical microscopy .....	144
IV.3.2.4. Hot Stage Microscopy (HSM) .....	144
IV.3.3. Results and discussion .....	146
IV.3.3.1. Nifedipine .....	146
IV.3.3.1.1. Identification of various polymorphic forms of NIF through Differential Scanning Calorimetry (DSC) .....	146
IV.3.3.1.2. Evaluation of drug crystalline state following particle size reduction - DSC .....	147
IV.3.3.1.3. Evaluation of drug crystalline state following particle size reduction - PXRD .....	149
IV.3.3.2. ucb-35440-3 .....	155
IV.3.3.3. UCB-A and UCB-B .....	160
IV.3.3.3.1. Investigations in UCB-A polymorphic transformations before and after particle size reduction - DSC .....	160
IV.3.3.3.2. Powder X-Ray Diffraction analysis .....	166
IV.3.4. Conclusion .....	167
<b>IV.4. In vitro evaluation - solubility/dissolution characteristics .....</b>	<b>169</b>
IV.4.1. Introduction .....	169
IV.4.2. Materials and Methods .....	171
IV.4.2.1. Materials .....	171
IV.4.2.2. Saturation solubility .....	172
IV.4.2.2.1. Nifedipine .....	172
IV.4.2.2.2. ucb-35440-3 .....	172
IV.4.2.2.3. UCB-A and UCB-B .....	173
IV.4.2.3. USP dissolution apparatus type II .....	173
IV.4.2.3.1. NIF .....	173
IV.4.2.3.2. ucb-35440-3 .....	174
IV.4.2.3.3. UCB-A and UCB-B .....	174
IV.4.2.4. USP dissolution apparatus type IV: Flow-Through dissolution apparatus .....	176
IV.4.2.5. HPLC methods .....	178
IV.4.2.5.1. ucb-35440-3 .....	178
IV.4.2.5.1.1. UCB M2 .....	178

IV.4.2.5.1.2. UCB M3 .....	178
IV.4.2.5.2. UCB-A and UCB-B.....	179
IV.4.2.5.2.1. UCBA M1 .....	179
IV.4.2.5.2.2. UCBA M2 .....	179
IV.4.2.5.2.3. UCBA M3 .....	180
IV.4.3. Results and discussion.....	181
IV.4.3.1. Saturation solubility evaluation before and following particle size reduction.....	181
IV.4.3.1.1. Nifedipine.....	181
IV.4.3.1.2. ucb-35440-3 .....	182
IV.4.3.1.3. UCB-A.....	184
IV.4.3.1.4. UCB-B .....	186
IV.4.3.2. Evaluation of dissolution rate characteristics before and following particle size reduction.....	188
IV.4.3.2.1. Nifedipine.....	188
IV.4.3.2.2. ucb-35440-3 .....	190
IV.4.3.2.2.1. USP type II apparatus .....	191
IV.4.3.2.2.2. USP type IV apparatus - Flow-through dissolution system .....	194
IV.4.3.2.3. UCB-A.....	204
III.4.3.2.4. UCB-B.....	210
IV.4.4. Conclusion .....	215
<b>IV.5. In vitro evaluation - permeation rate across Caco-2/HT29-5M21 cultures and co-cultures.....</b>	<b>217</b>
IV.5.1. Introduction .....	217
IV.5.2. Materials and Methods.....	222
IV.5.2.1. Materials .....	222
IV.5.2.2. Permeation studies.....	222
IV.5.2.2.1. Cell lines and culture conditions.....	222
IV.5.2.2.2. Transport studies .....	223
IV.5.2.2.3. Analytical procedure - HPLC method NIF M1 .....	224
IV.5.2.2.4. Statistical analysis .....	225
IV.5.3. Results and discussion.....	226
IV.5.3.1. Preparation of chitosan-coated NIF nanoparticles .....	226
IV.5.3.2. Transport studies across Caco-2/HT29-5M21 cultures and co-cultures.....	230
IV.5.4. Conclusion .....	238
<b>IV.6. In vivo evaluation - pharmacokinetic studies .....</b>	<b>239</b>
IV.6.1. Introduction .....	239
IV.6.2. Materials and methods.....	241
IV.6.2.1. ucb-35440-3: in vitro dissolution .....	241
IV.6.2.2. ucb-35440-3: in vivo pharmacokinetic studies.....	242
IV.6.2.2.1. Animals.....	242
IV.6.2.2.2. Experimental protocol .....	242
IV.6.2.2.3. Analysis .....	243
IV.6.2.2.3.1. Sample preparation procedure.....	243



IV.6.2.2.3.2. ucb-35440-3 analysis - UCB M4.....	243
IV.6.2.2.3.3. Data processing .....	244
IV.6.2.2.3.4. Statistical analysis .....	244
IV.6.2.3. Nifedipine .....	245
IV.6.2.3.1. Protocol A.....	245
IV.6.2.3.1.1. Animals .....	245
IV.6.2.3.1.2. Experimental protocol.....	245
IV.6.2.3.2. Protocol B.....	246
IV.6.2.3.2.1. Animals .....	246
IV.6.2.3.2.2. Experimental protocol.....	246
IV.6.2.3.3. Analysis .....	246
IV.6.2.3.3.1. Sample preparation procedure.....	246
IV.6.2.3.3.2. NIF analysis - HPLC method NIF M2 .....	247
IV.6.2.3.3.3. Data processing.....	247
IV.6.2.3.3.4. Statistical analysis .....	248
IV.6.3. Results and discussion.....	249
IV.6.3.1. ucb-35440-3 .....	249
IV.6.3.2. Nifedipine .....	254
IV.6.3.2.1. Suspension state - NIF protocol A.....	254
IV.6.3.2.2. Powder state (minicapsule) - NIF protocol B .....	256
IV.6.4. Conclusion .....	258
<b>IV.7. In vivo evaluation - evaluation of the antihypertensive effect of NIF nanoparticles on spontaneously hypertensive rats (SHR) .....</b>	<b>259</b>
IV.7.1. Introduction .....	259
IV.7.2. Materials and methods.....	259
IV.7.2.1. Animals .....	259
IV.7.2.2. NIF administration.....	260
IV.7.2.3. Systolic blood pressure measurements.....	260
IV.7.2.4. Statistical analysis.....	260
IV.7.3. Results and discussion.....	261
IV.7.4. Conclusion .....	263
<b>IV.8. Stability studies .....</b>	<b>265</b>
IV.8.1. Introduction .....	265
IV.8.2. Material and methods .....	266
IV.8.2.1. Capsule blistering .....	266
IV.8.2.2. Drug stability - HPLC method NIF M3.....	266
IV.8.2.3. Dissolution rate evaluation.....	267
IV.8.2.4. Redispersion analysis - Laser diffraction.....	267
IV.8.2.5. Differential scanning Calorimetry (DSC).....	268
IV.8.2.6. Powder X-Ray diffraction (PXRD).....	268
IV.8.3. Results and discussion.....	269

IV.8.3.1. Drug stability .....	269
IV.8.3.2. Drug dissolution.....	271
IV.8.3.3. NIF nanoparticle redispersion characteristics.....	273
IV.8.3.4. Crystalline state evaluation .....	275
IV.8.3.4.1. DSC.....	276
IV.8.3.4.2. PXRD.....	281
IV.8.4. Conclusion .....	285
<b>V. General conclusion.....</b>	<b>289</b>
<b>VI. References.....</b>	<b>295</b>
<b>VII. Annexes.....</b>	<b>311</b>

## **SUMMARY**



## I. Summary

When considering oral administration, drug release from its pharmaceutical form and its dissolution into gastrointestinal fluids generally precedes absorption and systemic availability. The solubility-dissolution behaviour of a drug is frequently the rate-limiting step to absorption of drugs from the gastrointestinal tract (BCS class II drugs). Poor aqueous solubility has always been a very challenging obstacle as it is, together with membrane permeability, an essential factor in the limitation of a drug's bioavailability following oral administration.. Since an increasing number of newly developed drug candidates in pre-clinical development phases present poor water-solubility characteristics, there is a great need for formulation approaches to overcome this factor.

Out of the many ways to increase a product's solubility/dissolution rate characteristics with the aim of enhancing its oral bioavailability, drug formulation as nanoparticles has received much-increased interest over the last decade. The hypothesis behind dissolution rate enhancement, considering drug particle size reduction to nanometer range, lies primarily in a much-increased effective surface area (Noyes-Whitney) presented by the resulting drug nanoparticles. Out of the various technologies available for drug particle size reduction to nanometer range, milling using high pressure homogenization is regarded as one of the simplest and most effective techniques. High pressure homogenization is a solvent-free process and is relatively rapid (time-saving). Furthermore, and most importantly, the scaling up of this technique is already established; processing capacities ranging from 3 l/h (e.g. EmulsiFlex C3<sup>®</sup>: minimum sample volume - 10 ml) to 1000 l/h (e.g. EmulsiFlex C1000<sup>®</sup>: minimum sample volume - 2 l).

Four model drugs were studied in this work. Nifedipine (NIF), an extensively studied poorly water-soluble drug in the literature, was used as the main model on which most of the development was done. In parallel to the work carried out on NIF, three UCB S.A. molecules currently under development were also studied as poorly water-soluble drugs: these being ucb-35440-3, UCB-A and UCB-B (salt of UCB-A). These three UCB S.A. model drugs are, contrarily to NIF, predicted highly dosed drugs and are weak bases, and thus present pH-dependent solubility profiles, which allowed us to investigate model drugs with different profiles.

Firstly, investigations regarding appropriate formulation development (stabilizer (surfactant) selection) and appropriate high pressure homogenization operating conditions (pre-milling cycles, influence of the number of high pressure homogenizing cycles, influence of homogenizing pressure, influence of sample temperature) were made. It has been shown, through this development, for the four studied model drugs, that high pressure

homogenization is an appropriate technique for reducing drug particle size to nanometer range (NIF ~ 290 nm, ucb-35440-3 ~ 180 nm, UCB-A ~ 350 nm and UCB-B ~ 250 nm). Investigations regarding water-removal from the nanosuspensions obtained and most importantly regarding the redispersion characteristics of the retrieved powders (i.e. nanoparticles) were then carried out. In that regard, it has been shown that the presence of carriers in the formulation is essential for limiting nanoparticles agglomeration during the water-removal operation.

Drug crystalline state characterizations before and following particle size reduction were then carried out on the three studied model drugs, mainly through DSC and PXRD studies. In fact, one of the advantages of this particle size reduction approach (using high pressure homogenization), versus other frequently studied solubility/dissolution rate enhancement technologies (e.g. such as solid dispersions), is that original crystalline state shall not be altered in such a way that the achieved increased solubility and dissolution rate characteristics do not rely on the presence of the amorphous form of the drug; this furthermore implying a greater time-stability of the developed formulations. Through the data obtained, it has been shown that original drug crystalline state seems to be unaltered following particle size reduction.

In vitro solubility and dissolution characteristics were then evaluated on the formulations developed in order to verify the posed hypothesis regarding effective surface area increase. It has been shown through these studies that drug solubility and most importantly drug dissolution rate can be significantly enhanced for nanoparticulate systems (verified for NIF, ucb-35440-3, UCB-A and UCB-B). For example, solubility was enhanced from 26 µg/ml vs. 19.5 µg/ml for NIF nanoparticles and the dissolution characteristics showed that 100% of the tested dose (equivalent to 10 mg NIF) was already dissolved following 10 min vs. less than 5% for un-milled NIF. Following these very interesting and promising results, and preliminary to the in vivo pharmacokinetic studies carried out, in vitro permeation studies (apical to basolateral transfer studies) across intestinal cell models (Caco-2 and HT29-5M21 cultures and co-cultures) were carried out. This evaluation was only carried out using NIF as a model drug and showed a 6-fold increase in the permeation rate for NIF nanoparticles. The influence of chitosan (permeability enhancer/bioadhesive polymer) in the NIF nanoparticle formulation with regard to in vitro NIF permeation rate was also evaluated.

In vivo pharmacokinetic studies in rats were conducted using NIF and ucb-35440-3 as model drugs. The very different profiles of these two model drugs allowed us to retrieve interesting information regarding the in vivo behaviour of the developed formulations. As expected from the in vitro (i.e. solubility/dissolution/permeation) studies and results obtained for NIF, an increased extent of exposure could be observed for NIF nanoparticles

versus un-milled NIF; the difference being more pronounced when the formulations were orally administered into capsules (2.5-fold increase in extent of exposure and 6-fold increase in C<sub>max</sub>). For ucb-35440-3, a poorly water-soluble weak base with a reported significant food effect considering oral bioavailability, an increased extent of exposure for nanoparticles, versus the un-milled drug, could only be observed in fasted state (4-fold increase in extent of exposure and 2.7-fold increase in C<sub>max</sub>). These different, diet-relative observations allowed us to put forward some limitations and precautions (considering poorly water-soluble weak bases) relative to the possibility of drug reprecipitation following stomach's emptying, particularly if dissolution in the stomach is quite fast (e.g. nanoparticulate systems).

In parallel to the *in vivo* pharmacokinetic evaluation of NIF nanoparticles, evaluation of the antihypertensive effect of the systems developed following oral administration, using spontaneously hypertensive rats, was also carried out and compared to un-milled NIF. The results obtained showed a significant drop in systolic blood pressure for NIF nanoparticles (32% reduction of initial SBP following 30 min vs. 1% for un-milled NIF) and nicely complemented the *in vitro* and *in vivo* results obtained for NIF nanoparticles.

Finally, a stability study of the optimized NIF nanoparticle formulation was carried out with respect to reported ICH conditions (25°C/60% RH; 30°C/65% RH; 40°C/75% RH). The results showed that the studied NIF nanoparticle formulation retains all its original characteristics (dissolution, crystalline state, redispersion characteristics); this being verified over time (12 months) and for each of the three storage conditions studied.





# INTRODUCTION



## II. Introduction

Because it is the easiest and most convenient way of non-invasive administration, the oral route has always, by far, been the preferred way of dosing. Oral drug delivery systems also being the most cost-effective to manufacture, they have always lead the worldwide drug delivery market.

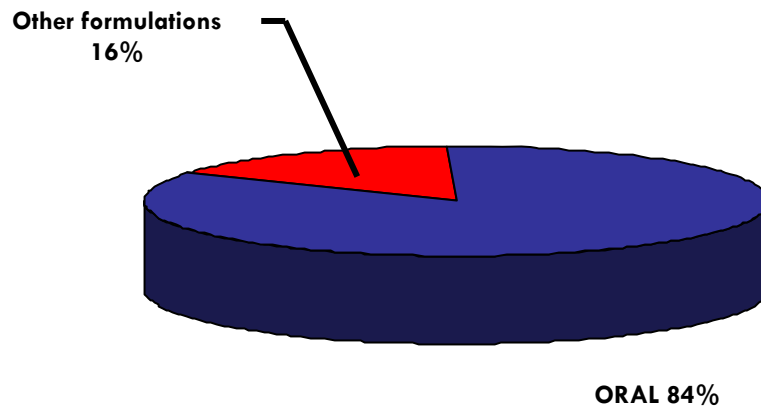


**Figure II 1.** Percent sales of orally administered drugs for the 50 most sold pharmaceutical products in US and Europe (from IMS Health 2001) (Lennernäs, 2005)

The most commonly encountered solid oral dosage forms on the market are tablets and capsules. All these oral dosage forms either follow an immediate or a modified drug release profile:

- **Immediate release (IR) drug delivery systems:**

IR drug delivery systems are dosage forms that allow the drug to dissolve in the gastrointestinal content with no intention of delaying or prolonging the drug dissolution or absorption. Specifications regarding dissolution characteristics of immediate release dosage forms indicate that at least 85% of the drug should be dissolved in a 60 min span (FDA CDER Guidance, 1997a).

Complete, rapid drug dissolution is advantageous for multiple reasons:

- Assuming that there is some relationship between drug concentration in the body and the magnitude of the therapeutic effect (which is often the case), the greater the concentration achieved, side-effects considerations apart, the greater the magnitude of response.
- Generally, the more rapidly the drug is dissolved and absorbed, the sooner the onset of the pharmacological response.

These forms are targeted mainly towards acute diseases or symptoms requiring rapid onset of action. These forms are generally dosed multiple times per day, depending of the pharmacokinetic half-life of the drug.

- **Modified release drug delivery systems:**

Modified-release drug delivery systems are solid dosage forms in which the active drugs are made available to a specified target at a rate and duration designed to accomplish therapeutic and/or convenience objectives (Qiu and Zhang, 2000). The two main modified drug delivery systems are delayed release dosage forms and extended release dosage forms.

- Delayed release dosage forms: Dosage forms that release the drug at a time other than promptly after administration, i.e. enteric drug delivery systems (Wilding, 2000; Cole et al., 2002) and colonic drug delivery systems (Sangalli et al., 2001, 2004; Yang et al., 2002; Minko, 2004).

Targeted delivery into the small intestine is used in a first hand to bypass the stomach environment in the case of pH sensitive drugs (i.e. degradation in acidic media) and in a second hand, to protect the stomach's mucosa from potentially aggressive drugs (e.g. NSAID-associated gastric ulcer). Targeted delivery into the colon represents an advantageous approach for the treatment of widespread inflammatory bowel disease (IBD) including ulcerative colitis and Crohn's disease, as well as tumoral, infective or neurovegetative colonic pathologies (Sangalli et al., 2001).

Furthermore, the colon is found to be a promising site for systemic absorption of peptides and proteins because of the less hydrolytic hostile environment in comparison with the stomach and small intestine as well as the existence of specific transporters (Minko, 2004).

- Extended release dosage forms: Dosage forms that provide an immediate drug release after administration with a continued controlled drug release over an extended period of time. The main advantage of these dosage forms over IR dosage forms lies in the fact that the plasmatic concentrations can easily be levelled in the therapeutic range of the drug for an extended period of time with a reduced dosing frequency (increased patient compliancy), thus limiting plasmatic peaks and reducing undesirable side effects. These forms are, however, of limited utility when considering highly dosed drugs (i.e. manufacturing reasons), drugs presenting an absorption window, drugs presenting a narrow therapeutic index, poorly water-soluble drugs (i.e. diffusion being the main encountered driving factor for drug release) and drugs with a long plasmatic half-life (Hamdani, 2005).

## II.1. Oral drug delivery

### II.1.1. Physiological and anatomical considerations

The gastrointestinal tract (GIT) is a highly specialized region of the body whose primary functions involve the processes of secretion, digestion and absorption. With the exception of oxygen, all nutrients needed by the body must first be ingested orally, processed by the GIT, and then made available for absorption into the bloodstream (Mayersohn, 2002). Orally administered drugs follow the same pathway as these nutrients and physiological/anatomical considerations are of high relevance, in complement to drug physicochemical characteristics, in determining the drug's fate in the GIT.

A schematic representation of the human GIT is shown in **Figure II 2**. It is possible to divide the gut in five sections, all presenting different and specific functions: the esophagus, stomach, small intestine, large intestine, and rectum.

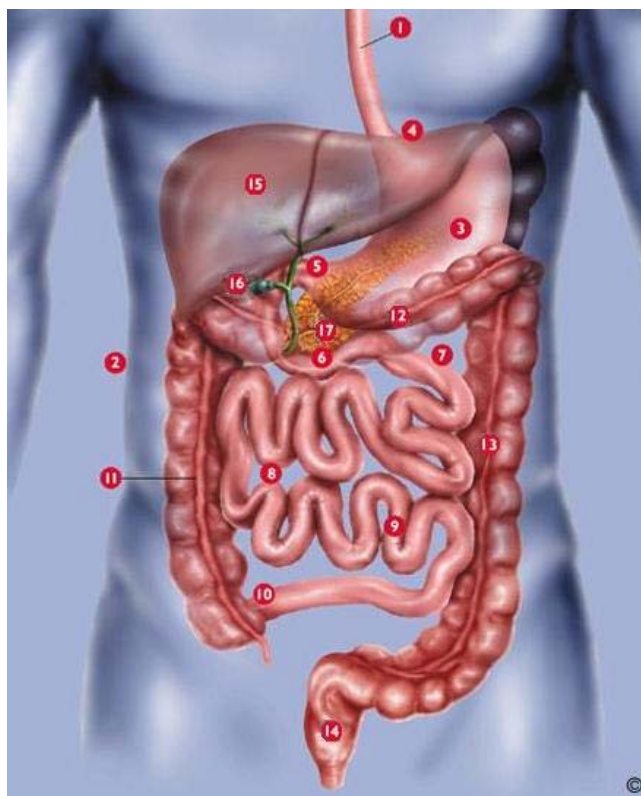


**Figure II 2.** Schematic representation of the human gastrointestinal tract (GIT): 1. Esophagus; 2. Abdomen; 3. Stomach; 4. Sphincter; 5. Pyloric sphincter; 6-7. Duodenum; 8. Jejunum; 9. Ileum; 10. Ileocecal valve; 11. Ascending colon; 12. Transverse colon; 13. Descending colon; 14. Rectum; 15. Liver; 16. Gallbladder; 17. Pancreas (adapted from **Genesis Health, 2006**).

**Esophagus:** The esophagus begins as an extension of the pharynx in the back of the oral cavity. It then runs down the neck next to the trachea, through the thoracic cavity, and penetrates the diaphragm to connect with the stomach in the abdominal cavity. Anatomically and functionally, the esophagus is the least complex section of the digestive tract. Its role is to convey boluses of food, and, in our case, drug formulations, from the pharynx to the stomach. In adults, the esophagus is about 25 centimeters long. Transit through the esophagus is normally complete within 5 to 15 seconds, depending on posture (**Wilson, 2000**).

The esophagus does not play a role in drug absorption and does not, in normal physiological conditions, interfere with the advance of drug formulations to the stomach. A few reported conditions such as disorders of normal motility (dysphagia), left-sided heart enlargement, or stricture of the esophagus might alter esophageal clearance of formulations (**Wilson, 2000**).

**Stomach:** The stomach, situated on the left side of the abdominal cavity, is the GIT section found between the esophagus and the duodenum. It has anatomically been divided into three parts: the fundus, the body and the antrum (**Figure II 3**). Its main functions involve the storage, the mixing and digestion of food intake and finally, the emptying of its content into the duodenum. In fed state, the stomach can distend to accommodate a meal of up to one liter (**Mayersohn, 2002**). The stomach is a highly acidic environment (mainly due to the secretion of hydrochloric acid by parietal cells) maintained at pH 1.5-2 in fasted state. There are complex variations in pH between the fed and fasted

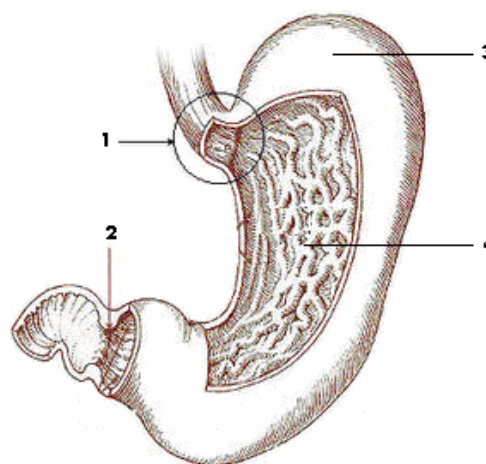


**Figure II 3.** Schematic representation of the stomach: (1) gastro-oesophageal junction (antrum), (2) pyloric sphincter, (3) fundus and (4) body (modified from **US NIH-NCI SEER, 2005**).

state. Upon ingestion of a meal, the gastric pH at first increases (up to pH 5.0 depending on meal type) because of the buffering effects of food components. In response to food ingestion, however, gastric acid is secreted, and by 3 to 4 hours after the meal intake, the fasted state pH has usually been re-established (**Hörter and Dressman, 2001**) (**Figure II 4**). These fasted/fed state pH variations are of great relevance when considering IR dosage forms containing drugs presenting a pH-dependent solubility profile. This is particularly important for weak bases (i.e. decrease in solubility when pH increases) as their stomachal solubility in fasted state is generally greater than in fed state and even greater than their intestinal solubility; reprecipitation of the dissolved drug

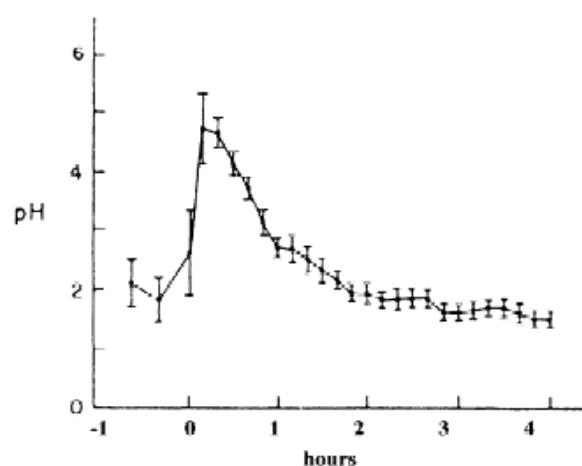


**Figure II 4.** Gastric pH in the fasted state and after food intake (pH6, 458 calories and 400ml total volume) in 10 healthy volunteers (**Hörter and Dressman, 2001**).

following exiting of the stomach being then a possible consideration (**Hecq et al, 2006**). The fasted and fed state (in addition to meal type) also influence gastric retention time (GRT) as gastric emptying is much faster in fasted state. This, depending on formulation type and size, also has an influence on the retention time of the dosage form in the stomach (**Hamdani, 2005**).

Absorption from the stomach, when compared to absorption from the small intestine, by virtue

of histological and anatomical considerations (larger intestinal surface area (**Table II 1**)), is very low. The stomach, nevertheless, contributes to the absorption, to a small extent, of water, electrolytes, alcohol (**Levitt et al., 1997**) and some drugs (i.e. acidic drugs such as acetylsalicylic acid (**Mayersohn, 2002**)).

**Table II 1.** GIT morphological and physiological aspects (**Qiu and Zhang, 2000; Wilding, 2000; Hörter and Dressman, 2001; Mayersohn, 2002**).

Section	Size diameter x length (cm)	Absorption surface (m <sup>2</sup> )	pH fasted	pH fed
Stomach	1.5 x 20	0.1	1.5-3	2-5
Duodenum	3-5 x 20-30	0.1	6.5	5.4
Jejunum	3-5 x 240	60	6.6	5.2-6
Ileum	3-5 x 360	60	7.4	unmodified
Large intestine	3-9 x 90-150	0.25	7-8	unmodified

**Small intestine:** The small intestine is the part of the gastrointestinal tract lying between the stomach and the large intestine. It has the shape of a convoluted tube and is situated in the central and lower part of the abdominal cavity. It is divided into three structural parts: the duodenum (20-30 cm), the jejunum ( $\pm 2.5$  m) and the ileum ( $\pm 3.6$  m). The duodenal pH is found to be around 5.5-6.5 in fasted state. This pH at first decreases in response to a meal with the arrival of acidic content from the stomach but it is progressively restored to its original value (**Figure II 5**). The small intestine pH increases up to  $\pm 7.4$  in distal ileum (**Table II 1**). The small intestine primary functions involve the completion of the digestion and the absorption of water, electrolytes, nutrients and most orally administered drug substances. The absorption function of the small intestine is principally

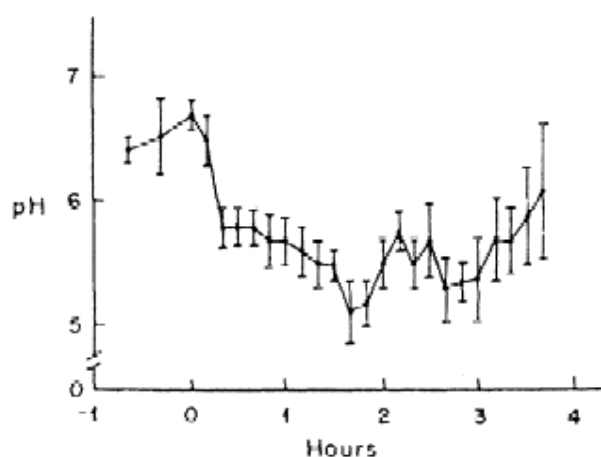


**Figure II 5.** Duodenal pH in the fasted state and after food intake (pH6, 458 calories and 400ml total volume) in 10 healthy volunteers (**Hörter and Dressman, 2001**).

enhanced, in comparison to other sections of the GIT, due to the increased effective luminal surface area. This particularly high absorption surface area is due to the specific structural aspect of the small intestine. In addition to the fact that the intestinal mucosa is folded over itself, the entire epithelial surface of the small intestine is folded into finger-like projections (0.5-1.5 mm in length) known as villi, which extend into the gut lumen. In turn, the epithelial cells which line these villi possess even



larger numbers of projections called microvilli (0.08  $\mu\text{m}$  in diameter and 1  $\mu\text{m}$  in length), which are simple extensions of the cell surface. The mucosal folds, the villi and the microvilli increase the effective surface area, in comparison to the surface area of a smooth cylinder, by a 3-, 30- and 600-fold factor (Mayersohn, 2002).

**Large intestine:** The large intestine (colon) is the part of the gastrointestinal tract lying between the end of the ileum (cecum) and the rectum. It is structurally similar to the small intestine although there is a loss of the villi. One of its main functions involves the storage and elimination of fecal material. Its role in absorption is limited to the absorption of the water remaining from the small intestinal transit and to the absorption of some electrolytes. As already reported in this introduction, absorption of peptides is also favoured in this location due to the less hydrolytic hostile environment in comparison with the stomach and the small intestine as well as the existence of specific transporters (Minko, 2004).

### II.1.2. Drug absorption from the gastrointestinal tract

Drug transposition from its dosage form into the general circulation, when considering oral administration of immediate-release dosage forms, is a multi-step process involving:

- Disintegration: the process by which the dosage form breaks up into primary particles, drug and excipients, when exposed to the dissolution media.
- Dissolution: the process by which drug molecules leave the solid drug particle and enter into the nearby dissolution media to form a solution.
- Absorption: the process by which dissolved drug molecules pass through the membranes of the gastrointestinal tract to reach the systemic circulation.

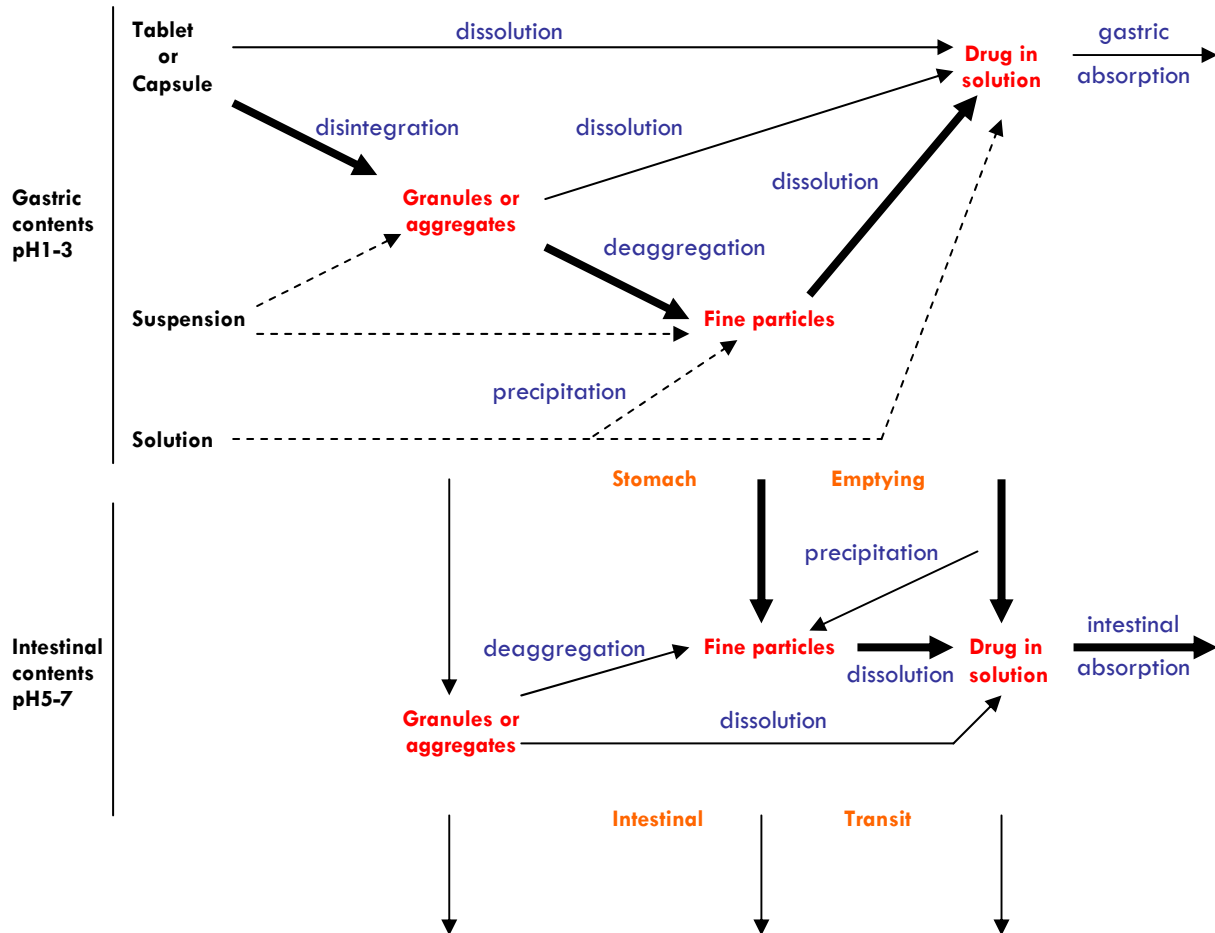


**Figure II 6.** Processes involved in getting a drug into solution in the gastrointestinal tract so that absorption may take place. Heavy arrows indicate primary pathways that the majority of drugs administered in a particular dosage form undergo. Dashed arrows indicate that the drug is administered in this state in the dosage form. Thin continuous arrows indicate secondary pathways, which are usually inconsequential in achieving therapeutic efficacy. (Reproduced from **Hoener and Benet, 2002**).

As we can clearly see in **Figure II 6**, drug absorption following its oral uptake can thus find a limitation either from the drug release from its pharmaceutical form (i.e. solubilization – dissolution) and/or in the permeation across the GIT membranes; tablet or capsule disintegration being generally a well-controlled manufacturing parameter.

As the overall rate of absorption of a drug is dictated by its solubility and permeability characteristics, a classification system based on those parameters has been introduced: the biopharmaceutical classification system (BCS).

### II.1.2.1. Biopharmaceutical Classification System (BCS)

A Biopharmaceutics Classification System (BCS) was introduced by Amidon et al. in 1995 as a basis for predicting the likelihood of in vitro-in vivo correlations for immediate release dosage forms, based on the recognition that drug solubility/dissolution properties and gastrointestinal permeability are the fundamental parameters controlling the rate and extent of drug absorption (Amidon et al., 1995).

The BCS classification scheme is subdivided into four groups with respect to aqueous solubility and intestinal permeability:

	Solubility	Permeability
<b>Class I</b>	High	High
<b>Class II</b>	Low	High
<b>Class III</b>	High	Low
<b>Class IV</b>	Low	Low

The FDA has set specifications regarding the solubility and permeability class boundaries used for this BCS classification (FDA CDER Guidance, 2000):

**Solubility:** a drug substance is considered *highly soluble* when the highest dose strength is soluble in 250 ml or less of aqueous media over a pH range of 1 to 7.5 (equilibrium solubility at 37°C).

**Permeability:** in the absence of evidence suggesting instability in the gastrointestinal tract, a drug substance is considered *highly permeable* when the extent of absorption in humans is determined to be 90% or more of an administered dose based on mass balance determination or in comparison to an intravenous reference dose (absolute bioavailability study). The permeability class of a drug may also be determined using in vivo intestinal perfusion approaches (human or appropriate animal models) or in vitro permeation studies (excised human or animal intestinal tissues or monolayers of cultured intestinal cells).

Specifications regarding the dissolution of the IR drug product are also added to this classification.

**Dissolution:** an IR drug product is considered *rapidly dissolving* when no less than 85% of the labeled amount of the drug substance dissolves within 30 min using USP type I apparatus at 100 rpm (or USP type II at 50 rpm) in a volume of 900 ml or less in each of the following media: (1) HCl 0,1N or USP SGF without enzymes, (2) a pH 4,5 buffer and (3) a pH 6,8 buffer or USP SIF without enzymes.

An in vitro-in vivo correlation (IVIVC) has been defined by the FDA as a predictive mathematical model describing the relationship between an in vitro property of a dosage form and an in vivo response. The objective behind the development and the evaluation of an IVIVC is to establish the dissolution test as a surrogate for human bioequivalence studies (i.e. biowaver – permission to replace pharmacokinetic studies by dissolution testing). Biowavers can actually be requested for solid, orally administered immediate-release products meeting the dissolution requirements described above and containing highly soluble and highly permeable drugs (Class I compound). For information, IVIVC can be expected for Class I drugs if the dissolution rate is slower than the gastric emptying rate (otherwise limited or no correlation) and for Class II drugs if the in vitro dissolution rate is similar to the in vivo dissolution rate (unless the dose is very high); limited or no correlations being expected for Class III and IV compounds as permeability is the rate controlling step in drug absorption (Amidon et al., 1995; Löbenberg and Amidon, 2000).

A well developed review by Lindenberg et al. made in association with the World Health Organization (WHO) (Lindenberg et al., 2004) establishes a classification of drugs belonging to the WHO model list of Essential Medicines. Examples of this classification are shown in **Table II 2**.

Although the Class IV is the most problematic, interest will be concentrated primarily on BCS Class II drugs since it is the most common combination as poor solubility of many drugs is directly associated with good lipophilicity which in turn ensures good membrane permeability. For BCS Class II drugs, the dissolution of the drug product is the rate limiting step to absorption as it is the parameter that changes the actual drug concentration in solution over time and that there is no limitation permeability-wise.

**Table II 2.** Classification of orally administered drugs on the WHO model list of Essential Medicines according to the BCS (Lindenberg et al., 2004). (NB: Class III drugs in bold are drugs with permeabilities corresponding to at least 80% absorption).

<b>Class I</b>	amoxicillin	propanolol	<b>Class III</b>	<b>ascorbic acid</b>	atenolol
	diazepam	riboflavin		<b>Abacavir</b>	captopril
	fluconazole	salbutamol		<b>Acetylsalicylic acid</b>	cimetidine
	levodopa	stavudine		<b>aciclovir</b>	hydrochlorthiazide
	metronidazole	theophylline		<b>allopurinol</b>	<b>paracetamol</b>
<b>Class II</b>	nitrofurantoin	phenytoin	<b>Class IV</b>	acetazolamide	
	carbamazepin	valproic acid		furosemide	
	griseofulvin			indinavir	
	ibuprofen			nelfinavir	
	nifedipine			ritonavir	

## II.2. Solubility / Dissolution rate theory

### II.2.1. Solubility

The saturation solubility of a drug compound is a key factor influencing its dissolution rate, as it determines, along with the concentration of the drug already dissolved, the concentration gradient across the boundary layer (see **part II.2.2**). This concentration gradient is the driving force behind dissolution. A limitation in solubility is in general, if no particular adequate formulation approaches are undertaken, translated into a limited dissolution.

Drug solubility ranges according to the European Pharmacopeia, from “very soluble” to “practically insoluble” (**Table II 3**).

The saturation solubility of a drug in the GIT is influenced by many physicochemical and physiological factors. Amongst the physicochemical factors, emphasis will be made in this introduction on the intrinsic aqueous solubility, the pKa (pH-dependent solubility profile of weak acids and weak bases) and the crystalline state of the drug.

**Table II 3.** Descriptive terms of solubility according to the European Pharmacopeia.

		equivalence in concentration
<b>Very soluble</b>	less than 1 volume of solvent (ml) per gram of solute	more than 1 g/ml
<b>Freely soluble</b>	from 1 to 10 volumes of solvent (ml) per gram of solute	100 mg/ml to 1 g/ml
<b>Soluble</b>	from 10 to 30 volumes of solvent (ml) per gram of solute	33 mg/ml to 100 mg/ml
<b>Sparingly soluble</b>	from 30 to 100 volumes of solvent (ml) per gram of solute	10 mg/ml to 33 mg/ml
<b>Slightly soluble</b>	from 100 to 1000 volumes of solvent (ml) per gram of solute	1 mg/ml to 10 mg/ml
<b>Very slightly soluble</b>	from 1000 to 10000 volumes of solvent (ml) per gram of solute	0.1 mg/ml to 1 mg/ml
<b>Practically insoluble</b>	more than 10000 volumes of solvent (ml) per gram of solute	less than 0.1 mg/ml

Considering physiological aspects, GIT pH variations and the possibility of drug solubilization by native surfactants will be discussed.

#### II.2.1.1. Theoretical background

The saturation solubility of a substance can be defined as the amount of that substance in a solution, under given conditions (temperature, pressure, etc.), that is at chemical equilibrium with an excess of the undissolved substance (i.e. the solid phase) (Tong, 2004). Solubility is thus a chemical equilibrium between the solid and dissolved states of a compound at saturation.

An unsaturated solution is a solution containing the dissolved solute in a concentration less than a saturated solution. A supersaturated solution is a solution that contains more of the dissolved solute than normal for a given temperature.

The solvation process of a solid into a liquid is a three-step process (Chen and Liu, 2000; Delaney, 2005). The first step is the separation of the solute molecule from its crystal lattice. This step requires a work that is dependent on the intermolecular forces of the solute (i.e. the solute affinity for itself) within the lattice. The second step involves the separation of the solvent molecules and the creation of a cavity in the solvent to accommodate a solute molecule. Here again, intermolecular forces of the solvent are very important. The third step is the placement of the separated solute molecule within the created cavity and we must here consider the importance

of the solute-solvent intermolecular forces, i.e. how strongly the molecule associates with the solvent. Compound and solvent entropy also play a role in the regulation of this multi-step operation; having a positive and a negative influence, respectively (Delaney, 2005).

We will differentiate between ionic and non ionic compounds:

#### - ionic compounds (salts)

Ionic compounds normally dissociate into their constituent ions (cations ( $C^{n+}$ ) and anions ( $A^{n-}$ )) following their dissolution.



The equilibrium expression of this equation can be written as follows where K is called the equilibrium (or solubility) constant:

$$K = \frac{[C^{n+}] [A^{n-}]}{[C A_{(s)}]}$$

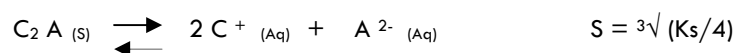
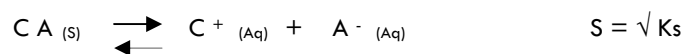
The concentration of solid phase can be considered constant and can be included into the equilibrium constant. The above equation can be simplified as:

$$K_s = [C^{n+}] [A^{n-}] = \text{Solubility product}$$

In this equation, the concentration of each ion is raised to a power equal to the number of ions appearing on dissociation.

When considering slightly soluble electrolytes:	- $[C^{n+}] [A^{n-}] > K_s$	: precipitation
	- $[C^{n+}] [A^{n-}] < K_s$	: no precipitation
	- $[C^{n+}] [A^{n-}] = K_s$	: equilibrium (saturated solution)

The relation between  $K_s$  and the solubility of an ionic compound will be dictated by the stoichiometry of the respective dissociating ions:

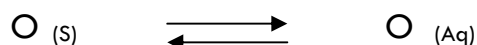


Given these two examples, a lower value of  $K_s$  does not always mean a lower solubility.

It has to be noted that the solubility of an ionic compound will decrease in the presence of an electrolyte possessing a common ion (Le Chatelier's principle) and will increase in the presence of an electrolyte without a common ion (increased ionic strength) (Amidon and Bermejo, 2003).

#### - non ionic compounds (salts)

The solubilization of a non ionic organic solid can be described as an equilibrium between the substance in its solid and dissolved forms.



Comparatively to ionic compounds, the equilibrium expression of this equation can be written as follows:

$$K = \frac{[O_{(aq)}]}{[O_{(s)}]}$$

The concentration of solid phase also being considered constant, this equilibrium equation can be reduced to:

$$K_s = [O_{(aq)}]$$



### II.2.1.2. Factors influencing solubility

#### II.2.1.2.1. Drug characteristics

Drug characteristics such as molecular size, structure and polarity are factors governing intrinsic solubility. Solutes (and solvents) can be broadly classified as polar (hydrophilic) and non-polar (lipophilic). The polarity can be measured as the dielectric constant or the dipole moment of a molecule. A dipole moment is defined as a non-uniform distribution of negative and positive charges amongst the various atoms of the molecule. Molecules with a permanent dipole moment are said to be polar. The polarity of a molecule is thus related to its atomic composition, its geometry, and its size.

Generally polar solute molecules will dissolve in polar solvents and non-polar solute molecules will dissolve in non-polar solvents (“like dissolves like” rule of thumb).

Dipole-dipole interactions (e.g. hydrogen bonding as water is the encountered solvent in vivo) are responsible for the dissolution of many pharmaceutical drugs; the solubility of the low molecular weight organic acids, alcohols, amides, amines, esters, ketones and sugars in polar solvents is a result of dipole-dipole interactions.

Structurally, as the number of polar groups (hydroxyl groups, carboxylic groups, amine groups, etc.) increases on a molecule, water solubility is enhanced as more solute-solvent interactions are made possible. Nevertheless, it has to be noted that strong inter and/or intramolecular bonds may possibly be a cause of poor water solubility (Beyers et al., 2000).

Concerning molecular size, generally, the larger the molecule (i.e. the higher its molecular weight) the less soluble the substance will be. For example, within alkanes, molecular size is the primary determinant of their solubility in water, and increasing molecular size results in a decrease in water solubility mainly due to the increased free energy penalty for cavity formation in water (Tolls et al., 2002).

### II.2.1.2.2. Temperature and pressure

#### - Temperature:

During the dissolution of a solid into a liquid, a change in the physical state of the solid takes place. Energy (e.g. in the form of heat) is necessary to break the intermolecular bonds in the solid and heat is given off during the formation of the new solute/solvent bonds (solvation). The first phenomenon is always endothermic and the second is always exothermic. The resulting enthalpy of this two-step phenomenon will determine if the overall dissolution is exothermic or endothermic.

If the heat given off in the solvation process is greater than the heat required to break apart the solid, the net dissolving reaction produces heat and the dissolution is called exothermic. In contrary, if the heat given off in the dissolving reaction is less than the heat required to break apart the solid, the net dissolving reaction requires heat and dissolution is then called endothermic.

The solubility of solutes is thus highly dependent on temperature. In the first case (i.e. exothermic dissolution), an external increase of temperature will inhibit the dissolution of the solid as an excess of heat is already being produced and a lower solubility will be achieved if temperature is increased. In the second case, on the contrary, an external increase of temperature will facilitate the dissolution of the solid and a higher solubility will be achieved if temperature is increased.

Endothermic dissolution is the most generally encountered phenomenon for organic drugs and thus, an increase in temperature will result in increased drug solubility.

#### - Pressure:

Unlike gases (Henry's law – increase in pressure yielding an increase in solubility), liquids and solids exhibit practically no change of solubility with modifications in pressure; the latter physical forms being barely compressible.

### II.2.1.2.3. pKa and GIT pH profile

The solubility of weak acids and weak bases is highly dependent on their acid-dissociation (or acid-ionization) constant ( $K_a$ ) and the pH of the medium they are placed in.  $K_a$  is the equilibrium constant for the reaction in which a weak acid is in equilibrium with its conjugate base in aqueous solution and it indicates the extent of dissociation of hydrogen ions from an acid. The higher the  $K_a$  value (or the lower the  $pK_a$  value –  $pK_a = -\log_{10} K_a$ ), the stronger the acid.

The intrinsic solubility of a compound is defined as the solubility of the compound in its free acid or base form and shall thus be evaluated at pH values more than one unit below the  $pK_a$  for weak acids and more than one unit above the  $pK_a$  for weak bases (Hörter and Dressman, 2001). As represented in **Figure II 7**, the solubility of weak acids increases with increasing pH and the solubility of weak bases increases with decreasing pH.

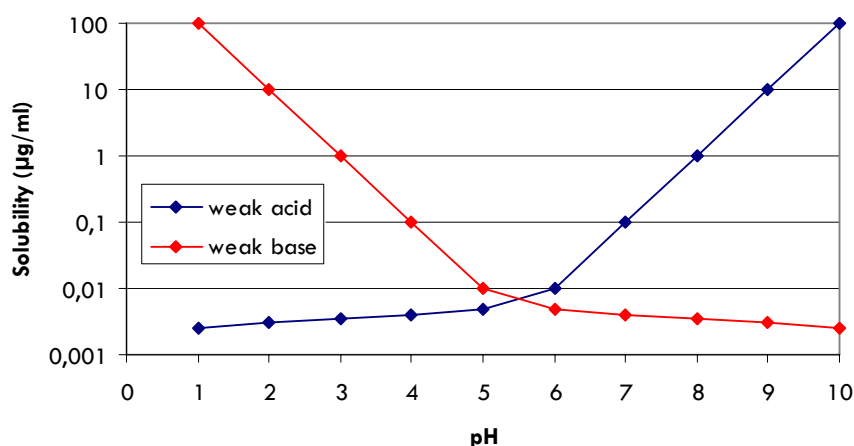


**Figure II 7.** Example of pH-dependent solubility profiles for a weak acid and a weak base.

Solubility pH-dependency and mathematical expressions of equilibriums for the dissociation of a weak acid compound and for the dissociation of the monoprotonated conjugate acid of a weak base can be written as follows (Hörter and Dressman, 2001; Amidon and Bermejo, 2003; Tong, 2004) :



$$K_A = \frac{[H_3O^+][A^-]}{[AH]}$$

$$K_A = \frac{[H_3O^+][B]}{[BH^+]}$$

$$[A^-] = K_A \frac{[AH]}{[H_3O^+]}$$

$$[BH^+] = [B] \frac{[H_3O^+]}{K_A}$$

Expressing the overall solubility (S) as the sum of the concentrations of the ionized (Si) and the unionized (So) species:

$$S = S_o + S_i = [AH] + [A^-]$$

$$S = S_o + S_i = [B] + [BH^+]$$

$$S = S_o \left( 1 + \frac{K_a}{[H_3O^+]} \right)$$

$$S = S_o \left( 1 + \frac{[H_3O^+]}{K_a} \right)$$

At pH values exceeding  $pH = pK_a + 1$  for weak acids and for pH values below  $pH = pK_a - 1$  for weak bases, there is a linear relationship between the logarithm of the solubility and the pH until the limiting solubility of the ionized specie is reached.

Considering these aspects, in vivo GIT pH profile (**Figure II 4 and Figure II 5, Table II 1**) is of high relevance when considering weak acids and weak bases as their solubility and thus their dissolution will be either greater in the intestinal fluids than in the stomach or greater in the stomach than in intestinal fluids, respectively. The fasted and fed state conditions also need to be taken into account as they are both characterized by different stomachal pH (**Figure II 4, Table II 1**), implying a resulting different behavior of these kind of compounds.

Furthermore, for poorly water-soluble weak bases, if rapid and complete dissolution occurs in the stomach, the possibility of reprecipitation following stomach exiting shall be considered (**Hecq et al, 2006**).

#### II.2.1.2.4. Crystalline state - polymorphism

Most organic and inorganic compounds of pharmaceutical relevance can exist in one or more crystalline forms. Because these different crystalline forms will differ in crystal packing, and/or molecular conformation as well as in lattice energy and entropy, there are usually significant differences in their physicochemical properties, such as density, hardness, tabletability, refractive index, melting point, enthalpy of fusion, hygroscopicity, vapor pressure, solubility, dissolution rate, chemical stability, as well as other thermodynamic and kinetic properties (Vippagunta et al, 2001; Huang and Tong, 2004; Singhal and Curatolo, 2004).

A crystal can be viewed as a solid in which the molecules are packed in a regularly ordered, indefinitely repeating pattern extending in all three spatial dimensions. In crystals the repeated structural units are called unit cells. Unit cells are defined by various parameters including the length of the cell edges and the angles between them, and are arranged in a specific order that describes the crystal. Crystalline solids can exist in the form of monocrystals or polycrystals. Monocrystals are crystalline solids in which the crystal lattice of the entire sample is continuous and unbroken to the edges of the sample. Polycrystals are crystalline solids where the regular pattern of arrangements is interrupted by crystal defects and are materials made up of numerous smaller crystals (called crystallites) that have an equivalent type of structure as monocrystals. Crystalline drugs are generally polycrystals (monocrystals are not easily found or obtained).

The most common crystalline forms in which a drug substance can be found are polymorphs and solvates (or pseudopolymorphs).

##### - Polymorphs:

By definition, crystalline polymorphs have identical chemical composition but possess different crystal structures. The differences in crystal structure allow, due to differences in energy states, for differences in physicochemical characteristics, notably in solubility (the lowest energy state polymorph being generally characterized by the lowest solubility). Examples of differences in solubility for different polymorphs of known crystalline drugs are reported in **Table II 4**. Polymorphs are classified, based on their differences in thermodynamic properties and their ability to transform reversibly one to another, as enantiotropes or monotropes; a reversible transformation between polymorphs being possible at a definite transition temperature below the melting point in the first case

(Vippagunta et al, 2001). Model drugs representing both monotropic and enantiotropic systems will be evaluated in this work.

#### - Solvates - pseudopolymorphs:

Solvates are crystalline solids that include solvent molecules into their crystalline lattice. Depending on the type of solvent used, the physicochemical properties of the substance will be modified. Solvates of drugs show, presumably by weakening of the crystal lattice, increased solubility characteristics (Henwood et al., 2001; Chawla et al, 2003). Based on the thermodynamic theory of solubility of solvates however, the rule applying to solubility behaviour is that solid solvates are always less soluble in the solvent forming the solvate than the original solid (Amidon and Bermejo, 2003; Huang and Tong, 2004; Pudipeddi et al, 2005). Solvates formed from other solvents however, if the solvent is water-miscible, are more soluble in water than the corresponding non-solvated form (Huang and Tong, 2004). Hydrates (i.e. solvates where the incorporated solvent is water) are thus less soluble in water. Examples of differences in solubility for different hydrates are reported in **Table II 5**.

**Table II 4.** Solubility ratio of polymorphs (in water): when more than two polymorphic forms are reported, the solubility ratio of each form was calculated relative to the least soluble form - examples from Pudipeddi et al, 2005.

compound	solubility ratio	compound	solubility ratio
Acemetacin (II/I)	1.7	Losartan	2.3
Acemetacin (III/I)	4.7	piroxicam (I/III)	1.3
Acemetacin (IV/I)	2.1	piroxicam (I/III)	1.3
Acemetacin (V/I)	2.8	propanolol	1.4
acetazolamide	1.1	Ranitidine (I/IV)	1.4
Chloramphenicol palmitate	4.2	Ranitidine (II/IV)	1.4
Diflunisal (I/IV)	1.4	Ranitidine (III/IV)	1.3
Diflunisal (II/IV)	1.3	Tenoxicam (I/III)	1.9
Diflunisal (III/IV)	1.3	Tenoxicam (II/III)	1.9
Etoposide	1.9		
Furosemide (II/I)	1		
Furosemide (III/I)	1.8		

**Table II 5.** Anhydrate (A)/ Hydrate solubility ratio (in water) - examples from Pudipeddi et al, 2005.

compound	solubility ratio	compound	solubility ratio
Ampicilline (A/Trihydrate)	1.6	Naproxen sodium	1.2
Caffeine	1.7	Nifedipine (A/Dihydrate)	1.8
Carbamazepine (A/Dihydrate)	1.6	Theophylline	1.9
Erythromycin (A/ Dihydrate)	2.2		

When no long-range order, as described for crystalline solids, can be found within the organization of the molecules of a specific substance, the substance is called amorphous. The amorphous state is characterized by an even greater energy state than some polymorphs (metastable polymorphs) and is much more thermodynamically unstable. The amorphous state of a compound can be obtained by various techniques such as rapid melting/cooling or precipitation techniques.

Since lattice energies of physical forms (amorphous, polymorphs or solvates) are responsible for the difference in solubility, the largest difference in solubility is observed between amorphous and crystalline materials (Huang and Tong, 2004). In fact, when considering polymorphs, the solubility ratio between polymorphs is rarely found to be above 5 (Table II 4). In the review from Pudipeddi and coworkers (Pudipeddi et al, 2005), out of 50 drugs investigated (comprising 81 polymorph comparisons), the solubility ratio never exceeded 5 (except for 1 compound). Similar conclusions could be made for solvates. However for amorphous drugs the solubility ratio can be increased up to several hundred times when compared to the stable crystalline drug (Table II 6) (Huang and Tong, 2004).

**Table II 6.** Comparison of apparent solubility (in water) of amorphous material (A) and crystalline material (C) (Huang and Tong, 2004).

compound	solubility ratio (A/C)	compound	solubility ratio (A/C)
Caffeine	5	Hydrochlorthiazide	1.1
Theophylline	50	Sulfamethoxydiazine	1.5
Morphine	270	Benzimidazole derivatives	500-1000

The use of metastable polymorphic forms and solvates, and to a greater extent of amorphous forms, is frequently relied upon when considering solubility/dissolution formulation enhancement technologies for poorly water-soluble

drugs (e.g. solid dispersions – see **part II.3.3.1**). However, the biggest problem associated with the use of the metastable polymorphs and amorphous forms is the risk of conversion of the higher energy, more soluble form into the crystalline form with the lowest energy state, characterized by a lower solubility. Without any stabilization strategy behind their utilization, their marketing possibility is limited due to the possible conversions during both manufacturing and storage.

The importance of the crystalline state (polymorphs, solvates, amorphous) in pharmaceuticals cannot thus be overlooked. It is important that crystalline forms of drug substances used in solid dosage forms be characterized, and the appropriate forms selected to ensure that the product performance with respect to manufacturability, stability, and of course desired properties (e.g. solubility/dissolution/bioavailability) remain unchanged (**Pudipeddi et al, 2005**).

As the polymorphism can affect the quality, safety, and efficacy of a drug product, the importance of controlling a crystal form, from a regulatory standpoint, is very well recognized and deep investigations in the crystalline state properties of a drug need to be furnished when considering a new drug application (**FDA CDER Guidance, 2004**).

#### **II.2.1.2.5. Surfactants**

Surfactants, both in vitro and in vivo, significantly influence the solubility of a poorly water-soluble drug substance by enhancing its solubilization. Surfactants also interfere with the interfacial transport of solute from the crystal to the bulk solution (enhanced wetting characteristics – Young's equation) (**Lee et al., 2000**).

Solubilization, in this case, can be defined as “the preparation of a thermodynamically stable solution of a substance that is normally insoluble or very slightly soluble in a given solvent, by the introduction of one or more amphiphilic component(s)” (**Hörter and Dressman, 2001**). The solubility enhancement properties of surfactants are the result of the dual nature of the surfactant molecules, i.e. possession of distinct hydrophobic and hydrophilic regions which allow them to orient at polar/non polar interfaces (**Liu et al., 2000**). In the absence of such interface or above a concentration known as the critical micelle concentration (CMC), surfactants self-associate to form micelles or other aggregates (depending on the surfactant concentration), where their hydrophobic regions



are separated from aqueous contact by their hydrophilic regions; this creating an hydrophobic environment (hydrophobic core) suitable for the solubilization of many hydrophobic compounds (Zana, 1997; Liu et al., 2000). The solubility of an hydrophobic poorly water-soluble drug will thus see its aqueous solubility increase above the CMC of the surfactant used for solubility enhancement.

In vivo, in the small intestine, drug solubility can be enhanced by amphiphilic bile components such as bile salts, lecithin and monooleins; for some reported poorly water-soluble compounds, increases in solubility of up to a hundred-fold upon addition of physiological concentrations of bile salts to aqueous media have been reported (Hörter and Dressman, 2001). In vivo solubility of a drug compound, at least for lipophilic drugs, is in fact generally greater than its referred in vitro aqueous solubility (Dressman, 2005).

#### II.2.1.2.6. Particle size

Drug particle size can also have an influence on saturation solubility; the size dependency, however, coming into effect only for particles having a size below approximately 1  $\mu\text{m}$  (Shefter, 1981; Müller et al., 2001; Hoener and Benet, 2002). The increase in the saturation solubility with respect to diminution of particle size is explained by the Ostwald-Freundlich equation and is illustrated in **Figure II 8**:

$$C_s = C_\infty e^{\frac{2 \gamma M}{R T \rho r}}$$

**C<sub>s</sub>**: Solubility (mg/ml)  
**C<sub>∞</sub>**: Solubility of infinite radius particles  
**γ**: Interfacial tension between drug particles and the solubilizing fluids  
**M**: Molecular weight  
**R**: Ideal gas constant  
**T**: Absolute temperature  
**ρ**: Density of the solid  
**r**: Radius of the particles

The Ostwald-Freundlich equation is the equation used to explain crystal growth in a dispersed system. Any particle system dispersed in a medium and having a certain degree of solubility in it is thermodynamically unstable due to its large interface area. One way of decreasing the high interfacial energy associated with this large interfacial area is through particle growth, and the mechanism most likely to achieve this reduction is called

the Ostwald ripening (Leite et al., 2003). This Ostwald ripening is due to the solubility difference between smaller and larger particles, i.e. enhanced solubility for smaller particles.

The saturation solubility increase which occurs for smaller particles is quite hard to explain for relatively low difference in particle size as it happens, and is definitely more pronounced, when particles are reduced to the nanometer range, and that except for the radius ( $r$ ) of the particles, the only possible variable parameter in this equation is the surface tension ( $\gamma$ ).

It has been reported that an increase in  $\gamma$  can take place during sample processing (i.e. particle size reduction operations such as high pressure homogenization in our case). The energy introduced during such process might lead to an increase in  $\gamma$  and thus to an increase in saturation solubility (Peters et al., 1999). Converting microparticles into nanoparticles might also lead to the formation of defects in the original crystals. These crystal defects, including dislocations, influence the crystal lattice energy and give rise to increased surface energy and thus to an increased saturation solubility (Müller and Peters, 1998; Lee et al., 2000). Another reported possible explanation is the change in radius curvature of the particles, meaning that the packing density of the surfactants at the surface is no longer optimal and is less dense due to the changed geometrics, resulting in an increased surface tension at the interface with the nanoparticles (Peters et al., 1999).

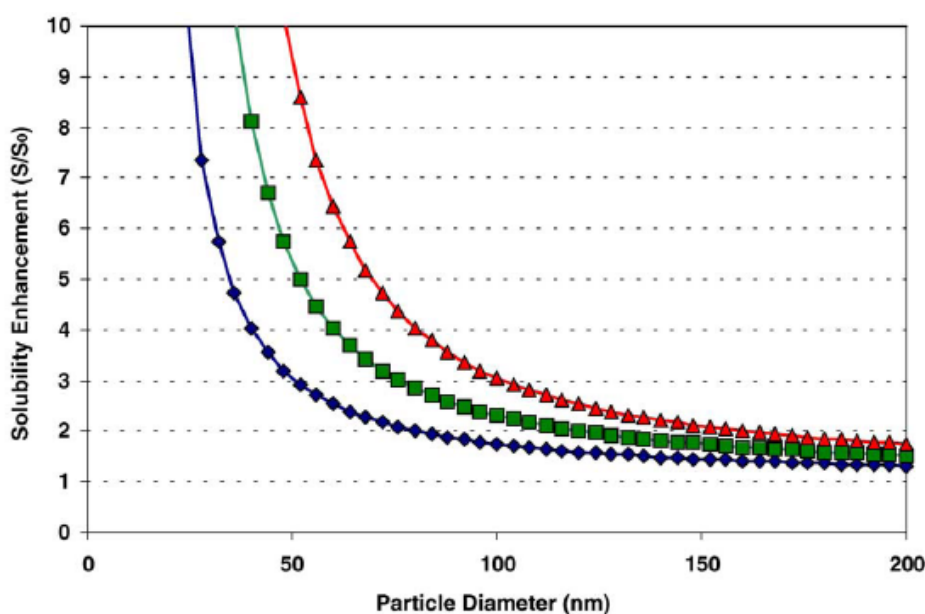


**Figure II 8.** Illustration of the calculated effect of particle radius on  $S/S_0$  (i.e.  $CS/C_\infty$ ) for a hypothetical particle with a molecular weight of 708, an interfacial surface tension of 50 (blue curve), 75 (green curve), or 100 (red curve) dyn cm<sup>-1</sup>, and a density of 1 g/mL (Kipp, 2004).

The size dependency of saturation solubility may also be explained through the Young-Laplace and Kelvin equations which define the relationship between particle radius and “vapor pressure” (Pellicer et al., 2000; Johnson, 2002).

$$(1) \quad p_i - p_e = \frac{2\gamma}{r}$$

$p_i$ : Internal pressure of the spherical surface (Pa)  
 $p_e$ : External pressure of the spherical surface  
 $\gamma$ : Interfacial tension  
 $r$ : Radius of the particles

$$(2) \quad p_s = p_o \exp\left(\frac{2\gamma M}{RT\rho r}\right)$$

$p_s$ : Saturation vapour pressure (Pa)  
 $p_o$ : Saturation vapour pressure of a plane surface  
 $\gamma$ : Surface tension  
 $M$ : Molecular weight  
 $R$ : Ideal gas constant  
 $T$ : Absolute temperature  
 $\rho$ : Density  
 $r$ : Radius of the particles



**Figure II 9.** (1) Young-Laplace equation and (2) Kelvin equation

According to these equation ( $\Delta P \approx 1/r$ ), the vapor pressure above a curved surface is increased compared to a flat surface (i.e. vapor pressure increases with decreasing particle size) (Figure II 9). Through these equations we can compare the transition of molecules from a liquid state to a surrounding gas phase to the transition of molecules from a solid phase to a surrounding liquid phase and say that, analogously to vapor pressure, the “dissolution pressure” of a product increases as particle size decreases. As saturation solubility depends on the tendency for a molecule to move from a solid phase to a liquid phase, we can assume that it increases with particle size reduction (Müller et al., 2000).

## II.2.2. Dissolution

### II.2.2.1. Theoretical background

Dissolution of a solid dispersed in a liquid takes place in two stages: the first stage is an interfacial interaction between the solid and the liquid phase leading to the formation of solute molecules from the solid phase, and the second is the transport of these molecules from the interface into the bulk medium under the influence of diffusion (Mosharraf and Nyström, 1995). The dissolution process is described by the Noyes-Whitney equation:

$$dm / dt = \frac{D \times A}{h} (S - C_b)$$

**dm/dt:** Dissolution rate (mg/min)

**D:** Diffusion coefficient of the solute

**A:** Effective surface area of the dispersed solid (surface area of the particles exposed to the solvent)

**h:** Diffusion boundary layer thickness

**S:** Saturation solubility (i.e. the equilibrium solubility)

**C<sub>b</sub>:** Concentration of the solute in the bulk medium at time "t"

The diffusion coefficient D being defined by the Stockes – Einstein equation:

$$D = \frac{R T}{6 \pi \eta r N}$$

**D:** Diffusion coefficient of the solute (m<sup>2</sup> s<sup>-1</sup>)

**R:** Ideal gas constant

**T:** Temperature (Kelvin)

**η:** Viscosity of the dissolution medium

**R:** Molecular radius of the solute

**N:** Avogadro's number.

The Noyes-Whitney equation is a model that assumes that (1) the drug is dissolved uniformly from all surfaces of the particles, that (2) the particles are spherical, that (3) the thickness of the diffusion boundary layer is constant

and that (4) the thickness of the diffusion boundary layer and the saturation solubility are independent of particle size (Hoener and Benet, 2002). **Figure II 10** illustrates the relationship of the terms of the Noyes – Whitney equation.

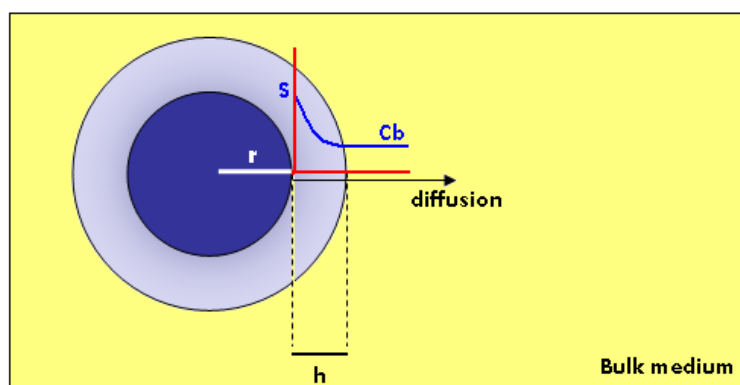


**Figure II 10.** Schematic representation including the parameters of the Noyes – Whitney equation.

#### II.2.2.2. Factors influencing dissolution rate

According to the Noyes-Whitney equation, there are many ways to enhance the dissolution rate of drug compounds. **Table II 7** summarizes the physicochemical characteristics and the in vitro-in vivo factors influencing the terms of the Noyes-Whitney equation.

**Table II 7.** Factors influencing dissolution rate (Bermejo, 2005). Temperature, also having an influence on drug dissolution, is not mentioned in this table.

Parameter	Physicochemical characteristic	Physiological variable - in vivo factor	In vitro factor
<b>A</b>	Particle size	Presence of surfactants	Presence of surfactants
<b>h</b>		GIT motility	Stirring rate System hydrodynamics
<b>D</b>	Molecular size	Viscosity of gastrointestinal fluids	Viscosity of medium
<b>S</b>	Hydrophilicity Crystalline state	pH Surfactants	pH Surfactants
<b>Cb</b>		Volume of gastrointestinal fluids	Volume of medium

Considerations regarding drug saturation solubility having been made in the previous chapter (**part II.2.1**), as well as the factors influencing its value (particularly drug polymorphism and crystal morphology and defects (**part II.2.1.2.6**)), our attention here will be placed on specific surface area, diffusion coefficient, and the thickness of the diffusion boundary layer. The wetting properties of the substance will also be an important factor.

#### II.2.2.2.1. Particle size - Specific surface area (SSA)

Drug particle size is parameter of great importance when considering its dissolution characteristics. In fact the smaller the particle size, the greater the specific surface area (**Figure II 11**), and thus, according to the Noyes-Whitney equation, agglomeration considerations apart, the greater the dissolution rate. The specific surface area, which is solely dependent on drug particle size shall in fact be distinguished from the effective surface area, which additionally takes into account particle agglomeration. The specific surface area is defined as the surface area divided by the volume. **Figure II 11** clearly shows the evolution of the specific surface area when decreasing particle size and indicates, for a given size reduction, a particularly strong enhancement for sub-micron particles.

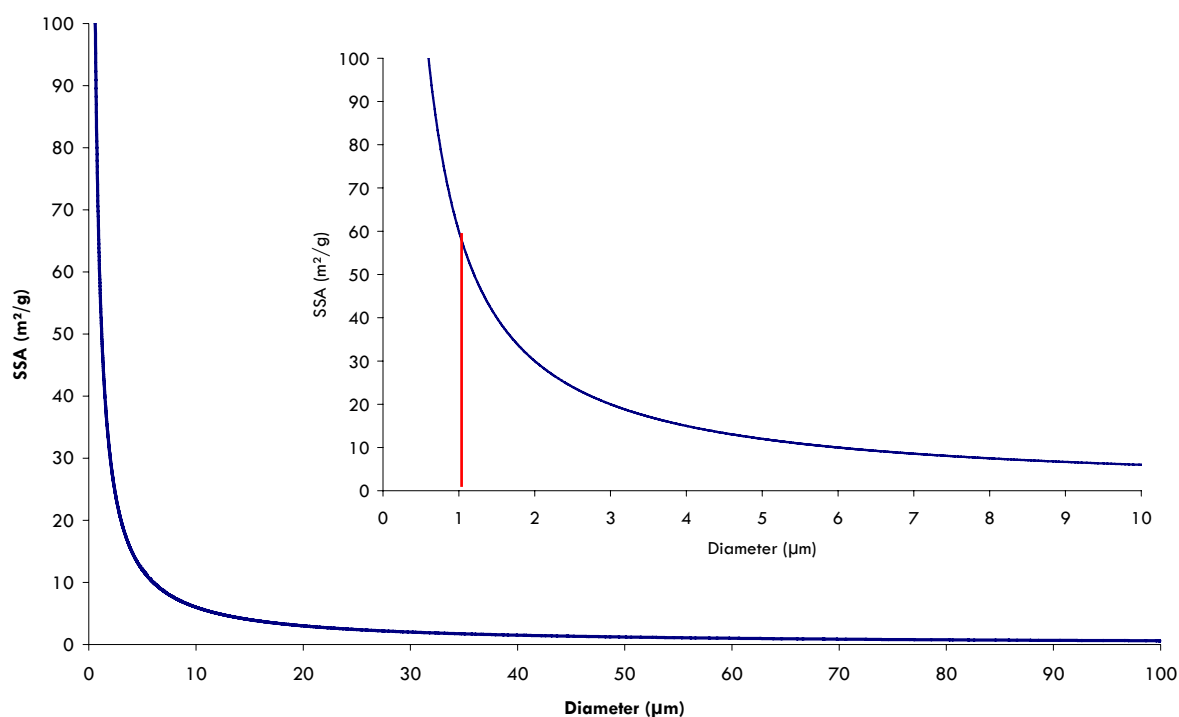


**Figure II 11.** Evolution of the specific surface area (m<sup>2</sup>/g) as a function of particle size (assuming a density of 1 g/cm<sup>3</sup>)

#### II.2.2.2.2. Diffusion coefficient and the thickness of the diffusion boundary layer

The diffusion coefficient (D) is compound-specific and depends largely on the molecular weight of the solute. Practically, with the exception of temperature and viscosity, no other factors affect this parameter. These factors being well controlled in vitro, they do not influence D and thus do not influence the in vitro dissolution characteristics. It has to be noted, however, that viscosity of gastrointestinal fluids varies between fasted and fed state (including type of meal) and that diffusion in these varying conditions might be different.

The thickness of the diffusion boundary layer is influenced by fluid motion at the solid liquid interface and is thinner when this motion is increased. If the thickness of the diffusion boundary layer decreases, according to the Noyes-Whitney equation, the dissolution rate increases. Practically, thus, the thickness of the diffusion boundary layer decreases when increasing the in vitro stirring rate during dissolution evaluations and will be influenced in vivo by the gastrointestinal motility (Hörter and Dressman, 2001).

The thickness of the diffusion boundary layer is also influenced by particle size; it decreases with particle size reduction (Mosharraf and Nyström, 1995; Galli, 2006). This phenomenon is explained by the Prandtl boundary layer equation. This equation, relative for flow passing a flat surface, expresses the hydrodynamic boundary layer thickness as equal to  $k (L^{1/2} / V^{1/2})$  where L is the length of the surface in the direction of flow, V the relative velocity of the flowing liquid against the surface and k is a constant (M. Mosharraf, C. Nyström, 1995). Nyström et al. have showed that, for solids dispersed in a liquid medium under agitation, a decrease in particle size probably leads to a decrease in both L and V, and that although these two parameters counteract each other, the net effect is a decreased thickness of the boundary layer around the particles and an increase in the surface-specific dissolution rate.

It is, in fact, known that for large particles, the effective diffusion boundary layer is constant with respect to particle size and its thickness is found to be around 30  $\mu\text{m}$  (Galli, 2006). Particles of diameter of less than 50  $\mu\text{m}$ , however, do not have sufficient surface area and associated friction force to support a hydrodynamic boundary layer of this magnitude and the Prandtl boundary layer theory postulates that for such particles, the effective hydrodynamic boundary layer is approximately equal to the particle radius or diameter (Galli, 2006).

### II.2.2.2.3. Wettability

The wettability of a drug substance may be defined as the surface affinity of its particles for the dissolving medium and is characterized by the contact angle ( $\theta$ ) a droplet of this medium would form at its surface (considering a horizontal surface). A contact angle inferior to  $90^\circ$  and a contact angle superior to  $90^\circ$  are indicative of good and poor wettability characteristics of a liquid for a given substance, respectively. A schematic representation of this phenomenon is shown in **Figure II 12**.

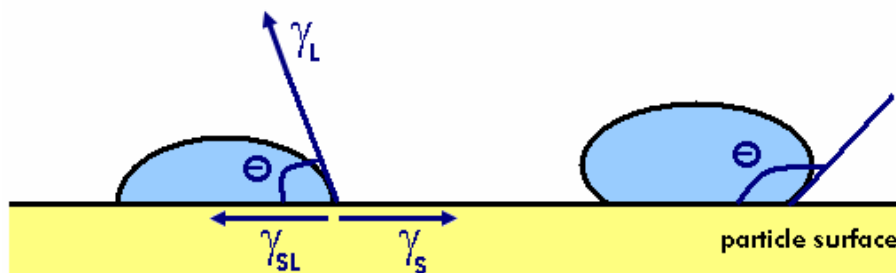


**Figure II 12.** Schematic representation of two different types of contact angles ( $< 90^\circ$  and  $> 90^\circ$ ) indicating good and poor wettability, respectively. The relationship of the terms of the Young equation is also represented in this Figure.

The contact angle ( $\theta$ ) is actually a thermodynamic variable that depends on the interfacial surface tensions (mN/m) (both liquid and solid) and can be expressed by the Young equation:

$$\gamma_s = \gamma_{SL} + \gamma_L (\cos \theta)$$

$\gamma_s$ : Surface tension of the solid  
 $\gamma_L$ : Surface tension of the liquid  
 $\gamma_{SL}$ : Interfacial tension of the solid/liquid  
 $\theta$ : Contact angle

As we can see in **Figure II 12** and from the Young equation, wettability thus depends on two factors: the surface tension at interface and the contact angle.

Because of their adsorption at water/air and solid/water interfaces, thus reducing the excess free energy of these interfaces, the presence of surfactants (and biosurfactants) in the wetting liquid causes variation in the



wettability of solids (Ozdemir and Malayoglu, 2004). The presence of surfactants is thus of great importance when assessing in vitro drug dissolution characteristics as their absence would fail to address the possibility of wetting by native GIT surfactants in vivo, where the dissolution rate would thus be enhanced (Hörter and Dressman, 2001).

### II.3. Dissolution rate/solubility enhancement technologies

The uses of high throughput screening, combinatorial chemistry and other tools in new drug development are resulting in the discovery of large numbers of new chemical entities (NCE), many of which are potential new drugs. The drawback of this extensive output, however, is that these NCE tend to be more and more water-insoluble. It is estimated, as of today, that 40% or more of these new NCE are poorly water-soluble (Merisko-Liversidge et al., 2003; Patravale et al., 2004). One of the many challenges in furthering the development of these drugs will be the development of appropriate drug formulations or drug delivery systems to enhance drug solubility characteristics. The role of solubility enhancement is to attempt to shift the classification of a drug (II → I) in order to eliminate the problems associated with dissolution-limited compounds.

There are numerous solubility enhancement technologies reported in the literature and numerous extensive reviews and books assessing poor water-solubility considerations and these technologies may be found.

Basically, drugs can be poorly soluble in aqueous media or simultaneously in aqueous and organic media. In the first case, a number of formulation approaches are available for saturation solubility enhancement such as specific or non specific complexation (solid solutions or dispersions in polymers or use of cyclodextrins) and solubilization techniques (solvent-mixtures, etc.). However, for drugs that are poorly soluble in both aqueous and organic media, most of these approaches are of limited success, if not unusable, as they rely on the use of solvents for formulation development, and other alternatives have to be used in order to lead to a dissolution rate increase (particle size reduction, prodrugs, salt formation, etc.).

The aim of this section is to review the general solubility/dissolution enhancement technologies available nowadays.

### II.3.1. Drug modification

The chemical structure of a drug is, in general, determinant of its aqueous solubility. As already discussed in part II.2.1.2.1 of this introduction, the presence and the relative number of polar/non polar groups in the structure will greatly influence drug solubility. Two different approaches, which are not formulation-related, for solubility enhancement of poorly water-soluble drugs are salt formation and prodrug synthesis.

#### II.3.1.1. Pharmaceutical salts

Salt formation is a simple means of modifying the properties of a drug with ionisable functional groups in order to overcome some undesirable feature of the parent drug (O'Connor and Corrigan, 2001). Effectively, due to strong interactions between the solute ion and the water molecules, which can overcome the drawback of large hydrophobic regions of drug molecules, the solubility of an organic molecule is frequently enhanced more by an ionized functional group than by any other single means (Neau, 2000). The salt form of a drug thus, in general, has an enhanced aqueous solubility compared to the non ionized drug. Solubility considerations of ionized species and non ionized species for poorly water-soluble weak bases and poorly water-soluble weak acids depend on the pKa of the ionized functions and the medium pH; these considerations have been taken into account in part II.2.1.2.3 of this report.

The solubility of a salt form of a drug depends largely on the counterion used in salt formation but the prediction of the solubility outcome with the change in the counterion is not simple as it can vary from drug to drug (Neau, 2000). Although it would be useful to be able to predict the influence of the salt-forming agent (counterion) on the parent drug compound, there is actually no reliable way of predicting this influence and the selection of an appropriate counterion to produce a salt with the desired combination of properties is still being carried out on an empirical basis (O'Connor and Corrigan, 2001).

Many known drugs are reported to have their solubility and thus their dissolution rate and oral bioavailability increased following salt formation; for example, mono-, di-, and triethanolamine salts of piroxicam yield an approximate 2-fold increase of C<sub>max</sub> and extent of exposure compared to piroxicam (Gwak et al., 2005).

Solubility enhancement through salt formation is also reported for haloperidol (Li et al., 2005), diclofenac (O'Connor and Corrigan, 2001) and many other drugs. Salt selection of poorly water-soluble NCE in the early phase of drug development is also frequently used as a way of enhancing drug solubility.

It has although to be noted that salt formation is not feasible for neutral compounds and that even when salts can be prepared (i.e. molecules with an ionisable function), an increased dissolution rate in the GIT cannot always be achieved due to the possible reconversion of salts into aggregates of their respective acid or base form (Serajuddin, 1999).

#### II.3.1.2. Prodrugs

A prodrug is a term used to describe a compound, comprising the drug and a covalently bound inactive moiety, which must undergo bioconversion prior to exerting its pharmacological effect (Neau, 2000b). These prodrugs can be used to increase drug gastrointestinal stability, drug permeability (Kakumanu et al., 2006; Li et al., 2006), and eventually drug solubility. Concerning solubility, enhancement can be achieved by the introduction of polar groups in the parent drug structure.

Many examples of prodrugs used for solubility enhancement can be found in the literature. To report a few of these, we can take the example of clindamycin hydrochloride which has a solubility of 3 mg/ml, while clindamycin-2-phosphate has a solubility of 150 mg/ml and is hydrolyzed in vivo with a reaction half-life of only 10 min (Neau, 2000b). Prodrugs for poorly soluble antiviral nucleoside analogues such as acyclovir (valacyclovir) (Granero and Amidon, 2006) and ganciclovir (Patel et al., 2006), and for anti-cancer drugs such as paclitaxel (Choi and Jo, 2004; Choi and Shin, 2005) have met success towards oral bioavailability enhancement, in comparison with the parent drug.

## II.3.2. Solubilization

### II.3.2.1. Solubilization using a cosolvent – solvent mixture

Many drugs are fairly soluble in the commonly used pharmaceutical solvents and the use of solvent mixtures is often exploited as a method to increase their solubility. Solvents used for drug solubilization need, of course, to be non-toxic and physically and chemically stable and inert. The biggest disadvantage of using a cosolvent is the toxicity of most of the water-miscible solvents that have a high potential for increasing drug solubility (Trivedi and Wells, 2000).

Solvents used for solubility enhancement are generally alcohol, glycerol, propylene glycol and polyethylene glycols (PEG) of low molecular weight (200-600), used alone or in mixed-solvent systems (Trivedi and Wells, 2000; Strickley, 2004).

The cosolvent approach for saturation solubility enhancement is primarily used for parenteral administration (injectables) of poorly water-soluble drug compounds. Cosolvent solubilization is particularly important for parenteral dosage forms as it is desirable to incorporate the required dose as a true solution in the smallest volume of liquid as possible (Millard et al., 2002). Examples of drugs being formulated in cosolvent systems for parenteral use are cox-2 inhibitors celecoxib, rofecoxib, meloxicam and nimesulide (H<sub>2</sub>O/EtOH/glycerol/PEG alone or in binary mixtures) (Seedher and Bhatia, 2003), Biphenyl dimethyl dicarboxylate (N,N'-dimethylacetamide (DMA)/alcohol/ H<sub>2</sub>O ternary solvent system) (Han et al., 1999), Fluasterone (EtOH) (Li et al., 1999), phenytoin (DMA, EtOH, PEG 400, glycerol) (Kawakami et al., 2006), diazepam (propylene glycol/EtOH) (Strickley, 2004), digoxin (propylene glycol/EtOH) (Strickley, 2004) and dihydroergotamine (glycerol/EtOH) (Strickley, 2004). Modulation of the pH in injectable formulations is also frequently relied upon for solubility enhancement of poorly water-soluble weak base or acids; the acceptable range is pH 2–12 for intravenous and intramuscular administration, pH 2.7–9.0 for subcutaneous administration (Strickley, 2004).

This cosolvent approach can also be used for oral administration for drugs formulated either as solutions or placed in soft gelatin capsules (Tabibi and Gupta, 2000). Although they have various disadvantages such as high production costs, soft gelatin capsules offer an interesting approach for the formulation of oily or aqueous solutions as a solid dosage form. Many drugs are commercially available using this formulation approach such as

nifedipine (PEG400/Glycerol), diphenhydramine HCl (PEG400/Glycerol), digoxin (PEG400/Glycerol/EtOH), etoposide (PEG400/Glycerol) and valproic acid (corn oil) (Trivedi and Wells, 2000; Strickley, 2004).

### II.3.2.2. Micellization

As it has already been described in **part II.2.1.2.5** of this introduction, surfactants have the ability to enhance the solubility of poorly water-soluble compounds. Surfactants are amphiphilic molecules capable, in the absence of polar/non polar interface or above a certain concentration known as the critical micelle concentration (CMC), to self-associate to form specific arrangements such as micelles (Zana, 1997; Liu et al., 2000). **Figure II 13** shows a schematic representation of different types of surfactant association including micelles.

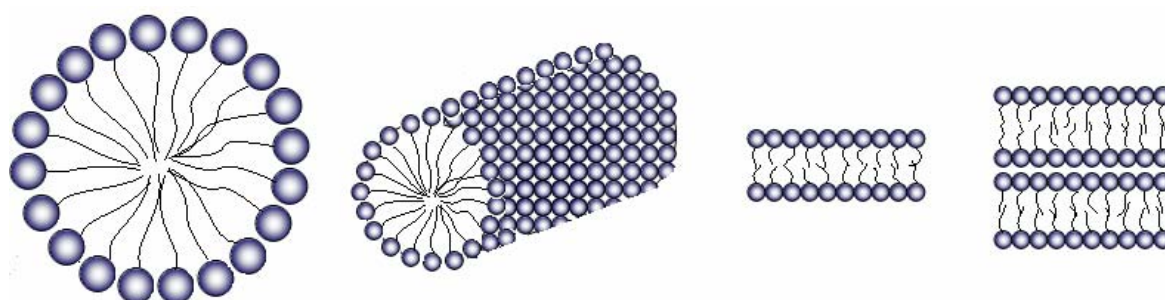


**Figure II 13.** Schematic representation of various types of surfactants self-association. From left to right (with increasing surfactant concentration): micelles, cylindrical (rod-shaped), unilamellar, bilamellar (blue circles and thin black lines represent hydrophilic and hydrophobic moieties of the surfactant molecule, respectively).

As we can clearly see in this figure, micelles are associations of surfactants where the hydrophobic region (core region) is separated from the surrounding aqueous media by the hydrophilic region. The solubilization of hydrophobic drugs by surfactants occurs by inclusion of these drugs into the hydrophobic regions of the micelles.

Depending on their polarity, the drugs will locate either totally in the hydrophobic region (case of non polar drugs) or more at the hydrophobic/hydrophilic interface. The solubilization capacity in the first case will thus be determined by the core volume and in the second case be dependent on the polar head groups (Liu et al., 2000).

Mixed micelles, or micelles formed by surfactant mixtures, are frequently used in many applications. Mixtures of surfactants in micelle formation are advantageous as synergism in a surfactant mixture can minimize the total surfactant monomer concentration, may enhance the micellar solubilization potential and are physiologically relevant (Liu et al., 2000).

Although the solubilization of poorly water-soluble drugs using surfactant or mixed-surfactant micelles has a long history and is a very interesting approach for drug solubility enhancement it has some drawbacks mainly linked to toxicological issues and to a relatively low solubilization capacity at acceptable surfactant concentration (surfactant “toxicity” is directly related to its concentration). Furthermore, another issue concerning micellar systems is the potential drug reprecipitation following dilution of the system, particularly upon intravenous and oral administration.

Micellization of drugs is frequently accompanied by another solubility enhancement technique such as cosolvents or complexation with cyclodextrins (Li et al., 1999b; Yang et al., 2004; Kawakami et al., 2004, 2006; Rao et al., 2006).

### **II.3.2.3. Emulsions – microemulsions – SEDDS/SMEDDS**

Emulsions are defined as a mixture of two immiscible phases (generally water and oil) with the addition of one (or more) emulsifiers to stabilize the droplets of the inner phase; droplets with a general diameter above 200 nm (<80 nm for microemulsions) (Gupta and Cannon, 2000). Emulsions are frequently-used formulations in drug delivery and find an interest primarily in dermal formulations and parenteral formulations. Concerning parenteral delivery, emulsions do, in fact, present an interesting alternative for drugs that cannot be formulated as an aqueous solution. The main limitation of emulsions comes from their stability and in conventional parenteral formulations, for example, nonaqueous solvents such as ethanol, and solubilizers such as surfactants, are often needed to enable adequate solubilization of highly insoluble drugs (Constantinides, 2004). Microemulsions provide an interesting approach as their stability is further increased; emulsion stability being dependent on the size and the homogeneity of the dispersed droplets (Agatonovic-Kustrin et al., 2004; Constantinides, 2004; Ghosh and Murthy, 2006).

Emulsions, and principally microemulsions, also have an interest regarding oral drug delivery as they can increase the solubility characteristics of lipophilic drugs and thus enhance their oral bioavailability (**Constantinides, 1995; Ghosh and Murthy, 2006**). Microemulsions are superior to simple micellar solutions in terms of solubilization potential (**Constantinides, 1995**).

An emerging technique for solubility enhancement of poorly water-soluble drugs that uses emulsions as a basis for drug incorporation are self-emulsifying drug delivery systems (SEDDS) and self-microemulsifying drug delivery systems (SMEDDS). SEDDS and SMEDDS are defined as isotropic mixtures of natural or synthetic oils, solid or liquid surfactants, or alternatively, one or more hydrophilic solvents and co-solvents/surfactants, which upon mild agitation (e.g. gastrointestinal motility) followed by dilution in aqueous media (e.g. gastrointestinal fluids) form fine oil-in-water (o/w) emulsions or microemulsions (**Gursoy and Benita, 2004**). SEDDS and SMEDDS are thus formulations that represent an efficient vehicle for the in vivo administration of emulsions as their thermodynamic stability offers advantages over unstable dispersions such as emulsions (longer shelf-life) (**Constantinides, 1995; Gursoy and Benita, 2004**).

Poorly water-soluble drugs that have been formulated as SEDDS or SMEDDS for which an enhanced oral bioavailability has been observed include itraconazole (**Hong et al., 2006**), carvedilol (**Wei et al., 2005**), chloramphenicol, ibuprofen, ketoprofen, tamoxifen, testosterone and tolbutamide (**Araya et al., 2005**).

#### II.3.2.4. Liposomes

Liposomes, or lipid vesicles, are spherical vesicular concentric bilayered structures composed of one or more phospholipids bilayer (**Figure II 14**). In general, the phospholipids used are phosphatidylcholine comprising C14 to C18 side chains with varying degree of saturation (**Lian and Ho, 2001**). Liposomes are very interesting drug carriers in that they can encapsulate drug compounds with varying polarities, hydrophilic drugs being entrapped in the aqueous spaces and the lipophilic drugs being entrapped into the lipid membranes (**Liu et al., 2000b**). Drug loading efficiencies of up to 100 percent often being achievable, the liposomal formulation of lipophilic poorly water-soluble drugs can significantly increase their apparent aqueous solubility (**Cullis and Chonn, 1998; Liu et al., 2000b**).

Liposomes are characterized as function of their size (dependent on the number of lamellae) and we can distinguish the following (Liu et al., 2000b) (**Figure II 14**): (1) Multilamellar vesicles (MLVs - size: 100-10000 nm - minimum 5 lamellae), (2) Small unilamellar vesicles (SUVs - size: 15-25 nm - 1 lamellae) and (3) Intermediate-sized and Large unilamellar vesicles (IUVs and LUVs - size: > 100 nm for LUVs - 1 lamellae).

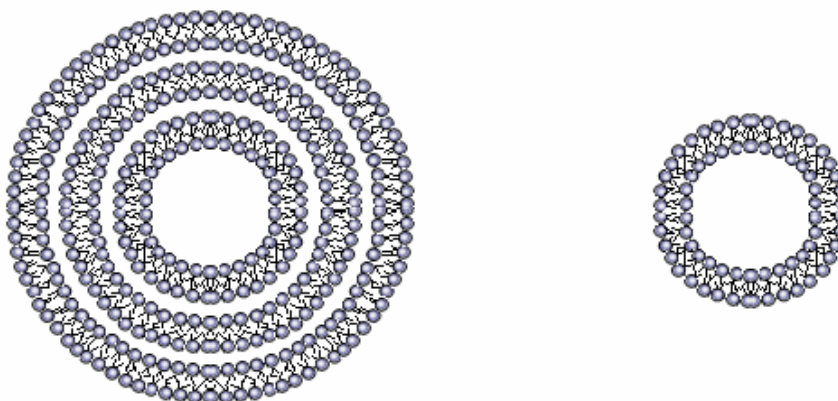


**Figure II 14.** Schematic representation of various types of liposomes: MLVs (left), SUVs (right).

Liposomal formulations are frequently used in parenteral delivery of numerous poorly water-soluble drugs. One of the best known and documented example is amphotericin B (ambisone<sup>®</sup> - Gilead/Nexstar - SUVs - IV). Most FDA-approved liposomal formulations concern antifungal and anticancer therapies, but many other types of products (analgesics, etc.) are being developed (Lian and Ho, 2001).

Despite their great advantage concerning drug solubility enhancement, liposomes, however, pose many problems in terms of physicochemical stability (aggregation, fusion, sedimentation, phospholipids hydrolysis/oxidation, etc.) as well as in product processing (sterilization, large-scale production, etc.) (Yan-Yu et al., 2006). To meet these stability concerns, development of proliposomes is of great interest. Similarly to SEDDS, proliposomes are defined as dry, free-flowing particles that immediately form a liposomal suspension when placed in aqueous media. These proliposomes find an interest as a formulation approach for solubility enhancement of poorly water-soluble orally administered drugs. Examples are progesterone (mixed micellar proliposomal system: 4-fold increase in transport in Caco-2 cell model) (Potluri and Betageri, 2006), cefotaxime (proliposomal system:  $\approx$  3-fold increase in extent of exposure in rats) (Ling et al., 2006) and sylmarin (proliposomal system:  $\approx$  4-fold increase in extent of exposure in beagle dogs) (Yan-Yu et al., 2006).



### II.3.3. Specific and non specific complexation

#### II.3.3.1. Solid dispersions or solutions in polymers

A solid dispersion can be defined as an intimate mixture of a drug substance (solute) with a carrier (i.e. diluent - solvent - continuous phase) and is called a solid solution when the drug is dispersed in the carrier at a molecular level (Serajuddin, 1999; Leuner and Dressman, 2000; Nanda et al., 2000). It is also defined that, based on the extent of miscibility of the solute and solvent species, these solid solutions are either called discontinuous (solute has a limited solubility in the solid solvent) or continuous (the two components are miscible or soluble in solid state at all proportions) (Leuner and Dressman, 2000; Nanda et al., 2000). These solid solutions are further described as substitutional or interstitial solid solutions and amorphous solid solutions; the latter being the most frequently encountered case as they are most likely to occur when using polymer carriers (Leuner and Dressman, 2000).

The different types of carrier that can be used for solid dispersion and solution preparation are listed in **Table II 8**.

Solid dispersions and solutions can be prepared, depending on the drug characteristics such as melting point and solubility in organic solvents, by either the fusion method (or hot melt method) or the solvent method. It has to be noted that it is not the preparation method but the molecular arrangement that governs the properties of solid dispersions.

**Table II 8.** Carriers used in the preparation of solid dispersions and solutions (Leuner and Dressman, 2000; Nanda et al., 2000).

Polymers	Small molecular weight carriers
Polyethylene Glycol (PEG) (MW 1500-20000)	Urea
Polyvinylpyrrolidone (PVP)	Sucrose
Polyvinylalcohol (PVA)	Mannitol
Cross-linked Polyvinylpyrrolidone (PVP-CL)	Organic acids (citric and succinic)
Polvinylpyrrolidone-polyvinylacetate copolymer (PVP-PVA)	
Cellulose derivatives	
Hydroxypropylmethylcellulose (HPMC)	
Hydroxypropylcellulose (HPC)	
Carboxymethylethylcellulose (CMEC)	
Hydroxypropylmethylcellulose phthalate (HPMCP)	
Polyacrylates and polymethacrylates	

**- Fusion method:**

The preparation of a solid dispersion or solution by the fusion method involves the melting of both the carrier and the drug followed by a rapid cooling of the well homogenized mix. The cooling process leads to supersaturation, but due to solidification the dispersed drug becomes trapped within the carrier matrix; the achievement of a molecular dispersion depending on the degree of supersaturation and rate of cooling attained in the process (Leuner and Dressman, 2000). Different methods of cooling have been used for this method including cooling in an ice bath, on dry ice and spraying of the melt on a cold surface. This method was the first method used for the preparation of solid dispersions (in polymer or smaller molecular weight carriers) but finds a major limitation in drug thermostability.

**- Solvent method:**

The preparation of a solid dispersion or solution by the solvent method involves the solubilization of the carrier and the drug in a common solvent system followed by a drying operation to remove the solvent. The solvent removal operation is generally a simple evaporation under vacuum or spray-drying. With the advent of the solvent method, the problem associated with the processing of thermolabile drugs through the fusion method is solved; the only problem of this method being toxicological issues due to the use of organic solvents.

Solid dispersions and solutions show enhanced solubility and dissolution properties due to the fact that drug particle size is generally very small for solid dispersions (in the case of solid solutions, the drug is dispersed at the molecular level) and that particle aggregation is limited due to the presence of the dispersing carrier. Wettability of the system is enhanced following modifications in drug particle surface characteristics and to the use of hydrophilic carriers representing the dispersing phase. Furthermore, and most importantly, in solid dispersions and solutions, the drug is generally found in a high energy state form which is characterized by an increased solubility, and thus dissolution rate, when compared to the low energy state crystalline drug (see **part II.2.1.2.4**). In addition to the reduced particle size, the formation of a drug's amorphous form, or a high energy state polymorph in case of multiple polymorphism, is in fact the basis on which solid dispersions and solid solutions are built. It is, although, one of its major limitations, when considering marketability of this type of formulations, as their main problem consists of the possible crystallization (amorphous form → lower energy state form) of the drug substance during

manufacturing processes and most importantly during the shelf-life of the drug product, implying modifications in the biopharmaceutical behaviour of the formulation. Batch to batch reproducibility of the drug physicochemical properties, scaling up issues and the amount of carrier generally required for enhancing drug dissolution are also limitations of this formulation approach.

In fact, despite the great potential of this formulation approach regarding solubility/dissolution rate enhancement, which has over 40 years of existence, very few marketed drug examples can be found: (1) a griseofulvin-PEG solid dispersion formulated as tablets (Gris-PEG® - Pedinol Pharmaceuticals - Novartis), (2) a nabilone-PVP solid dispersion (formerly developed by Eli Lilly (Cesamet®) in 1982 and withdrawn in 1989; acquired by Valeant Pharmaceuticals International in 2004 and reapproved by the FDA in May 2006) and (3) an itraconazole - HPMC/PEG solid dispersion (Sporanox® - Janssen Pharmaceutica).

Nevertheless, the field of solid dispersions and solutions in polymers is the object of much research as it offers an enhancement in solubility of several orders of magnitude when compared to other formulation approaches. The enhanced solubility characteristics are generally translated into enhanced in vitro dissolution behavior and into enhanced systemic exposure. Examples of poorly water-soluble drugs formulated with success as solid dispersions or solutions include nitrendipine (carbopol/HPMCP) (Wang et al., 2005), glibenclamide (microcrystalline cellulose) (Dastmalchi et al., 2005), ketoprofen (ternary systems using PEG-SDS) (Mura et al., 2005), flurbiprofen (nicotinamide) (Varma and Pandi, 2005), simvastatin (PVP) (Ambike et al., 2005), nifedipine (mannitol) (Zajc et al., 2005) (HPMC) (Cilurzo et al., 2002), valdecoxib (PEG 4000) (Liu et al., 2005) and carbamazepine (PEG 6000) (Zerrouk et al., 2001).

### II.3.3.2. Inclusion complexation (cyclodextrins)

Complexation is another frequently encountered technique for solubility enhancement of poorly water-soluble drugs. A complex can be defined as a species of definite substrate (S)-to-ligand (L) stoichiometry that can be formed in an equilibrium process in solution and that can exist in solid state ( $mS + nL \rightleftharpoons S_mL_n$ ) (Stella et al., 1999; Tong, 2000b). Interest regarding complexation in pharmaceuticals has arisen with the advent of cyclodextrins.

Cyclodextrins are a family of cyclic oligosaccharides consisting of a variable number of D-glucose residues (6, 7 and 8 residues for  $\alpha$ ,  $\beta$ , and  $\gamma$ -cyclodextrins, respectively) linked by  $\alpha$ -(1,4) bonds (Tong, 2000b; Strickley, 2004). Cyclodextrins are represented spatially as cone-shaped (Figure II 15). The hydroxyl groups (which can be substituted) in position 2 and 3 are displayed on the wider rim and the hydroxyl group in position 6 in the narrower rim of the cyclodextrins as represented in Figure II 15; these hydrophilic groups all being positioned on the outside of the molecular cavity. The inner surface of this cavity is lined with methylene groups and ethereal oxygens of the glucose units and is, in contrary, hydrophobic and is a perfect fit, if the molecule or a portion of that molecule is of appropriate size to fit inside the central cavity, for the noncovalent inclusion complexation of many hydrophobic poorly water-soluble drug compounds (Strickley, 2004; Challa et al., 2005).

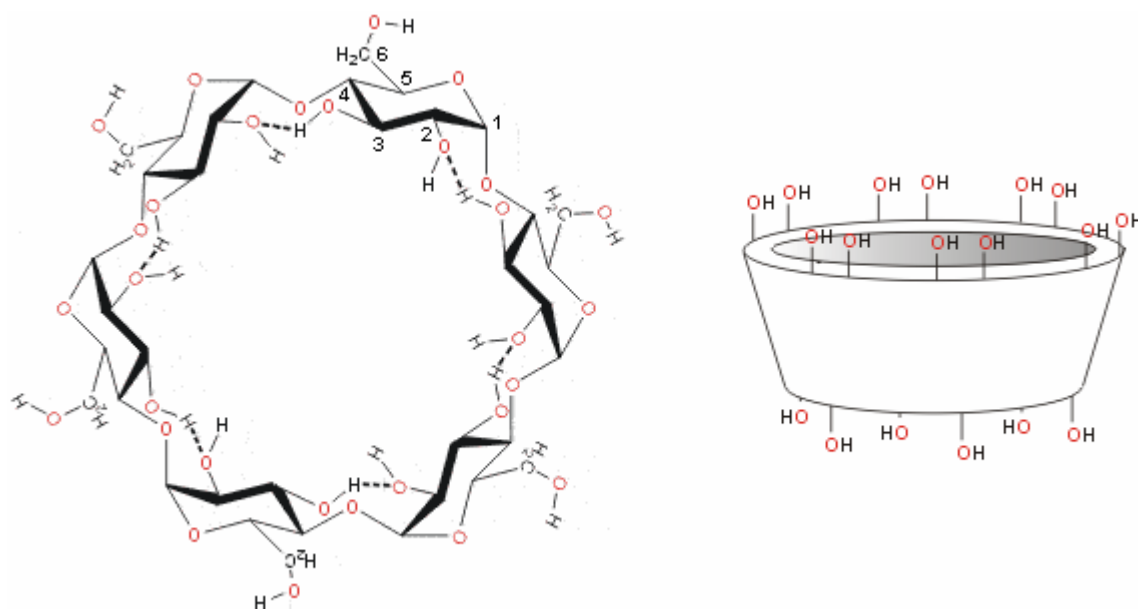


**Figure II 15.** Chemical structure of  $\alpha$  cyclodextrins with specific numbering (left). Cone-shaped spatial conformation of cyclodextrins (right) (LSBU, 2006).

The cavity size of  $\alpha$ -cyclodextrins being insufficient for many drugs and  $\gamma$ -cyclodextrins being very expensive, most pharmaceutical research focuses on the use of  $\beta$ -cyclodextrins and particularly on chemically modified  $\beta$ -cyclodextrins (e.g. hydroxypropyl- $\beta$ -cyclodextrin and sulfobutylether- $\beta$ -cyclodextrin) to extend the

physicochemical properties and inclusion capacity of the initial cyclodextrins (e.g. parent  $\beta$ -cyclodextrins having a reported low solubility ( $\approx 18$  mg/ml)) (Strickley, 2004; Challa et al., 2005).

Examples of poorly water-soluble drugs formulated with success, regarding solubility/dissolution rate enhancement, using cyclodextrins include diclofenac ( $\beta$ -cyclodextrin - up to a 5-fold increase in solubility) (Manca et al., 2005), rofecoxib (Hydroxypropyl- $\beta$ -cyclodextrin - up to a 10-fold increase in solubility) (Baboota et al., 2005), flurbiprofen ( $\beta$ -cyclodextrin/Hydroxyethyl- $\beta$ -cyclodextrin/Methyl- $\beta$ -cyclodextrin - up to a 120-fold increase in solubility for the latest) (Cirri et al., 2005) and lorazepam (Hydroxypropyl- $\beta$ -cyclodextrin - up to a 27-fold increase in solubility) (Holvoet et al., 2005).

Cyclodextrins utilization is not limited to the oral route, as development for the transdermal, ophthalmic and nasal route of administration is also referred (Matsuda and Arima, 2005; Merkus et al., 2005; Loftssona and Jarvinen, 2005) and it is not limited to the administration of small hydrophobic poorly water-soluble organic drugs as development concerning delivery of peptides and proteins is also studied (Irie and Uekama, 2005). In addition to their use regarding solubility enhancement, cyclodextrins are also frequently used to mask the bad taste of some orally administered drugs.

The use of cyclodextrins, however, has a few disadvantages in that the drug-loading capacity is quite low and that it only works for drugs which will fit in the cyclodextrin cavity and that possess a high complex-forming constant.

Other complexing agents have been reported to form inclusion complexes with poorly water-soluble drugs. 4-sulphonic calyx[n]arenes (water-soluble phenolic cyclooligomers) have been reported to enhance the solubility of nifedipine by up to a three-fold factor and the solubility of furosemide by up to a two-fold factor (Yang and de Villiers, 2004 and 2004b).

#### II.3.4. Particle size reduction

According to the Noyes-Whitney equation, out of the many ways to increase the dissolution rate of a poorly water-soluble drug, increase of the drug specific surface area by particle size reduction has a long history and

has been extensively studied for over 30 years (Fincher, 1968; Lin et al., 1968; Kaneniwa and Watari, 1974, 1978, 1978b; Jounela et al., 1975; Pendersen and Brown, 1975; Hintz and Jonhson, 1989; Mosharraf and Nyström, 1995). By 1968, many studies had been conducted to denote the influence of drug particle size reduction on various pharmacological parameters (plasma or blood concentrations, urinary excretion, etc.) and a positive influence could be observed for drugs such as chloramphenicol, griseofulvin, nitrofurantoin, procaine, spironolactone, sulfadiazine and tolbutamide (Fincher, 1968).

The positive influence of particle size reduction on the dissolution rate (SSA/solubility/diffusion boundary layer) of a drug has already been discussed in **part II.2.1.2.6**, **part II.2.2.2.1** and **part II.2.2.2.2** of this introduction.

A common method for enhancing the dissolution rate of poorly water-soluble compounds, and eventually the oral bioavailability (BCS class II drugs), through particle size reduction is simply called micronization. Micronized drug powders are fine powders with a mean particle size that is typically in the range of 2-5  $\mu\text{m}$  and that have an overall particle size distribution ranging from 0.1 to 25  $\mu\text{m}$  (fraction in the nanometer range being negligible) (Müller et al., 2001; Keck and Müller, 2006). Many drugs such as felodipine (Scholtz et al., 2002), griseofulvin (Reverchon et al., 2004; Wong et al., 2006), megestrol acetate (Farinha et al., 2000) and artemisinin (Van Nijlen et al., 2003) have been shown to have their dissolution and bioavailability enhanced following simple micronization when compared to the bulk drug.

Although micronization of drug powders effectively leads to an increase in surface area, it has no influence on the saturation solubility of a drug; the size dependency coming into effect only for particles that have a size below approximately 1  $\mu\text{m}$  (**part II.2.1.2.6** of this introduction) (Shefter, 1981; Müller et al., 2001; Hoener and Benet, 2002). For drugs that present very low water solubility, this increase in surface area and the eventual corresponding dissolution rate enhancement might not lead to a sufficiently high oral bioavailability (Müller et al., 2001; Keck and Müller, 2006). A solution for this problem is to further particle size reduction to the nanometer range ("nanoinisation"). Nanoparticulate systems (i.e. crystalline nanoparticles - nanocrystals) have the advantage of having an even greater surface area, and being characterized, unlike micronized drugs, by an increase in saturation solubility. By definition, drug nanocrystals are nanoparticles composed of 100 percent of drug without any matrix materials (e.g. lipids, carriers, etc.); nanoparticles being defined as particles with a mean particle size below 1  $\mu\text{m}$  (Keck and Müller, 2006).

In conclusion, the production of nanoparticles shall increase the drug dissolution rate by means of:

- Increase of surface area following particle size reduction (**part II.2.2.2.1** of this introduction).
- Increase of saturation solubility (**part II.2.1.2.6** of this introduction).
- Decrease in the diffusional distance  $h$  (**part II.2.2.2.2** of this introduction).
- Increase of the time available for dissolution following inherent adherence characteristics of nanoparticles to the gastrointestinal wall (high specific surface area being indicative of a high interactive potential with biological surfaces) (**Ponchel and Irache, 1998; Arangoa et al., 2000**).

Nanodispersed drug formulations also have the advantage over previously described solubility enhancement methods (particularly solid dispersions) in the way that drug initial crystalline state shall be maintained following the particle size reduction process. The solubility/dissolution rate enhancement occurring with particle size reduction to nanometer range not relying on the presence of the amorphous form of the drug, no long term time-stability considerations regarding crystalline state modifications are of concern. The maintain of original drug crystalline state following particle size reduction has been verified (DSC/PXRD) on the model drugs studied in this work using one particular technique (High Pressure Homogenization - see **part II.3.4.2.2**) and is reported for other nanoparticle engineering technologies such as ball milling (Nanocrystal<sup>®</sup> Technology - Nanosystems - Elan) and some technologies using supercritical fluids (**Thakur and Gupta, 2006; Shekunov et al., 2006**). It has, however, to be noted that not all micro/nanoparticle engineering technologies (e.g. SFL, EPAS, etc.) lead to the preparation of crystalline particles and that crystalline state evaluation following particle size reduction is a very important parameter to assess.

Nanoparticulate technology, unlike other solubility/dissolution enhancement technologies which are generally associated to one or more limitations (e.g. solubility in solvents or/and in carriers, molecular size, stability considerations, drug loading efficiency, etc.), offers, due to its flexibility and adaptability, a general approach applicable to most poorly water-soluble and poorly water- and lipid-soluble drugs (**Date and Patravale, 2004; Patravale et al., 2004**). Drug nanoparticles possess many advantages over other colloidal drug carriers and extensive research relative to their production, characterization and efficacy is carried out nowadays. Comparisons of drug nanoparticles with other colloidal drug carriers are represented in **Table II 9**.

**Table II 9.** Comparison of drug nanoparticles with other colloidal drug carriers (**Date and Patravale, 2004**).

	Liposomes	Microemulsions	Polymeric nanoparticles	Drug nanoparticles
Commercialization	Possible	Easily possible	Impossible	Easily possible
Drug loading capability	Varies	Varies	Varies	Very good
Cost efficiency	Costly	Moderate	Costly	Relatively cheaper
Carrier-associated side effects	Low	Moderate	Moderate	None or very less
Delivery of poorly water- and lipid-soluble drugs	Possible	Difficult	Possible	Easily possible

There are two basic principles for particle size reduction of a drug, either to micrometer or nanometer range (i.e. based on controlled production parameters). The most common method is the comminution of larger particles using milling techniques (i.e. jet mills, pearl/ball mills, homogenization, etc.) and the other being controlled production from solutions (e.g. spray-drying and spray-freezing technologies, precipitation from supercritical fluids, controlled crystallization, etc.) (**Rasenack et al., 2003, 2004**).

The aim of the following chapters will be to review and to summarize the main particle size reduction technologies available nowadays and to investigate their potential in nanoparticle engineering. Particular attention on the description of High Pressure Homogenization (HPH) will be given as it is the technique used for this work.

#### **II.3.4.1. Controlled production from solutions**

##### **II.3.4.1.1. Supercritical fluid-based technologies**

The use of supercritical fluids (SCFs), particularly in applications such as material processing, is becoming more and more important in the field of pharmaceuticals. SCF-based particle engineering technologies possess many advantages as they are easily scaled-up and that drug particle size and shape can easily be controlled (**Date and Patravale, 2004**). The most frequently used SCF is supercritical CO<sub>2</sub>, which is a relatively inert gas. Particle size reduction (to micrometer and to nanometer range for some) using SCFs has already been reported for many drugs such as phenytoin (**Muhrer et al., 2006; Thakur and Gupta, 2006**), griseofulvin (**Reverchon et al., 2004; Perrut et al., 2005**), nifedipine, felodipine and fenofibrate (**Kerc et al., 1999; Perrut et al., 2005**), phenylbutazone (**Moribe et al., 2004**) and ibuprofen and Lovastatin (**Perrut et al., 2005**). The article by Perrut et



al. (2005) reviews many examples from the literature and self-obtained results relative to the dissolution rate enhancement of many SCF processed drugs.

Several SCF particle engineering technologies can be found in the literature, these being classified according to the type of utilization of the SCF (i.e. as a solvent or as an anti-solvent). These techniques can be used for the production of neat (i.e. only the drug) or composite (drug-carrier) particles.

#### II.3.4.1.1.1. Rapid Expansion of Supercritical Solutions (RESS)

In the rapid expansion from supercritical fluids (RESS) process, the desired solute (i.e. the poorly water-soluble drug), is first solubilized in a SCF (generally CO<sub>2</sub>). This pressurized solution is then subjected to a rapid expansion (i.e. decompression-depressurization) by spraying through a nozzle into a collection chamber. This rapid expansion causes a supersaturation of the solute and subsequent precipitation (nucleation) of the solute as small particles with a narrow particle size distribution (Date and Patravale, 2004; Rogers et al., 2004; Perrut et al., 2005). Schematic representation of the RESS process is shown in **Figure II 16**. Particle size and morphology of the processed drug will depend on parameters such as the nature of the solute, pre- and post-expansion temperature and pressure, the nozzle geometry and the solution concentration (e.g. drug loading capability can be increased with an increase in pre-expansion temperature at high pressures, drug solubility and solvent density can be increased, at a given temperature, by increasing the SCF pressure, etc.) (Date and Patravale, 2004; Rogers et al., 2004).

Although this RESS process is fairly simple, it possesses some disadvantages in the fact that it is not applicable to drugs presenting poor solubility in selected SCFs (although alternatives such as PGSS (Precipitation from gas saturated solutions - modified RESS technology) exist) and in the fact that it is very hard to reach submicron sizes due to particle agglomeration during the expansion process (Date and Patravale, 2004).

To minimize this aggregation phenomenon and to allow this RESS technology to be used for nanoparticle engineering, RESS has evolved in RESAS (Rapid Expansion from Supercritical to Aqueous Solutions). Here the supercritical drug-containing solution is again expanded through a nozzle, but in this case into a stabilizer (i.e. surfactants) containing aqueous solution, and the drug is precipitated as a suspension (e.g. nanoparticulate

suspension) (Date and Patravale, 2004; Rogers et al., 2004; Hu et al., 2004). In the RESAS process, the surfactant rapidly diffuses to the newly-formed particle surface to impede particle agglomeration and growth.

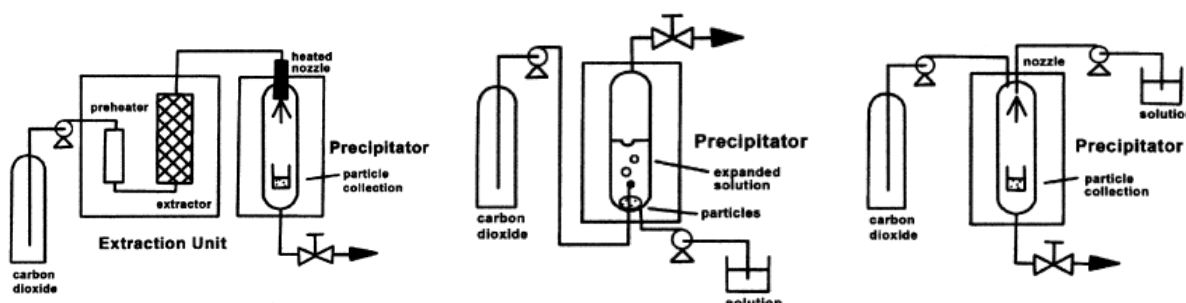


**Figure II 16.** Schematic representation of the RESS (left), GAS (middle) and SAS (right) processes (Rogers et al., 2004).

#### II.3.4.1.1.2. Gas anti-solvent (GAS) and Supercritical anti-solvent (SAS) precipitation method

In both Gas anti-solvent (GAS) and Supercritical anti-solvent (SAS) methods, the desired drug is solubilized in an appropriate organic solvent (or solvent mixture). The solvent(s) used need(s) to be chosen with respect to the drug's solubility in these solvents and also to the solvent(s) solubility in the SCF. In the GAS method, the addition of a SCF (typically supercritical CO<sub>2</sub>) as an antisolvent to the drug-containing solution will diminish the solvent strength, providing good SCF/solvent solubility, and lead to the drug's precipitation. Particle size using the GAS method will depend on the rate of addition of the SCF into the organic solution (Rogers et al., 2004). A schematic representation of the GAS process is shown in **Figure II 16**. Unlike the GAS technology, in the SAS technology, the drug-containing organic solution is atomized into an excess flowing continuum of SCF (typically supercritical CO<sub>2</sub>), with the high surface area atomized droplets allowing for an intimate contact with the excess anti-solvent (Date and Patravale, 2004; Rogers et al., 2004). In this process the bidirectional mass transfer (supercritical CO<sub>2</sub> ↔ organic solvent) again leads to a diminished solvent strength and to particle nucleation. A schematic representation of the SAS process is shown in **Figure II 16**. The success of the SAS process in drug nanosizing will mainly depend, in addition to the various controlled processing parameters (temperature, pressure, etc.), upon the efficiency of the atomization of the drug containing organic solution into the SCF; an increase in the extent of

atomization leading to an increase in surface area and thus to a more rapid bidirectional mass transfer and thus to smaller particle sizes (Date and Patravale, 2004). Further development of the SAS technology, with the aim of enhancing the bidirectional SCF/solvent mass transfer, has led to the SAS-EM technology (Supercritical anti-solvent enhanced mass transfer). The SAS-EM technology uses, like the SAS technology, a solvent and a SCF as an anti-solvent but here, the drug-containing solvent solution jet is deflected by a surface vibrating at an ultrasonic frequency in order to atomize the jet into nanodroplets, thus enhancing the bidirectional SCF/solvent mass transfer (Date and Patravale, 2004).

These techniques, and principally SAS and SAS-EM if we only consider nanoparticle engineering, have the advantage over RESS and RESAS technologies in that drugs that present poor solubility in SCFs can be processed.

#### **II.3.4.1.2. Spray-drying**

Spray-drying is a frequently used technique for particle size reduction to micrometer range. A solution of the drug to be micronized is atomized through a nozzle as fine droplets into a heated chamber, the solvent evaporation leading to the nucleation and growth of particles. This evaporation being almost instantaneous, and thus the particle formation being very rapid, this process generally leads to the formation of amorphous products. In the case of poorly water-soluble drugs, organic solvents need to be used.

Particles obtained through spray-drying are generally of micron range and show, in general, a homogenous particle size distribution. However this technique is of limited application for nanoparticle engineering. It is however, like freeze-drying, frequently used to transfer nanosuspensions into dry-state drug nanoparticles obtained with other techniques.

#### **II.3.4.1.2. Aerosol Flow reactor method**

In the aerosol flow reactor method, the drug is at first dissolved in a suitable volatile solvent (generally ethanol). The resulting drug-containing solution is then atomized into nanodroplets which are subsequently suspended in a pressurized inert carrier gas and passed through a heated tubular laminar flow reactor in order to evaporate the

solvent and to lead to the formation of drug nanoparticles (Date and Patravale, 2004; Eerikäinen et al., 2004). Processing parameters such as temperature and most importantly the atomization (necessity of atomizing the solution as nanodroplets in order to obtain nanoparticles) are critical in determining particle size and morphology. This technique has been described for the preparation of nanoparticles (with a mean diameter around 100 nm) for drugs such as ketoprofen, naproxen and beclomethasone dipropionate (Eerikäinen et al., 2003, 2004; Raula et al. 2004). All these described drug nanoparticles are, however, polymeric nanoparticles (i.e. drug/carrier nanoparticles) where the drugs are found in amorphous state. This very interesting technique is also limited to drugs presenting a fair solubility in organic solvents such as ethanol and cannot thus be used for the nanosizing of drugs that present limited solubility in both aqueous and organic media.

#### II.3.4.1.3. Controlled precipitation process

The controlled precipitation process (or continuous precipitation process) is a very simple method for the production of micro- and nanoparticles of poorly water-soluble drug compounds. It simply consists in dissolving the drug, and if necessary additional stabilizers, in a water-miscible organic solvent (e.g. ethanol, methanol, etc.) which is then dispersed under agitation at a controlled rate in an aqueous solution. The diffusion of the solvent into the aqueous phase leads to the generation, depending on operating conditions, of micro and/or nanoparticles (Date and Patravale, 2004). This technique has been reported for the preparation, with the aim of enhancing drug dissolution, of crystalline nanoparticles of drugs such as danazol and naproxen (Rogers et al., 2004).

#### II.3.4.1.4. Evaporative precipitation into aqueous solutions (EPAS)

The evaporative precipitation into aqueous solutions (EPAS) technique is a solution-based spray process to produce micron and submicron sized particles (Sarkari et al., 2002; Hu et al., 2004). In this technique, the studied drug is dissolved at first in a low boiling point organic solvent (e.g. dichloromethane, diethyl ether, etc.) and the

obtained drug-containing solution is then passed through a tube where it is heated under pressure at a temperature above the solvent's boiling point. This solution is subsequently sprayed as fine droplets into an heated stabilizer (e.g. polymers, surfactants, etc.) containing aqueous solution. A schematic representation of the EPAS process is shown in **Figure II 17**. This technique is also based, as are the previously described technologies, on the principle of rapid phase separation and subsequent nucleation of particles. The obtained micro- or nanosuspensions are then freeze- or spray-dried to obtain particles in dry state. This technique has been reported for the preparation, with the aim of enhancing drug dissolution, of micro- and nanoparticles of drugs such as carbamazepine (Sarkari et al., 2002), cyclosporine A (Chen et al., 2002) and itraconazole (Sinswat et al., 2005). This technique, due to the rapid phase separation, leads in general to the formation of amorphous drug particles. This technique is also limited to drugs presenting a fair solubility in organic solvents.

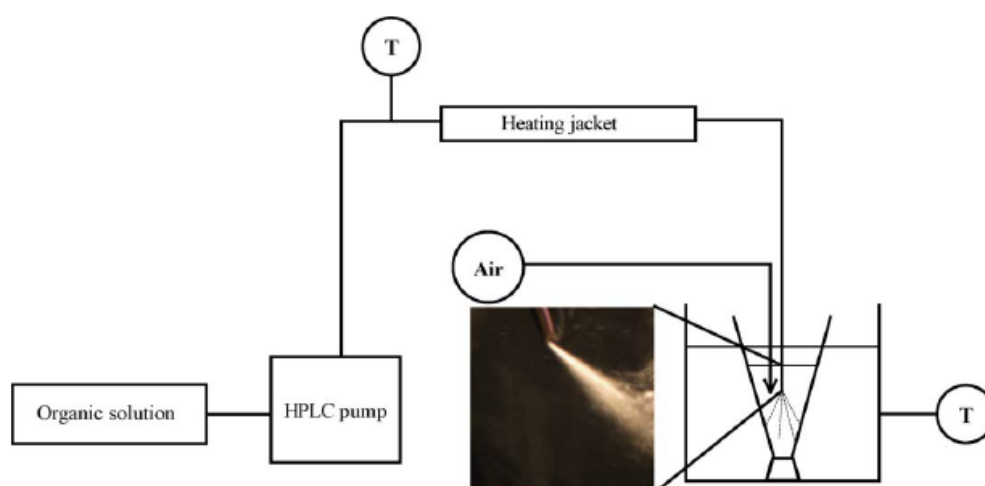


**Figure II 17.** Schematic representation of EPAS process and a photograph showing intense atomization of the spray (Sinswat et al., 2005).

#### II.3.4.1.5. Cryogenic Spray Process - Spray-freezing into liquids (SFL)

The cryogenic spray process and, more importantly, the process of spray-freezing into liquids (SFL) are very interesting techniques for producing drug micro- and nanoparticles. Both these processes involve the atomization of an aqueous, organic, or aqueous-organic co-solvent solution, aqueous-organic emulsion, or suspension containing a drug and eventually pharmaceutical excipients, into cryogenic liquids such as nitrogen (mainly), argon

or hydrofluoroethers (Rogers et al. 2002; Hu et al., 2004). The cryogenic spray process involves the atomization of such described types of solutions above the cryogenic liquid so that the atomized droplets gradually solidify while passing through the vapour of the cryogenic liquid and completely freeze when contact is made with the cryogenic liquid. In this case, due to the fact that atomization occurs in the vapour phase above the liquid gas, the solution droplets gradually agglomerate and solidify while passing through the vapour phase and then settle onto the surface of the cryogenic liquid and, as a result this agglomeration, broad particle size distributions and nonmicronized dry powders might be obtained (Hu et al., 2004). The SFL process is a derivative of the previously described general cryogenic spray process that was developed to erase the potential agglomeration limitation of this process. In the SFL process, the pressurized feed solution is directly atomized into the cryogenic liquid (i.e. not into the vapour phase) which gives advantages with regard to a more intense atomization (liquid-liquid impingement increases the degree of atomization) and a more rapid freezing rate (Hu et al., 2004). The SFL technology has been reported for the preparation of micro- and nanoparticles of poorly water-soluble drugs, with the aim of enhancing drug dissolution rate, such as carbamazepine (Rogers et al. 2002; Hu et al., 2003) and danazol (Rogers et al. 2002; Hu et al., 2004b, 2004c). SFL, due to the rapid freezing operation, leads to the formation of amorphous drug particles. This technique is also limited to drugs that present a fair solubility in organic solvents.

#### II.3.4.1.6. Microemulsion template methodology

Microemulsions can be defined as colloidal nanodispersions of water in oil (W/O) or oil in water (O/W) stabilized by a surfactant film (López-Quintela, 2003). Considering this microemulsion template methodology for drug nanoparticle engineering, two preparation methods are referred: a solvent diffusion method and a melt emulsification method. Both these technologies require the use of stabilizers such as surfactants to control particle growth.

- Solvent diffusion method:

In this case the microemulsion is generally composed of a surfactant containing aqueous phase (acting as an anti-solvent) and an organic solvent as the dispersed phase. The chosen solvent needs to be partially water miscible as

this technique is based on diffusion. The steps for obtaining a drug nanosuspension (further processing leading to drug nanoparticles) consist in the preparation of a microemulsion (using adequate technique such as high pressure homogenization) of the poorly water-soluble drug containing organic phase in water and the subsequent dilution of this emulsion in water; the diffusion of the solvent in the aqueous phase leading to the nucleation and growth of particles. This technique has been successfully used for the preparation of nanosuspensions of drugs such as ibuprofen (Kocbek et al., 2006) and mitotane (Trotta et al., 2001).

This simple precipitation method has, however, numerous drawbacks in that only drugs presenting fair solubility in solvents (which furthermore need to be water-miscible) can be processed, that it is very difficult to control nucleation and crystal growth to obtain a narrow size distribution and that the amorphous form is generally obtained (Kipp, 2004).

- Melt emulsification method:

This melt emulsification technique is well known for the production of solid lipid nanoparticles (SLN) but has also been referred for the production of drug nanosuspensions and subsequently drug nanoparticles for drugs such as ibuprofen (nanoparticles from 100-200 nm) (Kocbek et al., 2006). This technique has been described as the preparation of a microemulsion with the melted poorly water-soluble drug as the dispersed phase (e.g. using high pressure homogenization) and the subsequent cooling to solidify the droplets of the melted drug. This method is, however, only useful for drugs that present a melting point below the boiling point of water.

#### II.3.4.2. Mechanical micronization (“nanoisation”) processes

There are different kinds of mills available in the pharmaceutical industry for particle size reduction, such as the pearl/ball mill, fluid energy mill, cutter mill, hammer mill, vibration mill, etc. However, the fluid energy mill (also called air jet mill or air classifying mill) and the pearl/ball mill are the only two that can reduce the particle size to less than 5 µm by dry milling (Vatsaraj et al., 2003). Both these milling techniques rely on interparticular

collisions for drug particle size reduction and the second relies on additional collisions with the grinding media used (i.e. ceramic or steel spherical particles ( $\approx 3\text{mm}$ )).

There are four types of particle size reduction mechanism (FDA CDER Guidance, 1998):

- **Impact** - Particle size reduction by applying an instantaneous force perpendicular to the particle and/or agglomerate surface. The force can result from particle-to-particle or particle-to-mill surface collision.
- **Attrition** - Particle size reduction by applying a force parallel to the particle surface.
- **Compression** - Particle size reduction by applying a force slowly (as compared to impact) to the particle surface towards the center of the particle.
- **Cutting** - Particle size reduction by applying a shearing force to a material.

Contrarily to the fluid energy mill where only impact forces are present, the cascading action of the grinding media in pearl/ball mills affects particle size reduction via attrition, impact and compression (Lee et al., 2000). These two technologies, which work in dry state mode, do not allow sufficient particle size reduction to the nanometer range.

In order to obtain drug nanoparticles, the two milling technologies available nowadays which have shown very interesting results and promising applications (both are patented technologies) are media milling (i.e. pearl/ball wet milling) and high pressure homogenization.

#### II.3.4.2.1. Media milling

Media milling is a comminution process in which large micron size drug crystals are wet milled in the presence of grinding media and a surface modifier (i.e. pearl/ball milling in a stabilizer-containing solution) (Liversidge and



Cundy, 1995; Lee et al., 2000; Hu et al., 2004; Kipp, 2004; Patravale et al., 2004; Keck and Müller, 2006).

The grinding media (or milling beads - size range 0.4 to 3 mm) can be composed of glass, zirconium oxide, ceramics, stainless steel or plastics (e.g. cross-linked polystyrene resins) and the surface modifiers include various polymers (polyvinylpyrrolidone, cellulose derivatives, etc.) and/or surfactants. A schematic representation of the media milling process is shown in **Figure II 18**. The milling chamber is charged with the grinding media and with the previously formed drug suspension (in the stabilizer solution) and is then rotated (via the milling shaft) at very high rates ( $\pm 20000$  rpm) (Lee et al., 2000). The high energy and shear forces generated as a result of the impaction of the grinding media with the drug provides the energy input to break the drug microparticles into nanoparticles (Patravale et al., 2004). This technique has been reported not to interfere with the crystalline state of the processed drug and nanoparticles engineered through this method are reported to be crystalline (intended that the drug is crystalline prior to the milling operation).

Although the very high potential of this technique in drug nanoparticle engineering, a general reported problems using pearl mills is the potential erosion of materials from the grinding material and the subsequent contamination of the final drug product, even with the use of very hard grinding material (Kipp, 2004; Patravale et al., 2004; Keck and Müller, 2006). This erosion phenomenon will depend on the hardness of the drug and the hardness of the grinding material (could be limited when using polymers such as polystyrene resins) and the milling time required (e.g. from several hours up to a few days); contamination numbers from 0.05 ppm to 70 ppm have been reported (Keck and Müller, 2006). Scaling-up feasibility of the system, which although quite good to a certain degree, could find a limit in the size of the mill due to its weight (almost 80% of the volume of the milling chamber consists of the grinding media) (Lee et al., 2000; Keck and Müller, 2006).

This patent-protected technology, termed Nanocrystal<sup>®</sup>, was developed by Gary G. Liversidge and co-workers from the company Nanosystems and is now owned by Elan Pharmaceutical Technologies (Elan Group). Many drugs have been successfully formulated with success using this technique such as danazol (16-fold increase in oral bioavailability) (Liversidge and Cundy, 1995), ketoprofen (Vergote et al., 2001, 2002) and naproxen (Patravale et al., 2004). As of today, two marketed products using the Nanocrystal<sup>®</sup> technology can be found. The first approved drug is a tablet dosage form of the macrolide immunosuppressant sirolimus (Rapamune<sup>®</sup>, Wyeth Pharmaceuticals) and the second (approved by the FDA for marketing in the US in 2003) is a selective antagonist of substance P/neurokinin 1 receptors used in prevention of chemotherapy-induced nausea and vomiting (Emend<sup>®</sup>, Merck & Co.) (Wu et al., 2004).

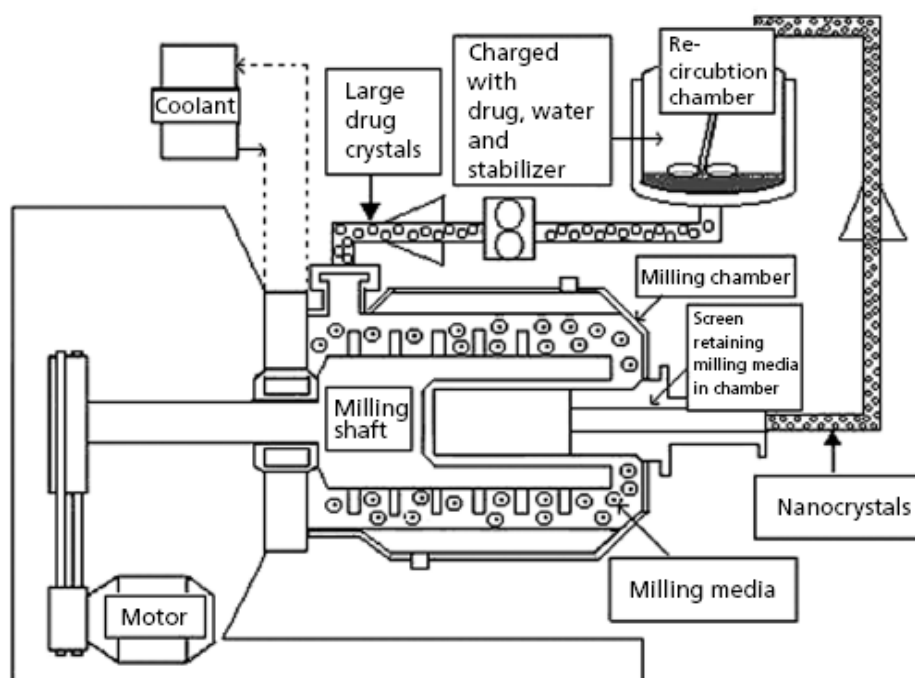


**Figure II 18.** Schematic representation of the media milling process (Patravale et al., 2004).

#### II.3.4.2.2. High Pressure (piston-gap) Homogenization (HPH)

High pressure homogenization (HPH) regroups two kinds of technologies, based on the homogenization principle and the homogenizer type, which are microfluidisation and piston-gap homogenization. Microfluidisation is a jet stream principle where the drug suspension is accelerated and passes at extremely high velocity through an especially designed homogenization chamber; this chamber being either z-shaped (the change in flow direction leads to important particle collision and high shear forces) or y-shaped (the suspension stream is divided into two streams which are subsequently collided frontally) (Keck and Müller, 2006). This technique is, however, limited by the high number of homogenizing cycles (up to 75) through the microfluidiser for sufficient particle size reduction. Piston-gap homogenization was subsequently developed to further the particle size reduction efficiency of microfluidisation. The piston-gap HPH of drugs in water (patented name DissoCubes® (US 5,858,410 - Peters et al., 1999) and, more recently, in non aqueous media or in dispersion media with a reduced water content (patented name Nanopure®) was developed by Rainer H. Müller and co-workers at the Free University of Berlin (Müller et al., 1998, 2000, 2001; Peters et al., 1999; Grau et al., 2000; Jacobs et al., 2000; Krause and

Müller, 2001; Keck and Müller, 2006). The DissoCubes® technology is now owned by the company SkyePharma and the Nanopure® technology is owned by the company PharmaSol GmbH (Berlin, Germany).

The DissoCubes® technology is the technique used in this work for the preparation of model drugs (i.e. nifedipine (Hecq et al, 2005) and UCB S.A. molecules ucb-35440-3 (Hecq et al, 2006), UCB-A and UCB-B). A complete description of the method including its principle will be made in this chapter.

#### II.3.4.2.2.1. Principle behind particle size reduction

Effective particle size reduction in piston-gap high pressure homogenizers, and possibly in microfluidizers as well, is the resultant of enormous impact forces brought in by intense interparticular collisions, high fluid shear forces and cavitation forces; the latest being far more pronounced for piston-gap homogenizers (Kipp, 2004).

Cavitation is the phenomenon where small and largely empty cavities are generated in a fluid when it is subjected to a low pressure and more precisely below its vapor pressure at the local ambient temperature. At this stage the liquid can undergo a phase change (liquid → vapor) and thus create empty voids termed cavitation bubbles. When the initial pressure is restored, these cavitation bubbles implode and the high energy accompanying this implosion (heat, turbulent flow, acoustic shockwaves) is responsible for the breaking of the drug particles (Kipp, 2004; Keck and Müller, 2006).

The cavitation forces arousal in piston-gap homogenizers is the consequence of the reduced tubular diameter through which the suspension is processed. In fact, the suspension reservoir (**Figure IV 2 1**) has a terminal diameter of approximatively 3 mm and the diameter at the homogenizing valve (**Figure II 19**) can be as narrow as 25 µm (size of the homogenizing gaps at an homogenizing pressure of 1500 bar (Müller et al., 2001)), thus leading to a very high streaming velocity. According to Bernoulli's Law, which states that the flow volume of a liquid in a closed system per cross-section is constant, the reduction of the diameter through which the suspension is passed leads to a tremendous increase in the fluid dynamic pressure and simultaneously to a decrease in the fluid static pressure at the homogenization gaps (Müller et al., 2001; Keck and Müller, 2006) (**Figure II 20**). This drop in static pressure goes below the vapor pressure of the liquid (water) at ambient temperature meaning that, as described

in the previous paragraph, water starts to “boil” at this temperature with the formation of gas bubbles (cavitation bubbles) which implode when the suspension leaves the gap and that normal pressure is restored.

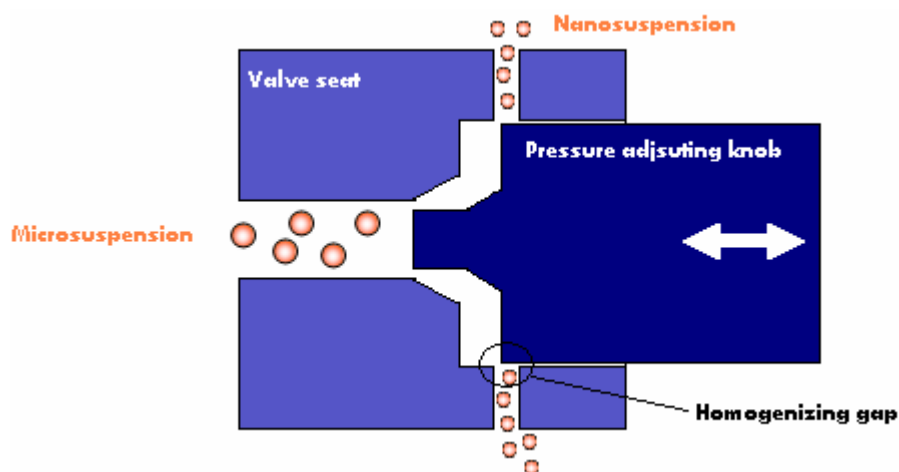


**Figure II 19.** Schematic representation of the homogenizing valve of an EmulsiFlex C5<sup>®</sup> type piston-gap high pressure homogenizer

The high pressure homogenization particle size reduction efficiency will be dependent upon the power density of the homogenizer (i.e. the homogenizing pressure applied - up to 30000 PSI as reported in part III.2.2.2.3.2 of this report), the number of homogenizing cycles, the drug hardness characteristics, and eventually the processing temperature.

Processing temperature has been shown, in this work, to have an influence on the particle size reduction efficiency of nifedipine and on UCB-A. For the latter the temperature effect is the result of polymorphic changes of the drug, probably leading to varying drug hardness characteristics.

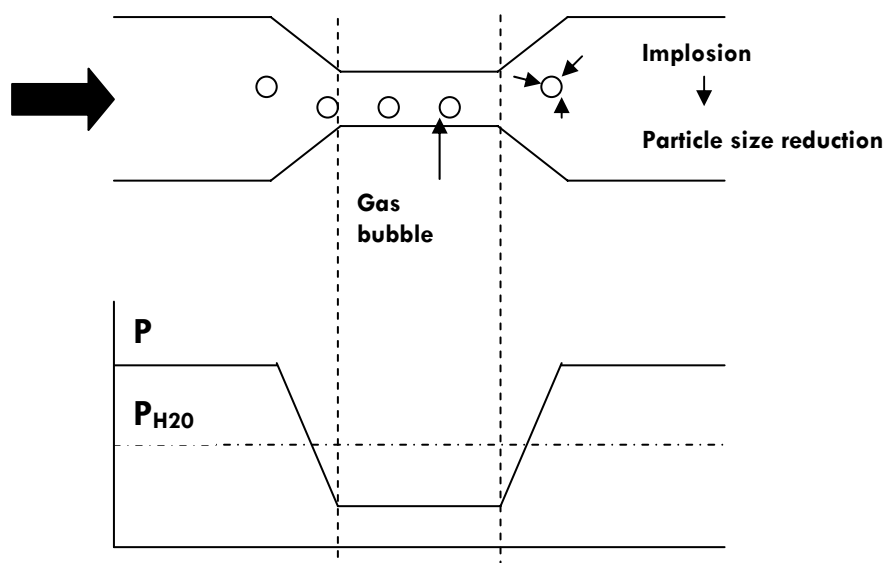


**Figure II 20.** Diagram showing the modification in static pressure following the decrease of the diameter of the streaming dispersion at the homogenizing valve:  $P$  = Pressure;  $P_{H_2O}$  = Vapor pressure of water at room temperature (reproduced from **Keck and Müller, 2006**).

Particle size reduction efficiency depends on the homogenizing pressure applied; the higher the power density, the more efficient the particle size reduction. In fact during milling operations such as high pressure homogenization, particle/crystal cleavage is favored at crystal dislocations. As the number of crystalline defects per particle is theoretically reduced as particle size is decreased, the force required to break the particles will increase with decreasing particle size (eventually if the power density in the homogenizer is  $\leq$  to the interaction forces in the crystal, particle size reduction will be stopped) (**Kipp, 2004; Keck and Müller, 2006**). When a limit in particle size reduction is reached, the homogenizing pressure should be increased if further particle size reduction is required; this however stopping at the limits of the apparatus used.

Considering the number of homogenizing cycles, as this number increases for a given pressure, further reduction in particle size can be achieved; this, however, to a limited extent for the same reason as explained in the previous paragraph (e.g. for some drugs 20 cycles at a given pressure will yield the same particle size as 10 cycles, meaning that maximum particle size reduction has been reached for the given pressure). Although this increasing number of homogenizing cycles will rapidly find a limitation with regard to the decrease of the mean particle size, it has been shown to be very interesting with regard to the decrease of other reported diameters such as  $d(v;0.9)$  and  $D[4,3]$  which are better representative of the presence of residual microparticles or nanoparticle

agglomerates in the resulting suspension. In fact, one or a few milling cycles at a given homogenizing pressure is generally not sufficient to obtain the desired particle size, and even at high homogenizing pressures some microparticles might be left in the suspension. This can be explained by the existence of a different turbulent flow profile at the homogenizer gap with the highest streaming velocity in the center of the gap and a decreasing streaming velocity when going from the center to the wall of this homogenization gap; a decreased streaming velocity resulting in lesser disruptive forces and leaving some “large” crystals to survive the passage of the gap (Keck and Müller, 2006). An extended number of cycles will increase the probability that these larger particles, having escaped the zone of high power density in the center of the homogenization gap, will pass this region.

High pressure homogenization is, in general, a rapid method for engineering drug nanosuspensions as, depending on drug hardness, reported protocols rarely exceed 20-30 homogenizing cycles. These protocols generally involve the processing of previously micronized drugs (jet-mills, high-speed stirrers/homogenizers, etc.) and a gradual increase in homogenizing pressure in order to prevent the blocking of the homogenizing gaps (since these get smaller as the homogenizing pressure is increased). The homogenizing protocol adopted in this work was 15 cycles at 7000 PSI, 10 cycles at 12000 PSI, 0-20 cycles at 23-24000 PSI and 0-10 cycles at 30000 PSI.

The use of stabilizers such as surfactants is, in general, a requisite for processing a drug microsuspension through HPH in order to reduce particle aggregation during the homogenization process in order to maintain a free-flow of the suspension through the homogenizer and, most importantly, to stabilize the newly-formed drug nanoparticles.

Unlike the wet-milling technique, where contamination of the final drug product following erosion of the grinding media occurs (although this can be limited by proper selection of this grinding media), this phenomenon is less of a concern for high pressure homogenization. Erosion of the homogenizing valve (primarily the valve seat and the stem) can in fact show a wearing due to cavitation forces and particle impact but only, in general, after a long time of usage (studies have reported a maximal contamination of 0.7 ppm of iron in processed suspensions under hard processing conditions) (Keck and Müller, 2006).

## **AIM OF THE WORK**





### III. Aim of the work

When considering oral administration, drug release from its pharmaceutical form and its dissolution into gastrointestinal fluids generally precede absorption and systemic availability. The solubility-dissolution behaviour of a drug is frequently the rate-limiting step to absorption of drugs from the gastrointestinal tract (BCS class II drugs). Poor aqueous solubility is thus a very challenging obstacle in formulation development as it is, together with membrane permeability, an essential factor in the limitation of a drug's bioavailability following oral administration.

The formulation of drugs as crystalline nanoparticles (i.e. drug nanosizing) is reported in the literature to be a successful approach for the enhancement of the *in vitro* solubility and the *in vitro* dissolution rate of poorly water-soluble drugs (BCS class II drugs). Crystalline NP are defined as particles with a mean particle size below 1  $\mu\text{m}$  and composed of 100 percent of drug without any matrix material. They offer primarily the advantage of a much increased surface area and increased solubility, both characteristics beneficial in regards to drug dissolution. Out of the many techniques available for drug particle size reduction to nanometer range, high pressure homogenization is coming out as one of the most promising technique as it is applicable to almost any kind of compounds.

The aim of this work was to evaluate the potential of high pressure homogenization in the development of crystalline NP formulations and to evaluate the potential of these formulations in enhancing the *in vitro* – *in vivo* properties (i.e. solubility, dissolution, bioavailability) of poorly water-soluble drugs.

In order to meet this objective, four model drugs (nifedipine and three UCB S.A. molecules under investigation) with different physicochemical properties were used and we have conducted various types of experiments. In the following chapters:

- The influence of production parameters such as the homogenizing pressure, the number of homogenizing cycles and temperature will be evaluated with regards to particle size reduction efficiency. The influence of the presence of various formulation additives (e.g. surfactants, carriers, etc.) with regards to the stabilization of NP will also be evaluated. As the aimed desired solubility/dissolution properties of NP shall not be the consequence of the presence of the amorphous form of the drug, investigations in the crystalline state of the developed NP formulations will be carried out.

-The *in vitro* solubility and the *in vitro* dissolution characteristics of the NP formulations developed will be evaluated to confirm the theoretical hypothesis of increased surface area (i.e. particle size reduction).

-An *in vitro* permeability study across intestinal cell models (Caco-2/HT29-5M21) will then be carried out preliminary to *in vivo* pharmacokinetic studies (using rats as models). An attempt to evaluate the *in vivo* pharmacological response of the NIF NP formulations (by measuring their antihypertensive effect on SHR rats) will also be made.

-Finally, a stability study (using NIF as a model) will be conducted (12 months: ICH conditions of 25°C/60%RH, 30°C/65%RH and 40°C/75%RH) with regards to the maintain of the original properties of an optimized NIF NP formulation (chemical stability, dissolution, redispersion characteristics and crystalline state).

## **EXPERIMENTAL PART**



## IV. Experimental Part

### IV.1. Model drugs

#### IV.1.1. Nifedipine

Nifedipine (NIF) is a cardiovascular drug that belongs to a group of drugs termed “calcium channel blocking agents”. It is frequently used in the prevention and treatment of angina pectoris (chest pain caused by lack of oxygen to the heart due to clogged arteries or spasm of the arteries), to help reduce blood pressure (“antihypertensive” drug), and for other cardiovascular disorders. The mechanism by which NIF operates is an inhibition of calcium ion influx notably in myocardic cells, in smooth muscle cells of coronary arteries and in peripheral vessels; this inhibition leading to the relaxation of arterial smooth muscles and thus to dilatation of coronary and peripheral arteries (R.M. Robertson and D. Robertson, 1996).

NIF was purchased from Chem-Spec Ind. (Newsmart, China). It has 99.25% purity. It comes as a yellow crystalline powder with a melting point of 172°C (Merck index 12<sup>th</sup> Ed., 1996). Its aqueous solubility at 25°C is approximately 10 µg/ml (practically insoluble) and it is classified as a BCS class II drug (Lindenberg et al., 2004). NIF solubility profile is pH-independent (considering GIT pH range).

Nifedipine is a molecule comprising a dihydropyridine cycle associated to a nitrophenyl aromatic cycle (Figure IV 1 1) which confers a high oxidation sensitivity to the molecule and makes it a highly photosensitive product. NIF is, in fact, extremely sensitive to ultraviolet radiation and to visible light up to 450 nm, the quantum yield for photodegradation being approximately 0.5 (meaning statistically that for every two photons absorbed, one causes decomposition of an NIF molecule) (de Vries and Beijersbergen van Henegouwen, 1998). The degradation products of nifedipine are of two types: 1) a nitrophenylpyridine derivative and 2) a nitrosophenylpyridine derivative (Figure IV 1 2) (Sansdrap, 1996). Studies have shown that UVA and daylight exposure give rise to the same photoproducts (the nitroso derivative being the main product obtained).

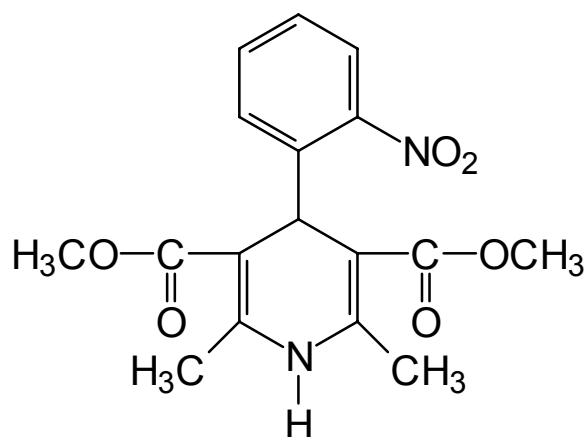


**Figure IV 1 1.** Chemical structure of nifedipine (1,4-dihydro-2,6-dimethyl-4-(2-nitrophenyl)-3,5-pyridine-dicarboxylic acid dimethyl ester)

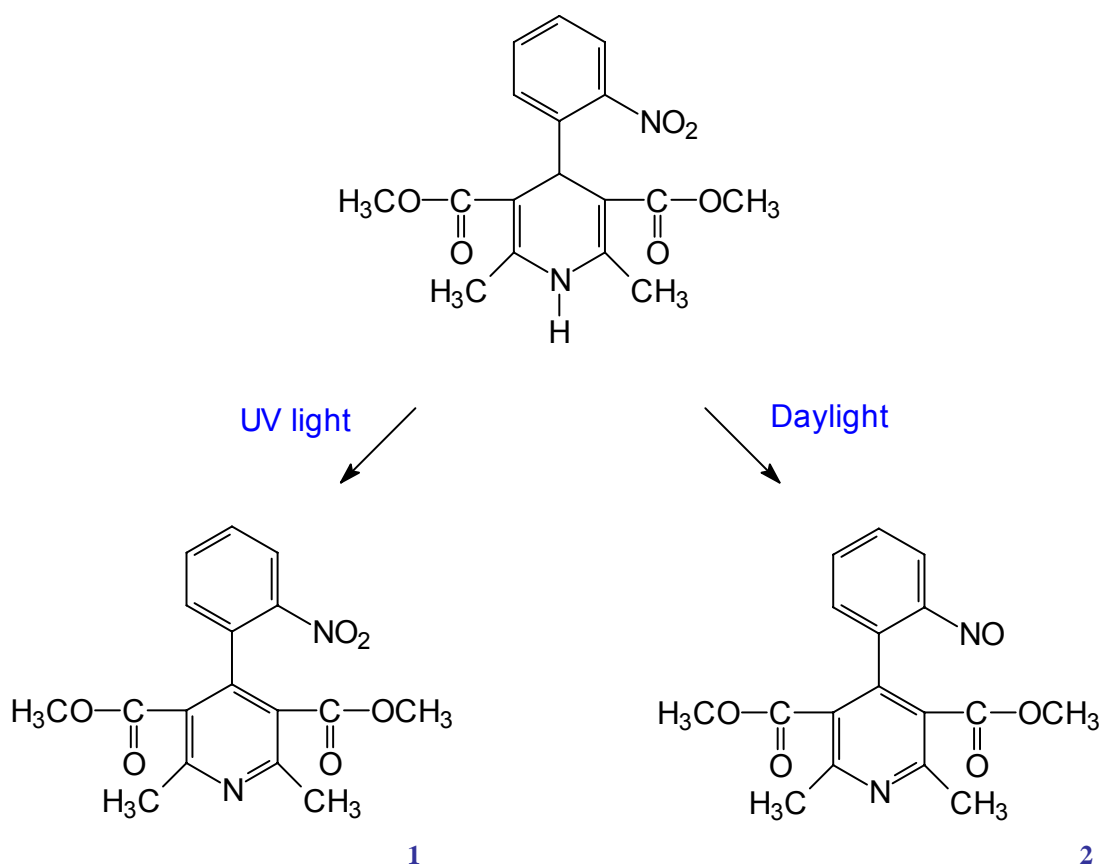


**Figure IV 1 2.** Photodegradation products of nifedipine: (1) nitrophenylpyridine derivative and (2) nitrosophenylpyridine derivative

NIF has two ultraviolet absorption maxima at 235 and 340 nm (in water – spectrum in ethanol readily identical) (**Figure IV 1 3**). NIF photodecomposition under natural daylight (or even artificial light of certain wavelengths) can easily be observed as one can see the evolution of the ultraviolet spectra following different exposition times to daylight and red light (dark room conditions) versus the spectra obtained for light protected (aluminum foil) NIF solutions (**Figure IV 1 4** and **Figure IV 1 5**).

Looking at these results, one can clearly see the evolution of the UV spectra of NIF solution following exposure to daylight. The maxima at 235 nm and 340 nm disappear after a 1-hour exposure, being substituted by two maxima at 280 nm and 313 nm. **Figure IV 1 5** shows that manipulation of NIF under red light (dark room conditions) does not lead to product photodecomposition (“red light” and “no light” spectra are identical) and that respecting these conditions is thus necessary in order not to alter NIF. The NIF photodegradation rate constant is indeed found to increase with decreasing particle size when NIF is in powder state (Teraoka et al., 1999).

The photodegradation of NIF can also be assessed with the HPLC methods used in this work (differences in retention times) but it is here represented through the showings of the UV spectrums taken under different exposure conditions, primarily for clearer visualization. Simple UV determinations were also used for NIF quantification (e.g. for the in vitro dissolution/solubility studies) and the spectrum aspect was considered a good indicator of NIF photodegradation and consequently a suitable control of our operating conditions with regard to light-protection of NIF samples.

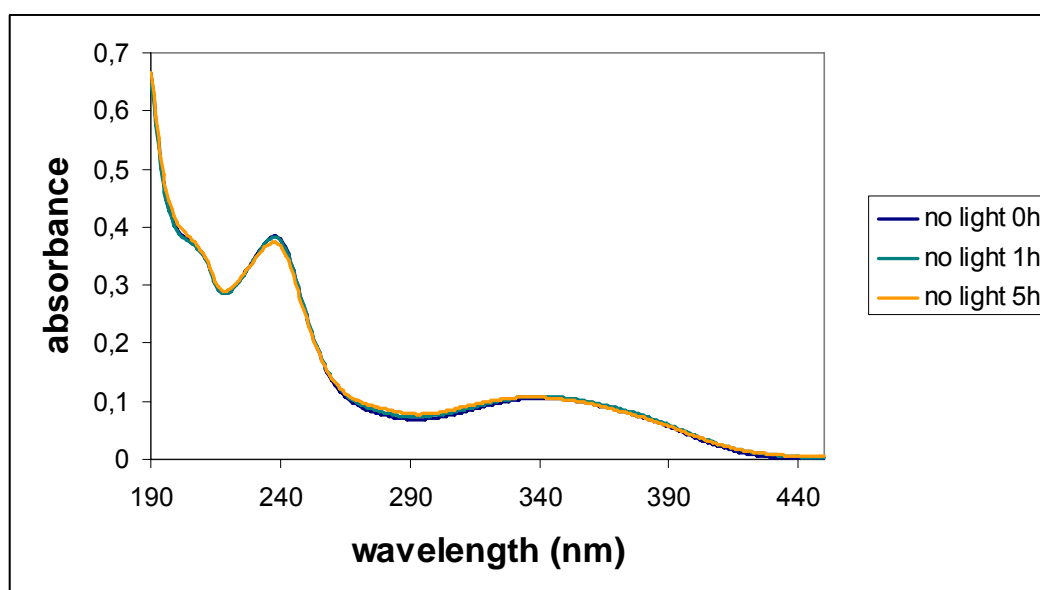


**Figure IV 1 3.** UV spectra of NIF solutions protected from light (aluminum foil) after 0, 1 and 5 hours.

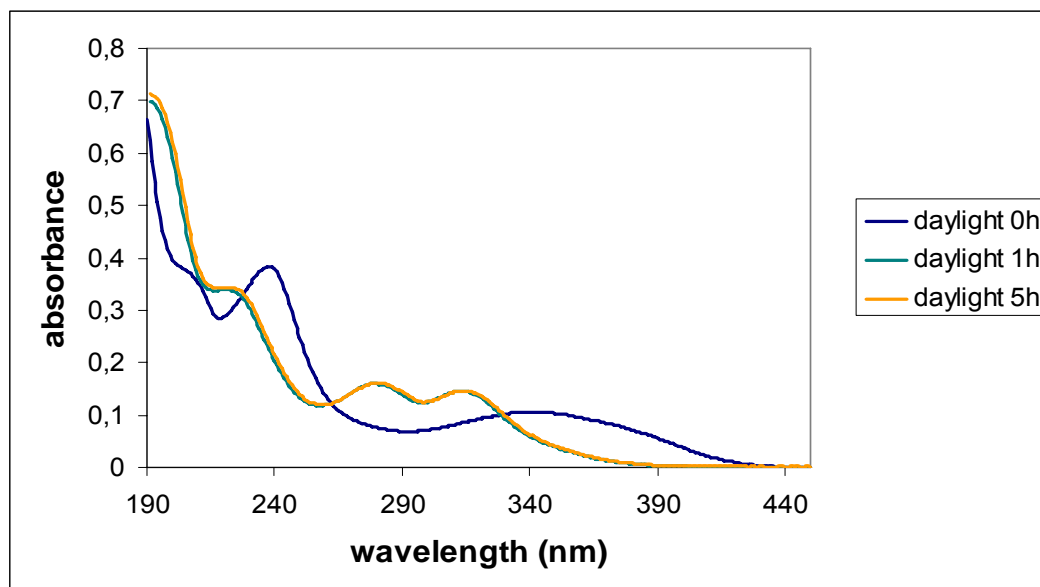


**Figure IV 1 4.** UV spectra of NIF solutions exposed to daylight after 0, 1 and 5 hours.

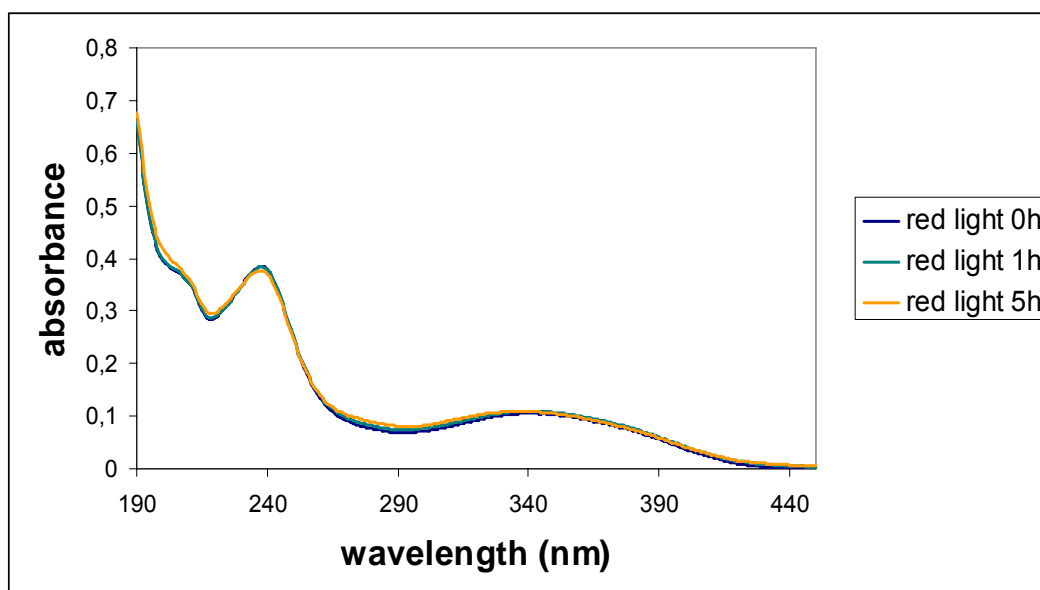


**Figure IV 1 5.** UV spectra of NIF solutions exposed to red light (dark room conditions) after 0, 1 and 5 hours.

NIF was used throughout this work as the main model drug on which most of the development was made. As it will be shown and extensively explained throughout this work, the aim of the formulation of NIF as nanoparticles was to increase its solubility and its dissolution rate and consequently enhance the systemic extent of exposure (with an increased  $C_{max}$  and a decreased  $T_{max}$ ) and ultimately the pharmacological response (enhanced drop in systolic blood pressure) following its oral administration. It has to be noted that NIF is only used here as a poorly water-



soluble model drug as there is no clinical interest in developing NIF formulations with such properties since NIF side effects are associated with the rapidity of the onset of action and the magnitude of the antihypertensive effect (Kim et al., 1997). These cited properties could, however, have real beneficial clinical implications for other poorly water-soluble drug models where a rapid onset of action and high blood concentrations are necessary. NIF is, however, frequently used as a poorly water-soluble model drug for the evaluation of various formulations that aim to enhance solubility and dissolution such as solid dispersions, inclusion complexes, etc. (Hirayama et al., 1994; Lin and Cham, 1996; Yamamura and Rogers, 1996; Sencar-Bozic et al., 1997; Portero et al., 1998; Sugimoto et al., 1998; Suzuki et al., 2001; Bayomi et al., 2002; Cilurzo et al., 2002; Vipagunta et al., 2002; Mitchell et al., 2003; Zajc et al., 2005).

#### IV.1.2. ucb-35440-3

ucb-35440-3 (patent N° WO 00/58295) is a new drug entity under investigation at UCB S.A. for the oral treatment of asthma and allergic rhinitis. It is an orally active dual 5-LO inhibitor/H<sub>1</sub> antagonist which could provide a valuable alternative to the currently available therapies, circumventing the poor compliance usually associated with multiple and/or inhalation therapies (Lewis et al., 2004a, 2004b). This molecule has effectively a dual-function compounds in which the H<sub>1</sub> scaffold (i.e. cyclizine) of cetirizine was linked to an *N*-hydroxyurea, the 5-LO inhibiting moiety of zileuton. A furan-based linker resulted in a compound demonstrating dual activities both in vitro and in vivo.

The molecule, a poorly water-soluble weak base (fumarate salt), presents two ionisable ternary nitrogens placed in a piperazine cycle (**Figure IV 1 6**). ucb-35440-3 comes as a white powder with a melting point around 160-166°C. Product decomposition is observed within this temperature range and no recrystallization is reported thereafter. ucb-35440-3 shows a pH-dependent solubility profile and is reported to be slightly soluble in water at pH 2.0 at 25°C (about 9 mg/ml). Solubility markedly decreases between pH 2.0 and pH 3.0 (about 0.7 mg/ml, very slightly soluble) and decreases further between pH 3.0 and pH 6.4 (0.04 mg/ml; practically insoluble) (**Figure IV 1 7 - Table IV 1 1**). The intrinsic dissolution rate is slow to very slow and is pH-dependent: 0.15 mg.min<sup>-1</sup>.cm<sup>-2</sup>, 0.044 mg.min<sup>-1</sup>.cm<sup>-2</sup> and 0.0025 mg.min<sup>-1</sup>.cm<sup>-2</sup> at pH 1.2, 4.0 and 7.5, respectively.

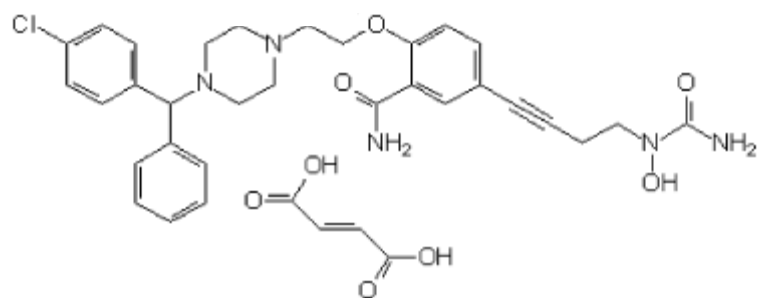


**Figure IV 1 6.** Chemical structure of ucb-35440-3 (5-{4-[(aminocarbonyl)(hydroxy)amino]but-1-ynyl}-2-{4-[(R)-(4-chlorophenyl) (phenyl) methyl]piperazin-1-yl} ethoxy) benzamide).

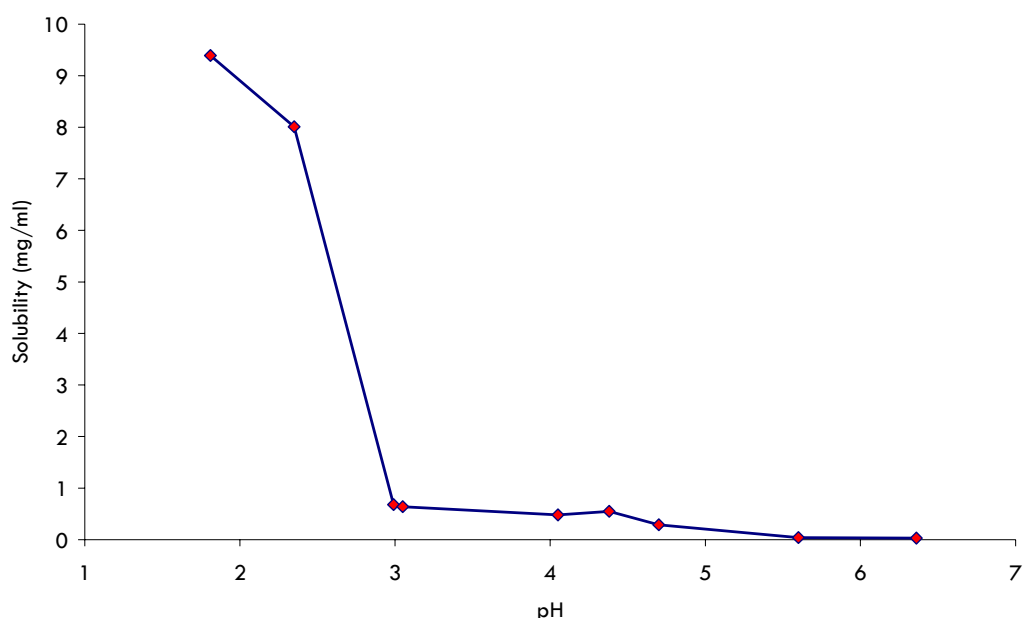


**Figure IV 1 7.** Aqueous solubility of ucb-35440-3 (25°C) versus pH.

**Table IV 1 1.** Values for **Figure IV 1 7.**

	pH (un-buffered media)	Solubility (mg/ml) (70h -25°C)
	1.81	9.39
	2.35	8.01
	2.99	0.68
	3.05	0.64
	4.05	0.48
	4.38	0.55
	4.70	0.29
	5.60	0.04
	6.36	0.03

ucb-35440-3 is an interesting poorly water-soluble drug model as, when compared to NIF, it presents a pH-dependent solubility profile and it is a highly dosed drug; the anticipated human pharmacologically active dose should be predicted at around 250-500 mg/day (NIF in its immediate-release dosage form is dosed at 10 mg).

The ucb-35440-3 batches supplied (UCB S.A. - Pharmaceutical R&D - Pharmaceutical & Galenic development, UCB S.A., Braine-L'Alleud, Belgium) for this work were batch N°C01HURU100 and batch N°01-06-1151.

#### IV.1.3. UCB-A and UCB-B

UCB-A and UCB-B (salt of UCB-A) are new drug entities under investigation at UCB S.A. for the oral treatment of inflammatory conditions such as asthma, multiple sclerosis (MS), and rheumatoid arthritis (RA) or Crohn's disease.

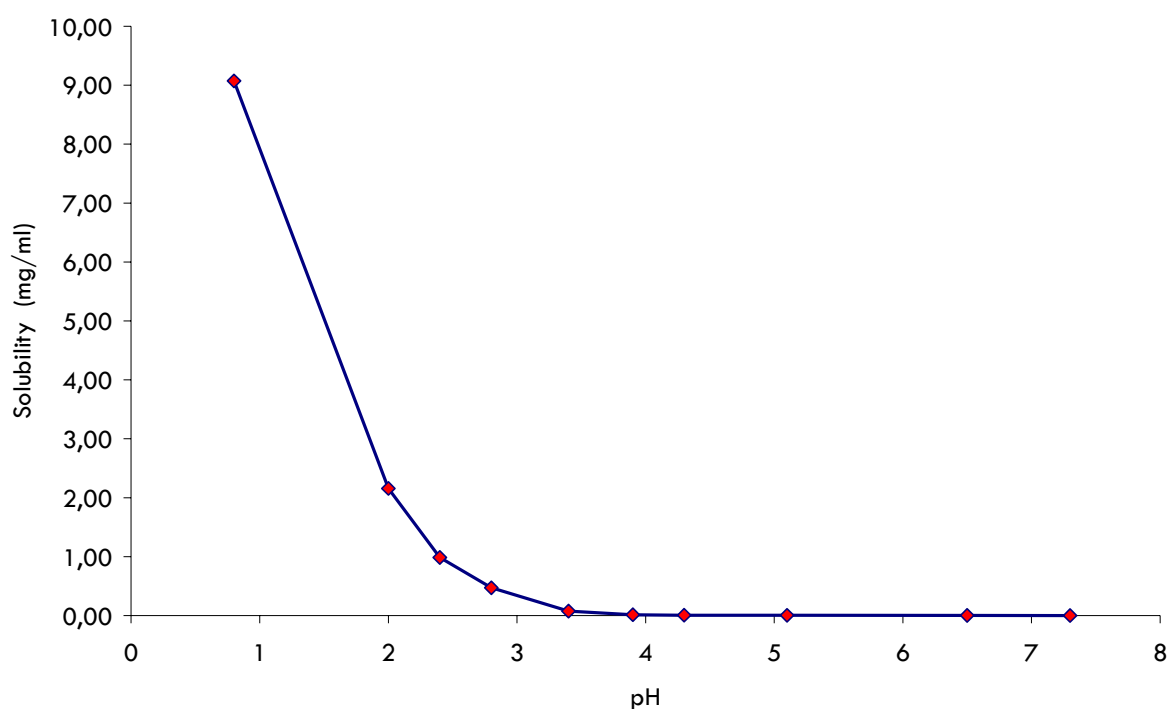
UCB-A, is a pro-drug ester that is hydrolyzed *in vivo* (tissue esterase) to its active form, UCB-A-Met1, which has been shown to be a potent and selective inhibitor of  $\alpha_4\beta_1$  and  $\alpha_4\beta_7$  integrins. Another major circulating human metabolite, UCB-A-Met2, has also been identified, and it has also been shown to be a potent inhibitor of  $\alpha_4\beta_1$  and  $\alpha_4\beta_7$  integrins. The drug is orally delivered as an ethyl ester prodrug to aid gastrointestinal absorption.

The integrins mediate several cell functions, including adhesion, migration, activation and cell survival. Lymphocytes, monocytes, eosinophils and mast cells all constitutively express  $\alpha_4\beta_1$  integrins and are capable of expressing the closely related integrin  $\alpha_4\beta_7$ . The  $\alpha_4$  integrin has been implicated as a major mediator in the leukocyte-endothelial cascade, a process whereby leukocytes, under the response of local inflammatory stimuli, emigrate out of the blood into inflamed tissues. Data from clinical and pharmacological studies have indicated a wide variety of diseases that may have some dependency on  $\alpha_4$  integrins.  $\alpha_4\beta_7$  is thought to be important in mucosal immunity. The ligands for both  $\alpha_4\beta_1$  and  $\alpha_4\beta_7$  are VCAM-1 (vascular adhesion molecule-1), expressed on the vascular endothelium, and an alternatively spliced connecting segment (CS1) region on fibronectin, expressed in extracellular matrices. In addition  $\alpha_4\beta_7$  integrins can also interact with the mucosal addressin cell adhesion molecule-1 (MAdCAM), the expression of which is limited to mucosal tissues. The interaction between the integrins and VCAM-1 is an essential step in facilitating the migration of white blood cells (WBC) into surrounding tissues where they are able to mediate the effects of inflammation. UCB-A-Met1 and UCB-B-Met2 bind to  $\alpha_4\beta_1$  and

$\alpha_4\beta_7$  integrins that are expressed on the surface of WBC. This binding prevents the interaction of the integrins with VCAM-1 thus reducing the ability of leucocytes to participate in the inflammatory response. Therefore, UCB-A, via integrin inhibition, is believed to be potentially effective at reducing tissue inflammation and symptoms seen in diseases such as asthma, MS, RA or Crohn's disease.

UCB-A comes as a white to slightly yellowish powder with a melting point around 197°C. UCB-B comes as bright orange powder with a melting point around 140°C. Both UCB-A and UCB-B are highly unstable in acidic media (pH < 3.5), with rapid product decomposition into UCB-A-Met1.

UCB-A shows a pH-dependent solubility profile and is reported to be slightly soluble in water around pH 1.0 at 25°C (about 9 mg/ml). Solubility markedly decreases between pH 1.0 and pH 2.0 (about 2 mg/ml, slightly soluble) and decreases further between pH 2.0 and pH 5.0 (0.006 mg/ml; practically insoluble) (**Figure IV 1 8 - Table IV 1 2**). UCB-A has two pKa: pKa1 = 1.8 and pKa2 = 5.5.

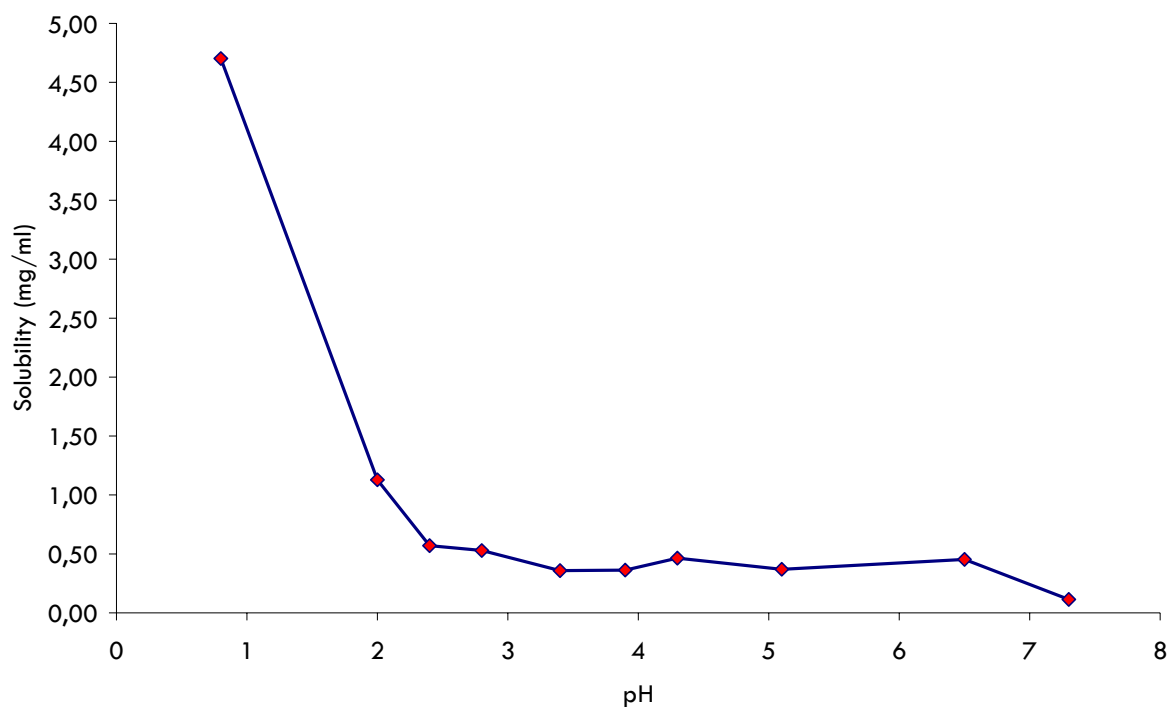


**Figure IV 1 8.** Aqueous solubility of UCB-A (25°C) versus pH.

**Table IV 1 2.** Values for **Figure IV 1 8.**

	pH (un-buffered media)	Solubility (mg/ml) (24h -25°C)
	0.8	9.07
	2.0	2.16
	2.4	0.986
	2.8	0.472
	3.4	0.076
	3.9	0.015
	4.3	0.007
	5.1	0.006
	6.5	0.003
	7.3	0.002

UCB-B also shows a pH-dependent solubility profile and is reported to be slightly soluble in water around pH 1.0 at 25°C (about 5 mg/ml). Solubility markedly decreases between pH 1.0 and pH 2.0 (about 1 mg/ml, slightly soluble) and decreases further between pH 2.0 and pH 5.0 (0.37 mg/ml; very slightly soluble) (**Figure IV 1 9** - **Table IV 1 3**). UCB-B is thus, comparatively to UCB-B, less soluble at highly acidic pH and more soluble at increased pH (e.g. intestinal pH values).

**Figure IV 1 9.** Aqueous solubility of UCB-B (25°C) versus pH.

**Table IV 1 3.** Values for **Figure IV 1 9**.

	pH (un-buffered media)	Solubility (mg/ml) (24h -25°C)
	0.8	4.70
	2.0	1.13
	2.4	0.571
	2.8	0.529
	3.4	0.358
	3.9	0.363
	4.3	0.465
	5.1	0.370
	6.5	0.453
	7.3	0.114

UCB-A was received as crystal form F. This crystal form F is in fact a solvate (DCM/THF). UCB-A shows a particular temperature-dependent behavior in that it shows reversible polymorphic transformations to form G below 16°C and to form H above 37°C. This reversible phenomenon ( $G \leftrightarrow F \leftrightarrow H$ ) is observed as many times as the definite cited temperature is crossed. UCB-A form F, G and H crystal structural data are given in **Table IV 1 4**. More details regarding this phenomenon will be given in **part IV.3.3.3** of this work. This phenomenon is not reported for UCB-B.

**Table IV 1 4.** UCB-A structural data.

Form	Temperature		N	Z	a	b	c	$\beta$
<b>G</b>	0°C	Orthorhombic P2 <sub>1</sub> 2 <sub>1</sub> 2 <sub>1</sub>	1	4	11.1	14.0	17.5	n/a
<b>F</b>	23°C	Monoclinic P2 <sub>1</sub>	4	8	17.5	17.8	17.9	103.4°
<b>H</b>	45°C	Orthorhombic P2 <sub>1</sub> 2 <sub>1</sub> 2 <sub>1</sub>	1	4	11.0	13.9	17.9	n/a

N: number of independent molecules in asymmetric unit; Z: number of molecules in the unit cell; a, b, c: unit cell dimensions (Angstrom).

UCB-A and UCB-B are interesting poorly water-soluble drug models as, comparatively to ucb-35440-3, they also presents a pH-dependent solubility profile and they are also projected highly dosed drugs. Their aqueous solubility is, however, lower for a given pH (particularly acidic pH), than the aqueous solubility of ucb-35440-3.

Due to the reported polymorphic transformations, UCB-A also constitute an interesting model considering high pressure homogenization processing. In fact, these transformations, occurring in HPH processing temperature range, might have implications with regard to particle size reduction efficiency (i.e. crystal hardness).

The UCB-A batch supplied (UCB S.A. - Pharmaceutical R&D - Pharmaceutical & Galenic development, UCB S.A., Braine-L'Alleud, Belgium) for this work was batch N°2002206024. The UCB-B batch supplied (UCB S.A. - Pharmaceutical R&D - Pharmaceutical & Galenic development, UCB S.A., Braine-L'Alleud, Belgium) for this work was batch N°0505001.





## IV.2. Particle size reduction using high pressure homogenization - nanoparticle preparation

### IV.2.1. Introduction

A description of the (piston-gap) high pressure homogenization (HPH) technique with regard to particle size reduction principles (cavitation, high shear forces and interparticular collisions) has been given in **part II.3.4.2.2** of this work.

The aim of this chapter is to go over the various parameters influencing drug particle size reduction using high pressure homogenization. Numerous very interesting review and research articles regarding drug processing through HPH and the various parameters influencing particle size reduction efficiency (number of milling cycles, homogenizing pressure, suspension drug content, etc.) have been published by Professor Rainer H. Müller and co-workers of the Free University of Berlin (Müller et al., 1998, 1999, 2000, 2001; Grau et al., 2000; Jacobs et al., 2000; Krause and Müller, 2001; Keck and Müller, 2006). HPH has been reported for the preparation of nanoparticles for many drugs. Examples are given in **Table IV 2 1**. In this chapter, we will investigate the various parameters influencing particle size reduction for the three drugs studied: Nifedipine, ucb-35440-3, UCB-A and UCB-B.

Drug nanoparticle production using high pressure homogenization involves the processing of the drug in suspension state (e.g. in water or eventually other solvents in which the processed drug is not soluble). The preparation of the initial drug suspension that is to be processed though HPH might in some cases be quite problematic as the studied poorly water-soluble drugs often show poor wettability characteristics (e.g. particularly UCB-A and UCB-B in our case - see **part IV.2.3.5**); the use of surfactant(s) being in general necessary. The surfactants used for the preparation of drug suspension are also necessary for stabilizing the newly formed micro-/nanoparticles and thus for the prevention of agglomeration of these particles following exiting of the homogenization gaps. Judicious stabilizer/surfactant selection and optimization of their concentrations are thus very important factors to take into account. The surfactants used need to be well-tolerated (i.e. with regard to the targeted route of administration - nanosuspensions can be used as parenteral, oral or dermal formulations) and need to have proper physicochemical characteristics with regards to further processing of the nanosuspensions (i.e. surfactants with low melting points such as polysorbates and poloxamers might be problematic for drying (water-removal) processes such as spray-drying). Tested stabilizers/surfactants in this work include polysorbates, poloxamers, sodium

dodecyl sulfate (SDS), hydroxypropylmethylcellulose (HPMC) of low viscosity grades, acaciae gum (AG) and polyvinyl alcohol (PA).

**Table IV 2 1.** Examples of drugs processed successfully (obtainment of drug nanoparticles) through HPH. All PCS diameters given as mean values and all LD diameters given as median values (d(0.5)) (except for hydrocortisone acetate - mean value). Surfactant/stabilizer percentages are expressed w/w relative to drug content.

Drug	Size (µm)	Surfactant system	Reference
Hydrocortisone acetate	~ 0.90 µm (LD)	Poloxamer 188 - 100% Chitosan Chloride - 50%	Moschwitzter and Müller, 2006
Buparvaquone	~ 0.79 µm (LD)	Poloxamer 188 - 20%	Müller and Jacobs, 2002
Budesonide	~ 0.70 µm (LD)	Lecithin - 50% Alkylaryl polyether alcohol - 20%	Jacobs and Müller, 2002
tarazepide	~ 0.60 µm (LD)	Poloxamer 188 - 5% Polysorbate 80 - 2.5%	Jacobs et al., 2000
clofazimine	~ 0.40 µm (PCS)	Poloxamer 188 - 25% Phosphatidylcholine derivatives - 30% Sodium cholic acid - 12.5% Mannitol - 280%	Peters et al. 2000
ibuprofen	~ 0.20 µm (PCS)	Poloxamer 188 - 50% Polysorbate 80 - 50%	Kocbek et al., 2006
Spironolactone	~ 0.54 µm (LD)	Diocylsulfosuccinate - 5%	Langguth et al., 2005
Omeprazole	~ 0.60 µm (PCS)	Poloxamer 188 - 10%	Moschwitzter et al., 2004

Prerequisite particle size reduction steps using high-speed stirrer homogenizers (i.e. Turrax® milling) and pre-milling low pressure homogenizing cycles using the piston-gap high pressure homogenizer will also be described in this chapter. These particle size reduction steps are often a requisite preliminary to the high pressure homogenization cycles when the processed drugs are characterized by large particles (d(v, 0.5) superior to 50-100 µm and d(v, 0.9) up to 250 µm for our processed drugs (for NIF and ucb-35440-3) - UCB-A was received as a micronized powder: d(v, 0.5) 3 µm). Since homogenizing gaps are characterized by an opening as low as 25 µm for homogenizing pressures around 22000 PSI (Müller et al., 2001), these preliminary size reduction steps are necessary to prevent the blocking of these gaps.

The influence of the number of high pressure homogenizing cycles and the influence of the homogenizing pressure (23-24000 PSI → 30000 PSI) will also be assessed in this chapter.

The influence of sample temperature on high pressure homogenization particle size reduction efficiency will also be studied in this chapter, particularly for UCB-A. In fact UCB-A, as described in **part IV.1.3** of this work, presents a particular temperature-dependent behaviour in that reversible polymorphic transformations occur below 16°C (form F ↔ G) and above 37°C (form F ↔ H). It is thus important to control sample temperature during UCB-A processing as these different polymorphic forms might behave differently (polymorphism ↔ crystal hardness) when considering drug particle size reduction.

Investigations into techniques such as freeze-drying and spray-drying for removal of the water from the nanosuspensions were also carried out in this work. Drug nanosuspensions need, in fact, to be “dried” following the high pressure homogenization operation in order to obtain nanoparticles in a “dried powder state”, this for the various in vitro/in vivo assays that need to be conducted for their characterization (DSC, PXRD, dissolution, etc.), and also for storage and stability considerations. Redispersion characteristics of these freeze- and/or spray-dried nanosuspensions were also evaluated. In fact, particle agglomeration during removal of the water from the nanosuspensions could be observed and additives such as water-soluble (e.g. mannitol) or water-insoluble (e.g. Emcompress® -  $\text{CaHPO}_4 \cdot 2\text{H}_2\text{O}$ ) carriers need to be added to the formulation prior to the water-removal operation to prevent this agglomeration. Drug chemical stability following the high pressure homogenization operation and the water removal operation (most importantly spray-drying) were also evaluated and results are presented in this chapter; this evaluation was carried out on ucb-354440-3.

It has to be noted that for comprehension reasons, not all results from all formulations tested will be presented in this chapter. In fact, the influence of various milling operations, be it for pre-milling or milling purposes, the number of homogenization cycles and the influence of homogenizing pressure for example, was generally evaluated on most of the formulations investigated and for each drug. Unless unexpected results for a given drug formulation were observed, in each of the sections of this chapter, the most representative results (generally for optimized formulations) will be presented.

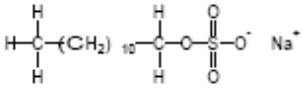
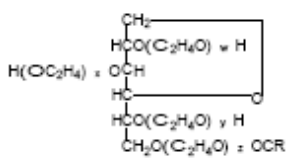
## IV.2.2. Materials and Methods

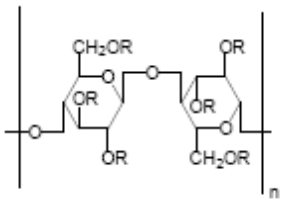
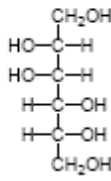
## IV.2.2.1. Materials used for nanosuspension preparation

## IV.2.2.1.1. Stabilizers/Surfactants - carriers

Surfactants and carriers used for nanosuspension preparation are listed in **Table IV 2 2**.

**Table IV 2 2.** List of excipients used for nanoparticle preparation.

	Synonym (obtained from)	Physicochemical characteristics (Handbook of Pharmaceutical Excipients, 2003)
Sodium dodecyl sulfate 	Texapon K12® Henkel (Düsseldorf, Germany)	MW: 288.38 CMC: 8.2 mmol/l (0.23 g/l) at 20°C HLB value: 40 mp: 204-207°C surface tension: 11.8 dynes/cm (0.05% w/v aq. solution 30°C) freely soluble in water (1% w/v aqueous sol pH 7.0-9.5) low solubility in acidic media
Poloxamer 407 $\text{HO}(\text{C}_2\text{H}_4\text{O})_a(\text{C}_3\text{H}_5\text{O})_b(\text{C}_2\text{H}_4\text{O})_a \text{H}$ $a = \pm 101 \quad b = \pm 56$	Lutrol F127® BASF (Ludwigsbafen, Germany)	MW: 9840-14600 mp: 52-57°C surface tension: 26 dynes/cm (0.001% w/v aq. solution 25°C) freely soluble in water (2.5% w/v aqueous sol pH 5.0-7.4)
Polysorbate 20 / 80 $w + x + y + z = 20$ R= lauric acid (20) / oleic acid (80)	Tween 20® / Tween 80® Certa (Braine-l'alleud, Belgium)	MW: 1128 (20) / 1310 (80) HLB value: 16.7 (20) / 15.0 (80) surface tension: 42.5 dynes/cm (0.1% w/v aq. solution 20°C) (80)
		
Polyvinyl alcohol	Aldrich chemical company Inc. (Milwaukee, WIS, USA)	MW: 13000-23000 87-89% hydrolyzed
Acaciae gum	Sigma-Aldrich Inc. (St-Louis, MO, USA)	Solubility: 1 in 2.7 of water, practically insoluble in ethanol

	synonym (obtained from)	Physicochemical characteristics
<b>Hydroxypropylmethylcellulose</b> R: H, CH <sub>3</sub> , [CH <sub>3</sub> CH(OH)CH <sub>2</sub> ] 	Methocel E15 LV Premium EP®  Methocel E5 LV Premium EP®  Colorcon (West Point, PA, USA)	mp: browns at 190-200°C (Tg:170-180°C) soluble in cold water viscosity (20°C- 2%w/v aq. solutions) E15: 12-18 mPa.s E5: 4-6 mPa.s
<b>Mannitol</b> 	Roquette (Roquette Frères, Lestrem, France)	MW: 182.17 mp: 166-168°C solubility in water (20°C): 1 in 5.5
<b>CaHPO<sub>4</sub>·2H<sub>2</sub>O</b> Calcium phosphate, dibasic dihydrate	Emcompress® (Penwest Pharmaceuticals, Patterson, NY, USA)	mp : decomposes below 100°C with loss of water  Practically insoluble in ethanol, ether and water; soluble in dilute acids

#### IV.2.2.1.2. Water

Water used is Milli-Q water. It was obtained from a CFOF 01205 Milli-Q Water purification System (Millipore, USA) with a 18 MΩcm resistivity.

#### IV.2.2.2. Nanoparticle preparation

##### IV.2.2.2.1. Drug suspension preparation

The drug firstly needs to be dispersed in the stabilizer/surfactant containing solution. All described stabilizers can be directly solubilized in water except for HPMC. In this case, water was heated at  $\pm 80^\circ\text{C}$  prior to the dispersion of the polymer. Once the dispersion is complete, the solution is allowed to cool to room temperature under

magnetic stirring. The dispersion of the drug in the surfactant solution is made under mild magnetic stirring (300-500 rpm for 10 to 20 min).

#### **IV.2.2.2.2. High speed stirrer-homogenizer**

The high-speed stirrer-homogenizer used is an ULTRA-TURRAX® T25 Basic (IKA®-Werke GMBH & CO.KG, Staufen, Germany) coupled to a S25N-8G stirring shaft.

- **Technical characteristics:**

- Stirring (homogenizing) speed for the ULTRA-TURRAX® T25 Basic range from 6500 rpm to 24000 rpm
- The S25N-8G stirring shaft (length 8.5 cm; stator diameter 0.8 cm; rotor diameter 0.61 cm) can be used for volumes ranging from 10 to 50 ml.

The stirring/homogenizing operation was used in a first hand to evaluate its potential in regards to drug particle size reduction. This particularly for NIF and ucb-35440-3 (characterized by relatively large particles -  $d(v, 0.9)$  up to 250  $\mu\text{m}$ ); UCB-A coming as a micronized powder of  $d(v, 0.5) \sim 3 \mu\text{m}$ . This operation is also useful for obtaining a complete and homogeneous dispersion of the drug to be processed using high pressure homogenization, be it at low or high homogenizing pressures, if simple magnetic stirring as described in **part IV.2.2.2.1** is not sufficient.

The procedure for this homogenizing operation was set with a homogenizing time of 10 min (for a 50 ml sample) and a stirring rate of 24000 rpm. This operation was run in an ice bath to prevent sample temperature increase. This high speed stirrer – homogenizer was also used during the high pressure homogenization operation as it was placed inside the sample reservoir (stirring rate of 8000 rpm) to ensure suspension homogeneity.

#### IV.2.2.2.3. High Pressure Homogenizer

The high pressure homogenizer used is an EmulsiFlex-C5® (Avestin Inc., Ottawa, Canada) (**Figure IV 2 1**). Technical characteristics (**part IV.2.2.2.3.1**) of the apparatus and adopted homogenizing protocol (**part IV.2.2.2.3.2**) are given in the next sections of this work

##### IV.2.2.2.3.1. Apparatus - Technical characteristics

- The EmulsiFlex-C5® possesses a 200 ml sample reservoir but samples as small as 10 ml can be processed. Flow rate ranges from 1 up to a maximum of 5 liters/hour (dependent of the inlet pressure, the homogenizing pressure applied and the viscosity of the sample). This flow rate must be checked for each batch produced and ranges between 50-60 ml/min at 7000 PSI and 12000 PSI and around 15 ml/min at 23-24000 PSI (data for an inlet pressure of 100 PSI)
- The EmulsiFlex-C5® possesses an air/gas (N<sub>2</sub>) driven high pressure pump. The required inlet pressure is 240 times less ( $\pm 10\%$ ) than the desired hydraulic pressure on the sample. Adjustment of the homogenizing pressure is operated manually by closing or opening the homogenizing valve by simply turning, respectively, clockwise or counter-clockwise the control knob. Homogenizing pressures range from 500 up to a maximum of 30000 PSI.
- In addition to the fact that the instrument can be immersed in a temperature-controlled water bath for cooling or heating purposes, inlet and outlet temperatures can also be controlled with installation of a heat exchanger after the homogenizing valves (homogenizing procedure causing an increase in sample temperature – increase of 20-30°C from initial temperature after 20 cycles at 23000 PSI).
- Majority of the EmulsiFlex-C5® parts are made of stainless steel, with no "O"-rings or gaskets in the entire path of the product. The only plastic seal is the plunger seal which is UHMWPE (Ultra High Molecular Weight Polyethylene). This makes the apparatus resistant to most solvents and inert relative to the samples passed.

All wetted parts are autoclavable. The inlet valve of the pump can be connected easily to steam at 120-130°C for SIP sterilization.



**Figure IV 2 1.** EmulsiFlex-C5 High Pressure Homogenizer

(1) Hose to connect to air/gas supply; (2) Safety valve; (3) air/gas regulator with air/gas inlet pressure gauge; (4) Sample cylinder body; (5) Inlet check valve; (6) Outlet check valve; (7) Pump motor; (8) Control valve and air/gas hose for pump motor; (9) Homogenizing pressure gauge; (10) Sample exit; (11) Homogenizing valve; (12) Heat exchanger (optional); (13) Homogenizing pressure control knob.

It has to be noted that compressed air (pressure 7-8 bar) was used for operating the EmulsiFlex C5® at pressures up to 23-24000 PSI; compressed N<sub>2</sub> (inlet pressure of ~10 bar) being necessary for processing up to 30000 PSI.



#### IV.2.2.2.3.2. Homogenizing protocol

The adopted protocol used for drug particle size reduction using the EmulsiFlex-C5<sup>®</sup> high pressure homogenizer is as follows:

- Pre-milling low pressure homogenizing cycles (PMC)

- 15 cycles (C) at 7000 PSI

- 10 cycles at 12000 PSI

- High pressure homogenizing cycles

- 0 to 20 cycles at 23-24000 PSI

- 0 to 10 cycles at 30000 PSI

These pre-milling low pressure homogenizing cycles and high pressure homogenizing cycles were conducted by re-circulating the processed suspension directly into the sample reservoir (“closed loop”). During all the cycles, agitation (ULTRA-TURRAX<sup>®</sup> T25 Basic - 8000 rpm (or equivalent)) was maintained in the sample reservoir to avoid sedimentation of the particles in suspension. Suspension flow rates were measured for each pressure used in order to calculate the equivalent number of cycles. About 0.5 ml samples were withdrawn following the two sets of pre-milling cycles and following different pre-determined number of high pressure cycles for size distribution analysis.

Product processing temperature was shown to have an influence on final drug particle size distribution and was finally set at 10°C. This observation was made when working with NIF and the NIF processing temperature of 10°C was kept for ucb-35440-3, UCB-B and UCB-A. For the latest, the processing temperature was also tested at

25°C and 45°C. These processing temperatures can easily be maintained using the EmulsiFlex-C5® heat exchanger and using an appropriate inlet temperature (cryostat). This is clearly represented in **Figure IV 2 2** (temperature recorded in the sample reservoir).

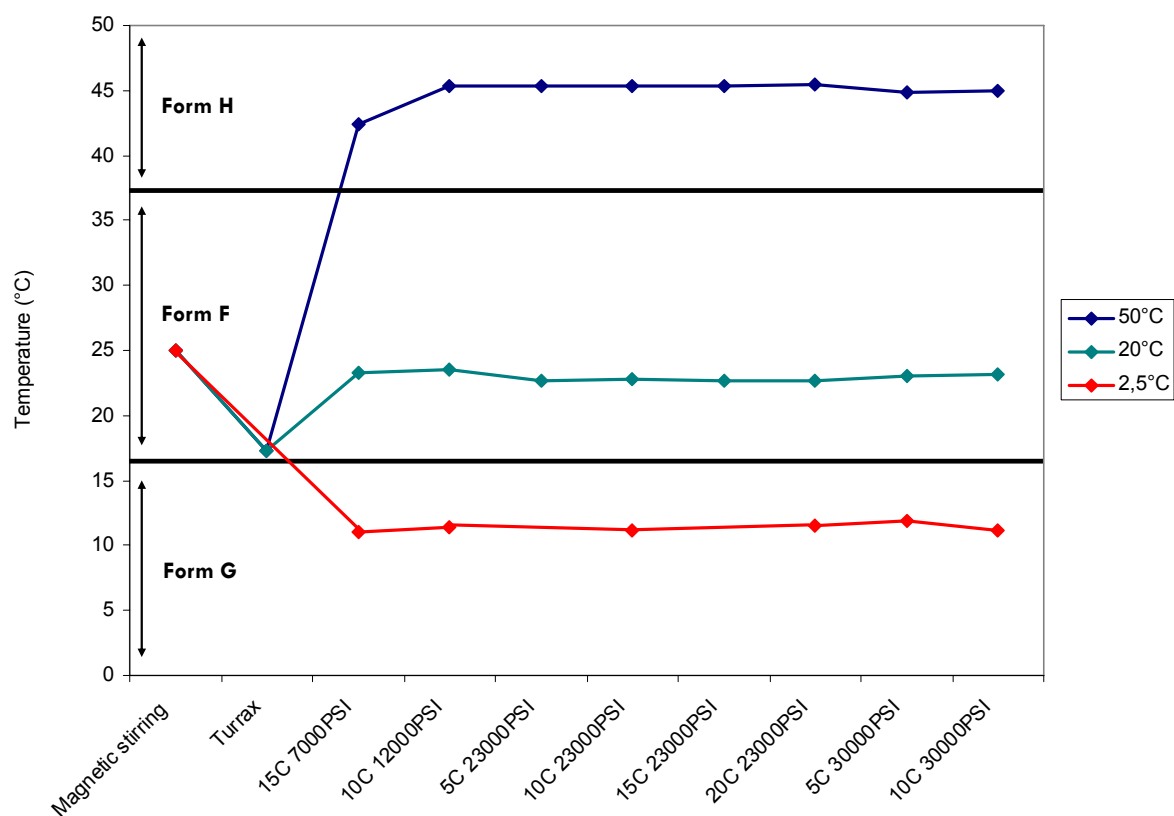


**Figure IV 2 2.** Sample temperature (°C) evolution following the different milling operations used for UCB-A particle size reduction (for a cryostat inlet temperature of 2.5°C (polymorphic form G), 20°C (polymorphic form F) and 50°C (polymorphic form H) - Heat exchanger)

#### **IV.2.2.3. Water-removal from the nanosuspensions**

In order to retrieve nanoparticles in dried-powder state from the nanosuspensions, water removal can be conducted through freeze-drying or spray-drying. Freeze-drying was used first as it is less material consuming (higher recovery) than spray-drying and because the first evaluations were carried out on ucb-35440-3 (available in small quantity). Spray-drying is however less time consuming and was the only technique used for NIF, UCB-A and UCB-B.

##### **IV.2.2.3.1. Freeze-drying**

The homogenized suspensions were frozen at -80°C overnight and freeze-dried using a Lyovac GT-2 apparatus (Leybold-Heraeus, Köln, Germany) under vacuum (pressure < 0.01 mbar) for 15 hours in open Petri dishes.

##### **IV.2.2.3.1. Spray-drying**

The homogenized suspensions were spray-dried using a Büchi B191a Mini Spray-Dryer (Büchi, Flawil, Switzerland). The spraying rate was set at 3.5 ml/min. The drying temperature was set at 115°C. The outlet temperature was measured at around 45°C. Spray airflow was set at 800 l/h and drying airflow was set at 35m<sup>3</sup>/h.

#### **IV.2.2.4. Nanoparticle size/morphology characterization**

##### **IV.2.2.4.1. Laser diffraction**

Laser diffraction (LD) methods are nowadays extensively used for particle sizing in different applications (pharmaceuticals, chemicals, cosmetics, biotechnology, food industry, etc.). Laser diffraction measurements are fast

and easy to accomplish but the proper use of the instrument and the interpretation of the results obtained require a deep understanding of the method.

The laser diffraction measurements are based on the phenomenon that particles scatter light in all directions with an intensity pattern dependent on particle size: the smaller the particle size, the higher the scattering angle ( $\theta$ ) and the smaller the scattering intensity (**Figure IV 2 3** and **Figure IV 2 4**). According to ISO 13320-1 (ISO, 1999), the principle behind the laser diffraction measurements is that a representative sample, dispersed at an adequate concentration in a suitable liquid or gas, is passed through the beam of a monochromatic light source followed by the subsequent recording of the light scattered by the particles at various angles by a multi-element detector. These numerical scattering values are then transformed, using an appropriate optical model, to yield the proportion of total volume to a discrete number of size classes forming a volumetric particle size distribution.

Since most materials exhibit strong absorption in the ultraviolet and infrared regions, which would strongly reduce the scattering intensity, most light scattering measurements use visible light ranging from 350 to 800 nm. The Mastersizer 2000 (Malvern Instruments Ltd., Worcestershire, United Kingdom) used in this work for particle size analysis uses a 2 mW 632.8 nm Helium Neon laser along with a shorter wavelength 466 nm blue light source for improved fine-particle resolution.

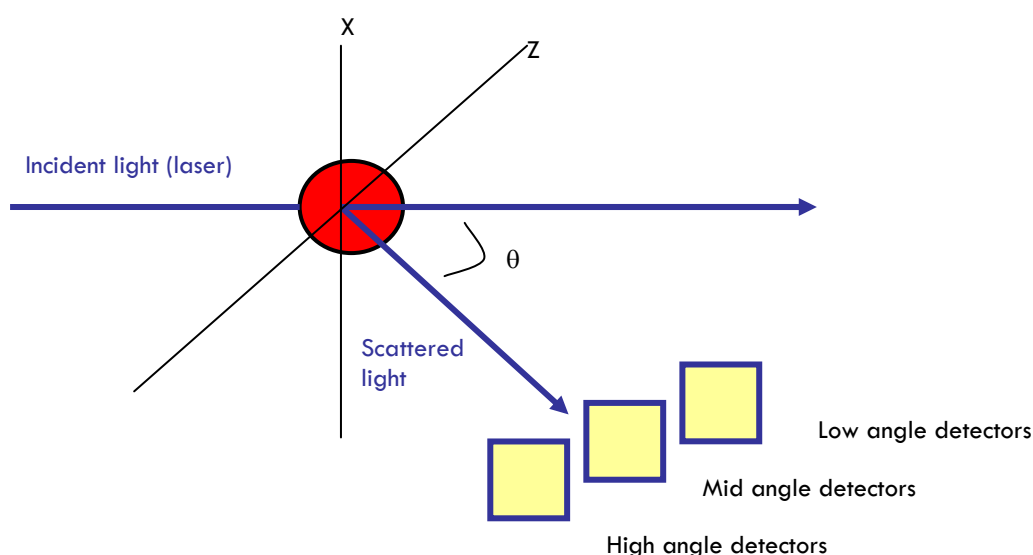


**Figure IV 2 3.** Schematic representation of laser diffraction measurement

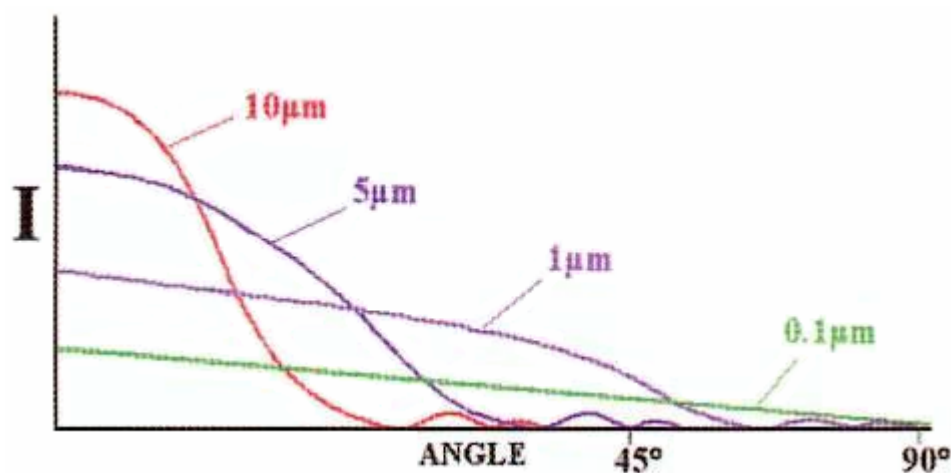


**Figure IV 2 4.** Schematic representation of scattering intensity vs. scattering angle for different sized particles: Large particles scatter light strongly at low angles and with readily detectable maxima and minima in the scattering pattern (detectors placed at low angles relative to the optical path will detect these large particles) (Beckman Coulter LS 13320 Data Sheet)

Mean particle size and particle size distribution are thus obtained through a matrix conversion of the scattered intensity measurements as a function of the scattering angle and the wavelength of light on applicable scattering theory (Mie theory for the Mastersizer 2000).

In this rather complex theory (Mie), the scattered light intensity of a particle is function of different variables:

- Particle size
- Particle refractive index (RI)
- Medium refractive index
- Light wavelength
- Scattering angle

The absorption index (AI) of the dispersed particles and the dispersing medium shall also be known or evaluated. A refractive index of 1.54 and an absorption index of 0 were used for measurements of NIF particles (data obtained from Bayer Health Care - Kuhnert-Brandstätter et al, 1980). For ucb-35440-3 and for both UCB-A and UCB-B, refractive and absorption indexes were evaluated as RI 1.61/AI 0.001 and RI 1.59/AI 0.001, respectively.

These refractive and absorption indexes have been approximated through data manipulation of different sized populations. This manipulation consisted of screening RI and AI values to find the combination yielding the best residual values (indication of the coherence between the theoretical and measured data) and fit data; this combination being kept for all measurements. These values, as indicated, represent approximate values that are most representative of the model used and might effectively differ from the real values (which are unknown). An example of the curves obtained (in our example for UCB-A) is illustrated in **Figure IV 2 5**.

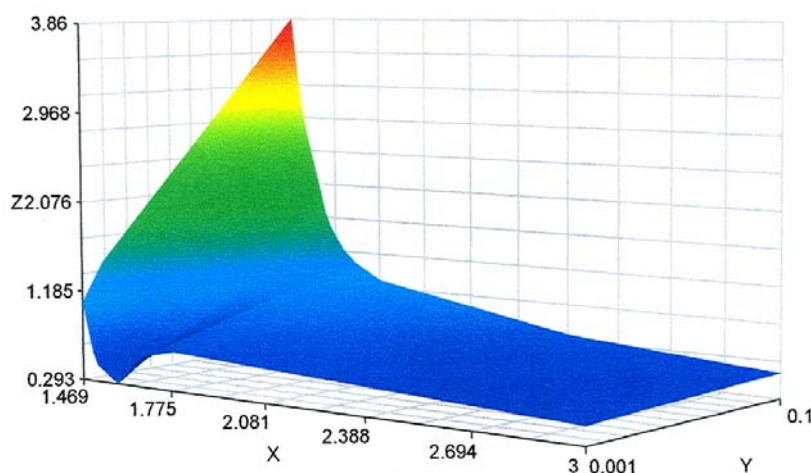


**Figure IV 2 5.** Refractive index/Absorption index evaluation for UCB-A laser diffraction analysis – Weighted residual (Z), refractive index (X), absorption index (Y).

Laser diffraction analysis yield a size distribution expressed in volume. Calculations are based on the theory of “equivalent spherical diameter” in order to determine particle sizes; that is to consider the diameter of a theoretical sphere that would produce the same signal as the studied particle. In fact, there are very few materials that present totally spherical particles and, although a sphere can be characterized by one unique number, which is its diameter, these types of irregular particles cannot be characterized without taking into account their three-dimensional aspect. Using this theory, numerous “equivalent diameters”, including other parameters such as surface, volume or weight, can be calculated. The main reported equivalent diameter is the  $D[4,3]$  which is the mean volume diameter. This diameter is calculated using the following formula (d being the measured theoretical diameter):

$$D[4,3] = \frac{\sum d^4}{\sum d^3}$$

Through the laser diffraction results obtained, other size characteristics can and will also be retrieved such as:

- **d (v, 0.5) or d(0.5):** size ( $\mu\text{m}$ ) of particle below which 50% of the sample lies (volume median diameter).
- **d (v, 0.1) or d(0.1):** size ( $\mu\text{m}$ ) of particle below which 10% of the sample lies.
- **d (v, 0.9) or d(0.9):** size ( $\mu\text{m}$ ) of particle below which 90% of the sample lies.
- **Span:** measurement of the width of the distribution.

$$\text{Span} = (d(0.9) - d(0.1)) / d(0.5)$$

The laser diffraction apparatus used for particle sizing was a Mastersizer 2000 (Malvern Instruments Ltd., Worcestershire, United Kingdom) equipped with dry and wet sampling systems (Scirocco 2000 and Hydro 2000 S, respectively), the latter being used for suspension measurements. The performances of the optical and the sample handling units were qualified by performing operational qualification procedures, as proposed by Malvern Instruments, using standard material (Duke Scientific 0.3  $\mu\text{m}$  and 1.0  $\mu\text{m}$  polystyrene DVB microsphere suspensions). Detection limits for the equipment range from 0.02  $\mu\text{m}$  to 2000  $\mu\text{m}$ .

- **Procedure for sample measurement:**
  - 10 cleaning cycles using deionized water.
  - Background measurement with the dispersant used (1 cleaning cycle with dispersant before measurement).
  - Measurements shall be made in a drug-saturated aqueous solution (in order to prevent variation in laser obscuration values due to dissolution of the particles - and thus variation in particle size).
  - Stirring of the sample being measured set at 2500 rpm.
  - No sonication during measurement.
  - Minimum of 2 sets of 5 measurements shall be made for each sample at laser obscuration values ranging from 4 to 6% (+ average measurements).
  - 1 cleaning cycle using alcohol (97%) and 5 cleaning cycles using deionized water.

Laser diffraction measurements were made after each particle size reduction step.

It has to be noted that Photon Correlation Spectroscopy (PCS), although more frequently used for submicron sized particles (detection limits 0.002-3  $\mu\text{m}$ ), was not used for particle size characterization in this work. In fact, due to the type of particle size distribution obtained for the three studied drugs (see **part IV.2.3**), size distribution evaluation shall better be reflected through LD measurements. Furthermore, due to the presence of residual microparticles or nanoparticle agglomerates in the final nanosuspensions, PCS results would be strongly affected (max limit 3  $\mu\text{m}$ ). LD was also chosen to allow comparison of equivalent diameters when considering un-milled drugs and results from pre-milling operations (not measurable by PCS in case of micron-sized drug populations) and drug nanoparticles. Furthermore, the Mastersizer 2000 equipment, characterized by a particle size detection limit down to 0.02  $\mu\text{m}$  (i.e. blue light source), allows for correct size determination of particles around 0.1 to 0.5  $\mu\text{m}$  (e.g. excellent reproducibility of the results observed for the standards (i.e. 0.3  $\mu\text{m}$ ) and our samples).

Redispersion analyses were conducted by adding the freeze- or spray-dried nanosuspensions (equivalent of 5 mg/ml) in surfactant-free deionized water. The suspension formed was placed under magnetic stirring for 10 min at 300 rpm (Variomag Multipoint HP15 magnetic stirrer-shaker 100-1000 rpm, Labortechnik GmbH, Munich, Germany). Particle size measurement was carried out using the protocol described above.

#### IV.2.2.4.2. Scanning Electron Microscopy (SEM) - SEM-EDS

Scanning electron microscopy (SEM) is a technique that uses electrons instead of light for image viewing. The electron beam is produced by heating (voltage induced) of a metallic filament that functions as the cathode, generally a loop of Tungsten (Tungsten hairpin gun). An anode placed right below the cathode forms powerful attractive forces for the electrons causing them to accelerate down the microscope column towards the sample to be analyzed. Before reaching the sample, the electron beam is condensed (condenser lens = electromagnetic lens) and focused (objective lens) as a very fine point on the material to be analyzed. Once the electron beam hits the sample, there is production of secondary electrons (or back-scattered electrons) which are collected (secondary detector or back-scattered detector), converted to voltage and amplified. The image viewed consists of thousands



of spots of varying intensity, dependent of the topography of the sample. The SEM column must always be in vacuum in order to prevent electron beam instability.

Since the SEM uses electrons to produce an image, it requires samples be electrically conductive (with the exception of ESEM - Environmental SEM - that can be used to view non-conductive or even wet samples). In order to view non conductive samples (case of most organic drugs), these must be covered with a thin layer of conductive material (gold, platinum, etc.) using a sputter coater.

The scanning electron microscope used was a JSM-6100 Scanning Electron Microscope (EDAX CDU "LEAP" detector, JEOL, Japan) and the sputter coater used was a SCD030 (Blazers Union, Liechtenstein), with the conductive metal used to cover the drug particles being Platinum (3 min deposition under vacuum). The material to be analyzed was previously taped onto a support and, after deposition of the Platinum, was placed in the microscope at a distance of 31 mm under the head of the electron beam before the vacuum was installed.

In addition to image viewing, analysis of the chemical composition of the particles observed can be achieved using the "mapping" technique (SEM-EDS: Scanning Electron Microscopy – Energy Dispersive Spectroscopy X-Ray phase analysis). This technique combines SEM with X-ray imaging (distribution of chemical elements as halogens (Cl, F, etc.), S, etc.). The mapping technique can give, if the proper elements are found in the molecule, deeper informative results relative to drug distribution in the system studied. In our case, this type of analysis shall yield information about drug localization in the drug/surfactant mix observed by SEM. Mapping studies were carried out using a combined mapping X-ray microscopy technique (JSM-6100 Scanning Electron Microscope, EDAX CDU 'LEAP' Detector, JEOL, Japan). This mapping analysis was used for a ucb-35440-3/Emcompress® formulation (chloride of ucb-35440-3 and calcium for Emcompress®).

#### **IV.2.2.5. Chemical stability - HPLC method UCB M1**

Chemical stability following the high pressure homogenization operation and the water-removal operations (particularly spray-drying) is an important parameter to assess. ucb-35440-3 was the model drug used to assess this characteristics as it is reported to be relatively labile, mainly temperature-wise. A specific validated

chromatographic purity HPLC method (UCB M1) for ucb-35440-3 is described below (UCB ref TDAAM0313/01-E).

ucb-35440-3 quantification was achieved using an Agilent series 1100 HPLC system (Palo Alto, CA, USA) comprising a solvent delivery pump, an autosampler, an UV-VIS variable wavelength detector and a data module integrator. Chromatographic separation was accomplished using a Chromspher C18 RP, 5  $\mu$ m, 250 mm X 4.6 mm stainless steel column (Varian Inc., Palo Alto, CA, USA). The mobile phase consisted of acetonitrile: sulfuric acid 0.12N (97:3 v/v). The mixture was filtered through 0.22  $\mu$ m Durapore® membrane filters (Millipore Corporation, Bedford, MA, USA) (or equivalent) under vacuum and degassed through sonication for 5 min. The mobile phase was pumped isocratically at a flow rate of 1.0 ml/min during analysis, at ambient temperature. The volume of injection was set at 20  $\mu$ l. The effluent was monitored at 230 nm. Retention time for ucb-35440-3 is 8 min.

As described by this chromatographic purity HPLC method, results shall be calculated as area percent, taking the total area of peaks as 100%. Impurities above 0.1% have to be reported.

### IV.2.3. Results and discussion

#### IV.2.3.1. Surfactant screening - influence of the type of surfactant

As described in the introductive part of this chapter (**part IV.2.1**), drug nanoparticle production using high pressure homogenization involves the processing of the drug in suspension state (e.g. in water or eventually other solvents in which the processed drug is not soluble). The preparation of the initial drug suspension that is to be processed through HPH might in some cases be quite problematic as the studied poorly water-soluble drugs often show poor wettability characteristics (e.g. particularly UCB-A in our case - see **part IV.2.3.5**); the use of surfactant(s) being in general necessary. The surfactants used for the drug suspension preparation are also necessary for the stabilization of the newly formed micro-/nanoparticles and thus for preventing agglomeration of these particles following exiting of the homogenization gaps.

Judicious stabilizer/surfactant selection and optimization of their concentrations are thus very important factors to take into account. The surfactants used need to be well tolerated and to have appropriate physicochemical characteristics with regard to further processing of the nanosuspensions (i.e. surfactants with low melting points such as polysorbates and poloxamers (**Table IV 2 2**) might be problematic for processes such as spray-drying).

For comprehension reasons, LD results (size distribution analysis) will already be shown in this chapter in order to complement and illustrate our choice of given surfactants. All LD results are representative of suspensions passed using pre-milling low pressure homogenizing cycles (15C 7000 PSI + 10C 12000 PSI) and 10 (ucb-35440-3) or 20 cycles at 23-24000 PSI (NIF, UCB-A and UCB-B).

This work was started using NIF as a model drug. NIF did not, as it is the case for UCB-A and UCB-B, show particular wettability problems when placed in various surfactants-containing solutions, even at very low concentrations. Various surfactants such as poloxamers (poloxamer 407), polysorbate 80, SDS, and cellulose derivatives such as Hydroxypropylmethylcellulose (HPMC) were tested and all yielded interesting results regarding NIF suspension stabilization. Some of these results are shown in **Figure IV 2 6**.

HPMC of low viscosity grade was rapidly chosen as the stabilizer of choice for NIF nanoparticulate system stabilization as, when compared to the other cited surfactants, it yielded very interesting results size-wise.

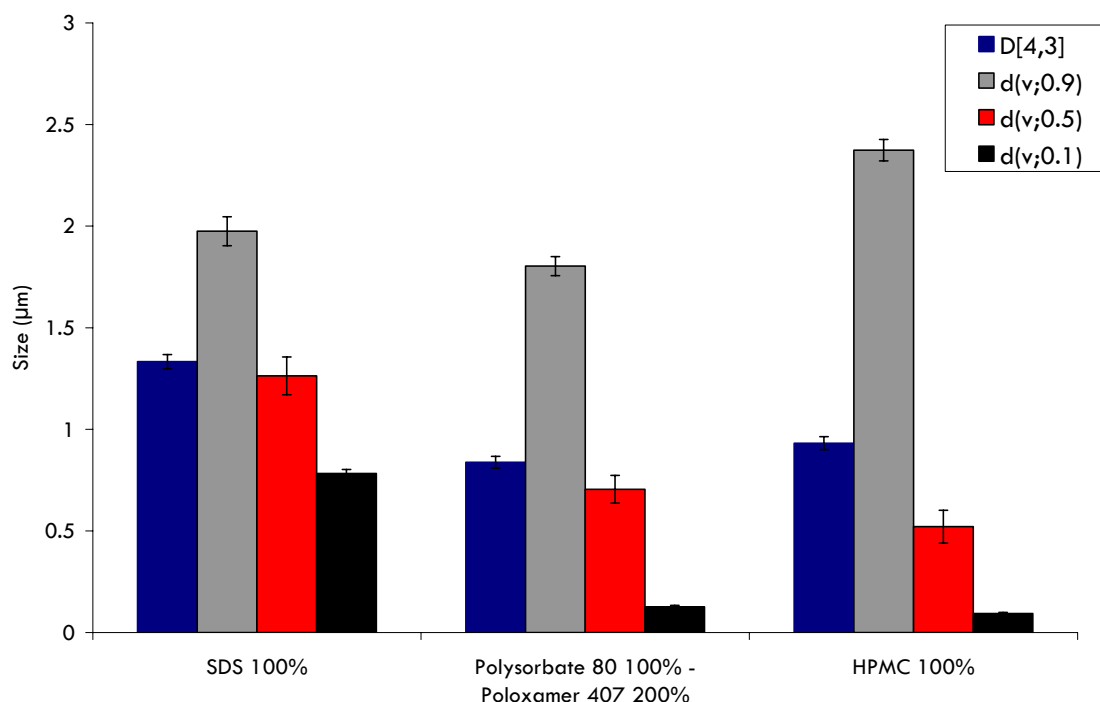


**Figure IV 2 6.** Influence of type of surfactant on NIF particle size reduction efficiency (% expressed relative to NIF content, w/w) (NIF % in suspension: 0.5-1% w/v) (PMC + 20C 23-24000 PSI). Data reported in annex 1 (**Table A1**).

Furthermore, HPMC also has the advantage of having a high melting point when compared to stabilizers such as polysorbates and poloxamers. Additives characterized by a low melting point might in fact be found problematic when considering further nanosuspension processing, as in the case of suspension water-removal operations such as spray-drying. In this case, softening or even fusion of these excipients (spray-drying temperature set at 115°C - melting point of poloxamer 407 being 52-57°C and polysorbate 80 being liquid at ambient temperature), particularly if their concentrations are found to be quite high, might lead to particle agglomeration, particularly if no carriers are used. It has to be noted that the spray-drying of polysorbate-containing suspensions led to powders that could not even be retrieved from the collecting device of the spray-drier because the powder stuck to the glass of the device.

The next step consisted in the evaluation of the optimal HPMC concentration regarding NIF nanoparticle stabilization. This evaluation was carried out by investigating NIF particle size distribution characteristics when increasing HPMC concentration (w/w relative to NIF). Results are shown in **Figure IV 2 7**. An HPMC concentration of 10% (w/w) relative to NIF content was found to be optimal, over a range of 2–200%, with regard to particle size reduction and to suspension processing (i.e. increase in sample viscosity with increasing HPMC %).

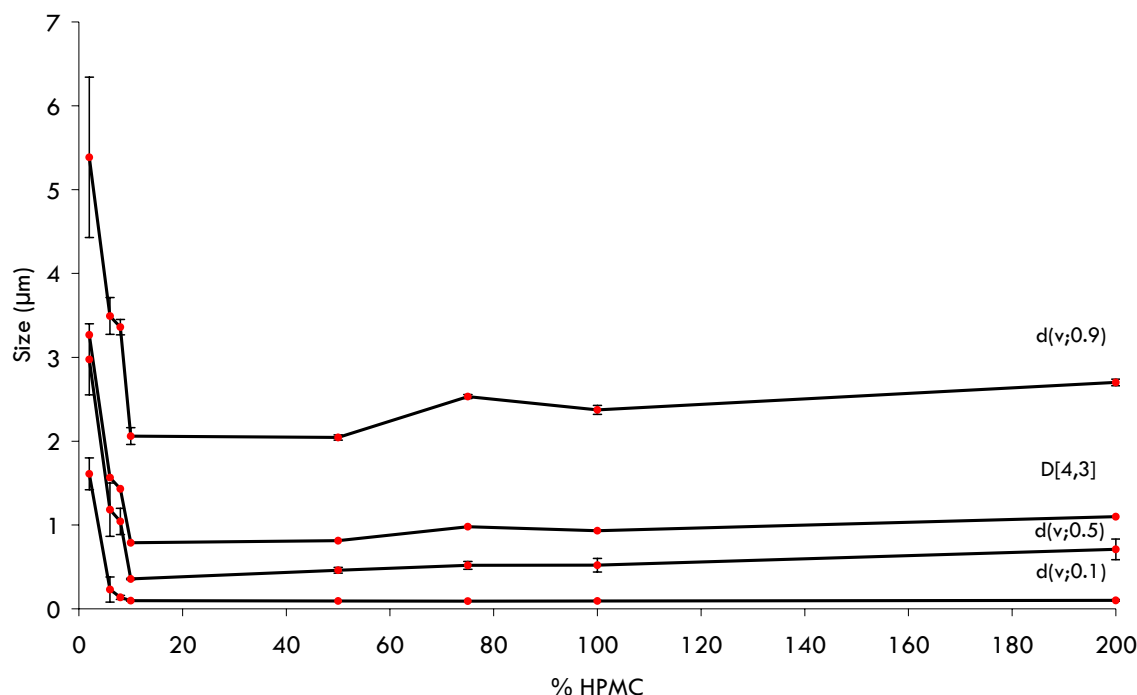


**Figure IV 2 7.** Influence of HPMC concentration on NIF particle size reduction efficiency (% expressed relative to NIF content, w/w) (NIF % in suspension: 5% w/v for HPMC % of 2 to 10% and 1% w/v for HPMC % of 50 to 200%) (PMC + 20C 23-24000 PSI). Data reported in annex 1 (**Table A2**).

Given the interesting results obtained with HPMC of low viscosity grade (Methocel E15<sup>®</sup>) for NIF, this stabilizer was first used in a particle size reduction feasibility study for ucb-35440-3. Due to the fact that this model drug is a projected highly dosed drug, aim in minimization of additives (stabilizers, carriers, etc.) used in formulation development was necessary. An HPMC concentration as low as 2% (w/w relative to ucb-35440-3) was shown sufficient for suspension preparation and stabilization as it can be seen from the results presented in **Figure IV 2 8**; this concentration showed a particle size distribution characterized by  $d(v,0.5)$  around 180 nm. No attempt was made to further minimize this concentration as poor wetting characteristics and subsequent problems in suspension preparation were observed below this concentration. No attempt was made to increase this concentration either, as in the case of NIF, due to the fact that the size results were even more promising than for NIF ( $d(v,0.5)$  of 180 nm versus 350 nm) and that, as previously said, attempt was made towards minimization of the concentration of the additives used.

Despite the interesting results obtained with HPMC, surfactant screening was also carried out for ucb-35440-3. Other surfactants tested were HPMC (Methocel E5<sup>®</sup>), SDS, polyvinyl alcohol (PVA), poloxamer 407 and acaciae gum. The stabilizer concentration was always kept at 2% w/w relative to ucb-35440-3. Results are represented in **Figure IV 2 8**.

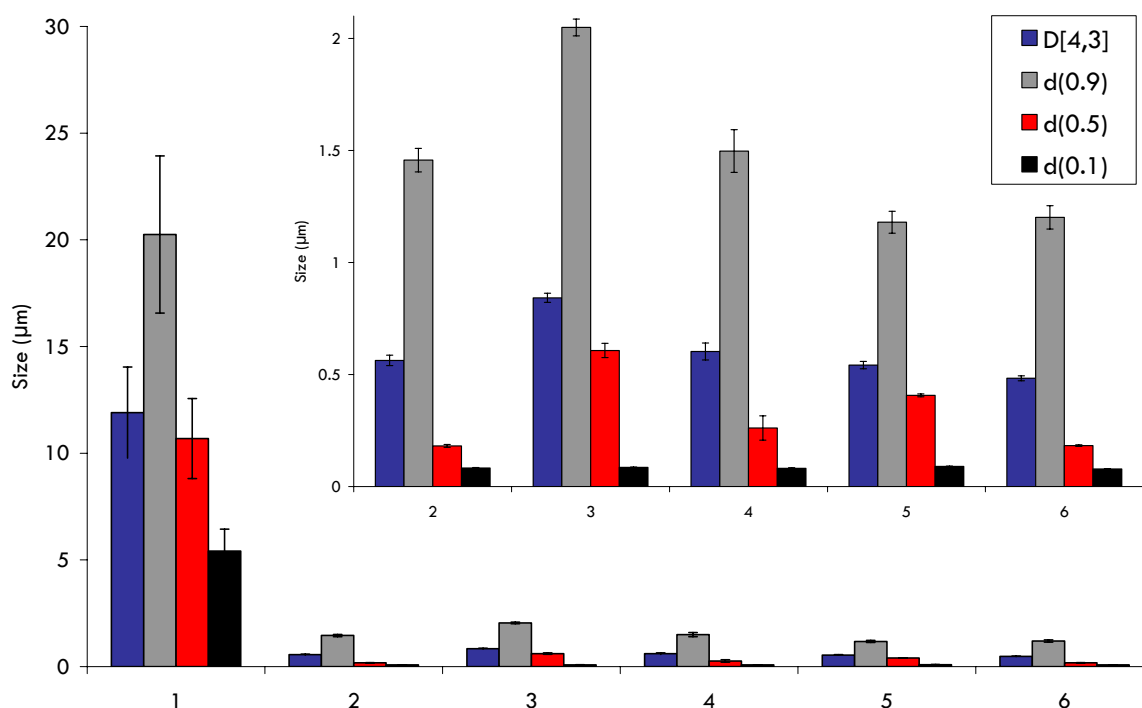


**Figure IV 2 8.** Influence of type of surfactant on ucb-35440-3 particle size reduction efficiency (2 % w/w relative to ucb-35440-3 content - 5% w/v ucb-35330-3 suspensions) (PMC + 10C 23-24000 PSI). (1) SDS, (2) HPMC (Methocel E15<sup>®</sup>), (3) HPMC (Methocel E5<sup>®</sup>), (4) PVA, (5) Acaciae gum and (6) Poloxamer 407. Data reported in annex 1 (**Table A3**).

We can clearly see that, except for SDS, all surfactants assayed yielded a particle size distribution in the nanometer range; the most interesting results coming with HPMC (Methocel E15<sup>®</sup>) and poloxamer 407.

As for UCB-A, adequate surfactant selection was shown to be a critical parameter in the fact that the drug presents very poor wettability characteristics, thus rendering suspension preparation impossible in surfactant-free media (powder floats on top of the liquid totally un-wetted if no surfactants are used - see **part IV.2.3.5**). Examples of tested surfactants for the preparation of UCB-A primary suspensions with mention of their concentration tested are listed in **Table IV 2 3**. UCB-B also presents poor wettability characteristics.

Contrarily to NIF and ucb-35440-3 where HPMC of low viscosity grade could easily be used alone and, furthermore, at relatively low concentrations, only SDS and poloxamer 407 were shown to be useful in the preparation of UCB-A suspensions.

**Table IV 2 3.** Surfactants tested for UCB-A suspension preparation (2% w/v UCB-A suspension): Estimation of UCB-A wettability (+: poor wettability → +++++: good wettability; -: not tested) (% expressed as w/v).

	2%	1%	0.5%	0.2%	0.1%	0.05%
<b>SDS</b>	+++++	+++++	++++	+++	++	-
<b>Poloxamer 407</b>	++++	+++	+++	+++	+++	-
<b>Poyorbate 20</b>	++++	++++	++++	++++	+++	++
<b>Polyvinyl alcohol</b>	++	-	-	-	-	-
<b>HPMC (Methocel E15)</b>	+	-	-	-	-	-

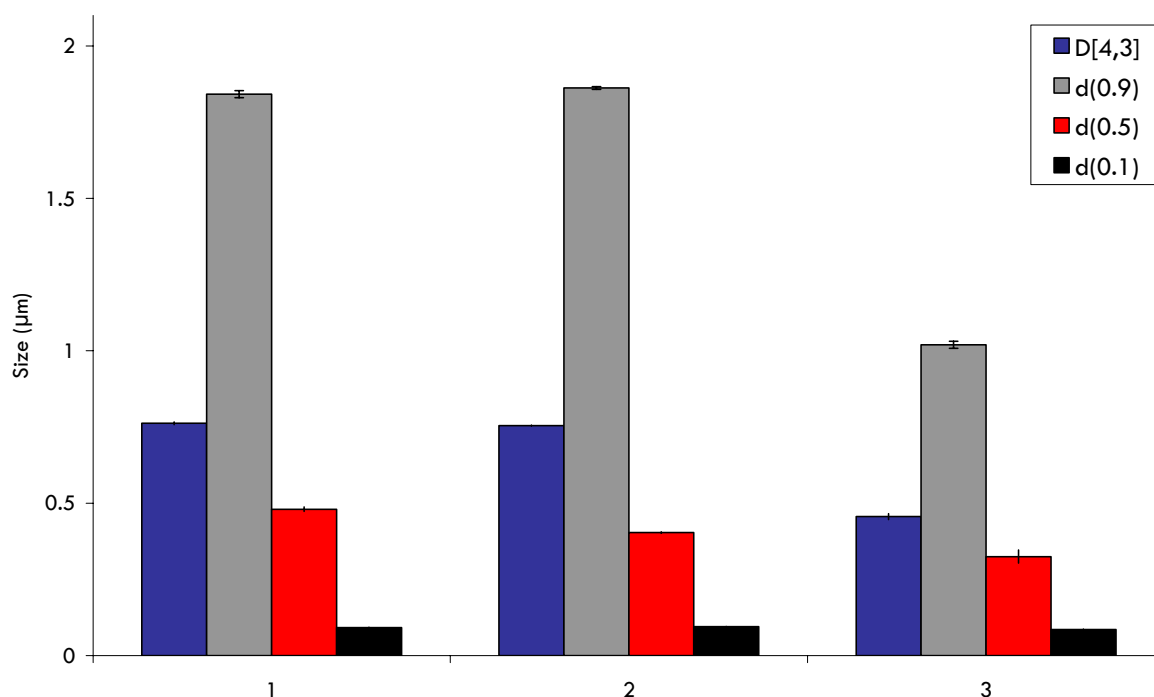


**Figure IV 2 9.** Influence of type of surfactant on UCB-A particle size reduction efficiency: (1) UCB-A 5%, Methocel E15® 0.5%, SDS 0.1%, w/v; (2) UCB-A 5%, Methocel E15® 0.5%, Poloxamer 407 0.25% w/v; and (3) UCB-B 5%, Methocel E15® 0.5%, Poloxamer 407 0.25%, w/v. Data reported in annex 1 (**Table A4**).

HPMC could only be used (and was used) in the development of UCB-A formulations in combination with either SDS or poloxamer 407, with both combinations yielding equivalent results size-wise (**Figure IV 2 9**). LD size distribution results for an equivalent UCB-B formulation are also represented in this figure.

### IV.2.3.2. Influence of pre-milling operations

Pre-milling operations such as high speed-stirrer homogenizer (i.e. Turrax® milling) homogenization and pre-milling low pressure homogenizing cycles using the EmulsiFlex C5® were shown to be necessary steps prior to homogenization at high pressures such as 23000 PSI to 30000 PSI. In fact, as the homogenizing gaps (inside the homogenizing valve - see **Figure II 19**) are characterized by an opening as low as 25 µm for homogenizing pressures around 22000 PSI (**Müller et al., 2001**), these preliminary size reduction steps are necessary to prevent the blocking of these gaps.

Un-milled purchased (NIF) or received (ucb-35440-3) model drugs were effectively characterized by relatively large particles. UCB-A and UCB-B were received as micronized powders. LD size distribution results for of all four model drugs as received are shown in **Figure IV 2 10** and **Table IV 2 4**. Particle size distributions of un-milled ucb-35440-3 was found to be highly variable from one sampling to another with  $d(v,0.5)$  ranging from 60 to 150 µm; the size distribution curve represented in **Figure IV 2 10** being, however, well-representative of the un-milled drug.

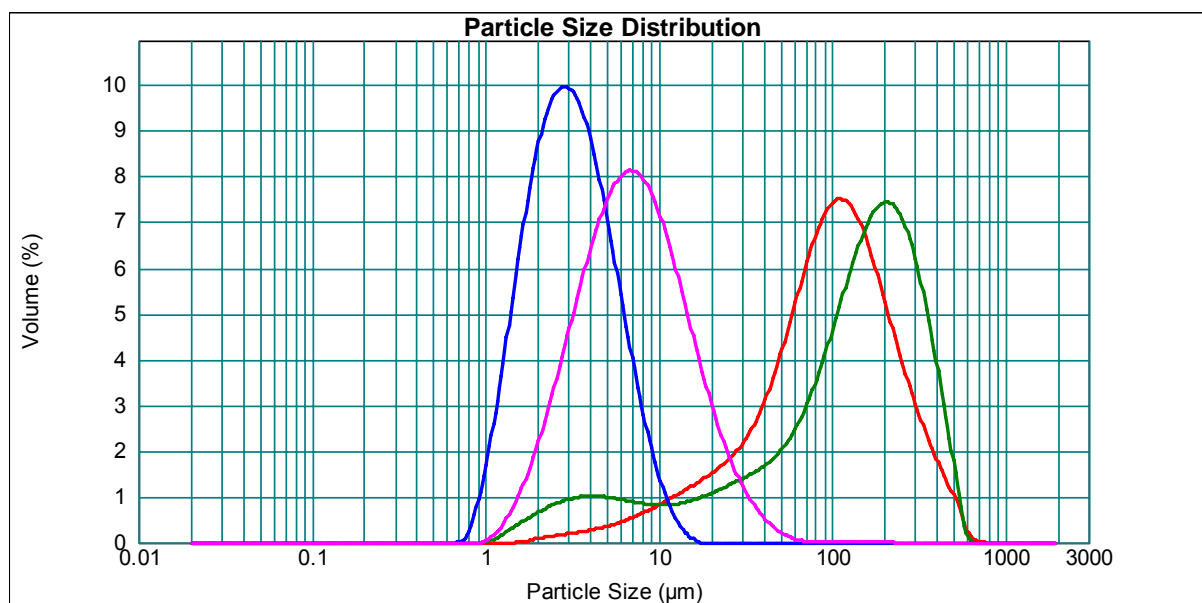


**Figure IV 2 10.** LD size distribution analysis for model drugs as received (prior to milling operations): NIF 5% , Methocel E15® 0.5%, w/v (**red**); ucb-35440-3 5%, Methocel E15® 0.1%, w/v (**green**); UCB-A 5%, Methocel E15® 0.5%, Poloxamer 407 0.25%, w/v (**blue**) and UCB-B 5%, Methocel E15® 0.5%, Poloxamer 407, 0.25%, w/v (**pink**).



**Table IV 2 4.** Data for Figure IV 2 10 (size in  $\mu\text{m}$ ).

	<b>d (0.1) <math>\pm</math> SD</b>	<b>d (0.5) <math>\pm</math> SD</b>	<b>d (0.9) <math>\pm</math> SD</b>	<b>D[4,3] <math>\pm</math> SD</b>	<b>span <math>\pm</math> SD</b>
<b>NIF</b>	<b>21.9 <math>\pm</math> 0.2</b>	<b>98.7 <math>\pm</math> 0.4</b>	<b>267.2 <math>\pm</math> 0.5</b>	<b>126.2 <math>\pm</math> 0.6</b>	<b>2.48 <math>\pm</math> 0.08</b>
<b>ucb-35440-3</b>	<b>8.78 <math>\pm</math> 2.10</b>	<b>140.5 <math>\pm</math> 11.3</b>	<b>340.6 <math>\pm</math> 15.1</b>	<b>160.4 <math>\pm</math> 9.4</b>	<b>2.37 <math>\pm</math> 0.11</b>
<b>UCB-A</b>	<b>1.47 <math>\pm</math> 0.03</b>	<b>3.00 <math>\pm</math> 0.02</b>	<b>6.52 <math>\pm</math> 0.21</b>	<b>3.59 <math>\pm</math> 0.06</b>	<b>1.68 <math>\pm</math> 0.07</b>
<b>UCB-B</b>	<b>2.75 <math>\pm</math> 0.04</b>	<b>6.97 <math>\pm</math> 0.03</b>	<b>18.3 <math>\pm</math> 0.5</b>	<b>9.24 <math>\pm</math> 0.23</b>	<b>2.23 <math>\pm</math> 0.07</b>

Through the results observed in **Figure IV 2 10** and **Table IV 2 4**, it is very clear that preliminary size reduction steps prior to the high pressure homogenization cycles are necessary for optimal drug processing. This is more evident for NIF and ucb-35440-3 and, to a lesser extent, for UCB-B as UCB-A is already characterized by a relatively low particle size with a mean volume particle size around 3  $\mu\text{m}$ . Turrax<sup>®</sup> milling was, however, evaluated for UCB-A in order to denote any positive influence regarding further particle size reduction of the drug. LD results regarding the influence of the Turrax<sup>®</sup> milling operation on the tested model drugs are shown in **Figure IV 2 11**. Through these results we can clearly see that the Turrax<sup>®</sup> milling operation has absolutely no consequence on reducing UCB-A and UCB-B particle size as the exact same particle size distributions were observed (d(v,0.5) around 3  $\mu\text{m}$  and 6  $\mu\text{m}$ , respectively). The Turrax<sup>®</sup> milling (10 min 24000 rpm - suspension placed in an ice bath) operation was not conducted on ucb-35440-3 suspensions due to excessive foam formation during the operation. Skipping this operation was, however, further shown not to be problematic for ucb-35440-3 as the pre-milling low pressure homogenization cycles conducted using the EmulsiFlex C5<sup>®</sup> were highly efficient considering preliminary size reduction; a d(v,0.5) around 0.6  $\mu\text{m}$  being obtained following PMC.

The Influence of pre-milling cycles (PMC) (15C 7000 PSI + 10C 12000 PSI) on drug particle size reduction is also represented in **Figure IV 2 11**. From these results, we can clearly see that preliminary size reduction was feasible for all tested drugs. These low-pressure homogenizing cycles are more efficient regarding particle size reduction efficiency than the Turrax<sup>®</sup> milling operation carried out. The largest reduction in particle size using these low pressure homogenizing cycles came with ucb-35440-3 with a d(v,0.5) around 0.6  $\mu\text{m}$  with 59% (in volume) of submicron particle being obtained following PMC. For NIF, a particle population characterized by a d(v,0.5) around 2.5  $\mu\text{m}$  with 18% (in volume) of submicron particle was obtained. A significant size reduction was also observed for UCB-A and UCB-B with obtained particle populations of d(v,0.5) around 1  $\mu\text{m}$  (48% (in volume) of submicron particle) and 2  $\mu\text{m}$  (5% (in volume) of submicron particle), respectively.

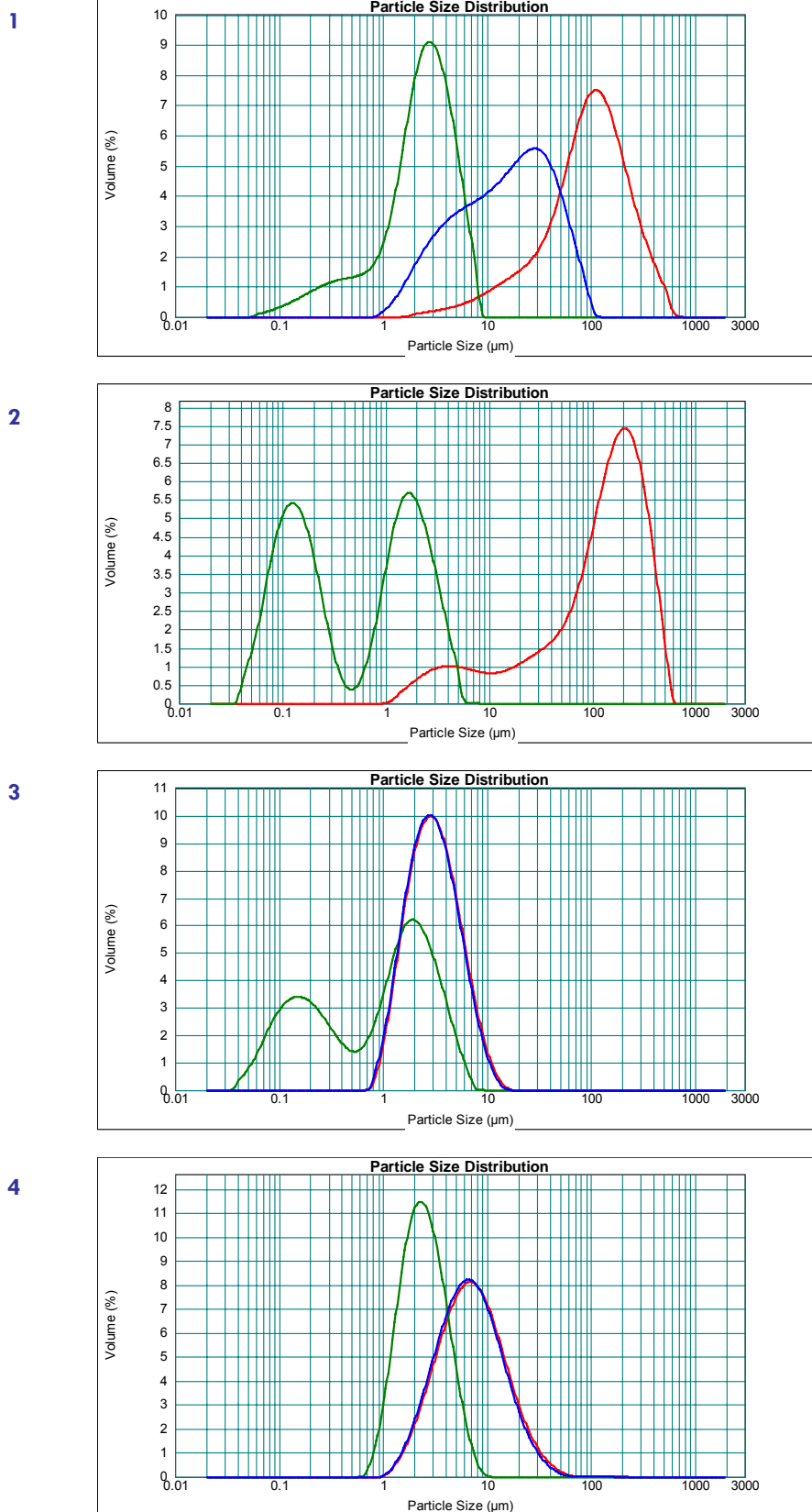


**Figure IV 2 11.** LD size distribution analysis following pre-milling operations: Drug as received (prior to milling operations (red), 10min 24000rpm Turrax® milling (blue) and PMC (15C 7000 PSI + 10C 12000 PSI) using the EmulsiFlex C5® (green). For **(1)** NIF 5%, Methocel E15® 0.5%, w/v; **(2)** ucb-35440-3 5%, Methocel E15® 0.1%, w/v; **(3)** UCB-A 5%, Methocel E15® 0.5%, Poloxamer 407 0.25%, w/v and **(4)** UCB-B 5%, Methocel E15® 0.5%, Poloxamer 407 0.25%, w/v. Data reported in annex 1 (**Table A5**).

It has to be noted that, for ucb-35440-3, important particle size reduction was already observed following the 15 cycles at 7000 PSI with a particle population characterized by a  $d(v,0.5)$  around 2  $\mu\text{m}$ . However, this particle population was characterized by less than 2% (in volume) of submicron particles. No major differences were observed between cycles at 7000 PSI and 12000 PSI for NIF, UCB-A, and UCB-B.

We can thus conclude that these pre-milling operations, be they the Turrax® milling operation and, most evidently, the EmulsiFlex C5® low pressure homogenizing cycles, are quite effective as preliminary size reduction operations which are requisites for high pressure homogenization at high homogenizing pressures. The Turrax® milling operation, when possible, should be conducted for drugs that are characterized by a  $d(v,0.5)$  above 100  $\mu\text{m}$  for a first significant particle size reduction. The EmulsiFlex C5® pre-milling low pressure homogenizing cycles were found to further particle size reduction from Turrax® milled suspensions and, more interestingly, for micronized drugs (UCB-A and UCB-B). The need for these operations, although seemingly evident for drugs with relatively large particle size (i.e. >100  $\mu\text{m}$ ), shall be dependent of the type of drug being processed (i.e. hardness) and should be used in the adopted particle size reduction protocols on a case-by-case basis.

#### **IV.2.3.3. Influence of high pressure homogenizing cycles**

##### **IV.2.3.3.1. Influence of the number of homogenizing cycles**

Cycles at a homogenizing pressure of about 23-24000 PSI were applied to the tested suspensions following the pre-milling operations cited above to see if further size reduction could be achieved. Suspensions were passed for a maximum of 20 cycles (closed loop operation – see **part IV.2.2.2.3**). Samples were withdrawn at various times to denote the influence of the number of cycles applied. LD results for NIF are shown in **Figure IV 2 12**, for ucb-35440-3 in **Figure IV 2 13**, for UCB-A in **Figure IV 2 14**, and for UCB-B in **Figure IV 2 15**.

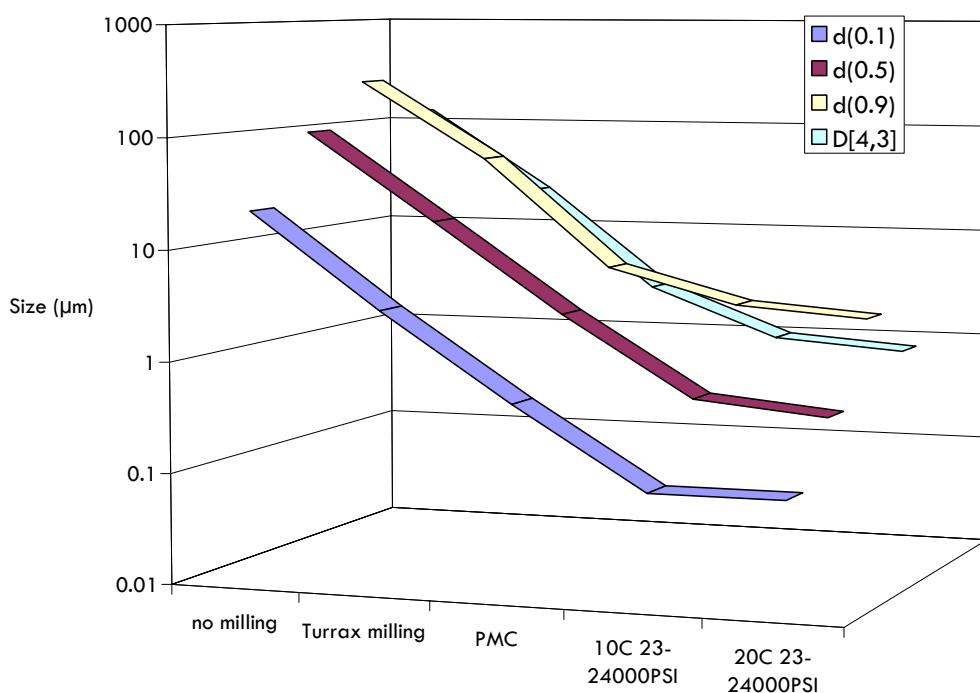


**Figure IV 2 12.** LD size distribution analysis following HPH cycles (10-20 cycles at 23-24000 PSI) for NIF (NIF 5%, Methocel E15® 0.5% suspension, w/v). Data reported in annex 1 (Table A6).

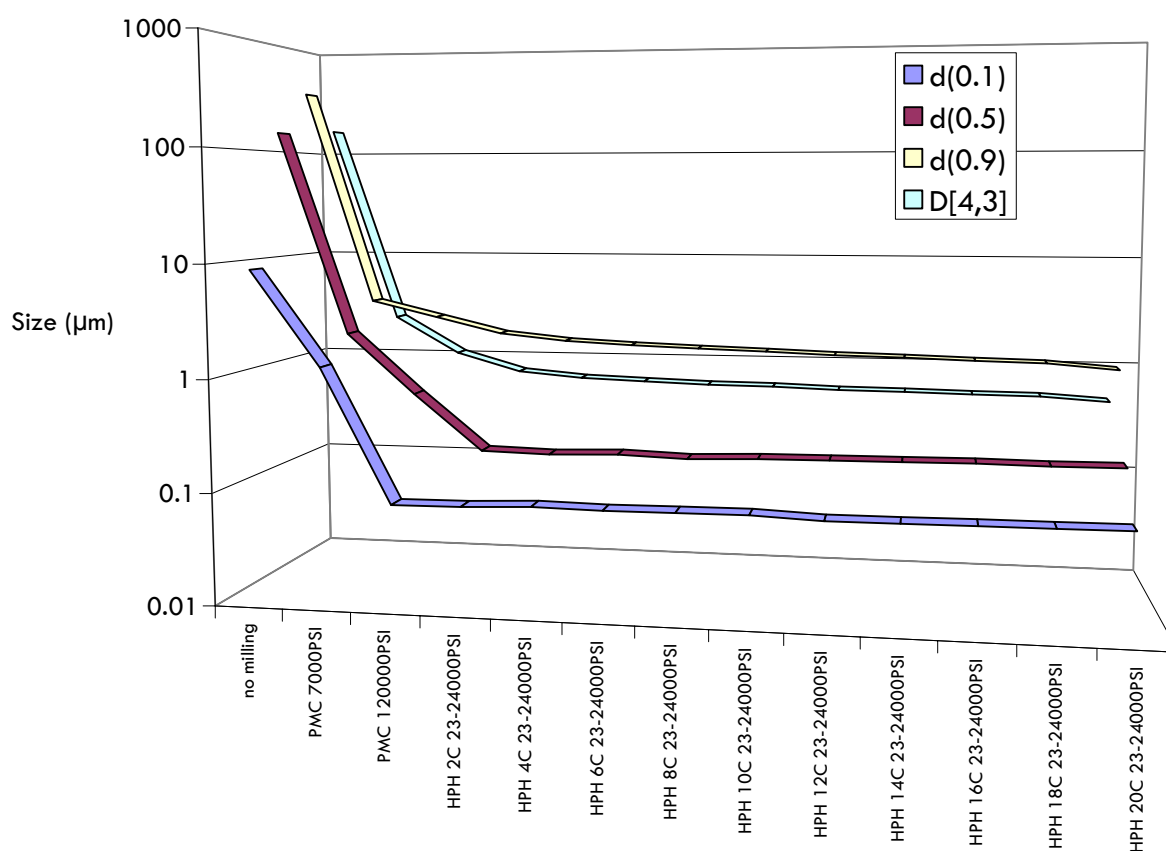


**Figure IV 2 13.** LD size distribution analysis following HPH cycles (up to 20 cycles at 23-24000 PSI) for ucb-35440-3 (ucb-35440-3 5%, Methocel E15® 0.1% suspension, w/v). Data reported in annex 1 (Table A7).

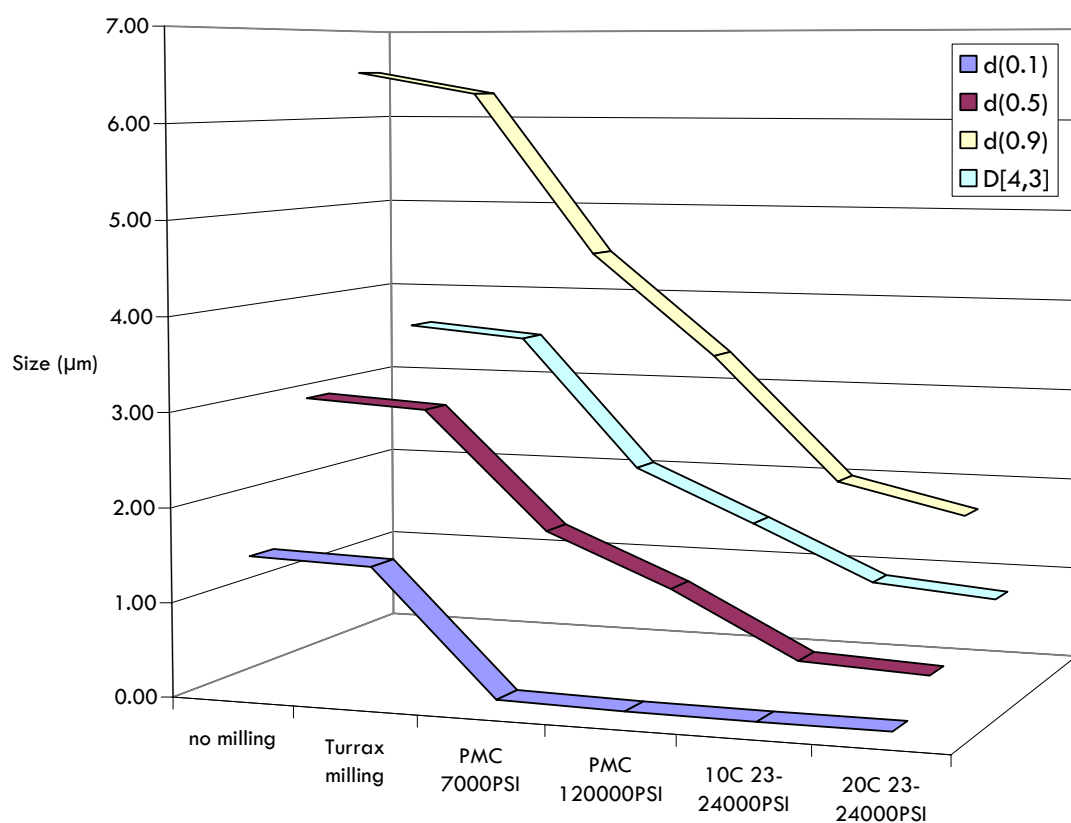


**Figure IV 2 14.** LD size distribution analysis following high pressure homogenization cycles (10 - 20 cycles at 23-24000 PSI) for UCB-A (UCB-A 5%, Methocel E15® 0.5%, Poloxamer 407 0.25% suspension, w/v). Data reported in annex 1 (**Table A8**).

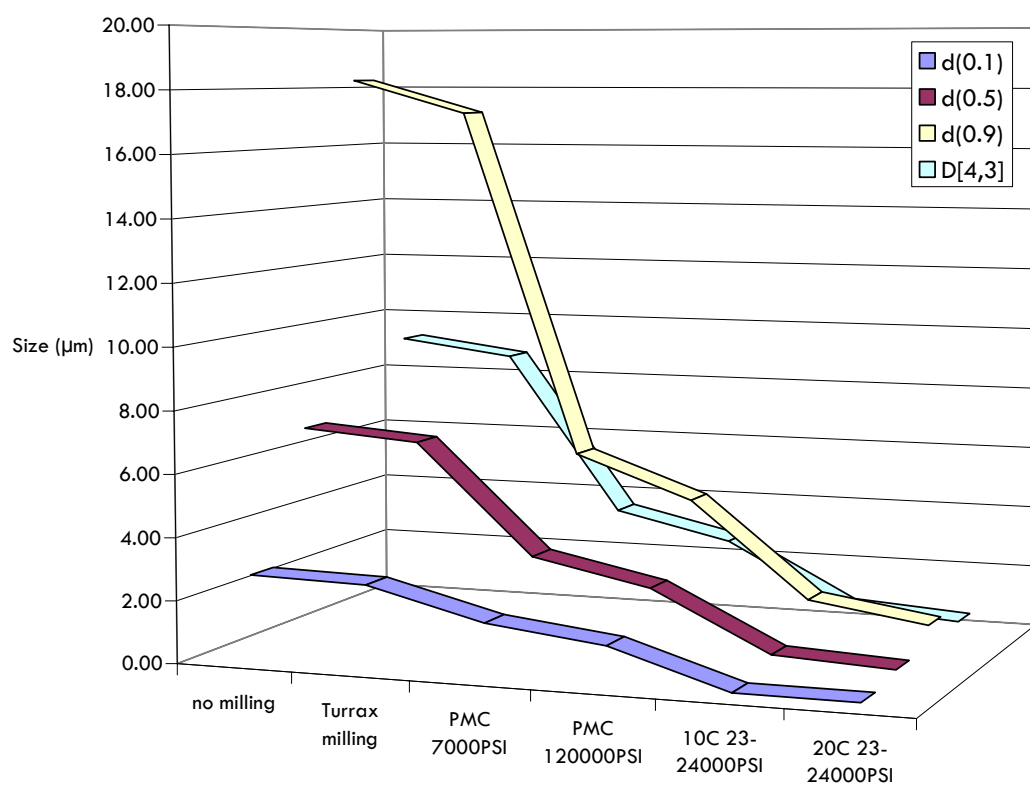


**Figure IV 2 15.** LD size distribution analysis following HPH cycles (10 - 20 cycles at 23-24000 PSI) for UCB-B (UCB-B 5% Methocel E15® 0.5% Poloxamer 407 0.25% suspension, w/v). Data reported in annex 1 (**Table A9**).

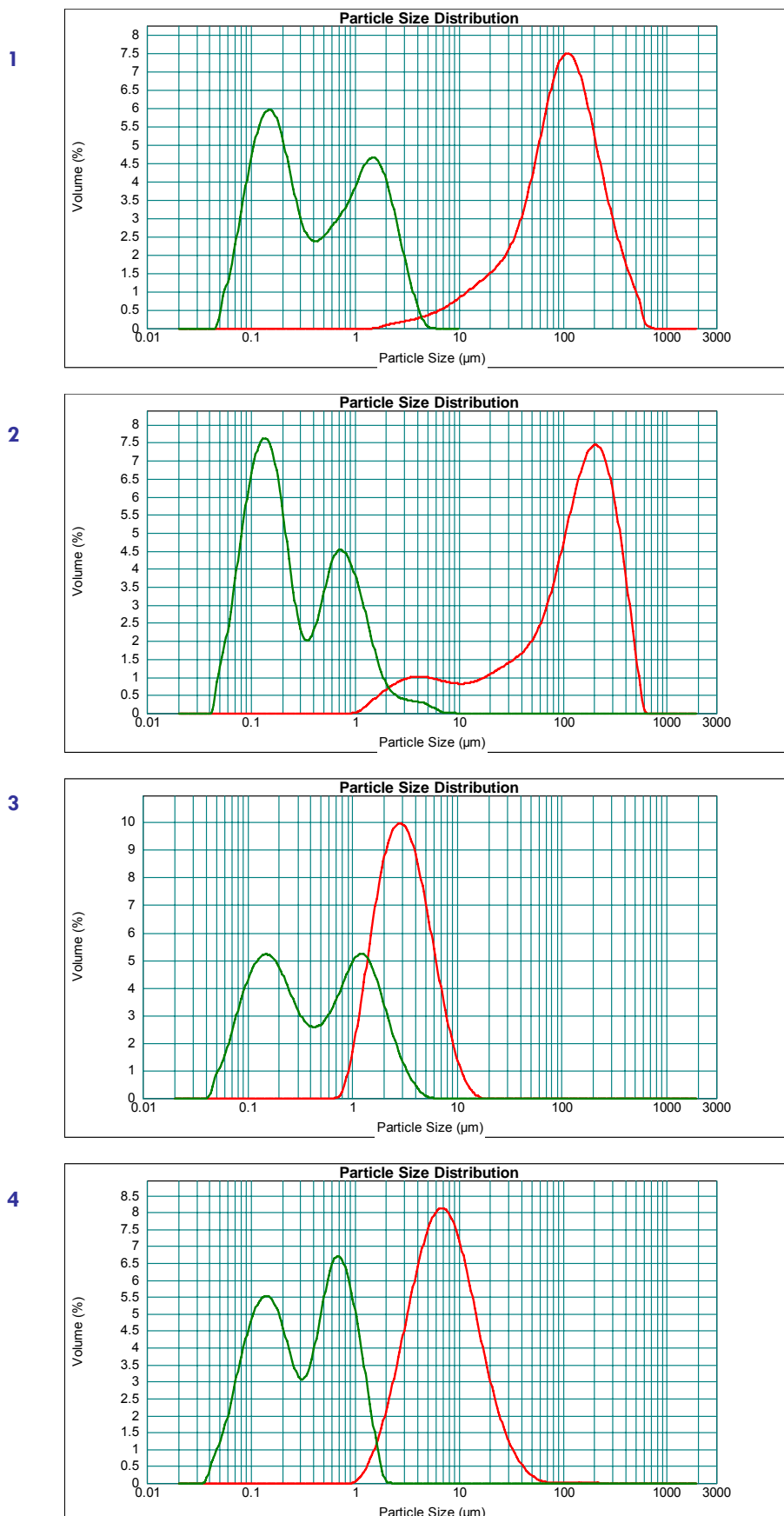


**Figure IV 2 16.** LD size distribution curves for drugs prior to milling operations (**red**) and following PMC + 20C 23-24000 PSI HPH (**green**): For (1) NIF 5%, Methocel E15<sup>®</sup> 0.5%, w/v; (2) ucb-35440-3 5%, Methocel E15<sup>®</sup> 0.1%, w/v; (3) UCB-A 5%, Methocel E15<sup>®</sup> 0.5%, Poloxamer 407 0.25%, w/v and (4) UCB-B 5%, Methocel E15<sup>®</sup> 0.5%, Poloxamer 407 0.25%, w/v.

Size distribution curves prior to milling operations and following pre-milling cycles and 20 cycles at 23-24000 PSI for all studied drugs are shown in **Figure IV 2 16**.

Through the results obtained, we can clearly see that further processing of the pre-milled drug suspensions allows for greater particle size reduction with achievement of a population with a  $d(v,0.5)$  around 350 nm and with about 70% (in volume) of submicron particles for NIF, a  $d(v,0.5)$  around 200 nm with about 90% (in volume) of submicron particles for ucb-35440-3, a  $d(v,0.5)$  around 400 nm with about 70% (in volume) of submicron particles for UCB-A and a  $d(v,0.5)$  around 325 nm and with about 90% (in volume) of submicron particles for UCB-B.

We can also see that particle size decreases when increasing the number of homogenization cycles and that except for  $d(v,0.1)$  and to a lesser extent for  $d(v,0.5)$ , we can still observe, at least for NIF, UCB-A and UCB-B, this decrease following the 20 cycles at 23-24000 PSI, primarily in parameters such as  $d(v, 0.9)$  and  $D[4,3]$ . The operation was stopped following these 20 cycles but one can assume that, although to a small extent, particle size could have been further reduced with additional homogenization cycles. In the case of ucb-35440-3 (**Figure IV 2 13**), however, rapid limitation in particle size reduction can be observed at homogenizing pressure of 23-24000 PSI. A significant decrease is observed after 2 cycles at 23-24000 PSI when compared to particle size following PMC ( $d(v,0.5) \pm 625 \text{ nm} \rightarrow 200 \text{ nm}$ ) and particle size does not seem to further decrease with additional cycles.  $d(v, 0.9)$  and  $D[4,3]$  are, however, shown to slightly decrease with the increase in the number of cycles for up to 20 cycles. The protocol for ucb-35440-3 particle size reduction was thus limited to 10 homogenizing cycles following the pre-milling size reduction operations, primarily for time-saving purposes.

It has to be noted that the particle size distribution curves obtained were always characterized by a bimodal distribution. This could be noticed for the four model drugs tested in this work. The second population, around the micron range, is thought to be the consequence of nanoparticle agglomerates or residual microparticles (the latter case being more probable). In fact, laser diffraction size curves represent a volume distribution meaning that even a very few residual microparticles will strongly influence the particle size distribution. Although this second “microparticle” population could in some cases, be lowered it could never be completely removed if no particular process was applied following the homogeneization operation. In that regard, simple centrifugation procedures have been showed to allow for the removal of this second population (data not shown). Also, given the results obtained (see following chapters) with the population obtained, no particular attempt was made to remove this second population. This evaluation could nevertheless be carried out to denote any eventual differences.

#### IV.2.3.3.2. Influence of additional cycles at higher homogenizing pressure

In the same way as the evaluation of the number of homogenizing cycles, the homogenizing pressure applied to the suspension was also evaluated to denote any influence on the efficiency of particle size reduction. In fact, from the results already presented in this chapter regarding pre-milling low pressure homogenizing cycles and high pressure homogenization cycles, we can clearly see and understand the effect of increasing homogenizing pressure (7000 PSI → 12000 PSI → 23-24000 PSI) on drug particle size reduction efficiency and foreshadow the effect of increasing the homogenizing pressure up to 30000 PSI. This evaluation was mainly conducted on UCB-A and UCB-B. LD results for UCB-A are shown in **Figure IV 2 17**, and for UCB-B in **Figure IV 2 18**.

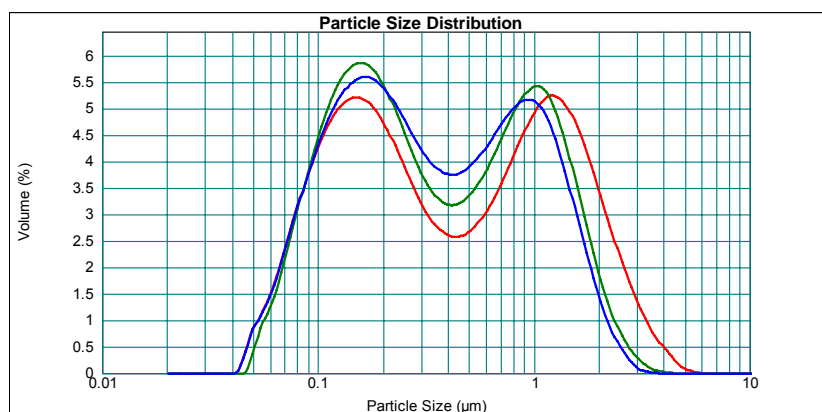


**Figure IV 2 17.** LD size distribution curves following high pressure homogenization cycles of UCB-A: 20 C 23-24000 PSI (red), 5C 30000 PSI (green) and 10C 30000 PSI (blue). (UCB-A 5%, Methocel E15® 0.5%, Poloxamer 407 0.25%, w/v). Data reported in annex 1 (**Table A10**).

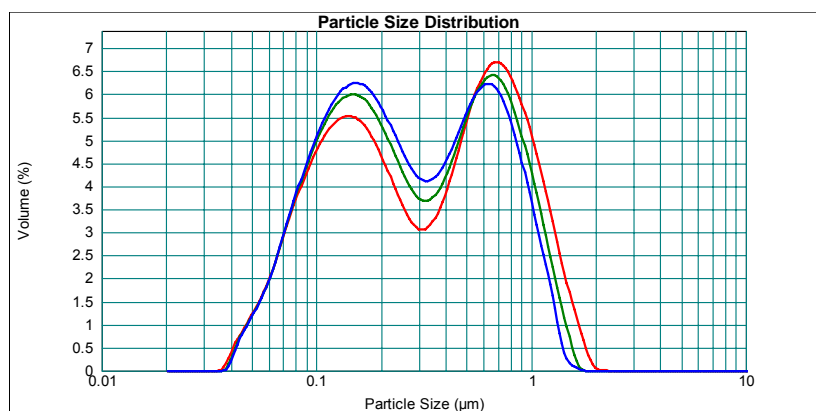


**Figure IV 2 18.** LD size distribution curves following high pressure homogenization cycles of UCB-B: 20 C 23-24000 PSI (red), 5C 30000 PSI (green) and 10C 30000 PSI (blue). (UCB-B 5%, Methocel E15® 0.5%, Poloxamer 407 0.25%, w/v). Data reported in annex 1 (**Table A11**).



As we can see from the results presented in these figures, UCB-A and UCB-B particle size can be further decreased by processing the suspensions at homogenizing pressures of 30000 PSI following the cycles at 23-24000 PSI. Most importantly, both  $d(v, 0.9)$  and  $D[4,3]$  can be further reduced and for example, as in the case of UCB-B, we can obtain a size distribution with approximately 97% (in volume) of submicron particles. Homogenizing cycles at 30000 PSI were not shown to have an influence on further particle size reduction of ucb-35440-3, possibly due to the fact that relatively low particle sizes were already obtained at 23-24000 PSI (e.g. already for 2 cycles at this homogenizing pressure - no further significant reduction for additional cycles - limit in particle size for the given system). The influence of additional homogenizing cycles at 30000 PSI on NIF was not evaluated.

It has to be noted that, even though these additional cycles at 30000 PSI can be interesting with regard to further particle size reduction from suspensions processed at 23-24000 PSI, the difference is relatively limited when compared to differences between sample processing at 12000 PSI and 23-24000 PSI (this observation based on our results - other drugs might behave differently). Although it needs to be verified, the slight difference observed (i.e. 23-24000 PSI/30000 PSI) might not be translated into significant differences in vitro-in vivo behaviour (dissolution, PK, etc.). If this is the case, these cycles might not be of real interest in drug formulation development as these additional cycles increase (depending on the desired number of cycles) the sample processing time.

#### IV.2.3.4. Influence of temperature

In addition to the influence of processing temperature on drug chemical stability, the influence of processing temperature on high pressure homogenization particle size reduction efficiency is a very important parameter to control and to assess. High pressure homogenization processing has been shown to increase sample temperature by approximately 25-30°C (following the described pre-milling low-pressure homogenizing cycles and 20 cycles at 23-24000 PSI) if it is run without using an heat exchanger with an appropriate inlet temperature or without placing the apparatus in an ice bath. The first evaluation of processing temperature on particle size reduction efficiency was carried out on NIF suspensions with the EmulsiFlex<sup>®</sup> placed in or out of an ice bath (no heat exchanger); sample temperature (measured in the sample reservoir) being then 10°C and 45°C, respectively. LD results for this evaluation are shown in **Figure IV 2 19**.

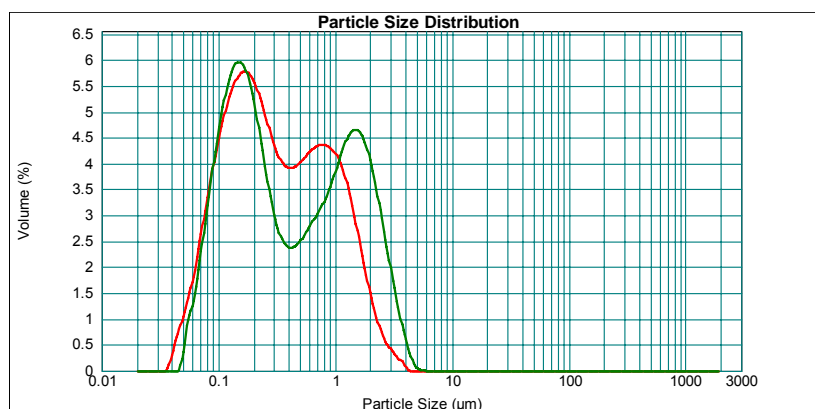


**Figure IV 2 19.** LD size distribution curves following suspension processing (PMC + 20C 23-24000 PSI) at 10°C (red) and 45°C (green). (NIF 5%, Methocel E15® 0.5%, w/v). Data reported in annex 1 (Table A12).

**Figure IV 2 19** clearly shows the positive influence of reducing sample temperature regarding NIF particle size reduction efficiency.  $d(v,0.5)$  was decreased from 350 nm to 290 nm and, most importantly,  $d(v,0.9)$  was decreased from 2  $\mu\text{m}$  to 1.3  $\mu\text{m}$  (decrease in span:  $5.5 \rightarrow 4.1$ ) and  $D[4,3]$  from 790 nm to 530 nm. Populations were characterized by 86% and 70% (in volume) of submicron particles when processing NIF at 10°C or 45°C, respectively. This observed difference could find an explanation in the fact that an increase in sample temperature might lead to an increase in drug solubility (i.e. drug nanoparticles) with subsequent recrystallization when sample temperature is decreased (i.e. after sample processing), thus leading to larger particle sizes. A possible difference in crystal hardness cannot be the explanation, as it will be the case for UCB-A, for this observation. Although this evaluation was carried out by immersing the EmulsiFlex® in an ice bath, similar results can be obtained using a heat exchanger placed ahead of the homogenizing valve (for a sample temperature of 10°C, the inlet cryostat temperature should be set around 2.5°C). The heat exchanger has, however, different advantages over apparatus immersion in that handling is facilitated (pressure regulation - the pressure adjusting knob being immersed when placing the EmulsiFlex C5® in an ice bath) and that optimal control of any desired temperature can be achieved by properly selecting the inlet cryostat temperature. A sample processing temperature of 10°C was thus adopted in our established high pressure homogenization protocol and was the temperature used for all ucb-35440-3, UCB-A and UCB-B suspensions. This is the case for the previously reported data for these drugs. As for NIF, the data already shown in this chapter are representative of suspensions passed without utilization of a heat exchanger (or immersion in an ice bath) and thus at a processing temperature of approximately 45°C.

The influence of sample processing temperature on particle size reduction efficiency was, as already mentioned, a critical parameter to assess for UCB-A. In fact, this drug, as described in **part IV.1.3** of this work, presents a particular temperature-dependent behaviour in that reversible polymorphic transformations occur below 16°C (form F  $\leftrightarrow$  G) and above 37°C (form F  $\leftrightarrow$  H). Since these polymorphic transformations occur in the temperature range in which the EmulsiFlex® can be run, it is thus important to control sample temperature during UCB-A processing as these different polymorphic forms might behave differently (polymorphism  $\leftrightarrow$  crystal hardness) when considering drug particle size reduction. To denote the influence of the presence of a particular polymorphic form of UCB-A on the milling efficiency of the EmulsiFlex-C5®, homogenization was carried out at controlled temperatures of about 11°C (milling of UCB-A as polymorphic form G), about 23°C (milling of UCB-A as polymorphic form F) and about 45°C (milling of UCB-A as polymorphic form H). Temperature was controlled using a heat exchanger and monitored throughout the homogenization operation (**Figure IV 2 2 - part IV.2.2.2.3.2**). LD results for this evaluation are shown in **Figure IV 2 20 A/B**.

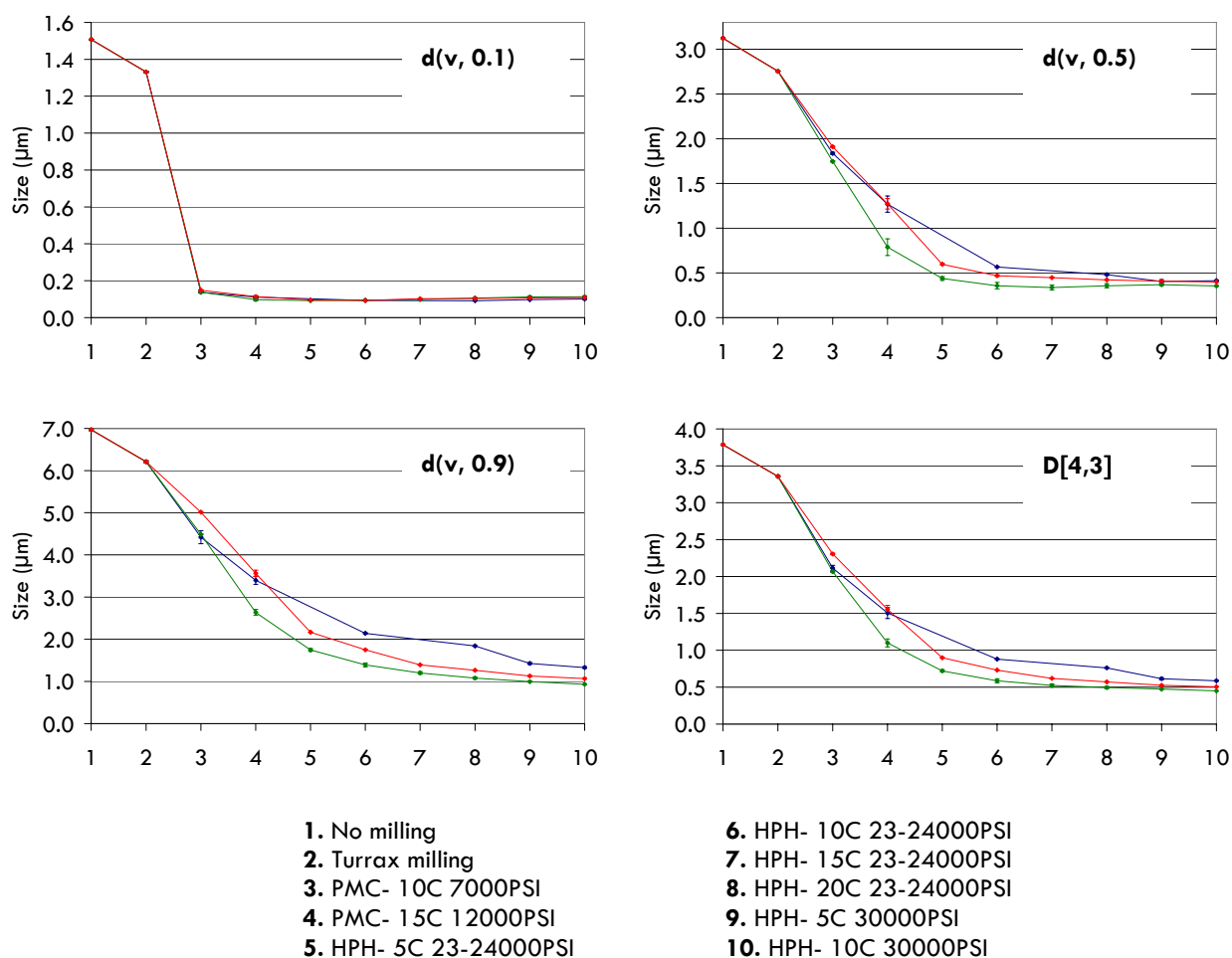


**Figure IV 2 20 A.** LD results: influence of processing temperature on UCB-A particle size: 11°C (blue), 23°C (green) and 45°C (red). (UCB-A 5%, Methocel E15® 0.5%, SDS 0.1%, w/v). Data reported in annex 1 (**Table A13**).

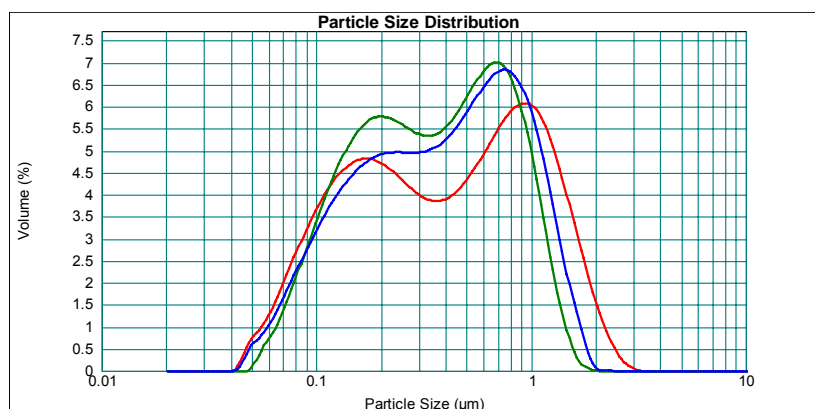


**Figure IV 2 20 B.** LD size distribution curves following sample processing (PMC + 20C 23-24000 PSI + 10C 30000 PSI) at 10°C (red), 23°C (green) and 45°C (blue). (UCB-A 5%, Methocel E15® 0.5%, SDS 0.1%, w/v). Data reported in annex 1 (Table A13).

As we can clearly see in **Figure IV 2 20 A/B**, temperature seems to influence the milling efficiency of UCB-A using high pressure homogenization. A smaller particle size can effectively be obtained by milling UCB-A when in polymorphic form F (i.e. 23°C); a  $d(v,0.5)$  of 350 nm being obtained with approximately 95% (in volume) of submicron particles. The  $d(v,0.5)$  is 410 nm and 400 nm and the volume percentage of submicron particles is 83% and 90% for polymorphic form G (11°C) and polymorphic form H (45°C), respectively. Complementing these data with the knowledge of the possibility of varying crystal hardness for the different UCB-A polymorphs would be very interesting in order to correlate the particle size reduction efficiency of the homogenizer with UCB-A crystal hardness.

#### IV.2.3.5. Redispersion analysis - influence of carriers

As drug nanoparticles are prepared in a suspension state, water needs to be removed after the homogenization operation in order to retrieve particles in a powder state; this is for the various *in vitro*/*in vivo* assays conducted for their characterization (DSC, PXRD, dissolution, etc.) and also for storage and stability considerations. Investigations into techniques such as freeze-drying and spray-drying for water-removal from the nanosuspensions were carried out in this work.

Redispersion characteristics of the spray- or freeze-dried powders are, in fact, an important parameter to assess as it is desirable to restore the particle size distribution achieved before the water-removal operation once the powders are again placed in an aqueous media; this in order to maintain the various presumed characteristics achieved through nanosizing (increased SSA → enhanced solubility/dissolution rate → enhanced oral bioavailability). The redispersion characteristics of the water-removed nanosuspensions is strongly influenced by the presence of the type of stabilizer (i.e. surfactant) in the formulation (i.e. modifications in drug particles surface properties) and the presence of a carrier in the formulation will be shown to be greatly beneficial towards enhancing these redispersion characteristics.

These redispersion characteristics of water-removed nanosuspensions were evaluated for the first time when starting the evaluation of ucb-35440-3 dissolution at pH 6.5 using the flow-through dissolution system (USP type IV apparatus). These characteristics were thus evaluated alongside the evaluation of the dissolution characteristics of various spray or freeze-dried nanosuspensions and this principally using NIF and ucb-35440-3 as model drugs. The influence of redispersion characteristics on drug dissolution will be discussed in **part IV.4** of this work.

In order to evaluate the extent of particle agglomeration following water-removal and the particle size distribution observed following redispersion of these “water-removed” nanosuspensions, scanning electron microscopy (SEM) and laser diffraction (LD) analyses were carried out. SEM allows for the visualization of the size and the morphology of the freeze- or spray-dried powders. LD evaluation of the redispersion characteristics was carried out using the protocol described in **part IV.2.2.4.1** of this work. SEM micrographs of NIF prior to milling operations and for a NIF spray-dried suspension are shown in **Figure IV 2 21**. SEM micrographs for a ucb-35440-3 freeze-dried suspension are shown in **Figure IV 2 22**.

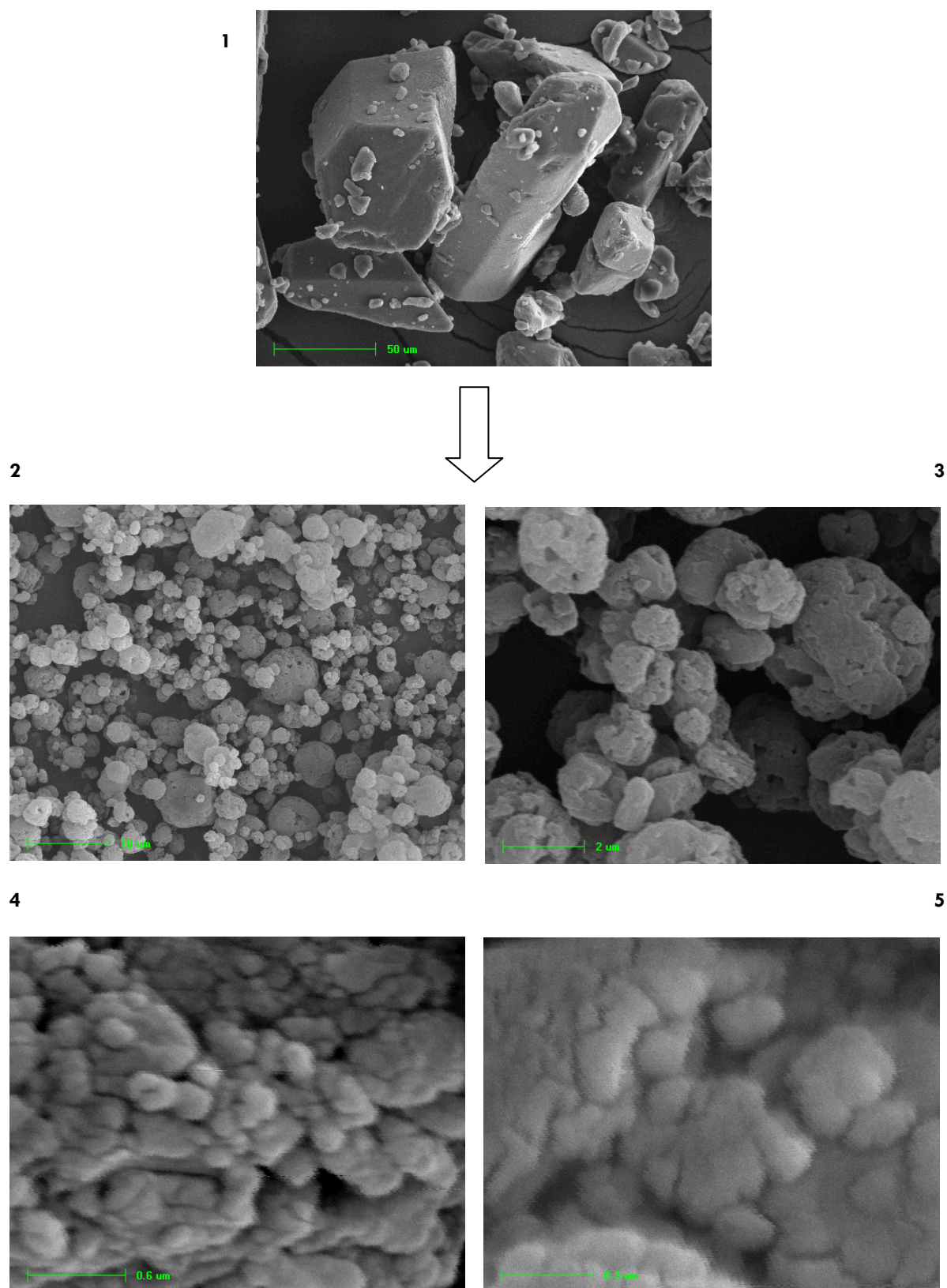


**Figure IV 2 21.** SEM micrograph of (1) un-milled NIF (magnification 500X - scale 50  $\mu\text{m}$ ) and (2-5) spray-dried 5% NIF 0,5% Methocel E15<sup>®</sup> nanosuspension (suspension following pre-milling cycles + 20C at 23-24000 PSI) - (2) magnification 2000X (scale 10  $\mu\text{m}$ ), (3) magnification 10000X (scale 2  $\mu\text{m}$ ), (4) magnification 40000X (scale 0.6  $\mu\text{m}$ ) and (5) magnification 75000X (scale 0.3  $\mu\text{m}$ ).

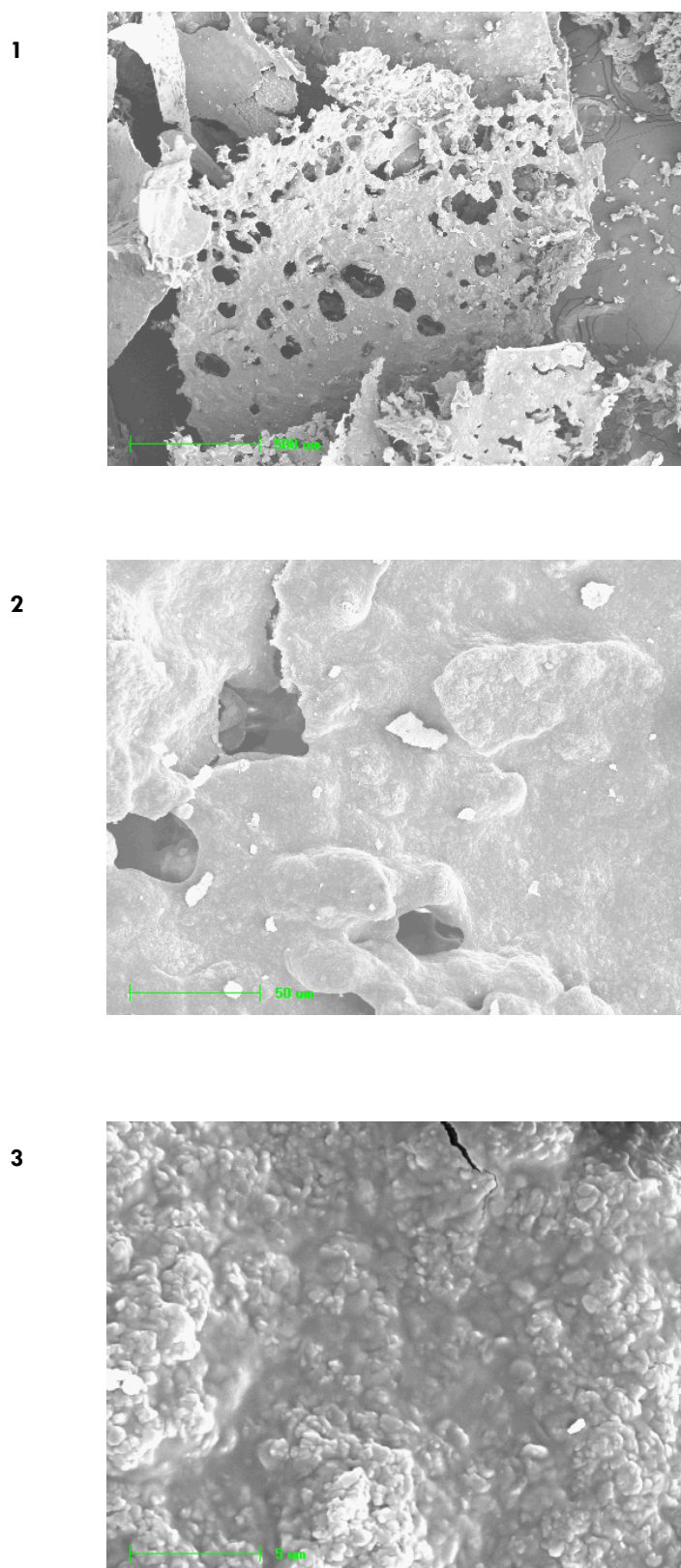


**Figure IV 2 22.** SEM micrograph of a freeze-dried 2% ucb-35440-3, 0,5% Methocel E15<sup>®</sup> nanosuspension (suspension following pre-milling cycles + 20C at 23-24000 PSI): (1) magnification 50X (scale = 500  $\mu\text{m}$ ), (2) magnification 500X (scale = 50  $\mu\text{m}$ ), (3) magnification 5000X (scale = 5  $\mu\text{m}$ ).



As it can easily be seen on these micrographs, drug nanoparticle agglomeration is a clear fact following water-removal operations, be it freeze-drying or spray-drying. This can further be shown when analyzing particle size distribution following redispersion of the freeze-or spray-dried powders. LD results for this evaluation are shown in **Figure IV 2 23** and **Table IV 2 5** for NIF and on **Figure IV 2 24** and **Table IV 2 6** for ucb-35440-3.

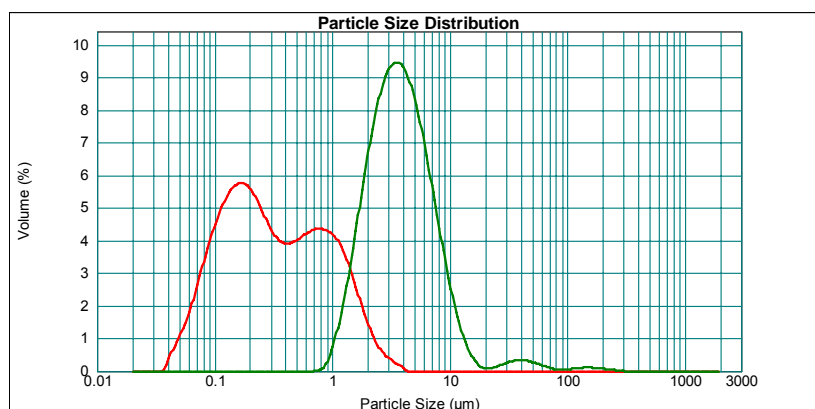


**Figure IV 2 23.** LD size distribution curves following sample processing (PMC + 20C 23-24000 PSI) (**red**) and following redispersion of the spray-dried processed suspension (**green**). (NIF 5%, Methocel E15® 0.5%, w/v).

**Table IV 2 5.** Data for Figure IV 2 23 (size in  $\mu\text{m}$ ) (SD: Spray-drying).

	$d(0.1) \pm \text{SD}$	$d(0.5) \pm \text{SD}$	$d(0.9) \pm \text{SD}$	$D[4,3] \pm \text{SD}$	$\text{span} \pm \text{SD}$
<b>Before SD</b>	$0.089 \pm 0.003$	$0.291 \pm 0.006$	$1.29 \pm 0.07$	$0.526 \pm 0.022$	$4.11 \pm 0.03$
<b>Following SD</b>	$1.73 \pm 0.04$	$3.7 \pm 0.09$	$8.6 \pm 0.33$	$5.49 \pm 0.41$	$1.82 \pm 0.05$

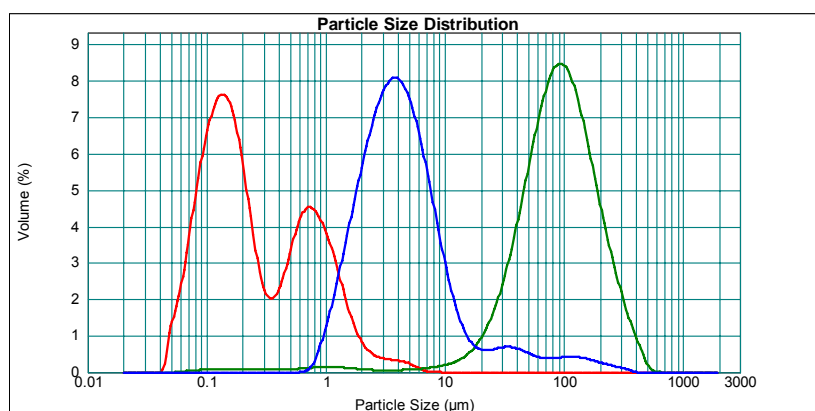


**Figure IV 2 24.** LD size distribution curves following sample processing (PMC + 20C 23-24000 PSI) (**red**) and following redispersion of the freeze-dried (**green**) and spray-dried (**blue**) processed suspension. (ucb-35440-3 5%, Methocel E15® 0.1%, w/v).

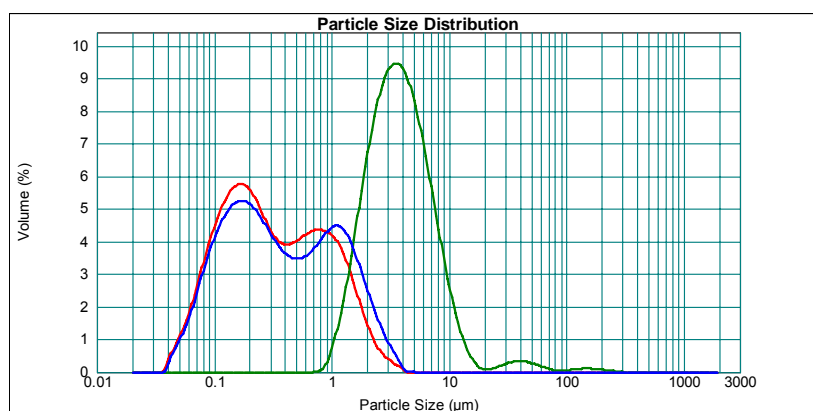


**Table IV 2 6.** Data for Figure IV 2 24 (size in  $\mu\text{m}$ ) (FD: Freeze-drying / SD: Spray-drying).

	$d(0.1) \pm \text{SD}$	$d(0.5) \pm \text{SD}$	$d(0.9) \pm \text{SD}$	$D[4,3] \pm \text{SD}$	$\text{span} \pm \text{SD}$
<b>Before water-removal</b>	<b>0.082 <math>\pm</math> 0.004</b>	<b>0.202 <math>\pm</math> 0.019</b>	<b>1.14 <math>\pm</math> 0.02</b>	<b>0.482 <math>\pm</math> 0.019</b>	<b>5.27 <math>\pm</math> 0.48</b>
<b>Following FD</b>	<b>89.8 <math>\pm</math> 2.7</b>	<b>34.6 <math>\pm</math> 2.0</b>	<b>221.8 <math>\pm</math> 10.1</b>	<b>112.2 <math>\pm</math> 3.7</b>	<b>2.08 <math>\pm</math> 0.09</b>
<b>Following SD</b>	<b>4.07 <math>\pm</math> 0.24</b>	<b>1.65 <math>\pm</math> 0.06</b>	<b>14.5 <math>\pm</math> 3.1</b>	<b>11.0 <math>\pm</math> 1.8</b>	<b>3.13 <math>\pm</math> 0.60</b>

These data confirm the strong agglomeration phenomenon that occurs during water-removal from the nanosuspensions, as less than 1% (in volume) of submicron particles are found following spray-drying of NIF nanosuspensions and less than 2% (in volume) of submicron particles for either freeze-dried or spray-dried ucb-35440-3 nanosuspensions (agglomeration being more important following freeze-drying than spray-drying).

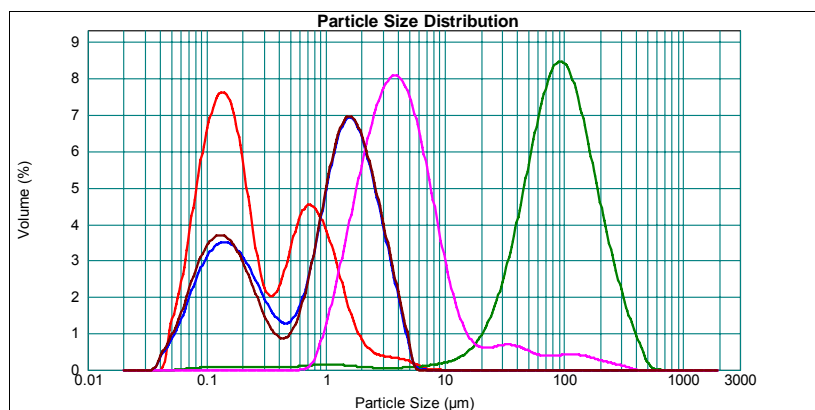
To prevent this rather problematic agglomeration phenomenon, water-soluble carriers such as mannitol can be added to the formulation prior to the water-removal operation. The role of mannitol is, in fact, to recrystallize around drug nanoparticles during the water-removal operation, thus preventing particle interaction and agglomeration (drug nanoparticles can be viewed as being entrapped in a crystalline mannitol matrix). Mannitol, being a highly water-soluble compound, also procures the advantage of creating a highly hydrophilic environment around NIF nanoparticles which might be shown to be beneficial with regard to drug dissolution characteristics. Mannitol was added to the suspension, at 100% w/w relative to drug content, following the high pressure homogenization and prior to the spray-drying or freeze-drying operation. The influence of mannitol in NIF and ucb-35440-3 formulations is shown in **Figure IV 2 25** and **Table IV 2 7** and on **Figure IV 2 26** and **Table IV 2 8**, respectively. Data for mannitol-free suspensions is again shown in these figures and tables.



**Figure IV 2 25.** LD size distribution curves following sample processing (PMC + 20C 23-24000 PSI) (**red**) and following redispersion of the spray-dried processed suspension: NIF 5%, Methocel E15® 0.5%, w/v (**green**) and NIF 5%, Mannitol 5%, Methocel E15® 0.5%, w/v (**blue**).

**Table IV 2 7.** Data for Figure IV 2 25 (size in  $\mu\text{m}$ ) (SD: Spray-drying).

	$d(0.1) \pm \text{SD}$	$d(0.5) \pm \text{SD}$	$d(0.9) \pm \text{SD}$	$D[4,3] \pm \text{SD}$	$\text{span} \pm \text{SD}$
<b>Before SD</b>	<b>0.089 <math>\pm</math> 0.003</b>	<b>0.291 <math>\pm</math> 0.006</b>	<b>1.29 <math>\pm</math> 0.07</b>	<b>0.526 <math>\pm</math> 0.022</b>	<b>4.11 <math>\pm</math> 0.03</b>
<b>no mannitol</b>	<b>1.73 <math>\pm</math> 0.04</b>	<b>3.7 <math>\pm</math> 0.09</b>	<b>8.6 <math>\pm</math> 0.33</b>	<b>5.49 <math>\pm</math> 0.41</b>	<b>1.82 <math>\pm</math> 0.05</b>
<b>mannitol</b>	<b>0.093 <math>\pm</math> 0.002</b>	<b>0.339 <math>\pm</math> 0.006</b>	<b>1.60 <math>\pm</math> 0.04</b>	<b>0.638 <math>\pm</math> 0.010</b>	<b>4.49 <math>\pm</math> 0.17</b>

**Figure IV 2 26.** LD size distribution curves following sample processing (PMC + 20C 23-24000 PSI) (**red**) and following redispersion of the freeze-dried processed suspension (ucb-35440-3 5%, Methocel E15® 0.1%, w/v (**green**) and ucb-35440-3 5%, Mannitol 5%, Methocel E15® 0.1%, w/v (**blue**)) and of the spray-dried processed suspension (ucb-35440-3 5%, Methocel E15® 0.1%, w/v (**pink**) and ucb-35440-3 5%, Mannitol 5%, Methocel E15® 0.1%, w/v (**brown**)).**Table IV 2 8.** Data for Figure IV 2 26 (size in  $\mu\text{m}$ ) (FD: Freeze-drying / SD: Spray-drying).

	$d(0.1) \pm \text{SD}$	$d(0.5) \pm \text{SD}$	$d(0.9) \pm \text{SD}$	$D[4,3] \pm \text{SD}$	$\text{span} \pm \text{SD}$
<b>Before water-removal</b>	<b>0.082 <math>\pm</math> 0.004</b>	<b>0.202 <math>\pm</math> 0.019</b>	<b>1.14 <math>\pm</math> 0.02</b>	<b>0.482 <math>\pm</math> 0.019</b>	<b>5.27 <math>\pm</math> 0.48</b>
<b>FD - no mannitol</b>	<b>89.8 <math>\pm</math> 2.7</b>	<b>34.6 <math>\pm</math> 2.0</b>	<b>221.8 <math>\pm</math> 10.1</b>	<b>112.2 <math>\pm</math> 3.7</b>	<b>2.08 <math>\pm</math> 0.09</b>
<b>FD - mannitol</b>	<b>0.101 <math>\pm</math> 0.001</b>	<b>1.06 <math>\pm</math> 0.04</b>	<b>2.79 <math>\pm</math> 0.07</b>	<b>1.22 <math>\pm</math> 0.04</b>	<b>2.62 <math>\pm</math> 0.06</b>
<b>SD - no mannitol</b>	<b>4.07 <math>\pm</math> 0.24</b>	<b>1.65 <math>\pm</math> 0.06</b>	<b>14.5 <math>\pm</math> 3.1</b>	<b>11.0 <math>\pm</math> 1.8</b>	<b>3.13 <math>\pm</math> 0.60</b>
<b>SD - mannitol</b>	<b>0.097 <math>\pm</math> 0.005</b>	<b>1.06 <math>\pm</math> 0.11</b>	<b>2.83 <math>\pm</math> 0.11</b>	<b>1.24 <math>\pm</math> 0.08</b>	<b>2.61 <math>\pm</math> 0.18</b>

As we can clearly see from the data presented in **Figures IV 2 25** and **IV 2 26**, the presence of mannitol in the formulation is highly beneficial in preventing drug nanoparticle agglomeration and in enhancing their redispersion characteristics. For NIF, the original particle size distribution (i.e. before spray-drying) is almost restored and, contrary to the mannitol-free formulation which was characterized by less than 1% (in volume) of submicron particles, the obtained population is characterized by 80% (in volume) of submicron particles (86% before spray-drying). For ucb-35440-3, although redispersed powders do not yield a particle size distribution that comes close

to what was observed before either freeze- or spray-drying, redispersion characteristics are nevertheless better with the presence of mannitol in the formulation. In fact, as the particle size distribution for the mannitol-free formulation was characterized by less than 2% (in volume) of submicron particles, approximately 50% (in volume) of submicron particles were retrieved in the presence of mannitol either for freeze-dried or spray-dried powders; practically no differences were found in this case between the two water-removal techniques.

As it will be seen in **part IV.4** of this work, these redispersion characteristics for ucb-35440-3 nanoparticles can be further enhanced by the addition of other types of carriers to the formulation. Here we will present the influence of the addition of a water-insoluble carrier such as Emcompress® ( $\text{CaHPO}_4 \cdot 2\text{H}_2\text{O}$ ) to the formulation. This type of carrier acts differently than mannitol: here, the large particles of the carrier (mean volume diameter around 100  $\mu\text{m}$  - **Figure IV 2 27**) are used as an insoluble matrix to which nanoparticles will adhere. This can clearly be seen on the SEM micrographs taken for an Emcompress®-containing ucb-35440-3 suspension - **Figure IV 2 28**. Mapping analyses, represented as well on **Figure IV 2 27**, also clearly indicate the homogeneous distribution of ucb-35440-3 nanoparticles on the surface of Emcompress® particles (mapping analyses were used in this case to discriminate between the calcium of Emcompress® and the chloride of ucb-35440-3). The presence of Emcompress® in the formulation is also very useful for decreasing the powder density and thus for possibly enhancing the rheological properties (flow properties) of the formulation obtained. No LD analyses regarding the redispersion characteristics of this formulation were retrieved due to the limited solubility of the Emcompress® in the dispersing media (no possible discrimination between ucb-35440-3 nanoparticles and the carrier's particles). Other types of additives can also be added in the formulations to further enhance the dispersion characteristics of freeze- or spray-dried nanosuspensions. Cross-linked PVP (super-desintegrant) was used in that regard and results for this formulation will be given in **part IV.4.3.2.2.2**.

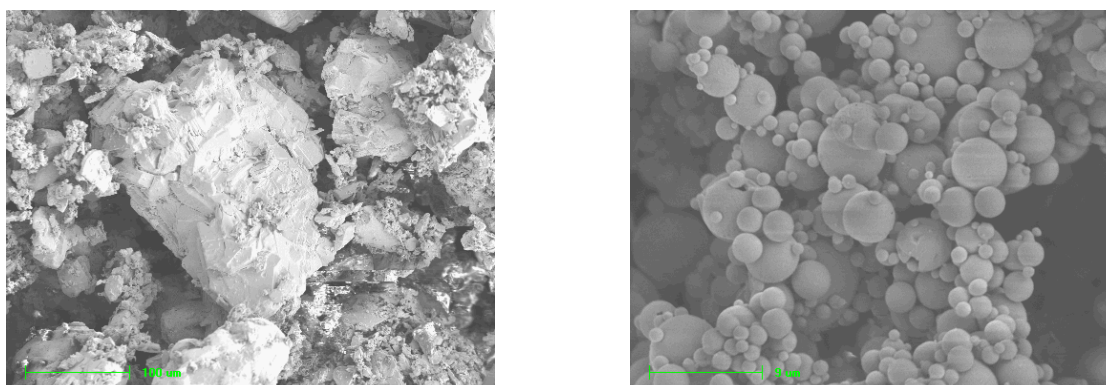


**Figure IV 2 27.** SEM micrographs of a spray-dried Emcompress® suspension (magnification 250X: right – scale = 100  $\mu\text{m}$ ) and of a spray-dried mannitol solution (magnification 3000X: left – scale = 9  $\mu\text{m}$ ).

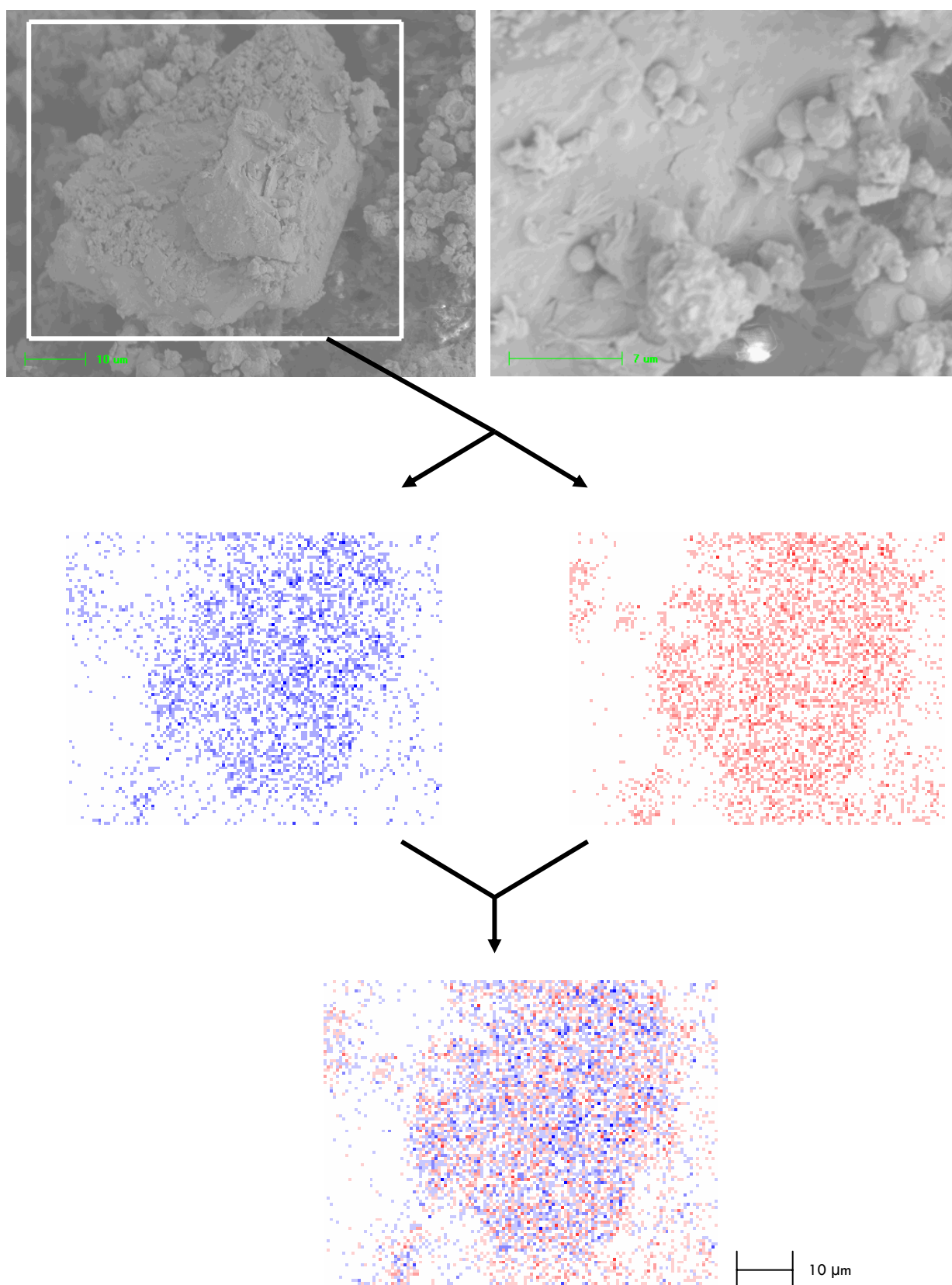


**Figure IV 2 28.** SEM micrographs of a spray-dried ucb-35440-3 5%, Mannitol 5%, Emcompress® 5%, acaciae gum 0.1% w/v suspension (**top left** - magnification 1500X - scale = 10 µm) and **top right** (magnification 4000X - scale = 7 µm). Mapping analysis (SEM-EDS) shows the calcium in blue and the chloride in red.

Investigation relative to the ucb-35440-3/Emcompress<sup>®</sup> formulation was complemented by PXRD analysis (**Figure IV 2 29**) and compared to diffractograms of spray-dried mannitol and Emcompress<sup>®</sup>. This analysis was made to evaluate the crystalline state of the various carriers of the formulation. PXRD diffractograms show that both carriers of the formulation, and as well ucb-35440-3, are crystalline and that most peaks for the individual components are found in the mixed formulation. These observations are very interesting as this crystalline state (particularly ucb-35440-3 and mannitol) should be advantageous regarding the stability of the formulation. The same remark can be made for mannitol-containing NIF formulations.

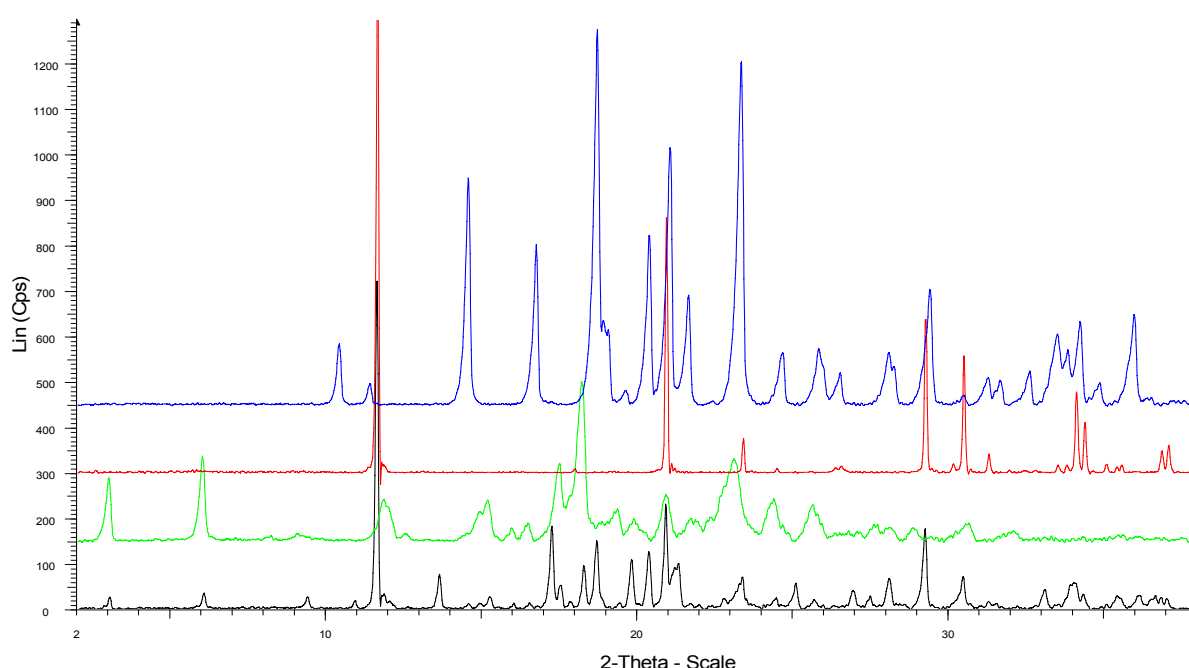


**Figure IV 2 29.** PXRD analysis: spray-dried mannitol solution (**blue**), spray-dried Emcompress<sup>®</sup> suspension (**red**), ucb-35440-3 (as received) (**green**) and spray-dried ucb-35440-3 5%, Mannitol 5%, Emcompress 5%, Acaciae gum 0.1% suspension (% expressed w/v) (**black**).

Although these carriers, be they water-soluble or water-insoluble, offer a real positive influence regarding enhancement of the redispersion characteristics of freeze-dried or spray-dried nanosuspensions, their presence might sometimes be quite problematic as their concentration is not negligible, especially for highly-dosed drugs where minimization of excipients used is necessary for further formulation development. Concentrations for NIF formulations could eventually be lowered although it is not much of a concern for NIF as the usual doses are quite low (IRDF of NIF doses at 10 mg) but might not be for ucb-35440-3.

As for UCB-A, the reported positive influence of mannitol on spray-dried nanosuspension redispersion characteristics was not observed as these characteristics were already very good in the absence of the water-soluble carrier. This observation was noted for all UCB-A tested formulations. LD results for this evaluation are shown in **Figure IV 2 30**.

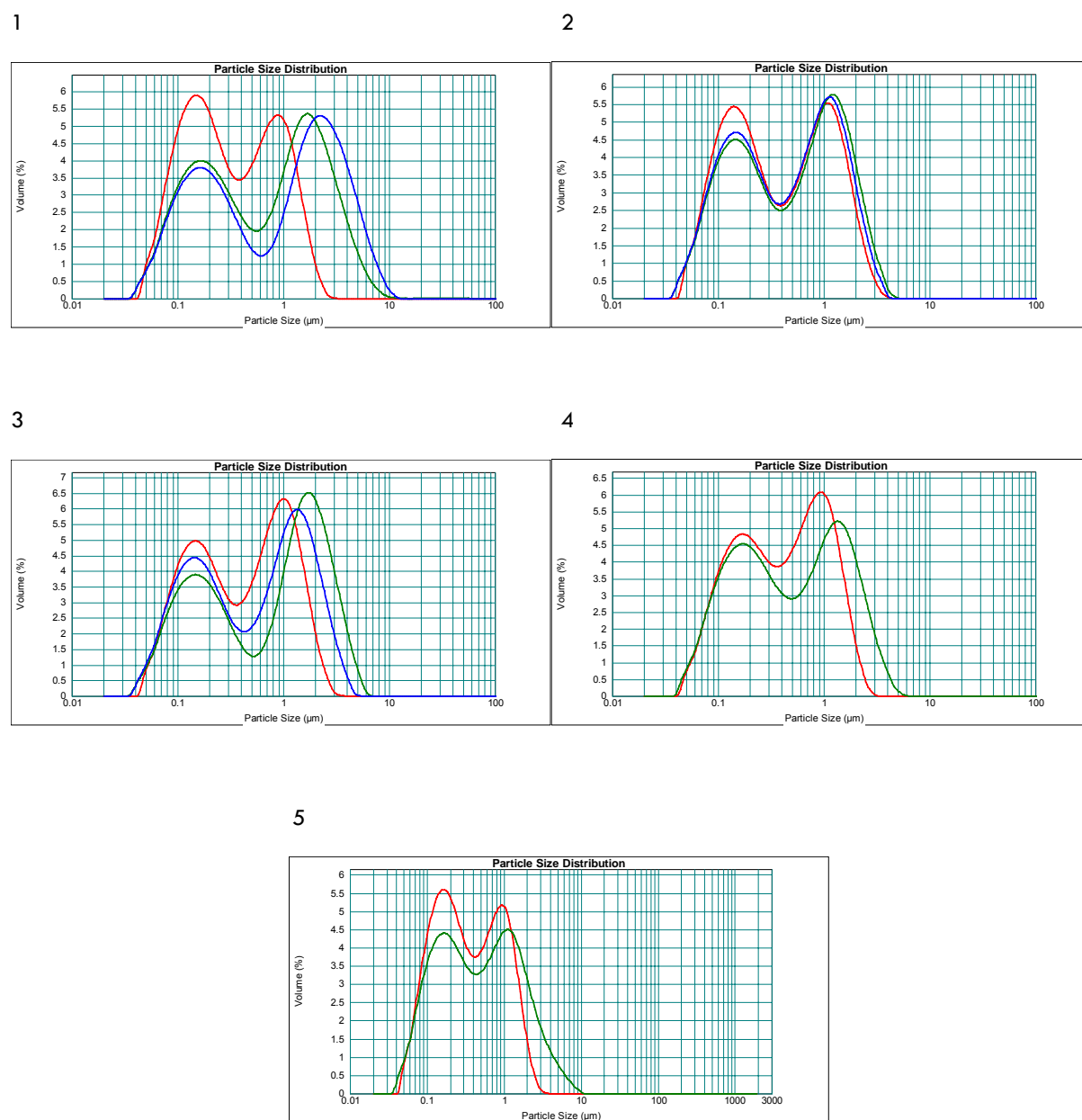


**Figure IV 2 30.** LD size distribution curves following sample processing (PMC + 20C 23-24000 PSI + 10C 30000 PSI (for 4 and 5 only)) (red) and following redispersion of the spray-dried processed suspension in absence of mannitol (green) and presence of mannitol (100% w/w relative to UCB-A content) (blue): (1) UCB-A 2%, SDS 2%, w/v; (2) UCB-A 2%, Methocel E15® 0.5%, SDS 0.06%, w/v; (3) UCB-A 2%, Methocel E15® 0.5%, Poloxamer 407 1%, w/v; (4) UCB-A 5%, Methocel E15® 0.5%, SDS 0.1%, w/v and (5) UCB-A 5%, Methocel E15® 0.5%, Poloxamer 407 0.25%, w/v. Data reported in annex 1 (**Table A14**).

When looking at the results presented in **Figure IV 2 30**, we can see that the redispersion characteristics of the spray-dried UCB-A nanosuspensions are quite good and that, except for formulation F1, the initial particle size distributions are practically restored. Furthermore, mannitol seems to have very little influence when considering minimization of particle reagglomeration as agglomeration in the absence of mannitol is, apparently, limited. When considering these results, in combination to the fact that UCB-A is a projected highly dosed drug and that minimization of formulation additives is certainly necessary for further formulation development, mannitol does not need to be added to UCB-A nanosuspensions prior to spray-drying (as it is the case for formulations F4 and F5 and as it will be further discussed, for the preparation of the only tested UCB-B formulation).

In addition to the fact that the original particle size distribution is practically restored following redispersion of the spray-dried nanosuspensions, the rate of this redispersion was found to be very fast. In fact when compared to micronized UCB-A (where the powder is found to be totally un-wetted when placed in surfactant-free water), UCB-A nanoparticle formulations spontaneously go in suspension (without stirring). Although the surfactants present in the formulations studied certainly influence UCB-A's wettability (modifications in surface properties), as in the case of formulation F1 where SDS is found in an equivalent concentration to UCB-A, this observation was made for all four formulations, with the surfactant concentration in F4 and F5 (i.e. SDS 2% and poloxamer 407 5% w/w relative to UCB-A content) being greatly reduced when compared to the other three formulations. Representation of this observation is shown on **Figure IV 2 31**.

Although it is here applied to UCB-A, the observation made and represented in **Figure IV 2 31** can also be made for NIF and ucb-35440-3 as the freeze- or spray-dried powders of these drugs also present very rapid redispersion characteristics.

Redispersion characteristics of the only tested UCB-B formulation, although similar, in composition, to the UCB-A formulation F5 shown in **Figure IV 2 30**, were not good. LD results for this evaluation are shown in **Figure IV 2 32**. Mannitol might have a positive influence with regard to the drug redispersion characteristics, as it has been shown for NIF and ucb-35440-3, but was not tested on this drug.

Although there is certainly a significant decrease in the specific surface area enhancement achieved by nanosizing the tested drugs due to this particle agglomeration,, it is believed, as for NIF and ucb-35440-3 mannitol-free formulations, that these are large agglomerates of drug nanoparticles which certainly present quite high porosity.

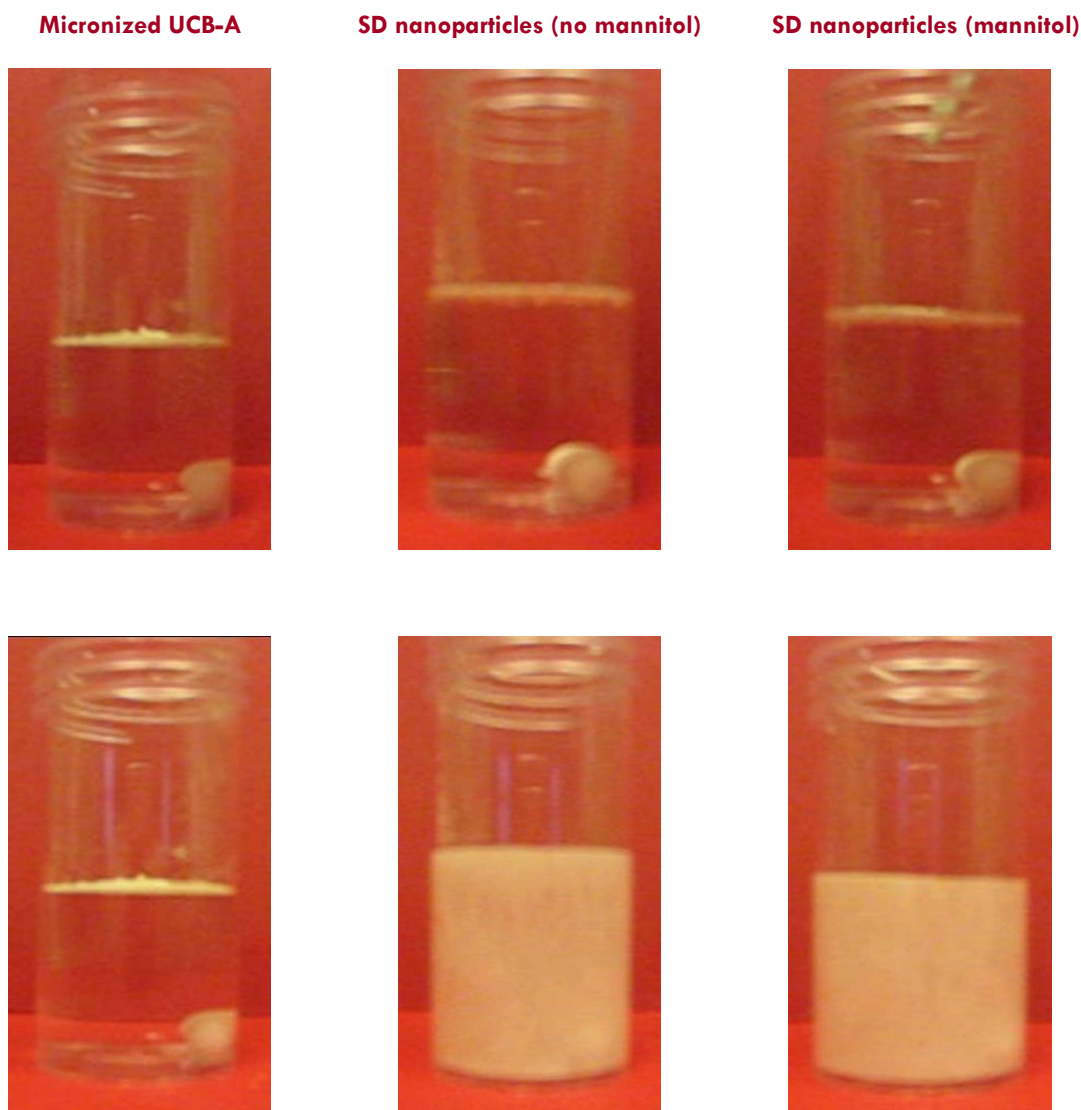


**Figure IV 2 31.** Observation of redispersion characteristics (surfactant-free deionized water – no stirring) for UCB-A micronized drug and UCB-A nanoparticles (SD formulation F3): Time 0 second (top) and 30 seconds (bottom). These observations were similar for all the tested UCB-A suspensions (F1, 2, 3, 4 and 5).

In this case, not all the benefits from increased surface area would be lost through particle agglomeration. In fact, as it will be shown in **part IV.4**, these agglomerated nanoparticles also show, although to a lesser extent than well redispersed powders (i.e. with mannitol), better dissolution characteristics than the un-milled or micronized drugs.

From all the data presented in this section, we can see that no possible generalizations can be drawn regarding drug nanoparticle redispersion characteristics (influence of mannitol: NIF, ucb-35440-3 and UCB-B vs. UCB-A). These characteristics and their possible optimization have to be evaluated on a case-by-case basis. The use of carriers, although clearly beneficial regarding particle agglomeration prevention, might see limitations when considering the formulation development of highly-dosed drugs.



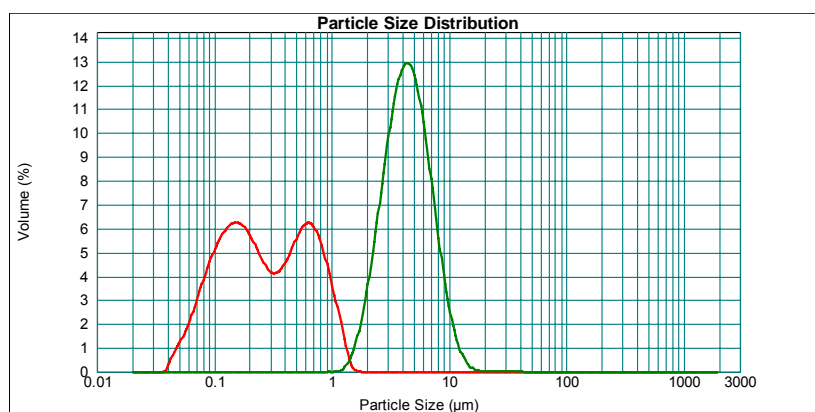


**Figure IV 2 32.** LD size distribution curves following sample processing (PMC + 20C 23-24000 PSI + 10C 30000 PSI (**red**) and following redispersion of the spray-dried processed suspension in absence of mannitol (**green**): UCB-B 5%, Methocel E15® 0.5%, Poloxamer 407 0.25%, w/v. Data reported in annex 1 (**Table A15**).

#### IV.2.3.6. Chemical stability

Drug chemical stability following the high pressure homogenization operation and, when necessary, following other processes such as water removal operations from the nanosuspensions (particularly spray-drying for heat sensitive drugs) is another critical parameter to assess, in particular for labile drugs. This evaluation was made using ucb-35440-3 as a model as it is reported to be relatively labile under stress conditions such as temperature. Although sample temperature is maintained at approximately 10°C throughout the homogenization process, ucb-35440-3 chemical stability following the high pressure operation had to be assayed in order to denote any possible product degradation that might be associated with the particle size reduction process.

Chemical stability was, at first, assayed on a freeze-dried ucb-35440-3 nanosuspension (ucb-35440-3 5%, HPMC 0.1% (w/v) following PMC and 20 cycles at 23-24000 PSI). In this case, freeze-drying was the only step, other than high pressure homogenization, that was conducted on ucb-35440-3. As this water-removal operation was not thought to be a cause of product degradation, the results obtained yielded stability information relative to the homogenization process only. A chromatograph of the un-processed un-milled drug using the chromatographic purity method UCB M1 is shown in **Figure IV 2 33 A**. A chromatograph of a freeze-dried nanosuspension using the same method is shown in **Figure IV 2 33 B**.

As described in this chromatographic purity HPLC method (UCB M1), results are calculated as area percent, taking the total area of peaks as 100% and impurities above 0.1% being reported. On the chromatograms obtained, be it for un-milled ucb-35440-3 or ucb-35440-3 nanoparticles, one major peak could be observed for each run (three runs for each sample yielding equivalent results) at a retention time of approximately 8.3-8.4 min and one minor peak at a retention time of about 11-12 min (**Table IV 2 9**) . This latter peak was found to be above the 0.1% limit over which impurities have to be reported, but it was also found in the un-milled product coming from the sponsor.

Since chromatograms for un-milled ucb-35440-3 and homogenized ucb-35440-3 were found to be nearly identical and since no other major peaks could be found in the chromatograms for the homogenized ucb-35440-3, we can assume that the high pressure homogenization process does not cause any product degradation.

The same evaluation was carried out on an equivalent suspension following spray-drying. In fact, as ucb-35440-3 is heat-sensitive, chemical stability also needs to be verified following this operation if it is to be used (a spraying temperature of 115°C being used). A representative chromatograph of a spray-dried nanosuspension using the chromatographic purity method UCB M1 is shown in **Figure IV 2 33 C**.

Here again, the same observations that were reported for the freeze-dried nanoparticle can be made relative to the un-milled ucb-35440-3, letting us assume that no product degradation occurs during the spray-drying process (at least at the temperature used). These conclusions are only applied to the chemical stability of ucb-35440-3 as chiral purity following the high pressure homogenization operation and the spray-drying operation were not assayed.

The chemical stability of NIF, UCB-A and UCB-B were not directly assayed using appropriate chromatographic purity HPLC methods. However, during the many in vitro-in vivo characterizations of the respective drug formulations (stability study for NIF, degradation into UCB-A-Met1 for UCB-A and UCB-B, etc.), no particular degradation products were observed (considering mainly photodegradation products for NIF and UCB-A-Met1 for UCB-A).

We can thus conclude that, at least when using the homogenizing protocol described in **part IV.2.2.2.3.2** of this chapter (primarily with the control of the processing temperature), high pressure homogenization does not seem to cause any product degradation. This evaluation should of course be carried out on a case-by-case basis.

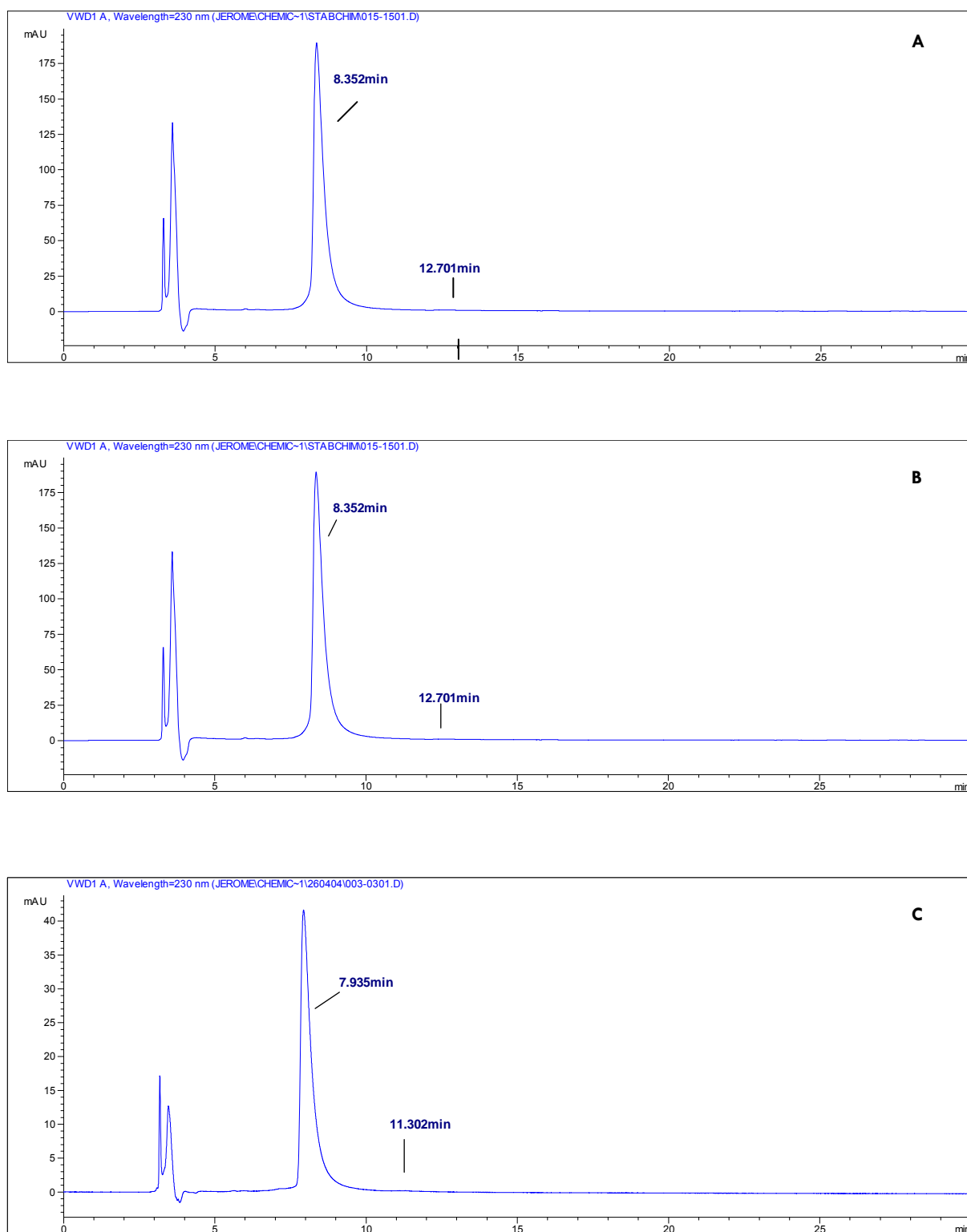


**Figure IV 2 33.** Representative chromatographic purity (UCB M1) HPLC chromatograms: un-milled ucb-35440-3 (A), freeze-dried ucb-35440-3 5%, HPMC 0,1% w/v nanosuspension (PMC + 20C 23-24000 PSI) (B) and spray-dried ucb-35440-3 5%, HPMC 0,1% w/v nanosuspension (PMC + 20C 23-24000 PSI) (C). (about 5 mg ucb-35440-3/ml).

**Table IV 2 9.** Values for Figure IV 2 33 A/B/C.

		<b>% area of peak at 11-12min RT (relative to ucb-35440-3 peak)</b>
		<b>Mean <math>\pm</math> SD (n=3)</b>
	un-milled ucb-354440-3	<b>0.36 <math>\pm</math> 0.04</b>
	freeze-dried nanosuspension	<b>0.29 <math>\pm</math> 0.11</b>
	spray-dried nanosuspension	<b>0.32 <math>\pm</math> 0.10</b>

#### IV.2.4. Conclusion

From the results presented in this chapter, we can conclude that high pressure homogenization is a technique that has been successfully used for particle size reduction to nanometer range for all four tested model drugs. In fact, NIF, ucb-35440-3, UCB-A and UCB-B have seen their particle size ( $d(v, 0.5)$ ) decrease from 100  $\mu\text{m}$  to 290 nm, from 140  $\mu\text{m}$  to 180 nm, from 3  $\mu\text{m}$  to 350 nm and from 7  $\mu\text{m}$  to 250 nm following HPH processing, respectively.

Pre-milling operations were shown to be important, necessary steps prior to the high pressure homogenizing cycles. Other than for homogenizing reasons (i.e. suspension preparation), the Turrax<sup>®</sup>-milling operation was only shown appropriate, considering drug particle size reduction, for particle populations characterized with mean diameters superior to 50  $\mu\text{m}$ ; this operation having been shown to be inefficient for micronized drugs such as UCB-A and UCB-B. The pre-milling low pressure homogenizing cycles using the EmulsiFlex C5<sup>®</sup> were, however, contrarily to the Turrax<sup>®</sup>-milling operation, shown to be efficient as a preliminary size reduction step for all four tested model drugs. From the results presented in this chapter, it was also shown that the number of high pressure homogenizing cycles and the homogenizing pressure used (i.e. 23-24000 PSI and 30000 PSI) have a clear influence on particle size reduction efficiency. Sample processing temperature was also shown to be relevant regarding particle size reduction efficiency and this more so in the case of UCB-A which is characterized by temperature-dependent polymorphic transformations (i.e. which might imply varying crystal hardness).

Redispersion characteristics of the water-removed (i.e. spray- or freeze-drying) drug nanosuspensions have been shown to be relatively limited, except in the case of UCB-A, when no carriers were used in the formulations developed. These carriers, either water-soluble (e.g. mannitol) or water-insoluble (e.g. Emcompress<sup>®</sup>), were shown to limit, to some extent, nanoparticle agglomeration during the water-removal operations and are thus necessary additives in development of the formulations.

Chemical stability following high pressure homogenization was also checked and this operation was not shown to be responsible for drug degradation; this evaluation being carried out on ucb-35440-3, which was reported to be particularly labile (heat-sensitive).

It has to be noted that no specific trends were followed by the four tested model drugs, except maybe for the influence of the number of homogenizing cycles and for the homogenizing pressure applied which were both

characterized by an increased particle size reduction efficiency. The homogenizing protocol (e.g. number of cycles, pressure, temperature, etc.) and the resulting formulation characteristics (e.g. redispersion characteristics following water-removal operations) should thus be evaluated on a case-by-case basis.

### **IV.3. Crystalline state evaluation**

#### **IV.3.1. Introduction**

Crystalline state of the model drugs studied, before and after particle size reduction to nanometer range using high pressure homogenization, is an important parameter to assess. All three model drugs studied are crystalline. Furthermore, UCB-A presents particular characteristics as it undergoes reversible temperature dependent polymorphic transformations to form G (below 16°C) and to form H (above 37°C).

The original aim of this work was to maintain the drug's original crystalline state following the particle size reduction operation in order not to rely on the presence of the amorphous form, characterized by long term time instability, and only on particle size reduction (i.e. increased surface area) for the targeted solubility/dissolution enhancement of these poorly water-soluble drugs. There have been recent assumptions (Kipp, 2004; Keck and Müller, 2006) that milling processes, including piston-gap high pressure homogenizers, might lead to the formation of partially or even totally amorphous products. This chapter will show that, at least for our model drug studied, original drug crystalline state seems to be maintained following particle size reduction using high pressure homogenization.

The development and the evaluations were mainly made using NIF, using primarily DSC and PXRD. Crystalline state evaluations for ucb-35440-3, UCB-A and UCB-B were also made to complement the data observed for NIF.

#### **IV.3.2. Materials and Methods**

##### **IV.3.2.1. Differential Scanning Calorimetry (DSC)**

DSC can be used to measure any kind of phase transition, for a given compound, that is associated with heat transfer. The principle behind DSC is that two cups, placed in an oven, one containing the sample and the other

nothing (or an inert material), are heated and kept at the same temperature (**Figure IV 3 1**). Once an endothermic or an exothermic phase transition occurs within the sample, the heat flow provided to keep the two cups at the same temperature needs to be respectively increased or decreased giving thus rise to an endotherm or an exotherm.

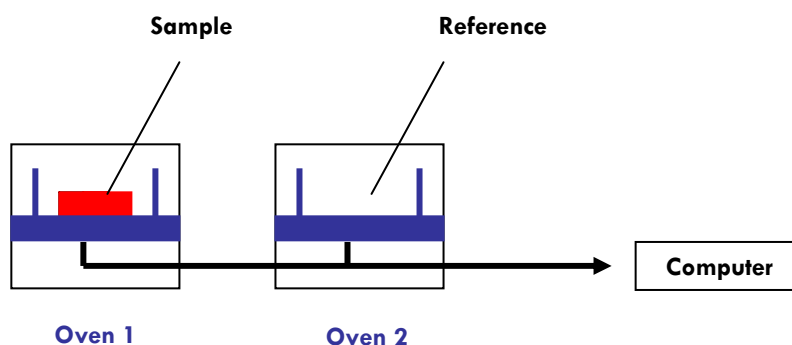


**Figure IV 3 1.** Schematic representation of a DSC apparatus (Clas et al., 2002).

DSC is a technique that is frequently used in preformulation studies in order to evaluate the crystalline state of newly developed drugs. DSC can also be used to reveal, with appropriate heat and cooling runs, the presence of different polymorphs of a given substances (e.g. UCB-A F/G/H) and to evaluate the influence of different parameters (formulation approach, production parameters, etc.) on the existence and maintain of these polymorphs or even of the amorphous form of a given compound. DSC is also frequently used to study drug/excipient interactions (complex, eutectics, etc.).

DSC was used in this research to lay out results relative to the crystalline state of the model drugs studied before and following the high pressure homogenization operation.

The DSC apparatus used was a Perkin Elmer DSC-7 differential scanning calorimeter/TAC-7 thermal analysis controller with an intracooler-2 cooling system (Perkin Elmer Instruments, USA). Temperature control was regulated in both ovens with an N<sub>2</sub> flux. The apparatus was Indium/Cyclohexane calibrated. The amount of product analyzed ranged from 3 mg to 5 mg and the sample was placed in aluminum perforated pans.



The various characterization parameters that were retrieved from the DSC thermograms include:

- **Peak temperature (°C)**
- **Onset (°C):** beginning of the endo/exotherm
- **End (°C):** end of the endo/exotherm
- **Peak area:**      Peak area (J.°C/s) = heat flux x temperature  
                                  Heat flux is the difference in heat quantity per unit of time needed by the two ovens  
                                  to keep their temperature equal (= dq/dt (J/s)).
- **Enthalpy (ΔH):**    ΔH (J/g) = peak area / (heating rate x sample weight)

#### IV.3.2.2. Powder X-Ray Diffraction (PXRD)

Powder X-ray diffraction (PXRD) is another powerful and widely used tool for crystalline state evaluation. X-rays are part of the electromagnetic spectrum lying between ultraviolet and gamma rays (wavelength expressed in Angstrom units - 0.01 to 100 Å). When X-rays are incident on a crystalline sample, they are scattered in all directions (scattering occurring due to the radiation wavelength being of the same order of magnitude as the interatomic distances within the crystal structure) and in some of these directions, the scattered beams are completely in phase and reinforce one another to form the diffracted beams (Suryanarayanan and Rastogi, 2002). As defined by Bragg's Law, diffraction will occur if a perfectly parallel and monochromatic X-ray beam, of wavelength  $\lambda$ , is incident on a crystalline sample at an angle  $\theta$  that satisfies the Bragg equation :

$$n\lambda = 2 d \sin \theta$$

$n$  = order of reflection (= an integer usually 1)  
 $\lambda$  = wavelength of X-ray  
 $d$  = distance between planes in crystals  
 $\theta$  = angle of incidence / reflection

The PXRD pattern, also called the diffractogram, consists of a series of peaks collected at different scattering angles (graph of scattering intensity vs.  $2\theta$ ). If the sample is amorphous (no long range order), then X-rays are not coherently scattered and no peaks can be observed.

The PXRD apparatus used was a Siemens Diffractometer D5000 (Siemens, Germany) (Cu radiation –  $WL1 = 1,5406 \text{ \AA}$ ,  $WL2 = 1,54439 \text{ \AA}$ ). Standard procedure was generally followed for the various model drugs analyzed:

- Voltage 40kV
- Current 40mA
- $2\theta$  range of 3 to  $40^\circ$
- Scanning rate  $0.02^\circ/\text{min}$

#### **IV.3.2.3. Polarized-light optical microscopy**

Optical microscopy analysis were conducted on an Olympus-BX 60 microscope (Olympus – Nihon Kodan, Japan) (magnification 5 up to 100 times) equipped with a JVC TK-C1381 colour video camera (JVC, Japan). A U-POT Polaroid filter was used for light polarization.

#### **IV.3.2.4. Hot Stage Microscopy (HSM)**

Hot stage microscopy (HSM) is a technique that combines the information retrieved by optical microscopy and calorimetric analysis (e.g. DSC). This technique allows the visualization of the temperature-dependent phase transition occurring in a sample (fusion, crystallization, etc.). Multiple heat and cooling runs can be applied to the studied sample.

Although HSM cannot be used for the characterization of drug nanoparticles (phenomenon linked to the limitation of the optical microscope used - microparticles (2-5 $\mu$ m) being already barely visualized), it yields very informative complementary data regarding phase transitions of the model drug studied.

The HSM was conducted using a Linkam THMS 600 hot stage (Linkam Scientific Instruments, Waterfield, United Kingdom) coupled to a temperature module Linkam LNP/TMS 94 (Linkam Scientific Instruments, Waterfield, United Kingdom). The apparatus was linked to an Olympus-BX 60 microscope (Olympus – Nihon Kodan, Japan) equipped with a JVC TK-C1381 colour video camera (JVC, Japan). Data was recorded using the Olympus Microlmage v4.0 software (Olympus – Nihon Kodan, Japan). Samples can be cooled using a liquid nitrogen inlet.

### IV.3.3. Results and discussion

#### IV.3.3.1. Nifedipine

##### IV.3.3.1.1. Identification of various polymorphic forms of NIF through Differential Scanning Calorimetry (DSC)

It is well known that variation of the polymorphic forms of a particular drug substance can alter chemical and physical stability (in our concern – solubility) due to altered reactivity (Ford and Timmins, 1989). Crystalline state evaluation, i.e. search for evidence of polymorphism, is thus very important to carry out, be it before and following the particle size reduction process used.

Three NIF polymorphs (Form I, II and III) have already been described in literature (Keymolen et al., 2002). These were re-identified in our laboratory through DSC measurements. Polymorphic form I present a melting peak at around 172°C, polymorphic Form II at around 163°C and polymorphic Form III at around 140°C. These can be revealed through DSC scans by varying the heating rate of the sample after rapid cooling (25°C/min → 0°C) from a melted sample – the melted sample being represented by the orange curve on **Figure IV 3 2** (heating rate: 5°C/min). DSC curves showing the three NIF polymorphic forms are represented in **Figure IV 3 2**. Initially, a sample of crystalline NIF was heated from 30°C to 185°C at a heating rate of 5°C/min (orange curve). We can clearly see through this run that NIF is present as polymorphic form I (i.e. highest stable polymorphic form). In a first study, rapid cooling of the melted sample obtained above (25°C/min: 185°C → 0°C) was carried out followed by an heating run (5°C/min: 0°C → 185°C) (green curve). This run allowed for the visualization of NIF polymorphic form II (polymorphic form I also visualized). The next evaluation consisted, as above, to proceed to another heating run after rapid cooling from the melted sample (same cooling run, i.e. 25°C/min: 185°C → 0°C). In this case, the sample was re-heated from 0°C to 100°C at 5°C/min (with a holding time of 10 min) and then from 100°C to 185°C at 25°C/min (blue curve). This run allowed for the visualization of NIF polymorphic form III (polymorphic form I also visualized). NIF polymorphic form III is hard to observe as it is relatively unstable and as during heating, it is probably transformed to polymorphic forms I or II.

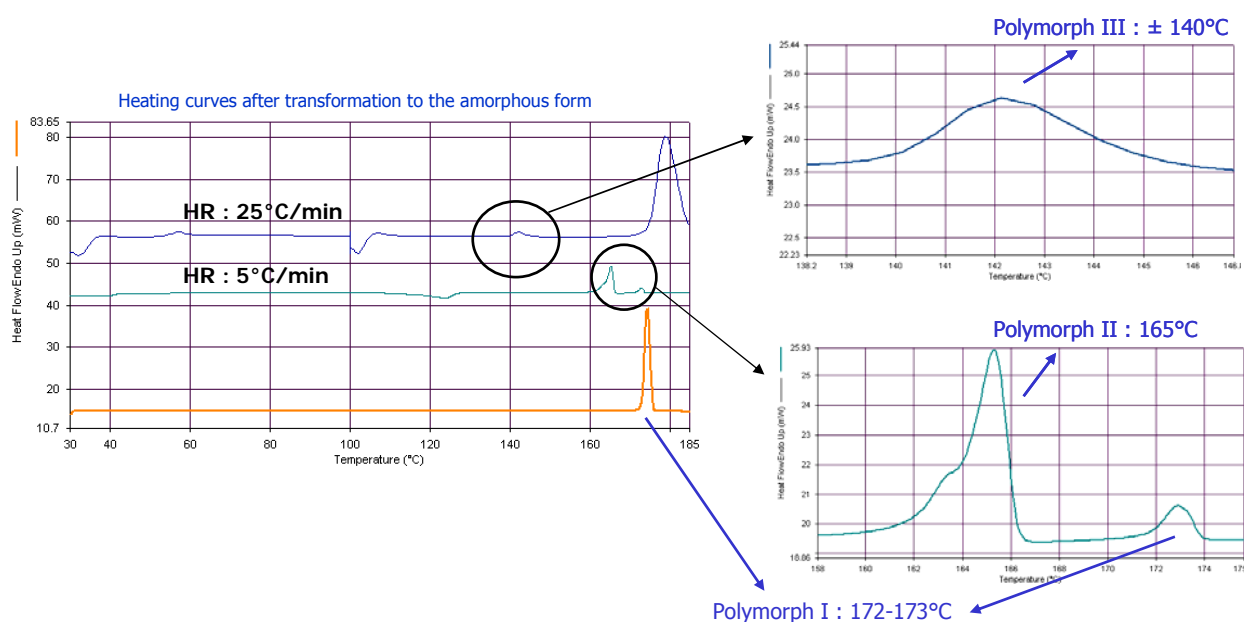


**Figure IV 3 2.** DSC identification of NIF polymorphs I, II and III (analysis of un-milled commercial NIF).

#### IV.3.3.1.2. Evaluation of drug crystalline state following particle size reduction - DSC

Evaluation of the crystalline state of the NIF nanoparticulate formulations through DSC analyses was carried out using heat runs going from 40°C to 200°C at a heating rate of 5°C/min. Comparisons with the unprocessed un-milled drug and along with the excipients used in the formulations were made. Physical mixtures of un-milled NIF and the excipients used in formulation development were also used as comparisons. Finally, comparisons with a Turrax<sup>®</sup> milled suspension (d(v,0.5) 15 µm versus 100 µm for un-milled NIF) and with a spray-dried un-milled NIF HPMC containing suspension were also made. All these evaluations are shown in **Figure IV 3 3**.

As it can be seen on the DSC curves of **Figure IV 3 3**, both NIF un-milled commercial product and NIF nanoparticles are present as polymorphic form I. The peaks were found to be nearly identical, with a calculated Delta H around 110 J/g for both un-milled NIF and NIF nanoparticles. The only differences observed were a slight shift in melting temperature (174°C to 173°C) and a broadening of the peaks. These modifications were attributed to the presence of HPMC as we can clearly see on the other DSC curves (**Figure IV 3 3 - D and E**). These differences were further enhanced in the presence of mannitol (**Figure IV 3 3 - J and K**), where the dilution of NIF particles was even higher. The physical properties of the spray-dried powders (i.e. NIF nanoparticles) are also responsible for this peak broadening. In fact, the spray-dried nanoparticles show a very low density, which is responsible for a decreased heat conduction throughout the studied sample.

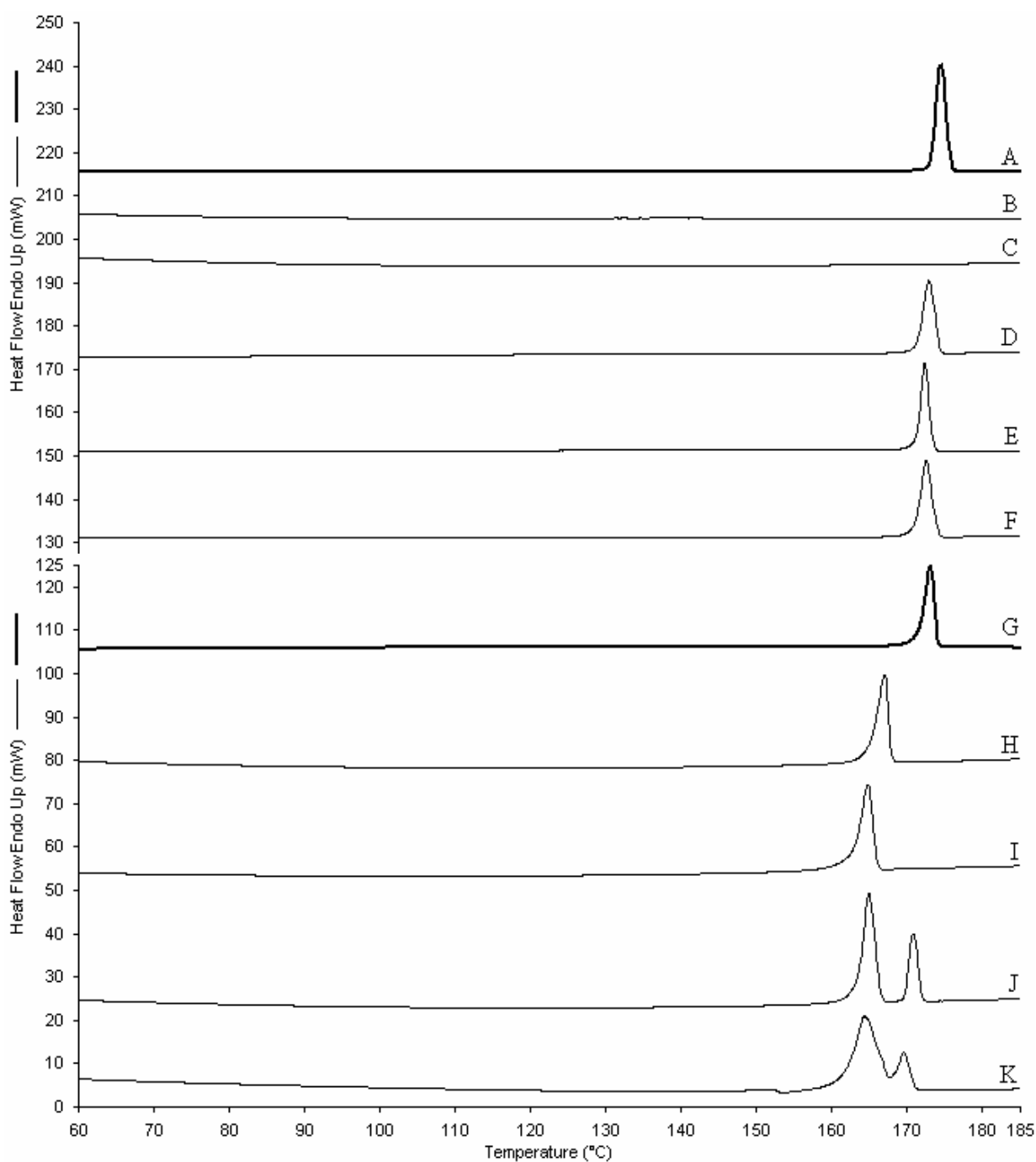


**Figure IV 3 3.** DSC curves for: **(A)** un-milled commercial NIF; **(B)** Methocel E15<sup>®</sup>; **(C)** Spray-dried Methocel E15<sup>®</sup>; **(D)** NIF/Methocel E15<sup>®</sup> 10:1 w/w physical mixture (mortar); **(E)** Spray-dried NIF 5%, Methocel E15<sup>®</sup> 0.5% w/v suspension (no-milling); **(F)** Spray-dried NIF 5%, Methocel E15<sup>®</sup> 0.5% w/v suspension (Turrax<sup>®</sup> milling); **(G)** Spray-dried NIF 5%, Methocel E15<sup>®</sup> 0.5% w/v suspension (HPH - nanoparticles); **(H)** Mannitol; **(I)** Spray-dried Mannitol; **(J)** NIF/Methocel E15<sup>®</sup>/Mannitol 10:1:10w/w physical mixture (mortar) and **(K)** Spray-dried NIF 5%, Mannitol 5%, Methocel E15<sup>®</sup> 0.5% w/v suspension (HPH - nanoparticles).

The preliminary particle size reduction operation using Turrax® milling (pre-milling operation (**part IV.2.3.2**) un-milled NIF: d(v,0.5) 100 µm → Turrax® milled NIF: d(v,0.5) 1.5 µm) (**Figure IV 3 3 - F and G**) was not shown to have any influence.

From the observations made in **Figure IV 3 3**, we can conclude that high pressure homogenization does not interfere with the original crystalline state of NIF. This statement can further be confirmed by crystalline state analysis by X-ray diffraction (**part IV.3.3.1.3**)

#### IV.3.3.1.3. Evaluation of drug crystalline state following particle size reduction - PXRD

Evaluation of the crystalline state of the NIF nanoparticulate formulations was also carried out using powder X-ray diffraction (PXRD). Comparisons with the unprocessed un-milled drug and along with the excipients used in the formulations were made. Physical mixtures of un-milled NIF and the excipients used in formulation development were also used as comparisons. And finally, comparisons with a Turrax® milled suspension (d(v,0.5) 1.5 µm versus 100 µm for un-milled NIF) and with a spray-dried un-milled NIF HPMC-containing suspension were also made. All these evaluations are shown in **Figure IV 3 4**.

The PXRD patterns of **Figure IV 3 4** confirm that the high pressure homogenization operation does not interfere with NIF crystalline state as the diffraction pattern for NIF is maintained for nanoparticles. The only difference observed between un-milled NIF and NIF nanoparticles lies in peak intensities, which were found to be smaller for nanoparticles. Here again, this difference was attributed to the presence of HPMC in the formulation. As we can see on **Figure IV 3 4**, and more clearly on **Figures III 3 5** and **III 3 6**, peak intensities, when compared to the diffractograms of NIF alone, are in fact reduced for a NIF/HPMC physical mixture (**Figure IV 3 4 - F / Figure IV 3 5**) and even further reduced for a spray-dried NIF/HPMC suspension prior to milling operations (**Figure IV 3 4 - H / Figure IV 3 6**), where HPMC is thought to be more evenly distributed around NIF particles. The diffraction pattern and indeed the peak intensity for the latter was found to be nearly similar for the spray-dried NIF nanoparticles (NIF 5%, Methocel E15® 0.5% w/v SD suspension) (**Figure IV 3 4 - J / Figure IV 3 7**).

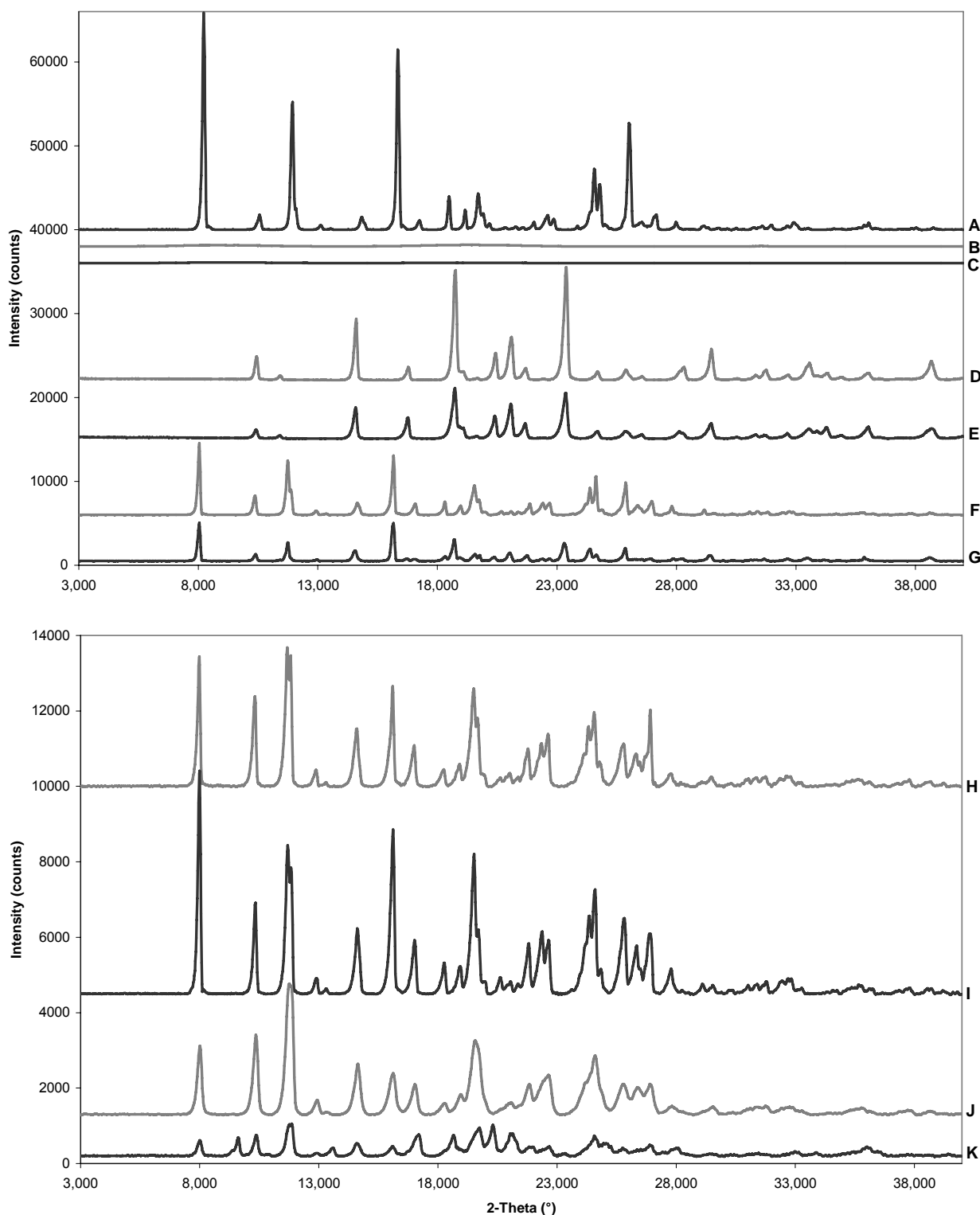


**Figure IV 3 4.** PXRD patterns for: (A) un-milled commercial NIF; (B) HPMC; (C) Spray-dried Methocel E15<sup>®</sup>; (D) Mannitol; (E) Spray-dried Mannitol; (F) NIF/Methocel E15<sup>®</sup> 10:1 w/w physical mixture (mortar); (G) NIF/Methocel E15<sup>®</sup>/Mannitol 10:1:10 w/w physical mixture (mortar); (H) Spray-dried NIF 5%, Methocel E15<sup>®</sup> 0.5% w/v suspension (no-milling); (I) Spray-dried NIF 5%, Methocel E15<sup>®</sup> 0.5% w/v suspension (Turrax<sup>®</sup> milling); (J) Spray-dried NIF 5%, Methocel E15<sup>®</sup> 0.5% w/v suspension (HPH - nanoparticles) and (K) Spray-dried NIF 5%, Mannitol 5%, Methocel E15<sup>®</sup> 0.5% w/v suspension (HPH - nanoparticles).



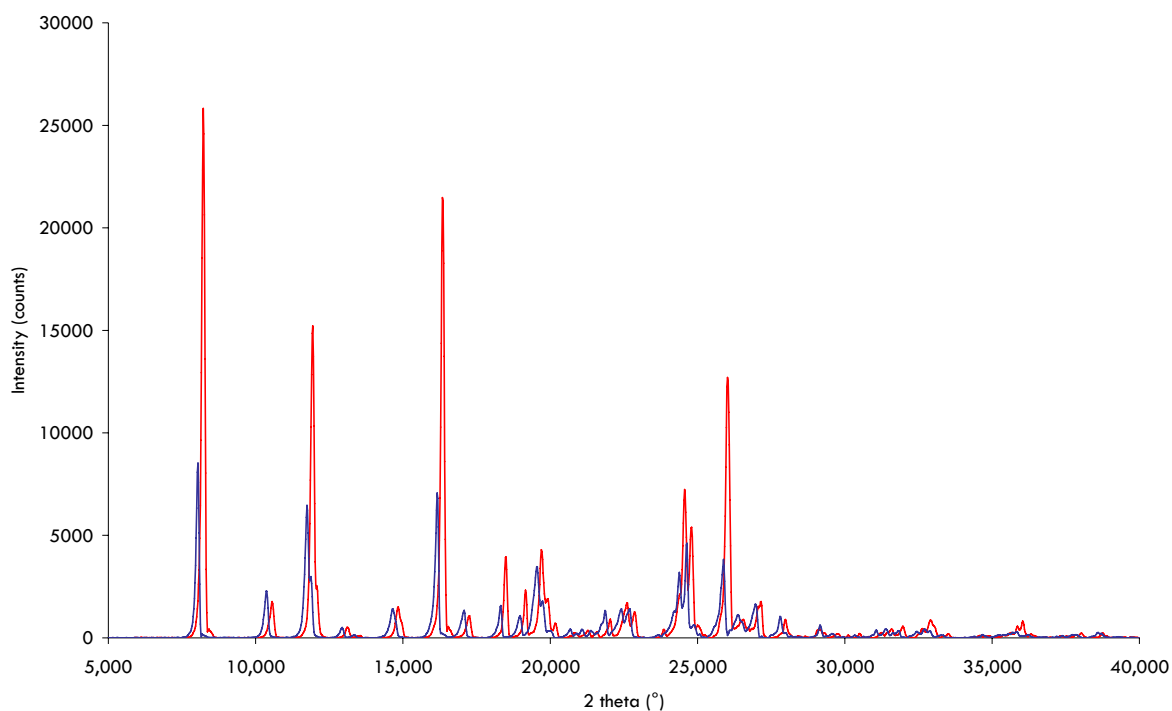


**Figure IV 3 5.** PXRD patterns for un-milled commercial NIF (as received) (**red**) and for a NIF/Methocel E15<sup>®</sup> 10:1 w/w physical mixture (mortar) (**blue**).

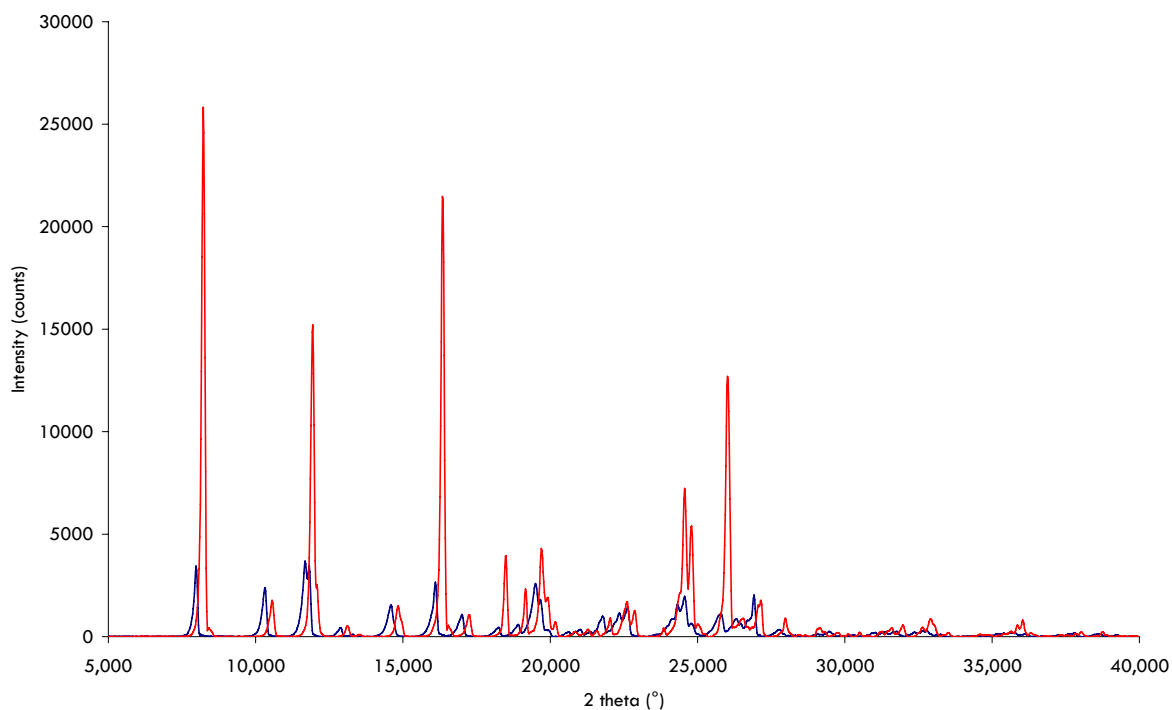


**Figure IV 3 6.** PXRD patterns for un-milled commercial NIF (as received) (**red**) and for a spray-dried NIF 5%, Methocel E15<sup>®</sup> 0.5% w/v suspension (prior to milling operations) (**blue**).

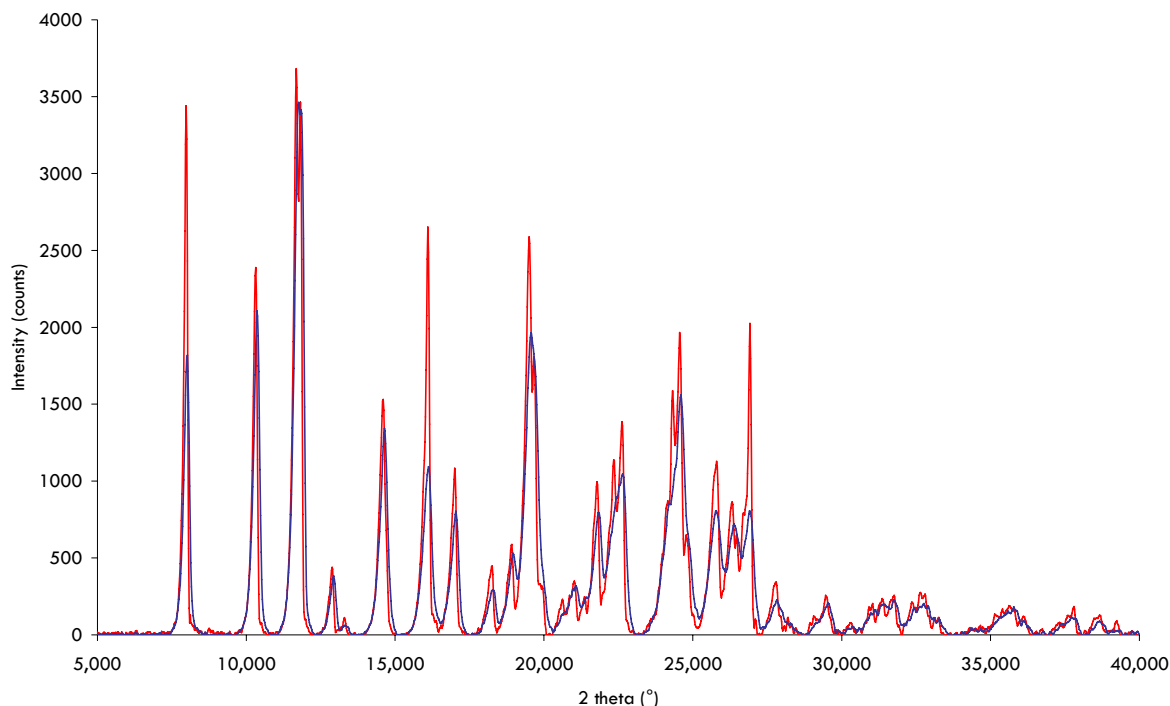


**Figure IV 3 7.** PXRD patterns for a spray-dried NIF 5%, Methocel E15<sup>®</sup> 0.5% w/v suspension (prior to milling operations) (**red**) and for a spray-dried NIF 5%, Methocel E15<sup>®</sup> 0.5% w/v suspension (HPH - nanoparticle) (**blue**).

When looking at the results in **Figures IV 3 5, IV 3 6 and IV 3 7**, HPMC has a clear influence on the reduction of peak intensity. This can be explained by the fact that HPMC, an amorphous polymer, surrounds drug particles, as it is represented in **Figure IV 8**, where SEM micrographs clearly show the morphology of obtained particles (following the high pressure homogenization operation) with an increasing percentage (w/w relative to NIF content) of HPMC. When looking at **Figures IV 3 5, IV 3 6 and IV 3 7**, this influence is progressively more pronounced as the polymer dispersion around the particles is more homogeneous (spray-dried drug particles following homogenization > spray-dried drug particles before homogenization > physical mixture). To further investigate the influence of HPMC on peak intensity reduction, diffractograms of spray-dried NIF nanosuspensions with varying HPMC percentages (% w/w relative to NIF content) were taken. The results of this evaluation are shown in **Figure IV 3 9. Table IV 3 1** shows the influence of HPMC % relative to NIF with regard to peak intensity, which is clearly shown to decrease with increasing HPMC %. These results suggest that the reduction in peak intensity is essentially due to dilution of the particles in the additives rather than from particle size reduction or any change of the polymorphic form (or presence of the amorphous form) of the active ingredient.

Investigations were carried out to evaluate the amorphous percentage present in the formulations studied and presented in **Figures IV 3 4, IV 3 5, IV 3 6 and IV 3 7**. This evaluation consisted of measuring the diffraction pattern deviation from the measured baseline. Knowing that the diffraction pattern of a totally crystalline compound presents no deviation from the baseline, the measured area (i.e. diffraction pattern vs. baseline) is thus indicative of the percentage of amorphous material in the formulation. It has to be noted that the excipients used in the formulation will, of course interfere, with this evaluation (more importantly if they are amorphous themselves) and that the reported percentages are thus not representative, in the case of the presence of these excipients, of the exact amorphous/crystalline percentage of the studied drug (i.e. NIF in our case).

Considering the studied formulations reported in **Figures IV 3 4, IV 3 5, IV 3 6 and IV 3 7**, un-milled NIF (i.e. NIF alone), the NIF/Methocel E15<sup>®</sup> 10:1 w/w physical mixture, the spray-dried NIF 5%, Methocel E15<sup>®</sup> 0.5% w/v suspension (no-milling - prior to HPH) and the spray-dried NIF 5%, Methocel E15<sup>®</sup> 0.5% w/v suspension (HPH - nanoparticles) were characterized by an amorphous percentage of 5.5%, 7.3%, 11.8% and 13.3%, respectively.

As we can see from these results, “un-milled NIF” (i.e. drug as received) is characterized by an amorphous percentage of 5.5% meaning that the drug is almost completely crystalline. This percentage was shown to increase in the presence of HPMC (amorphous polymer) and this gradually as this polymer is more evenly distributed around NIF particles. The amorphous percentage increase for the NIF/HPMC physical mixture, from NIF alone, is clearly indicative of the influence of HPMC on the estimated amorphous percentage.

When comparing the spray-dried NIF 5%, Methocel E15<sup>®</sup> 0.5% w/v suspension before and after HPH, we can assume that the high pressure homogenization and thus particle size reduction to nanometer range, is not responsible for an increase in the amorphous fraction in the formulation developed. Considering this information, we can assume that high pressure homogenization does not interfere with the processed drug original crystalline state (this statement verified in this case for NIF).

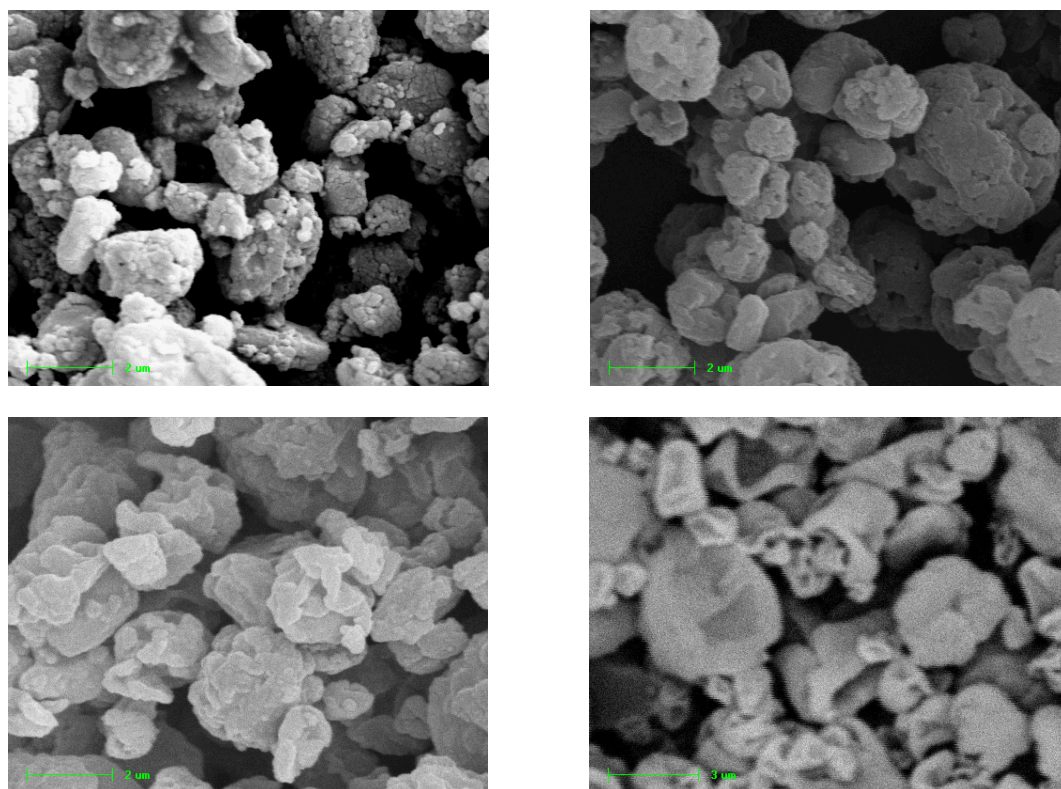


**Figure IV 3 8.** SEM micrographs of spray-dried NIF/Methocel E15<sup>®</sup> nanosuspensions (suspensions following pre-milling cycles + 20C at 23-24000 PSI) (magnification 10000X): (top left) **2% w/w** (scale=2  $\mu$ m), (top right) **10% w/w** (scale=2  $\mu$ m), (bottom left) **40% w/w** (scale=2  $\mu$ m) and (bottom right) **200% w/w** (scale=3  $\mu$ m) (% HPMC w/w relative to NIF content).

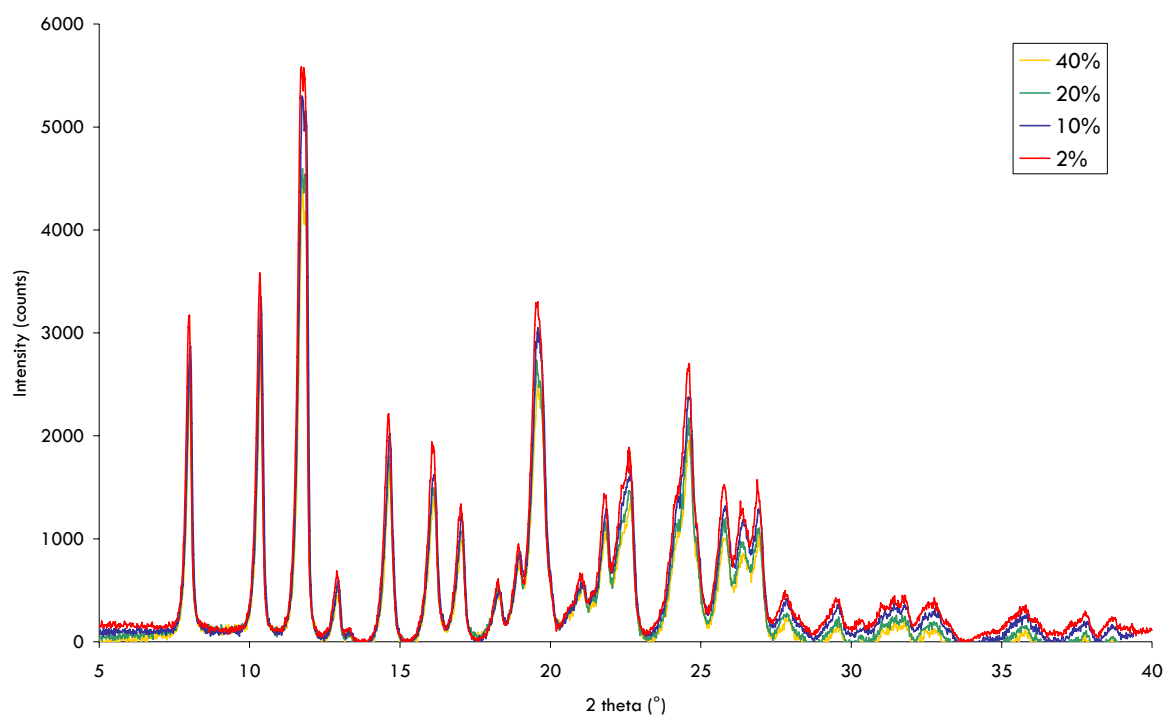


**Figure IV 3 9.** PXRD patterns for spray-dried NIF nanosuspensions (PMC + 20C 23-24000 PSI) - influence of HPMC (Methocel E15<sup>®</sup>) % (w/w relative to NIF content): 2% (**red**), 10% (**blue**), 20% (**green**) and 40% (**orange**).

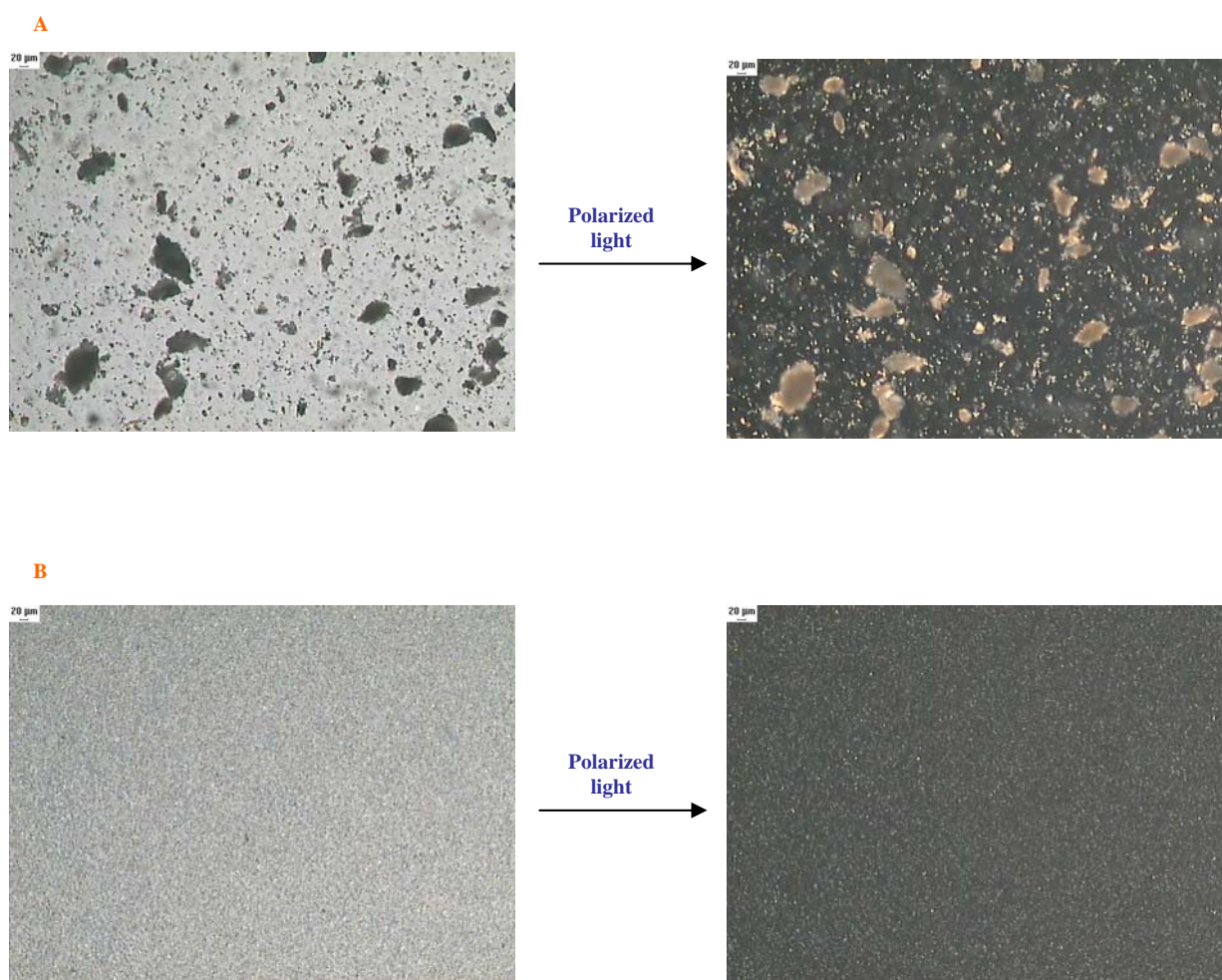
**Table IV 3 1.** Influence of HPMC % (w/w relative to NIF content) on PXRD peak intensity (counts - height) of NIF nanoparticles for given diffraction angles ( $2\theta$ ).

HPMC %	8.00°	10.34°	11.72°	14.62°	16.04°	19.58°	22.62°	24.60°
2	3171	3581	5586	2216	1703	3301	1888	2703
10	2783	2976	4950	1873	1319	3049	1600	2354
20	2687	2963	4528	1806	1294	2600	1462	2171
40	2428	2542	4144	1586	1174	2455	1278	1957

#### IV.3.3.2. ucb-35440-3

ucb-354440-3 crystalline state before and following high pressure homogenization was also evaluated in order to denote any influence of the milling operation on modifications of the original drug crystalline state. ucb-35440-3, as it can clearly be seen on **Figure IV 3 10**, comes as a crystalline powder. **Figure IV 3 10** shows optical microscopy micrographs, with and without light polarization, of un-milled ucb-35440-3 (drug as received) and a ucb-35440-3 nanosuspension.

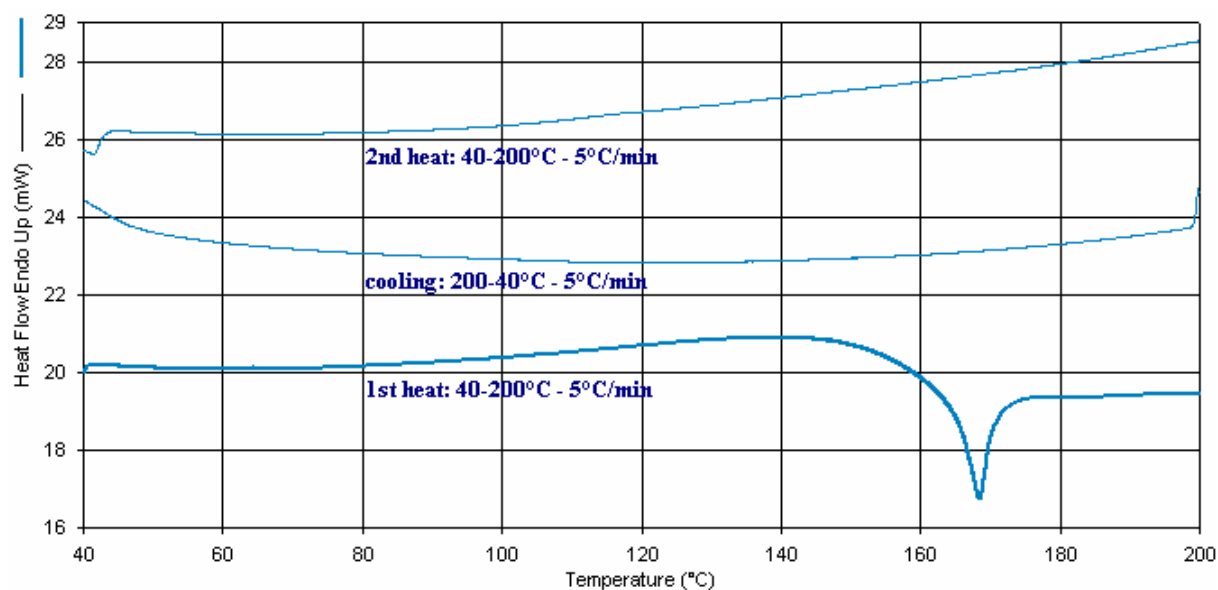
Although optical microscopy is of no utility regarding nanoparticle size and shape characterization (i.e. limited resolution  $\sim 1 \mu\text{m}$ ), it can be used to yield useful information, with polarization of the light source (as it will be shown), regarding the crystalline nature of the studied material. The polarized-light optical microscopy analysis (**Figure IV 3 10**) clearly shows the anisotropic nature of the un-milled drug and the drug nanoparticles, indicating that crystalline state seems to be unaltered following the homogenization operation. The bright colors, or in fact the interference colors, viewed in **Figure IV 3 10** following polarization of light are characteristic of anisotropic materials such as crystallite substances. Isotropic materials, or the amorphous form of drugs, do not interfere with polarized light, so that such images cannot be viewed.



**Figure IV 3 10.** Optical microscopy – polarized light analysis of ucb-35440-3 (magnification 50X – scale = 20µm) A: un-milled ucb-35440-3; B: ucb-35440-3 2%, Methocel E15<sup>®</sup> 0.5% w/v nanosuspension (PMC + 20C 23-24000 PSI).

Confirmation of this observation was made by DSC. ucb-35440-3 is referred by the sponsor as having a melting point in the range of 160°C to 166°C, with decomposition observed within this temperature range and no recrystallisation thereafter. A first DSC run was made on un-milled ucb-35440-3 consisting of a first heating from 40°C to 200°C at a heating rate of 5°C/min and a subsequent cooling from 200°C to 40°C (5°C/min) and a second heating from 40°C to 200°C (5°C/min). Results from this evaluation are represented in **Figure IV 3 11**. As observed on the first heat run in **Figure IV 3 11**, thermal behavior of ucb-35440-3 is rather uncharacteristic as an exotherm is observed around 166°C-170°C, which corresponds to the reported drug melting point. The fusion transition phase being in general an endothermic process, this peak could result from product degradation (although DSC degradation peaks are not usually represented by uniform peaks such as the one found).

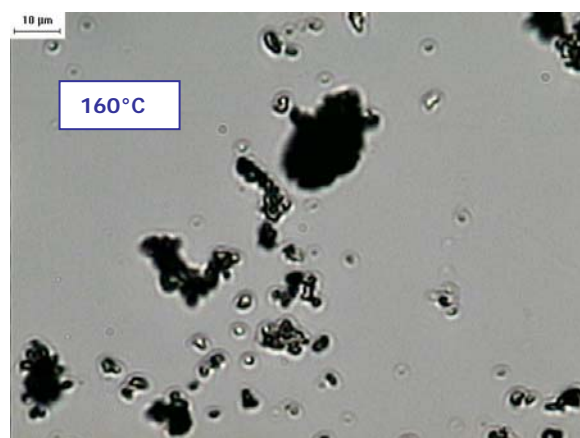
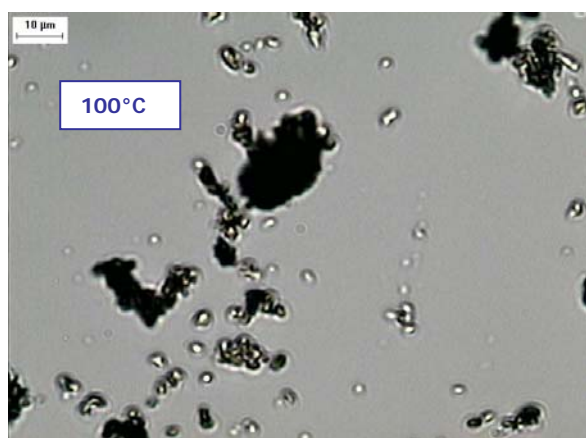




**Figure IV 3 11.** DSC run for un-milled ucb-35440-3: First heating from 40°C to 200°C (5°C/min) followed by cooling of the heated sample from 200°C to 40°C (5°C/min) and re-heating from 40°C to 200°C (5°C/min).

Complementary data relative to the visualization of this observed transition phase was obtained through hot stage microscopy (HSM) analysis, while conducting a similar heat run to the one used for DSC analysis. Micrographs taken using HSM are shown in **Figure IV 3 12**. As we can see on this figure, although the temperatures are slightly shifted upwards, the phase transition occurring around 170°C does coincide with the product's fusion.

A similar DSC heat run was thus conducted on ucb-35440-3 nanoparticles (freeze-dried nanosuspension) in order to compare the thermal behavior of the drug before and after particle size reduction. Results are shown in **Figure IV 3 13** and **Table IV 3 2**.



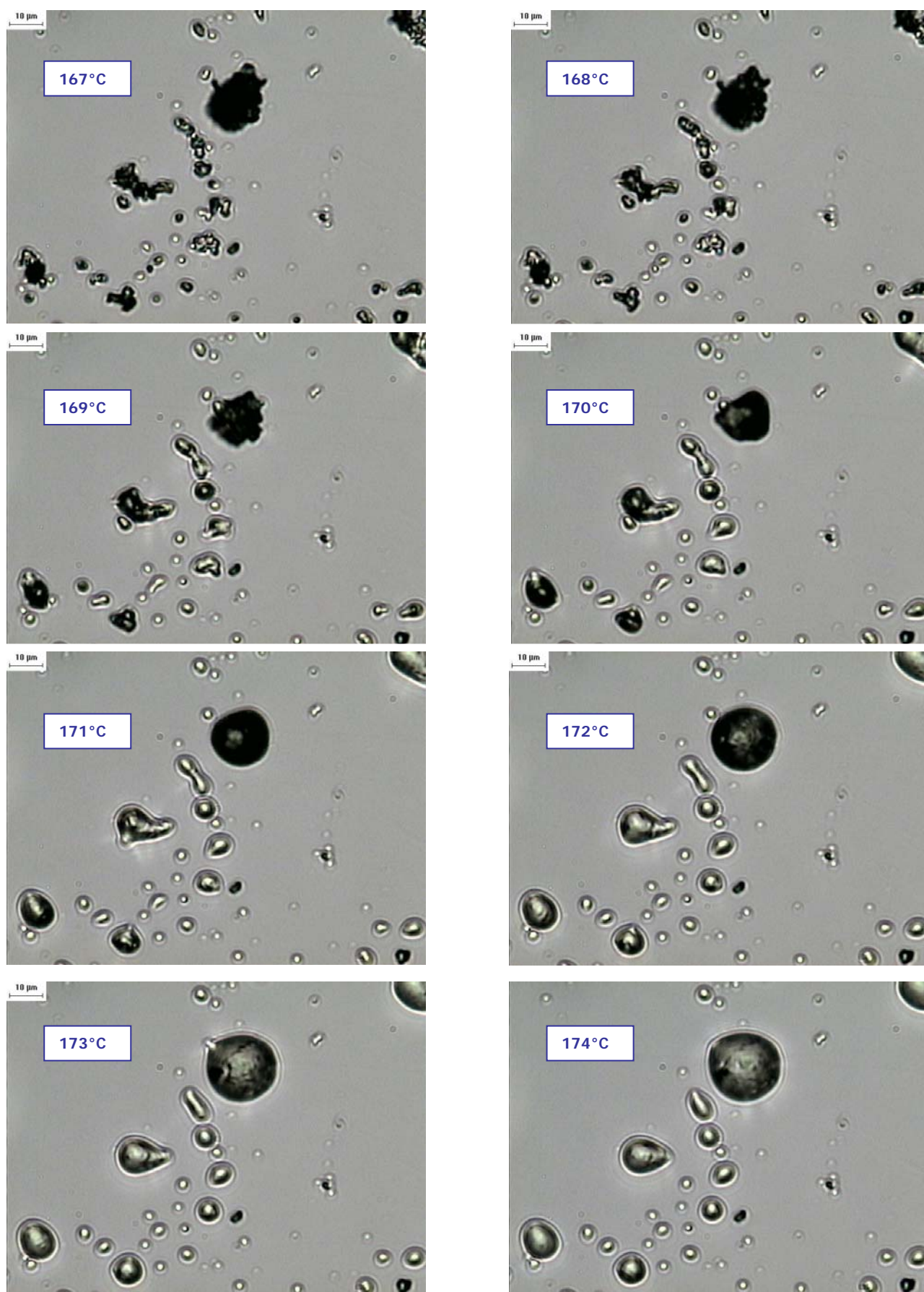


**Figure IV 3 12.** HSM micrographs for un-milled ucb-35440-3: heating 25°C → 140°C (5°C/min), 140°C → 200°C (2°C/min).



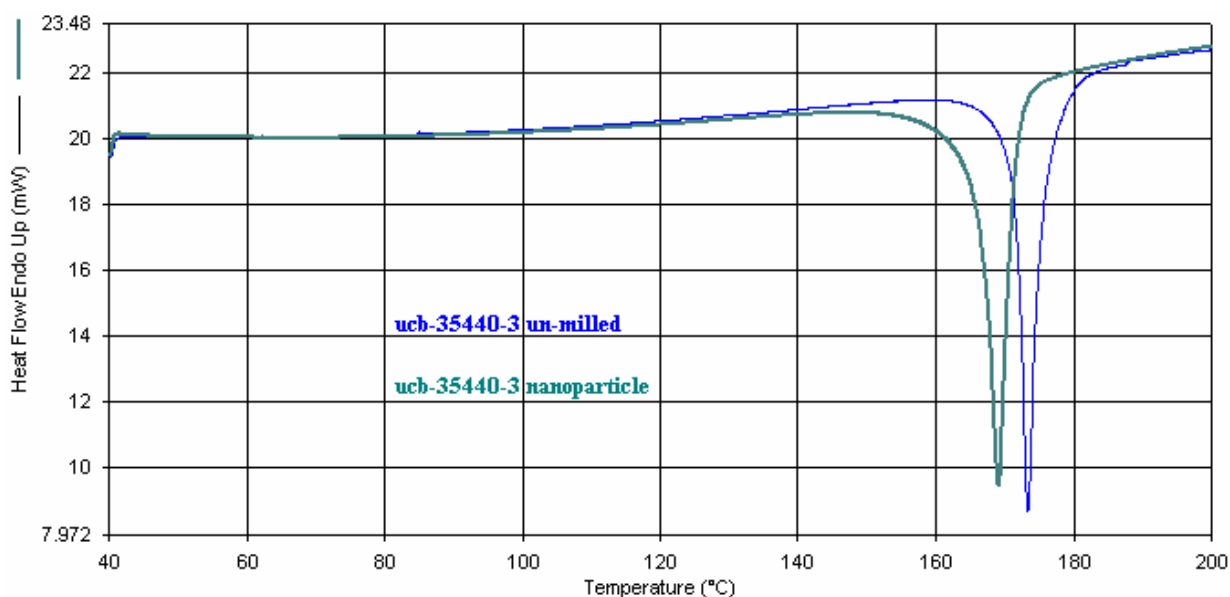


**Figure IV 3 13.** DSC runs (40°C to 200°C at 5°C/min) for un-milled ucb-35440-3 (**blue**) and for a ucb-35440-3 5%, Methocel E15<sup>®</sup> 0.1% w/v freeze-dried nanosuspension (**green**). DSC runs were conducted a minimum of three times for each samples with equivalent results being yielded.

**Table IV 3 2.** Values for Figure IV 3 13.

	ucb-35440-3 (un-milled)	ucb-35440-3 (nanoparticle)
<b>Onset</b>	171.4°C	166.4°C
<b>End</b>	175.4°C	171.5°C
<b>Peak</b>	173.3°C	169.2°C
<b>Peak height</b>	-13.1 mW	-12.1 mW
<b>Area</b>	-625.4 mJ	-717.0 mJ
<b>Delta H</b>	-147.9 J/g	-168.1 J/g

As we can see from the data shown in **Figure IV 3 13** and **Table IV 3 2**, the thermal behavior of ucb-35440-3 nanoparticles is nearly identical to that of the un-milled drug. The crystalline state is better represented through PXRD analysis of the un-milled drug and drug nanoparticles, as it was the case for NIF. The PXRD diffractograms are shown in **Figure IV 3 14**. The results obtained for un-milled ucb-35440-3 show a rather complex diffraction pattern indicating the crystalline structure of the drug. As the diffraction pattern for the freeze-dried nanosuspension is identical to that of the un-milled drug, crystalline state can be said to be unaffected by the high pressure homogenization operation. The only difference to be noted between the two products lies again in the

diffraction intensities. Diffraction intensities, regarding the scattering angle, are in fact found to be smaller for the homogenized ucb-35440-3. This is, however, as it has been discussed in **part IV.3.3.1.3** of this work, is due to the presence of HPMC in the case of ucb-35440-3 nanoparticles.

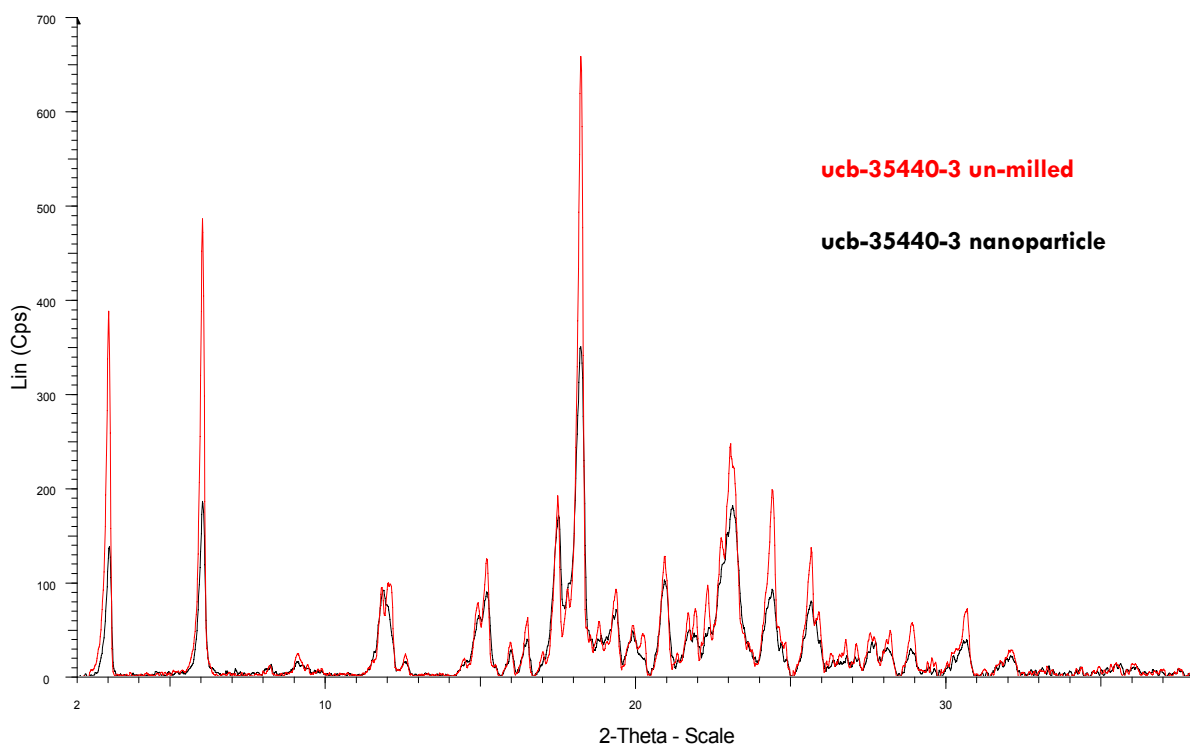


**Figure IV 3 14.** PXRD diffractograms for un-milled ucb-35440-3 (**red**) and for a ucb-35440-3 5%, Methocel E15<sup>®</sup> 0.1% w/v freeze-dried nanosuspension (**black**).

#### IV.3.3.3. UCB-A and UCB-B

##### IV.3.3.3.1. Investigations in UCB-A polymorphic transformations before and after particle size reduction - DSC

UCB-A has been reported to exhibit reversible temperature-dependent polymorphic transformations. In fact, below 16°C, UCB-A has been reported to be present as polymorphic form G, between 16°C and 37°C it has

been reported to be present as polymorphic form F and above 37°C as polymorphic form H, with totally reversible passage from one form to the other occurring when crossing the cited temperature range. These three polymorphs might behave, from a physicochemical standpoint, differently from one another (solubility, etc.). In fact, these polymorphic transformations have been shown in this work to be of relevant importance when considering the milling properties of UCB-A (possible crystal hardness differences between form G/F/H) (**part IV.2.3.5** of this work).

Investigations into these polymorphic transformations were mainly carried out using DSC analysis of micronized UCB-A (batch N° 200206024). The influence of UCB-A nanosizing on these transformations was also evaluated. Multiple subsequent heating and cooling runs were carried out in order to denote the fully reversible occurring polymorphic transformations of UCB-A. The DSC curves representing this evaluation are represented in **Figure IV 3 15**.

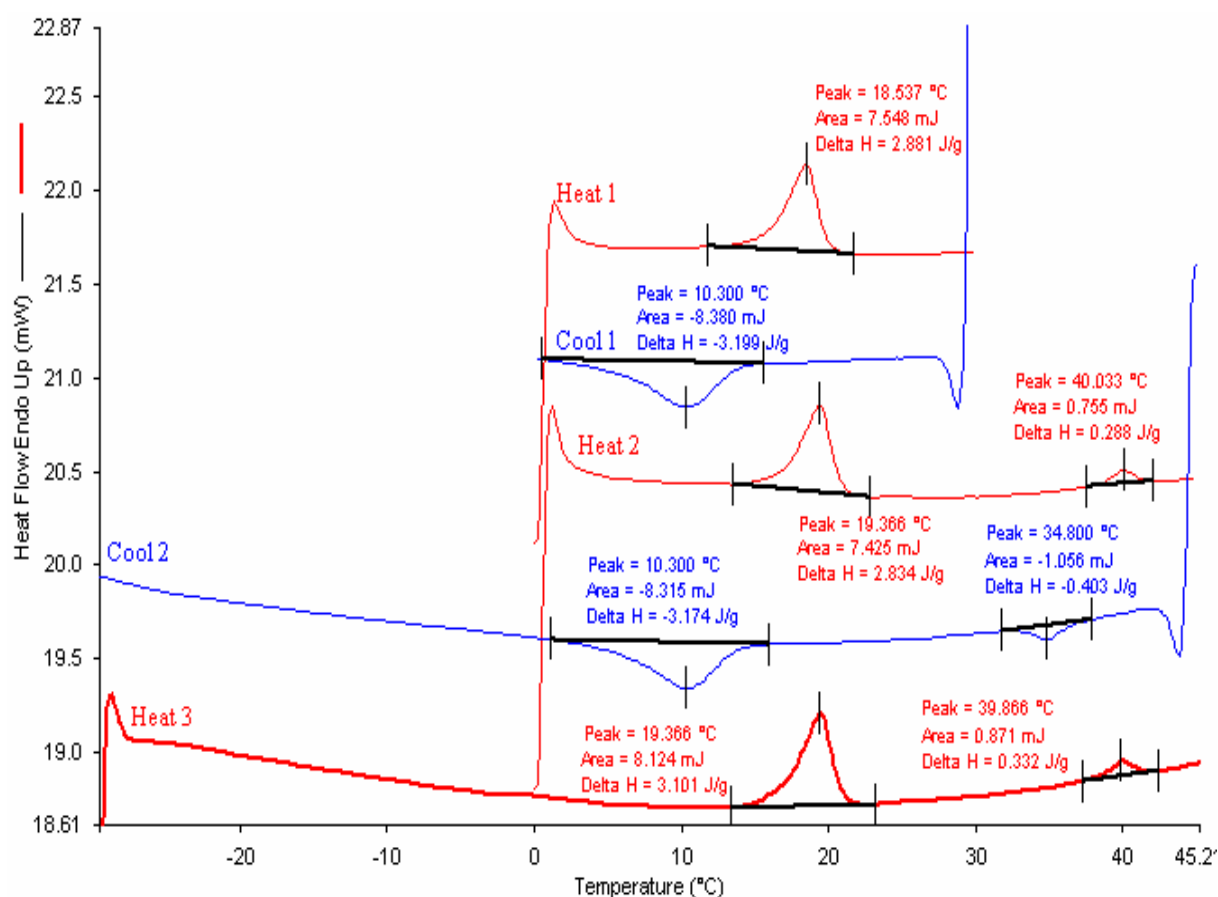


**Figure IV 3 15.** DSC run for micronized UCB-A (batch N° 200206024): (**heat 1**): heat 0°C → 30°C (10°C/min), (**cool 1**): cool 30°C → 0°C (10°C/min), (**heat 2**) heat 0°C → 45°C (10°C/min), (**cool 2**) cool 45°C → -30°C (10°C/min), (**heat 3**): heat -30°C → 250°C (10°C/min).

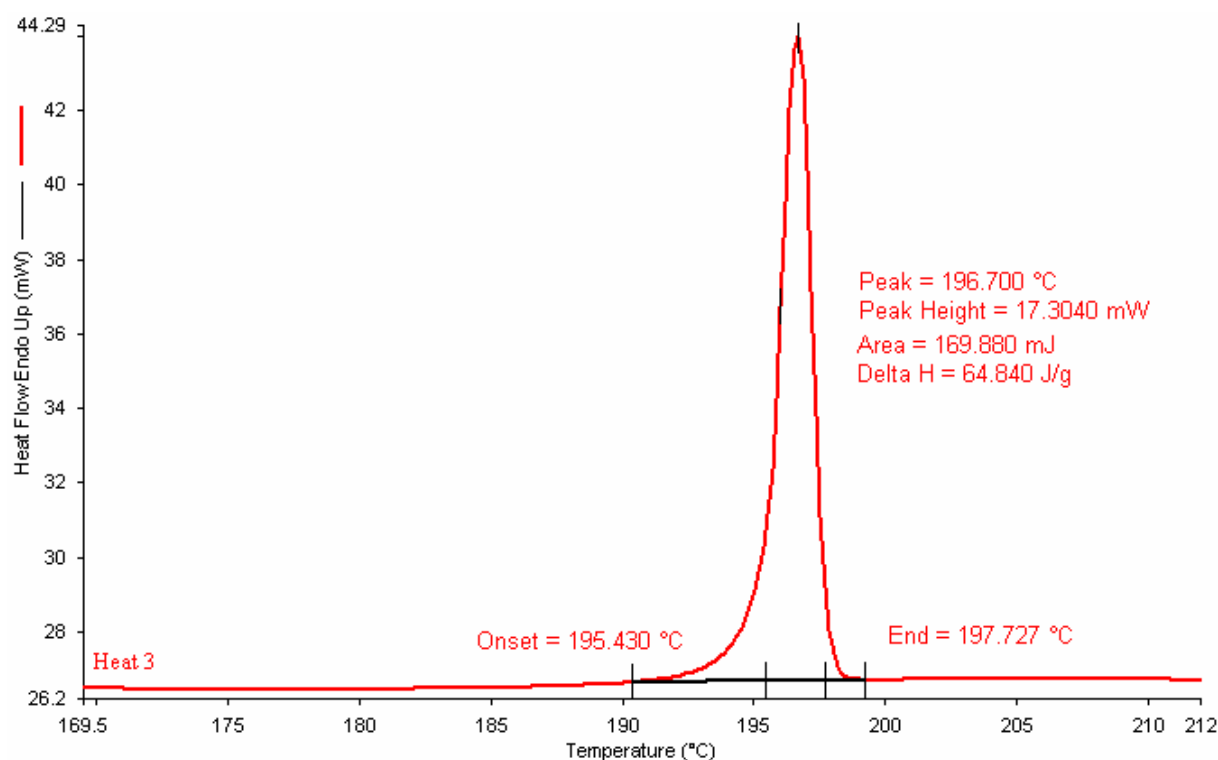
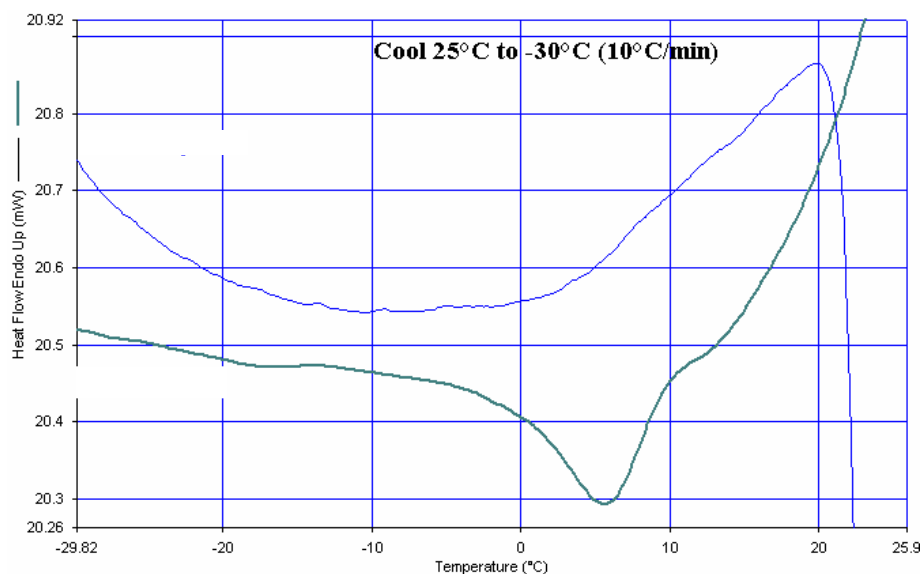


**Figure IV 3 15.** DSC run for micronized UCB-A (batch N° 200206024): (**heat 3** - followed): heat  $-30^{\circ}\text{C} \rightarrow 250^{\circ}\text{C}$  ( $10^{\circ}\text{C}/\text{min}$ ).

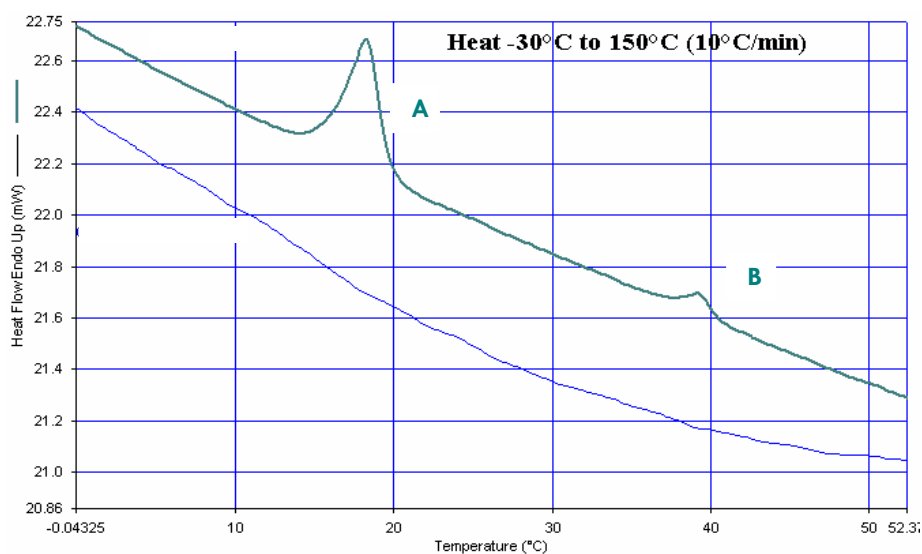
**Figure IV 3 15** clearly shows the two phase transition endotherms (heat 2/heat 3) and exotherms (cool 2) representative of the transitions from form G  $\leftrightarrow$  F and F  $\leftrightarrow$  H. The endotherm represented on “heat 1” and the first endotherm represented on “heat 2” and “heat 3” ( $\sim 19^{\circ}\text{C}$ ) are representative of the polymorphic transition from form G to F. The second endotherms represented on “heat 2” and “heat 3” ( $\sim 40^{\circ}\text{C}$ ) are representative of the polymorphic transition from form F to H. The exotherm represented on “cool 1” and the second exotherm represented on “cool 2” ( $\sim 10^{\circ}\text{C}$ ) are representative of the polymorphic transition from form F to G. The first exotherm represented on “cool 2” ( $\sim 35^{\circ}\text{C}$ ) is representative of the polymorphic transition from form H to F. The endotherm represented on “heat 3” at  $\sim 197^{\circ}\text{C}$  corresponds to the UCB-A melting point. As we can see through these results, UCB-A’s polymorphic transformations are totally reversible by varying the heat runs and going over the cited temperature ranges.

To investigate the presence of these polymorphic transformations for UCB-A nanoparticles, similar heat runs were conducted on the spray-dried UCB-A nanosuspension (tested on a spray-dried UCB-A 5%, Methocel E15<sup>®</sup> 0.5%,

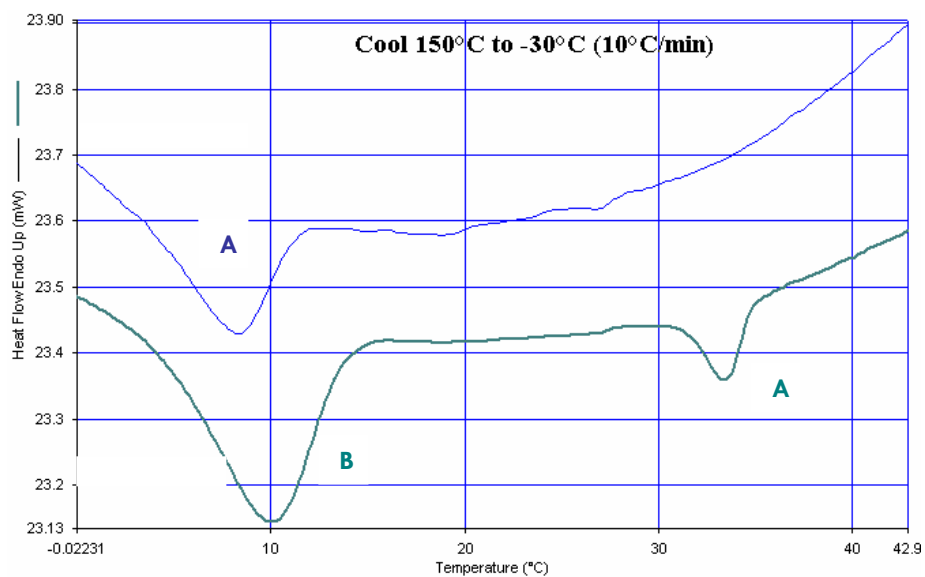
SDS 0.1% nanosuspension). The results, comparing micronized UCB-A and this spray-dried UCB-A nanosuspension, are shown on **Figure IV 3 16**.



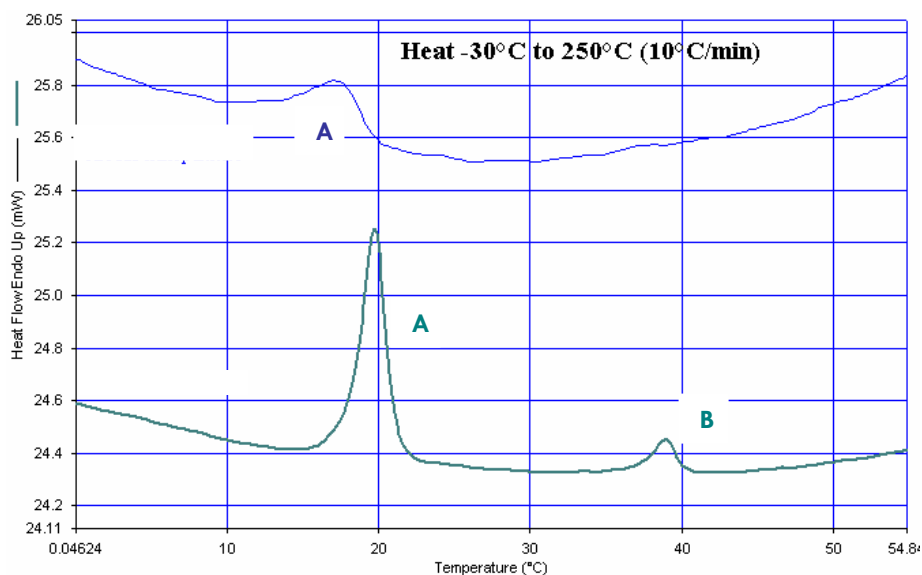
		Peak (°C)	onset (°C)	end (°C)	Delta H (J/g)
Micronized UCB-A		5.66	10.14	- 1.14	- 2.90
UCB-A nanoparticles		-	-	-	-



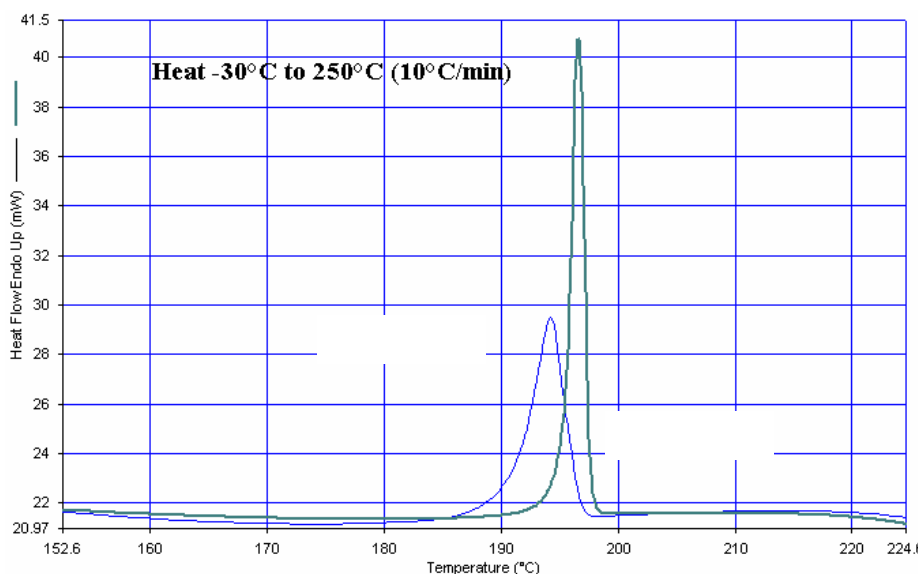
		Peak (°C)	onset (°C)	end (°C)	Delta H (J/g)
Micronized UCB-A	A	18.87	16.18	20.51	2.90
	B	39.70	38.29	41.14	0.28
UCB-A nanoparticles		-	-	-	-



		Peak (°C)	onset (°C)	end (°C)	Delta H (J/g)
Micronized UCB-A	A	33.47	34.85	31.43	- 0.51
	B	9.97	13.90	3.73	- 4.32
UCB-A nanoparticles	A	8.13	11.41	1.09	- 3.22



		Peak (°C)	onset (°C)	end (°C)	Delta H (J/g)
Micronized UCB-A	A	19.70	17.98	21.13	4.15
	B	38.87	37.06	40.16	0.55
UCB-A nanoparticles	A	17.20	12.27	19.77	2.12



	Peak (°C)	onset (°C)	end (°C)	Delta H (J/g)
Micronized UCB-A	196.70	195.41	197.55	61.02
UCB-A nanoparticles	194.20	190.95	196.51	66.36

**Figure IV 3 16.** DSC thermograms for micronized UCB-A (batch N° 200206024) (**green curves**) and UCB-A nanoparticles (spray-dried UCB-A 5%, Methocel E15<sup>®</sup> 0.5%, SDS 0.1% w/v nanosuspension) (**blue curves**): Run: Cool 25°C → -30°C (10°C/min), heat -30°C → 150°C (10°C/min), cool 150°C → -30°C (10°C/min), heat -30°C → 250°C (10°C/min).

As we can observe in **Figure IV 3 16**, the thermal behavior of UCB-A nanoparticles is different than the thermal behavior of micronized UCB-A. In fact, when considering the first cooling (25°C → -30°C (10°C/min)) and the first heating (-30°C → 150°C (10°C/min)), the polymorphic transformations (G/F/H) of UCB-A have disappeared. These polymorphic transformations, however, reappear after re-cooling the heated sample and after subsequent re-heating. On those last two runs, however, only the polymorphic transformation from form F to G (second cool) and G to F (second heat) were visible; the reversible transformation from polymorphic form G to H and H to G not being observed. This last transformation (i.e. F ↔ H), although it might be present, is much less energetic than the transition F ↔ G and might thus, simply, not have been detected.

The explanation for these observed results (absence of phase transitions G ↔ F ↔ H in the first run) might lie in the physical state of the UCB-A spray-dried nanoparticles as the powder obtained has a very low density and is highly porous, thus limiting proper heat conduction throughout the sample. The UCB-A polymorphic transformations

might thus be effectively present for UCB-A nanoparticles, but the DSC sensitivity might not be high enough to visualize these polymorphic transformations. These polymorphic transformations are not reported for UCB-B.

#### IV.3.3.3.2. Powder X-Ray Diffraction analysis

Preliminary investigations into UCB-A and UCB-B nanoparticles crystalline state were also carried out using X-ray diffraction. As the apparatus available for X-ray diffraction analysis does not allow for temperature modulation, analyses were made at room temperature and no investigation in UCB-A's polymorphic transformations could be carried out for nanoparticulate systems in order to complement the observed DSC behavior. The information obtained thus only served for a comparison between the un-milled drug and drug nanoparticles and therefore will only be made to denote any eventual modifications following the high pressure homogenization operation. As we can see in **Figures IV 3 17** and **IV 3 18**, the diffraction pattern for spray-dried UCB-A and UCB-B nanosuspensions are found to be identical to the diffraction patterns prior to the high pressure homogenization operation, for UCB-A and UCB-B respectively. A decrease in peak intensity is, however, observed for nanoparticles but can again be attributed to the presence of the stabilizer (in this case HPMC and SDS - dilution of the particles in the additives - cf. **part IV.3.3.1.3**).

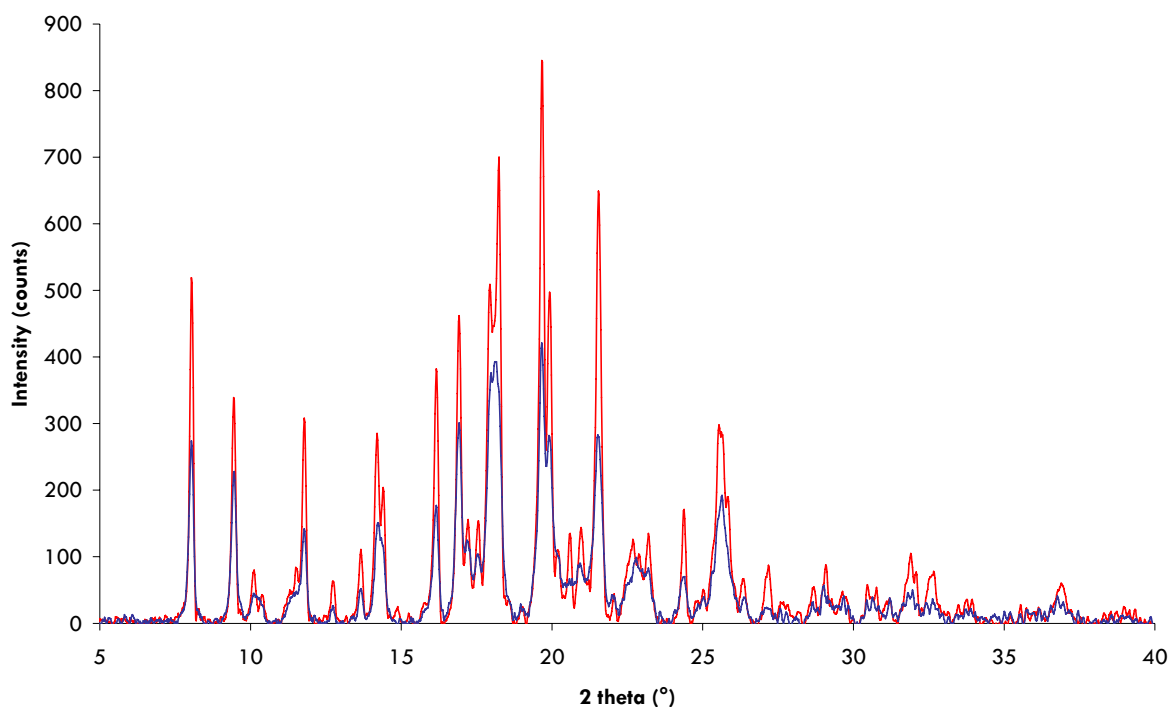


**Figure IV 3 17.** PXRD diffractograms for UCB-A prior to milling operations (**red**) and UCB-A nanoparticles (spray-dried UCB-A 5%, Methocel E15<sup>®</sup> 0.5%, SDS 0.1% w/v nanosuspension) (**blue**).



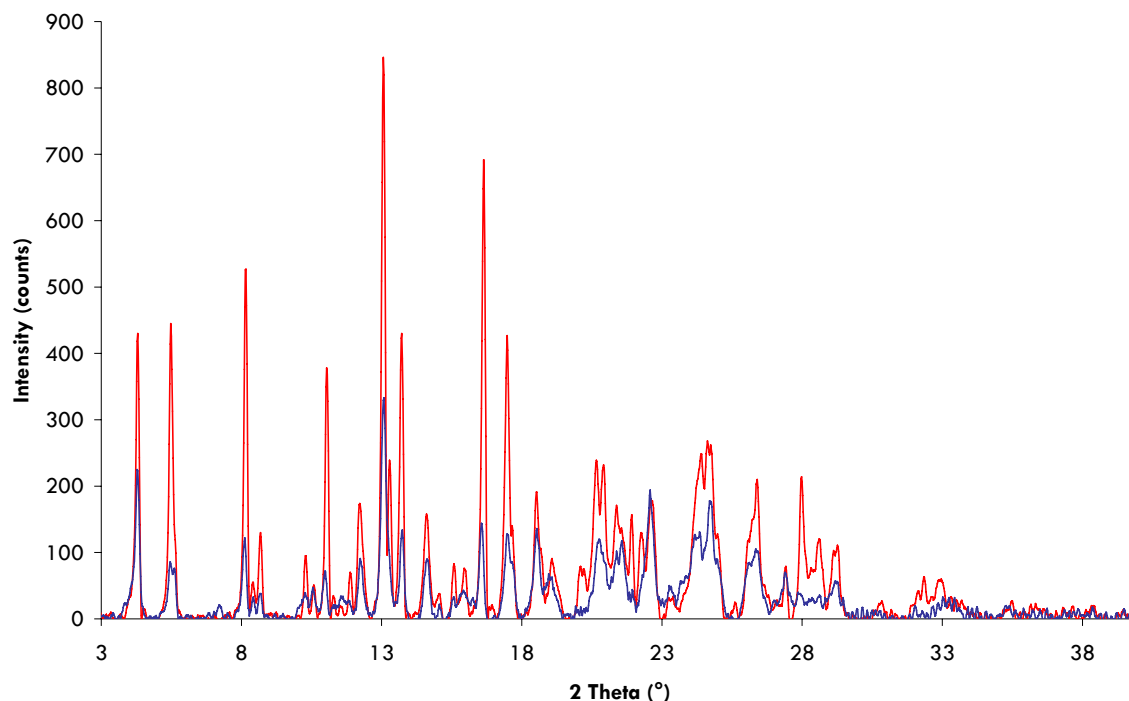


**Figure IV 3 18.** PXRD diffractograms for UCB-B prior to milling operations (**red**) and UCB-B nanoparticles (spray-dried UCB-B 5%, Methocel E15<sup>®</sup> 0.5%, Poloxamer 407 0.25% w/v nanosuspension) (**blue**).

#### IV.3.4. Conclusion

From the results presented in this chapter, we can conclude that high pressure homogenization is a technique that does not seem to interfere with the original crystalline state of the processed drugs. Considering NIF as a model drug, no differences in the amorphous/crystalline percentage (evaluated through PXRD analysis) could be observed following HPH processing. The results obtained for the other three model drugs (i.e. ucb-35440-3, UCB-A and UCB-B) suggest the same conclusion.



## IV.4. In vitro evaluation - solubility/dissolution characteristics

### IV.4.1. Introduction

Solubility and dissolution rate evaluations of the nanoparticulate systems produced were conducted to investigate the theoretical hypothesis behind drug particle size reduction and specific surface area enhancement. Solubility and dissolution rate characteristics have already been reported to be enhanced for numerous drugs by formulating them as nanoparticles. To give a few examples, cilostazol's solubility was increased by 6 percent by reducing particle size (media milling) from 2.4  $\mu\text{m}$  to 0.22  $\mu\text{m}$  ( $d(v;0.5)$ ) (Jinno et al., 2006) and RMKP22 (HPH) has seen its solubility increase from 1.97 mg/ml to 3.29 mg/ml and to 3.52 mg/ml for micronized particles (3.6 $\mu\text{m}$ ) reduced to 0.8  $\mu\text{m}$  and 0.3  $\mu\text{m}$  ( $d(v;0.5)$ ), respectively (Peters et al., 1999). Considering dissolution characteristics, enhanced dissolution rate has been reported for many drugs following nanosizing such as cilostazol (media milling) (100% of drug dissolved following 2 min for 0.22  $\mu\text{m}$  ( $d(v;0.5)$ ) particles vs. 40% for 2.4  $\mu\text{m}$  particles and vs. 5% for 13  $\mu\text{m}$  particles) (Jinno et al., 2006), ibuprofen (HPH - melt emulsification) (70% of drug dissolved following 10 min for 0.3  $\mu\text{m}$  (mean diameter) particles vs. 15% for 45  $\mu\text{m}$  particles) (Kocbek et al., 2006), danazol (SFL) (95% of drug dissolved following 2 min for 0.1  $\mu\text{m}$  particles vs. 30% for the micronized drug) (Hu et al., 2004b) and RMKP22 (HPH) (65% of drug dissolved following 10 min for 0.3  $\mu\text{m}$  ( $d(v;0.5)$ ) particles vs. 0% for 3.6  $\mu\text{m}$  particles - test in drug saturated solution) (Peters et al., 1999).

As NIF presents a pH-independent solubility profile, solubility and dissolution rate characteristics were evaluated in un-buffered aqueous media. In contrary, the solubility and dissolution characteristics of ucb-35440-3, UCB-A and UCB-B, which all present a pH-dependent solubility profile, were investigated in buffered media of three different pHs (phosphate buffers at pH 3.0, pH 5.0 and pH 6.5 for ucb-35440-3; HCl 0.1N, acetate buffers pH 4.0 and pH 5.0 and phosphate buffer pH 6.8 for UCB-A and UCB-B).

USP type II (paddle method) was mainly used for drug dissolution evaluation (NIF, ucb-35440-3, UCB-A and UCB-B). USP type IV (flow-through dissolution apparatus) was also used but only for ucb-35440-3 and for a dissolution medium pH of 6.5, which is less favourable to drug dissolution. This test was used as ucb-35440-3 rapidly showed saturation of the dissolution media using the type II apparatus (at pH 6.5). Optimization of ucb-35440-3 nanoparticle formulations (influence of carriers) and of the conditions used (media, dissolution cell filling,

etc.) were carried out with regard to the dissolution characteristics observed using the flow-through dissolution apparatus.

Nanoparticle redispersion characteristics have already been discussed in **part IV.2.3.5** of this work and will, here again in this chapter, be shown relevant when considering drug dissolution. This evaluation was mainly carried out for NIF (USP type II apparatus) and ucb-35440-3 (USP type IV apparatus).

## IV.4.2. Materials and Methods

### IV.4.2.1. Materials

The products used for the various solubility and dissolution tests and the described HPLC methods are listed in

**Table IV 4 1.** Types of media used are listed in **Table IV 4 2.**

**Table IV 4 1.** Products used for solubility/dissolution/HPLC assays.

Product	Origin
polysorbate 20	Certa (Belgium)
K <sub>2</sub> HPO <sub>4</sub>	Merck (Germany)
KH <sub>2</sub> PO <sub>4</sub>	Merck (Germany)
Sodium acetate	Merck (Germany)
HCl 37%	Carlo Erba (France)
NaOH pellets	Merck (Germany)
H <sub>3</sub> PO <sub>4</sub>	Sigma-Aldrich (Germany)
H <sub>2</sub> SO <sub>4</sub>	Merck (Germany)
Acetic acid	Sigma-Aldrich (Germany)
KCl	Sigma (Belgium)
Sodium taurocholate	Sigma (Belgium)
Lecithin	Lipoid GmbH (Germany)
Acetonitrile	Sigma-Aldrich (Germany)
Methanol	Sigma-Aldrich (Germany)
Sodium heptane sulfonate	Sigma-Aldrich (Germany)

**Table IV 4 2.** Dissolution media used (continued on next page).

<b>M1</b>	DI H <sub>2</sub> O Polysorbate 20      0.05% (NaOH/HCl - pH 7.0)	<b>M3</b>	DI H <sub>2</sub> O Polysorbate 20      0.05% KH <sub>2</sub> PO <sub>4</sub> /K <sub>2</sub> HPO <sub>4</sub> 50mM pH 5.0
<b>M2</b>	DI H <sub>2</sub> O Polysorbate 20      0.05% KH <sub>2</sub> PO <sub>4</sub> /K <sub>2</sub> HPO <sub>4</sub> 50mM pH 3.0	<b>M4</b>	DI H <sub>2</sub> O Polysorbate 20      0.05% KH <sub>2</sub> PO <sub>4</sub> /K <sub>2</sub> HPO <sub>4</sub> 50mM pH 6.5

<b>M5</b>	FaSSiF media ( <b>Galia et al., 1998</b> )	<b>M7</b>	DI H <sub>2</sub> O Sodium acetate /acetic acid 2M pH 5.0
	Sodium taurocholate 1.6g Lecithin 0.6g KH <sub>2</sub> PO <sub>4</sub> 3.9g KCl 7.7g NaOH → pH 6.5 DI H <sub>2</sub> O → 1l	<b>M8</b>	DI H <sub>2</sub> O KH <sub>2</sub> PO <sub>4</sub> 50mM NaOH ad pH 6.8
<b>M6</b>	DI H <sub>2</sub> O Sodium acetate /acetic acid 2M pH 4.0	<b>M9</b>	HCl 0.1N

#### IV.4.2.2. Saturation solubility

##### IV.4.2.2.1. Nifedipine

Saturation solubility measurements were assayed through ultraviolet absorbance determination at 235 nm using an Agilent 8453 UV/Vis Spectrophotometer (Agilent Technologies, USA). Fifty millilitres of suspension (water pH 7.0–0.05% polysorbate 20) (NIF content = 2 mg/ml) prepared from NIF in powder state, were placed at a temperature of  $37 \pm 0.1^{\circ}\text{C}$  and shaken (speed 150/min) using a GFL 1086 shaker-thermostatic cabinet (Labortechnik, Burgwedel, Germany). Both micro- and nanosuspensions were filtered using 0.1  $\mu\text{m}$  Millex-VV PVDF filters (Millipore Corporation, Bedford, MA, USA) prior to analysis. The mean results of triplicate measurements and the standard deviations are reported. Kinetics up to saturation solubility achievement were assayed for the un-milled product and for the nanoparticles with withdrawals taken at times 1, 3, 7, 24, 48 and 72 h.

##### IV.4.2.2.2. ucb-35440-3

Saturation solubility of ucb-35440-3 nanoparticles was assayed by HPLC (HPLC method UCB M2 of this work - **part IV.4.2.5.1.1**) at pH 3.0, 5.0 and 6.5. Thirty millilitres of suspension (50 mmol phosphate buffers pH 3.0, 5.0 and 6.5 (surfactant-free)) (ucb-35440-3 content = 8 mg/ml) prepared from ucb-35440-3 in powder state, were

placed at a temperature of  $25 \pm 0.1^{\circ}\text{C}$  and shaken (speed 150/min) using a GFL 1086 shaker-thermostatic cabinet (Labortechnik, Burgwedel, Germany). Solutions were filtered using  $0.1\ \mu\text{m}$  Millex®-VV PVDF filters (Millipore Corporation, Bedford, MA, USA) prior to analysis (out of a 4 ml filtered withdrawal, the first 2 ml were rejected). The mean results of triplicate measurements and the standard deviations are reported. Kinetics up to saturation solubility achievement were assayed with withdrawals taken at times 2, 24, 48 and 72 h.

The data obtained for ucb-35440-3 nanoparticles was compared to solubility data obtained for un-milled ucb-35440-3 during preformulation studies (evaluation of the pH-dependent solubility profile of ucb-35440-3 - HPLC method UCB M3 of this work - **part IV.4.2.5.1.2**)

#### **IV.4.2.2.3. UCB-A and UCB-B**

Saturation solubility of UCB-A and UCB-B was assayed by HPLC (HPLC method UCBA M3 of this work - **part IV.4.2.5.2.3**) at pH 0.8, 2.0, 2.4, 2.8, 3.4, 3.9, 4.3, 5.1, 6.5 and 7.3 (surfactant-free media). An equivalent of 15 mg/ml of UCB-A or UCB-B was placed in 5 ml glass tubes (except UCB-A and UCB-B nanoparticles pH 0.8 – 20 mg/ml). Suspensions were placed under slight agitation (15/min) using a Labinco Rotary Mixer (Vel, Belgium) during a 24-hour period at room temperature ( $25^{\circ}\text{C}$ ) (samples were protected from light). Suspensions were centrifuged at 10000 rpm for 5 min and at 15000 rpm for an additional 5 minutes using an ALC microcentrifuge 4214. The supernatant was assayed through HPLC method UCBA M3.

#### **IV.4.2.3. USP dissolution apparatus type II**

##### **IV.4.2.3.1. NIF**

Drug dissolution determinations were carried out at  $37 \pm 0.2^{\circ}\text{C}$  using USP 25, number II dissolution testing apparatus (paddle method), at a rotational speed of 60 rpm. The apparatus was a DISTEK Dissolution System

2100C equipped with a DISTEK TCS0200C thermostat (DISTEK Inc., North Brunswick, NJ, USA). The dissolution volume was always set at 900ml. The dissolution medium consisted of deionized water (pH 7.0 - 0.05% polysorbate 20). All dissolution tests were carried out on an equivalent of 10 mg of NIF (in powder state - not filled into capsules). Automatic withdrawals at fixed times were filtered in-line and assayed through ultraviolet absorbance determination at 235 nm using an Agilent 8453 UV/visible Dissolution Testing System (Agilent Technologies, USA). The mean results of a minimum of three measurements and the standard deviations are reported.

#### **IV.4.2.3.2. ucb-35440-3**

Drug dissolution determinations were carried out at  $37 \pm 0.2^{\circ}\text{C}$  using USP 25, number II dissolution testing apparatus (paddle method), at a rotational speed of 60 rpm. The apparatus was a DISTEK Dissolution System 2100C equipped with a DISTEK TCS0200C thermostat (DISTEK Inc., North Brunswick, NJ, USA). The dissolution volume was always set at 900 ml. The dissolution medium consisted of 50 mM phosphate buffers at pH 3.0, 5.0 and 6.5 (0.05% polysorbate 20). All dissolution tests were carried out on an equivalent of 200 mg of ucb-35440-3 (in powder state - placed into size 00 HPMC capsules and then into sinkers). Automatic withdrawals at fixed times were filtered in-line and assayed through ultraviolet absorbance determination at 255 nm using an Agilent 8453 UV/visible Dissolution Testing System (Agilent Technologies, USA). The mean results of a minimum of three measurements and the standard deviations are reported.

#### **IV.4.2.3.3. UCB-A and UCB-B**

Drug dissolution determinations were carried out at  $37 \pm 0.2^{\circ}\text{C}$  using USP 25, number II dissolution testing apparatus (paddle method), at a rotational speed of 75 rpm. The apparatus was a VanKel VK 7000 Dissolution System (VanKel Industries Inc). The dissolution volume was always set at 900 ml. All dissolution runs were conducted in surfactant-free media. All dissolution tests were carried out on an equivalent of 25 mg of UCB-A or UCB-B (in powder state - placed into size 00 gelatin capsules and then into sinkers). As UCB-A nanoparticulate systems showed very good dispersion characteristics in the media tested, coupled to the fact that the drug is



characterized by a very low solubility (at  $\text{pH} \geq 3.0$  - media saturation - presence of a very fine suspension in the dissolution baths), conventional in-line withdrawals using  $10\text{ }\mu\text{m}$  or  $45\text{ }\mu\text{m}$  filters were shown inappropriate for adequate particle separation and interference in simple UV detection (baseline deviation) was clearly observed (**Figure IV 4 1**). This was never observed for NIF and ucb-35440-3 when using conventional in-line filtration for the dissolution tests (**part IV.4.3.1.1**). This can be explained by the fact that all NIF or ucb-35440-3 formulations tested using the protocol described in **part IV.4.3.1.1** consisted of drug microparticles or did not show, as UCB-A does, good redispersion characteristics (presence of large agglomerates of drug nanoparticles - up to  $10\text{ }\mu\text{m}$  and  $100\text{ }\mu\text{m}$  for NIF and ucb-35440-3, respectively). The only exception to this explanation is the optimized NIF/mannitol formulation where, in this case, although the redispersion characteristics are very good, drug dissolution is practically instantaneous and the dissolution media is not saturated, thus enabling proper UV measurement following conventional in-line filtration.

Samples (5 ml) were thus withdrawn manually at fixed times and filtered (first 3 ml rejected) on Millex GV  $0.22\text{ }\mu\text{m}$  PVDF filters (Millipore) prior to analysis (UV / HPLC - UCBA M1 ( $\text{pH} \geq 5.0$ ) / UCBA M2 ( $\text{pH} 4.0$ ) / UCBA M3 (HCl  $0.1\text{N}$ )) (evaluation of different filtration devices was carried out – **Table IV 4 3**). The mean results of triplicate measurements and the standard deviations are reported.

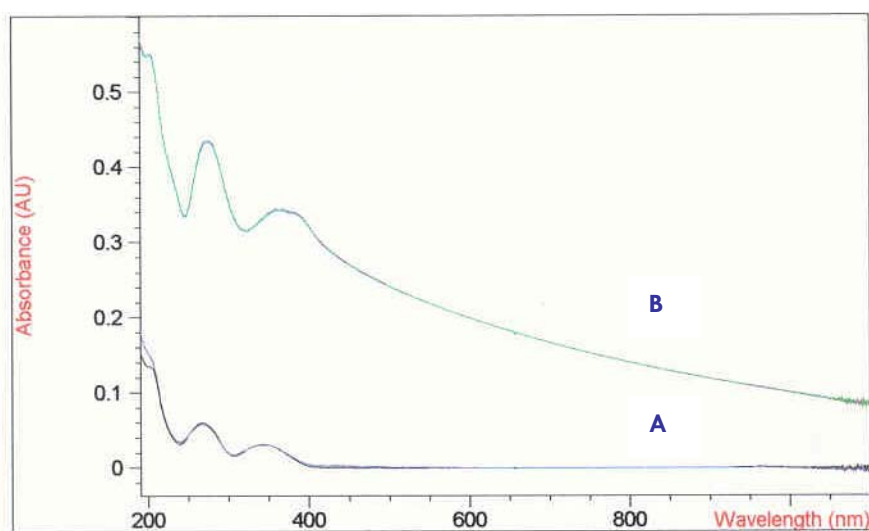


**Figure IV 4 1.** UV spectra of a dispersed spray-dried UCB-A nanosuspension following 10 min magnetic stirring: analysis following filtration on Millex VV PVDF  $0.1\text{ }\mu\text{m}$  filters (A) (Millex GV PVDF  $0.22\text{ }\mu\text{m}$  filters yielding the same observation) and following filtration using conventional  $10$  or  $45\text{ }\mu\text{m}$  pore size dissolution filters (B).

**Table IV 4 3.** Evaluation of filtration devices for optimization of particle separation during dissolution assays. (Withdrawal at time 2 hour – UCB-A 25 mg/900 ml deionized H<sub>2</sub>O)

		Concentration (µg/ml) UV	Concentration (µg/ml) HPLC UCBA M2	HPLC/UV
Millex VV PVDF 0.1µm	Millipore	0.516	0.992	1.924
Whatman PVDF 0.2µm	Whatman	0.703	0.694	0.987
Whatman 0.45µm Autotop Nylon	Whatman	0.273	0.346	1.267
Millex GV PVDF 0.22µm	Millipore	0.772	0.898	1.164
Chromafil 0.45µm PTFE (Macherey-Nagel)	Macherey-Nagel	0.884	0.872	0.986
Merck Eurolab 0.45µm PTFE	Merck	1.878	1.601	0.852
Millipore PVDF 0.45µm + 1µm APFB glass fiber prefilter	Millipore	0.977	1.020	1.044
GelmanGlass fiber 1,0µm	Gelman	3.073	2.496	0.812
Centrifugation - Ultrafree CL PMNL 100000	Millipore	2.960	0.493	0.167
Centrifugation - no filtration		3.039	3.337	1.098

Millex GV 0.22 µm PVDF filters were used as they have been reported not to interfere (adsorption, etc.) with UCB-A. They were shown to be adequate as the filtrate seemed “particle free” and concentrations obtained were in the range of most other systems with even smaller pore sizes.

Contrarily to NIF and ucb-35440-3, UCB-A and UCB-B concentrations were assayed by HPLC in order to characterize UCB-A-Met1 (degradation product of UCB-A - active moiety) (NIF photodegradation being clearly observed by looking at the UV spectra (**part IV.1.1**)). HPLC methods for UCB-A and UCB-B are described in **part IV.4.2.5.2** of this work.

#### IV.4.2.4. USP dissolution apparatus type IV: Flow-Through dissolution apparatus

The USP 25 type IV dissolution apparatus (also called Flow-Through dissolution apparatus) was used for the evaluation of ucb-35440-3 nanoparticle formulations. A Sotax Dissotest CE6 dissolution apparatus (Sotax AG Basel, Allschwil, Switzerland) Type IV (flow-through dissolution system) was used for in vitro testing of drug dissolution from the various formulations using a tablet dissolution cell. This apparatus houses six vertically mounted cells maintained at the desired test temperature by a heated water jacket. The two available cells used

for the evaluation of orally administered dosage forms are the powder cell (12 mm diameter) and the tablet cell (22.6 mm diameter) (**Figure IV 4 2**). Due to the large amount of powder used for the dissolution assays (i.e. equivalent of 200mg ucb-35440-3), powder cells rapidly showed limitations due to cell volume and tablet cells were thus used for all the assays. Each cell was prepared by placing a 5 mm ruby bead in the apex of the cone to protect the inlet tube and then, by filling the cone with 1 mm glass beads to create laminar media flow. 50mmol phosphate buffers (0.05% polysorbate 20) at pH 6.5 or FaSSiF media (**Table IV 4 2**) were used as dissolution media. The dissolution media was conveyed to the bottom of the dissolution cell by a CY-7 piston pump. Dissolution was carried out on an equivalent of 200 mg of ucb-35440-3 (in powder state). Drug loading into the dissolution cell has been shown to be an important parameter; homogeneous mixing of the drug with the glass beads being inferred as the best loading method (**Bhattachar et al., 2002**). The volume and temperature of the dissolution medium were 5 l and  $37.0 \pm 0.2^{\circ}\text{C}$  respectively. The flow rate ranged from 20-40 ml/min. Dissolution was evaluated in a closed loop system (media passed through the dissolution cell directly re-circulated in the media reservoir). The solution was filtered in-line using a series of filters with retention sizes of respectively 2.7 and  $0.7 \mu\text{m}$  (GF/D, GF/F filters, Whatman International Ltd., Maidstone, UK) placed at the top of the dissolution cell, in that order. 5 ml samples were withdrawn at definite times and were further filtered on  $0.1 \mu\text{m}$  Millex®-VV PVDF filter (Millipore Corporation, Bedford, MA, USA) prior to analysis (out of a 5 ml withdrawal, the first 3 ml were rejected). Drug concentration was assayed using the HPLC method UCB M2 described in **part IV.4.2.5.1.1** of this work. The mean results of triplicate measurements and the standard deviations are reported.

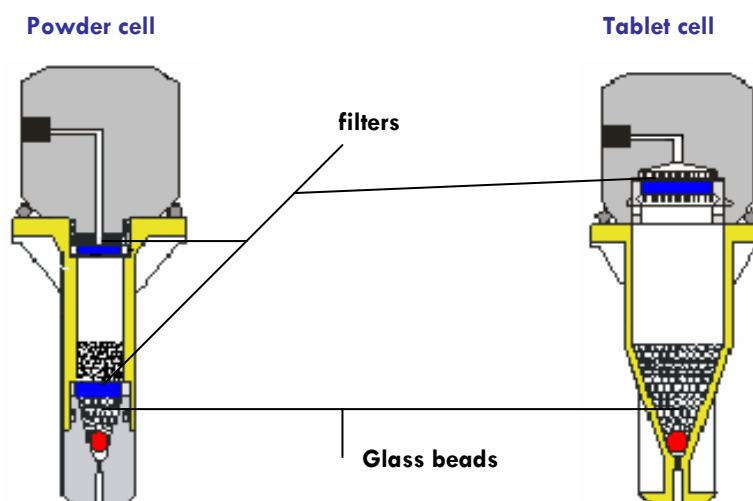


**Figure IV 4 2.** Schematic representation of powder (left) and tablet (right) flow-through dissolution cells: visualization of filters, ruby bead and glass beads.

#### **IV.4.2.5. HPLC methods**

##### **IV.4.2.5.1. ucb-35440-3**

###### **IV.4.2.5.1.1. UCB M2**

ucb-35440-3 quantification was realized using an Agilent series 1100 HPLC system (Palo Alto, CA, USA) comprising a solvent delivery pump, an autosampler, an UV-VIS variable wavelength detector and a data module integrator. Chromatographic separation was accomplished using a Nucleosil C18, 5  $\mu$ m, 250 x 4.0 mm stainless steel column (Macherey-Nagel, Düren, Germany). The mobile phase consisted of acetonitrile: H<sub>2</sub>O (50:50 v/v) added of 0.05% (w/v) sodium heptane sulphonate. The pH of the mixed solvent system was adjusted to pH 4.0 with sulfuric acid 0.12N. The mixture was filtered through 0.22  $\mu$ m Durapore® membrane filters (Millipore Corporation, Bedford, MA, USA) (or equivalent) under vacuum and degassed through sonication for 5 min. The mobile phase was pumped isocratically at a flow rate of 1.5 ml/min during analysis, at ambient temperature. The volume of injection was set at 20  $\mu$ l. The effluent was monitored at 210 nm. ucb-35440-3 concentrations were determined using appropriate external standards.

###### **IV.4.2.5.1.2. UCB M3**

ucb-35440-3 quantification was carried out using a Kontron chromatograph HPLC system type 400 (Kontron Instruments, Eching, Germany) comprising a solvent delivery pump, an autosampler, an UV-VIS variable wavelength detector and a data module integrator. Chromatographic separation was accomplished using a Kromasil C18, 3.5  $\mu$ m, 250 mm x 4.6 mm stainless steel column (AIT Chromato, France). The mobile phase consisted of a solvent A (ACN 10%/phosphate buffer pH 3.0 90%)/solvent B (ACN 75%/phosphate buffer pH 3.0 25%) mixture (50:50 v/v). The mixture was filtered through 0.22  $\mu$ m Durapore® membrane filters (Millipore Corporation, Bedford, MA, USA) (or equivalent) under vacuum and degassed through sonication for 5 min. The mobile phase was pumped isocratically at a flow rate of 1.0 ml/min during analysis, at 25°C. The volume of injection was set at 20  $\mu$ l. The effluent was monitored at 210 nm. ucb-35440-3 concentrations were determined using appropriate external standards.

#### IV.4.2.5.2. UCB-A and UCB-B

##### IV.4.2.5.2.1. UCBA M1

Drug quantification was carried out using a Waters HPLC system (Alliance 2690, PDA 996, Millenium 32) comprising a solvent delivery pump, an autosampler, an UV-VIS variable wavelength detector and a data module integrator. Chromatographic separation was accomplished using a Hypersil C18 BDS, 5  $\mu$ m, 100 mm X 4.6 mm stainless steel column (Thermo Hypersil Keystone). The mobile phase consisted of acetonitrile: 20 mmol phosphate buffer ( $\text{KH}_2\text{PO}_4/\text{K}_2\text{HPO}_4$ ) pH 6.0 (50:50 v/v). The mixture was filtered through 0.22  $\mu$ m Durapore® membrane filters (Millipore Corporation, Bedford, MA, USA) (or equivalent) under vacuum and degassed through sonication for 5 min. The mobile phase was pumped isocratically at a flow rate of 1.0 ml/min during analysis, at 30°C. The volume of injection was set at 10  $\mu$ l. The effluent was monitored at 270 nm. Drug concentrations were determined using appropriate external standards. This HPLC method is not suitable for discriminating UCB-A from UCB-A-Met1.

##### IV.4.2.5.2.2. UCBA M2

Drug quantification was carried out using a Waters HPLC system (Alliance 2690, PDA 996, Millenium 32) comprising a solvent delivery pump, an autosampler, an UV-VIS variable wavelength detector and a data module integrator. Chromatographic separation was accomplished using a Hypersil C18 BDS, 5  $\mu$ m, 100 mm X 4.6 mm stainless steel column (Thermo Hypersil Keystone). Mobile phase A consisted of acetonitrile:20mmol phosphate buffer ( $\text{KH}_2\text{PO}_4/\text{K}_2\text{HPO}_4$ ) pH 6.0 (5:95 v/v). Mobile phase B consisted of acetonitrile:20mmol phosphate buffer ( $\text{KH}_2\text{PO}_4/\text{K}_2\text{HPO}_4$ ) pH 6.0 (75:25 v/v). These mobile phases were filtered through 0.22  $\mu$ m Durapore® membrane filters (Millipore Corporation, Bedford, MA, USA) (or equivalent) under vacuum and degassed through sonication for 5 min. Mobile phase A/B composition was changed during the run as described in **Table IV 4 4**. The mobile phase combination was pumped isocratically at a flow rate of 1.5 ml/min during analysis, at 45°C. The volume of injection was set at 5  $\mu$ l. The effluent was monitored at 270 nm. Drug concentrations were determined using appropriate external standards. This HPLC method is suitable for

discriminating UCB-A from UCB-A-Met1, with retention times (RT) being found to be  $\pm 16$  min and  $\pm 6$  min, respectively.

**Table IV 4 4.** Mobile phase gradient in HPLC method UCBA M2

Time (min)	Solvent A (%)	Solvent B (%)
0	75	25
22.0	0	100
28.0	0	100
28.1	75	25
34.0	75	25

#### IV.4.2.5.2.3. UCBA M3

Drug quantification was carried out using a Waters HPLC system (Alliance 2690, PDA 996, Millenium 32) comprising a solvent delivery pump, an autosampler, an UV-VIS variable wavelength detector and a data module integrator. Chromatographic separation was accomplished using a Sun Fire RP18, 3.5  $\mu$ m, 150 X 2.1 mm stainless steel column (Waters, Belgium). Mobile phase A consisted of 900 ml aqueous phase (770 mg ammonium acetate/900 ml water. The pH was adjusted to 6.0 with glacial acetic acid) mixed with 100 ml acetonitrile. Mobile phase B consisted of 100 ml aqueous phase (770 mg ammonium acetate/900 ml water. pH adjusted to 6.0 with acetic acid glacial) mix with 900 ml acetonitrile. These mobile phases were filtered through 0.22  $\mu$ m Durapore® membrane filters (Millipore Corporation, Bedford, MA, USA) (or equivalent) under vacuum and degassed through sonication for 5 min. Mobile phase A/B composition was changed during the run as described in **Table IV 4 5**. The mobile phase combination was pumped isocratically at a flow rate of 0.25 ml/min during analysis, at 35°C. The volume of injection was set at 10  $\mu$ l. The effluent was monitored at 270 nm. Drug concentrations were determined using appropriate external standards. This HPLC method is suitable for discriminating UCB-A from UCB-A-Met1, with retention times (RT) being found to be  $\pm 24$  min and  $\pm 14$  min, respectively.

**Table IV 4 5.** Mobile phase gradient in HPLC method UCBA M3

Time (min)	Solvent A (%)	Solvent B (%)
0	100	0
29.0	0	100
30.0	100	0
40.0	100	0

### IV.4.3. Results and discussion

#### IV.4.3.1. Saturation solubility evaluation before and following particle size reduction

Saturation solubility assays were conducted using the protocols described in **part IV.4.2.2** of this work.

##### IV.4.3.1.1. Nifedipine

Saturation solubility measurements and kinetics up to saturation solubility achievement for un-milled NIF and NIF nanoparticles are shown on **Figure IV 4 3**. We can clearly see on this figure the enhanced achieved solubility for NIF nanoparticles when compared to the un-milled drug, with water-solubilities (37°C) of  $26 \pm 1 \mu\text{g/ml}$  and  $19.5 \pm 0.1 \mu\text{g/ml}$  being found, respectively.

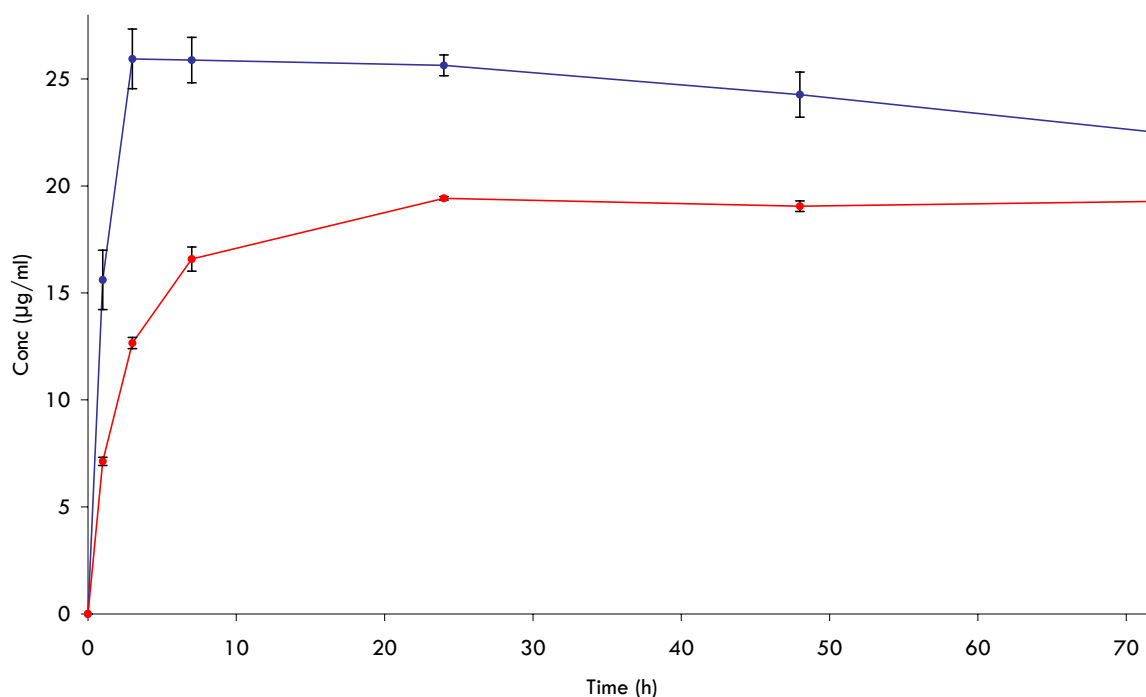


**Figure IV 4 3.** Kinetics to saturation solubility achievement (37°C) for un-milled commercial NIF (**red**) and for a spray-dried NIF 5%, Mannitol 5%, Methocel E15<sup>®</sup> 0.5% w/v suspension (PMC + 20C 23-24000 PSI HPH milling - nanoparticles) (**blue**). Mean  $\pm$  SD (n=3).

**Table IV 4 6.** Values for Figure IV 4 3. Mean  $\pm$  SD (n=3).

Time (h)	un-milled NIF ( $\mu\text{g/ml}$ )	NIF nanoparticles ( $\mu\text{g/ml}$ )
0	0 $\pm$ 0	0 $\pm$ 0
1	7.1 $\pm$ 0.2	15.6 $\pm$ 1.4
3	12.7 $\pm$ 0.3	25.9 $\pm$ 1.4
7	16.6 $\pm$ 0.6	25.9 $\pm$ 1.1
24	19.4 $\pm$ 0.1	25.6 $\pm$ 0.5
48	19.1 $\pm$ 0.2	24.3 $\pm$ 1.1
72	19.3 $\pm$ 0.1	22.5 $\pm$ 0.5

Furthermore, and most importantly, kinetics up to saturation solubility achievement was clearly enhanced for NIF nanoparticles as the measured  $26 \pm 1 \mu\text{g/ml}$  value was reached after only 3 h (equivalent concentration at time 3 h for un-milled NIF:  $12.7 \pm 0.3 \mu\text{g/ml}$ ); the maximum value of  $19.5 \pm 0.1 \mu\text{g/ml}$  being measured for un-milled NIF was only reached after 24 h. It has to be noted that the concentration reached for NIF nanoparticles was further shown to slowly decrease over time (up to 72 h), indicating achievement of a super-saturated NIF media for the nanoparticle formulation.

#### IV.4.3.1.2. ucb-35440-3

Saturation solubility assaying of ucb-354440-3 following particle size reduction has been accomplished to investigate theoretical enhancement predictions for nanoparticulate systems, which have been verified for NIF. ucb-35440-3's solubility is known to be pH-dependent, with this parameter decreasing with increase of pH as it can be seen on **Figure IV 1 7**. Saturation solubility determinations have thus been made with adequate control of the medium pH. Tests have been realized in 50 mmol phosphate buffers of pH 3.0, 5.0 and 6.5 as those were the pH values used for dissolution rate evaluation of ucb-35440-3 (see **part IV.4.3.2.2.1** of this work). Kinetics up to saturation solubility achievement was also assayed for these given pH. Results are shown in **Figure IV 4 4**.



As we can see in **Figure IV 4 4**, and when compared to the data from **Figure IV 1 7** and **Table IV 1 1**, saturation solubility of ucb-35440-3 seems to be enhanced when compared to the un-milled drug, particularly as pH increases (i.e. where the drug shows solubility limitations). In fact, the solubility values at pH 3.0 (0.72 mg/ml), although slightly enhanced, are very close to the solubility values for un-milled ucb-35440-3. Considering pH 5.0, solubility around 0.53 mg/ml has been found, which, when compared to the un-milled drug, might imply a 2-fold increase (reported solubility of 0.29 mg/ml at pH 4.7). As for pH 6.5, a maximum solubility around 0.24 mg/ml is reported for ucb-35440-3 nanoparticles. This, if we refer to the solubility values reported in **Figure IV 1 7** and **Table IV 1 1** (solubility at pH 6.36 - 0.03 mg/ml), would imply an 8-fold increase. This solubility result at pH 6.5 was rather unexpected as, when compared to the dissolution results at this same pH for ucb-35440-3 nanoparticles, sursaturation of the medium already seemed to appear around 0.05 mg/ml. As it had already been observed for NIF nanoparticles, and although we have no comparison for un-milled ucb-35440-3, kinetics up to saturation solubility achievement are again found to be very fast (except pH 6.5).

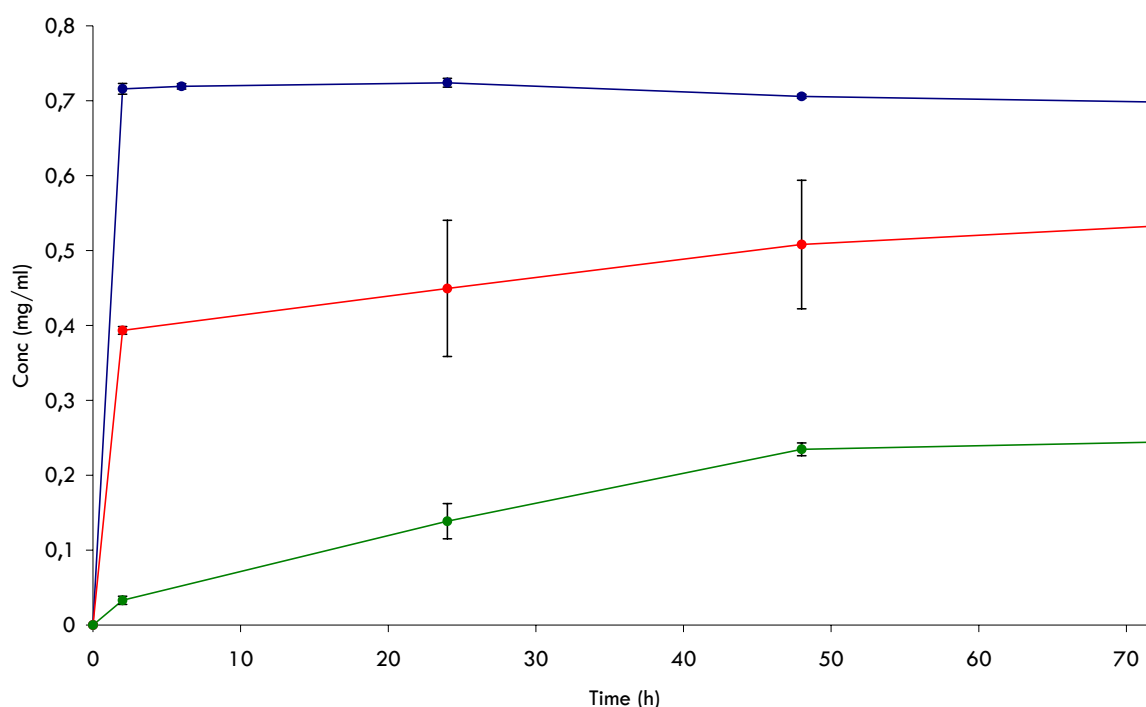


**Figure IV 4 4.** Kinetics to saturation solubility achievement (25°C) for a ucb-35440-3 5%, Methocel E15® 0.1% freeze dried nanosuspension (PMC + 20C 23-24000 PSI): pH 6.5 (green), pH5.0 (red) and pH3.0 (blue). Mean  $\pm$  SD (n=3).

**Table IV 4 7.** Values for Figure IV 4 4.

Time (h)	pH 3.0 (mg/ml)	pH 5.0 (mg/ml)	pH 6.5 (mg/ml)
0	0 ± 0	0 ± 0	0 ± 0
2	0.716 ± 0.007	0.393 ± 0.005	0.033 ± 0.006
6	0.719 ± 0.004		
24	0.724 ± 0.006	0.449 ± 0.091	0.139 ± 0.023
48	0.706 ± 0.003	0.508 ± 0.086	0.235 ± 0.008
72	0.698 ± 0.003	0.533 ± 0.075	0.244 ± 0.014

#### IV.4.3.1.3. UCB-A

UCB-A saturation solubility was assayed as function of pH as this drug, a poorly water-soluble weak base, is reported to have a pH-dependent solubility profile (solubility decreasing with increasing pH). Comparison between the micronized drug (drug as received - prior to high pressure homogenization) and drug nanoparticles was made. UCB-A-Met1 was also analyzed (HPLC method UCBA M3) in all samples to denote possible UCB-A degradation. Results are shown in **Figure IV 4 5** and **Table IV 4 8**.

As we can see from the results presented in **Figure IV 4 5** and **Table IV 4 8**, the pH-solubility profiles obtained for both micronized UCB-A and UCB-A nanoparticles are quite similar. We can also observe that there is an increase in saturation solubility for UCB-A nanoparticles for pH > 4. In fact, we can find a 4-fold increase at pH 4.3, a 6-fold increase at pH 5.1, a 10-fold increase at pH 6.5 and a 20-fold increase at pH 7.3. This observation can be attributed to the fact that, in addition to the reported theoretical saturation solubility enhancement for nanoparticulate systems, wettability of the UCB-A nanoparticles is also increased; micronized UCB-A being almost totally un-wetted in the media above pH 4 (even after the 24-hour test period).

On the other hand, saturation solubility at pH < 4 for UCB-A nanoparticles was found to be equivalent or inferior to the values obtained for the micronized UCB-A. This can find an explanation, as it will also be discussed for the dissolution profiles obtained in HCl 0.1N (**part IV.4.3.2.3** of this chapter), in the fact that the UCB-A nanoparticle formulation studied contains SDS. This surfactant, used for UCB-A nanoparticle stabilization during the highpressure homogenization operation, shows very poor solubility at acidic pH (< 4.0). UCB-A nanoparticles solubilization is thus limited at acidic pH as in fact SDS is found around UCB-A nanoparticles after spray-drying of

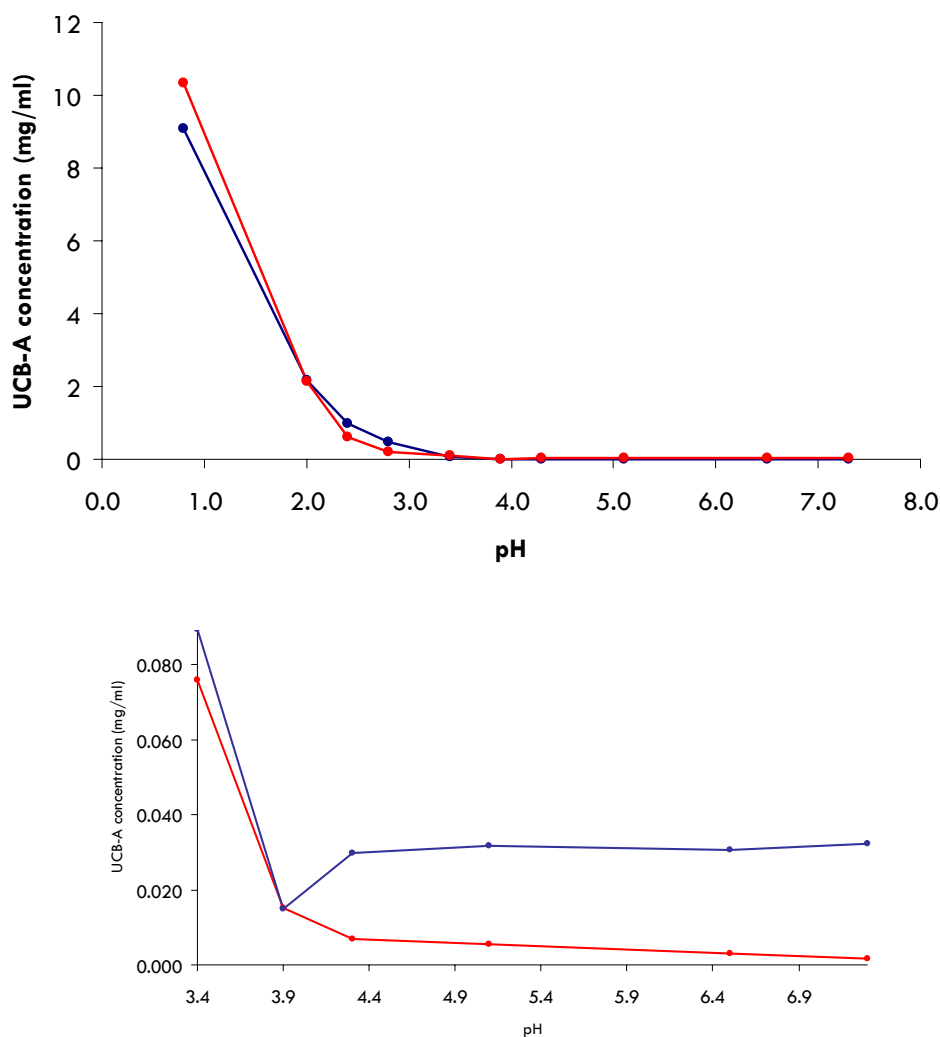


**Figure IV 4 5.** Aqueous solubility (25°C) versus pH (un-buffered media) for micronized UCB-A (product as received - prior to high pressure homogenization) (**red**) and for a spray-dried UCB-A 5%, Methocel E15<sup>®</sup> 0.5%, SDS 0.1% w/v nanosuspension (PMC + 20C 23-24000 PSI + 10C 30000 PSI) (**blue**). (n=1).

**Table IV 4 8.** Values for Figure IV 4 5 (ND: not detected).

pH	Solubility (mg/ml) micronized UCB-A	Solubility (mg/ml) UCB-A nanoparticles	UCB-A-Met1 (mg/ml) micronized UCB-A	UCB-A-Met1 (mg/ml) UCB-A nanoparticles
0.8	9.0718	10.3261	5.9780	5.6769
2.0	2.1569	2.1338	0.0453	0.0370
2.4	0.9858	0.6146	ND	ND
2.8	0.4721	0.2112	ND	ND
3.4	0.0759	0.0894	ND	ND
3.9	0.0153	0.0149	ND	ND
4.3	0.0069	0.0299	ND	ND
5.1	0.0056	0.0319	ND	ND
6.5	0.0030	0.0308	ND	ND
7.3	0.0017	0.0323	ND	ND

the nanosuspension. During this solubility evaluation assay, UCB-A nanoparticle samples at pH 0.8 to 2.4 did not in fact disperse properly, as it is the case for pH values higher than 2.4, indicating that this phenomenon (i.e. limitation in particle solubilization) might have occurred. We can also observe from these results, that solubility values at  $\text{pH} \geq 3.9$ , tend to increase gradually when going up to pH 7.3 (i.e. when SDS is freely soluble).

#### IV.4.3.1.4. UCB-B

The evaluation of UCB-B solubility profile against pH was carried out in a similar way to that of UCB-A. UCB-A-Met1 quantification was also carried out for each formulation and at all tested pH. Results from this evaluation are shown in **Figure IV 4 6** and **Table IV 4 9**. From these results, we find that, similarly to UCB-A, there are no differences in the pH-solubility profile between the un-milled UCB-B and the drug nanoparticles. No differences were found either for the physical mixture corresponding to the tested nanoparticle formulation. No differences in solubility values, except maybe at pH 0.8 for UCB-B nanoparticles, can be found through the tested pH range between the three models. Interestingly, for UCB-B nanoparticles, UCB-A-Met1 was found, at very low concentrations, for all tested pH. This is not the case for the other two models as no more UCB-A-Met1 could be detected above pH 2.8; in the case of UCB-A nanoparticles, no more UCB-A-Met1 could be detected above pH 2.0.

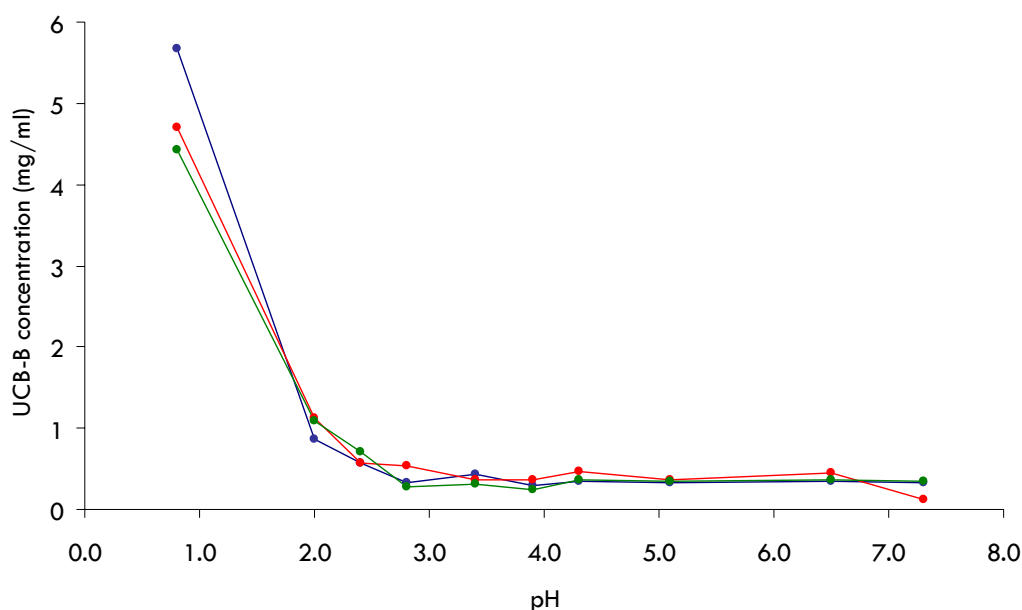


**Figure IV 4 6.** Aqueous solubility (25°C) versus pH (un-buffered media) for un-milled UCB-B (product as received - prior to high pressure homogenization) (**red**), for a spray-dried UCB-B 5% Methocel E15<sup>®</sup> 0.5% Poloxamer 407 0.25% w/v nanosuspension (PMC + 20C 23-24000 PSI + 10C 30000 PSI) (**blue**) and a UCB-B Methocel E15<sup>®</sup> 10% Poloxamer 407 5% w/w (relative to UCB-B content) physical mixture (**green**). (n=1).

**Table IV 4 9.** Values for Figure IV 4 6 (ND: not detected).

pH	Solubility (mg/ml) UCB-B nanoparticles	Solubility (mg/ml) un-milled UCB-B	Solubility (mg/ml) physical mixture
0.8	5.670	4.702	4.433
2.0	0.864	1.129	1.094
2.4	0.574	0.571	0.713
2.8	0.330	0.529	0.278
3.4	0.431	0.358	0.314
3.9	0.300	0.363	0.250
4.3	0.354	0.465	0.356
5.1	0.330	0.370	0.349
6.5	0.346	0.453	0.358
7.3	0.333	0.114	0.342

pH	UCB-A-Met1 (mg/ml) UCB-B nanoparticles	UCB-A-Met1 (mg/ml) un-milled UCB-B	UCB-A-Met1 (mg/ml) physical mixture
0.8	5.314	4.506	4.212
2.0	0.045	0.057	0.054
2.4	0.013	0.005	0.047
2.8	0.010	ND	0.009
3.4	0.011	ND	ND
3.9	0.007	ND	ND
4.3	0.018	ND	ND
5.1	0.013	ND	ND
6.5	0.016	ND	ND
7.3	0.006	ND	ND

#### IV.4.3.2. Evaluation of dissolution rate characteristics before and following particle size reduction

##### IV.4.3.2.1. Nifedipine

Dissolution rate characteristics of NIF nanoparticles were assayed and compared to un-milled NIF. As reported in **Table IV 4 10**, two NIF formulations were assayed. These two formulations (i.e mannitol-free and mannitol-added formulations), already described in **part IV.2.3.5** of this work, were evaluated for comparison of their redispersion characteristics. As described in **Table IV 4 10** and **part IV.2.3.5** of this work, NIF formulation A (mannitol-free formulation) shows very poor water-redispersion characteristics when compared to NIF formulation B (mannitol-added formulation). The dissolution rate characteristics of a physical mixture (NIF:Methocel E15<sup>®</sup> - 10:1 w/w), of a spray-dried NIF 5%, Methocel E15<sup>®</sup> 0.5% w/v suspension (prior to milling operations) and of a spray-dried NIF 5%, Methocel E15<sup>®</sup> 0.5% w/v suspension (Turrax<sup>®</sup> milling - prior to high pressure homogenization operation) were also used as comparisons. The first two formulations served as a basis for the evaluation of HPMC on drug dissolution and the Turrax<sup>®</sup> milled spray-dried suspension served as a basis for the evaluation of a first size reduction to micrometer range for NIF; this suspension being characterized by a d(v,0.5) around 15 µm versus 100 µm for un-milled NIF. Dissolution results for these evaluations are shown in **Figure IV 4 7**.

**Table IV 4 10.** Studied NIF formulations (PMC + 20C 23-24000 PSI HPH)

**Formulation A:** Spray-dried NIF 5%, Methocel E15<sup>®</sup> 0.5% w/v nanosuspension

**Formulation B:** Spray-dried NIF 5%, Mannitol 5%, Methocel E15<sup>®</sup> 0.5% w/v nanosuspension

	d (0.1) ± SD	d (0.5) ± SD	d (0.9) ± SD	D[4,3] ± SD	span ± SD
Before spray-drying	0.089 ± 0.003	0.291 ± 0.006	1.29 ± 0.07	0.526 ± 0.022	4.11 ± 0.03
NIF formulation A	1.73 ± 0.04	3.7 ± 0.09	8.6 ± 0.33	5.49 ± 0.41	1.82 ± 0.05
NIF formulation B	0.093 ± 0.002	0.339 ± 0.006	1.60 ± 0.04	0.638 ± 0.010	4.49 ± 0.17

	% below 1 µm (in volume)	Estimated specific surface area (SSA) (m <sup>2</sup> /g)
Before spray-drying	86%	29.9
NIF formulation A	< 1 %	1.88
NIF formulation B	80%	27.5

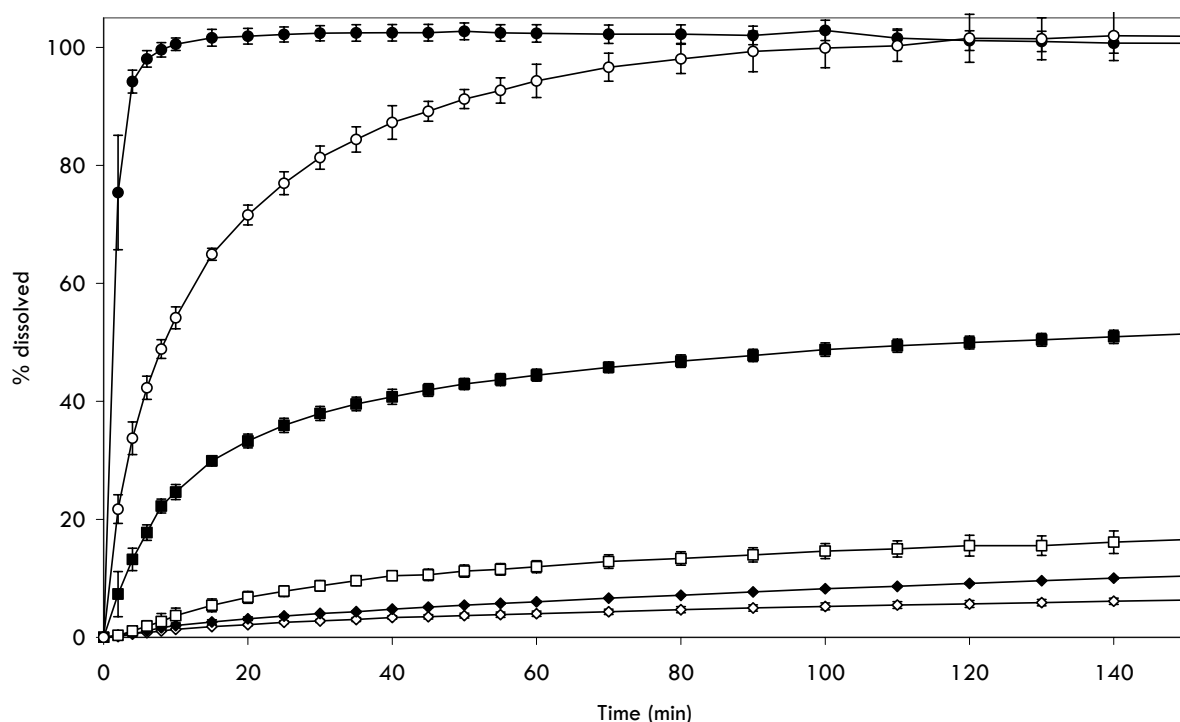


**Figure IV 4 7.** Dissolution profiles (mean  $\pm$  SD;  $n=3$ ) for (◇) un-milled commercial NIF, (◆) NIF/HPMC 10:1 m/m physical mixture (mortar), (□) spray-dried formulation A (no milling), (■) spray-dried formulation A (Turrax® milling), (○) spray-dried formulation A (HPH milling) and (●) spray-dried formulation B (HPH milling).

Comparison of the profiles obtained for the mannitol-free formulation (NIF formulation A) and un-milled NIF clearly shows the dissolution rate enhancement obtained with nano-sized systems as 95% of the drug was dissolved following 60 min compared to 5% for the un-milled drug. Complete dissolution came after about 90 min for nifedipine nanoparticles. **Figure IV 4 7** also reports the influence of HPMC, a hydrophilic polymer, on un-milled drug dissolution characteristics. HPMC was shown to only slightly enhance the dissolution of un-milled nifedipine when both were physically mixed; the effect being more pronounced following hydrophylisation of the drug particles (spray-dried formulation A prior to size reduction operations), as these are now homogeneously coated with the water-soluble polymer.

NIF micron-sized particles, obtained after Turrax® milling ( $d(v; 0.5) = 15 \mu\text{m}$ ), were also assayed for their dissolution behaviour. The approximate 10-fold decrease in particle size from the un-milled commercial NIF, accompanied by an estimated surface area increase from 0.134 to 0.758  $\text{m}^2/\text{g}$ , yielded a 19-fold increase in the dissolution rate at the beginning of dissolution (0.019 mg/min to 0.366 mg/min). Although the dissolution rate

enhancement is clearly shown, it is still limited and smaller than the one obtained for NIF nanoparticles (1.09 and 3.77 mg/min for formulation A and B, respectively), this being mainly due to the higher specific surface area achieved with the latter (1.88 and 27.5 m<sup>2</sup>/g, for formulations A and B, respectively – **Table IV 4 10**).

Dissolution profiles for mannitol-free (NIF formulation A) and mannitol-added (NIF formulation B) NIF formulations are also compared on **Figure IV 4 7**. This water-soluble additive is shown to further increase the NIF nanoparticle dissolution rate as 75% of the drug is already dissolved after 2 min versus 20% for formulation A. Complete dissolution being reached after only 10 min versus 90 min for formulation B and A, respectively. The difference observed between formulation A and B is attributed to the facts that mannitol acts as a carrier preventing particle agglomeration during the spray-drying operation (**Figure IV 2 25** - **Table IV 4 10**) and that it creates a highly hydrophilic environment around NIF nanoparticles beneficial for drug dissolution. No correlations can be made between surface areas and dissolution rates for the two systems as surface areas have been estimated from LD data (surface area of an equivalent sphere) and, for formulation A, the estimated surface area is not representative of the effective surface area directly in contact with the dissolution medium. Formulation A is in fact represented by agglomerates of nanoparticles (**Figure IV 2 20**) thought to show high porosity and thus having an effective surface area greater than the 1.88 m<sup>2</sup>/g value found. However, it should be noted that, when comparing un-milled NIF and NIF formulation B, where the agglomeration phenomenon is limited, an approximate 200-fold increase in surface area is shown to result in a 200-fold increase in DR.

#### IV.4.3.2.2. ucb-35440-3

Un-milled ucb-35440-3 and ucb-35440-3 nanoparticles dissolution rate characteristics were evaluated using both the USP type II (paddle method) dissolution apparatus and the USP type IV flow-through dissolution apparatus. The latter was used to evaluate drug dissolution characteristics in media at pH 6.5 (phosphate buffer, FaSSiF media), i.e. a pH not favorable to drug dissolution due to the drug's very low solubility (cf. **part IV.4.3.1.2** of this chapter). The flow-through dissolution apparatus, using ucb-35440-3 as a model drug, allowed us to put forward the problems associated with the nanoparticle reagglomeration phenomenon already discussed and studied in **part IV.2.3.5** of this work.



## IV.4.3.2.2.1. USP type II apparatus

The USP type II (paddle method) apparatus was used to evaluate the dissolution characteristics of un-milled ucb-35440-3 and ucb-35440-3 nanoparticles at pH 3.0, 5.0 and 6.5 (equivalent of 200 mg of ucb-35440-3/capsule). According to the drug's solubility profile, these pHs were used to evaluate drug dissolution characteristics in media progressively less favorable to drug dissolution. Comparison between un-milled ucb-35440-3 and a freeze-dried ucb-35440-3 5%, Methocel E15<sup>®</sup> 0.1% w/v nanosuspension was made. Comparisons of the dissolution profiles at pH 3.0, pH 5.0 and pH 6.5 are shown in **Figures IV 4 8, IV 4 9 and IV 4 10**, respectively.

As we can clearly see in **Figures IV 4 8, IV 4 9 and IV 4 10**, dissolution rate characteristics are clearly enhanced for ucb-35440-3 nanoparticles when compared to the un-milled drug at all tested pHs. We can further note that this observed difference increases with increasing pH (pH 3.0 → pH 5.0 → pH 6.5), meaning in an environment increasingly unfavorable to drug dissolution.

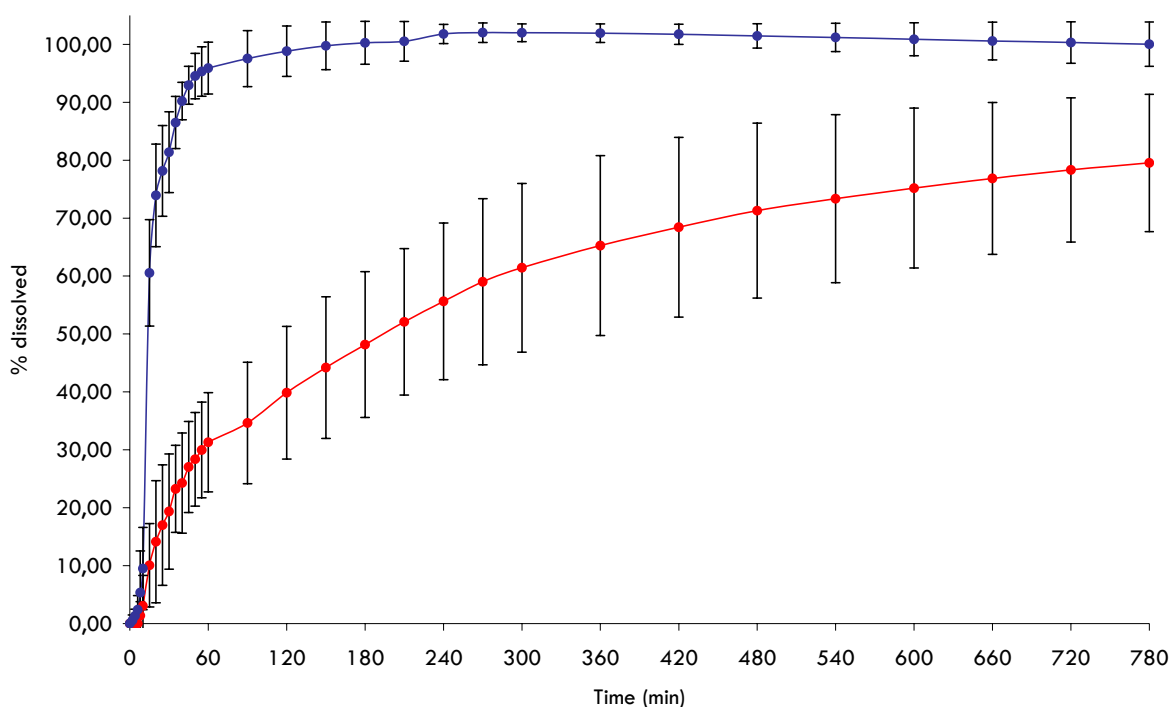


**Figure IV 4 8.** Dissolution profiles for ucb-35440-3 200 mg samples (mean  $\pm$  SD; n=3) (medium: 50 mmol phosphate buffer pH 3.0 - 0.05% polysorbate 20): un-milled ucb-35440-3 (**red**) and ucb-35440-3 5%, Methocel E15<sup>®</sup> 0.1% freeze-dried nanosuspension (PMC + 20C 23-24000 PSI) (**blue**).

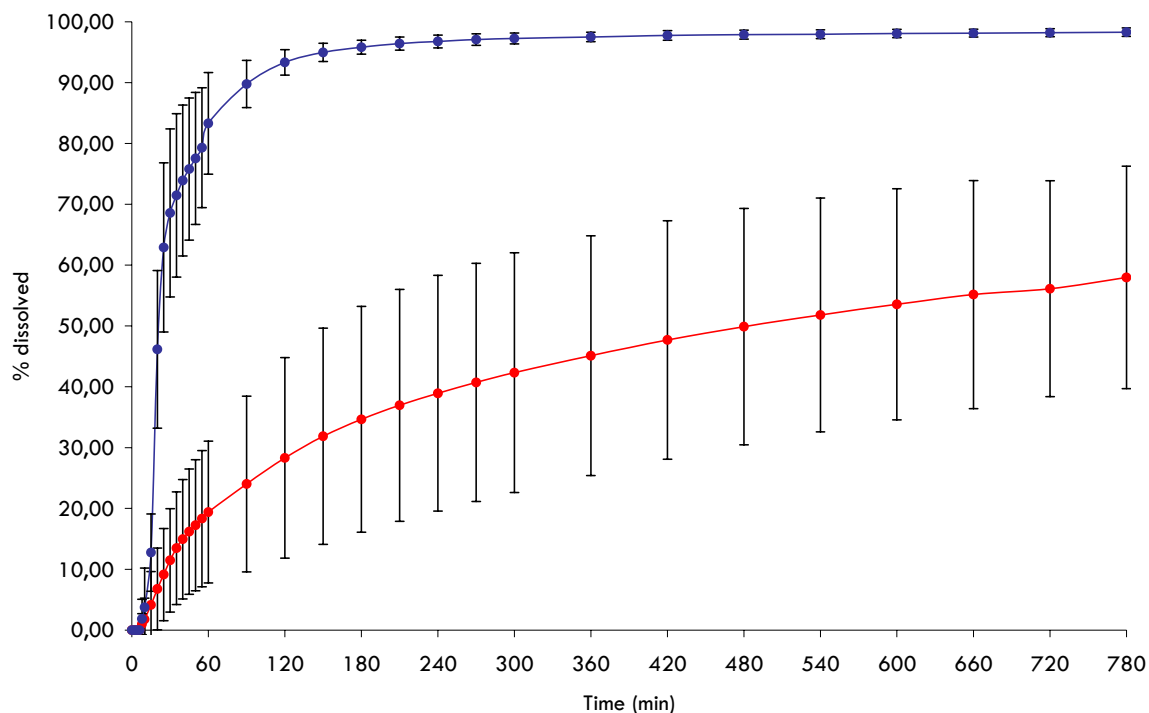


**Figure IV 4 9.** Dissolution profiles for ucb-35440-3 200 mg samples (mean  $\pm$  SD; n=3) (medium: 50 mmol phosphate buffer pH 5.0 - 0.05% polysorbate 20): un-milled ucb-35440-3 (**red**) and ucb-35440-3 5%, Methocel E15<sup>®</sup> 0.1% freeze-dried nanosuspension (PMC + 20C 23-24000 PSI) (**blue**).

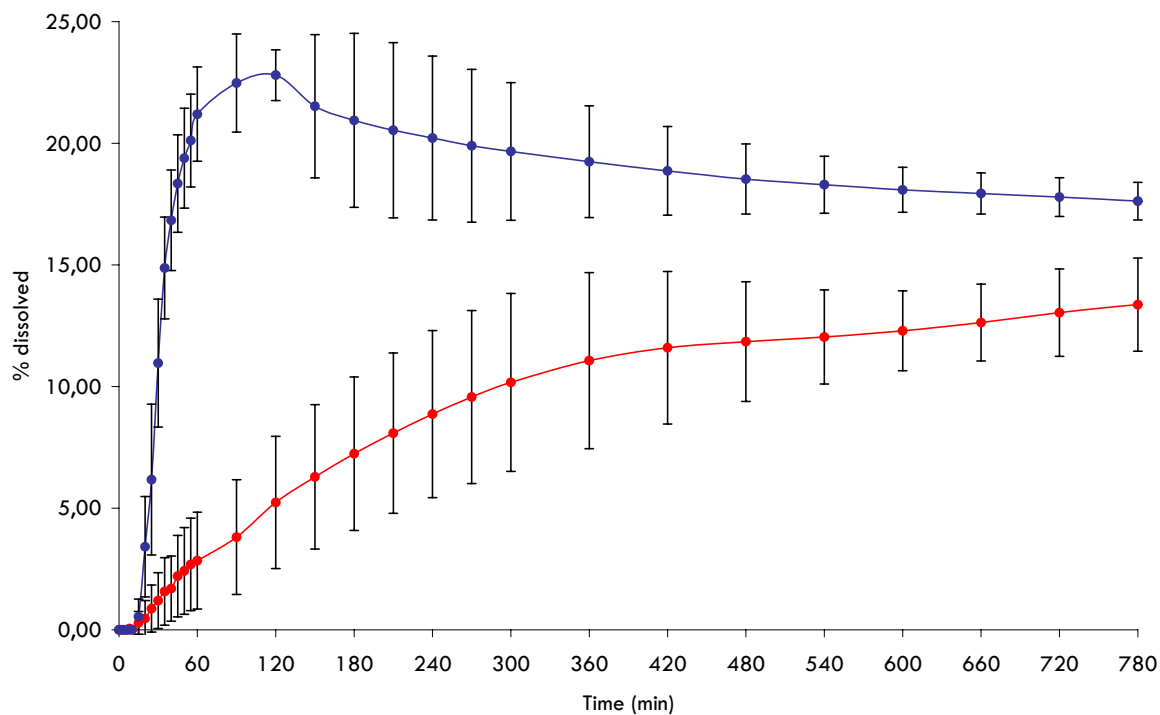


**Figure IV 4 10.** Dissolution profiles for ucb-35440-3 200 mg samples (mean  $\pm$  SD; n=3) (medium: 50 mmol phosphate buffer pH 6.5 - 0.05% polysorbate 20): un-milled ucb-35440-3 (**red**) and ucb-35440-3 5%, Methocel E15<sup>®</sup> 0.1% freeze-dried nanosuspension (PMC + 20C 23-24000 PSI) (**blue**).

The approximate 10 min lag time observed for each formulation can be attributed to capsule disintegration. At pH 3.0, more than 95% of the drug was already dissolved after 60 min for ucb-35440-3 nanoparticles compared to dissolution of around 30% of the un-milled ucb-35440-3 after the same time period and complete dissolution being unachieved for the latter over a span of 13 h. Similar observations could be made for dissolution at pH 5.0 (which is less favorable to ucb-35440-3 dissolution) as after 60 min 85% of the drug nanoparticles were already dissolved compared to 20% of un-milled ucb-35440-3, with the same observation regarding complete dissolution as for pH 3.0. An increased dissolution rate for ucb-35440-3 nanoparticles was also observed at pH 6.5 (**Figure IV 4 10**), where after 60 min approximately 20% of the drug was dissolved compared to 3% for un-milled ucb-35440-3. As it is shown in **Figure IV 4 11**, the dissolution rate at the beginning of the test (first 25 minutes if we subtract capsule disintegration time and consider the real beginning of drug dissolution) is enhanced by an 11-fold factor for ucb-35440-3 nanoparticles when compared to the un-milled drug (i.e. 1.38 mg/min vs. 0.12 mg/min). Due to the low saturation solubility at pH 6.5, saturation of the dissolution media is rapidly reached for nanoparticles at this pH, and recrystallization is observed. Drug dissolution at this pH has to be evaluated under different conditions (e.g. flow-through dissolution). Results from this evaluation are shown and described in **part IV.4.3.2.2.2** of this chapter. Finally, the standard deviations observed in the dissolution profiles (**Figures IV 4 8, IV 4 9 and IV 4 10**) were also shown to be smaller for ucb-35440-3 nanoparticles; the un-milled drug being received as a coarse powder with a large polydispersity with the resulting observed dissolution profiles showing high variations.

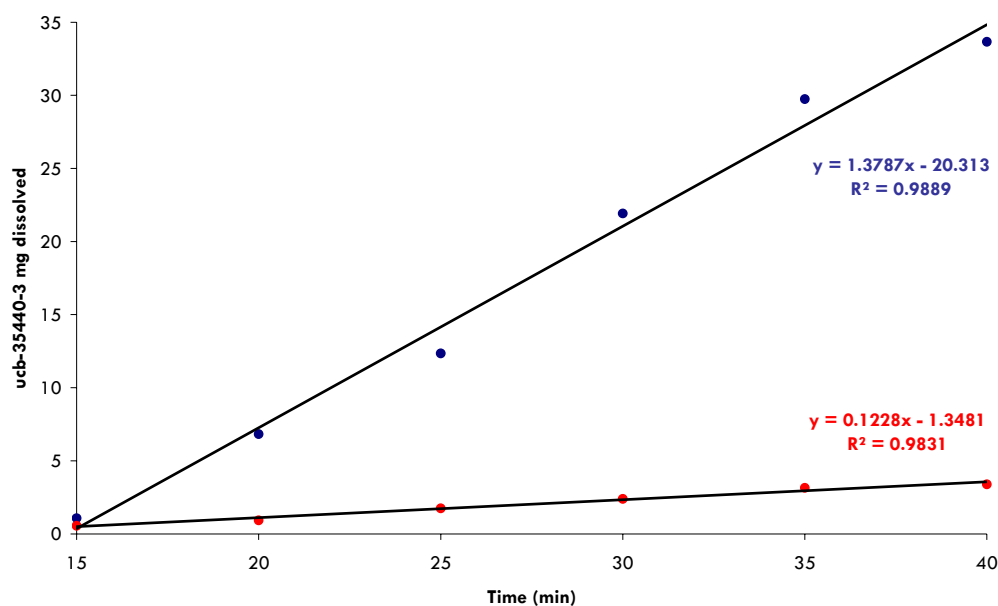


**Figure IV 4 11.** Evaluation of ucb-35440-3 dissolution rate at pH 6.5 (50 mmol phosphate buffer - 0.05% polysorbate 20): un-milled ucb-35440-3 (red) and ucb-35440-3 5%, Methocel E15<sup>®</sup> 0.1% freeze-dried nanosuspension (PMC + 20C 23-24000 PSI) (blue). (data calculated from mean values of Figure IV 4 10).

It has to be noted, when referring to the results presented in **part IV.2.3.5** of this work, that the ucb-35440-3 5%, Methocel E15<sup>®</sup> 0.1% freeze-dried nanosuspension used for assaying ucb-35440-3 dissolution characteristics using the USP type II apparatus (**Figures IV 4 8, IV 4 9 and IV 4 10**) does not present good redispersion characteristics (agglomeration during the water-removal operation - see **Figures IV 2 22 and IV 2 24**). This formulation, however, similarly to the spray-dried NIF formulation A described in **part IV.4.3.2.1** of this chapter, is certainly represented by large agglomerates presenting relatively high porosity. In this way, the desired benefits from increased surface area through particle size reduction are not completely lost during the agglomeration of the nanoparticles in suspension so that, as it is observed, the dissolution rate can still be enhanced for these formulations. The presence of carriers added in the formulation prior to the water-removal operation, particularly mannitol, has been shown to be greatly beneficial with regard to redispersion characteristics enhancement (NIF and ucb-35440-3 - see **part IV.2.3.5** and **Figure IV 2 26** for ucb-35440-3 redispersion in the presence of mannitol) and to further dissolution rate enhancement of NIF nanoparticles (**Figure IV 4 7**). The influence of the presence of mannitol in the formulation with regard to the dissolution characteristics of ucb-35440-3 nanoparticles was not evaluated in this section. This is explained by the fact that these problems regarding redispersion characteristics appeared using the flow-through dissolution system and that, time-wise, these flow-through dissolution assays were conducted after the USP type II dissolution assays. Furthermore, the intention was, in a first approach, to minimize the number of additives in the formulation, particularly their concentration, as the anticipated human pharmacologically active dose was predicted at around 250-500 mg. Mannitol was in fact used at a concentration of 100% (w/w relative to ucb-35440-3 content) for enhancing the redispersion characteristics, which could be problematic for further sample processing. We can, however, predict that the ucb-35440-3 dissolution rate, although already clearly enhanced, might be further enhanced with the presence of mannitol in the formulation.

#### **IV.4.3.2.2.2. USP type IV apparatus - Flow-through dissolution system**

In order to further investigate ucb-35440-3 dissolution characteristics at pH 6.5, the least favourable pH to drug dissolution (as it can be seen from **Figures IV 4 8, IV 4 9 and IV 4 10**), evaluations using the flow-through dissolution apparatus were carried out (equivalent of 200 mg of ucb-35440-3 in powder state). The flow-through (USP type IV) dissolution apparatus is a valuable and very useful tool for evaluating the dissolution profile of

poorly water-soluble compounds with regard to the maintenance of sink conditions as, contrarily to the USP type II apparatus, large volumes of dissolution media can be processed (no limitation, although these volumes still need to be representative of in vivo conditions - USP type II limited to 1l). We used a volume of 5 l for ucb-35440-3 dissolution evaluation. It should be noted that sink conditions are still not respected at pH 6.5 with this tested volume and the quantity of drug assayed (i.e. 200 mg); saturation solubility at pH 6.5 being approximately 0.03mg/ml, a dissolution volume of 66.6 l would be needed to respect sink conditions. The volume of 5 l was chosen following the observation of the dissolution profile shown in **Figure IV 4 10** where, in 0.9 l, dissolution of 25% of drug (i.e. 50 mg of ucb-35440-3) was reached. **Table IV 4 11** summarizes all the ucb-35440-3 formulations assayed in this section.

**Table IV 4 11.** Studied ucb-35440-3 formulations (PMC + 10C 23-24000 PSI HPH) - additives other than surfactants were added following the high pressure homogenization and prior to the water-removal operation.

	Surfactant	Mannitol	Emcompress®	Kollidon CL®	Water-removal operation
<b>Formulation A</b>	HPMC 2%	-	-	-	Freeze-drying
<b>Formulation B</b>	HPMC 2%	100%	-	-	Freeze-drying
<b>Formulation C</b>	AG 2%	100%	-	-	Freeze-drying
<b>Formulation D</b>	AG 2%	200%	-	-	Freeze-drying
<b>Formulation E</b>	AG 2%	100%	100%	-	Spray-drying
<b>Formulation F</b>	HPMC 2%	100%	-	100%	Spray-drying

AG: Acaciae gum; HPMC: Hydroxypropylmethylcellulose (Methocel E15®)

Similarly to the dissolution test (**USP type II**) represented in **Figure IV 4 10**, comparison between un-milled ucb-35440-3 and a freeze-dried ucb-35440-3 5%, Methocel E15® 0.1% w/v nanosuspension was made using the flow-through dissolution apparatus. In a first approach, the conditions of the test were as follows: 5 l of a pH 6.5 50 mM phosphate buffer, flow rate 20 ml/min and tablet cell half-filled with glass beads (**Figure IV 4 2**). The dissolution profiles obtained for both un-milled ucb-35440-3 and ucb-35440-3 nanoparticles are shown in **Figure IV 4 12**.

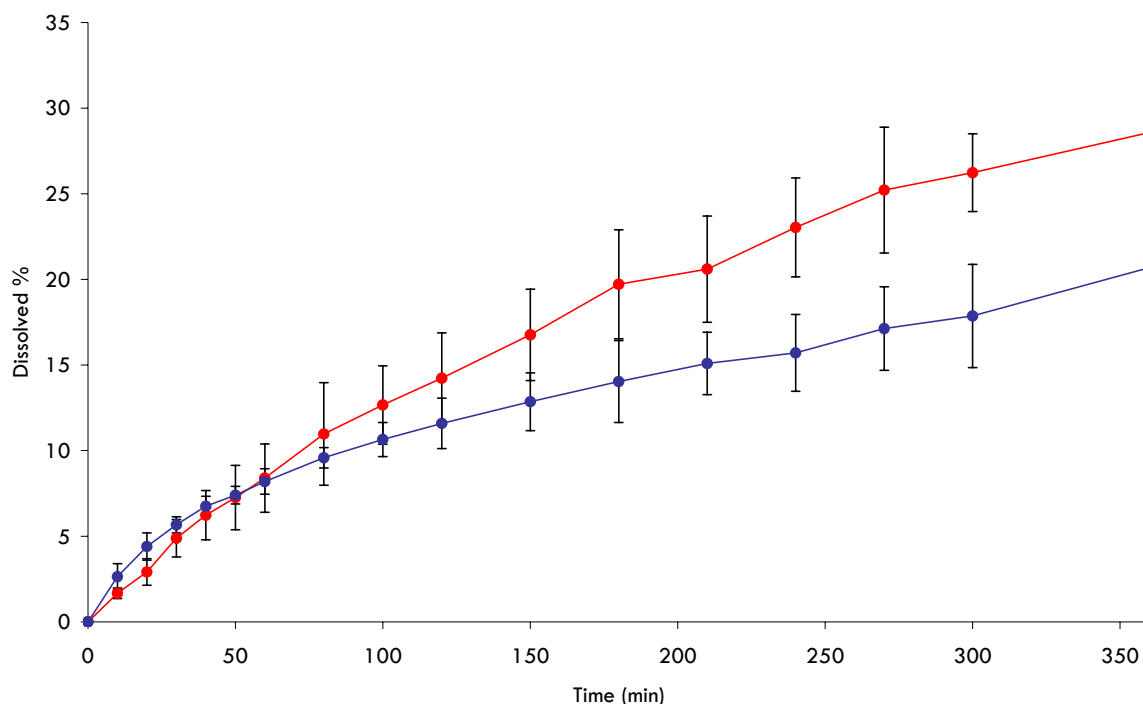


**Figure IV 4 12.** Flow-through dissolution assay for ucb-35440-3 200 mg sample (FR: 20 ml/min): un-milled ucb-35440-3 (red) and ucb-35440-3 NP formulation A (blue). Mean  $\pm$  SD; n=3.

From the data shown in **Figure IV 4 12**, we can see that no dissolution rate enhancement was observed for ucb-35440-3 nanoparticles when compared to the un-milled drug; the profile was very similar over the first hour of the test, a period where a difference, if they were any, should have been observed when looking at the results from **Figure IV 4 10** (USP type II apparatus). More surprisingly, a slight decrease was even observed following this one hour period. This observation, rather contradictory to the results obtained with the USP method II dissolution apparatus, was first thought to be the consequence of the poor redispersion characteristics of the water-removed nanosuspension (formulation A) (see **Figure IV 2 22** and **Figure IV 2 24 - part IV.2.3.5** of this work). Furthermore, agglomeration of the powder inside the dissolution cell was clearly visible. To overcome this problem, a formulation containing mannitol (100% w/w relative to ucb-35440-3), added as a water-soluble carrier (see **part IV.2.3.5** and **Figure IV 2 26** for ucb-35440-3 redispersion in the presence of mannitol), was assayed as redispersion characteristics were much improved from the previous, mannitol-free formulation. The dissolution profile obtained for ucb-35440-3 nanoparticles (formulation B) is shown in **Figure IV 4 13**. The dissolution profiles for un-milled ucb-35440-3 and ucb-35440-3 nanoparticles (formulation A) are again shown in this figure for comparison.

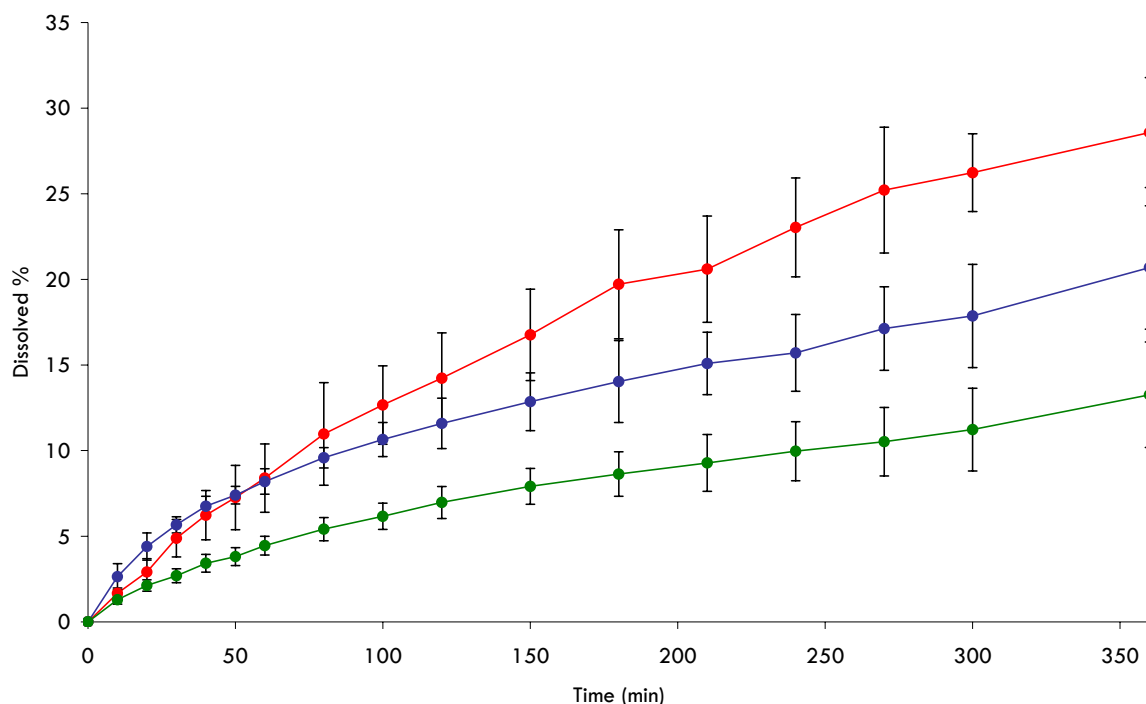


**Figure IV 4 13.** Flow-through dissolution assay for ucb-35440-3 200 mg sample (FR: 20 ml/min): un-milled ucb-35440-3 (red), ucb-35440-3 NP formulation A (blue) and ucb-35440-3 NP formulation B (green). Mean  $\pm$  SD; n=3.

Contrarily to what was expected if the problem was to come from redispersion characteristics, the dissolution rate is shown to be even slower for the mannitol-added formulation (ucb-35440-3 NP formulation B). Here again, though, agglomeration could still be observed inside the dissolution cell at the beginning of the dissolution run.

The influence of the flow rate of the dissolution medium was then investigated in order to evaluate its possible implication in limiting particle agglomeration. The medium flow rate was increased from 20 ml/min to 40 ml/min.

**Figure IV 4 14** shows the flow-through dissolution profiles for un-milled ucb-35440-3 and ucb-35440-3 nanoparticles (formulation B) at both tested flow rates. From the results shown on this figure, we can clearly see that the flow rate has no effect on un-milled ucb-35440-3 dissolution. However, for ucb-35440-3 nanoparticles (formulation B), flow rate has a clear influence as 13% and 27% of the drug was dissolved, following the 6-hour test, for a flow rate of 20 ml/min and 40 ml/min, respectively. Increased flow rate has thus, as it was expected, a beneficial effect in limiting particle agglomeration inside the dissolution cell. However, for a flow rate of 40 ml/min, there is still no difference between ucb-35440-3 nanoparticles and un-milled ucb-35440-3. The influence of the type of surfactant in the formulation was thus investigated, with HPMC being replaced by acaciae gum (AG). Results from this evaluation are shown in **Figure IV 4 15**.

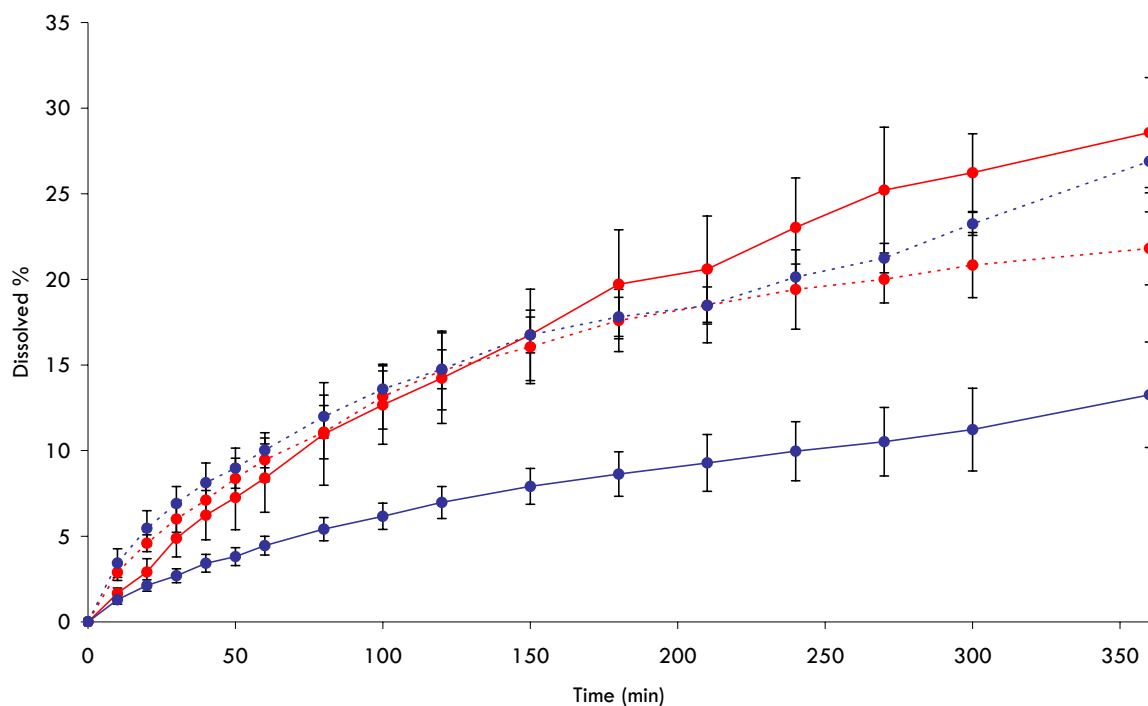


**Figure IV 4 14.** Flow-through dissolution assay for ucb-35440-3 200 mg sample (influence of flow rate): un-milled ucb-35440-3: FR 20 ml/min (**red - plain**) and FR 40 ml/min (**red - dashed**); ucb-35440-3 NP formulation B: FR 20 ml/min (**blue - plain**) and FR 40 ml/min (**blue - dashed**). Mean  $\pm$  SD; n=3.

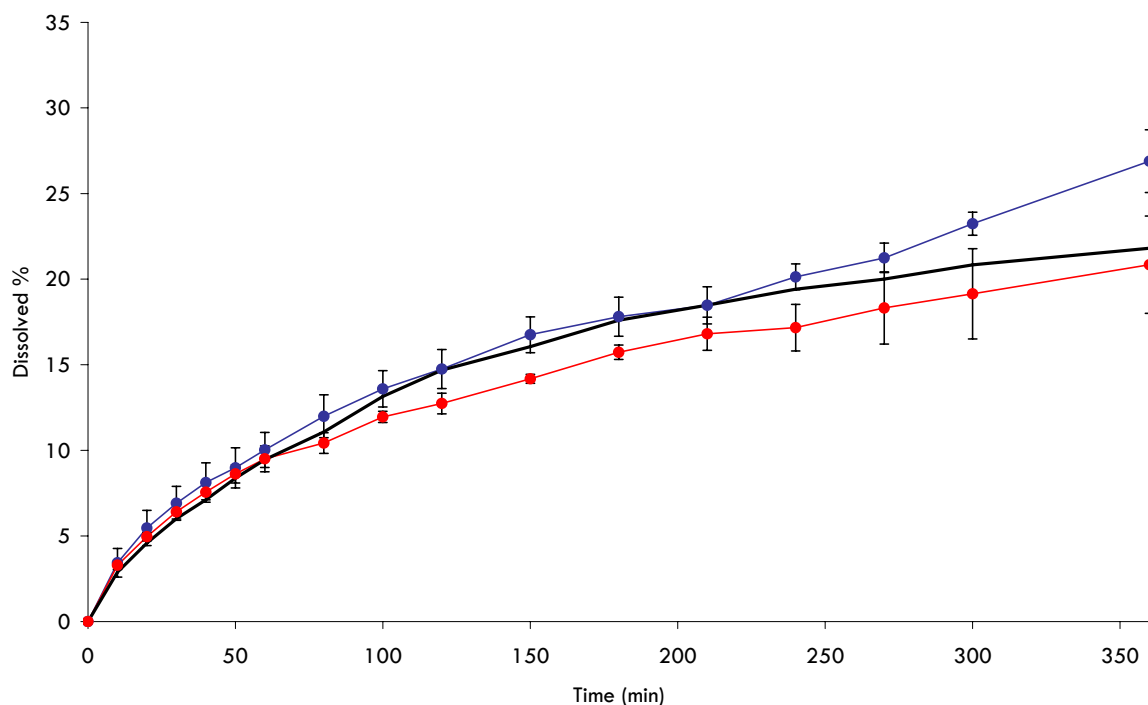


**Figure IV 4 15.** Flow-through dissolution assay for ucb-35440-3 200 mg sample (FR 40 ml/min) (influence of surfactant): ucb-35440-3 NP formulation B (**blue**) and ucb-35440-3 NP formulation C (**red**). Un-milled ucb-35440-3 (**black**) placed as a reference. Mean  $\pm$  SD; n=3 (n=2 for formulation C).



From the results observed in **Figure IV 4 15**, we can see that the type of surfactant used for nanoparticle stabilization (i.e. during high pressure homogenization) has no influence on the dissolution of ucb-35440-3 nanoparticles. Powder agglomeration on top of the glass beads could still be observed in this evaluation.

The next evaluation consisted of increasing the percentage of carrier used and in changing the type of carrier. First, the percentage of mannitol (relative to ucb-35440-3 content) in the AG/mannitol formulation presented above (ucb-35440-3 formulation C) was increased to 200% (ucb-35440-3 formulation D). In a next step, Emcompress® (CaHPO<sub>4</sub>·2H<sub>2</sub>O) was added at 100% w/w relative to ucb-35440-3 (ucb-35440-3 formulation E) to the ucb-35440-3 formulation C as a water-insoluble carrier to prevent particle agglomeration inside the flow-through dissolution cell. This Emcompress®-added formulation has already been characterized (SEM/SEM-EDS/PXRD - cf. **Figures IV 2 27, IV 2 28 and IV 2 29**) and described in **part IV.2.3.5** of this work. The dissolution profiles for ucb-35440-3 nanoparticle formulations D and E are represented in **Figure IV 4 16**. As we can see from the results presented in this figure, here again, although it was slightly enhanced for the Emcompress®-containing formulation, the dissolution rate achieved with ucb-35440-3 nanoparticles is comparable to the dissolution rate of un-milled ucb-35440-3. An increase in the percentage of mannitol was shown to have practically no influence on drug dissolution. Emcompress®, as it was expected from the data presented in **part IV.3.3.6**, limits to some extent particle agglomeration inside the dissolution cell and thus allows for a slight increase in dissolution, with 29% of the drug being dissolved following 300 min versus 21% for un-milled ucb-35440-3. As Emcompress® was shown, to some extent, to limit particle agglomeration further development was made in that regard using Kollidon CL® (cross-linked polyvinyl pyrrolidone (PVP)) as a carrier in the ucb-35440-3 nanoparticle formulation B, added at 100% w/w relative to ucb-35440-3 (ucb-35440-3 formulation F). Cross-linked PVP belongs to a class of pharmaceutical excipients called “super-desintegrants”, primarily used in tablet manufacture. Although no results regarding ucb-35440-3 nanoparticle redispersion characteristics were presented in **part IV.2.3.5** of this work (cross-linked PVP interfering with LD measurements due to limited water-solubility and no SEM/SEM-EDS analysis possible), ucb-35440-3 nanoparticles are thought to surround the excipient particles homogeneously, as it was the case for Emcompress®. Cross-linked PVP was thought to be useful in solving the problem of “agglomeration inside the dissolution cell” problem as this excipient will swell when put in contact with the dissolution media, thus limiting particle-particle interactions and thus agglomeration. Cross-linked PVP was, as for mannitol and Emcompress®, added to the ucb-35440-3 suspension after the high pressure homogenization (i.e. to the nanosuspension) and prior to the water-removal operation (in this case spray-drying). The dissolution profile for ucb-35440-3 nanoparticles E is represented in **Figure IV 4 16**.

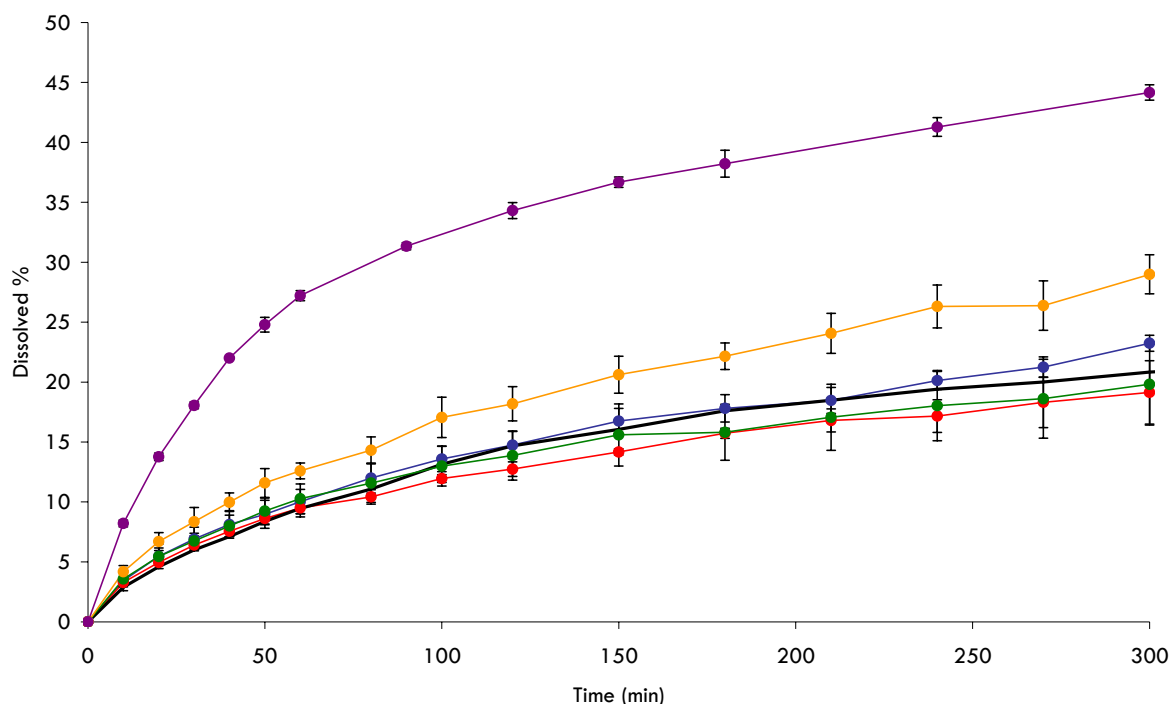


**Figure IV 4 16.** Flow-through dissolution assay for ucb-35440-3 200 mg sample (FR 40 ml/min) (influence of carrier): ucb-35440-3 NP formulation D (**green**), ucb-35440-3 NP formulation E (**orange**), ucb-35440-3 NP formulation F (**purple**). Un-milled ucb-35440-3 (**black**), ucb-35440-3 NP formulation B (**blue**) and ucb-35440-3 NP formulation C (**red**) placed as references. Mean  $\pm$  SD; n=3 (n=2 for formulation C).

As we can see in this figure, drug dissolution can clearly be enhanced using cross-linked PVP in ucb-35440-3 nanoparticle formulations when compared to the un-milled drug, with 44% of the drug being dissolved following 300 min versus 22% for un-milled ucb-35440-3.

Following the observations made for ucb-35440-3 formulations E and F (Emcompress®, cross-linked PVP), particle agglomeration inside the flow-through dissolution cell is the clear factor limiting drug dissolution from ucb-35440-3 nanoparticle formulations. This agglomeration was attributed to the fact that the surfactants and hydrophilic carriers used in the formulations are rapidly dissolved by the dissolution media and rapidly leave the dissolution cell, thus creating an unstable system (the ucb-35440-3 nanoparticles being more hydrophobic), which leads to particle agglomeration inside the cell. From all dissolution evaluations made and from what could be observed through the dissolution runs, the problem encountered for nanoparticulate formulations would thus be inherent to the flow-through dissolution test conditions and, more precisely, to the agitation conditions and to the small volume characterizing the dissolution cells: this one is approximately of 11 cm<sup>3</sup>, a volume thought to be insufficient for adequate particle dispersion and thus leading to the agglomeration phenomenon observed.

To further limit particle agglomeration inside the dissolution cells, dissolution runs comparing ucb-35440-3 nanoparticle formulation F and un-milled ucb-35440-3 were carried out by filling the flow-through dissolution powder cell with glass beads up to the top (**Figure IV 4 17**). In fact the visible agglomeration phenomena occurring at the beginning of the dissolution tests occurred after the incoming dissolution media had displaced the assayed formulations to the top of the bead bed; the formulations being homogeneously mixed with the glass beads in sample and dissolution bath preparation - cf. **part IV.4.2.4** of this section.

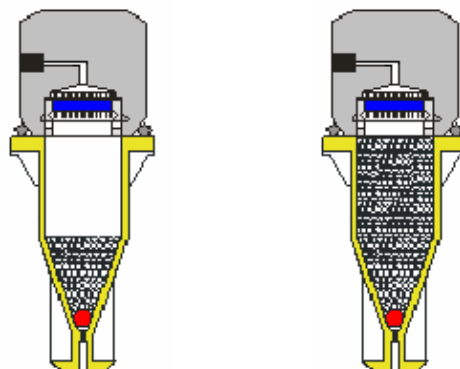


**Figure IV 4 17.** Schematic representation Tablet cells half-filled with glass beads (normal filling) (**left**) and fully-filled with glass beads (normal filling) (**right**). The assayed formulations are homogeneously mixed with these glass beads.

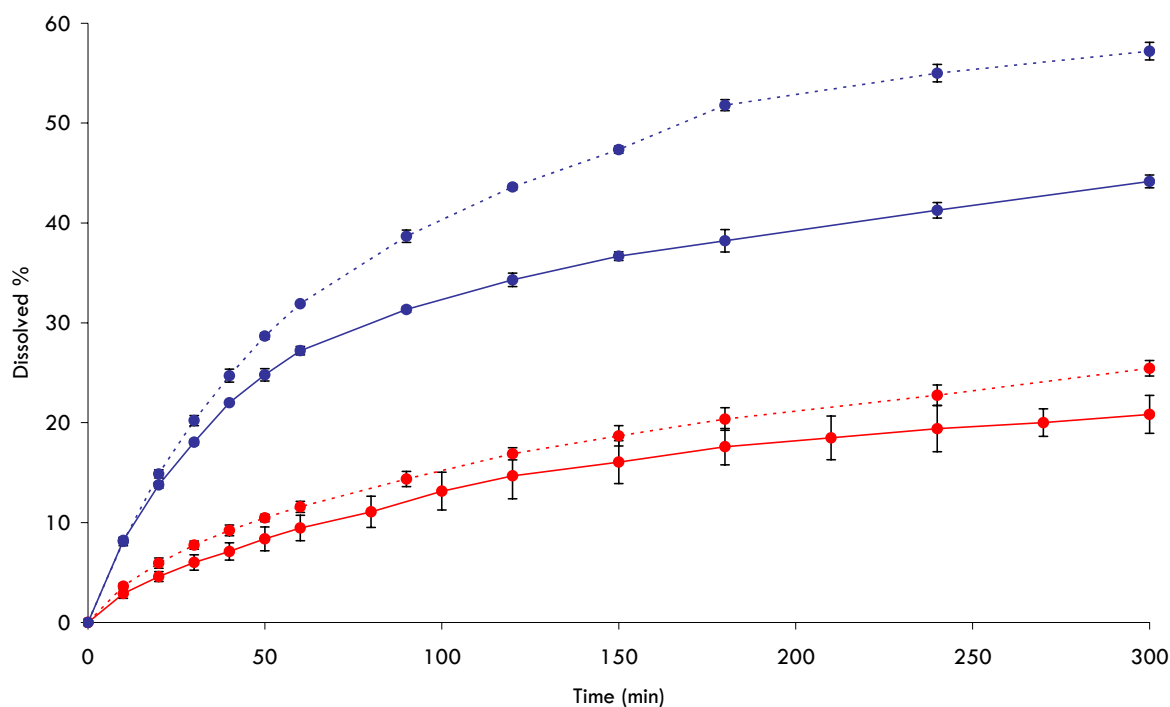


**Figure IV 4 18.** Flow-through dissolution assay for ucb-35440-3 200 mg sample (FR 40 ml/min) (influence of filling - flow-through dissolution cell): Un-milled ucb-35440-3: half-filled (**red - plain**) and fully-filled (**red - dashed**) and ucb-35440-3 NP formulation F: half-filled (**blue - plain**) and fully-filled (**blue - dashed**) Mean  $\pm$  SD; n=3.

Fully filling the dissolution cell with glass beads was thought to be a possible limitation to this phenomenon. The dissolution profiles for ucb-35440-3 nanoparticle formulation F and un-milled ucb-35440-3 using half-filled and fully-filled dissolution cells are shown in **Figure IV 4 18**. We can clearly see from these results that cell filling has an influence on drug dissolution, in particular for ucb-35440-3 nanoparticles, with 57% of the drug being dissolved following 300 min for fully-filled dissolution cells versus 44% for half-filled dissolution cells. For un-milled ucb-35440-3, 25% of the drug was dissolved following 300 min for fully-filled dissolution cells versus 21% for half-filled cells. This difference can be explained, as we hypothesized, by the fact that glass beads limit, to some extent, particle-particle interactions (powder being homogeneously mixed with the glass beads) and thus subsequent agglomeration, more so if the dissolution is fully-filled with these glass beads (powder is no longer left on top of the glass beads bed, as it is the case for half-filled cells). In the case of drug nanoparticles, the agglomeration inside the dissolution cell seems to be the limitation to drug dissolution, along with, of course, the poor solubility and poor dissolution characteristics at the tested pH.

In addition to the small dissolution cell volume, the type of dissolution media could also have an influence on the observed particle agglomeration phenomenon. In fact, the presence of surfactants might also limit, to some extent, this agglomeration. To denote this influence, drug dissolution was carried out using the fasted state simulated intestinal fluid (FaSSiF) media. This dissolution media, a pH 6.5 media containing sodium taurocholate and lecithin as surfactants, is more and more frequently used for drug dissolution evaluation (in association to FeSSiF media - fed state simulated intestinal fluid (pH 5.0)) as it is fairly simple to prepare (**Table IV 4 2**) and has a composition close to the in vivo intestinal conditions in fasted state. This media was used for the evaluation of the dissolution properties of un-milled ucb-35440-3 and ucb-35440-3 nanoparticle formulation B (spray-dried ucb-35440-3 5%, Mannitol 5%, Methocel E15<sup>®</sup> 0.1% w/v nanosuspension) and formulation F (spray-dried ucb-35440-3 5%, Mannitol 5%, Kollidon CL<sup>®</sup> 5%, Methocel E15<sup>®</sup> 0.1% w/v nanosuspension). The results from this evaluation are shown in **Figure IV 4 19**. Comparisons with the results obtained in phosphate buffer pH 6.5 for the cited formulations are also made in this figure. As it is clearly shown from the results presented on this figure, drug dissolution is clearly enhanced in the FaSSiF media when compared to drug dissolution in the phosphate buffer; this is the case for un-milled ucb-35440-3 and for both assayed ucb-35440-3 nanoparticle formulations (B and F). The percentages of drug dissolved following 300 min in phosphate buffer and in FaSSiF media were 21% and 28%, 23% and 61%, and 44% and 69% for un-milled ucb-35440-3, ucb-35440-3 nanoparticle formulation B and ucb-35440-3 nanoparticle formulation F, respectively. As expected, since the surfactants present in the FaSSiF media (sodium taurocholate and lecithin) are certainly more efficient than polysorbate 20 in limiting particle agglomeration (their concentrations being also higher than the polysorbate concentration used in the

phosphate buffer assayed), the difference in drug dissolution between the two dissolution media was higher for ucb-35440-3 nanoparticles (formulation B and formulation F) than for un-milled ucb-35440-3. This observation, along with what was observed from **Figures IV 4 16** and **IV 4 18**, allows us to conclude that one of the main limiting factors to drug dissolution from the ucb-35440-3 nanoparticle formulations comes from particle agglomeration inside the flow-through dissolution cell; this is probably due to the small volume characterizing these cells (i.e.  $\sim 11 \text{ cm}^3$ ). This can also be complemented by the observation made in **Figures IV 4 10** and **IV 4 11**, where the relatively fast dissolution rate for ucb-35440-3 nanoparticles (1.38 mg/min vs. 0.12 mg/min for un-milled ucb-35440-3) could certainly be achieved as drug particles were allowed to disperse in a volume equivalent to 900ml (i.e. this achieved dissolution rate and the difference observed could not be reproduced using flow-through dissolution as the dissolution volume inside the dissolution cell is probably too small).

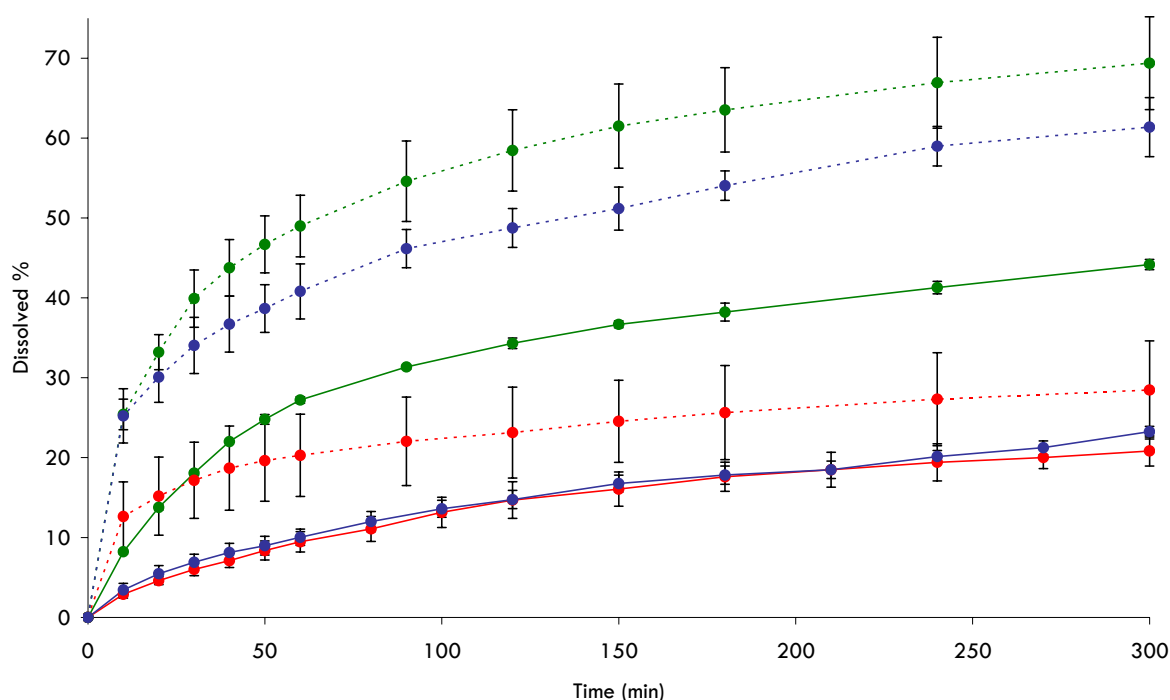


**Figure IV 4 19.** Flow-through dissolution assay for ucb-35440-3 200 mg sample (FR 40 ml/min) (influence of dissolution medium): Un-milled ucb-35440-3; 50 mM phosphate buffer pH 6.5 (0.05% polysorbate 20) (**red - plain**) and FaSSiF media (**red - dashed**); ucb-35440-3 (NP) formulation B; 50 mM phosphate buffer pH 6.5 (0.05% polysorbate 20) (**blue - plain**) and FaSSiF media (**blue - dashed**); ucb-35440-3 (NP) formulation F; 50 mM phosphate buffer pH 6.5 (0.05% polysorbate 20) (**green - plain**) and FaSSiF media (**green - dashed**). Mean  $\pm$  SD; n=3 (n=2 for un-milled ucb-35440-3 in FaSSiF).

## IV.4.3.2.3. UCB-A

The dissolution rate of UCB-A was assayed on micronized UCB-A particles and on UCB-A nanoparticles (UCB-A formulation A and B - **Table IV 4 12**) placed into 00 gelatin capsules (equivalent of 25 mg UCB-A/capsules). Dissolution was first evaluated on UCB-A formulation A. All dissolution assays were run in controlled-pH media. The dissolution profile of both samples was assayed at pH 4.0, pH 5.0 and in HCl 0.1N. All dissolution media were surfactant-free.

**Table IV 4 12.** Studied UCB-A formulations (PMC + 20C 23-24000 PSI + 10C 30000 PSI HPH). SDS: Sodium dodecyl sulphate, HPMC: Hydroxypropylmethylcellulose (Methocel E15®).

	UCB-A	Methocel E15®	SDS	Poloxamer 407	Water-removal operation
<b>Formulation A</b>	5%	0.5%	0.1%	-	Spray-drying
<b>Formulation B</b>	5%	0.5%	-	0.25%	Spray-drying

Keeping in mind the pH-dependent solubility profile of UCB-A (**Figure IV 4 5** - **Table IV 4 8**), the dissolution profile was first evaluated at pH 5.0, a pH less favorable to UCB-A dissolution and where the difference, if we were to find one, between the two systems might be greater. The dissolution profile was also evaluated at pH 4.0 to evaluate the dissolution profiles of the two systems in a more dissolution-friendly medium. Dissolution profiles for micronized UCB-A and UCB-A nanoparticles at pH 5.0 and pH 4.0 are shown on **Figures III 4 20** and **III 4 21**, respectively.

When comparing the dissolution profiles of both systems, either at pH 5.0 and pH 4.0, we can clearly see the enhancement brought by particle size reduction. At pH 5.0, although the achieved dissolution is still relatively poor, we can observe an approximate 6-fold increase in the percentage dissolved following 2 hours for UCB-A nanoparticles vs. that of UCB-A micronized particles (5.5% vs. 0.85%). The same observation can be made for the dissolution profiles of both systems at pH 4.0 as we can also observe an approximate 6-fold increase in the percentage dissolved following 2 hours for UCB-A nanoparticles vs. that of UCB-A micronized particles (32% vs. 5%). **Figure IV 4 21** also shows that, at pH 4.0, dissolution of 50% of the dose assayed can be achieved following 24 hours for UCB-A nanoparticles, vs. only 20% for the micronized drug.

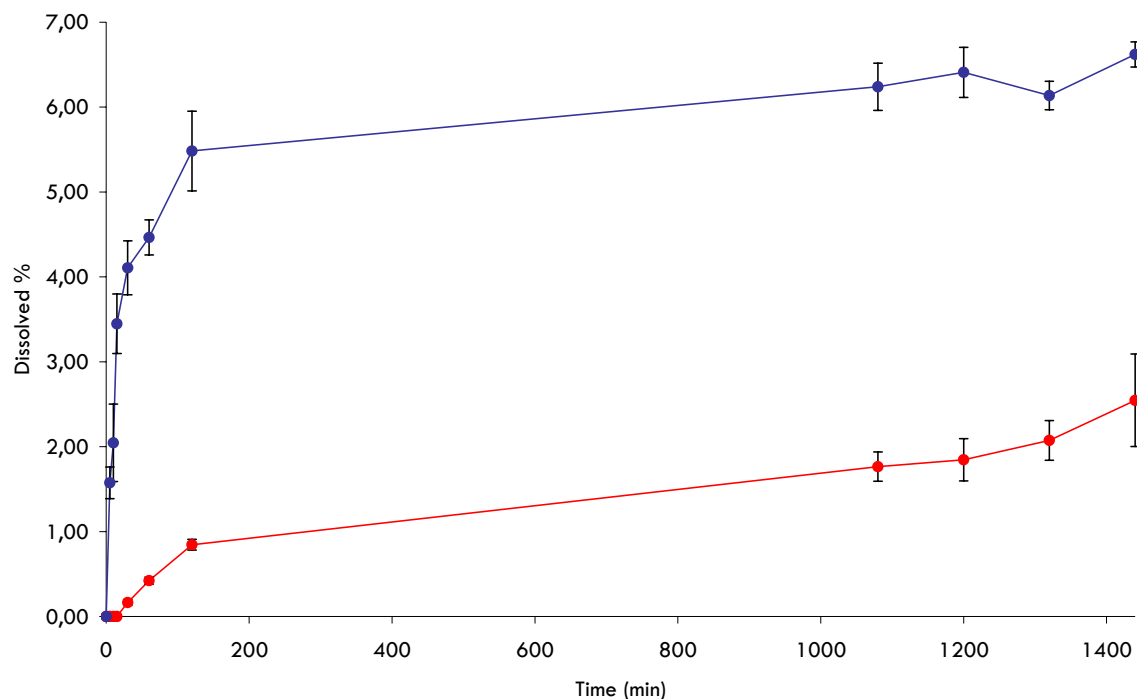


**Figure IV 4 20.** UCB-A dissolution profile in acetate buffer pH 5.0: micronized UCB-A (**red**) and spray-dried UCB-A formulation A nanosuspension (**blue**). Mean  $\pm$  SD; n=3.

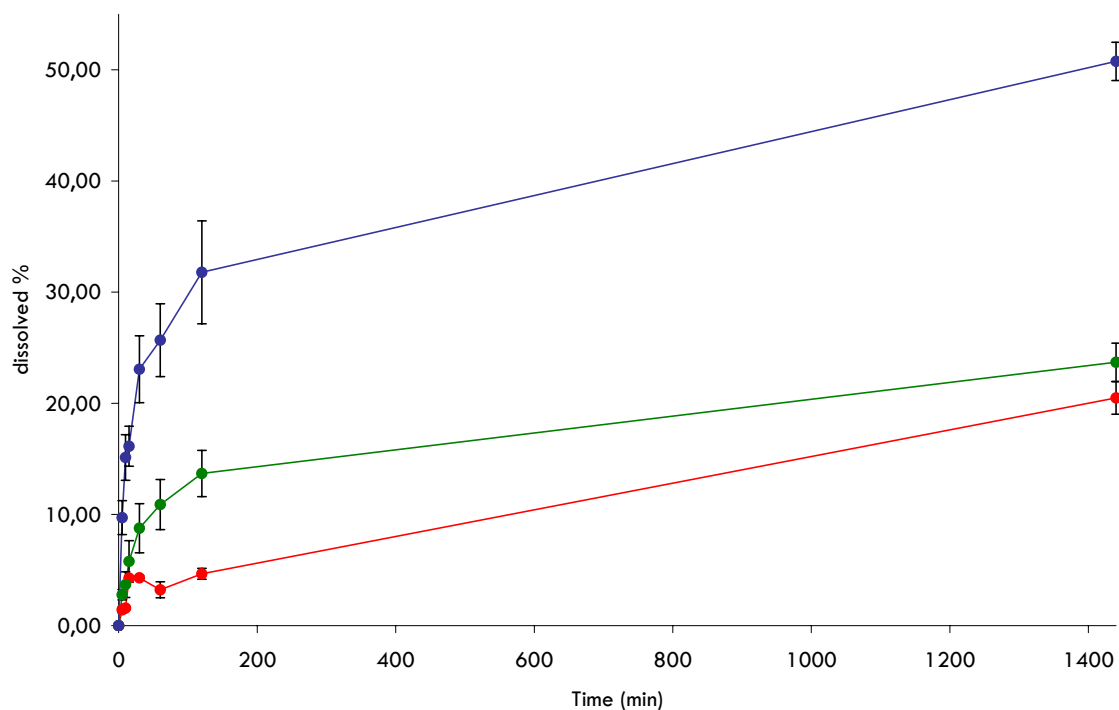


**Figure IV 4 21.** UCB-A dissolution profile in acetate buffer pH 4.0: micronized UCB-A (**red**), spray-dried UCB-A formulation A nanosuspension (**blue**) and spray-dried UCB-A formulation A prior to milling operations (**green**). Mean  $\pm$  SD; n=3.

When comparing the dissolution profiles of the spray-dried UCB-A formulation A before (**Figure IV 4 21** - green curve) and after (**Figure IV 4 21** - blue curve) high pressure homogenization, we can see that the excipients used for nanoparticle stabilization during the high pressure homogenization, although having a positive influence on micronized UCB-A dissolution (hydrophilisation - approximate 3-fold increase in percentage dissolved following 2 hours for the spray-dried UCB-A suspension prior to milling operations vs. UCB-A micronized particles (14% vs. 5%)), are not totally responsible for the dissolution rate enhancement offered by UCB-A nanoparticle formulation A.

Although the data is not shown, it also has to be noted that at pH 4.0, no degradation of UCB-A into UCB-A-Met1 was observed (no degradation peaks in the chromatograms); in fact, as it is shown by the solubility results of **Figure IV 4 5** and **Table IV 4 8**, degradation of UCB-A into UCB-A-Met1 seems to occur only at pH < 2.4. Although the HPLC method used for the dissolution test at pH 5.0 (HPLC method UCBA M1 - **part IV.4.2.5.2.1**) does not allow for the detection of UCB-A-Met1, degradation of UCB-A into UCB-A-Met1 is not of a concern at this pH.

The dissolution profiles of micronized UCB-A and UCB-A nanoparticles were also compared in acidic media (HCl 0.1N). Although the UCB-A dissolution rate should be very fast for both systems due to the increased solubility at this pH range, this evaluation was still carried out to denote any difference. Due to the drug's instability in acidic media (i.e. degradation in UCB-A-Met1), concentrations of both UCB-A and UCB-A-Met1 were quantified. The dissolution profiles in HCl 0.1N are represented in **Figure IV 4 22**. Investigation of the dissolution profile of spray-dried formulation A prior to milling operations to evaluate the influence of the excipients used is also represented in this figure. The sum of dissolved UCB-A and UCB-A-Met1 formed for all three formulations assayed is also represented on this figure. As we can see when observing the UCB-A dissolution profiles of **Figure IV 4 22**, the dissolution rate was found to be greater for micronized UCB-A than for UCB-A nanoparticles, inversely to what was observed at pH 4.0 and pH 5.0. The fast dissolution rate observed for micronized UCB-A, keeping in mind the pH-dependent solubility profile of the drug, is totally understandable as sink conditions are more than respected (solubility pH 1.0 ~ 10 mg/ml - UCB-A in bath (900 ml): 25 mg). For UCB-A nanoparticles, however, the dissolution rate would have been thought to be greater than or equivalent (the dissolution rate being already very fast) to that of the micronized drug. This observation can, however, find an explanation in the type of additives used for the UCB-A nanoparticle preparation. In fact the surfactant used for UCB-A nanoparticles stabilization during high pressure homogenization processing for this formulation (**formulation A - Table IV 4 12**) is sodium dodecyl sulfate (SDS).



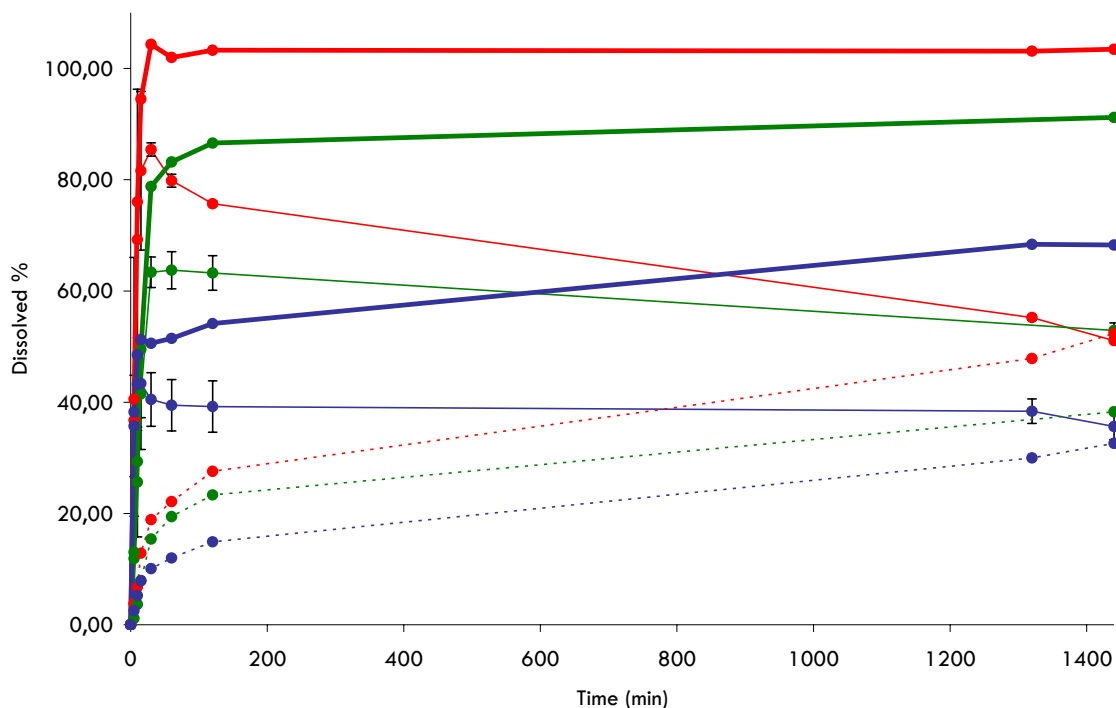


**Figure IV 4 22.** UCB-A dissolution profile in HCl 0.1N: micronized UCB-A (**red**), spray-dried UCB-A formulation A (prior to milling operations) (**green**) and spray-dried UCB-A formulation A (nanoparticles) (**blue**). Plain curves (UCB-A), dotted curves (UCB-A-Met1) and thick plain curves (UCB-A + UCB-A-Met1). Mean  $\pm$  SD; n=3.

This excipient, although showing very interesting properties regarding UCB-A nanoparticle stabilization, has, however, limited solubility in acidic media. As mentioned in **part IV.4.3.1.3** of this work, SDS, present at the particle surface following the spray-drying operation, limits UCB-A solubilization at acidic pH (i.e. HCl 0.1N) and thus diminishes its dissolution rate. This observation, although to a lower extent, is also reported for the spray-dried formulation A prior to milling operations (i.e. spray-dried micronized UCB-A in the presence of HPMC and SDS), which thus supports our given conclusion relative to the dissolution characteristics of spray-dried UCB-A nanoparticle formulation A. When comparing the cumulated UCB-A/UCB-A-Met1 profiles, we find a decrease in the percentage of dissolved drug when comparing the micronized UCB-A (no excipients) (100% following 30 min and up to the end of the 24-h test), the spray-dried UCB-A formulation A prior to milling operations (91% at the end of the 24-h test) and the spray-dried UCB-A formulation A nanosuspension (68% at the end of the 24-h test). **Figure IV 4 22** also shows that the degradation of UCB-A into UCB-A-Met1, for all three formulations studied, is very fast. Evaluation of the dissolution profile of UCB-A nanoparticles in HCl 0.1N shall thus be made on an SDS-free formulation.

Drug dissolution from the UCB-A nanoparticle formulation B (containing HPMC and poloxamer 407 as stabilizers) was thus evaluated in HCl 0.1N. Here again, comparison with micronized UCB-A and a spray-dried equivalent formulation prior to the milling operations was made. Results of this evaluation are shown in **Figure IV 4 23**.

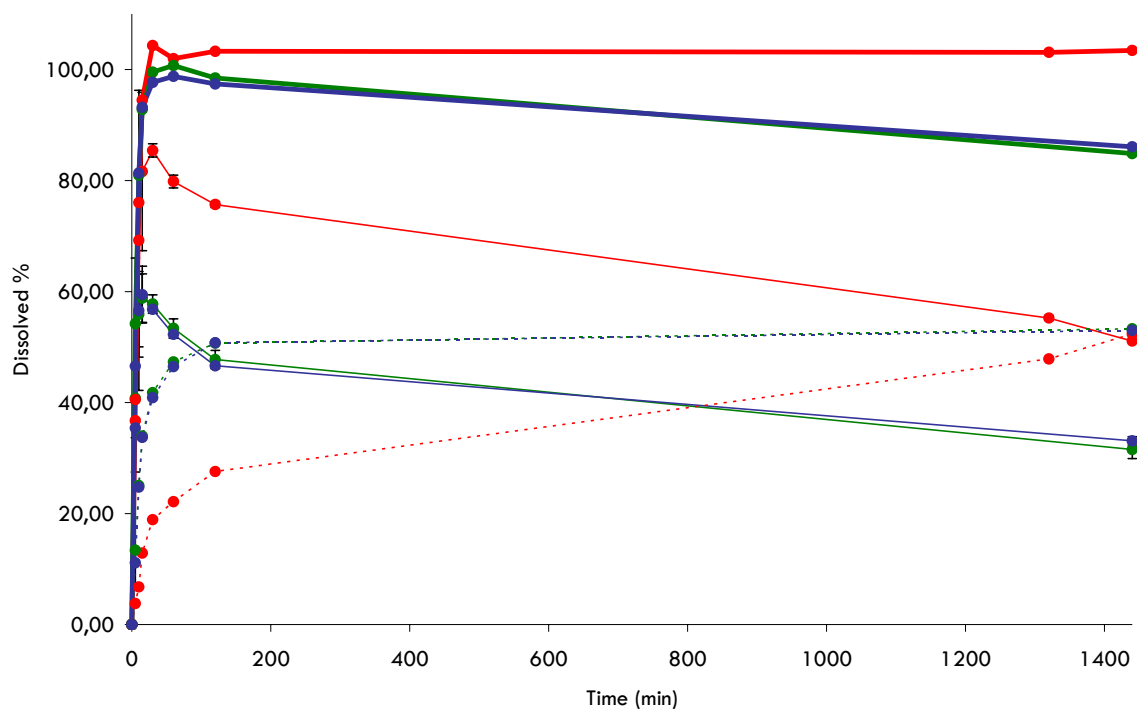


**Figure IV 4 23.** UCB-A dissolution profile in HCl 0.1N: micronized UCB-A (**red**), spray-dried UCB-A formulation B (prior to milling operations) (**green**) and spray-dried UCB-A formulation B (nanoparticles) (**blue**). Plain curves (UCB-A), dotted curves (UCB-A-Met1) and thick plain curves (UCB-A + UCB-A-Met1). Mean  $\pm$  SD; n=3.

As expected from the discussion above, when compared to the results obtained with UCB-A formulation A (SDS-containing), we do not find, at least during the first two hours of the test, any differences between the three formulations when comparing the cumulated UCB-A/UCB-A-Met1 dissolution profiles: “100%” of the drug had already dissolved following 30 min. There is however a difference between micronized UCB-A and spray-dried UCB-A formulation B, be it before or after the high pressure homogenization (i.e. micronized and nanosized drug, respectively). In fact, UCB-A dissolved percentages are found to be lower for the latter when compared to micronized UCB-A, with around 55% of UCB-A dissolved following 30 min for spray-dried formulation B before and following high pressure homogenization (no differences) versus 85% for micronized UCB-A. However, hydrolysis into UCB-A-Met1 is faster for the two spray-dried formulations than for micronized UCB-A, explaining the fact that the cumulated curves look similar for the three formulations. Contrarily to micronized UCB-A, there is a drop, from time 2 h to 24 h, in the percentage of UCB-A dissolved and the cumulated percentage dissolved

(UCB-A-Met1 not evolving) for both spray-dried formulations (before and following high pressure homogenization). This drop was unexplained but might imply the degradation of UCB-A in a compound other than UCB-A-Met1 (this was however not verified).

Evaluation of the dissolution characteristics of UCB-A formulation B, both nanoparticles and prior to milling operations (i.e. to denote the influence of the additives in the formulation on drug dissolution), in an acetate buffer pH 4.0 was also carried out. Since this media is less friendly to drug dissolution than HCl 0.1N, enhancement of dissolution rate for UCB-A nanoparticles, as it was the case for formulation A (**Figure IV 4 21**), was observed. Results from this evaluation are shown in **Figure IV 4 24**.

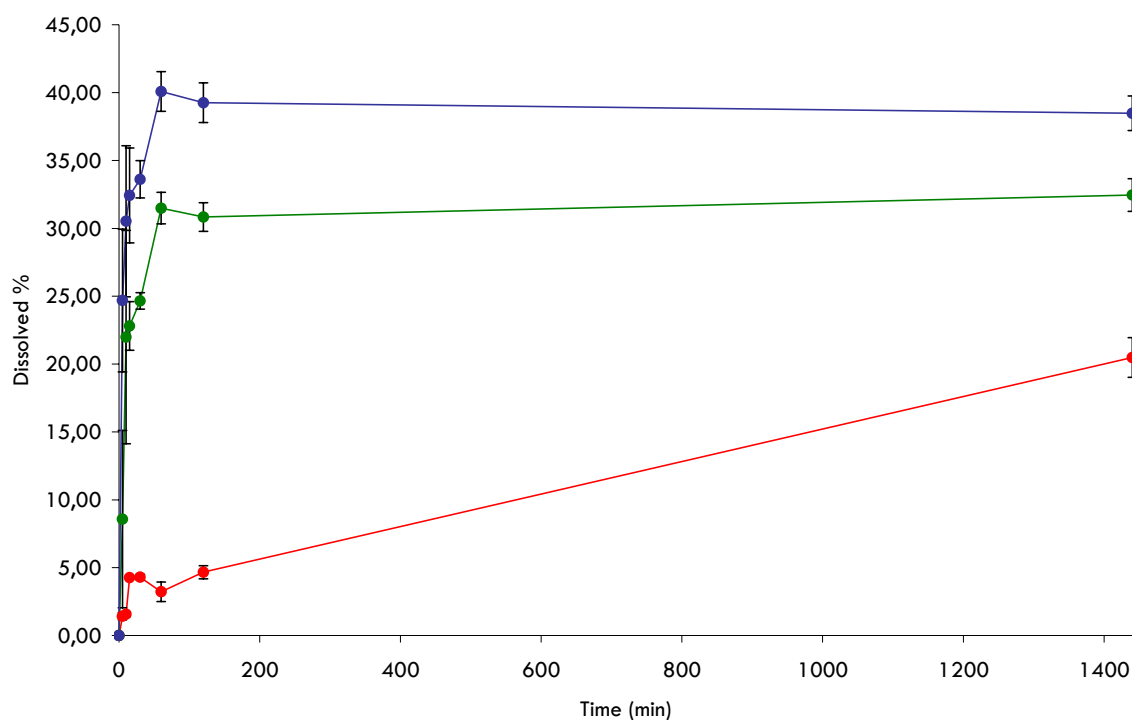


**Figure IV 4 24.** UCB-A dissolution profile in acetate buffer pH 4.0: micronized UCB-A (**red**), spray-dried UCB-A formulation B nanosuspension (**blue**) and spray-dried UCB-A formulation B prior to milling operations (**green**). Mean  $\pm$  SD; n=3.

When comparing the dissolution profiles of micronized UCB-A and UCB-A formulation B (nanoparticles), we can clearly see the enhancement brought by particle size reduction. At this pH we can observe an approximate 8-fold increase in the percentage dissolved following 2 hours for UCB-A nanoparticles vs. UCB-A micronized particles (40% vs. 5%). This is slightly better than the results obtained for UCB-A formulation A (nanoparticles) where an approximate 6-fold increase in the percentage dissolved was found following 2 hours for UCB-A nanoparticles vs. UCB-A micronized particles (32% vs. 5%) (**Figure IV 4 21**). In the case of formulation B, however, no further increase in dissolved percentage up to the end of the 24-h test can be seen; an increase up to 50% for formulation A (nanoparticles) had been observed. The main difference between the two formulations, however, lies in the much more rapid dissolution rate for formulation B, which is probably the consequence of better redispersion characteristics (i.e. SDS vs. poloxamer). The dissolution profile, obtained with the spray-dried formulation B prior to milling operations (i.e. micronized UCB-A in the presence of additives - HPMC/poloxamer 407), presented in this figure shows that the additives used in formulation development are also responsible for the observed enhanced dissolution rate of UCB-A (6-fold increase: percentage dissolved following 2 hours vs. UCB-A micronized particles being 30% vs. 5%, respectively). However, the dissolution profile obtained for this formulation is still lower than that for the equivalent spray-dried formulation that presents the drug as nanoparticles, meaning that particle size reduction has an additional beneficial effect on the influence of the presence of the additives. When comparing the results from **Figure IV 4 21** and **Figure IV 4 24**, considering the influence of surfactants in the formulation, it seems that poloxamer allows for better UCB-A dissolution than SDS. Here again, as it was mentioned for **Figure IV 4 21**, no degradation of UCB-A into UCB-A-Met1 was observed throughout the test period.

#### IV.4.3.2.4. UCB-B

As for UCB-A, the dissolution rate of UCB-B was assayed on un-milled UCB-B ( $d(v,0.5) \sim 7 \mu\text{m}$  - **Figure IV 2 9** / **Table IV 2 7**) and on UCB-B nanoparticles (spray-dried UCB-B 5%, Methocel E15<sup>®</sup> 0.5%, poloxamer 407 0.25% w/v nanosuspension - PMC + 20C 23-24000 PSI + 10C 30000 PSI) placed into 00 gelatin capsules (equivalent of 25 mg UCB-B /capsules). All dissolution assays were run in controlled-pH media. The dissolution profiles of both samples were assayed at pH 4.0, 6.8 and in HCl 0.1N. All dissolution media were surfactant-free. It should be noted that the studied UCB-B nanoparticle formulation shows relatively poor redispersion characteristics (**Figure**

**IV 2 32 - Table IV 2 23).** This, however, as it will be shown through the dissolution results presented in this section, did not withdraw all the benefits resulting from formulating UCB-B as nanoparticles. As it was shown for NIF and ucb-35440-3, the agglomerates responsible for the poor redispersion are certainly highly porous agglomerates so that the real surface area in contact with the dissolution medium is much greater than that of the un-processed drug. The presence of a carrier might have been shown to be beneficial in enhancing UCB-B nanoparticle redispersion characteristics but this evaluation was not carried out; the reason being that minimization of additives in formulation development was requested as UCB-B is a projected highly dosed drug.

Keeping in mind the pH-dependent solubility profile of UCB-B (**Figure IV 4 6 - Table IV 4 9**), the dissolution profiles were, at first, evaluated at pH 6.8, a pH less favorable to UCB-B dissolution. Dissolution was also evaluated at pH 4.0 to evaluate the dissolution profiles of the two systems in a more dissolution-friendly medium. The dissolution profiles for un-milled UCB-B and UCB-B nanoparticles at pH 6.8 and pH 4.0 are shown on **Figure IV 4 25** and **Figure IV 4 26**, respectively.

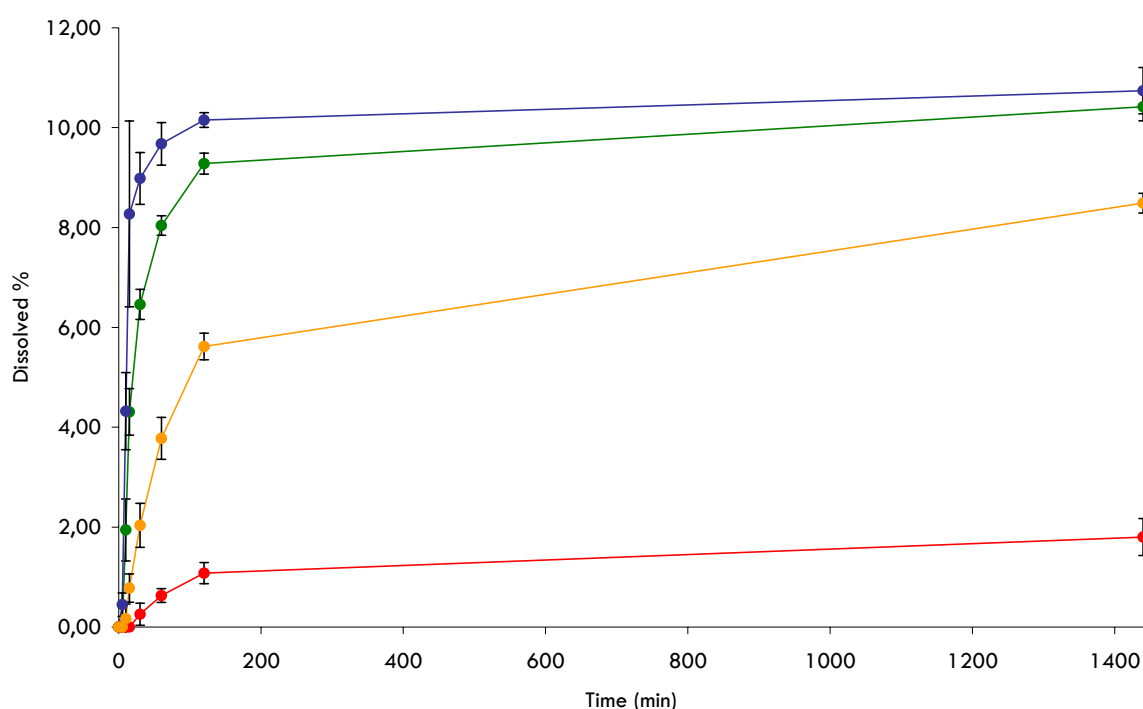


**Figure IV 4 25.** UCB-B dissolution profile in phosphate buffer pH 6.8: un-milled UCB-B (**red**), spray-dried UCB-B 5%, Methocel E15® 0.5%, poloxamer 407 0.25% w/v nanosuspension (**blue**), spray-dried UCB-B 5%, Methocel E15® 0.5%, poloxamer 407 0.25% w/v suspension prior to milling operations (**green**) and UCB-B: Methocel E15®: poloxamer 407 20:2:1 w/w physical mixture (**orange**). Mean  $\pm$  SD; n=3.

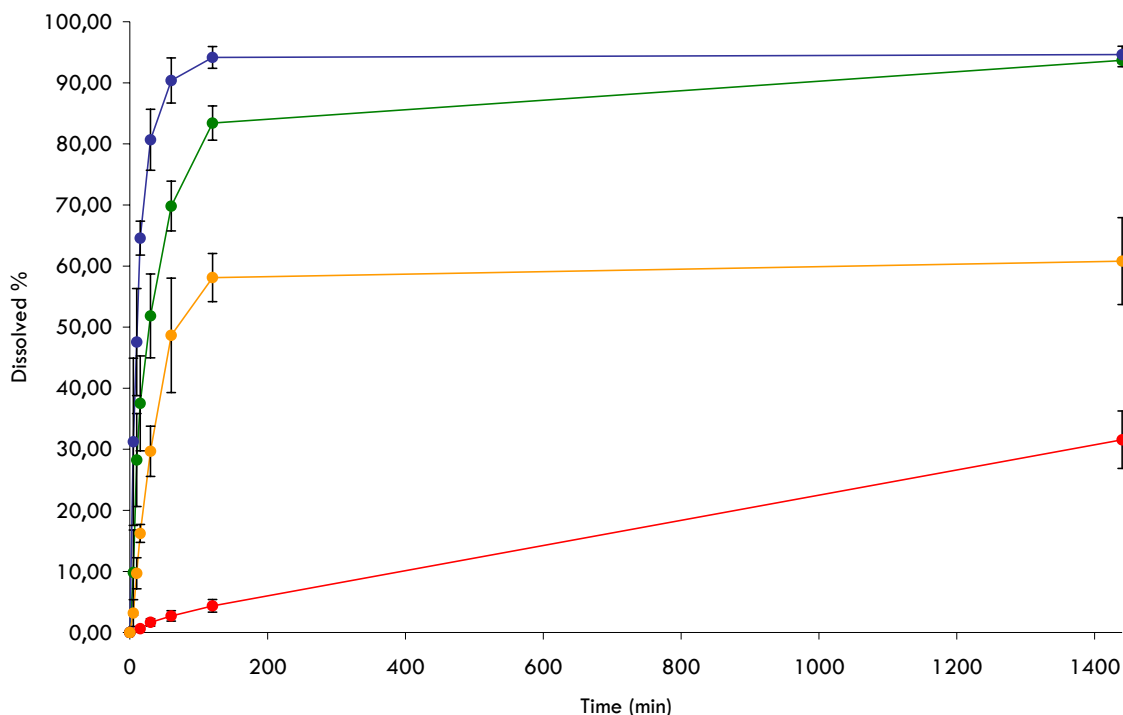


**Figure IV 4 26.** UCB-B dissolution profile in acetate buffer pH 4.0: un-milled UCB-B (**red**), spray-dried UCB-B 5%, Methocel E15<sup>®</sup> 0.5%, poloxamer 407 0.25% w/v nanosuspension (**blue**), spray-dried UCB-B 5%, Methocel E15<sup>®</sup> 0.5%, poloxamer 407 0.25% w/v suspension prior to milling operations (**green**) and UCB-B: Methocel E15<sup>®</sup>: poloxamer 407 20:2:1 w/w physical mixture (**orange**). Mean  $\pm$  SD; n=3.

When comparing the dissolution profiles of both systems, either at pH 6.8 or pH 4.0, we can clearly see the enhancement brought by particle size reduction. At pH 6.8, although the achieved dissolution is still relatively poor, we can observe an approximate 9-fold increase in the percentage dissolved following 2 hours for UCB-B nanoparticles vs. un-milled UCB-B (10.1% vs. 1.1%). When evaluating the spray-dried formulation prior to milling operations (i.e. UCB-B + HPMC and poloxamer 407) and the physical mixture equivalent to this formulation, we can observe the positive influence of HPMC and poloxamer on drug dissolution; the percentages of drug dissolved following 2 hours being 9.3% and 5.6%, respectively. The increased percentage in the case of the spray-dried suspension (prior to milling operations) is due to the fact that HPMC and poloxamer are more homogeneously distributed around UCB-B particles than following simple physical mixing. However, although the clear beneficial influence of the formulation surfactants can be seen when comparing the spray-dried formulation before and after high pressure homogenization (i.e. un-milled UCB-B and UCB-B nanoparticles), we can also clearly see the direct beneficial influence of particle size reduction on UCB-B dissolution.

Although it is even more pronounced, the same observation can be made for the dissolution profiles of both systems at pH 4.0 (**Figure IV 4 26**) as we can observe an approximate 21-fold increase in percentage dissolved following 2 hours for UCB-B nanoparticles vs. un-milled UCB-B (94.1% vs. 4.4%). When comparing the dissolution profiles of the spray-dried UCB-B formulation before (**Figure IV 4 26** - green curve) and after (**Figure IV 4 26** - blue curve) high pressure homogenization, as well as the physical mixture equivalent to the tested formulation (**Figure IV 4 26** - orange curve), we can see that the excipients used for nanoparticle stabilization during the high pressure homogenization, as it was already shown for pH 6.8 (**Figure IV 4 25**), have a clear positive influence on un-milled UCB-B dissolution, but are not totally responsible for the dissolution rate enhancement offered by the UCB-B nanoparticle formulation. Although the data is not shown, it also has to be noted that at pH 4.0 no degradation of UCB-B into UCB-A-Met1 was observed (no degradation peaks in the chromatograms).

The dissolution profiles of micronized UCB-B and UCB-B nanoparticles were also compared in acidic media (HCl 0.1N). Although the UCB-B dissolution rate should, analogously to UCB-A, be very fast for both systems due to the increased solubility at this pH range, this evaluation was still carried out to denote any difference. Due to the drug's instability in acidic media (i.e. degradation in UCB-A-Met1), both UCB-B and UCB-A-Met1's concentrations were quantified. The dissolution profiles in HCl 0.1N are represented in **Figure IV 4 27**. Investigation of the dissolution profiles of a spray-dried equivalent formulation prior to milling operations and of the physical mixture equivalent to the formulation to evaluate the influence of the excipients used are also represented in this figure. The cumulated dissolved percentages of UCB-B and UCB-A-Met1 for all four formulations assayed is also represented on this figure.

As we can see when observing the UCB-B dissolution profiles in **Figure IV 4 27**, we do not find, at least during the first two hours of the test, any differences between the four formulations when comparing the added UCB-B/UCB-A-Met1 dissolution profiles; "100%" of the drug being already dissolved following 30 min. There is, however, a difference between un-milled UCB-B and the spray-dried UCB-B formulations, be it before or after the high pressure homogenization (i.e. micronized and nanosized drug, respectively). In fact, the percentages of dissolved UCB-B were found to be lower for the latter when compared to un-milled UCB-B, with around 55% and 81% of UCB-B dissolved following 30 min for the spray-dried formulation before and after high pressure homogenization, respectively, versus 90% for un-milled UCB-B. The physical mixture equivalent to the tested formulation behaved similarly to un-milled UCB-B. However, hydrolysis into UCB-A-Met1 was faster for the two spray-dried formulations than for un-milled UCB-B, explaining the fact that the cumulated curves look similar for the four formulations. When looking at the results in **Figure IV 4 27**, there is a drop, from time 2 h to 24 h, in

UCB-B percentage dissolved and cumulated percentage dissolved (UCB-A-Met1 not evolving) for both spray-dried formulations (before and following high pressure homogenization) as well as for un-milled UCB-B. This was not observed for the tested physical mixture. This drop was unexplained but might imply the degradation of UCB-B in a compound other than UCB-A-Met1 (this was, however, not verified).

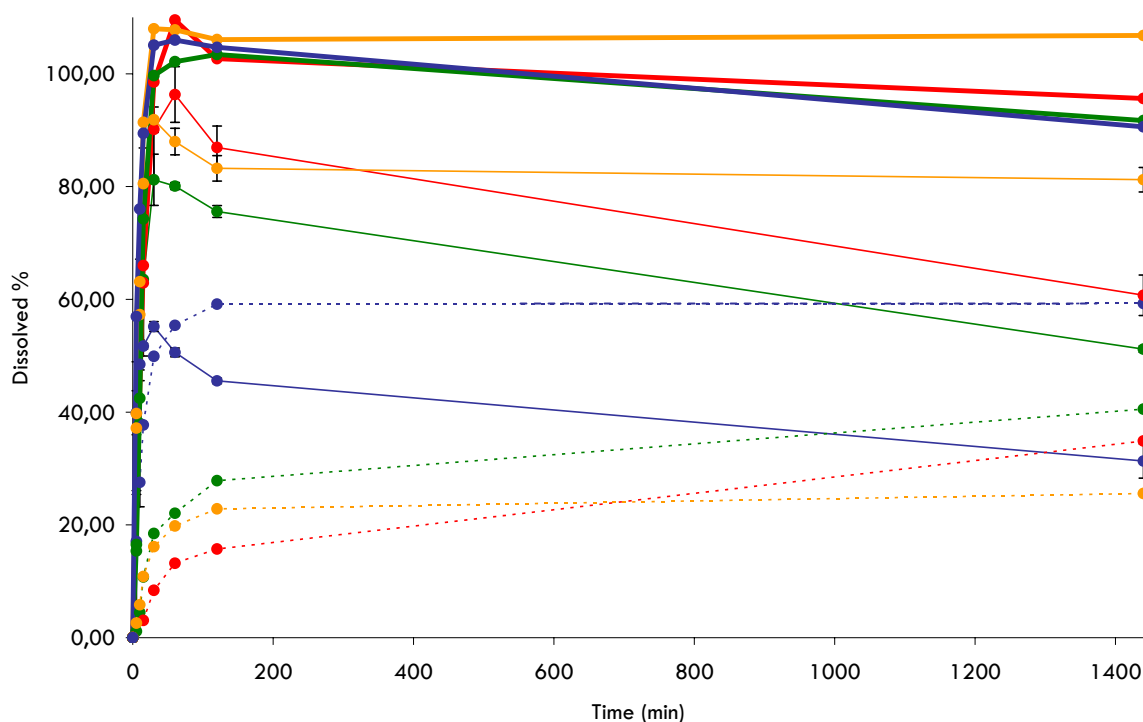


**Figure IV 4 27.** UCB-B dissolution profile in HCl 0.1N: un-milled UCB-B (**red**), spray-dried UCB-B 5%, Methocel E15<sup>®</sup> 0.5%, poloxamer 407 0.25% w/v suspension prior to milling operations (**green**), spray-dried UCB-B 5%, Methocel E15<sup>®</sup> 0.5%, poloxamer 407 0.25% w/v nanosuspension (**blue**) and UCB-B: Methocel E15<sup>®</sup> : poloxamer 407 20:2:1 w/w physical mixture (**orange**). Plain curves (UCB-B), dotted curves (UCB-A-Met1) and thick plain curves (UCB-B + UCB-A-Met1). Mean  $\pm$  SD; n=3.



#### IV.4.4. Conclusion

From the results presented in this chapter, we can conclude that formulating poorly water-soluble drugs as crystalline nanoparticles has a clear, beneficial, influence on both their solubility and dissolution characteristics.

Solubility-wise, a clear enhancement has been reported for NIF nanoparticles with a measured solubility of 26 µg/ml vs. 19.5 µg/ml for un-milled NIF. Most interestingly, these solubility values were achieved much more rapidly for NIF nanoparticles than for un-milled NIF; 3 h vs. 24 h, respectively. For ucb-35440-3, a poorly water-soluble weak base presenting a pH-dependent solubility profile, solubility was enhanced by a 1.1-fold, a more than 2-fold and by an 8-fold factor for nanoparticles at pH 3.0, 5.0 and 6.5, respectively. Considering UCB-A, which also presents a pH-dependent solubility profile, solubility enhancement for drug nanoparticles has been observed above pH 4.0 by factors ranging from 4 to 20-fold.

To a greater extent, dissolution characteristics of the four tested model drugs were also shown to be clearly enhanced for the drugs formulated as nanoparticles. Considering NIF nanoparticles, 100% of the tested dose (equivalent to 10 mg NIF) was already dissolved following 10 min vs. less than 5% for un-milled NIF. For ucb-35440-3 nanoparticles, more than 95% and 85% of the tested dose (equivalent to 200 mg ucb-35440-3) were already dissolved following 60 min vs. 30% and 20% for un-milled ucb-35440-3 at pH 3.0 and 5.0, respectively. At pH 6.5, a pH less favorable to ucb-35440-3 dissolution, an 11-fold increase in the dissolution rate was observed in the first 30 min of the test. For UCB-A nanoparticles, a 6-fold and a 6 to 8-fold increase in dissolved percentage (dose equivalent to 25 mg UCB-A) following 120 min was observed when compared to the un-milled drug at pH 5.0 and 4.0, respectively. For UCB-B nanoparticles, a 9-fold and a 21-fold (94% vs. 4%) increase in dissolved percentage (dose equivalent to 25 mg UCB-B) following 120 min was observed when compared to the un-milled drug at pH 6.8 and 4.0, respectively.

The redispersion characteristics of the freeze- or spray-dried nanosuspensions have also been shown, in this chapter, to be highly relevant when considering their dissolution characteristics. In fact, for NIF, the influence of mannitol, a water-soluble carrier added prior to the spray-drying operation in order to prevent particle agglomeration, was clearly shown beneficial in enhancing drug dissolution rate as dissolution of 100% of the tested dose (equivalent to 10 mg NIF) could be reached after only 10 min vs. 50% in its absence (i.e. agglomerated NIF nanoparticles). In addition to preventing NIF nanoparticle agglomeration, it has to be noted that mannitol also acts as a highly water-soluble matrix surrounding NIF nanoparticles which is clearly beneficial

for further drug dissolution. The clear enhancement observed for mannitol-free formulations, when compared to the un-milled drug, was however explained by the fact that the nanoparticle agglomerates present in the spray-dried powder show relatively high porosity. The redispersion characteristics and the particle agglomeration phenomena were also clearly shown to be relevant for ucb-35440-3 dissolution using the flow-through dissolution apparatus. In this case, although characteristics inherent to the apparatus used, such as particularly the limited dissolution cell volume available for particle redispersion, have to be taken into account, the presence of carriers, be they water-soluble or water-insoluble (Emcompress®, Cross-linked PVP), were shown to be clearly beneficial in preventing particle agglomeration and thus in enhancing the dissolution rate of ucb-35440-3.

It has to be noted that these carriers were used in non negligible amounts (i.e. equivalent amount to the drug substance) which could, in some cases, be quite problematic. For highly dosed drugs for example, such as it is anticipated for ucb-35440-3 and UCB-A or UCB-B, an attempt towards minimization of the use of additives in formulation development shall be made for future processing. As for mannitol (and possibly other water-soluble carriers), one of the drawback to its utilization lies in the fact that it further decreases the powder density of the spray-dried nanosuspensions (which are already characterized by a relatively low powder density).

The influence of the stabilizers (i.e. surfactants) used for nanosuspension preparation was also shown to be relevant when considering the dissolution properties of drug nanoparticles. This observation was principally noticed for UCB-A but shall be considered for each studied model.

## IV.5. In vitro evaluation - permeation rate across Caco-2/HT29-5M21 cultures and co-cultures

### IV.5.1. Introduction

This section, contrarily to the previous three sections, will only refer to NIF as a model drug. The in vitro solubility and dissolution behaviour of NIF has been shown to be greatly influenced by particle size and significantly enhanced for NIF nanoparticles (**part IV.4.3.1.1 (Figure IV 4 3)** and **part IV.4.3.2.1 (Figure IV 4 7)** of this work). To further investigate the benefits brought by NIF particle size reduction and as a complementary preliminary evaluation of the systems prior to the in vivo studies, studies of NIF transfer across intestinal in vitro cellular models were carried out in this work comparing un-milled NIF, Turrax® milled NIF and NIF nanoparticles. Turrax® milled NIF ( $d(v,0.5) \sim 15 \mu\text{m}$  vs  $100 \mu\text{m}$  for un-milled NIF - **part IV.2.3.2** of this work (**Figure IV 2 10**)) was evaluated in this study as, although to a lesser extent than for NIF nanoparticles, it also showed improvement, dissolution-wise, vs. un-milled NIF (**Figure IV 4 7**).

Amongst the various cell types constituting the human intestinal epithelium we can cite enterocytes, goblet cells, paneth cells, endocrine cells and stem cells; the first two cited being the main encountered cellular types (Nollevaux et al, 2006).

In vitro models are increasingly being developed to study drug transport across the intestinal epithelium (Pinto et al., 1983; Walter et al., 1996; Hilgendorf et al., 2000; Balimane et al., 2005; Nollevaux et al, 2006). The most commonly used cell culture models are listed in **Table IV 5 1**. The intestinal cell lineage Caco-2, obtained from human colon adenocarcinoma, is the cell model most commonly used to reproduce the features of the bowel epithelium and the most extensively used in the field of drug permeability studies. Despite its colonic origin, the Caco-2 cell line differentiates spontaneously, when grown to confluence, into polarized, columnar cells which are considered phenotypically representative of in vivo encountered enterocytes (Boulenc et al., 1992). These Caco-2 cells effectively exhibit TEER (transepithelial electrical resistance) similar to intestinal enterocytes (i.e.  $200\text{--}400 \Omega\cdot\text{cm}^2$  - the typical overall small intestinal TEER is estimated to be in the range of  $25\text{--}40 \Omega\cdot\text{cm}^2$ ) (Balimane et al., 2005) and exhibit a well defined brush border, microvilli and well-established tight junctions. The Caco-2 model is known to express adequate amounts of hydrolase, esterase and brush-border enzymes. However, they fail to

**Table IV 5 1.** Cell culture models commonly used for permeability assessment (Balimane et al., 2005).

Cell line	Species or origin	Special characteristics
Caco-2	Human colon adenocarcinoma	Most well-established cell model Differentiates and expresses some relevant efflux transporters Expression of influx transporters is variable (differs laboratory-to-laboratory)
MDCK	MDCK epithelial cells	Polarized cells with low intrinsic expression of ABC transporters Ideal for transfections
LLC-PK1	Pig kidney epithelial cells	Polarized cells with low intrinsic transporter expression Ideal for transfections
2/4/A1	Rat fetal intestinal epithelial cells	Temperature-sensitive Ideal for paracellularly absorbed compounds (leakier pores)
TC-7	Caco-2 subclone	Similar to Caco-2
HT-29	Human colon	Contains mucus-producing goblet cells
IEC-18	Rat small intestine cell line	Provides a size-selective barrier for paracellularly transported compounds

simulate the complete *in vivo* intestinal environment because they do not express appreciable quantities of CYP3A4, the principle CYP present in human epithelial cells (Schmiedlin-Ren et al., 1997; Hu et al., 1999; Engman et al., 2001; Thummel et al., 2001; Pfrunder et al., 2003). Furthermore Caco-2 cells are also known to underexpress (when compared to *in vivo* conditions) intrinsically pharmaceutically important transporters such as peptide transporters, organic cation transporter and organic anion transporter. This model is thus likely to generate false negatives with drug candidates that are known to be absorbed by a carrier-mediated process facilitated by transporter proteins (Balimane et al., 2005). These authors referred to the example of some  $\beta$ -lactam antibiotics (such as cephalexin and amoxicillin) and some angiotensin-converting enzyme (ACE) inhibitors, both classes being known substrates of dipeptide transporters, which were characterized by relatively poor permeability across Caco-2 cell monolayers despite being completely absorbed *in vivo*.

The adenosine triphosphate (ATP)-binding cassette (ABC) transmembrane transporter P-glycoprotein (P-gp) and some multidrug resistance related proteins (MRPs) (e.g. MRP1, MRP2, MRP3, MRP4 and MRP5) are however found to be normally expressed in the Caco-2 cell line (Pfrunder et al., 2003). P-gp, the gene product of the multidrug resistance protein 1 (MDR1) gene, is an efflux transporter with wide substrate specificity. The protein is expressed on the brush-border membrane of enterocytes where it extrudes its substrates back into the gut lumen (Pfrunder et al., 2003). MRPs are integral membrane glycoproteins and function as organic anion transporters, which transport a wide range of drugs.

Given these informations, the Caco-2 cell line model might show some limitations metabolization and transport-wise in order to be considered an ideal cell model totally representative of *in vivo* conditions. However, for “intrinsic permeability” measurements, these drawbacks might in fact be turned into an advantage for the model, as in our case for NIF (i.e. typical substrate for CYP3A4).

Considering these “intrinsic permeability” evaluations, the Caco-2 model, again in contrast to the *in vivo* intestinal epithelium, presents further limitations as it is characterized by relatively low paracellular permeability and by a great ease of access to the microvilli owing to an almost complete lack of mucus production (Nollevaux et al, 2006). In fact, the tight junctions in the Caco-2 cell line appear relatively tighter than the tight junctions in the human intestinal epithelial cells (estimated pore size in Caco-2 being in the range of  $3.7 \pm 0.1$  Å versus  $9.0 \pm 0.2$  Å for human intestinal epithelial cells), thus not making it an ideal model for the evaluation of compounds that are passively absorbed via the paracellular route (Balimane et al., 2005). The lack of mucus production, combined with the presence of a very thin unstirred water layer (UWL) above the cell surface is, in fact, another drawback of the model as it allows an increased access, in comparison to *in vivo* conditions, to highly diffusible small molecules (i.e. lipophilic drugs).

Given these last considerations, and primarily that of mucus production, co-culturing the Caco-2 cells with a HT29 cell lineage, a mucin-secreting cellular population issued from human colorectal cancer, has been reported and proposed to better represent *in vivo* conditions (Walter et al., 1996; Hilgendorf et al., 2000; Nollevaux et al. 2006). In this line, the best model representing the intestinal epithelium actually appears to be a confluent co-culture of Caco-2 and HT29-5M21 cells seeded at a 3:1 ratio (Nollevaux et al. 2006). This model was developed by Nollevaux et al. by evaluating different proportions of these two cell lineages. Caco-2/HT29-5M21 cultures and co-cultures characterized by proportions of 1:3, 2:2 and 3:1, respectively, have been evaluated. These cultures, and principally the co-cultures developed, need to be well characterized in terms of proportions of both cellular types as they can evolve during culture. The phenotype of each cell type and the reproducibility of the models were assayed with the characterization of specific markers (Caco-2 → differentiation marker is the alkaline phosphatase (membrane-bound enzyme localized in the brush border) activity associated with the microvilli (**Figure IV 5 1**)). According to the results obtained by Nollevaux et al. and considering the approximate *in vivo* enterocyte/goblet cell ratio, the 3:1 proportion was used for co-culture preparation.

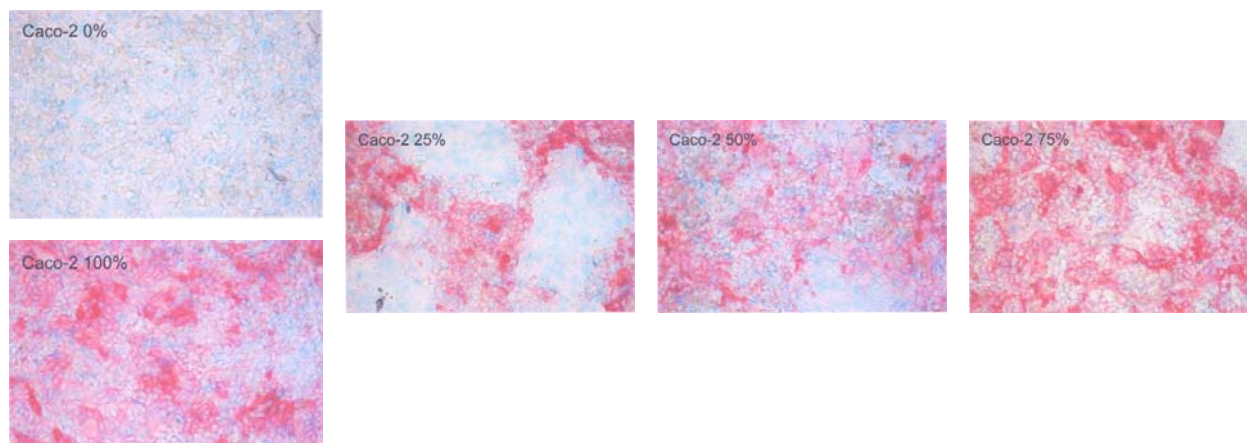


**Figure IV 5 1.** Localization of alkaline phosphatase activity (in red) by cytochemistry in a co-culture of Caco-2 and HT29-5M21 - results show a good relationship between alkaline phosphatase activity and percentage of Caco-2 and a good homogeneity between the two cell lines used in the co-cultures (reproduced from **Nollevaux et al. 2006**).

In this study, the influence of particle size on NIF permeation rate (apical to basolateral transfer) was thus analysed across Caco-2 and HT29-5M21 cultures and across a co-culture (3:1 ratio) of these two cell lineages. Evaluation of chitosan-coated NIF nanoparticles was also carried out in this section. Chitosan is a natural polysaccharide comprising co-polymers of glucosamine and N-acetylglucosamine (**Figure IV 5 2**). It is a natural hydrophilic polymer obtained by deacetylation of chitin (fungi, insects, crustaceans). Depending on the degree of deacetylation (ranging from 40% to 98%), chitosan shows basic properties that lead, in slightly acidic media, to a polycationic and swellable structure of the polymer. This polymer shows strong mucoadhesive properties (**Smart, 2005**); these properties being due to the formation of hydrogen and ionic bonds between the positively charged amino groups of the polymer and the negatively charged sialic acid residues of mucin glycoproteins. As chitosan has the ability to loosen the inter-cellular tight junctions of enterocytes (**Figure IV 5 3**) (thus facilitating the paracellular transport of hydrophilic compounds), it is also frequently used as a permeability enhancer (**Thanou et al., 2001**).

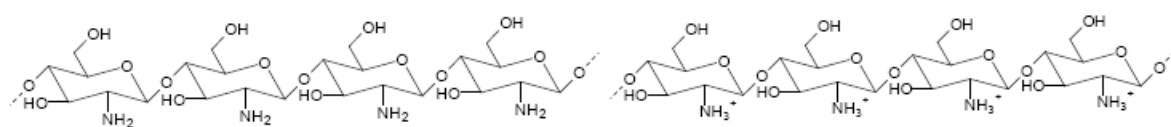


**Figure IV 5 2.** Chitosan (100% deacetylated)

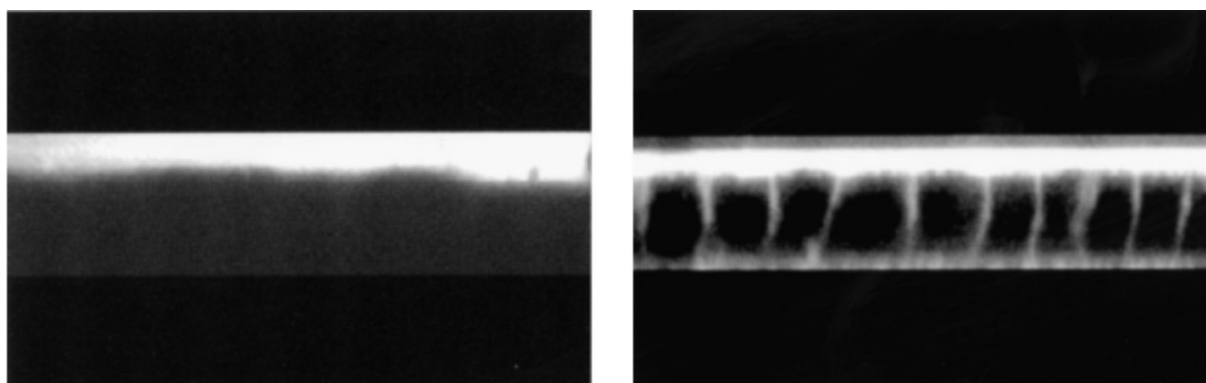


**Figure IV 5 3.** Confocal laser scanning electron microscopy vertical cross-sections through Caco-2 cell monolayers. Visualization of the paracellular transport of the fluorescent marker Texas red dextran 10000 (4h incubation) in the absence (left) and the presence (right) of chitosan derivatives (Trimethyl chitosan chloride (TMC) in this study) (Thanou et al., 2001).

## IV.5.2. Materials and Methods

### IV.5.2.1. Materials

Chitosan<sup>®</sup> was purchased from Aldrich (Aldrich Chemical Company Inc., Milwaukee, WI, USA). Acetonitrile and methanol (HPLC grade) were acquired from Sigma-Aldrich (St-Louis, MO, USA). All chemicals used for cell culture were purchased from Sigma-Aldrich (Poole, Dorset, UK) and from VWR (Brussels, Belgium). Cell culture media were obtained from Gibco BRL (Gaithersburg, USA) and from Sigma-Aldrich (Poole, Dorset, UK). The other materials were of analytical reagent grade.

### IV.5.2.2. Permeation studies

#### IV.5.2.2.1. Cell lines and culture conditions

The HT29-5M21 cell line, derived from the HT29-MTX 10-5 M cell line (Lesuffleur et al., 1993), was obtained at passage 9 from Dr. T. Lesuffleur (INSERM U505, Villejuif, France). Caco-2 cells were obtained at passage 22 from Cambrex Bio Science (Verviers, Belgium). These cells were progressively adapted (until passage 30 for HT29-5M21 and passage 40 for Caco-2) to a serum-free medium: the basal defined medium (BDM) (Schneider, 1989) supplemented with a mixture of non-essential amino acids and growth factors (Halleux et al., 1991). Initially, Caco-2 and HT29-5M21 cells were cultured in Dulbecco's Modified Eagle Medium (DMEM) containing glucose (4.15 mg/l), buffered with HEPES (25 mM) containing fetal calf serum (10%) and antibiotics (1%: penicillin [1 U/ml], streptomycin [1 µg/ml] and amphotericin as fungizone<sup>®</sup> [2.5 ng/ml]). These cells were then progressively sub-cultured in BDM containing glucose (4.15 mg/l) supplemented with non-essential amino acids and growth factors (Halleux et al., 1991). Cells were used at passages 30 (HT29-5M21) and 40 (Caco-2) to avoid dedifferentiation (Yu et al., 1997). The cells were seeded at  $4 \times 10^4$  cells/cm<sup>2</sup> in plastic flasks (Greiner labortechnik SA, Wemmel, Belgium) and cultured at 37°C in a CO<sub>2</sub>-air (5:95) atmosphere (Heraeus EK incubator). The culture medium was changed every day.



A Caco-2 culture, a HT29-5M21 culture and a Caco-2/HT29-5M21 co-culture at a seeding ratio of 3:1 (seeding of  $4 \times 10^4$  cells/cm<sup>2</sup> per flask) were maintained in BDM supplemented with non-essential amino acids, a mixture of growth factors and antibiotics (see above). The medium was changed every two days. Co-cultures were confluent 7 days after seeding. The Caco-2 and HT29-5M21 cells were maintained in culture for 21 days after confluence for differentiation. Cells were grown on Thincerts PET 0.4 µm inserts. Under these conditions, the maximum expression of intestinal differentiation-specific markers was achieved (alkaline phosphatase and mucin synthesis for Caco-2 and HT29-5M21 cells, respectively) (Nollevaux et al, 2006).

#### IV.5.2.2.2. Transport studies

NIF transfer from the apical to the basolateral side (A→B) of (co-) cultures of Caco-2/HT29-5M21 cells was studied (Figure IV 5 4). Hanks media were used for both (co-)culture sides during the study (Table IV 5 2). 100 µl of each formulation studied (susp 1 mg/ml in Hanks) were placed on the apical side and samples (200 µl) were withdrawn from the basolateral side at time 20, 40, 60, 80, 100, 120, 150, 180, 210 and 240min. Withdrawals were directly replaced by fresh media. Inserts were placed on an IKA Labortechnik KS250 basic stirring plate (50/min) (IKA® Werke GmbH, Staufen, Germany). Experiments were replicated five times for each formulation studied.

Cell layer integrity was controlled by measurement of transepithelial electrical resistance (TEER) values (millicell-ERS, Millipore, Brussels, Belgium) before and following experimentation. Cell viability was checked by microscopy analysis following ethidium bromide/acrydine orange DNA staining (Foglieni et al., 2001).

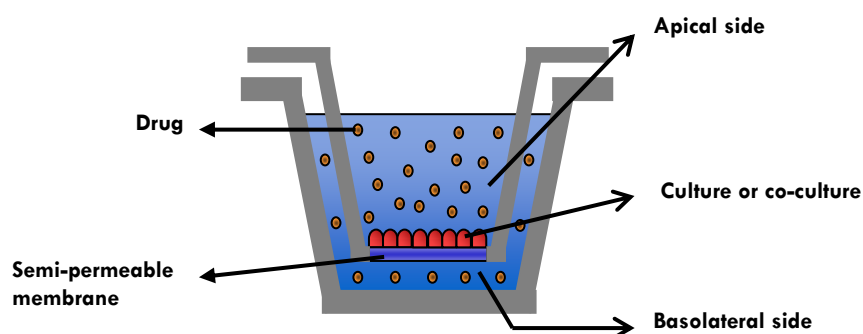


**Figure IV 5 4.** Schematic representation of inserts used for NIF permeability studies.

**Table IV 5 2.** Composition of Hanks media placed on the apical side (1.9 ml) and on the basolateral side (3 ml) of the cell (co-) cultures assayed

	Apical side	Basolateral side
glucose	9.9 g	9.9 g
NaCl	16 g	16 g
CaCl <sub>2</sub> 2H <sub>2</sub> O	0.37 g	0.37 g
KH <sub>2</sub> PO <sub>4</sub>	0.12 g	0.12 g
NaHCO <sub>3</sub>	0.7 g	0.7 g
KCl	0.8 g	0.8 g
MgCl <sub>2</sub> .2 H <sub>2</sub> O	0.2 g	0.2 g
MgSO <sub>4</sub> .7 H <sub>2</sub> O	0.2 g	0.2 g
Na <sub>2</sub> HPO <sub>4</sub> .2 H <sub>2</sub> O	0.12 g	0.12 g
HEPES	-	13.04 g
H <sub>2</sub> O	ad 2l (pH 6.8)	ad 2l (pH 7.4)

**IV.5.2.2.3. Analytical procedure - HPLC method NIF M1**

Samples were assayed by HPLC using a Lachrom Elite HPLC system (Hitachi High-Technologies Corporation, London, UK) consisting of a model L2130 solvent delivery pump, a model L2200 autosampler and a model L2400 UV-VIS variable wavelength detector. Chromatographic separations were accomplished using a Prevail Select C18, 5 µm, 15 cm x 4.6 mm stainless steel column (Alltech Inc., Deerfield, IL, USA) with a guard precolumn of the same packing material. The mobile phase consisted of a mixture of acetonitrile, methanol and water (35:17:48, v/v). The pH of the mixed solvent system was adjusted to pH 3.8 with phosphoric acid. The mixture was filtered through a 0.22 µm membrane (Millipore, Bedford, USA) under vacuum and then degassed with 5 min ultrasounds. The mobile phase was pumped isocratically at a flow rate of 1.2 ml/min during analysis, at ambient temperature. Aliquots of 80 µl were injected into the column. The effluent was monitored at 240 nm. Retention time for NIF was around 6 min. The method used showed good linearity ( $R^2$ : 0.9997) between 0.01-10 µg/ml and was capable of separating NIF from its photodegradation product and oxidized metabolite; NIF being a substrate for CYP3A4 (Patki et al., 2003). Cytochrome P450, present in small intestinal epithelial cells, is implicated in the metabolic elimination of many drugs (Schmiedlin-Ren et al., 1997). Its expression in native Caco-2 cells is, however, low to very low and needs to be induced (Schmiedlin-Ren et al., 1997; Hu et al., 1999; Engman et al., 2001; Thummel et al., 2001; Pfrunder et al., 2003). The rate of NIF oxidation has, in fact, been reported to be low in

Caco-2 cells (Boulenc et al., 1992). In contrast, CYP3A4 expression in HT-29 cells is constitutive (Chun et al., 2003) but is significantly lower than the in vivo colonic expression (Pool-Zobel et al., 2005).

#### **IV.5.2.2.4. Statistical analysis**

Statistical analyses were carried out using the Kruskal-Wallis (non parametric ANOVA) test. Multiple comparisons using the Dunn procedure were carried out when results from this test were found to be significant. Comparisons were evaluated for each formulation and each culture type for data time points at 180 min.

### IV.5.3. Results and discussion

#### IV.5.3.1. Preparation of chitosan-coated NIF nanoparticles

As described in the introductive part of this chapter, chitosan was evaluated for its permeability-enhancing properties with regard to NIF transfer across Caco-2/HT29-5M21 cultures and co-cultures. This polymer also shows very interesting mucoadhesive properties but the insert model used in this study is certainly not appropriate for its evaluation; a dynamic model such as Ussing chamber type cells (**Figure IV 5 5**) would be more appropriate in that regard. This type of cell might also be interesting for the evaluation of the inherent bioadhesive properties characteristic of nanoparticulate systems.

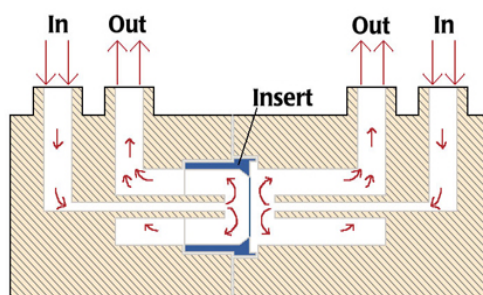


**Figure IV 5 5.** Schematic representation of an Ussing chamber type cell.

Concerning the preparation of chitosan-coated NIF nanoparticles, preliminary work has been done to evaluate the possibility of directly using the polymer for NIF nanoparticle stabilization (i.e. during the high pressure homogenization), similarly to the use of hydroxypropylmethylcellulose (HPMC - Methocel E15<sup>®</sup>) (see **part IV.2.3.1** of this work). Although the chitosan used is reported to be of a low viscosity grade, viscosity was seen, as reported in **Figure IV 5 6**, to increase rapidly with increasing chitosan percentage (w/v solutions). As 2% w/v chitosan solutions had a reported measured viscosity around 160 mPa.s, this percentage was not evaluated for NIF nanosuspension preparation as this viscosity is certainly too high for sample processing through the high pressure homogenizer. Chitosan solutions ranging from 0.1% to 1% were thus evaluated for NIF nanosuspension

preparation, the viscosities (< 40 mPa.s) characterizing these tested chitosan solutions being acceptable for high pressure homogenization processing.

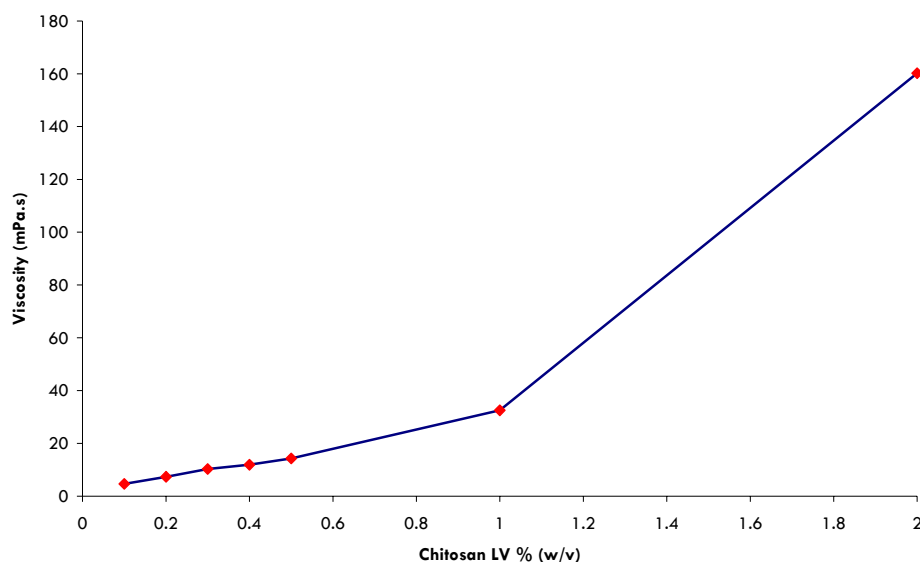


**Figure IV 5 6.** Evaluation of the viscosity (mPa.s) (25°C) of different chitosan solutions (% w/v) (dispersion in Hac 1% v/v - glacial acetic acid 1% v/v solution). Evaluation of the viscosity made using a Brookfield DV-II+ viscosimeter (S18 spindle) (Brookfield Engineering Labs Inc., Middleboro, MA, USA).

Chitosan rapidly showed limited properties, when compared to Methocel E15®, regarding NIF suspension stabilization, and this already following the pre-milling Turrax® milling operation (operation carried out preliminary to the high pressure homogenization for a first significant particle size reduction - see **part IV.2.3.2** of this work). Results from laser diffraction size analysis following the Turrax® milling operation are shown in **Table IV 5 3**. We can clearly see from these results that, except maybe for the 1% w/v chitosan solution which nevertheless yields very limited results, the performed Turrax® milling operation had absolutely no effect on NIF particle size reduction. Since significant size reduction can be achieved using Methocel E15®, these limited observed results are due to the ineffective properties of chitosan in stabilizing NIF particles in suspension. Pre-milling low pressure homogenizing cycles (**part IV.2.3.2**) and subsequent high pressure (23-24000 PSI) homogenizing cycles were then attempted on the 1% w/v chitosan Turrax® milled NIF suspension. Processing through HPH was, however, shown not possible for this suspension due to the frequent stalling of the apparatus (i.e. possible clogging at the homogenization gaps), even at low-pressure homogenizing cycles at 7000 PSI.

**Table IV 5 3.** LD size parameters for un-milled NIF and for chitosan-stabilized 5% NIF suspensions following 10min Turrax milling 24000 rpm (ice bath). Methocel E15®-stabilized equivalent NIF suspension indicated as a reference. (% expressed w/v).

	<b>d (0.1) ± SD</b>	<b>d (0.5) ± SD</b>	<b>d (0.9) ± SD</b>	<b>D[4,3] ± SD</b>	<b>span ± SD</b>
<b>NIF no milling</b>	<b>21.9 ± 0.2</b>	<b>98.7 ± 0.4</b>	<b>267.2 ± 0.5</b>	<b>126.2 ± 0.6</b>	<b>2.48 ± 0.08</b>

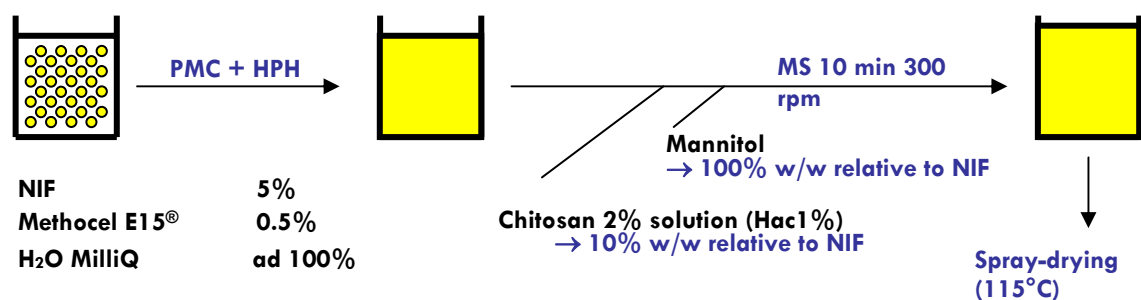
  

<b>Chitosan %</b>	<b>d (0.1) ± SD</b>	<b>d (0.5) ± SD</b>	<b>d (0.9) ± SD</b>	<b>D[4,3] ± SD</b>	<b>span ± SD</b>
<b>0.1</b>	<b>23.7 ± 1.1</b>	<b>138.3 ± 5.1</b>	<b>372.1 ± 20.9</b>	<b>175.1 ± 8.1</b>	<b>2.52 ± 0.07</b>
<b>0.2</b>	<b>14.2 ± 0.6</b>	<b>96.4 ± 4.0</b>	<b>269.5 ± 13.6</b>	<b>124.1 ± 5.3</b>	<b>2.65 ± 0.08</b>
<b>0.3</b>	<b>14.7 ± 0.7</b>	<b>109.7 ± 3.7</b>	<b>273.8 ± 8.7</b>	<b>131.7 ± 4.3</b>	<b>2.36 ± 0.05</b>
<b>0.4</b>	<b>10.7 ± 0.5</b>	<b>108.4 ± 4.5</b>	<b>283.1 ± 13.2</b>	<b>132.4 ± 5.6</b>	<b>2.51 ± 0.10</b>
<b>0.5</b>	<b>12.8 ± 0.6</b>	<b>105.6 ± 4.6</b>	<b>278.4 ± 18.3</b>	<b>131.9 ± 7.8</b>	<b>2.51 ± 0.09</b>
<b>1</b>	<b>5.02 ± 0.11</b>	<b>21.8 ± 0.6</b>	<b>151.3 ± 6.9</b>	<b>54.8 ± 2.8</b>	<b>6.71 ± 0.18</b>

<b>Methocel E15® %</b>	<b>d (0.1) ± SD</b>	<b>d (0.5) ± SD</b>	<b>d (0.9) ± SD</b>	<b>D[4,3] ± SD</b>	<b>span ± SD</b>
<b>0.5</b>	<b>3.07 ± 0.17</b>	<b>15.7 ± 0.3</b>	<b>51.6 ± 0.4</b>	<b>22.3 ± 0.3</b>	<b>3.07 ± 0.04</b>

Following these observed results, NIF nanoparticles were thus prepared using Methocel E15® as a stabilizer, as described in **part IV.2** of this work. Chitosan was then added, subsequently to the high pressure homogenization and prior to the spray-drying operation, as an “external” solution (2% w/v solution in Hac 1%) to the NIF nanosuspension. The chitosan solution was added in order to have 10% w/w of chitosan relative to NIF. Mannitol, when used in the formulation, should also be added following the high pressure homogenization and prior to the spray-drying operation. As it was explained in **part IV.2** and **part IV.3** of this work, chitosan, similarly to HPMC, will be found around NIF nanoparticles following the spray-drying operation (i.e. NIF nanoparticles being entrapped in a HPMC/chitosan matrix). This operation is schematically represented in **Figure IV 5 7**.



**Figure IV 5 6.** Schematic representation of the preparation of chitosan-coated NIF nanoparticles.

Chitosan-coated NIF nanoparticles were assayed for their redispersion characteristics in the presence or absence of mannitol; this hydrophilic carrier having been shown to significantly enhance this characteristic for spray-dried NIF nanoparticles (cf. **part IV.2.3.5 - Figure IV 2 25**). As it can be seen from the results presented in **Figure IV 5 7** and **Table IV 5 4**, the redispersion characteristics of spray-dried chitosan-coated nanoparticles are relatively poor, and this in the absence or presence of mannitol in the formulation. These two formulations (i.e. mannitol-free and mannitol-added formulations) show important particle agglomeration as it was previously shown in the evaluation of the redispersion characteristics of NIF spray-dried nanoparticles (cf. **part IV.2.3.5 - Figure IV 2 21** and **Figure IV 2 23**). It should be noted that the advantages (increased dissolution rate, etc.) offered by particle size reduction to nanometer range are not completely lost as a consequence of these poor redispersion characteristics (see **part IV.4.3.2 - Figures IV 4 8, 9, 10, 11, 26 and 27**) as the agglomerates, as already discussed in **part IV.2.3.5**, show relatively high porosity (**Figure IV 2 21**) and represent drug nanoparticles entrapped in a highly hydrophilic matrix (mannitol, HPMC, etc.). It should be noted that these redispersion characteristics are not due to the poor solubility of the chitosan in the redispersion media used (DI H<sub>2</sub>O in our case - **Figure IV 5 7** - chitosan showing poor solubility at neutral or alkaline pH) as redispersion in Hac 1% showed the same redispersion results as in DI H<sub>2</sub>O (**Figure IV 5 8**), with agglomeration probably occurring before the spray-drying operation.

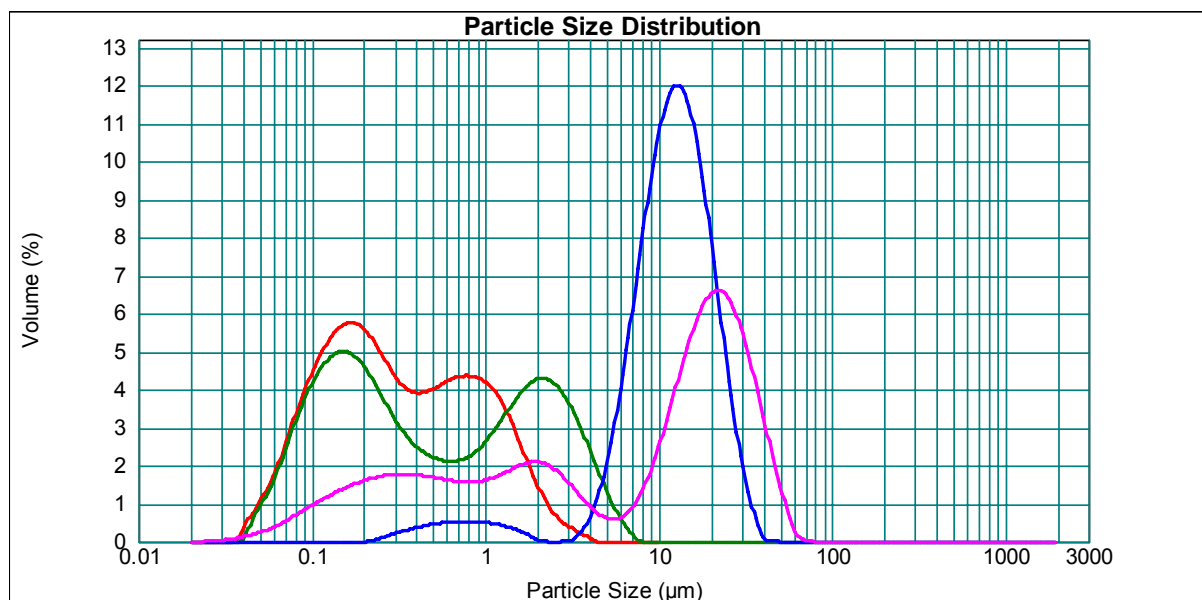


**Figure IV 5 7.** LD size distribution curves for (1) a NIF 5%, Methocel® 0.5% w/v suspension following PMC + 20C 23-24000 PSI HPH (red), (2) following addition of chitosan (10% w/w relative to NIF) to the nanosuspension described in 1 (green), (3) spray-dried suspension (Methocel®/chitosan) in the absence of mannitol (blue) and (4) spray-dried obtained suspension (Methocel®/chitosan) in the presence of mannitol (10% w/w relative to NIF) (pink). Data reported in annex 1 (**Table A16**).

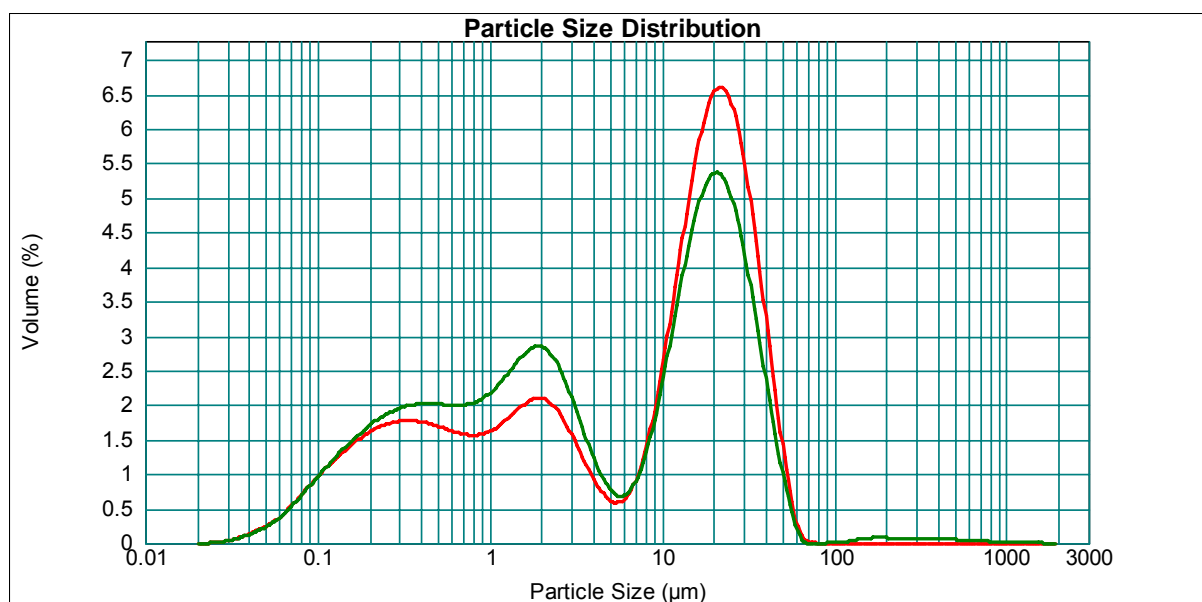


**Figure IV 5 8.** LD size distribution curves for a spray-dried NIF/Mannitol/Methocel E15®/Chitosan 10:10:1:1 w/w suspension: redispersion in deionized water (**red**) and in Hac 1% (**green**). Data reported in annex 1 (**Table A17**).

#### IV.5.3.2. Transport studies across Caco-2/HT29-5M21 cultures and co-cultures

Nifedipine studied formulations for transport studies across Caco-2/HT29-5M21 cultures and co-cultures are listed in **Table IV 5 4**.

**Table IV 5 4.** Studied NIF formulations for transport studies across Caco-2/HT29-5M21 cultures and co-cultures (% expressed w/w relative to NIF).

	Methocel E15®	Mannitol	Chitosan	Milling operation	Water-removal operation
<b>Formulation A</b>		-	-	no milling	-
<b>Formulation B</b>	10%	-	-	Turrax milling	Spray-drying
<b>Formulation C</b>	10%	100%	-	HPH (nano)	Spray-drying
<b>Formulation D</b>	10%	100%	10%	HPH (nano)	Spray-drying

**Figures IV 5 9, IV 5 10 and IV 5 11** represent NIF apical to basolateral transfer across cultures of Caco-2 cells alone, HT29-5M21 cells alone and across co-cultures (3:1 ratio) of Caco-2 and HT29-5M21 cells for the different NIF formulations studied, respectively. When looking at the results presented in these figures, NIF transport is significantly enhanced for NIF nanoparticles (formulation C and formulation D) when compared to un-milled NIF,



be it across Caco-2 cultures ( $p < 0.0025$ ), HT29-5M21 cultures ( $p < 0.0015$ ) and across Caco-2 75 %/HT29-5M21 25 % co-cultures ( $p < 0.001$ ). NIF permeation rate ( $\mu\text{g}/\text{cm}^2\cdot\text{h}$ ) for NIF nanoparticles (formulation C) was increased by an approximate 6-fold factor across all three models studied when compared to un-milled NIF (**Table IV 5 5**). This observation nicely complements the in vitro data obtained solubility- and dissolution-wise for NIF NP (**part IV.4.3.1.1 - Figure IV 4 3 / part IV.4.3.2.1 - Figure IV 4 7**). Particle size reduction to micron range (i.e. Turrax®-milled NIF) also seemed to result in an improved permeation rate (**Table IV 5 5**), but no significant differences ( $p > 0.5$ ) were observed vs. un-milled NIF. Significant differences ( $p < 0.03$ ) were detected between Turrax®-milled NIF and NIF nanoparticles (formulation C) for both Caco-2 and HT29-5M21 cultures but not for the Caco-2/HT29-5M21 co-culture, although a tendency toward a difference can be noted.

Investigation into the influence of chitosan on NIF permeation rate is also represented on **Figures IV 5 9, IV 5 10** and **IV 5 11**, with NIF formulation D representing chitosan-coated NIF nanoparticles. As the permeability enhancement of chitosan is usually considered as resulting from an increase of the aperture degree of intercellular tight junctions (thus enhancing the paracellular passage route), a positive influence could be expected in Caco-2 cells containing models (Caco-2 100% > Caco-2 75%/HT29-5M21 25% > HT29-5M21 100%).

**Table IV 5 5.** NIF permeation rate ( $\mu\text{g}/\text{cm}^2\cdot\text{h}$ ) across cell models for four different NIF formulations (calculated on mean values of Figure IV 5 9, III 5 10 and III 5 11).

	Caco-2 100 %	Caco-2 75 % - HT29-5M21 25 %	HT29-5M21 100 %
<b>Formulation A</b>	<b>1.60 10<sup>-2</sup></b>	<b>1.53 10<sup>-2</sup></b>	<b>1.45 10<sup>-2</sup></b>
<b>Formulation B</b>	<b>4.20 10<sup>-2</sup></b>	<b>5.37 10<sup>-2</sup></b>	<b>3.25 10<sup>-2</sup></b>
<b>Formulation C</b>	<b>8.57 10<sup>-2</sup></b>	<b>8.80 10<sup>-2</sup></b>	<b>8.29 10<sup>-2</sup></b>
<b>Formulation D</b>	<b>7.37 10<sup>-2</sup></b>	<b>7.74 10<sup>-2</sup></b>	<b>7.13 10<sup>-2</sup></b>

No influence of chitosan on NIF permeability was observed in the case of the three cell models tested ( $p > 0.5$  in all cases). TEER values, which were expected to decrease for formulation D in Caco-2 cells containing models (Caco-2 100% > Caco-2 75%/HT29-5M21 25% > HT29-5M21 100%), did not show significant differences from the other formulations tested (**Figure IV 5 12**). These observations could probably be explained by chitosan's intrinsic low solubility at the experimental pH (i.e. pH 6.8). Evaluation using formulation D dispersed at a lower pH (pH 4.5) was also carried out but no data could be retrieved due to the large amount of cell damage incurred at this pH (significant drop in TEER values combined with limited cell viability - Ethidium Bromide/acrydine orange test - **Figure IV 5 17**).

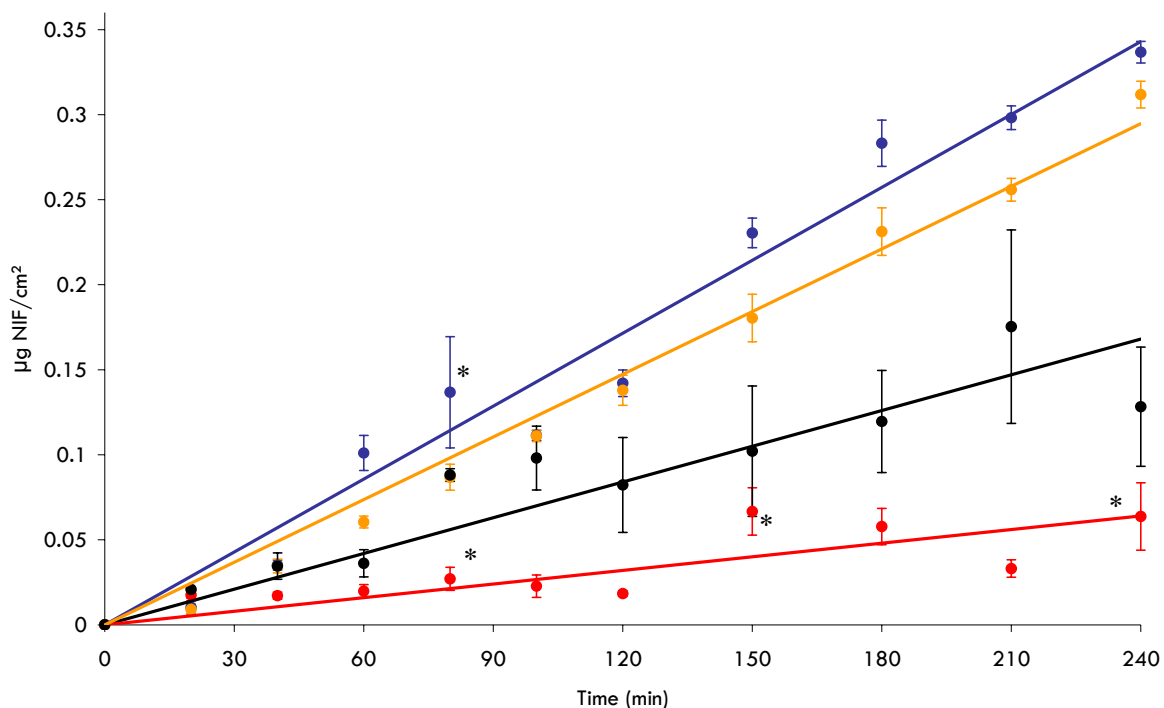


**Figure IV 5 9.** NIF transfer (apical to basolateral) across Caco-2 cultures, for un-milled NIF (formulation A) (red), Turrax-milled NIF (formulation B) (black), NIF nanoparticles (formulation C) (blue) and chitosan-coated NIF nanoparticles (formulation D) (orange). Mean  $\pm$  sem – n=5 (\* n=4)).

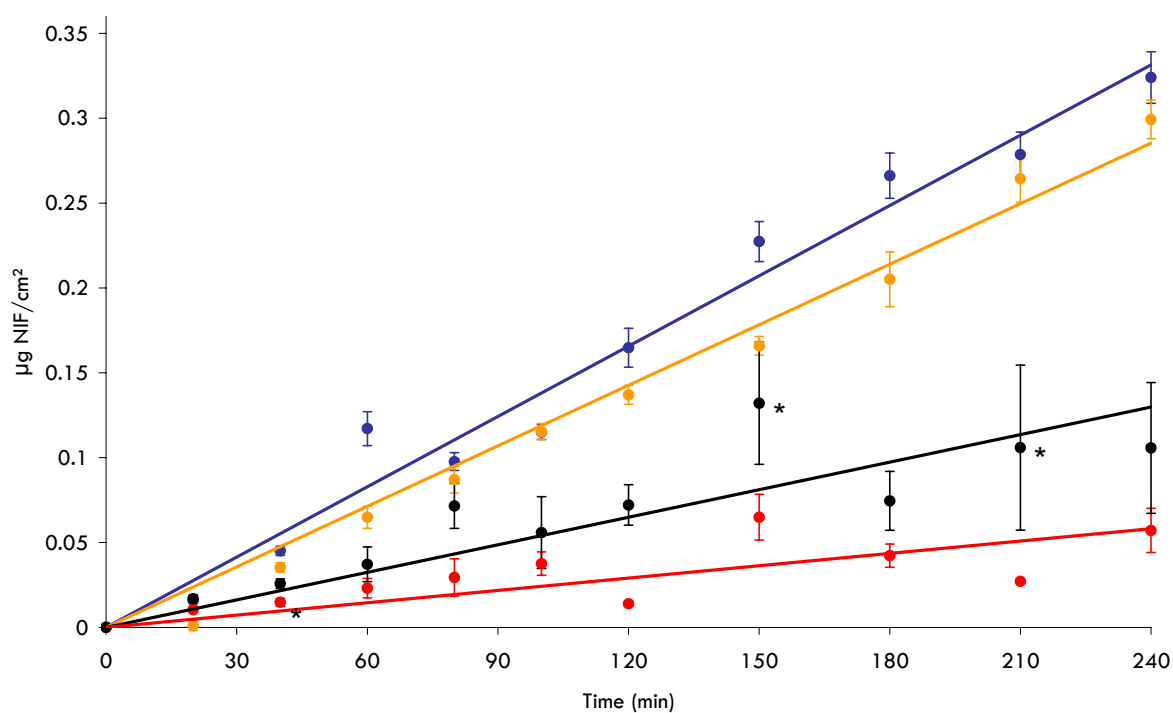


**Figure IV 5 10.** NIF transfer (apical to basolateral) across HT29-5M21 100% cultures, for un-milled NIF (formulation A) (red), Turrax-milled NIF (formulation B) (black), NIF nanoparticles (formulation C) (blue) and chitosan-coated NIF nanoparticles (formulation D) (orange). Mean  $\pm$  sem – n=5 (\* n=4)).

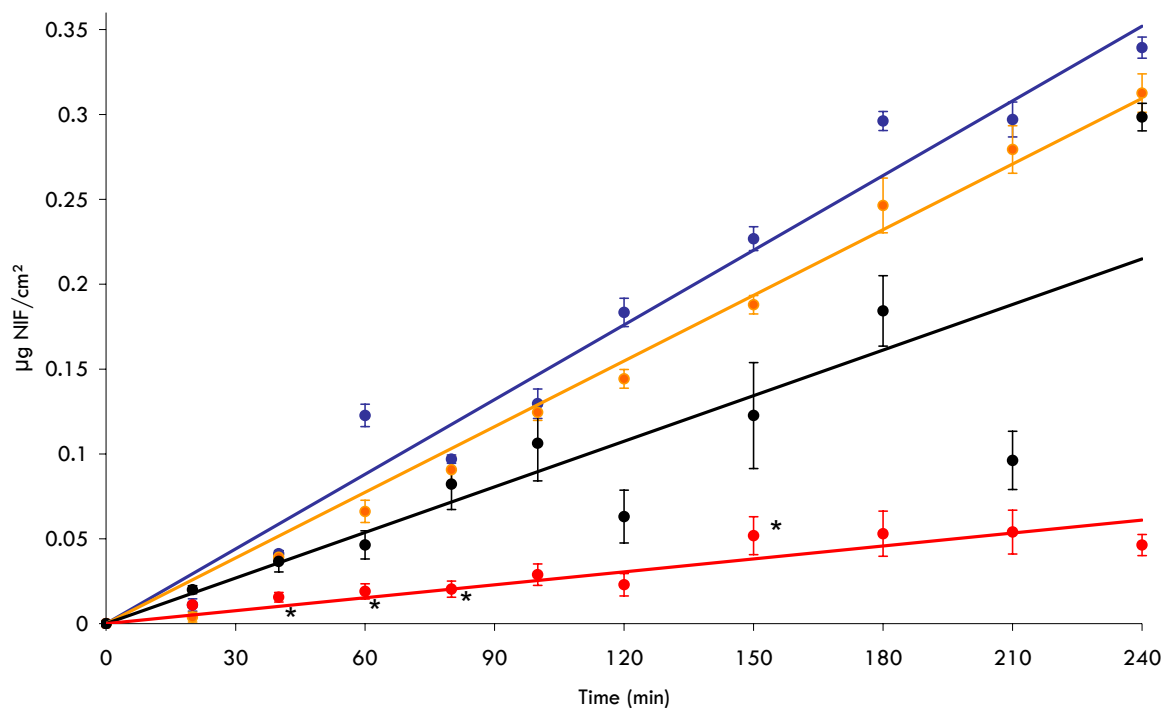


**Figure IV 5 11.** NIF transfer (apical to basolateral) across Caco-2 75% / HT29-5M21 25% co-cultures, for unmilled NIF (formulation A) (red), Turrax-milled NIF (formulation B) (black), NIF nanoparticles (formulation C) (blue) and chitosan-coated NIF nanoparticles (formulation D) (orange). Mean  $\pm$  sem – n=5 (\* n=4)).

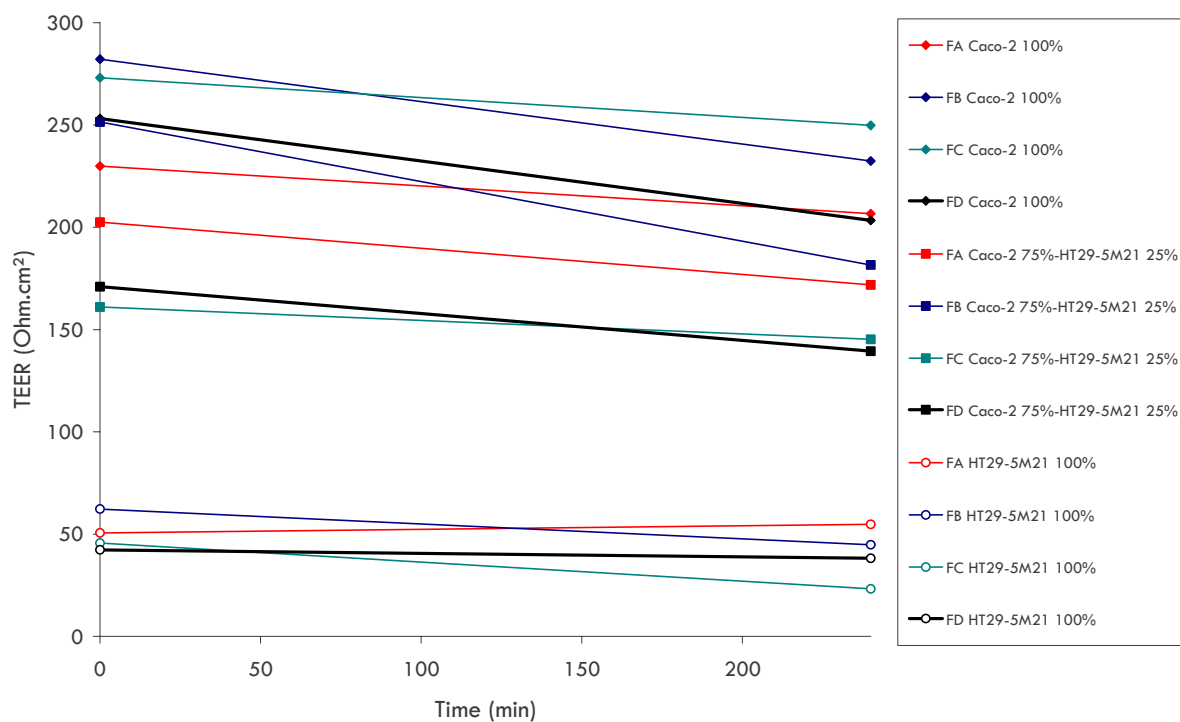


**Figure IV 5 12.** Mean TEER values before (0 min) and after (240 min) NIF transport studies on Caco-2/HT29-5M21 (co-) cultures using NIF formulation A, B, C, and D. Mean (n=5).

When comparing the results represented in **Figures IV 5 9, IV 5 10, IV 5 11** and **Table IV 5 5**, no significant differences were observed in the results of transfer studies across Caco-2 culture, HT29-5M21 culture or the Caco-2 75%/HT29-5M21 25% co-culture (all  $p$  values  $> 0.05$ ). Only Turrax®-milled NIF showed a significant difference ( $p < 0.05$ ) between the HT29-5M21 culture and the Caco-2 75%/HT29-5M21 25% co-culture: this could be the consequence of the higher variability observed for this formulation. These evaluations, which compare the three studied cell models relative to a given formulation and compared to a blank measurement (used as a control for the assays conducted), are also reported in **Figures IV 5 13, IV 5 14, IV 5 15** and **IV 5 16**.

Since the established Caco-2/HT29-5M21 co-culture is well characterized and seemingly better representative of *in vivo* intestinal conditions, it could therefore be of great interest when considering *in vitro* permeation studies in drug development. Furthermore, the formulation of drugs as nanoparticles in order to increase their solubility and dissolution rate could be an interesting alternative to the use of solvents for the evaluation of poorly water-soluble compounds in these kinds of transport/permeability studies.

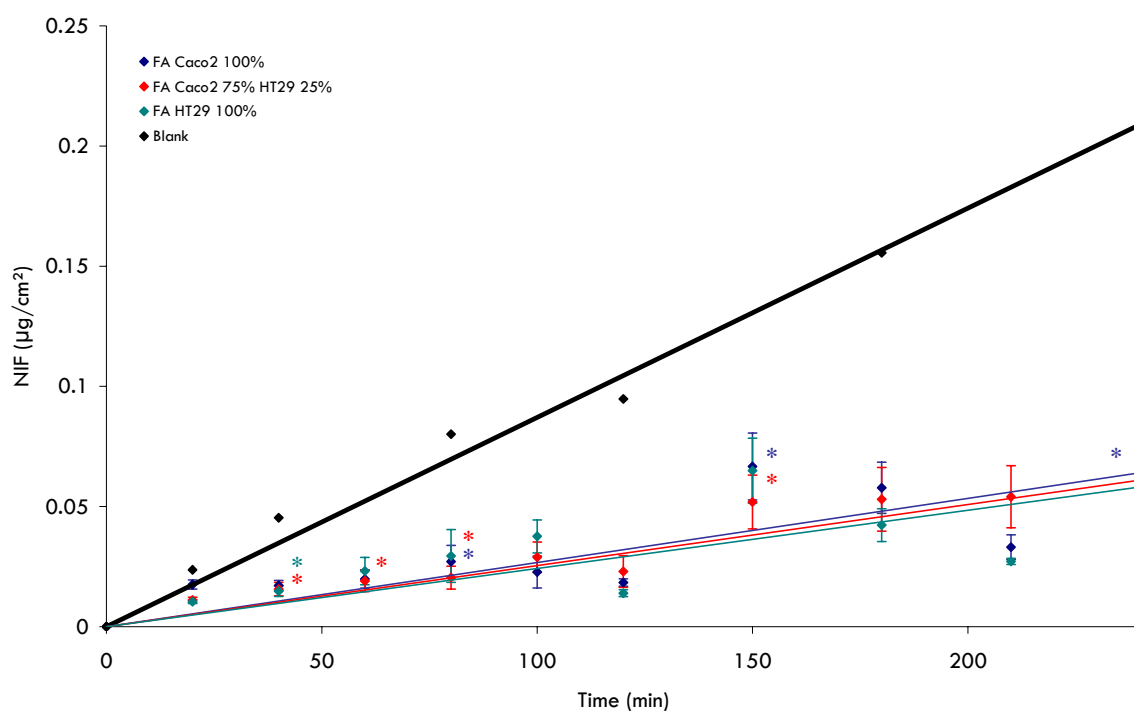


**Figure IV 5 13.** NIF transfer (apical to basolateral) (**formulation A**) across Caco-2 cultures (**blue**), HT29-5M21 cultures (**green**) and Caco-2 75%/HT29-5M21 25% co-cultures (**red**). Blank measurement (NIF transport across “blank” inserts - no cells) is represented in black. Mean  $\pm$  sem –  $n=5$  (\*  $n=4$ )).

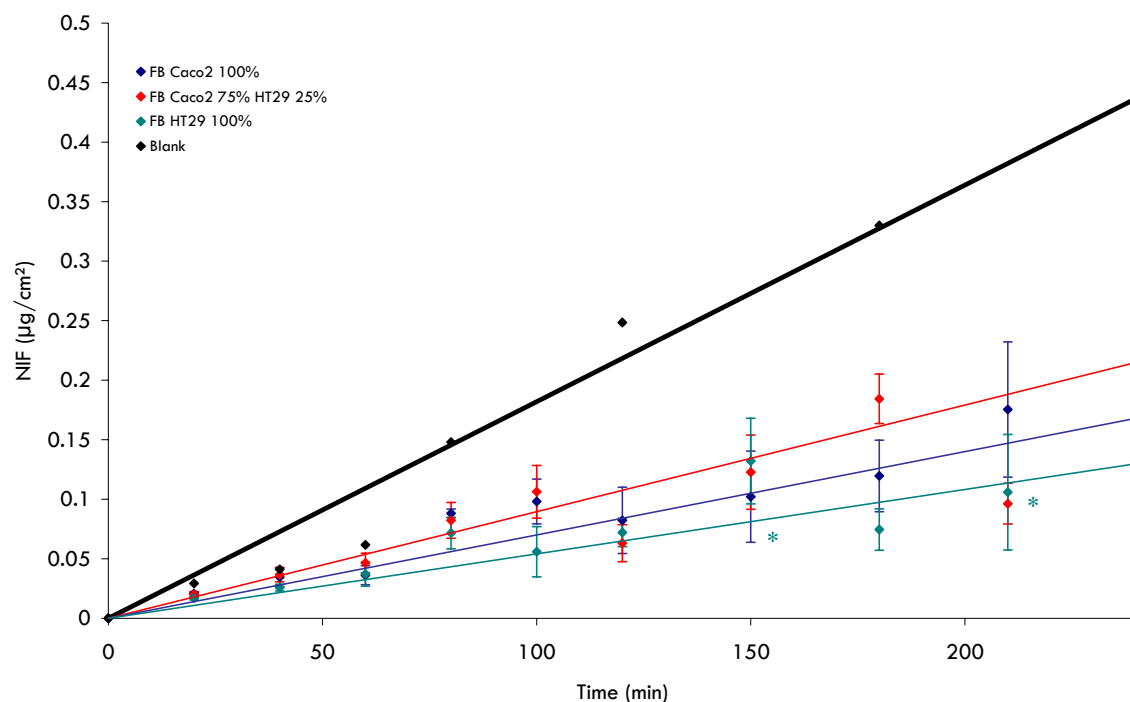


**Figure IV 5 14.** NIF transfer (apical to basolateral) (**formulation B**) across Caco-2 cultures (**blue**), HT29-5M21 cultures (**green**) and Caco-2 75%/HT29-5M21 25% co-cultures (**red**). Blank measurement (NIF transport across “blank” inserts - no cells) is represented in black. Mean  $\pm$  sem – n=5 (\* n=4)).

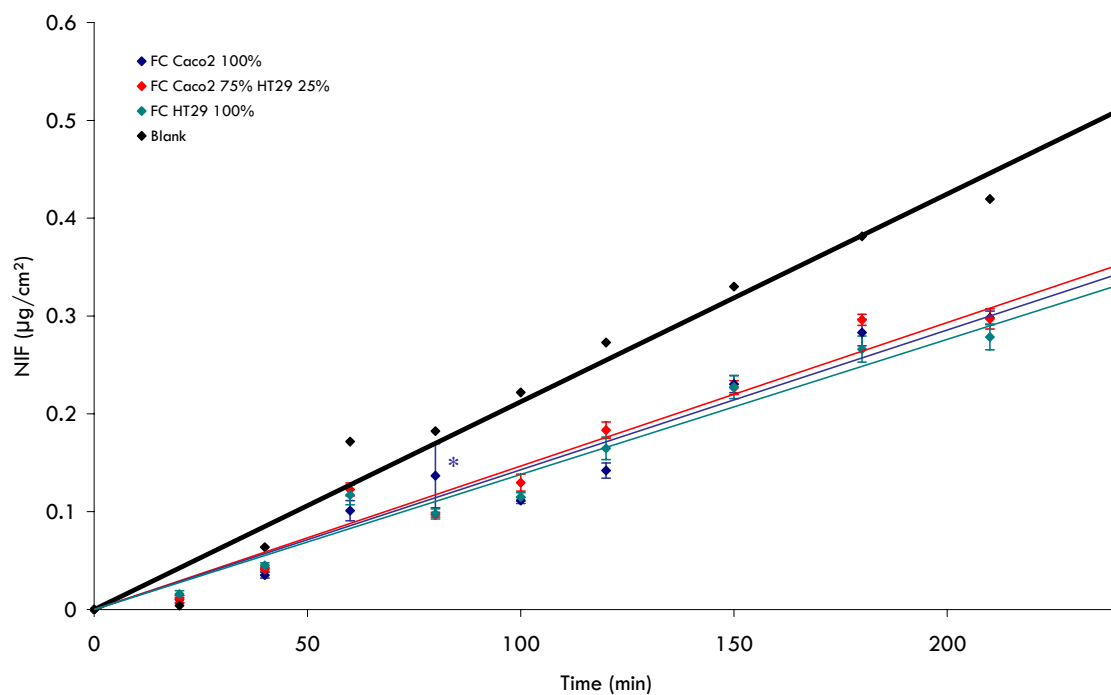


**Figure IV 5 15.** NIF transfer (apical to basolateral) (**formulation C**) across Caco-2 cultures (**blue**), HT29-5M21 cultures (**green**) and Caco-2 75%/HT29-5M21 25% co-cultures (**red**). Blank measurement (NIF transport across “blank” inserts - no cells) is represented in black. Mean  $\pm$  sem – n=5 (\* n=4)).

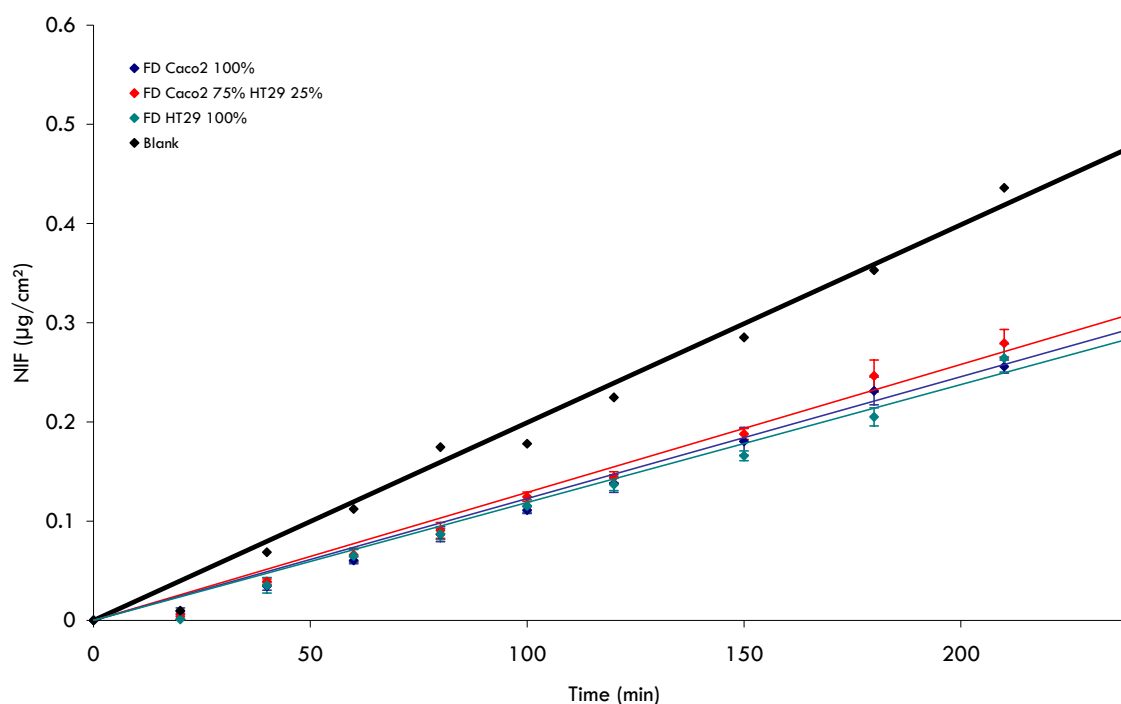


**Figure IV 5 16.** NIF transfer (apical to basolateral) (**formulation D**) across Caco-2 cultures (**blue**), HT29-5M21 cultures (**green**) and Caco-2 75%/HT29-5M21 25% co-cultures (**red**). Blank measurement (NIF transport across “blank” inserts - no cells) is represented in black. Mean  $\pm$  sem – n=5 (\* n=4)).

Through the results presented in **Figures IV 5 13, IV 5 14, IV 5 15 and IV 5 16**, we can also observe that the (co-) cultures monolayers are effectively limiting, to some extent (depending on the formulation studied), drug transport across the inserts (top to bottom). The measurement of drug transport across “blank” inserts is an important parameter to assess in order to fully characterize and validate the data obtained. In fact this evaluation, in combination with the measurement of TEER values, is a good indicator of complete homogeneous cell development along the entire proposed insert surface.

Cell monolayer integrity and cell viability (Ethidium Bromide/acrydine orange test) was also assessed for all tested formulations and for all cell models. The type of results obtained are shown in **Figure IV 5 17**.

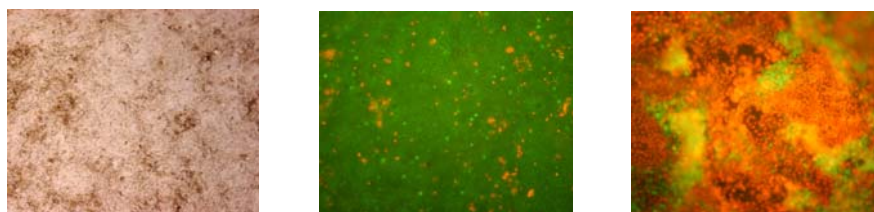


**Figure IV 5 17.** Cell layer integrity (optical microscopy) evaluation (**left**) and cell viability (Ethidium Bromide/acrydine orange staining - red: dead cells/green: viable cells) following NIF transport studies (**middle and right**). For the transport studies carried out in this work (NIF formulation A, B, C and D) across Caco-2/HT29-5M21 (co-) cultures, all the observations were similar to the first two micrographs (left and middle). The micrograph on the right-side is representative of an assay carried out when dispersing NIF formulation D in a pH 4.5 media which was further placed on top of the (co-) cultures.

#### IV.5.4. Conclusion

From the results presented in this chapter, we can conclude that permeability across intestinal cell models can be significantly enhanced for NIF nanoparticles when compared to the permeability values obtained for un-milled NIF ( $d(v,0.5) \sim 100 \mu\text{m}$ ). This conclusion can be made following the data obtained with the three cell models used as a 5.4-fold, a 5.7-fold and a 5.8-fold increase in permeation rate across was observed for Caco-2 cultures, HT29-5M21 cultures and for Caco-2 75%/HT29-5M21 25% co-cultures, respectively. This significant enhancement in permeation rate is explained by the difference of the dissolution characteristics of the two studied formulations. Although no significant differences could be found when compared to un-milled NIF, the Turrax®-milled NIF formulation ( $d(v,0.5) \sim 15 \mu\text{m}$ ), which was also characterized by enhanced dissolution rate when compared to un-milled NIF, was also found to show increased permeation rates across the three studied cell models.

No significant differences could be found for chitosan-containing nanoparticulate formulations when compared to NIF nanoparticles. This result was attributed to the resulting poor solubility of chitosan, which was evaluated for its permeability enhancement properties, in the media used during the permeability studies. Chitosan derivatives that present better solubility characteristics around pH 7 should thus preferably be used for this evaluation. The bioadhesive properties of chitosan-containing formulations, as well as the bioadhesive characteristics of nanoparticulate systems, should be evaluated on dynamic systems such as the Ussing chamber.

It has to be noted that no significant differences could be found between the three tested cell models. Since the established Caco-2/HT29-5M21 co-culture is well characterized and seemingly better representative of in vivo intestinal conditions, it could therefore be of great interest when considering in vitro permeation studies in drug development. Furthermore, the formulation of drugs as nanoparticles in order to increase their solubility and dissolution rate could be an interesting alternative to the use of solvents for the evaluation of poorly water-soluble compounds in these kinds of transport/permeability studies.



## IV.6. In vivo evaluation - pharmacokinetic studies

### IV.6.1. Introduction

Pharmacokinetic parameters such as extent of exposure and  $C_{max}$  have been reported in the literature to be enhanced for numerous drugs through nanosizing. To give a few examples, cilostazol's extent of exposure (fasted state) in Beagle dogs was increased from 2.72  $\mu\text{g}\cdot\text{h}/\text{ml}$  to 2.88  $\mu\text{g}\cdot\text{h}/\text{ml}$  and to 17.83  $\mu\text{g}\cdot\text{h}/\text{ml}$  and its  $C_{max}$  was increased from 0.58  $\mu\text{g}/\text{ml}$  to 1.03  $\mu\text{g}/\text{ml}$  and to 5.37  $\mu\text{g}/\text{ml}$  for a hammer-milled product ( $d(v,0.5)$  13  $\mu\text{m}$ ), a jet-milled product ( $d(v,0.5)$  2.4  $\mu\text{m}$ ) and a media-milled product ( $d(v,0.5)$  0.22  $\mu\text{m}$ ), respectively (Jinno et al., 2006). Danazol's extent of exposure (fasted state) in Beagle dogs was increased from 1.0  $\mu\text{g}\cdot\text{h}/\text{ml}$  to 16.5  $\mu\text{g}\cdot\text{h}/\text{ml}$  and its  $C_{max}$  was increased from 0.20  $\mu\text{g}/\text{ml}$  to 3.01  $\mu\text{g}/\text{ml}$  when decreasing particle size from 10  $\mu\text{m}$  to 0.17  $\mu\text{m}$  (media-milling) (Liversidge and Cundy, 1995). Aprepitant's extent of exposure (fasted state) in Beagle dogs was increased from 5.89  $\mu\text{g}\cdot\text{h}/\text{ml}$  to 25.29  $\mu\text{g}\cdot\text{h}/\text{ml}$  and its  $C_{max}$  was increased from 0.31  $\mu\text{g}/\text{ml}$  to 1.16  $\mu\text{g}/\text{ml}$  when decreasing particle size from 5.5  $\mu\text{m}$  to 0.48  $\mu\text{m}$  (media-milling) (Wu et al., 2004). Spironolactone's extent of exposure and  $C_{max}$  in rats was increased by a 3.3-fold and a 3-fold factor (measurement of canrenone) following nanosizing (HPH) (Langguth et al., 2005).

This section will only refer to NIF and ucb-35440-3 as model drugs (a comparative pharmacokinetic evaluation in Beagle dogs being underway for UCB-B). As solubility and, to a greater extent, dissolution characteristics were shown to be greatly influenced by particle size and significantly enhanced for drug nanoparticles (part IV.4 of this work), in vivo pharmacokinetic studies (rats) were carried out on the formulations developed to see if these enhanced characteristics could be translated into an enhanced extent of exposure in vivo.

The totally different profiles of the two model drugs (ucb-35440-3, contrarily to NIF, is a projected highly dosed drug and shows a pH-dependent solubility profile) allowed us to retrieve interesting information regarding the in vivo behaviour of the developed nanoparticulate formulations.

Considering ucb-35440-3 pharmacokinetic studies, the pH-solubility profile of the drug (Figure IV 1 7 - Table IV 1 1) allowed us to suspect the possibility of drug reprecipitation following stomach's exiting, particularly if, as expected for ucb-35440-3 nanoparticles, drug dissolution at relatively low pH (i.e. stomach - beneficial to ucb-35440-3 dissolution) is very fast. This assumption was complemented by the evaluation of the in vitro dissolution

profile of ucb-35440-3 when mimicking the GIT pH profile. To limit the possibility of this described phenomenon, ucb-35440-3 nanoparticles (administered to the rats as a suspension) were formulated in a phosphate buffer (0.5M pH 6.5) in order to limit drug dissolution in the stomach. This formulation was compared to an equivalent ucb-35440-3 nanosuspension in un-buffered media.

Considering NIF nanoparticles, a preliminary in vivo pharmacokinetic study was carried out by administering NIF (un-milled versus nanoparticles (spray-dried NIF 5%, Mannitol 5%, Methocel E15® 0.5% w/v nanosuspension)) in suspension state. A further study consisted in the evaluation of the same formulations administered into mini-capsules to the rats. The latter evaluation was carried out as the difference between the two systems was anticipated to be greater.

## IV.6.2. Materials and methods

### IV.6.2.1. ucb-35440-3: in vitro dissolution

ucb-35440-3 dissolution characteristics were evaluated, in complement to the dissolution data presented in **part IV.4.3.2.2** of this work, by varying the dissolution medium pH in order to mimic the GIT pH conditions. As ucb-35440-3 is characterized by a pH-dependent solubility profile (**part IV.1.2** of this work), this evaluation was carried out as a preliminary test to the in vivo pharmacokinetic studies in order to investigate the possibility of drug reprecipitation with increasing pH (i.e. modelling of potential in vivo drug reprecipitation following stomach exiting)

Drug dissolution determinations were carried out at  $37 \pm 0.2^\circ\text{C}$  using USP 25, number II dissolution testing apparatus (paddle method), at a rotational speed of 60 rpm. The apparatus was a DISTEK Dissolution System 2100C equipped with a DISTEK TCS0200C thermostat (DISTEK Inc., North Brunswick, NJ, USA). The dissolution medium consisted of a phosphate ( $\text{KH}_2\text{PO}_4$  50mM)/acetate ( $\text{CH}_3\text{COOH}$  50 mM) buffer adjusted to pH 1.3 and containing 0.05% polysorbate 20. The dissolution volume was initially set at 900 ml. pH was gradually increased (NaOH 8M) (volume added was taken into account for concentration evaluation) in accordance with the following scheme:

- |          |   |                  |
|----------|---|------------------|
| • pH 1.3 | → | 1 h              |
| • pH 5.0 | → | 30 min           |
| • pH 6.3 | → | 3 h              |
| • pH 6.9 | → | 3 h              |
| • pH 7.2 | → | till end of test |

All dissolution tests were carried out on an equivalent of 200 mg of ucb-35440-3 (in powder state - placed into size 00 HPMC capsules and then into sinkers) with comparison of un-milled ucb-35440-3 and ucb-35440-3 nanoparticles (freeze-dried ucb-35440-3 5%, Methocel E15® 0.1% w/v nanosuspension). Automatic withdrawals at fixed times were filtered in-line and assayed through ultraviolet absorbance determination at 255 nm for ucb-35440-3 using an Agilent 8453 UV/visible Dissolution Testing System (Agilent Technologies, USA). The mean results of a minimum of three measurements and the standard deviations are reported.

#### **IV.6.2.2. ucb-35440-3: in vivo pharmacokinetic studies**

##### **IV.6.2.2.1. Animals**

Male Wistar rats (6-7 weeks old) were obtained from Charles River Laboratories (Charles River, Brussels, Belgium). The rats' weights ranged from 180 to 200 g. All animals had free access to tap water and pelleted diet. Fasted rats were deprived of food 18 h before the experiment and food was reoffered 4 h post-dosing.

##### **IV.6.2.2.2. Experimental protocol**

ucb-35440-3 suspensions were administered orally to 6 male Wistar rats at a dose of 100 mg/kg. Suspensions of un-milled drug and drug nanoparticles (ucb-35440-3 1%, Methocel E15® 0.1% w/v nanosuspension: un-buffered suspension/0.5M phosphate pH 6.5 buffered suspension) were dosed at 10 ml/kg. For homogeneity reasons, un-milled ucb-35440-3 suspensions were prepared in 1% (w/v) Methocel A400® solutions (i.e. particle sedimentation). 600 µl blood samples were withdrawn from the caudal vein at predose, 30 min, 1, 2, 4, 8, 12 and 24 h post dosing and placed into Li Heparin plastic tubes. Blood samples were held on ice (+4°C) until centrifuged at 3000g, 4°C for 5 min. Plasma was transferred to individual Eppendorfs and stored at -20°C until analysed. This study protocol complies with particular recommendations and was approved by an internal UCB S.A. ethical committee.

#### IV.6.2.2.3. Analysis

##### IV.6.2.2.3.1. Sample preparation procedure

Plasma samples were prepared by liquid-liquid extraction. 200 µl of plasma sample were pipetted into an Eppendorf tube and fortified with 50 µl of the internal standard (ucb-46680) working solution (100 ng/ml). 300 µl of a glycine-sodium chloride 2.0 mol/l buffer adjusted at pH 10.0 with sodium hydroxide 2.0 mol/l were added. The content of the tube was gently mixed and then extracted with 1 ml of hexane-isopropanol 1:1 (v/v). This involved thorough vortex mixing for 10 min and subsequent centrifugation at 13000 rpm ( $\approx$  14750 g) for 10 min. The upper organic phase was transferred into another Eppendorf tube and evaporated to dryness in a preheated concentrator-evaporator (JOUAN RC 10.22; Saint-Herblain, France). The residue was reconstructed with 75 µl of acetonitrile-water 23:77 (v/v) containing 0.1% trifluoroacetic acid and adjusted to pH 3.0 with ammonium hydroxide, vortex mixed and then filtered on a Ultrafree MC 0.45 µm device at 13000 rpm ( $\approx$  14750 g) for 15 min using an ALC microcentrifuge 4214 (Milan, Italy). An aliquot (10 µl) was injected into the LC/ESI/MS/MS system described below.

##### IV.6.2.2.3.2. ucb-35440-3 analysis - UCB M4

A HP1100 HPLC system (Hewlett Packard, Palo Alto, USA), coupled to a Quattro Ultima mass spectrometer (Micromass, Manchester, UK) was used to measure ucb-35440-3 in plasma samples. The analytical column (Inertsil ODS 3, 5 µm, 50 x 2.1 mm ID (Varian, Harbor City, USA)) was protected by a guard column (Inertsil ODS 3, 5 µm, 10 x 2.1 mm ID (Varian, Harbor City, USA)). The column and the pre-column were placed in an oven set to a temperature of 40°C. Analyses were performed in a binary gradient mode. Solvents A and B consisted of acetonitrile-water 5:95 and 95:5 (v/v), respectively, both containing 0.1% trifluoroacetic acid and adjusted to pH 3.0 with ammonium hydroxide. The HPLC gradient started at 25% B and was linearly increased to 50% B over 7 min. It was then increased to 100% B over 0.1 min (0.9 min hold) before returning to 25% B over 0.1 min. The system was allowed to re-equilibrate for 1.9 min before injection of the next sample. The flow was adjusted to 0.250 ml/min and split post-column (ratio of 1:5) in order to get 0.050 ml/min into the electrospray source.

Electrospray experiments used a capillary voltage set at 4.00 kV. The source temperature was kept at 100°C and the desolvation temperature at 350°C. The cone gas flow (N<sub>2</sub>) was adjusted to ca 90 l/h and the desolvation gas flow (N<sub>2</sub>) to ca 850 l/h. The collision gas pressure (argon) was adjusted to about 2.10<sup>-3</sup> mbar. Spectra were acquired at ca. 1 mass unit resolution (10% valley definition) for parent and daughter ions. The inter-channel delay was fixed at 0.1s. ucb-35440-3 concentrations were determined by the peak area ratio technique. Calibration curves were established over a range of 0.5 to 100 ng/ml ( $r^2 > 0.997$ ) and study samples were diluted with blank human plasma when required.

#### IV.6.2.2.3.3. Data processing

Individual plasma concentrations and nominal sampling times were used to assess the pharmacokinetic parameters by non-compartmental analysis using the Watson Lims (6.4.0.03, Innaphase, Philadelphia, PA, USA).  $C_{\max}$  refers to the peak plasma level and  $t_{\max}$  refers to the time at which  $C_{\max}$  occurred. The area under the curve AUC(0-t) (i.e. area under the concentration-time curve calculated from zero up to time corresponding to the last measurable concentration) was calculated using the linear trapezoidal rule using mean concentrations. Concentration results on PK curves are presented as mean  $\pm$  standard deviation (SD).

#### IV.6.2.2.3.4. Statistical analysis

Statistical analysis was performed using an unpaired Student's t-test at each time points. The standard level of significance used to justify a claim of a statistically significant difference is  $p \leq 0.05$ .

### IV.6.2.3. Nifedipine

#### IV.6.2.3.1. Protocol A

##### IV.6.2.3.1.1. Animals

Male Sprague-Dawley rats were obtained from Charles River Laboratories (Charles River, Brussels, Belgium). The rats' weights ranged from 290 to 315 g. All animals had free access to tap water and pelleted diet. Fasted rats were deprived of food 18 h before the experiment and food was reoffered 4 h post-dosing.

##### IV.6.2.3.1.2. Experimental protocol

NIF suspensions were administered orally in suspension state to 4 male Sprague-Dawley rats at a dose of 25 mg/kg. Suspensions of un-milled NIF and NIF nanoparticles were dosed at 10 ml/kg. Suspensions were prepared by dispersing NIF (un-milled NIF and the spray-dried NIF 5%, Mannitol 5%, Methocel E15<sup>®</sup> 0.5% nanosuspension) in 1% w/v Methocel A400<sup>®</sup> solutions (i.e. homogeneity - particle sedimentation particularly for un-milled NIF). 240 µl blood samples were automatically withdrawn using an AccuSampler (DiLab<sup>®</sup>, Lund, Sweden) (**Annex 1**) from the femoral artery (UCB S.A. internal report regarding animal surgery reported in **Annex 2**) at predose, 30 min, 1, 2, 4, 8, and 12 h post dosing, and placed into Li Heparin plastic tubes. Blood samples were held at + 4°C until centrifuged at 3000 g, 4°C for 5 min. Plasma was transferred to individual Eppendorfs and stored at -20°C until analysis. This study protocol complies with particular recommendations and was approved by an internal UCB S.A. ethical committee.

#### **IV.6.2.3.2. Protocol B**

##### **IV.6.2.3.2.1. Animals**

Male Wistar rats were obtained from Charles River Laboratories (Charles River, Brussels, Belgium). The rats' weights ranged from 300 to 350 g. The animals were housed in a controlled environment (21 °C, 60% relative humidity and 12 h light and dark cycle) and had free access to tap water and pelleted diet (experiment was not conducted in fasted rats).

##### **IV.6.2.3.2.2. Experimental protocol**

In this protocol, NIF formulations (in powder state - un-milled NIF/spray-dried NIF 5%, Mannitol 5%, Methocel E15<sup>®</sup> 0.5% nanosuspension) were placed into mini-capsules (Elanco Capsules, Japan Elanco Co., Ltd., Osaka, Japan). The rats were administered subcutaneously Rimadyl<sup>®</sup> (40 mg/Kg; (15 min before administration of the capsule) and Heparine (500UI/kg; 30 min before administration of the capsule). The capsules were administered orally to the rats using an appropriate dosing syringe. NIF was administered at a dose of 5 mg/kg. 250 µl blood samples were withdrawn, in a non-serial mode (2 animals/time curve), from the animal's tail at time 15, 20, 30, 45, 60, 90, 120, 240, 480 and 1440 min post dosing and placed into plastic tubes. Blood samples were held at + 4°C and rapidly centrifuged at 10000 g, 4°C for 10 min. Plasma was transferred to individual Eppendorfs and stored at -20°C until analysed. This study protocol complies with particular recommendations and was approved by an internal ULB ethical committee (CEBEA - Commission d'éthique du bien-être animal de la Faculté de Médecine - ULB).

##### **IV.6.2.3.3. Analysis**

###### **IV.6.2.3.3.1. Sample preparation procedure**

NIF concentrations in rat plasma were determined by means of the method reported by Yoshioka et al. (**Yoshioka**



et al., 2004) with a slight modification. Plasma samples were prepared by liquid-liquid extraction. One hundred microlitres of plasma sample were pipetted into a polypropylene centrifuge tube (Nalge Nunc. Int., Rochester, NY, USA), and fortified with 100  $\mu$ L of the internal standard (Nicardipine - NIC; Sigma-Aldrich, Inc., St-Louis, MO, USA) working solution (5  $\mu$ g/mL – in toluene) and with 100  $\mu$ L of 0.1 M sodium hydroxide. The contents of the tube were gently mixed and then extracted with 5 mL of toluene. This involved shaking the solution for 20 min using a rotary mixer at 50 rpm (Labinco, Breda, The Netherlands) and subsequent centrifugation at 800 g for 15 min using a Sigma 3-10 centrifuge (Sigma Labozentrifugen GmbH, Osterode, Germany). The upper organic phase (4 mL) was transferred into glass vials and evaporated to dryness at 65°C. The residue was reconstructed with 200  $\mu$ L of the mobile phase used for HPLC analysis. An aliquot (100  $\mu$ L) was injected into the LC/UV system described below.

#### IV.6.2.3.3.2. NIF analysis - HPLC method NIF M2

An Agilent series 1100 HPLC system (Agilent Inc., Palo Alto, USA) consisting of a model G1311A solvent delivery pump, an autosampler (model ALS G1313A) and a model G1314A UV-VIS variable wavelength detector was used to measure NIF in plasma samples. Chromatographic separations were accomplished using a Nucleosil C18, 5  $\mu$ m, 25 cm x 4,0 mm stainless steel column (Macherey-Nagel GmbH, Düren, Germany) with a guard precolumn of the same packing material. The column and the pre-column were placed in an oven set to 40°C. The mobile phase consisted of methanol - 0.1M sodium acetate - 0.1M acetic acid (48:51:1 v/v). The pH of the mixed solvent system was adjusted to 5.0. The mixture was filtered through a 0.22  $\mu$ m membrane (Millipore, Bedford, USA) under vacuum and then degassed with 5 min ultrasounds. The mobile phase was pumped isocratically at a flow rate of 1.0 mL/min during analysis. The effluent was monitored at 350 nm. The retention times for NIF and NIC were approximately 17 and 24 min, respectively. Linearity of the method was established over a range of 0.05  $\mu$ g/mL – 8  $\mu$ g/mL ( $R^2 = 0.9898$ ) (NIF concentration vs. NIF/NIC peak area).

#### IV.6.2.3.3.3. Data processing

Individual plasma concentrations and nominal sampling times were used to assess the descriptive pharmacokinetic parameters using GraphPad Prism™ (GraphPad Software Inc., San Diego, CA, USA). The area under the curve

AUC (0-t) (i.e. area under the concentration-time curve calculated from zero up to time corresponding to the last measurable concentration) was calculated using the linear trapezoidal rule using the mean concentrations for each formulation. Concentration results on PK curves are presented as mean  $\pm$  standard error mean (sem).

#### **IV.6.2.3.3.4. Statistical analysis**

Statistical analysis was performed using an unpaired Student's t-test at each time points. The standard level of significance used to justify a claim of a statistically significant difference is  $p \leq 0.05$ .

### IV.6.3. Results and discussion

#### IV.6.3.1. ucb-35440-3

Pharmacokinetic evaluation following an oral dose of 100 mg/kg (suspension state) of both ucb-35440-3 un-milled drug and nanoparticles was carried out on male Wistar rats in fed and fasted states as a positive food effect on the drug absorption has been reported. Based on the pH-dependent solubility profile of the drug and as it is clearly shown when mimicking GIT pH conditions through in vitro dissolution tests (**Figure IV 6 1**), reprecipitation upon entering the small intestine should be expected. **Figure IV 6 1** clearly shows the difference between the two ucb-35440-3 systems regarding dissolution at pH 1.3. It shows that the fast dissolution behaviour at this pH for the nanoparticulate formulation should allow for rapid drug disposal in the stomach (particularly if the stomach residence time is prolonged as it is the case in fed state).

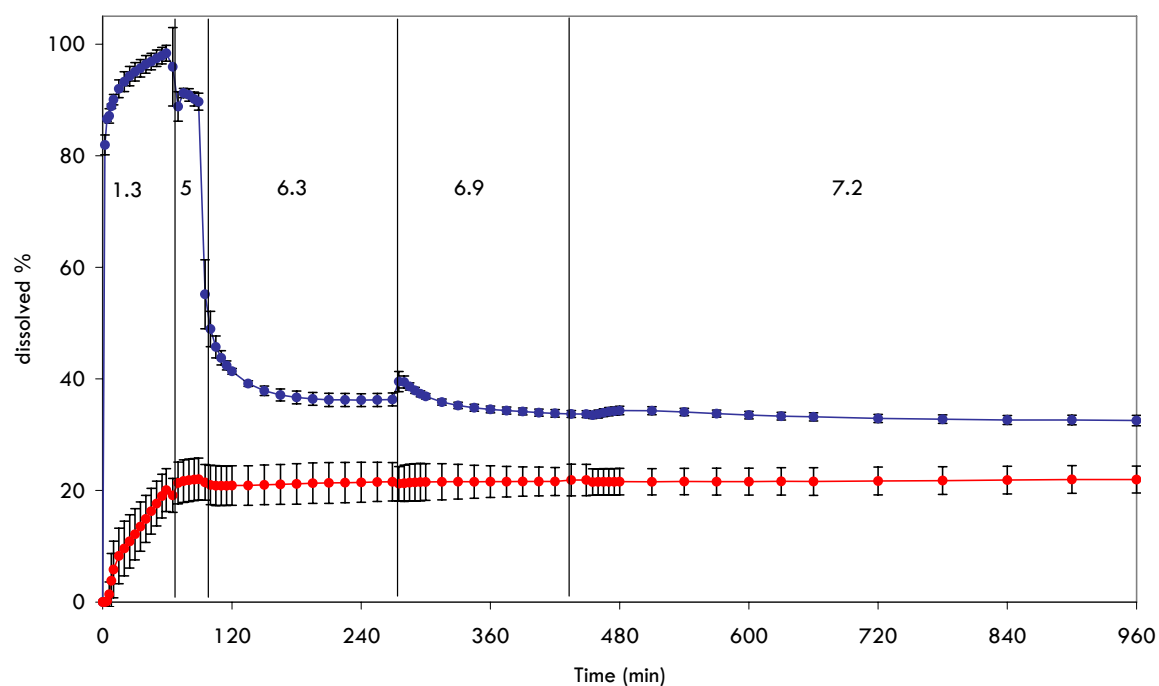


**Figure IV 6 1.** Dissolution assay for ucb-35440-3 200 mg samples: GIT pH variation simulation: un-milled ucb-35440-3 (red) and ucb-35440-3 5%, Methocel E15<sup>®</sup> 0.1% w/v freeze-dried nanosuspension (PMC + 20C 23-24000 PSI) (blue). Mean  $\pm$  SD; n=3.

These results also suggest that when drug dissolution is so fast at acidic pH, reprecipitation will occur when pH increases (based on the in vitro data shown in **Figure IV 6 1**). Laser diffraction analysis of the dissolution media after passage from pH 5.0 to pH 6.3, where most of the reprecipitation occurs, show a population of particles with a  $d(v,0.5)$  around 2.7  $\mu\text{m}$  and no submicron particles (**Figure IV 6 2 - Table IV 6 1**). Photograph of the dissolution bath before and following pH increase (pH 5.0 to pH 6.3) are shown in **Figure IV 6 3**. We can anticipate that this phenomenon might also be observed in vivo when entering the small intestine. Except for particle size, no other data regarding the particles in the precipitate were retrieved; the physicochemical state of the drug in the precipitate being unknown.

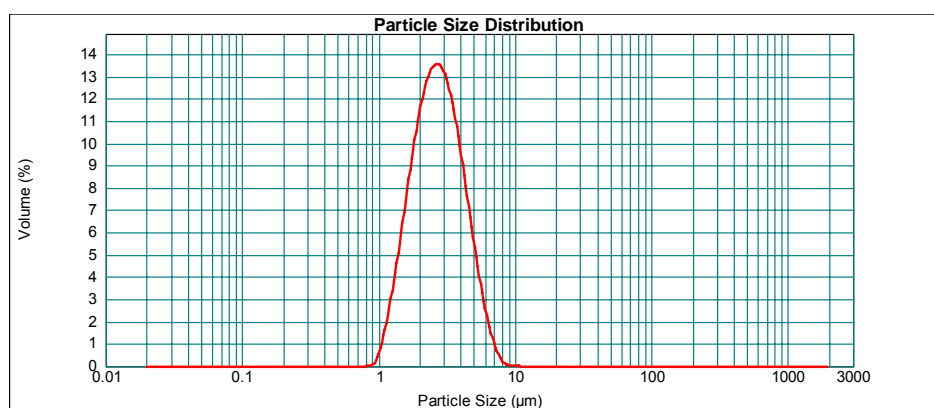


**Figure IV 6 2.** LD size distribution curve following drug reprecipitation inside the dissolution bath (pH 5.0 → 6.3).

**Table IV 6 1.** Data for Figure IV 6 2 (size in  $\mu\text{m}$ ).

	$d(0.1) \pm \text{SD}$	$d(0.5) \pm \text{SD}$	$d(0.9) \pm \text{SD}$	$D[4,3] \pm \text{SD}$	$\text{span} \pm \text{SD}$
reprecipitation	$1,57 \pm 0,12$	$2,68 \pm 0,13$	$4,66 \pm 0,30$	$2,93 \pm 0,14$	$1,18 \pm 0,10$



**Figure IV 6 3.** Photograph of dissolution baths - before (pH 1.3) and following (pH 6.3) drug reprecipitation.

To investigate the possibility of drug reprecipitation following stomach exiting, as well as its consequence on drug absorption, formulation of ucb-35440-3 nanoparticles in a 0.5M pH 6.5 phosphate buffer was assayed. This formulation was expected to limit drug dissolution in the stomach and thus prevent the presumed drug reprecipitation following its exit. This limitation was expected to be observed particularly in fasted conditions where the stomach's pH is at its lowest (e.g. the rat stomach pH in fasted state and fed state being of 3 and 5 respectively (Chu et al., 1999)).

Figures IV 6 4 and IV 6 5 show the pharmacokinetic profiles for un-milled ucb-35440-3 and for both ucb-35440-3 nanoparticle formulations in fed and fasted state, respectively. The results shown on Figure IV 6 4, Figure IV 6 5 and in Table IV 6 2 clearly indicate a positive food effect on ucb-35440-3 absorption. An extent of exposure of 7100 ng.h/ml was found for fed animals compared to 327 ng.h/ml for fasted animals (un-milled drug). The same conclusions could be drawn for ucb-35440-3 nanoparticles as extents of exposure of 3736 ng.h/ml and 2614 ng.h/ml were found for fed animals compared to 1282 ng.h/ml and 1366 ng.h/ml for fasted animals, in un-buffered and buffered conditions, respectively.

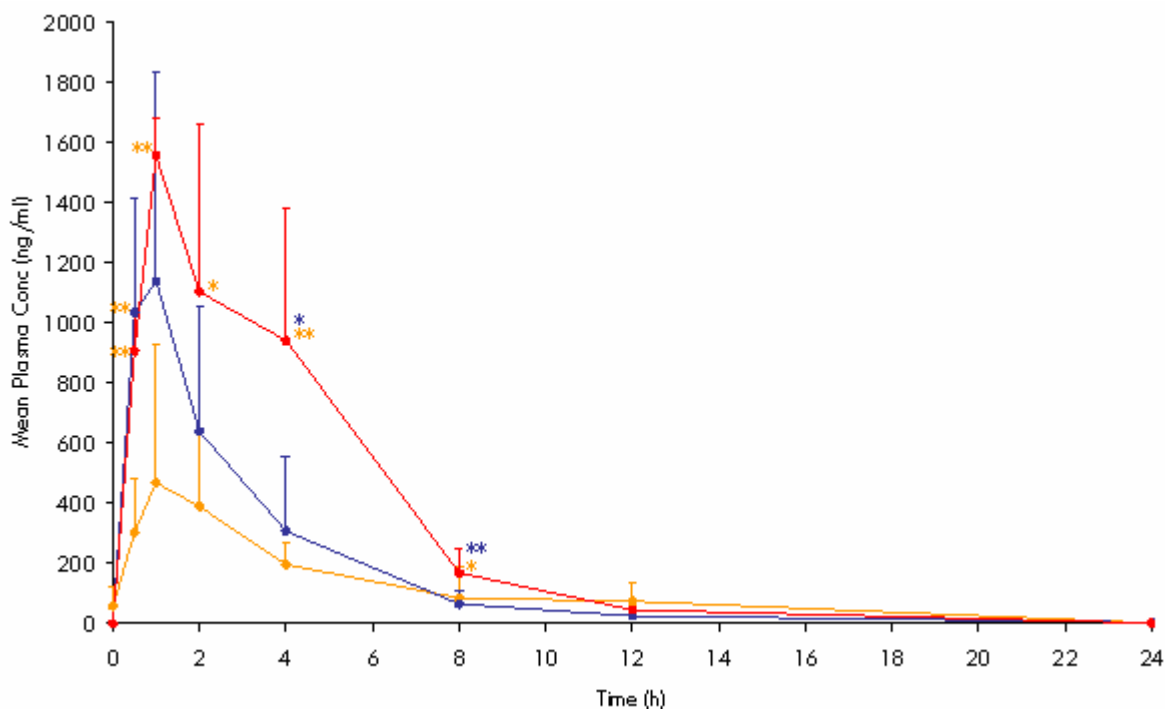


**Figure IV 6 4.** Mean plasma concentrations ( $\pm$  SD) (**fed state**) for un-milled ucb-35440-3 (**red**) (n=3); ucb-35440-3 nanoparticles (un-buffered suspension) (**blue**) (n=6) and ucb-35440-3 nanoparticles (buffered suspension) (**orange**) (n=6). (\*  $p \leq 0.05$ , \*\*  $p \leq 0.01$  - star colour indicative of the formulation to which the data is compared).

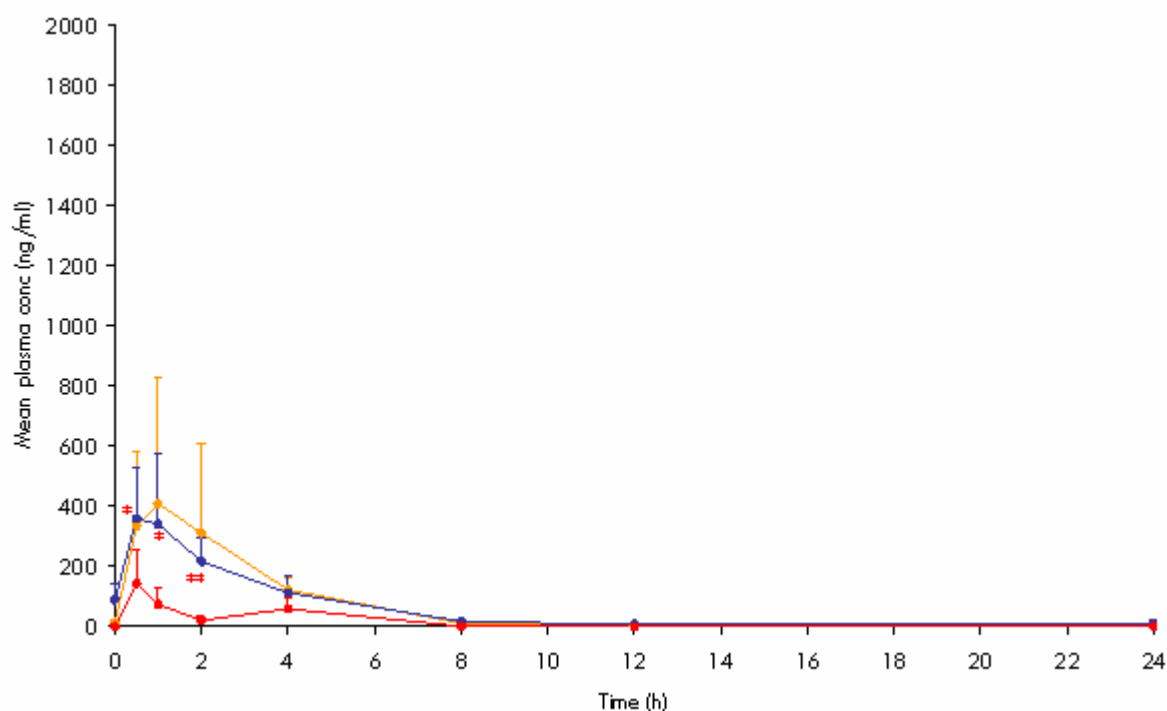


**Figure IV 6 5.** Mean plasma concentrations ( $\pm$  SD) (**fasted state**) for un-milled ucb-35440-3 (**red**) (n=3); ucb-35440-3 nanoparticles (un-buffered suspension) (**blue**) (n=6) and ucb-35440-3 nanoparticles (buffered suspension) (**orange**) (n=5). (\*  $p \leq 0.05$ , \*\*  $p \leq 0.01$  - star colour indicative of the formulation to which the data is compared).

**Table IV 6 2.** Mean plasma pharmacokinetic parameter values for ucb-35440-3 in the Wistar rat after single oral administration (100 mg/kg) of different tested ucb-35440-3 formulations: influence of particle size and media buffering.

	fed			fasted		
	Cmax (ng/ml)	Tmax	Mean AUC (0-t) (ng.h/ml)	Cmax (ng/ml)	Tmax	Mean AUC (0-t) (ng.h/ml)
<b>Un-milled</b>	1554 $\pm$ 127	1h	7100	144 $\pm$ 112	0.5h	327
<b>Nano (un-buffered suspension)</b>	1244 $\pm$ 594	0.75h	3736	383 $\pm$ 202	0.75h	1282
<b>Nano (buffered suspension)</b>	555 $\pm$ 396	1h	2614	443 $\pm$ 390	0.5h	1366

When comparing the PK profile of the un-milled ucb-35440-3 formulation and the ucb-35440-3 nanoparticle formulations in both fed and fasted state, we observe, respectively, a decrease and an increase of the drug extent of exposure for ucb-35440-3 nanoparticles. Keeping in mind the pH-dependent solubility profile of the drug (**part IV.1.2** of this work - **Figure IV 1 6** / **Table IV 1 1**), these observations can be explained by the amount of drug dissolved in the stomach and by the time given for this dissolution. As the gastric residence time (GRT) is

longer in fed state than in fasted state, the amount of dissolved ucb-35440-3 will be lower for the latter condition, even though gastric pH is lower.

When comparing the three formulations in fasted state, where GRT is short and where only the dissolution rate limits the amount of drug dissolved, we can clearly understand the increased extent of exposure for ucb-35440-3 nanosuspensions. No significant differences were observed between the buffered and un-buffered nanosuspension in fasted state. This could be explained by the fact that the amount of drug dissolved in the stomach for the un-buffered suspension might be higher than for the buffered suspension, but that drug reprecipitation might take place following stomach's emptying. Intestinal drug concentrations would thus be similar for the two suspensions. This observation could also find an explanation in the fact that gastric emptying is very fast in fasted state and that drug dissolution might mostly take place in intestinal media. Contrarily to stomach's conditions where the buffered suspension should play a role in limiting drug dissolution, no differences were expected to be observed between the two systems in this case. In fact, the lower extent of exposure observed in fed state for the buffered ucb-35440-3 nanosuspension (2614 ng.h/ml) compared to the un-buffered nanosuspension (3736 ng.h/ml) can be explained by a smaller dissolved amount due to the higher pH of the buffer compared to the nominal stomach pH in fed state. The GRT in both cases was thought to be the same.

When comparing the pharmacokinetic profile of both un-milled ucb-35440-3 and ucb-35440-3 nanoparticles in un-buffered media, we observe an approximate twofold decrease (7100 ng.h/ml → 3736 ng.h/ml) in extent of exposure for the latter in fed state. This rather unexpected result could be explained by the fact that un-milled ucb-35440-3, unlike ucb-35440-3 nanoparticles, was administered as a viscous suspension (i.e. suspension homogeneity – sedimentation of large particles). This might increase the GRT of the drug and thus increase the time available for ucb-35440-3 dissolution. The arrival of the drug in dissolved state in the intestine being more progressive, the chance of drug reprecipitation is smaller than for nanoparticulate formulations.

From the data obtained, we can see that a highly dosed, poorly water-soluble weak base, such as ucb-35440-3, represents a model with great complexity when considering nanoparticulate systems as a formulation approach for systemic exposure enhancement. We can see that for basic compounds there is an interest in increasing drug solubilization in the stomach and in increasing GRT. Investigations into the occurrence of in vivo drug reprecipitation, which was only posed as an hypothesis, shall of course be deepened.

### IV.6.3.2. Nifedipine

#### IV.6.3.2.1. Suspension state - NIF protocol A

In vivo pharmacokinetic evaluation of NIF nanoparticulate systems (i.e. optimized spray-dried NIF 5%, Mannitol 5%, Methocel E15® 0.5% w/v nanosuspension) was carried out to complement the promising data obtained through the in vitro studies described in previous chapters (solubility/dissolution - **part IV.4**; permeability studies - **part IV.5**). A preliminary study was conducted on male Sprague-Dawley rats with comparison of un-milled NIF and NIF nanoparticles (spray-dried NIF 5%, Mannitol 5%, Methocel E15® 0.5% w/v nanosuspension) administered orally (gavage) in suspension state.

**Figures IV 6 6** and **IV 6 7** show the pharmacokinetic profiles of NIF nanoparticles and of un-milled NIF in both fed and fasted animals. Results relative to the different pharmacokinetic parameters are given in **Table IV 6 3**. Although no significant differences could be observed between the two formulations studied, a clear tendency towards a systemic extent of exposure enhancement, in fed and fasted state, for NIF nanoparticles vs. un-milled NIF was observed. The double peak observed in fed state, for both formulations, was unexplained.

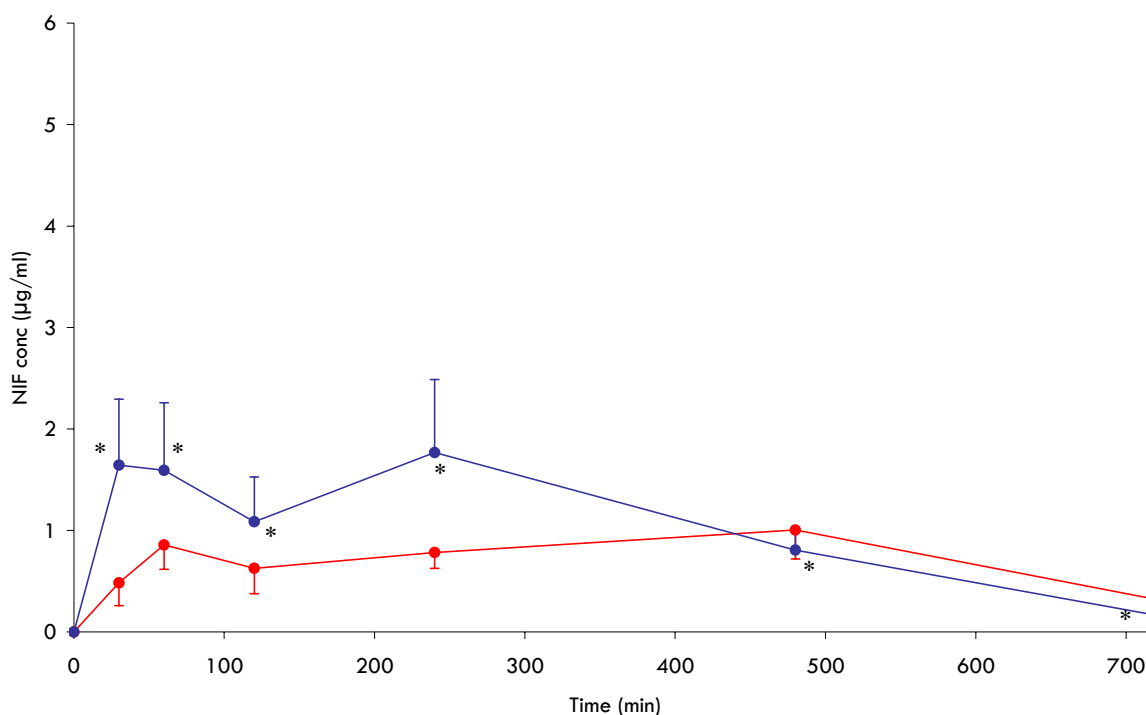


**Figure IV 6 6.** Pharmacokinetic profiles following oral administration (suspension state) (25 mg/kg) (**fed state**) of un-milled NIF (**red**) and NIF nanoparticles (spray-dried NIF 5%, Mannitol 5%, Methocel E15® 0.5% w/v nanosuspension) (**blue**). (Mean  $\pm$  sem (n=4; \* n=3)).



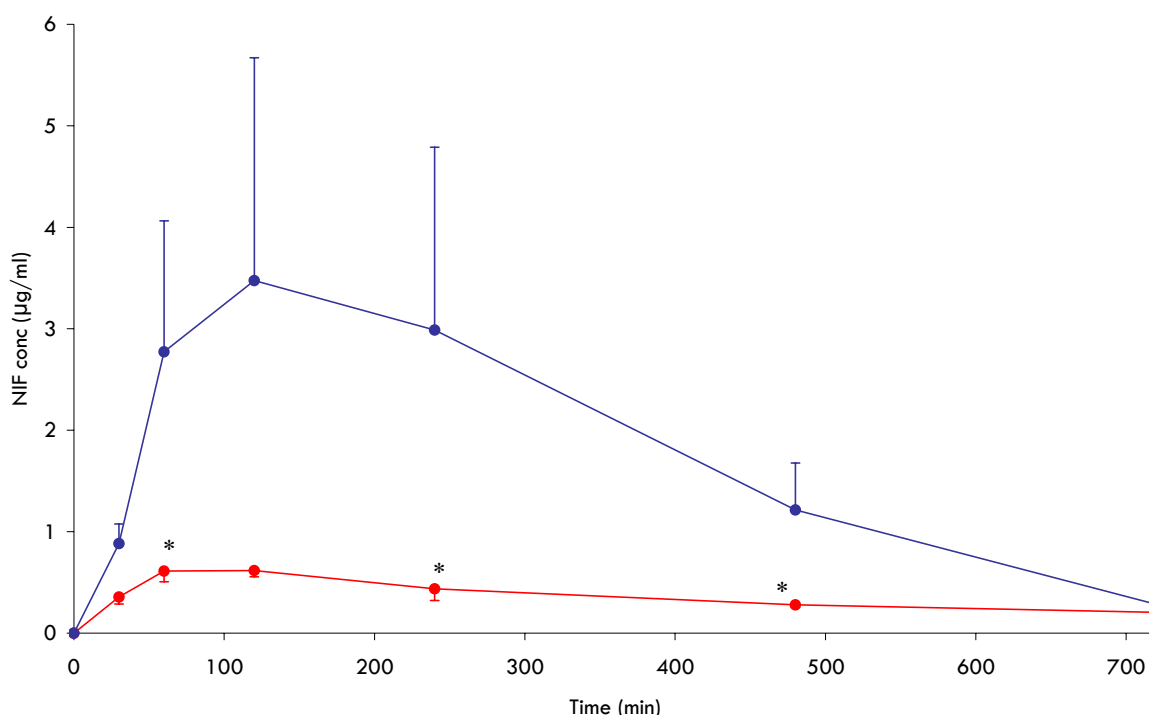


**Figure IV 6 7.** Pharmacokinetic profiles following oral administration (suspension state) (25 mg/kg) (**fasted state**) of un-milled NIF (**red**) and NIF nanoparticles (spray-dried NIF 5%, Mannitol 5%, Methocel E15® 0.5% w/v nanosuspension) (**blue**). (Mean  $\pm$  sem (n=4; \* n=3)).

**Table IV 6 3.** Mean plasma pharmacokinetic parameter values for NIF in male Sprague-Dawley rats after single oral administration (25mg/kg) for un-milled NIF and NIF nanoparticles in fed and fasted state.

	fed			fasted		
	Mean AUC (0-t) ( $\mu\text{g}\cdot\text{min}/\text{ml}$ )	C <sub>max</sub> ( $\mu\text{g}/\text{ml}$ ) Mean $\pm$ sem	T <sub>max</sub> (min)	Mean AUC (0-t) ( $\mu\text{g}\cdot\text{min}/\text{ml}$ )	C <sub>max</sub> ( $\mu\text{g}/\text{ml}$ ) Mean $\pm$ sem	T <sub>max</sub> (min)
Un-milled NIF	530	1.01 $\pm$ 0.57	480	264	0.62 $\pm$ 0.06	120
NIF nanoparticles	751	1.77 $\pm$ 0.72	240	1327	3.47 $\pm$ 2.20	120

This tendency towards enhancement was particularly marked in fasted state where extents of exposure of 1327  $\mu\text{g}\cdot\text{min}/\text{ml}$  and 264  $\mu\text{g}\cdot\text{min}/\text{ml}$  were found (5-fold increase) for NIF nanoparticles and un-milled NIF, respectively. The extents of exposure in fed state were found to be 751  $\mu\text{g}\cdot\text{min}/\text{ml}$  and 530  $\mu\text{g}\cdot\text{min}/\text{ml}$  for NIF nanoparticles and un-milled NIF, respectively.

The difference observed, for a given formulation, between fed and fasted animals was unexpected as diet has not been reported to interfere appreciably with the extent of systemic exposure for NIF (Reitberg et al., 1987).

This could possibly be explained by the increased sensitivity of NIF nanoparticles to the increased stomach medium viscosity in fed state. As the dissolution rate is so fast for NIF nanoparticles, NIF dissolution from nanosuspensions might be decreased if viscosity increases, with drug diffusion becoming, in this case, the limiting factor in the dissolution process. The pharmacokinetic profile obtained in this case is thus closer to that observed for un-milled NIF. Furthermore, it has to be noted that drug formulation as nanoparticles has been reported to decrease the food effect of compounds characterized by such phenomenon. This was reported for cilostazol (Jinno *et al.*, 2006) and felodipine (Scholz *et al.*, 2002).

#### IV.6.3.2.2. Powder state (minicapsule) - NIF protocol B

To complement the preliminary in vivo pharmacokinetic evaluation carried out on NIF nanoparticulate systems in the previous section and to compare a different dosage form thought to be more discriminating for the systems studied, in vivo pharmacokinetic profile evaluation of NIF nanoparticulate systems formulated in powder state (formulation placed into minicapsules) was carried out. In fact, when considering drug administration in powder state (i.e. into capsules), the difference in pharmacokinetic profiles between un-milled NIF and the studied NIF nanoparticle formulation was expected to be greater when compared to drug administration as a suspension (i.e. by gavage) where the drug is already wetted and probably already dissolved, to some extent (more so for NIF nanoparticles), prior to drug administration. In the case of capsule administration, drug wetting and drug dissolution have to take place after administration to the rats - these characteristics being much enhanced for NIF nanoparticles vs. un-milled NIF.

Pharmacokinetic profiles for NIF nanoparticles (spray-dried NIF 5%, Mannitol 5%, Methocel E15® 0.5% w/v nanosuspension) and of un-milled NIF following oral administration (powder state - minicapsules) are shown in **Figure IV 6 8**. Results relative to the different pharmacokinetic parameters are given in **Table IV 6 4**.

Through the results shown in **Figure IV 6 8** and **Table IV 6 4**, we can clearly see the difference between un-milled NIF and the studied NIF nanoparticle formulation. There is a reported 2.5-fold increase in the systemic extent of exposure for NIF nanoparticles versus the un-milled drug; 490 µg.min/ml versus 200 µg.min/ml, respectively. More interestingly, the C<sub>max</sub> was significantly enhanced by a 6-fold factor for NIF nanoparticles (2.58 µg/ml)

versus un-milled NIF ( $0.43 \mu\text{g/ml}$ ).  $T_{\text{max}}$  was reduced from 90 min to 20 min when considering un-milled NIF and the studied NIF nanoparticle formulation, respectively. These results are much more interesting regarding the behavior difference of NIF nanoparticles and un-milled NIF than the results obtained in suspension state and allow for a nice parallelism with the results obtained in vitro on Caco-2/HT29-5M21 (co-) cultures (**part IV.5** of this work).

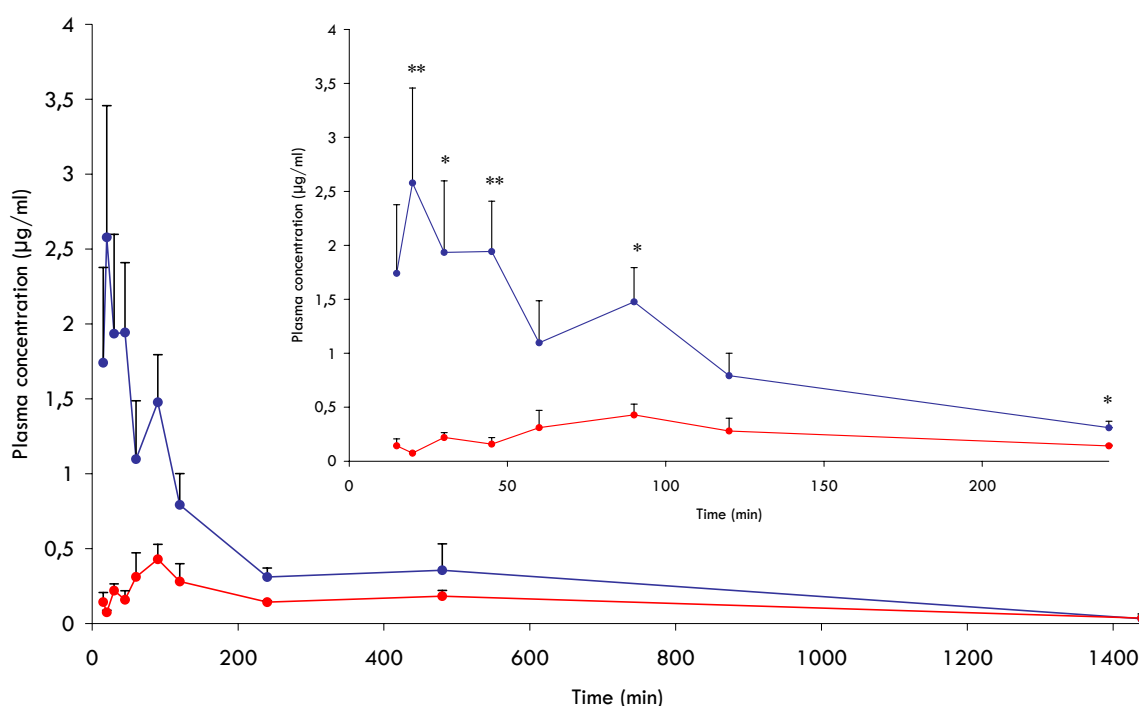


**Figure IV 6 8.** Pharmacokinetic profiles following oral administration (capsules) (5 mg/kg) (**fed state**) of un-milled NIF (n=5) (**red**) and NIF nanoparticles (spray-dried NIF 5%, Mannitol 5%, Methocel E15® 0.5% w/v nanosuspension) (n=6) (**blue**). (Mean  $\pm$  sem) (\*  $p < 0.05$ ; \*\*  $p < 0.01$ ).

**Table IV 6 4.** Mean plasma pharmacokinetic parameter values (calculated on the mean curves) for NIF in the Wistar rat after single oral administration (5 mg/kg - powder state (capsule)) of un-milled NIF (n=5) and NIF nanoparticles (n=6).

	$C_{\text{max}}$ ( $\mu\text{g/ml}$ )	$T_{\text{max}}$	Mean AUC (0-t) ( $\mu\text{g}\cdot\text{min/ml}$ )
<b>Un-milled</b>	$0.43 \pm 0.10$	90min	199.1
<b>Nano</b>	$2.58 \pm 0.88$	20min	489.8

#### IV.6.4. Conclusion

The results presented in this chapter showed the great complexity brought in by the different physicochemical characteristics (i.e. mainly solubility - pH-dependent/pH-independent) of the model drugs tested.

Considering ucb-35440-3, the extent of exposure following oral administration in fasted state was enhanced by a 4-fold factor and the C<sub>max</sub> was significantly enhanced from 144 ng/ml to 383 ng/ml following particle size reduction to nanometer range. It has to be noted that this observation could not be made for ucb-35440-3 in fed state as no enhancement could be reached for drug nanoparticles but the rather unexpected results were explained by the drug characteristics and by formulation considerations. The results obtained with ucb-35440-3 allowed us to show the high complexity of the model studied (poorly water-soluble weak base) and to raise the question of possible drug reprecipitation in vivo.

Considering NIF formulated in suspension state, extent of exposure was enhanced from 530 µg.min/ml to 751 µg.min/ml and from 264 µg.min/ml to 1327 µg.min/ml and C<sub>max</sub> was enhanced from 1.01 µg/ml to 1.77 µg/ml and from 0.62 µg/ml to 3.47 µg/ml following particle size reduction to nanometer range in fed and fasted state, respectively. Following NIF administration in powder state (i.e. in capsules) (fed state), the extent of exposure was enhanced from 199 µg.min/ml to 490 µg.min/ml and C<sub>max</sub> was significantly enhanced from 0.43 µg/ml to 2.58 µg/ml following particle size reduction to nanometer range. This dosage form was thought to be more discriminating between the two assayed formulations (i.e. NIF nanoparticles/un-milled NIF) as in this case, both wetting and drug dissolution has to take place following administration.

## **IV.7. In vivo evaluation - evaluation of the antihypertensive effect of NIF nanoparticles on spontaneously hypertensive rats (SHR)**

### **IV.7.1. Introduction**

This section will only refer to NIF as a model drug. In order to complement the very promising results obtained in vitro (solubility, dissolution, permeation rate across in vitro intestinal cell models - **part IV.4** and **part IV.5** of this work) and in vivo (pharmacokinetic profile - **part IV.6.3.2** of this work), the evaluation of the antihypertensive effect of NIF nanoparticles (spray-dried NIF 5%, Mannitol 5%, Methocel E15® 0.5% w/v nanosuspension) on spontaneously hypertensive rats (SHR), with comparison to un-milled NIF, was carried out.

This evaluation is to be compared with the pharmacokinetic profiles shown in **Figure IV 6 8** (same dose, same formulation and administration procedure). Systolic blood pressure (SBP) measurements were taken before (mean initial SBP) and 30, 60 and 120 min after administration. These time points were chosen according to the calculated pharmacokinetic parameters of **Table IV 6 4** to evaluate SBP around the C<sub>max</sub> obtained for the tested formulations (**part IV.6.3.2** of this work - **Figure IV 6 8** / **Table IV 6 4**).

### **IV.7.2. Materials and methods**

#### **IV.7.2.1. Animals**

Spontaneously hypertensive rats (SHR) were obtained from Charles River Laboratories (Charles River, Brussels, Belgium). The rats' weights ranged from 300 to 350 g. The animals were housed in a controlled environment (21°C, 60% relative humidity and 12-h light and dark cycle) and had free access to tap water and pelleted diet (experiment was not conducted in fasted rats).

#### **IV.7.2.2. NIF administration**

NIF formulations (in powder state - un-milled NIF/spray-dried NIF 5%, Mannitol 5%, Methocel E15® 0.5% w/v nanosuspension) were placed into mini-capsules (Elanco Capsules, Japan Elanco Co., Ltd., Osaka, Japan). The capsules were administered orally to the rats using an appropriate dosing syringe. NIF was administered at a dose of 5 mg/kg. This study protocol complies with particular recommendations and was approved by an internal ULB ethical committee (CEBEA - Commission d'éthique du bien-être animal de la Faculté de Médecine - ULB).

#### **IV.7.2.3. Systolic blood pressure measurements**

Systolic blood pressure (SBP) was measured non-invasively using a tail-cuff method (Apollo 179, IITC Life Science Instruments, Woodland Hills, CA, USA) on conscious, restrained animals. The animals were accommodated to the restrainers during one hour (per day) for one full week without taking any blood pressure measurements.

Systolic blood pressure (SBP) measurements were taken before (mean initial SBP) and 30, 60 and 120 min after administration. All SBP were calculated as the mean value of 4 measurements. The study design was a single dose, two-treatment, two-period cross-over study with a wash-out period of at least 7 days between the two phases of the study. Results are presented as mean  $\pm$  sem (n=8).

#### **IV.7.2.4. Statistical analysis**

Statistical analysis was performed using a paired Student's t-test at each time points. The standard level of significance used to justify a claim of a statistically significant difference is  $p \leq 0.05$ .

### IV.7.3. Results and discussion

Evaluation of the antihypertensive effect of un-milled NIF and of the optimized studied NIF nanoparticle formulation (spray-dried NIF 5%, Mannitol 5%, Methocel E15® 0.5% w/v nanosuspension) was carried out on male spontaneously hypertensive rats (SHR). Data relative to the measurement of the systolic blood pressure (SBP) before (measurement of the mean initial SPB) and following oral administration of the studied NIF formulations is shown in **Figure IV 7 1**. Evaluation of the percentage of SBP reduction (relative to initial SBP) for the two studied formulations is shown in **Figure IV 7 2**.

Through the results presented in **Figure IV 7 1**, we can clearly see the influence of particle size reduction on SBP following oral administration of the studied formulations to SHR rats. In fact, when comparing un-milled NIF and NIF nanoparticles, highly significant differences were found in SBP following 30 and 60 min (SBP at time 120 min not found significantly different -  $p$ : 0.052). Furthermore, when compared to the initial SBP ( $147 \pm 12$  mmHg), SBP was significantly (highly significant) decreased at time points 30 min ( $101 \pm 10$  mmHg -  $p$ : 0.005) and 120 min ( $109 \pm 13$  mmHg -  $p$ : 0.006) for NIF nanoparticles (no significant difference at time 60 min -  $121 \pm 7$  mmHg -  $p$ : 0.06) whereas no significant drop in SBP (vs. initial SBP) could be observed for un-milled NIF.

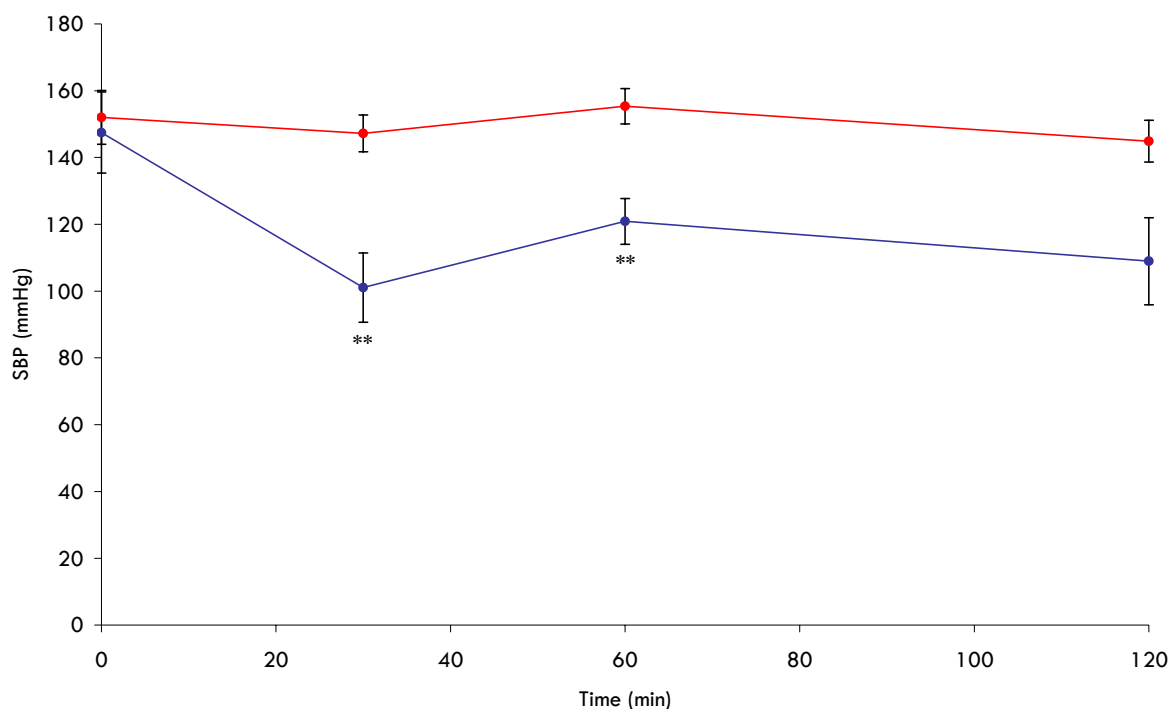


**Figure IV 7 1.** Evolution of SBP following oral administration (capsules) (5 mg/kg) (**fed state**) of un-milled NIF (n=8) (**red**) and NIF nanoparticles (spray-dried NIF 5%, Mannitol 5%, Methocel E15® 0.5% w/v nanosuspension) (n=8) (**blue**). (Mean  $\pm$  sem (n=8)) (\*  $p$  < 0.05; \*\*  $p$  < 0.01).

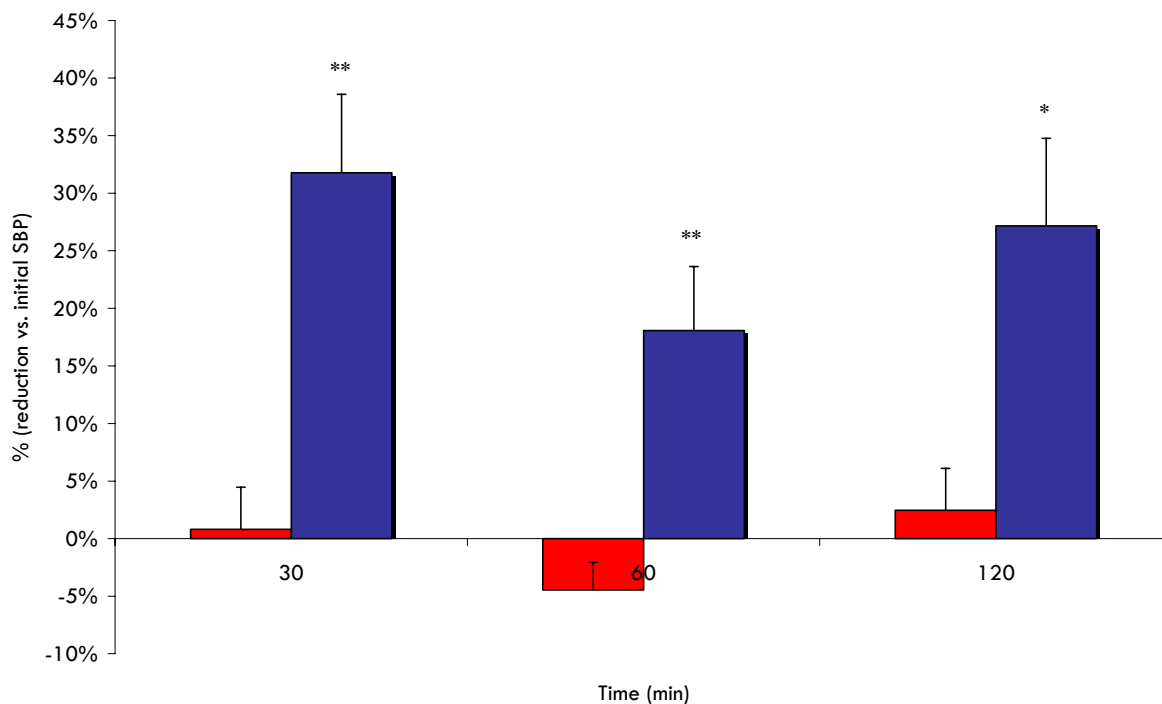


**Figure IV 7 2.** Reduction of initial SBP at each time points following oral administration (capsules) (5 mg/kg) (**fed state**) of un-milled NIF (n=8) (**red**) and NIF nanoparticles (spray-dried NIF 5%, Mannitol 5%, Methocel E15® 0.5% w/v nanosuspension) (n=8) (**blue**). (Mean ± sem (n=8)) (\* p < 0.05; \*\* p < 0.01).

As it can be better visualized from the data presented in **Figure IV 7 2**, the initial SBP was significantly reduced, 30 min after administration, by  $32 \pm 7\%$  for NIF nanoparticles versus  $1 \pm 4\%$  for un-milled NIF. According to the pharmacokinetic profiles presented in **part IV.6.3.2** of this work (**Figure IV 6 8** / **Table IV 6 4**), a significant drop in SBP was expected around this time (i.e.  $\sim C_{max}$ ) and is thus confirmed from the results obtained in this section.

This evaluation of the antihypertensive effect of the NIF nanoparticle formulation developed nicely complements the data already obtained both in vitro (solubility, dissolution, permeation rate, etc.) and in vivo (pharmacokinetic) and allows us to see the great potential of these systems considering poorly water-soluble drugs such as NIF.



#### IV.7.4. Conclusion

From the results presented in this chapter, we can see that the formulation of NIF, an antihypertensive drug, as crystalline nanoparticles allowed for a significant reduction in systolic blood pressure (SBP) following oral administration to spontaneously hypertensive rats (SHR). The initial SBP was, in fact, significantly reduced, 30 min after administration, by 32% for NIF nanoparticles versus 1% for un-milled NIF; this time of 30 min corresponding to the C<sub>max</sub> of the pharmacokinetic profile of NIF nanoparticles following oral administration (same conditions - see **part IV.6.3.2.2 (Figure IV 6 8 and Table IV 6 4)** of this work).



## IV.8. Stability studies

### IV.8.1. Introduction

Stability can be defined as the ability of a pharmaceutical product and/or a drug substance not to undergo specific chemical, physical, microbiological or biopharmaceutical alterations during the product shelf-life. The purpose of stability testing is to provide evidence on how the quality of a drug substance or drug product varies with time under the influence of a variety of environmental factors such as, mainly, temperature and humidity (and eventually light), and to establish a re-test period for the drug substance or a shelf-life for the drug product and recommended storage conditions (ICH - Q1A (R2), 2003). Recommendations considering stability studies are the object of an ICH guideline (ICH - Q1A (R2), 2003). Test conditions (time, temperature, relative humidity (RH)) are reported in **Table IV 8 1**. The storage conditions and the lengths of studies are generally chosen to be sufficient to cover storage, shipment, and subsequent use. Data from the accelerated storage condition and, if appropriate, from the intermediate storage condition can be used to evaluate the effect of short term excursions outside the labeled storage conditions (such as might occur during shipping).

**Table IV 8 1.** ICH recommendations regarding stability studies and test conditions.

Study	Storage condition	Minimum time period covered by data at submission
Long term	25°C ± 2°C/60% RH ± 5% RH	12 months
Intermediate	30°C ± 2°C/65% RH ± 5% RH	6 months
Accelerated	40°C ± 2°C/75% RH ± 5% RH	6 months

In the case of NIF nanoparticles, other than the parameters generally evaluated in conventional stability studies, redispersion characteristics were an important characteristic to assess. Other tests compared un-milled NIF (i.e. drug alone) and NIF nanoparticles (spray-dried NIF 5%, Mannitol 5%, Methocel E15® 0.5% w/v nanosuspension). NIF chemical stability and drug dissolution characteristics were evaluated over a 12-month period. Crystalline state evaluation through DSC and PXRD analysis was also carried out to denote any modifications, primarily for NIF nanoparticles.

## IV.8.2. Material and methods

### IV.8.2.1. Capsule blistering

Un-milled NIF and NIF nanoparticles (spray-dried NIF 5%, Mannitol 5%, Methocel E15® 0.5% w/v nanosuspension) were placed into size 00 gelatin capsules. Capsules were placed in Aluminium-Aluminium blisters. Blisters were formed and sealed using a Fantasy Plus model Blister Mac VT170W blistering unit (OMAR di Cericola Giorgio, Milan, Italy). The sealing temperature was set at 150°C. The sealing time was set at 2.5 seconds. Blisters were then placed into ovens at varying controlled temperature and relative humidity (i.e. ICH conditions - 25°C/60% RH, 30°C/65% RH and 40°C/75% RH).

### IV.8.2.2. Drug stability - HPLC method NIF M3

Samples were prepared by accurately weighting an amount of NIF equivalent to around 1.5 mg and by dissolving this amount in 25 ml of methanol. This solution was placed for 5 min under ultrasounds and completed to 250 ml with deionized water. Samples were prepared in triplicate for each conditions tested (2 injections/sample). The standard deviation was reported.

Samples were assayed by HPLC using an Agilent series 1100 HPLC system (Agilent Inc., Palo Alto, USA) consisting of a model G1311A solvent delivery pump, a model ALS G1313A autosampler and a model G1314A UV-VIS variable wavelength detector. Chromatographic separations were accomplished using a Prevail Select C18, 5 µm, 15 cm x 4.6 mm stainless steel column (Alltech Inc., Deerfield, IL, USA) with a guard precolumn of the same packing material. The mobile phase consisted of a mixture of acetonitrile, methanol and water (35:17:48, v/v). The pH of the mixed solvent system was adjusted to pH 3.8 with phosphoric acid. The mixture was filtered through a 0.22 µm membrane (Millipore, Bedford, USA) under vacuum and then degassed with 5 min ultrasounds. The mobile phase was pumped isocratically at a flow rate of 1.2 ml/min during analysis, at ambient temperature. Aliquots of 80 µl were injected into the column. The effluent was monitored at 240 nm. Retention time for NIF was around 6 min. The method used showed good linearity ( $R^2 > 0.999$ ) between 0.1-10 µg/ml.

#### IV.8.2.3. Dissolution rate evaluation

Drug dissolution determinations were carried out at  $37 \pm 0.2^\circ\text{C}$  using USP 25, number II dissolution testing apparatus (paddle method), at a rotational speed of 60 rpm. The apparatus was a DISTEK Dissolution System 2100C equipped with a DISTEK TCS0200C thermostat (DISTEK Inc., North Brunswick, NJ, USA). The dissolution volume was always set at 900 ml. Dissolution medium consisted of deionized water (pH 7.0 - 0.05% polysorbate 20). All dissolution tests were carried out on an equivalent of 10 mg of NIF (in powder state - not filled into capsules). Automatic withdrawals at fixed times were filtered in-line and assayed through ultraviolet absorbance determination at 235 nm using an Agilent 8453 UV/visible Dissolution Testing System (Agilent Technologies, USA). The mean results of a minimum of three measurements and the standard deviations are reported.

The similarity factor  $f_2$  was used as a determination tool for assessing the similarity of the dissolution profiles obtained (FDA CDER Guidance, 1997a; Shah et al., 1998). The compared dissolution profiles were obtained under the same test conditions and their dissolution time points were the same, e.g. for immediate-release dosage forms, the compared time points include 15, 30, 45 and 60 min. As indicated by Shah et al. (Shah et al., 1998), the similarity factor  $f_2$  value has to be higher than 50 in order to assess the similarity between two dissolution profiles.

#### IV.8.2.4. Redispersion analysis - Laser diffraction

Redispersion analyses were conducted by adding the spray-dried powder (equivalent of 5 mg/ml) in surfactant-free deionized water. The suspension formed was placed under magnetic stirring for 10 min at 300 rpm (Variomag Multipoint HP15 magnetic stirrer-shaker 100-1000 rpm, Labortechnik GmbH, Munich, Germany). Particle size measurement was carried out using the protocol described below.

The laser diffraction apparatus used for particle sizing was a MasterSizer 2000 (Malvern Instruments Ltd., Worcestershire, United Kingdom) equipped with a wet sampling system (Hydro 2000 S). The performances of the optical and the sample handling units were qualified by performing operational qualification procedures, as proposed by Malvern Instruments, using standard material (Duke Scientific 0,3  $\mu\text{m}$  and 1  $\mu\text{m}$  polystyrene DVB microsphere suspensions). Detection limits for the equipment range from 0,02  $\mu\text{m}$  to 2000  $\mu\text{m}$ .

- **Procedure for sample measurement:**

- 10 cleaning cycles using deionized water.
- Background measurement with the dispersant used (1 cleaning cycle with dispersant before measurement).
- Measurements shall be made in a drug-saturated aqueous solution (in order to prevent variation in laser obscuration values due to dissolution of the particles - and thus variation in particle size).
- Stirring of the sample being measured set at 2500 rpm.
- No sonication during measurement.
- Minimum of 2 sets of 5 measurements shall be made for each sample at laser obscuration values ranging from 4 to 6% (+ average measurements).
- 1 cleaning cycle using alcohol (97%) and 5 cleaning cycles using deionized water.

#### **IV.8.2.5. Differential scanning Calorimetry (DSC)**

The DSC apparatus used was a Perkin Elmer DSC-7 differential scanning calorimeter/TAC-7 thermal analysis controller with an intracooler-2 cooling system (Perkin Elmer Instruments, USA). Temperature control was regulated in both ovens with an N<sub>2</sub> flux. The apparatus was Indium/Cyclohexane calibrated. The amount of product to be analyzed ranged from 1 to 5 mg and was placed in aluminum perforated pans. Heat runs were conducted for each samples as follows: 40°C to 210°C at 5°C/min.

#### **IV.8.2.6. Powder X-Ray diffraction (PXRD)**

PXRD diffractograms were recorded using a Siemens diffractometer D5000 (Siemens, Germany) with a Cu line as the source of radiation (WL1 = 1,5406 Å, WL2 = 1,54439 Å). Standard runs using a 40 kV voltage, a 40 mA current and a scanning rate of 0.02°/min over a 2θ range of 3 to 40° were used.

### IV.8.3. Results and discussion

#### IV.8.3.1. Drug stability

Drug stability was assessed for the three ICH conditions reported in the introductive part of this section. Results from stability studies at 25°C/60% RH are shown in **Figure IV 8 1** and **Table IV 8 2**. Results from stability studies at 30°C/65% RH are shown in **Figure IV 8 2** and **Table IV 8 2**. Results from stability studies at 40°C/75% RH are shown in **Figure IV 8 3** and **Table IV 8 2**. Each figure compares un-milled NIF and NIF nanoparticles (spray-dried NIF 5%, Mannitol 5%, Methocel E15® 0.5% w/v nanosuspension). From these results, we can clearly see that no degradation of NIF could be observed over a span of 12 months for both formulations tested and for all tested conditions. The NIF percentage in the formulations following 12 months of storage were 98.9% and 101.8%, 97.5% and 99.3%, and 96.7% and 103.8 % for NIF nanoparticles and un-milled NIF at storage conditions of 25°C/60% RH, 30°C/65% RH and 40°C/75% RH, respectively. NIF, alone or in the nanoparticle formulation developed, was thus found to be unaltered by 12 months exposure to the tested temperatures. The results obtained also seem to indicate that NIF, alone or in the nanoparticle formulation developed, is stable under the various tested relative humidity values. However, no conclusion can be drawn from these results as the

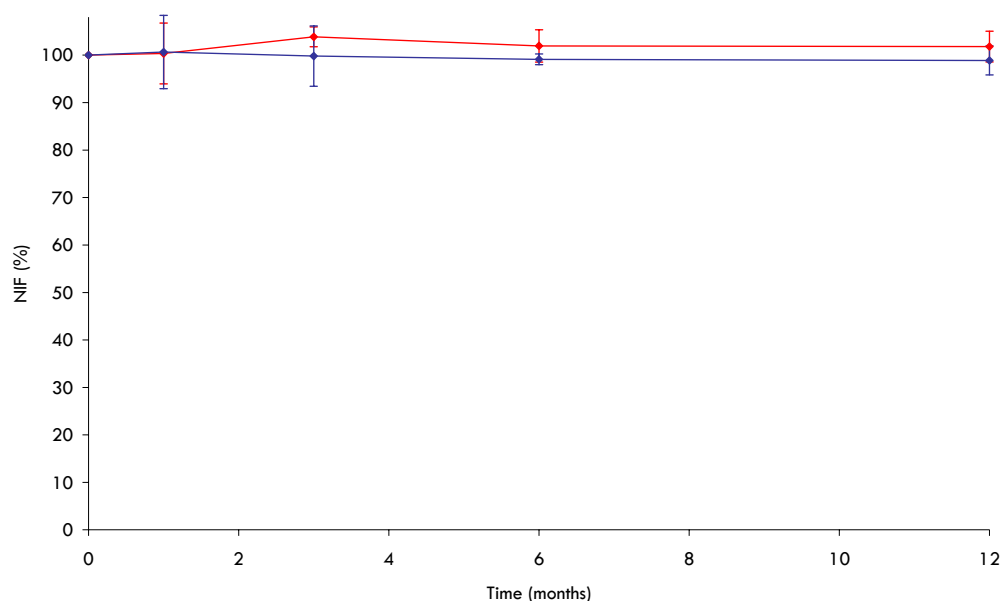


**Figure IV 8 1.** Evolution of drug content (expressed in percent - relative to values at time 0 months) as function of time for storage conditions of 25°C and 60% RH. Un-milled NIF (red) and NIF nanoparticles (blue). Mean  $\pm$  SD; n=3. Data reported in annex 1 (Table A18).

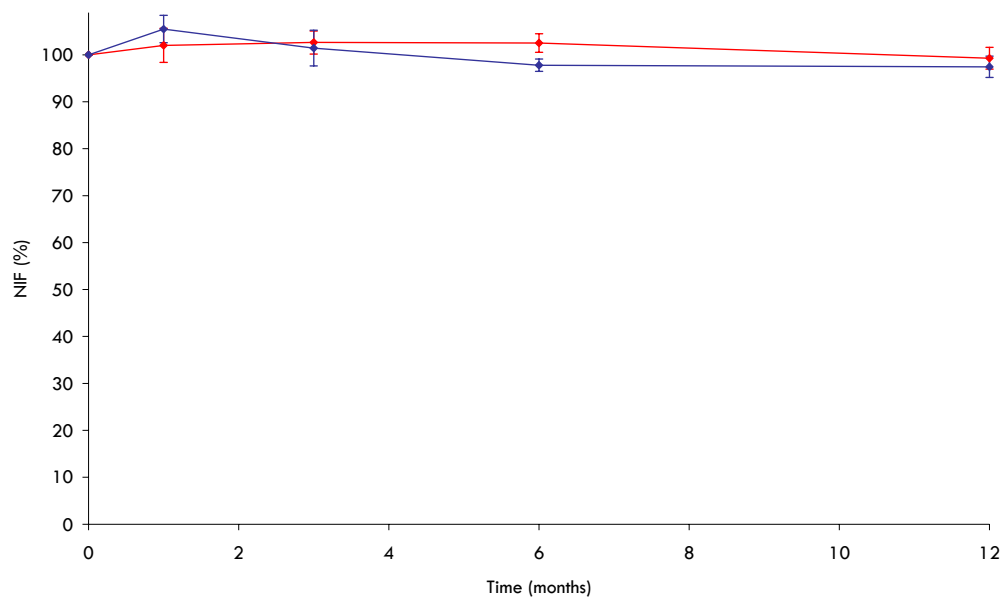


**Figure IV 8 2.** Evolution of drug content (expressed in percent - relative to values at time 0 months) as function of time for storage conditions of **30°C** and **65% RH**. Un-milled NIF (**red**) and NIF nanoparticles (**blue**). Mean  $\pm$  SD; n=3. Data reported in annex 1 (**Table A18**).

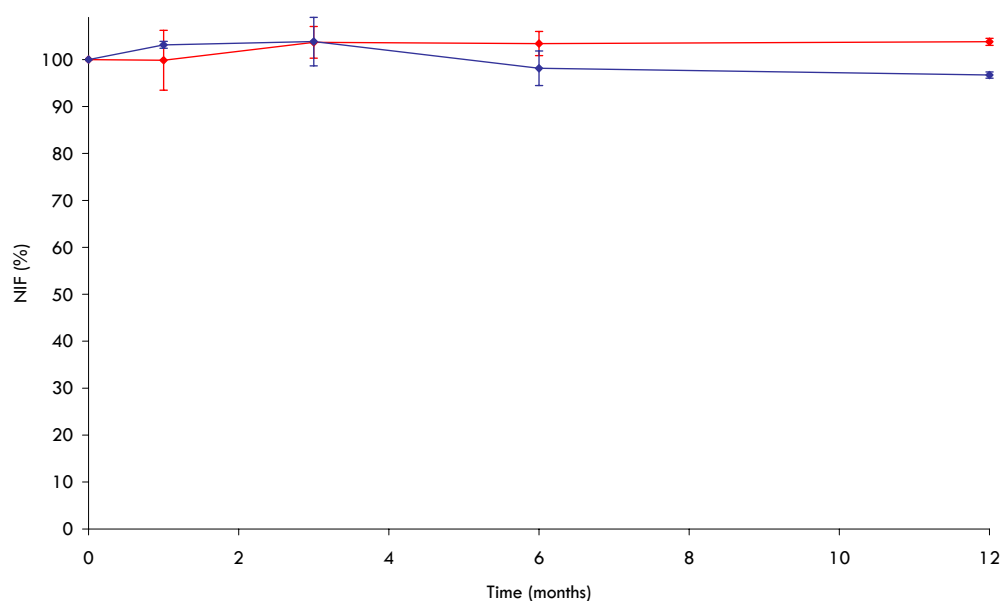


**Figure IV 8 3.** Evolution of drug content (expressed in percent - relative to values at time 0 months) as function of time for storage conditions of **40°C** and **75% RH**. Un-milled NIF (**red**) and NIF nanoparticles (**blue**). Mean  $\pm$  SD; n=3. Data reported in annex 1 (**Table A18**).



conditioning of the capsules in aluminium-aluminium blisters limited, to some extent, the contact of NIF with the ambient relative humidity. In order to clearly denote any influence of relative humidity on NIF stability, similar studies shall be conducted without conditioning the capsules in blisters.

#### IV.8.3.2. Drug dissolution

The NIF dissolution characteristics are an important parameter to assess, primarily for NIF nanoparticles, as the original dissolution profile obtained has to be maintained over time. The NIF dissolution characteristics were assessed for the three ICH conditions reported in the introductive part of this section. Results from dissolution studies at 25°C/60% RH are shown in **Figure IV 8 4**. Results from dissolution studies at 30°C/65% RH are shown in **Figure IV 8 5**. Results from dissolution studies at 40°C/75% RH are shown in **Figure IV 8 6**. Each figure compares un-milled NIF and NIF nanoparticles (spray-dried NIF 5%, Mannitol 5%, Methocel E15® 0.5% w/v nanosuspension). From the results presented in these figures we can again, as it was already observed and discussed in **part IV.4.3.2.1 (Figure IV 4 7 and Table IV 4 10)** of this work, see the clear dissolution rate enhancement procured by NIF particle size reduction. From all the data obtained, drug dissolution was complete for NIF nanoparticles following less than 10 min, whereas after this time, for un-milled NIF, less than 2% of drug was dissolved. No significant differences (similarity factors  $f_2$  determination - Annex 1 - **Table A19**) were found between dissolution curves of a given formulation; this being verified over time and for the three studied storage conditions.

From these results, we can conclude that NIF dissolution rate characteristics are, especially in the case of the nanoparticle formulation studied, unaffected by the various storage conditions and remain nearly the same over a year of storage.

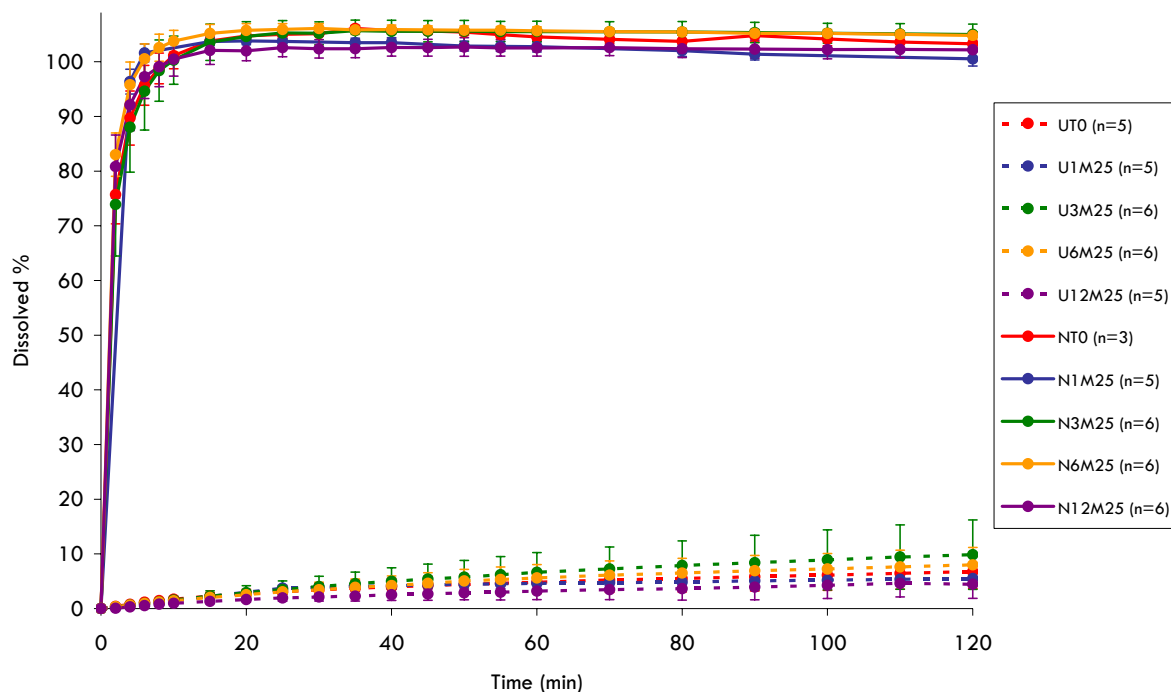


**Figure IV 8 4.** Dissolution profiles (mean  $\pm$  SD) for un-milled NIF (**dotted lines**) and NIF nanoparticles (**plain lines**) following storage conditions of **25°C** and **60% RH**. 0 months (**red**), 1 month (**blue**), 3 months (**green**), 6 months (**orange**) and 12 months (**purple**). Data reported in annex 1 (**Table A19**).

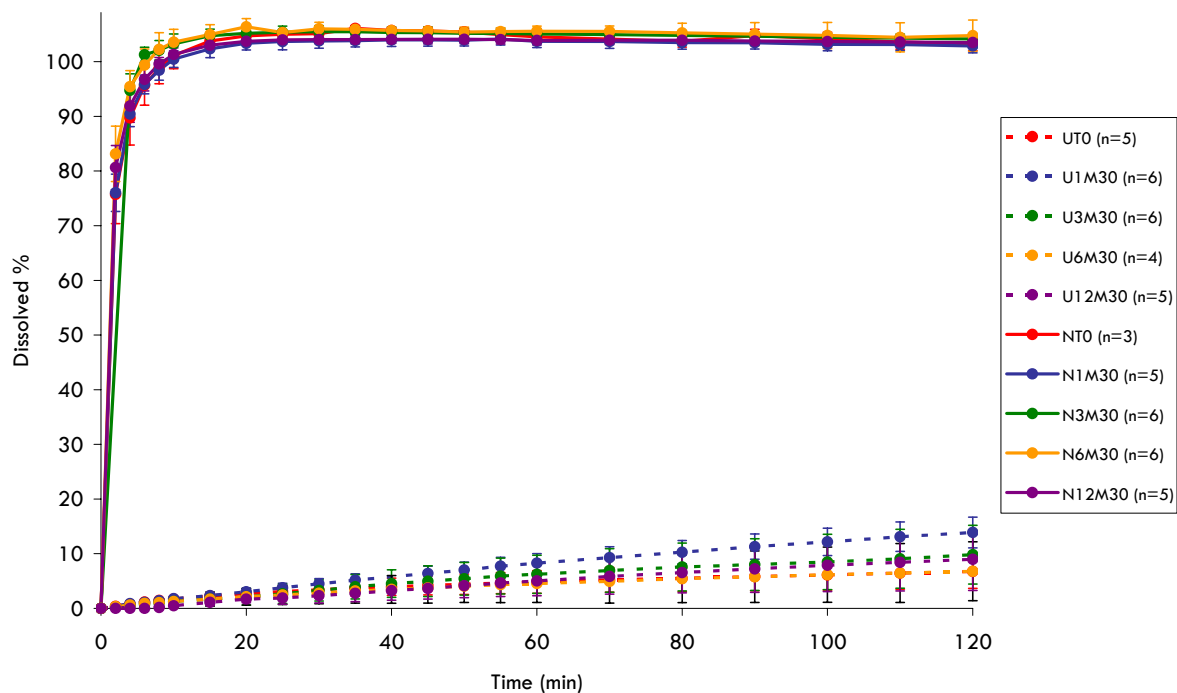


**Figure IV 8 5.** Dissolution profiles (mean  $\pm$  SD) for un-milled NIF (**dotted lines**) and NIF nanoparticles (**plain lines**) following storage conditions of **30°C** and **65% RH**. 0 months (**red**), 1 month (**blue**), 3 months (**green**), 6 months (**orange**) and 12 months (**purple**). Data reported in annex 1 (**Table A19**).

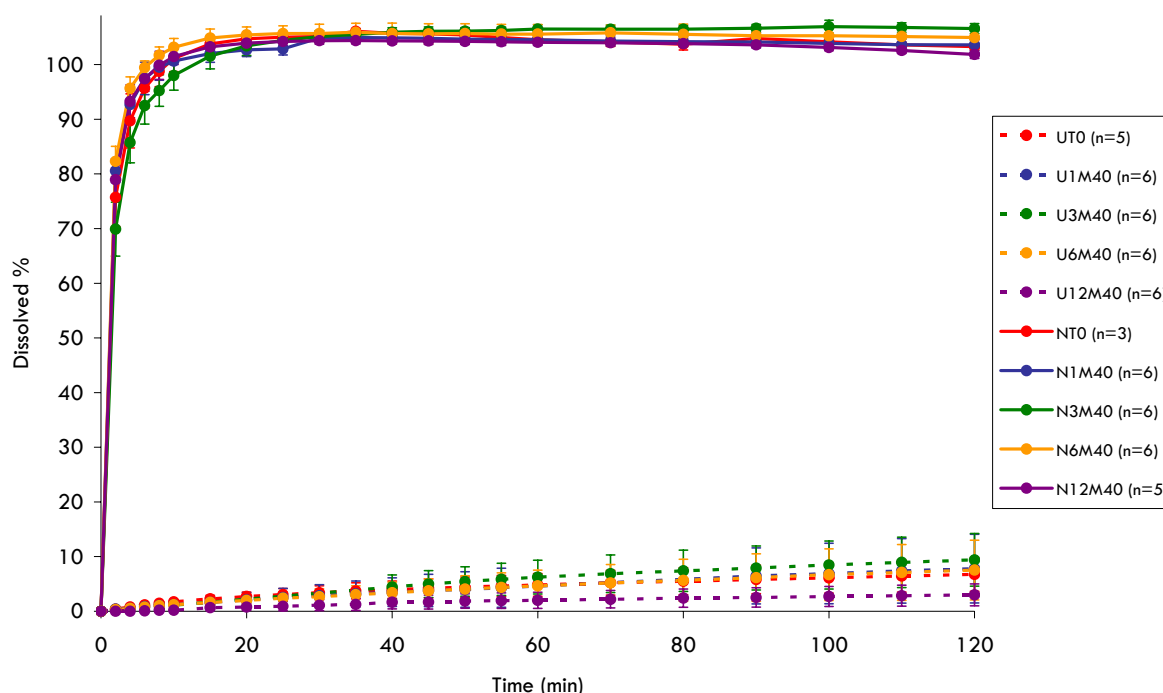


**Figure IV 8 6.** Dissolution profiles (mean  $\pm$  SD) for un-milled NIF (**dotted lines**) and NIF nanoparticles (**plain lines**) following storage conditions of **40°C** and **75% RH**. 0 months (**red**), 1 month (**blue**), 3 months (**green**), 6 months (**orange**) and 12 months (**purple**). Data reported in annex 1 (**Table A19**).

#### IV.8.3.3. NIF nanoparticle redispersion characteristics

NIF nanoparticle redispersion properties are important to assess as the original characteristics have to be maintained over time. As it has already been discussed in **part IV.2.3.5 (Figure IV 2 25)** of this work, the presence of mannitol in the NIF nanoparticle formulations was shown to be essential with regard to prevention of nanoparticle agglomeration following the water-removal operation (i.e. spray-drying) from the nanosuspension. In the presence of mannitol, the original particle size distribution (i.e. before spray-drying) could almost be restored (**Figure IV 2 25**).

The NIF nanoparticle (spray-dried NIF 5%, Mannitol 5%, Methocel E15® 0.5% w/v nanosuspension) redispersion characteristics were assessed for the three ICH conditions reported in the introductive part of this section. Results from redispersion studies at 25°C/60% RH are shown in **Figure IV 8 7**. Results from redispersion studies at 30°C/65% RH are shown in **Figure IV 8 8**. Results from redispersion studies at 40°C/75% RH are shown in **Figure IV 8 9**.

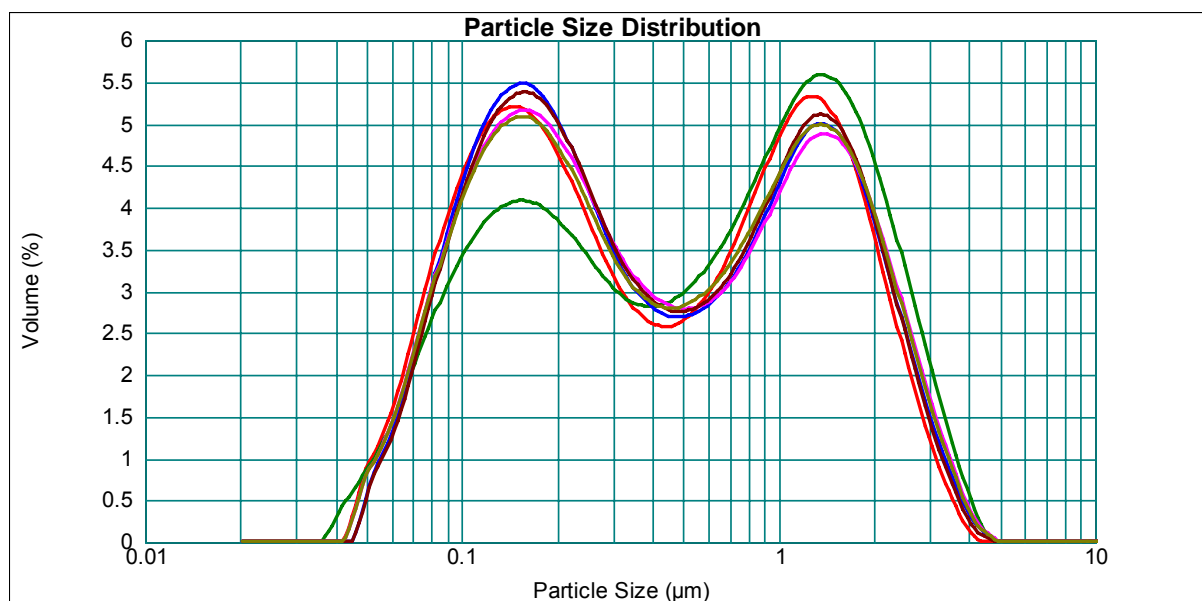


**Figure IV 8 7.** LD size distribution curves following sample processing (before spray-drying) (PMC + 20C 23-24000 PSI) (red) and following redispersion of the spray-dried processed suspension: T0 (green) and following storage (25°C/60% RH) - 1 month (blue), 3 months (pink), 6 months (brown) and 12 months (dark yellow). Data reported in annex 1 (Table A20).

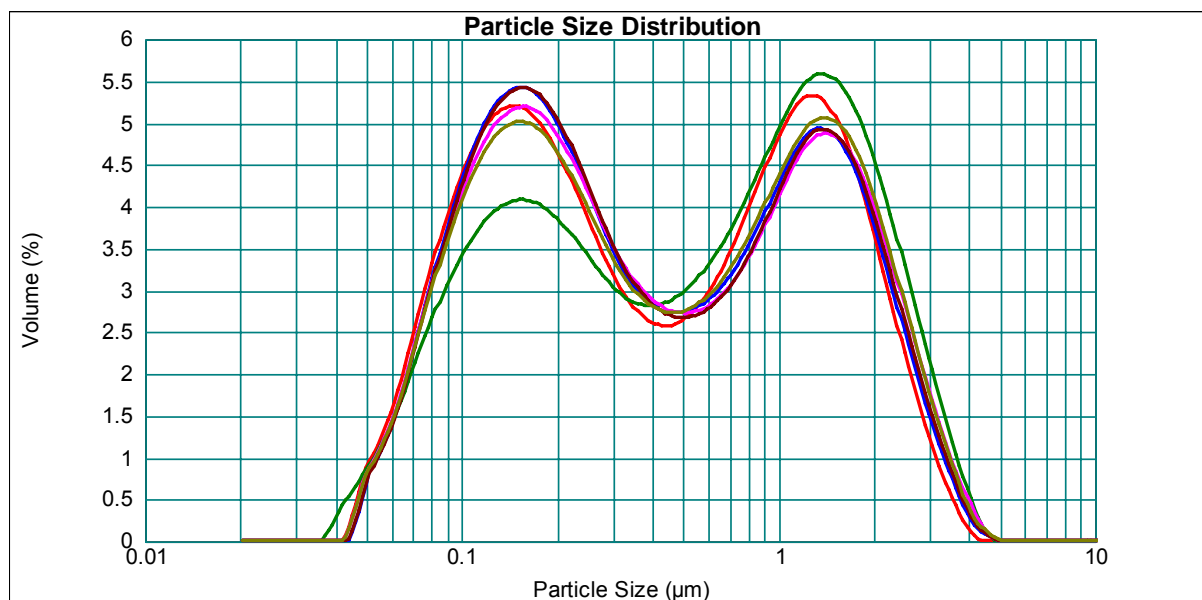


**Figure IV 8 8.** LD size distribution curves following sample processing (before spray-drying) (PMC + 20C 23-24000 PSI) (red) and following redispersion of the spray-dried processed suspension: T0 (green) and following storage (30°C/65% RH) - 1 month (blue), 3 months (pink), 6 months (brown) and 12 months (dark yellow). Data reported in annex 1 (Table A20).

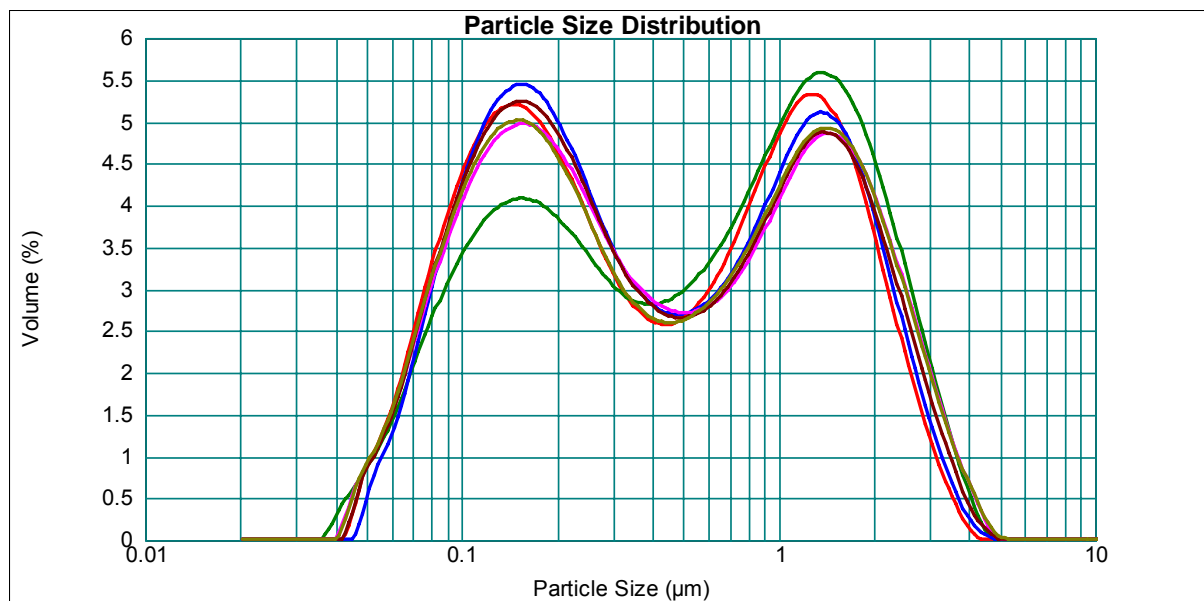


**Figure IV 8 9.** LD size distribution curves following sample processing (before spray-drying) (PMC + 20C 23-24000 PSI) (**red**) and following redispersion of the spray-dried processed suspension: T0 (**green**) and following storage (40°C/75% RH) - 1 month (**blue**), 3 months (**pink**), 6 months (**brown**) and 12 months (**dark yellow**). Data reported in annex 1 (**Table A20**).

From the results observed in **Figures IV 8 7, IV 8 8, IV 8 9** and **Table IV 8 4**, we can clearly see that the redispersion characteristics of NIF nanoparticles (spray-dried nanosuspension) remain very good over a year of storage at all tested temperature and relative humidity conditions. Except for the redispersion characteristics at time 0, all data retrieved show that the original particle size distribution (i.e. before the spray-drying operation) can be restored, with a median volume diameter and a mean volume diameter around 400 nm and 750 nm being obtained, respectively.

#### IV.8.3.4. Crystalline state evaluation

Discussion relative to the crystalline state evaluation of NIF (DSC, PXRD) before and following high pressure homogenization (i.e. un-milled NIF and NIF nanoparticles, respectively) has been made in **part IV.3.3.1 (Figures IV 3 2, IV 3 3 and IV 3 4)** of this work. From the results presented in **part IV.3.3.1**, it has been shown that NIF original crystalline state (i.e. NIF polymorphic form I - most stable polymorphic form) was not modified following

the high pressure homogenization operation and most importantly following particle size reduction to nanometer range. Although no physical state modifications are expected during storage as NIF is already present as polymorphic form I (which would not have been the case for polymorphic form II, III and certainly not for amorphous NIF), DSC and PXRD studies were carried out to assess NIF physical state, primarily in the case of the NIF nanoparticle formulation studied (spray-dried NIF 5%, Mannitol 5%, Methocel E15® 0.5% w/v nanosuspension).

#### IV.8.3.4.1. DSC

NIF thermal behavior was assessed for the three ICH conditions reported in the introductive part of this section. Results from DSC studies for un-milled NIF and NIF nanoparticles (spray-dried NIF 5%, Mannitol 5%, Methocel E15® 0.5% w/v nanosuspension) at 25°C/60% RH are shown in **Figure IV 8 10** and **Figure IV 8 13**, respectively, and in **Table IV 8 2**. Results from DSC studies for un-milled NIF and NIF nanoparticles at 30°C/65% RH are shown in **Figure IV 8 11** and **Figure IV 8 14**, respectively, and in **Table IV 8 2**. Results from DSC studies for un-milled NIF and NIF nanoparticles at 40°C/75% RH are shown in **Figure IV 8 12** and **Figure IV 8 15**, respectively, and in **Table IV 8 2**.

From the results observed on **Figures IV 8 10, IV 8 11, IV 8 12, IV 8 13, IV 8 14, IV 8 15** and **Table IV 8 2**, we can see that NIF, be it in the case of the un-milled drug or drug nanoparticles, is always present as polymorphic form I (endotherm ~ 171-172°C). For un-milled NIF, delta H (enthalpy) was found similar over time and for all tested conditions (~ 110 J/g). No enthalpy data was retrieved in the case of the NIF nanoparticle formulation as the mannitol present in the formulation would not allow for complete quantification of the NIF endotherms; the mannitol endotherm (~ 166-168°C) being too close to the NIF polymorphic form I endotherm (**Figures IV 8 13, IV 8 14** and **IV 8 15**). However, it should be noted that the NIF endotherms had comparable profiles at all tested conditions and that enthalpy values are seemingly close to 110 J/g. We can here conclude that NIF is thus, in the nanoparticle formulation, present as polymorphic form I and that no modifications in the crystalline state take place over time (12 month period).

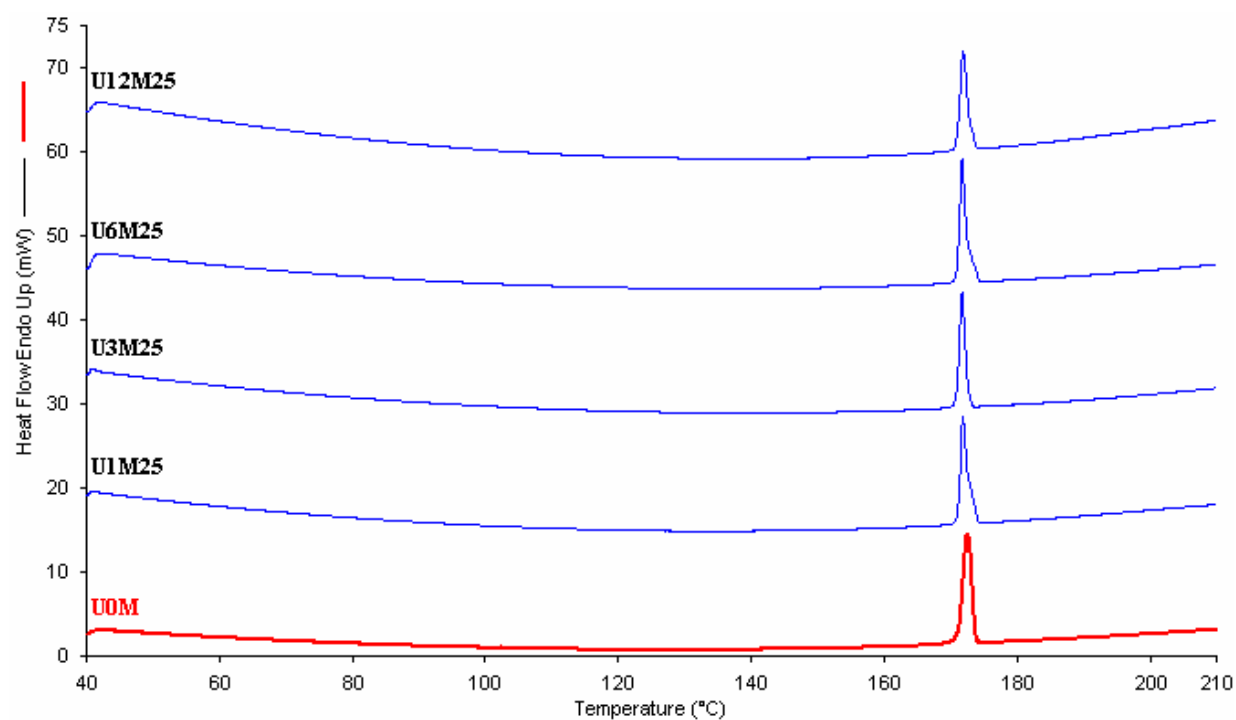


**Figure IV 8 10.** DSC heating curves (40°C → 210°C - 5°C/min) for un-milled NIF. Storage conditions: **25°C - 60% RH** - 0, 1, 3, 6 and 12 months.

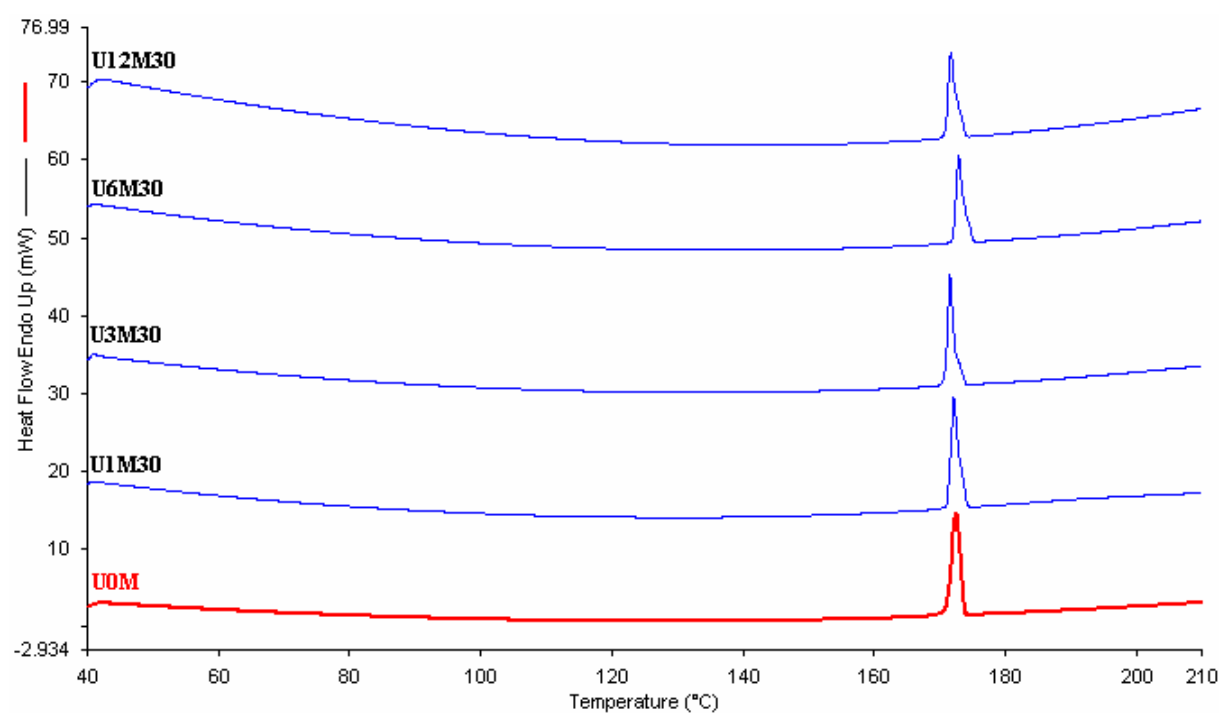


**Figure IV 8 11.** DSC heating curves (40°C → 210°C - 5°C/min) for un-milled NIF. Storage conditions: **30°C - 65% RH** - 0, 1, 3, 6 and 12 months.

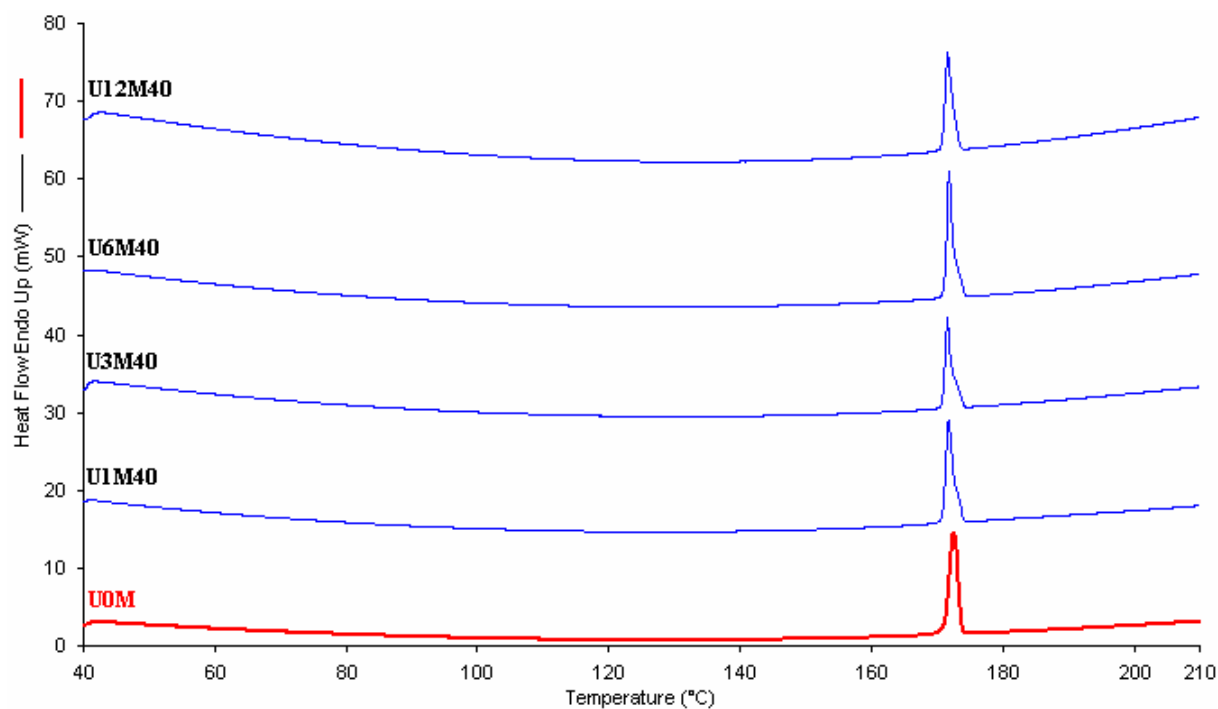


**Figure IV 8 12.** DSC heating curves (40°C → 210°C - 5°C/min) for un-milled NIF. Storage conditions: 40°C - 75% RH - 0, 1, 3, 6 and 12 months.

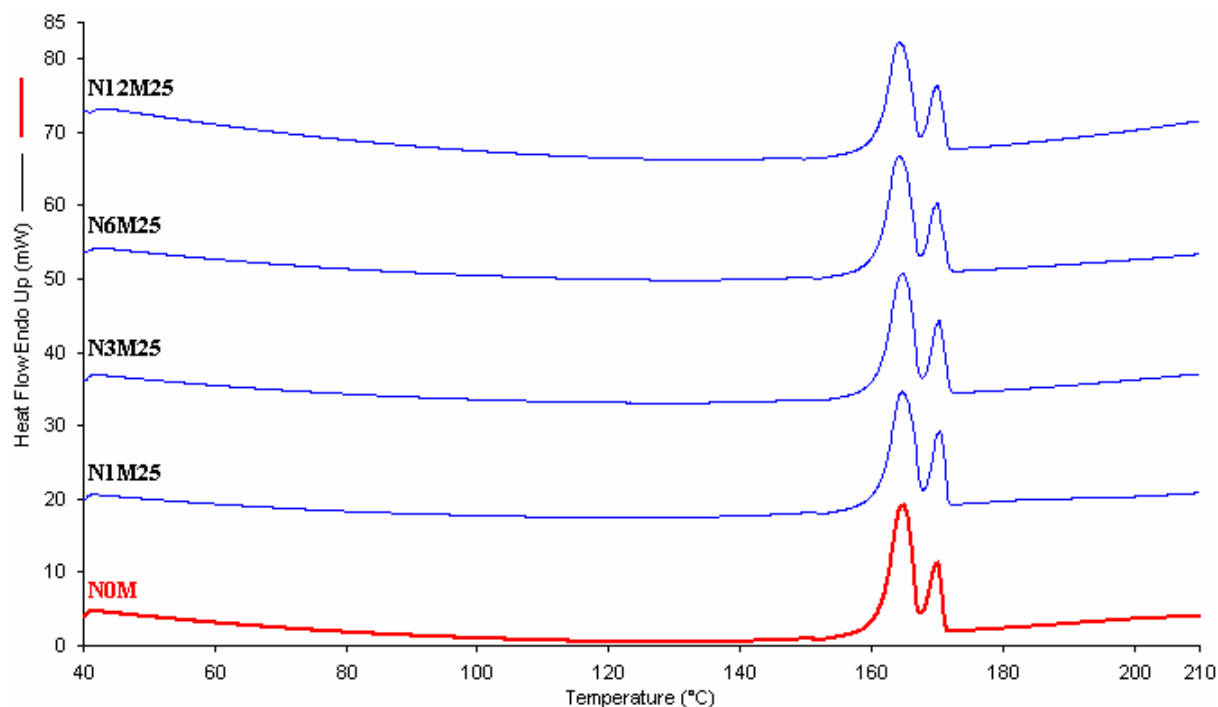


**Figure IV 8 13.** DSC heating curves (40°C → 210°C - 5°C/min) for NIF nanoparticles (spray-dried NIF 5%, Mannitol 5%, Methocel E15® 0.5% w/v nanosuspension). Storage conditions: 25°C - 60% RH - 0, 1, 3, 6 and 12 months.



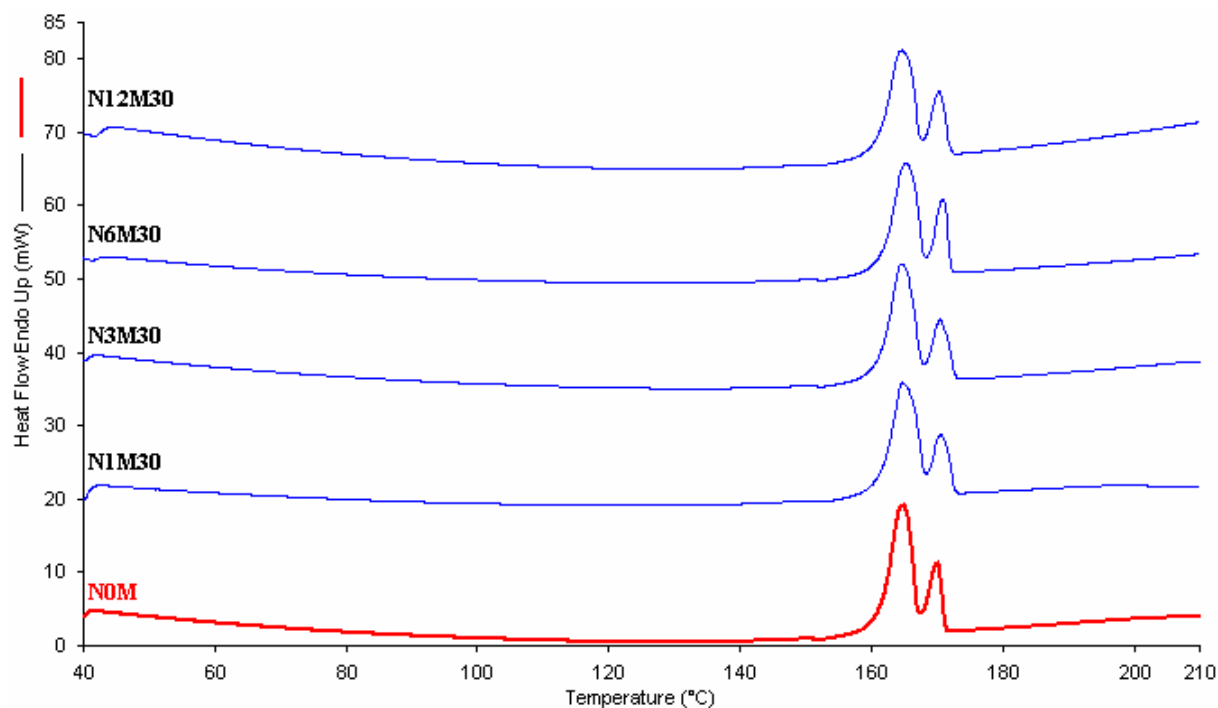


**Figure IV 8 14.** DSC heating curves (40°C → 210°C - 5°C/min) for NIF nanoparticles (spray-dried NIF 5%, Mannitol 5%, Methocel E15® 0.5% w/v nanosuspension). Storage conditions: **30°C - 65% RH** - 0, 1, 3, 6 and 12 months.

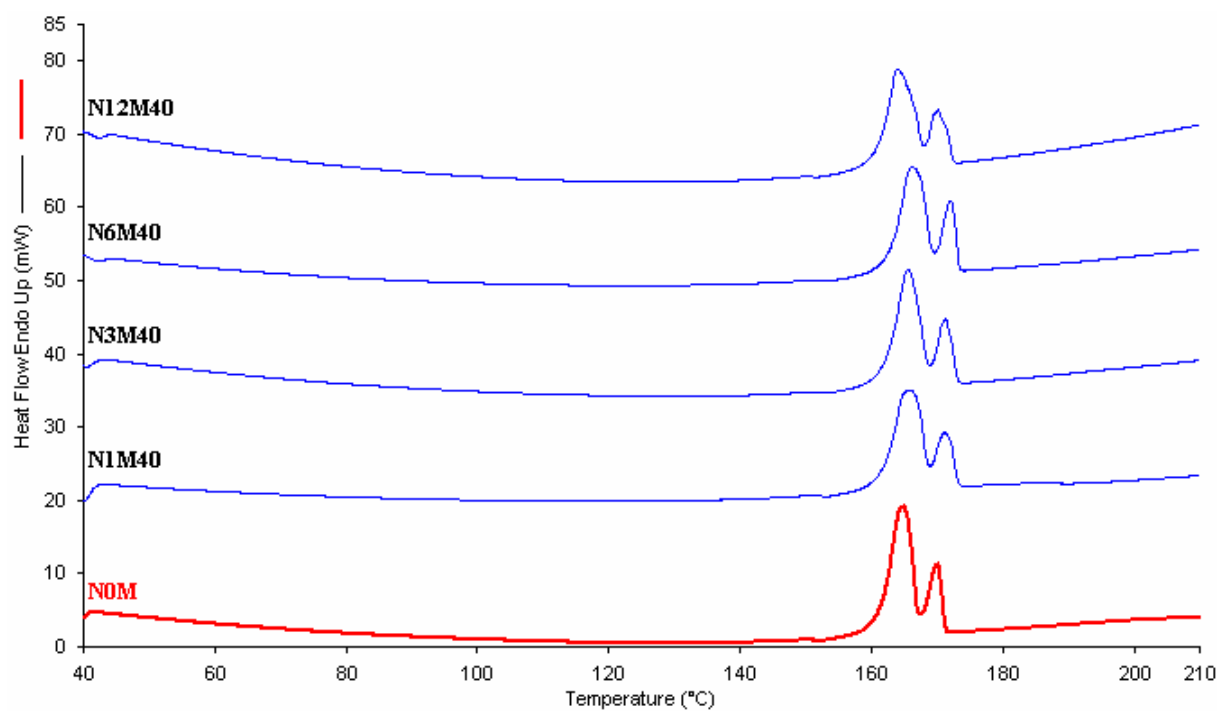


**Figure IV 8 15.** DSC heating curves (40°C → 210°C - 5°C/min) for NIF nanoparticles (spray-dried NIF 5%, Mannitol 5%, Methocel E15® 0.5% w/v nanosuspension). Storage conditions: **40°C - 75% RH** - 0, 1, 3, 6 and 12 months.

**Table IV 8 2.** Data for **Figures III 8 10, III 8 11, III 8 12, III 8 13, III 8 14 and III 8 15.**

	peak (°C)	onset (°C)	end (°C)	Delta H (J/g)
<b>UT0</b>	172.6	171.3	173.8	109.8
<b>U1M 25°C - 60% RH</b>	171.8	171.1	173.0	111.5
<b>U3M 25°C - 60% RH</b>	171.8	170.9	172.6	119.4
<b>U6M 25°C - 60% RH</b>	171.8	171.0	172.7	123.4
<b>U12M 25°C - 60% RH</b>	171.9	170.9	173.0	109.0
<b>U1M 30°C - 65% RH</b>	172.2	171.2	173.4	105.3
<b>U3M 30°C - 65% RH</b>	171.6	170.9	172.5	112.7
<b>U6M 30°C - 65% RH</b>	172.9	172.1	174.0	106.7
<b>U12M 30°C - 65% RH</b>	171.8	170.9	173.0	113.4
<b>U1M 40°C - 75% RH</b>	171.8	170.9	173.0	107.9
<b>U3M 40°C - 75% RH</b>	171.6	170.9	172.4	112.9
<b>U6M 40°C - 75% RH</b>	171.8	171.1	172.7	108.1
<b>U12M 40°C - 75% RH</b>	171.6	170.8	172.9	110.7

	peak (°C)	onset (°C)	end (°C)	Delta H (J/g)
<b>NT0</b>	170.2	168.2	171.3	-
<b>N1M 25°C - 60% RH</b>	170.4	168.6	171.6	-
<b>N3M 25°C - 60% RH</b>	170.3	168.4	171.9	-
<b>N6M 25°C - 60% RH</b>	170.0	168.2	171.8	-
<b>N12M 25°C - 60% RH</b>	170.0	168.2	171.6	-
<b>N1M 30°C - 65% RH</b>	170.7	168.8	172.6	-
<b>N3M 30°C - 65% RH</b>	170.6	168.6	172.7	-
<b>N6M 30°C - 65% RH</b>	170.9	169.0	172.1	-
<b>N12M 30°C - 65% RH</b>	170.3	168.4	171.9	-
<b>N1M 40°C - 75% RH</b>	171.2	169.3	173.1	-
<b>N3M 40°C - 75% RH</b>	171.3	169.5	173.0	-
<b>N6M 40°C - 75% RH</b>	172.1	170.1	173.3	-
<b>N12M 40°C - 75% RH</b>	170.1	168.5	172.3	-

## IV.8.3.4.2. PXRD

NIF diffraction patterns were assessed for the three ICH conditions reported in the introductive part of this section. Results from PXRD studies for un-milled NIF and NIF nanoparticles (spray-dried NIF 5%, Mannitol 5%, Methocel E15® 0.5% w/v nanosuspension) at 25°C/60% RH are shown in **Figure IV 8 16** and **Figure IV 8 19**, respectively. Results from PXRD studies for un-milled NIF and NIF nanoparticles at 30°C/65% RH are shown in **Figure IV 8 17** and **Figure IV 8 20**, respectively. Results from PXRD studies for un-milled NIF and NIF nanoparticles at 40°C/75% RH are shown in **Figure IV 8 18** and **Figure IV 8 21**, respectively.

From the results observed on these figures, it can be seen that NIF crystalline state seems unaltered following 12 months of storage at all tested temperature/relative humidity conditions (i.e. 25°C/60% RH; 30°C/65% RH; 40°C/75% RH); this most importantly considering the optimized NIF nanoparticulate formulation. The NIF diffraction patterns are in fact, from all the data presented, readily identical over time (considering one type of storage condition) and between the different storage conditions.

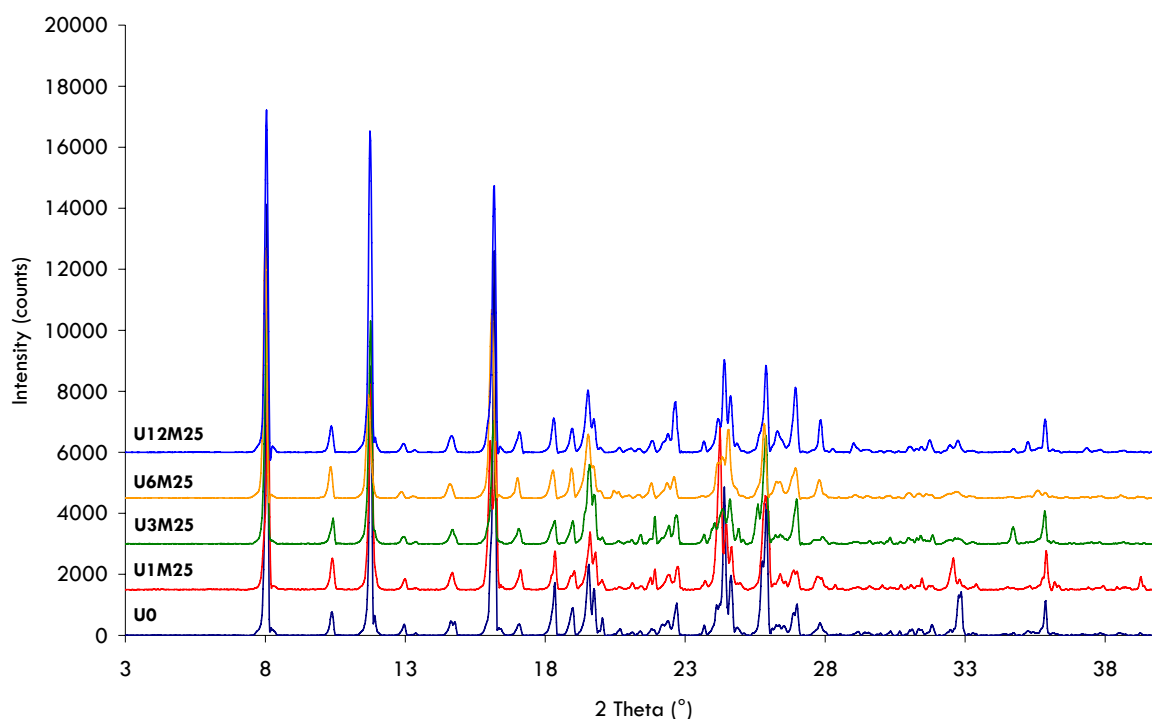


**Figure IV 8 16.** PXRD diffractograms for un-milled NIF. Storage conditions: 25°C - 60% RH - 0, 1, 3, 6 and 12 months.

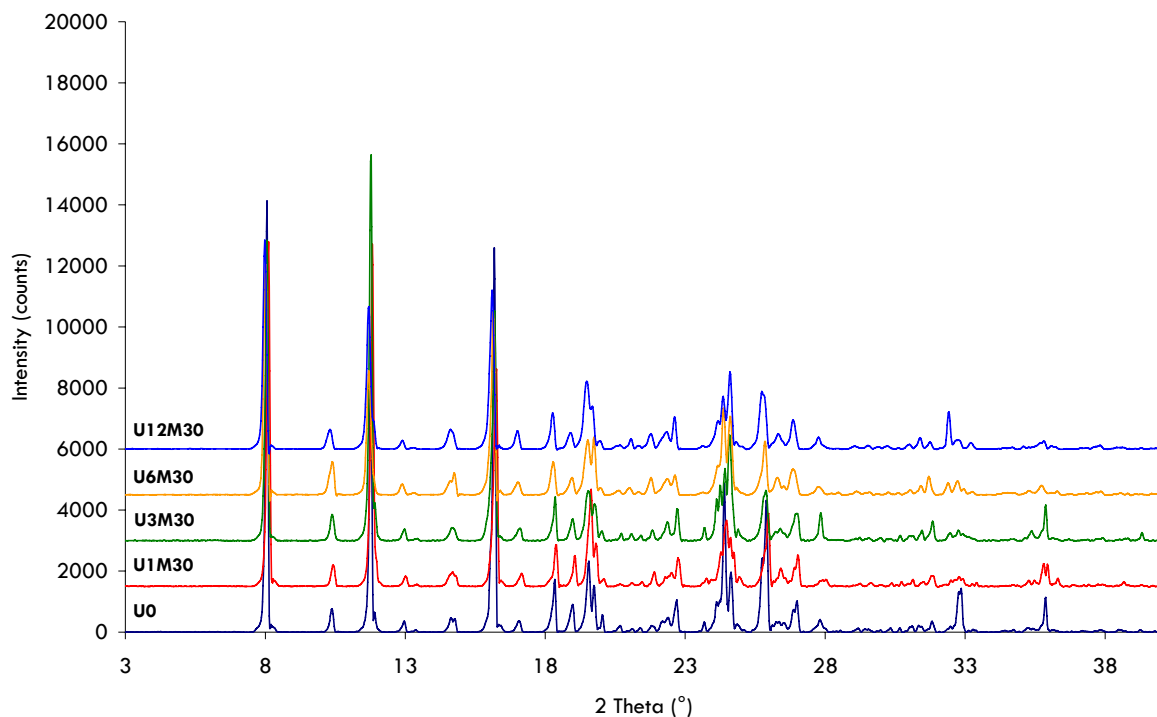


**Figure IV 8 17.** PXRD diffractograms for un-milled NIF. Storage conditions: 30°C - 65% RH - 0, 1, 3, 6 and 12 months.

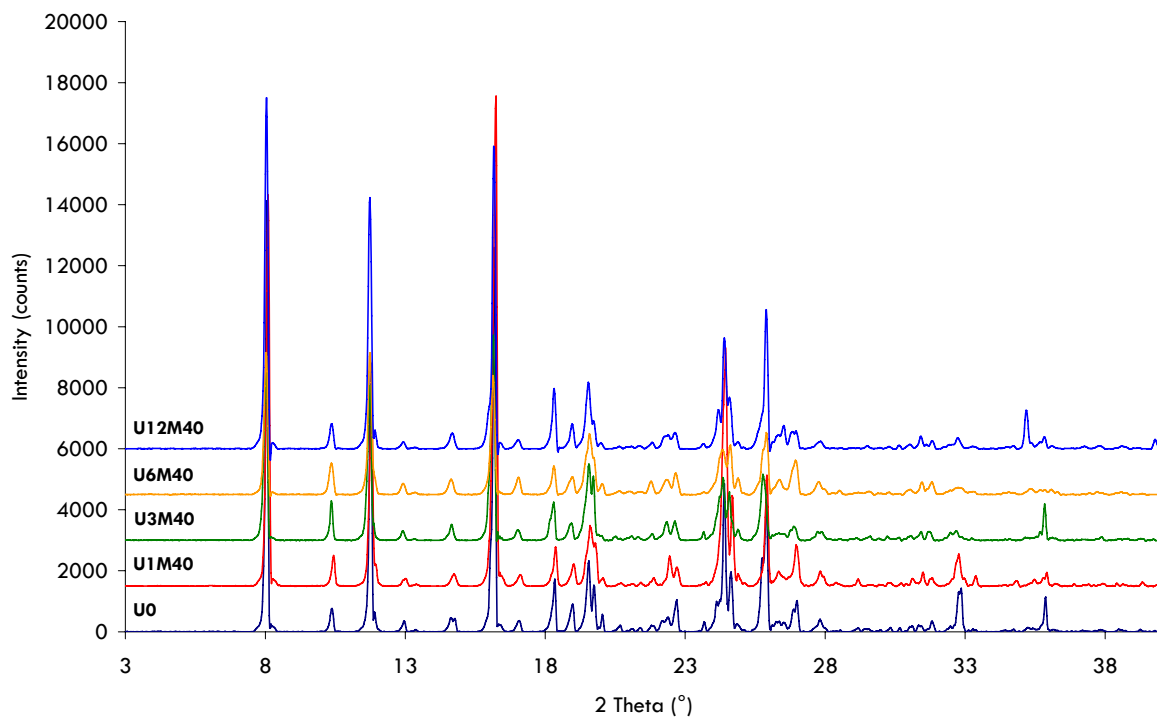


**Figure IV 8 18.** PXRD diffractograms for un-milled NIF. Storage conditions: 40°C - 75% RH - 0, 1, 3, 6 and 12 months.

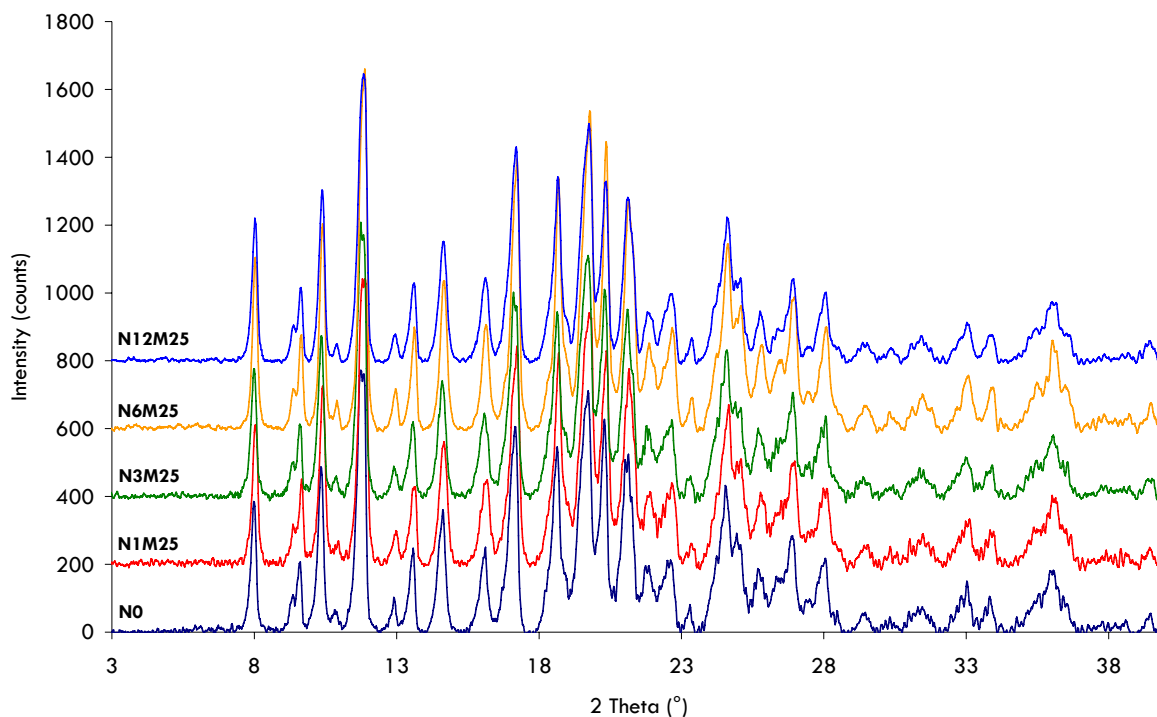


**Figure IV 8 19.** PXRD diffractograms for NIF nanoparticles (spray-dried NIF 5% Mannitol 5% Methocel E15® 0.5% nanosuspension). Storage conditions: 25°C - 60% RH - 0, 1, 3, 6 and 12 months.

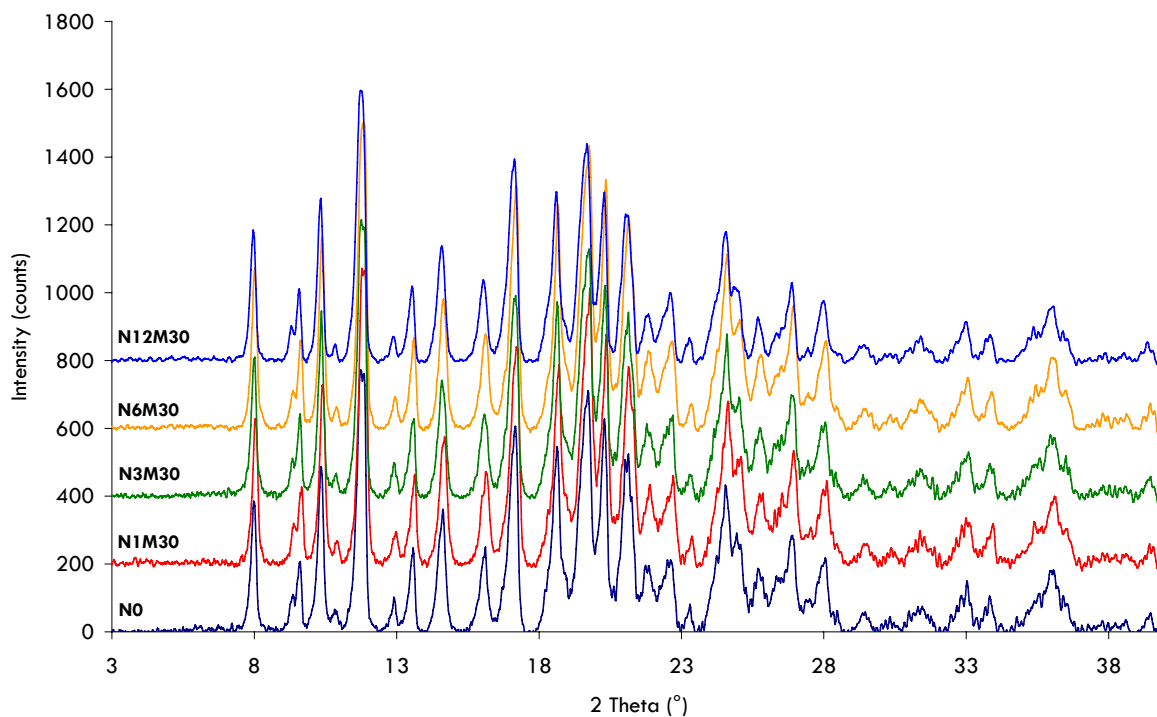


**Figure IV 8 20.** PXRD diffractograms for NIF nanoparticles (spray-dried NIF 5% Mannitol 5% Methocel E15® 0.5% nanosuspension). Storage conditions: 30°C - 65% RH - 0, 1, 3, 6 and 12 months.

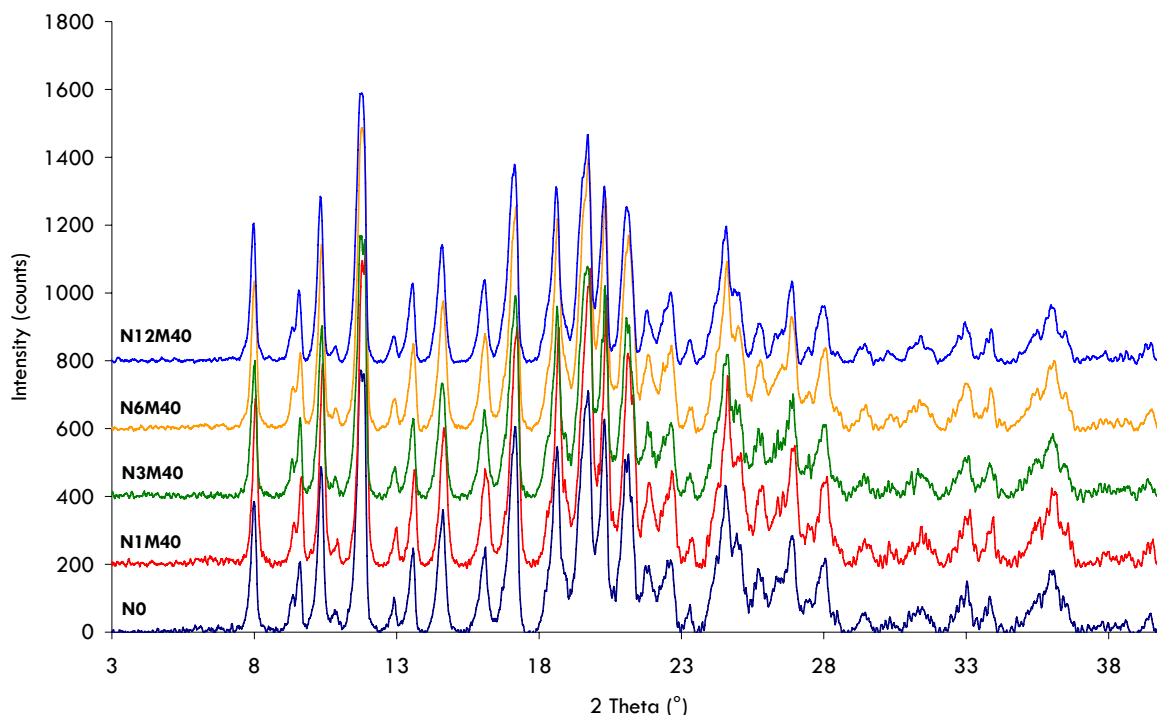


**Figure IV 8 21.** PXRD diffractograms for NIF nanoparticles (spray-dried NIF 5% Mannitol 5% Methocel E15® 0.5% nanosuspension). Storage conditions: **40°C - 75% RH** - 0, 1, 3, 6 and 12 months.

The decrease in peak intensity when comparing un-milled NIF and NIF nanoparticulate formulation, as it has already been discussed and explained in **part IV.3.3.1.3** of this work (**Figure IV 3 9 - Table IV 3 1**), is attributed to NIF dilution in the various formulation additives (in this case hydroxypropylmethylcellulose and mannitol). It should be noted that, considering the optimized NIF nanoparticulate formulation (i.e. spray-dried NIF 5%, Mannitol 5%, Methocel E15® 0.5% w/v nanosuspension), some of the peaks observed in the diffractograms should be attributed to mannitol which is also present in crystalline form in the spray-dried formulation (cf. **Figure IV 2 29**).

Similarly to the investigations carried out in **part IV.3.3.1.3** of this work, evaluation of the amorphous percentage present in the formulations studied was also made with comparison of the data obtained at time 0 and following 12 months of storage at 25°C/60% RH, 30°C/65% RH and 40°C/75% RH. The evaluated amorphous percentage in the formulations was of 28.7%, 30.8%, 31.4% and 31.3%, respectively. These values are higher than the value found for mannitol-free NIF nanoparticle formulations (i.e. 13.5% - **part IV.3.3.1.3**) and are simply explained by the dilution of the NIF nanoparticles in the mannitol matrix and not by modification in NIF amorphous/crystalline proportions. We can, however, see from these results that the optimized NIF nanoparticle formulation is stable, crystalline state-wise, over a 12-month period.

#### IV.8.4. Conclusion

From the results presented in this chapter, we can conclude that the optimized developed NIF nanoparticle formulation (i.e. spray-dried NIF 5%, Mannitol 5%, Methocel E15® 0.5% w/v nanosuspension) is stable over a 12-month period at ICH storage conditions of 25°C/60% RH, 30°C/65% RH and 40°C/75% RH. The NIF nanoparticle formulation was shown to keep its initial redispersion characteristics and dissolution properties. In fact, it has been shown that, for all tested storage conditions, the original particle size distribution (i.e. before the spray-drying operation) could be restored with a median volume diameter and a mean volume diameter around 400 nm and 750 nm being retrieved, respectively. Considering dissolution characteristics, no modifications in the observed profiles could be noticed over 12 months at the three tested storage conditions, with complete drug dissolution being achievable with NIF nanoparticles in less than 10 min (vs. less than 2% for un-milled NIF). The NIF crystalline state was also shown to be unaltered following 12 months at the three tested conditions. NIF was, in fact, shown, through DSC analysis, to be maintained as polymorphic form I (the most stable NIF polymorphic form) and the NIF formulation was not shown, through PXRD analysis, to have its amorphous/crystalline percentage changed.





## **GENERAL CONCLUSION**



## V. General conclusion

Together with membrane permeability, the solubility/dissolution behavior of a drug is a key determinant to its oral bioavailability; the latter frequently being the rate-limiting step to absorption of drugs from the gastrointestinal tract (BCS class II compounds). Since an increasing number of newly-developed drug candidates present poor water-solubility (as of today, it is estimated that more than 40% of NCE are poorly-water soluble), approaches to overcome this factor are of great importance in drug formulation. Out of the numerous formulation approaches to overcome these poor solubility/dissolution issues, drug particle size reduction to nanometer range has received, over the last decade, much increased interest. The hypothesis behind dissolution rate enhancement, considering drug particle size reduction to nanometer range, lies primarily in the much-increased effective surface area (Noyes-Whitney) presented by the resulting drug nanoparticles.

High pressure homogenization has been demonstrated in this work to be a simple, rapid, efficient and reproducible technique for drug nanosizing. It is a solvent-free process for which the scaling up is already established. Drug particle size can easily be modified and controlled with proper selection of the homogenizing pressure and the number of homogenizing cycles applied. It has to be noted that the use of surfactants as stabilizers for the newly formed nanoparticles is a requisite of this formulation approach and that their nature and concentration will also influence the resulting obtained particle sizes. The influence of processing temperature, which can easily be controlled through the use of a heat exchanger, was also shown relevant with regard to particle size reduction efficiency, particularly in the case of drugs presenting temperature-dependent physical modifications (e.g. UCB-A polymorphism - crystal hardness). Moreover, the control of sample processing temperature is also critical for thermolabile compounds. High pressure homogenization was, in that regard, shown not to interfere with the processed drug chemical stability. High pressure homogenization was also shown not to interfere with the processed drug original crystalline state as no variations in the degree of crystallinity (amorphous/crystalline percentage) could be noticed through X-ray analysis.

The processed drug “nanocrystals” (i.e. by definition nanoparticles composed of 100 percent of drug without any matrix materials) are thus, following high pressure homogenization, obtained in suspension state (i.e. nanosuspension). These suspensions need, before any further processing, to be dried using water-removal techniques such as spray-drying or eventually freeze-drying. In that regard, particle agglomeration during and following these operations has been shown to be of a concern, particularly if no carriers (water-soluble and/or water-insoluble) are used in the processed formulations. These carriers have been shown to significantly reduce

particle agglomeration by limiting particle-particle interactions simply by recrystallizing around drug nanoparticles (e.g. water-soluble carriers such as mannitol) or by acting as an inert support (e.g. water-insoluble carriers such as Emcompress®). Although there is a clear beneficial influence of these carriers with regard to nanoparticle agglomeration prevention, it has to be said that these formulation additives have to be used at non-negligible concentrations (up to 100% w/w relative to drug content) which can, in some cases such as highly dosed drugs where minimization of additives is in general necessary, be quite problematic.

The *in vitro* dissolution assays carried out to confirm the theoretical enhancement predictions clearly showed the beneficial influence of particle size reduction to nanometer range for the four tested model poorly water-soluble drugs. The redispersion characteristics of the water-removed drug nanosuspensions were shown to be highly relevant, dissolution-wise, as further enhancement could be achieved when particle agglomeration was limited, be it before dissolution as it is the case for the evaluations carried out using the USP type II apparatus or during dissolution when the evaluations were carried out using the USP type IV apparatus. The solubility studies carried out also showed enhanced characteristics for drug nanoparticles when compared to the un-milled drugs.

In order to confirm and further investigate the clear solubility/dissolution enhancement offered by the nanoparticulate systems developed and prior to investigating its possible translation into enhanced *in vivo* exposure following oral administration, permeability studies across intestinal cell models were carried out. Apical to basolateral transfer studies were carried out across Caco-2 and HT29-5M21 cultures and co-cultures. Caco-2/HT29-5M21 co-cultures (seeding ratio 3:1) were evaluated to better represent *in vivo* intestinal conditions. It has been shown that the nifedipine permeation rate across the three culture models can be significantly enhanced for nifedipine nanoparticles when compared to the un-milled drug; the difference being directly related to the observed dissolution behaviour of both systems. Investigation into the presence of chitosan in the nifedipine nanoparticle formulation in order to evaluate its potential permeability-enhancing properties showed no influence. It has to be noted that no significant differences could be found between the three tested cell models. Since the established Caco-2/HT29-5M21 co-culture is well characterized and seemingly better representative of *in vivo* intestinal conditions, it could therefore be of great interest when considering *in vitro* permeation studies in drug development. Furthermore, the formulation of drugs as nanoparticles in order to increase their solubility and dissolution rate could be an interesting alternative to the use of solvents or other solubilizing additives for the evaluation of poorly water-soluble compounds in these kinds of transport/permeability studies.

Considering these very promising *in vitro* results (solubility/dissolution/permeability), *in vivo* pharmacokinetic studies following oral administration of the nanoparticulate systems developed and using rats as a model were carried out. These *in vivo* pharmacokinetic studies showed that, as a general remark, both the extent of exposure and the  $C_{max}$  can be clearly enhanced when reducing drug particle size to nanometer range. Investigations in the *in vivo* behavior of two different models, i.e. a poorly water-soluble drug presenting a pH-independent solubility profile (nifedipine) and another presenting a pH-dependent solubility profile (ucb-35440-3 (weak base)), allowed us to underline the complexity of the latter with regard to the fed and fasted state and to raise the question of possible drug reprecipitation *in vivo*. Two types of dosage forms (i.e. suspension/minicapsule) were also evaluated to investigate their influence on the pharmacokinetic profiles obtained (evaluation using nifedipine as a model drug). The latter dosage form was evaluated as it was thought to be more discriminating between the two assayed formulations (i.e. nifedipine nanoparticles/un-milled nifedipine) as in this case, both wetting and drug dissolution took place following administration.

To confirm and to emphasize the promising results obtained both *in vitro* and *in vivo* for nifedipine nanoparticles, evaluation of the antihypertensive effect on spontaneously hypertensive rats, with comparison to the response obtained with un-milled nifedipine as a control, were carried out. A significant drop in systolic blood pressure, corresponding to the  $C_{max}$  of the pharmacokinetic profile obtained following a similar administrating protocol, was achieved for nifedipine nanoparticles.

Finally, the optimized nifedipine nanoparticle formulation was shown to be stable, chemically and physically, following 12 month storage at recommended ICH stability testing conditions (25°C/60% RH, 30°C/65% RH and 40°C/75% RH). The formulation was shown to keep its original redispersion and dissolution characteristics at all tested conditions. Nifedipine original crystalline state was also shown to be unaltered at all tested conditions.

We can thus conclude that the development of crystalline nanoparticles is an efficient approach for enhancing solubility, dissolution rate and oral bioavailability of poorly water-soluble drug compounds. The high pressure homogenization operation has been shown to be a very simple, rapid and efficient technique for drug nanosizing which shall be applicable to most newly developed poorly water-soluble drug entities. This work was done with the hope of contributing to this very promising drug particle size reduction technique and most importantly, to the very promising formulation approach that is crystalline nanoparticles.



## REFERENCES





## VI. References

- Agatonovic-Kustrin, S., Glass, B.D., Wisch, M.H., **2004**. Strategy for the development of a thermodynamically stable oral microemulsion. *Curr. Drug Discov. Technol.*, 1 (2), 165-171.
- Ambike, A.A., Mahadik, K.R., Paradkar, A., **2005**. Spray-dried amorphous solid dispersions of simvastatin, a low tg drug: in vitro and in vivo evaluations. *Pharm. Res.*, 22 (6), 990-998.
- Amidon, G.L., Bermejo, M., **2003**. Modern Biopharmaceutics: version 6.03, TSRL Inc., Ann Arbor, MI, USA.
- Amidon, G.L., Lennernäs, H., Shah, V.P., Crison, J.R., **1995**. A theoretical basis for a biopharmaceutic drug classification: the correlation of in vitro drug product dissolution and in vivo bioavailability. *Pharm. Res.*, 12 (3), 413-420.
- Arangoa, M.A., Ponchel, G., Orecchioni, A.M., Renedo, M.J., Duchêne, D., Irache, J.M., Peters, K., **2000**. Bioadhesive potential of gliadin nanoparticulate systems. *Eur. J. Pharm. Sci.*, 11 (4), 333-341.
- Araya, H., Nagao, S., Tomita, M., Hayashi, M., **2005**. The novel formulation design of self-emulsifying drug delivery systems (SEDDS) type O/W microemulsion I: enhancing effects on oral bioavailability of poorly water soluble compounds in rats and beagle dogs. *Drug Metab. Pharmacokinet.*, 20 (4), 244-256.
- Avestin. Glen Creston Ltd. EmulsiFlex-C5 High Pressure Homogeniser Data Sheet. Avestin, Ottawa, Canada.
- Baboota, S., Dhaliwal, M., Kohli, K., **2005**. Physicochemical characterization, in vitro dissolution behavior, and pharmacodynamic studies of rofecoxib-cyclodextrin inclusion compounds. preparation and properties of rofecoxib hydroxypropyl beta-cyclodextrin inclusion complex: a technical note. *AAPS Pharm. Sci. Tech.*, 6 (1), E83-90.
- Balimane, P.V., Chong S., **2005**. Cell-culture-based models for intestinal permeability: a critique. *Drug Discov. Today*, 10 (5), 335-343.
- Bhattachar, S.N., Wesley, J.A., Fioritto, A., Martin, P.J., Babu, S.R., **2002**. Dissolution testing of a poorly soluble compound using the flow-through cell dissolution apparatus. *Int. J. Pharm.*, 236 (1-2), 135-143.
- Bayomi, M.A., Abanumay, K.A., Al-Angary, A.A., **2002**. Effect of inclusion complexation with cyclodextrins on photostability of nifedipine in solid state. *Int. J. Pharm.*, 243 (1-2), 107-117.
- Beckman Coulter LS 13320 Data Sheet. Beckman Coulter, Inc. (Fullerton, CA, USA).
- Bermejo, M., **2005**. Dissolution methodologies and IVIVC. Strategies in Oral Drug Delivery. Oral drug delivery foundation meeting 2005. Garmisch-Partenkirchen, Germany.
- Beyers, H., Malan, S.F., van der Watt, J.G., de Villiers, M.M., **2000**. Structure-solubility relationship and thermal decomposition of furosemide. *Drug Dev. Ind. Pharm.*, 26 (10), 1077-1083.
- Boulenc, X., Bourrie, M., Fabre, I., Roque, C., Joyeux, H., Berger, Y., Fabre, G., **1992**. Regulation of cytochrome P450IA1 gene expression in a human intestinal cell line, Caco-2. *J. Pharmacol. Exp. Ther.*, 263 (3), 1471-1478.
- Challa, R., Ahuja, A., Ali, J., Khar, R.K., **2005**. Cyclodextrins in drug delivery: an updated review. *AAPS Pharm. Sci. Tech.*, 6 (2), E329-357.
- Chawla, G., Gupta, P., Thilagavathi, R., Chakraborti, A.K., Bansal, A.K., **2003**. Characterization of solid-state forms of celecoxib. *Eur. J. Pharm. Sci.*, 20 (3), 305-317.
- Chen, Y., Liu, R., **2000**. Prediction of solubility. In: Water-insoluble drug formulation. Ed. R. Liu; Interpharm Press, Denver, CO, USA; 25-64.

- Chen, X., Timothy J. Young, T.J., Sarkari, M., Williams III, R.O., Johnston, K.P., **2002**. Preparation of cyclosporine A nanoparticles by evaporative precipitation into aqueous solution. *Int. J. Pharm.*, 242 (1-2), 3-14.
- Choi, J.S., Jo, B.W., **2004**. Enhanced paclitaxel bioavailability after oral administration of pegylated paclitaxel prodrug for oral delivery in rats. *Int. J. Pharm.*, 280 (1-2), 221-227.
- Choi, J.S., Shin, S.C., **2005**. Enhanced paclitaxel bioavailability after oral coadministration of paclitaxel prodrug with naringin to rats. *Int. J. Pharm.*, 292 (1-2), 149-156.
- Chu, S., Tanaka, S., Kaunitz, J.D., Montrose, M.H., **1999**. Dynamic regulation of gastric surface pH by luminal pH. *J. Clin. Invest.*, 103 (5), 605-612.
- Chun, Y.J., Park, S., Yang, S.A., **2003**. Activation of Fas receptor modulates cytochrome P450 3A4 expression in human colon carcinoma cells. *Toxicol. Lett.*, 146 (1), 75-81.
- Cilurzo, F., Minghetti, P., Casiraghi, A., Montanari, L., **2002**. Characterization of nifedipine solid dispersions. *Int. J. Pharm.*, 242 (1-2), 313-317.
- Cirri, M., Rangoni, C., Maestrelli, F., Corti, G., Mura, P., **2005**. Development of fast-dissolving tablets of flurbiprofen-cyclodextrin complexes. *Drug Dev. Ind. Pharm.*, 31 (7), 697-707.
- Clas, S.D., Dalton, C.R., Hancock, B., **2002**. In: *Calorimetry in Pharmaceutical research and development. Encyclopaedia of Pharmaceutical Technology*, 2<sup>nd</sup> Edition. Swarbrick, J., Boylan, J., Vol 1, Marcel Dekker, New York, USA, 289-301.
- Cole, E.T., Scott, R.A., Connor, A.L., Wilding, I.R., Petereit, H.U., Schminke, C., Beckert, T., Cade, D., **2002**. Enteric coated HPMC capsules designed to achieve intestinal targeting. *Int. J. Pharm.*, 231 (1), 83-95.
- Constantinides, P.P., **1995**. Lipid microemulsions for improving drug dissolution and oral absorption: physical and biopharmaceutical aspects. *Pharm Res.*, 12 (11), 1561-1572.
- Constantinides, P.P., Tustian, A., Kessler, D.R., **2004**. Tocol emulsions for drug solubilization and parenteral delivery. *Adv. Drug Del. Rev.*, 56 (9), 1243-1255.
- Cullis, P.R., Chonn, A., **1998**. Recent advances in liposome technologies and their applications for systemic gene delivery. *Adv. Drug. Deliv. Rev.*, 30 (1-3), 73-83.
- Dastmalchi, S., Garjani, A., Maleki, N., Sheikhee, G., Baghchevan, V., Jafari-Azad, P., Valizadeh, H., Barzegar-Jalali, M., **2005**. Enhancing dissolution, serum concentrations and hypoglycemic effect of glibenclamide using solvent deposition technique. *J. Pharm. Pharm. Sci.*, 8 (2), 175-181.
- Date, A.A., Patravale, V.B., **2004**. Current strategies for engineering drug nanoparticles. *Cur. Op. Coll. Int. Sci.*, 9, 222-235.
- Delaney, J.S., **2005**. Predicting aqueous solubility from structure. *Drug Discov. Today*, 10 (4), 289-295.
- de Vries, H., Beijersbergen van Henegouwen, G.M.J., **1998**. Photoreactivity of nifedipine in vitro and in vivo. *J. Photochem. Photobiol. B : Biology*, 43 (3), 217-221.
- Dressman, J.B., **2005**. Applications of biorelevant dissolution testing. *Strategies in Oral Drug Delivery. Oral drug delivery foundation meeting 2005. Garmisch-Partenkirchen, Germany.*
- Eerikäinen, H., Kauppinen, E.I., **2003**. Preparation of polymeric nanoparticles containing corticosteroid by a novel aerosol flow reactor method. *Int. J. Pharm.*, 263 (1-2), 69-83.
- Eerikäinen, H., Kauppinen, E.I., Kansikas, J., **2004**. Polymeric drug nanoparticles prepared by an aerosol flow reactor method. *Pharm. Res.*, 21 (1), 136-143.

- Engman, H.A., Lennernas, H., Taipalensuu, J., Otter, C., Leidvik, B., Artursson, P., **2001**. CYP3A4, CYP3A5, and MDR1 in human small and large intestinal cell lines suitable for drug transport studies. *J. Pharm. Sci.*, 90 (11), 1736-1751.
- Farinha, A., Bica, A., Tavares, P., **2000**. Improved bioavailability of a micronized megestrol acetate tablet formulation in humans. *Drug Dev. Ind. Pharm.*, 26 (5), 567-570.
- Fincher, J.H., **1968**. Particle size of drugs and its relationship to absorption and activity. *J. Pharm. Sci.*, 57 (11), 1825-1835.
- Foglieni, C., Meoni, C., Davalli, A.M., **2001**. Fluorescent dyes for cell viability: an application on prefixed conditions. *Histochem. Cell Biol.*, 115 (3), 223-229.
- Ford, J.L., Timmins, P., **1989**. In: Thermal analysis in the characterization of pharmaceutical solids. *Pharmaceutical thermal analysis: Techniques and applications*; Ellis Horwood Limited, Halsted Press, New York, 136-149.
- Galia, E., Nicolaides, E., Hörter, D., Löbenberg, R., Reppas, C., Dressman, J.B., **1998**. Evaluation of various dissolution media for predicting in vivo performance of class I and II drugs. *Pharm. Res.*, 15 (5), 698-705.
- Galli, C., **2006**. Experimental determination of the diffusion boundary layer width of micron and submicron particles. *Int. J. Pharm.*, 313 (1-2), 114-122.
- Ghosh, P.K., Murthy, R.S., **2006**. Microemulsions: a potential drug delivery system. *Curr. Drug Deliv.*, 3 (2), 167-80.
- Granero, G.E., Amidon, G.L., **2006**. Stability of valacyclovir: Implications for its oral bioavailability. *Int. J. Pharm.*, 317 (1), 14-18.
- Grau, M.J., Kayser, O., Müller, R.H., **2000**. Nanosuspensions of poorly soluble drugs--reproducibility of small scale production. *Int. J. Pharm.*, 196 (2), 155-159.
- Gupta, P.K., Cannon, J.B., **2000**. In: Emulsions and microemulsions for drug solubilization and delivery. *Water-insoluble drug formulation*. Ed. R. Liu; Interpharm Press, Denver, CO, USA; 609-633.
- Gursoy, R.N., Benita, S., **2004**. Self-emulsifying drug delivery systems (SEDDS) for improved oral delivery of lipophilic drugs. *Biomed. Pharmacother.*, 58 (3), 173-182.
- Gwak, H.S., Choi, J.S., Choi, H.K., **2005**. Enhanced bioavailability of piroxicam via salt formation with ethanolamines. *Int. J. Pharm.*, 297 (1-2), 156-161.
- Halleux, C., Schneider, Y.J., **1991**. Iron absorption by intestinal epithelial cells: 1. Caco-2 cells cultivated in serum-free medium, on polyethyleneterephthalate microporous membranes, as an in vitro model. *In Vitro Cell. Dev. Biol.*, 27A, 293-302.
- Hamdani, J., **2005**. Développement de formes orales divisées à libération prolongée par la technique de la pelletisation thermoplastique; Thèse de doctorat en Sciences Pharmaceutiques, Institut de Pharmacie, Laboratoire de Pharmacie Galénique et Biopharmacie, Université Libre de Bruxelles.
- Han, S.K., Kim, G.Y., Park, Y.H., **1999**. Solubilization of biphenyl dimethyl dicarboxylate by cosolvency. *Drug. Dev. Ind. Pharm.*, 25 (11), 1193-1197.
- Handbook of Pharmaceutical Excipients, 4<sup>th</sup> Edition, **2003**. Ed. Rowe, R.C., Sheskey, P.J., Weller, P.J., Pharmaceutical Press, London, UK.
- Hecq, J., Deleers, M., Fanara, D., Vranckx, H., Amighi, K., **2005**. Preparation and characterization of nanocrystals for solubility and dissolution rate enhancement of nifedipine. *Int. J. Pharm.*, 299 (1-2), 167-177.
- Hecq, J., Deleers, M., Fanara, D., Vranckx, H., Boulanger P., Le Lamer, S., Amighi, K., **2006**. Preparation and in vitro/in vivo evaluation of nano-sized crystals for dissolution rate enhancement of ucb-35440-3, a highly-dosed poorly water-soluble weak base. *Eur. J. Pharm. Biopharm.* 64 (3), 360-368.

- Henwood, S.Q., Liebenberg, W., Tiedt, L.R., Lotter, A.P., de Villiers, M.M., **2001**. Characterization of the solubility and dissolution properties of several new rifampicin polymorphs, solvates, and hydrates. *Drug Dev. Ind. Pharm.*, 27 (10), 1017-1030.
- Hilgendorf, C., Spahn-Langguth, H., Regardh, C.G., Lipka, E., Amidon, G.L., Langguth, P., **2000**. Caco-2 versus Caco-2/HT29-MTX co-cultured cell lines: permeabilities via diffusion, inside- and outside-directed carrier-mediated transport. *J. Pharm. Sci.*, 89 (1), 63-75.
- Hintz, R.J., Johnson, K.C., **1989**. The effect of particle size distribution on dissolution rate and oral absorption. *Int. J. Pharm.*, 51 (1), 9-17.
- Hirayama, F., Wang, Z., Uekema, K., **1994**. Effect of 2-hydroxypropyl-beta-cyclodextrin on crystallisation and polymorphic transition of nifedipine in solid state. *Pharm. Res.*, 11 (12), 1766-1770.
- Hoener, B-A., Benet, L.Z., **2002**. In: Factors influencing drug absorption and drug availability. *Drugs and the Pharmaceutical Sciences: Modern Pharmaceutics; Volume 121*; Ed. G.S. Banker, C.T. Rhodes; Marcel Dekker, New York, 93-117.
- Holvoet, C., Vander Heyden, Y., Plaizier-Vercammen, J., **2005**. Inclusion complexation of lorazepam with different cyclodextrins suitable for parenteral use. *Drug Dev. Ind. Pharm.*, 31 (6), 567-575.
- Hong, J.Y., Kim, J.K., Song, Y.K., Park, J.S., Kim, C.K., **2006**. A new self-emulsifying formulation of itraconazole with improved dissolution and oral absorption. *J. Control. Release.*, 110 (2), 332-338.
- Hörter D., Dressman J.B., **2001**. Influence of physicochemical properties on dissolution of drugs in the gastrointestinal tract. *Adv Drug Deliv Rev.*, 46 (1-3), 75-87.
- Hu, M., Li, Y., Davitt, C.M., Huang, S-M., Thummel, K., Penman, B.W., Crespi, C.L., **1999**. Transport and metabolic characterization of Caco-2 cells expressing CYP3A4 and CYP3A4 plus oxydoreductase. *Pharm. Res.*, 16 (9), 1352-1359.
- Hu, J., Johnston, K.P., Williams III, R.O., **2003**. Spray freezing into liquid (SFL) particle engineering technology to enhance dissolution of poorly water soluble drugs: organic solvent versus organic/aqueous co-solvent systems. *Eur. J. Pharm. Sci.*, 20 (3), 295-303.
- Hu, J., Johnston, K.P., Williams III, R.O., **2004**. Nanoparticle engineering processes for enhancing the dissolution rates of poorly water soluble drugs. *Drug Dev. Ind. Pharm.*, 30 (3), 233-245.
- Hu, J., Johnston, K.P., Williams III, R.O., **2004b**. Rapid dissolving high potency danazol powders produced by spray freezing into liquid process. *Int J. Pharm.*, 271 (1-2), 145-154.
- Hu, J., Johnston, K.P., Williams III, R.O., **2004c**. Stable amorphous danazol nanostructured powders with rapid dissolution rates produced by spray freezing into liquid. *Drug Dev. Ind. Pharm.*, 30 (7), 695-704.
- Huang, L.F., Tong, W.Q., **2004**. Impact of solid state properties on developability assessment of drug candidates. *Adv. Drug Deliv. Rev.*, 56 (3), 321-334.
- Irie, T., Uekama, K., **1999**. Cyclodextrins in peptide and protein delivery. *Adv. Drug Deliv. Rev.*, 36 (1), 101-123.
- ISO, **1999**. International Organization for Standardization. Particle size analysis - Laser diffraction methods - Part 1: General Principles. Ref N° ISO 13320-1 :1999(E)
- Jacobs, C., Kayser, O., Müller, R.H., **2000**. Nanosuspensions as a new approach for the formulation of the poorly soluble tarazepide. *Int. J. Pharm.*, 196 (2), 161-164.
- Jacobs, C., Müller, R.H., **2002**. Production and characterization of a budesonide nanosuspension for pulmonary administration. *Pharm. Res.*, 19 (2), 189-194.

- Jinno, J., Kamada, N., Miyake, M., Yamada, K., Mukai, T., Odomi, M., Toguchi, H., Liversidge, G.G., Higaki, K., Kimura, T., **2006**. Effect of particle size reduction on dissolution and oral absorption of a poorly water-soluble drug, cilostazol, in beagle dogs. *J. Control. Release.*, 111 (1-2), 56-64.
- Johnson, A.E., **2002**. Analysis of the Young equation and the use of the Kelvin equation in calculating the Gibbs excess. *Colloids Surf. A*, 202, 33-39.
- Jounela, A.J., Pentikainen, P.J., Sothmann, A., **1975**. Effect of particle size on the bioavailability of digoxin. *Eur. J. Clin. Pharmacol.*, 8 (5), 365-370.
- Kakumanu, V.K., Arora, V., Bansal, A.K., **2006**. Investigation of factors responsible for low oral bioavailability of cefpodoxime proxetil. *Int. J. Pharm.*, 317 (2), 155-160.
- Kaneniwa, N., Watari, N., **1974**. Dissolution of slightly soluble drugs. I. Influence of particle size on dissolution behavior. *Chem. Pharm. Bull.*, 22 (8), 1699-1705.
- Kaneniwa, N., Watari, N., **1978**. Dissolution of slightly soluble drugs. IV. Effect of particle size of sulfonamides on in vitro dissolution rate and in vivo absorption rate, and their relation to solubility. *Chem. Pharm. Bull.*, 26 (3), 813-826.
- Kaneniwa, N., Watari, N., Iijima, H., **1978b**. Dissolution of slightly soluble drugs. V. Effect of particle size on gastrointestinal drug absorption and its relation to solubility. *Chem. Pharm. Bull.*, 26 (9), 2603-2614.
- Kawakami K., Miyoshi K., Ida Y., **2004**. Solubilization behavior of poorly soluble drugs with combined use of Gelucire 44/14 and cosolvent. *J. Pharm. Sci.*, 93 (6), 1471-1479.
- Kawakami, K., Oda, N., Miyoshi, K., Funaki, T., Ida, Y., **2006**. Solubilization behavior of a poorly soluble drug under combined use of surfactants and cosolvents. *Eur. J. Pharm. Sci.*, 28 (1-2), 7-14.
- Keck, C.M., Müller, R.H., **2006**. Drug nanocrystals of poorly soluble drugs produced by high pressure homogenisation. *Eur. J. Pharm. Biopharm.*, 62 (1), 3-16.
- Kerc, J., Srcic, S., Knez, Z., Sencar-Bozic, P., **1999**. Micronization of drugs using supercritical carbon dioxide. *Int. J. Pharm.* 182 (1), 33-39.
- Keymolen, B., Ford, J.L., Powell, M.W., Rajabi-Siahboomi, A.R., **2003**. Investigation of the polymorphic transformations from glassy nifedipine. *Thermochim. Acta*, 397 (1), 103-117.
- Kim, Y.I., Fluckiger, L., Hoffman, M., Lartaud-Idjouadiene, I., Atkinson, J., Maincent, P., **1997**. The antihypertensive effect of orally administered nifedipine-loaded nanoparticles in spontaneously hypertensive rats. *Br. J. Pharmacol.*, 120 (3), 399-404.
- Kipp, J.E., **2004**. The role of solid nanoparticle technology in the parenteral delivery of poorly water-soluble drugs. *Int. J. Pharm.*, 284 (1-2), 109-122.
- Kocbek, P., Baumgartner, S., Kristl, J., **2006**. Preparation and evaluation of nanosuspensions for enhancing the dissolution of poorly soluble drugs. *Int. J. Pharm.*, 312 (1-2), 179-186.
- Krause, K.P., Müller, R.H., **2001**. Production and characterization of highly concentrated nanosuspensions by high pressure homogenization. *Int. J. Pharm.*, 214 (1-2), 21-24.
- Kuhnert-Brandstätter, M., Geller, M., Wurlan, I., **1980**. Microscopic characterization and identification of drugs: part 14. *Sci. Pharm.*, 48 (3), 250-258.
- Langguth, P., Hanafy, A., Frenzel, D., Grenier, P., Nhamias, A., Ohlig, T., Vergnault, G., Spahn-Langguth, H., **2005**. Nanosuspension formulations for low-soluble drugs: pharmacokinetic evaluation using spironolactone as model compound. *Drug Dev. Ind. Pharm.*, 31 (3), 319-329.
- Lee, R.W., Shaw, J.M., McShane, J., Wood, R.W., **2000**. In: Particle size reduction. Water-insoluble drug formulation. Ed. R. Liu; Interpharm Press, Denver, CO, USA; 455-492.

- Leite, E.R., Giralaldi, T.R., Pontes, F.M., Longo, E., A. Beltrán, A., J. Andrés, J., **2003**. Crystal growth in colloidal tin oxide nanocrystals induced by coalescence at room temperature. *Appl. Phys. Lett.*, 83 (8), 1566-1568.
- Lennernäs, H., **2005**. Mechanisms of intestinal membrane permeation. Strategies in Oral Drug Delivery. Oral drug delivery foundation meeting 2005. Garmisch-Partenkirchen, Germany.
- Lesuffleur, T., Porchet, N., Aubert, J.P., Swallow, D., Gum, J.R., Kim, Y.S., Real, F.X., Zweibaum, A., **1993**. Differential expression of the human mucin genes MUC1 to MUC5 in relation to growth and differentiation of different mucus-secreting HT-29 cell subpopulations. *J. Cell. Sci.*, 106 (Pt 3), 771-783.
- Leuner, C., Dressman, J., **2000**. Improving drug solubility for oral delivery using solid dispersions. *Eur. J. Pharm. Biopharm.*, 50 (1), 47-60.
- Levitt, M.D., Li, R., DeMaster, E.G., Elson, M., Furne, J., Levitt, D.G., **1997**. Use of measurements of ethanol absorption from stomach and intestine to assess human ethanol metabolism. *Am. J. Physiol.* 273 (4), G951-957.
- Lewis, T.A., Bayless, L., Eckman, J.B., Ellis, J.L., Grewal, G., Libertine, L., Marie Nicolas, J., Scannell, R.T., Wels, B.F., Wenberg, K., Wypij, D.M., **2004a**. 5-lipoxygenase inhibitors with histamine H(1) receptor antagonist activity. *Bioorg. Med. Chem. Lett.*, 14 (9), 2265-2268.
- Lewis, T.A., Young, M.A., Arrington, M.P., Bayless, L., Cai, X., Collart, P., Eckman, J.B., Ellis, J.L., Ene, D.G., Libertine, L., Nicolas, J.M., Scannell, R.T., Wels, B.F., Wenberg, K., Wypij, D.M., **2004b**. Cetirizine and loratadine-based antihistamines with 5-lipoxygenase inhibitory activity. *Bioorg. Med. Chem. Lett.*, 14 (22), 5591-5594.
- Li, P., Tabibi, S.E., Yalkowsky, S.H., **1999**. Solubilization of flavopiridol by pH control combined with cosolvents, surfactants, or complexants. *J. Pharm. Sci.*, 88 (9), 945-947.
- Li, P., Zhao, L., Yalkowsky, S.H., **1999b**. Combined effect of cosolvent and cyclodextrin on solubilization of nonpolar drugs. *J. Pharm. Sci.*, 88 (11), 1107-1111.
- Li, S., Wong, S., Sethia, S., Almoazen, H., Joshi, Y.M., Serajuddin, A.T., **2005**. Investigation of solubility and dissolution of a free base and two different salt forms as a function of pH. *Pharm. Res.*, 22 (4), 628-635.
- Li, F., Hong, L., Mau, C.I., Chan, R., Hendricks, T., Dvorak, C., Yee, C., Harris, J., Alfredson, T., **2006**. Transport of levovirin prodrugs in the human intestinal Caco-2 cell line. *J. Pharm. Sci.*, 95 (6), 1318-1325.
- Lian, T., Ho, R.J., **2001**. Trends and developments in liposome drug delivery systems. *J. Pharm. Sci.*, 90 (6), 667-680.
- Lin, S.L., Menig, J., Lachman, L., **1968**. Interdependence of physiological surfactant and drug particle size on the dissolution behavior of water insoluble drugs. *J. Pharm. Sci.*, 57 (12), 2143-2148.
- Lin, C.-W., Cham, T.-M., **1996**. Effect of particle size on the available surface area of nifedipine from nifedipine-polyethylene glycol 6000 solid dispersions. *Int. J. Pharm.*, 127 (2), 261-272.
- Lindenberg, M., Knopp, S., Dressman, J.B., **2004**. Classification of orally administered drugs on the World Health Organization model list of essential medicines according to the biopharmaceutics classification system, *Eur. J. Pharm. Biopharm.*, 58 (2), 265-278.
- Ling, S.S., Magosso, E., Khan, N.A., Yuen, K.H., Barker, S.A., **2006**. Enhanced oral bioavailability and intestinal lymphatic transport of a hydrophilic drug using liposomes. *Drug Dev. Ind. Pharm.*, 32 (3), 335-345.
- Liu, R., Sadrzadeh, N., Constantinides, P.P., **2000**. In : Micellization and drug solubility enhancement. Water-insoluble drug formulation. Ed. R. Liu; Interpharm Press, Denver, CO, USA; 213-354.
- Liu, R., Cannon, J.B., Li, Y., **2000b**. Liposomes in solubilization. In: Water-insoluble drug formulation. Ed. R. Liu; Interpharm Press, Denver, CO, USA; 355-404.

- Liu, C., Liu, C., Desai, K.G., **2005**. Enhancement of dissolution rate of valdecoxib using solid dispersions with polyethylene glycol 4000. *Drug. Dev. Ind. Pharm.*, 31 (1), 1-10.
- Liversidge, G.G., Cundy, C.C., **1995**. Particle size reduction for improvement of oral bioavailability of hydrophobic drugs: I. Absolute oral bioavailability of nanocrystalline danazol in beagle dogs. *Int. J. Pharm.*, 125 (1), 91-97.
- Löbenberg R., Amidon G.L., **2000**. Modern bioavailability, bioequivalence and biopharmaceutics classification system. New scientific approaches to international regulatory standards; *Eur. J. Pharm. Biopharm.*, 50 (1), 3-12.
- Loftsson, T., Jarvinen, T., **1999**. Cyclodextrins in ophthalmic drug delivery. *Adv. Drug Deliv. Rev.*, 36 (1), 59-79.
- López-Quintela, M.A., **2003**. Synthesis of nanomaterials in microemulsions: formation mechanisms and growth control. *Curr. Op. Coll. Int. Sci.*, 8, 137-134.
- Manca, M.L., Zaru, M., Ennas, G., Valenti, D., Sinico, C., Loy, G., Fadda, A.M., **2005**. Diclofenac-beta-cyclodextrin binary systems: physicochemical characterization and in vitro dissolution and diffusion studies. *AAPS Pharm. Sci. Tech.*, 6 (3), E464-472.
- Matsuda, H., Arima, H., **1999**. Cyclodextrins in transdermal and rectal delivery. *Adv. Drug Deliv. Rev.*, 36 (1), 81-99.
- Mayersohn, M., **2002**. In: Principles of drug absorption. *Drugs and the Pharmaceutical Sciences: Modern Pharmaceutics; Volume 121*; Ed. G.S. Banker, C.T. Rhodes; Marcel Dekker, New York, 23-66.
- Merck index, Twelfth Edition, **1996**. Merck & Co., Inc., Withehouse Station, NJ, USA, 6617, 1121.
- Merisko-Liversidge, E., Liversidge, G.G., Cooper, E.R., **2003**. Nanosizing: a formulation approach for poorly-water-soluble compounds. *Eur. J. Pharm. Sci.*, 18 (2), 113-120.
- Merkus, F.W., Verhoef, J.C., Martin, E., Romeijn, S.G., van der Kuy, P.H., Hermens, W.A., Schipper, N.G., **1999**. Cyclodextrins in nasal drug delivery. *Adv. Drug Deliv. Rev.*, 36 (1), 41-57.
- Millard, J., Alvarez-Nunez, F., Yalkowsky, S., **2002**. Solubilization by cosolvents. Establishing useful constants for the log-linear model. *Int. J. Pharm.*, 245 (1-2), 153-166.
- Minko, T., **2004**. Drug targeting to the colon with lectins and neoglycoconjugates. *Adv. Drug Deliv. Rev.*, 56 (4), 491-509.
- Mitchell, S.A., Reynolds, T.D., Dasbach, T.P., **2003**. A compaction process to enhance dissolution of poorly water-soluble drugs using hydroxypropyl methylcellulose. *Int. J. Pharm.*, 250 (1), 3-11.
- Moribe, K., Tsutsumi, S., Morishita, S., Shinozaki, H., Tozuka, Y., Ogushi, T., Yamamoto, K., **2005**. Micronization of Phenylbutazone by Rapid Expansion of Supercritical CO<sub>2</sub> Solution. *Chem. Pharm. Bull.*, 53 (8), 1025-1028.
- Mosharraf, M., Nyström, C., **1995**. The effect of particle size and shape on the surface specific dissolution rate of micro-sized practically insoluble drugs. *Int. J. Pharm.*, 122 (1-2), 35-47.
- Moschitz, J., Achleitner, G., Pomper, H., Müller, R.H., **2004**. Development of an intravenously injectable chemically stable aqueous omeprazole formulation using nanosuspension technology. *Eur. J. Pharm. Biopharm.*, 58 (3), 615-619.
- Moschitz, J., Müller, R.H., **2006**. Spray coated pellets as carrier system for mucoadhesive drug nanocrystals. *Eur. J. Pharm. Biopharm.*, 62 (3), 282-287.
- Müller, R.H., Peters, K., **1998**. Nanosuspensions for the formulation of poorly water soluble drugs. I. Preparation by a size reduction technique. *Int. J. Pharm.*, 160 (2), 229-237.

- Müller, R.H., Böhm, B.H.L., Grau, M.J., **2000**. In: Nanosuspensions: A formulation approach for poorly soluble and poorly bioavailable drugs. Handbook of Pharmaceutical Controlled Release Technology; Ed. D.L. Wise; Marcel Dekker, New York, 345-357.
- Müller, R.H., Jacobs, C., Kayser, O., **2001**. Nanosuspensions as particulate drug formulations in therapy. Rationale for development and what we can expect for the future. *Adv. Drug Deliv. Rev.*, 47 (1), 3-19.
- Müller, R.H., Jacobs, C., **2002**. Buparvaquone mucoadhesive nanosuspension: preparation, optimisation and long-term stability. *Int. J. Pharm.*, 237 (1-2), 151-161.
- Mura, P., Moyano, J.R., Gonzalez-Rodriguez, M.L., Rabasco-Alvarez, A.M., Cirri, M., Maestrelli, F., **2005**. Characterization and dissolution properties of ketoprofen in binary and ternary solid dispersions with polyethylene glycol and surfactants. *Drug Dev. Ind. Pharm.*, 31 (4-5), 425-434.
- Muhrer, G., Meier, U., Fusaro, F., Albano, S., Mazzotti, M., **2006**. Use of compressed gas precipitation to enhance the dissolution behaviour of a poorly water-soluble drug: Generation of drug microparticles and drug-polymer solid dispersions. *Int. J. Pharm.*, 308 (1-2), 69-83.
- Nanda, R.N., Rowlings, C.E., Barker, N.P., Sheen, P.-C., **2000**. In: Immediate release solid dispersions for oral drug delivery. Water-insoluble drug formulation. Ed. R. Liu; Interpharm Press, Denver, CO, USA; 493-523.
- Neau, S.H., **2000**. In : Pharmaceutical salts. Water-insoluble drug formulation. Ed. R. Liu; Interpharm Press, Denver, CO, USA; 405-425.
- Neau, S.H., **2000b**. In: Prodrugs for improved aqueous solubility. Water-insoluble drug formulation. Ed. R. Liu; Interpharm Press, Denver, CO, USA; 427-454.
- Nollevaux, G., Devillé, C., El Moulaj, B., Zorzi, W., Deloyer, P., Schneider, Y.G., Peulen, O., Dandrifosse, G., **2006**. Development of a serum-free co-culture of human intestinal epithelium cell-lines (Caco-2/HT29-5M21). *BMC Cell Biol.*, 7 (1), 20.
- O'Connor, K.M., Corrigan, O.I., **2001**. Preparation and characterisation of a range of diclofenac salts. *Int. J. Pharm.*, 226 (1-2), 163-179.
- Ozdemir, G., Malayoglu, U., **2004**. Wetting characteristics of aqueous rhamnolipids solutions. *Colloids Surf. B Biointerfaces*, 39 (1-2), 1-7.
- Patel, K., Trivedi, S., Luo, S., Zhu, X., Pal, D., Kern, E.R., Mitra, A.K., **2005**. Synthesis, physicochemical properties and antiviral activities of ester prodrugs of ganciclovir. *Int. J. Pharm.*, 305 (1-2), 75-89.
- Patki, K.C., Von Moltke, L.L., Greenblatt, D.J., **2003**. In vitro metabolism of midazolam, triazolam, nifedipine, and testosterone by human liver microsomes and recombinant cytochromes p450: role of cyp3a4 and cyp3a5. *Drug Metab Dispos.*, 31 (7), 938-944.
- Patravale, V.B., Date, A.A., Kulkarni, R.M., **2004**. Nanosuspensions: a promising drug delivery strategy. *J. Pharm Pharmacol.*, 56 (7), 827-840.
- Pellicer, J., Garcia-Morales, V., Hernandez, M.J., **2000**. On the demonstration of the Young–Laplace equation in introductory physics courses. *Phys. Educ.*, 35 (2), 126-129.
- Pedersen, P.V., Brown, K.F., **1975**. Dissolution profile in relation to initial particle distribution. *J. Pharm. Sci.*, 64 (7), 1192-1195.
- Perrut, M., Jung, J., Leboeuf, F., **2005**. Enhancement of dissolution rate of poorly-soluble active ingredients by supercritical fluid processes. Part I: Micronization of neat particles. *Int. J. Pharm.*, 288 (1), 3-10.
- Peters, K., Kruss, B., Becker, R., Müller, R.H., **1999**. Pharmaceutical nanosuspensions for medicament administration as systems with increased saturation solubility and rate of solution. Patent number: 5.858.410; Jan 12, 1999; US005858410A.



- Peters, K., Leitzke, S., Diederichs, J.E., Borner, K., Hahn, H., Müller, R.H., Ehlers, S., **2000**. Preparation of a clofazimine nanosuspension for intravenous use and evaluation of its therapeutic efficacy in murine *Mycobacterium avium* infection. *J. Antimicrob. Chemother.*, 45 (1), 77-83.
- Pfrunder, A., Gutmann, H., Beglinger, C., Drewe, J., **2003**. Gene expression of CYP3A4, ABC-transporters (MDR1 and MRP1-MRP5) and hPXR in three different human colon carcinoma cell lines. *J. Pharm. Pharmacol.*, 55 (1), 59-66.
- Pinto, M., Robine-Léon, S., Appay, M.D., Kedinger, M., Triadou, N., Dussaulx, E., Lacroix, B., Simon-Assmann, P., Haffen, K., Fogh, J., Zweibaum, A., **1983**. Enterocyte-like differentiation and polarization of the human colon carcinoma cell line Caco-2 in culture. *Biol. Cell*, 47, 323-330.
- Ponchel, G., Irache, J., **1998**. Specific and non-specific bioadhesive particulate systems for oral delivery to the gastrointestinal tract. *Adv. Drug Deliv. Rev.*, 34 (2-3), 191-219.
- Pool-Zobel, B.L., Selvaraju, V., Sauer, J., Kautenburger, T., Kiefer, J., Richter, K.K., Soom, M., Wolf, S., **2005**. Butyrate may enhance toxicological defence in primary, adenoma and tumor human colon cells by favourably modulating expression of glutathione S-transferases genes, an approach in nutrigenomics. *Carcinogenesis*, 26 (6), 1064-1076.
- Potluri, P., Betageri, G.V., **2006**. Mixed-micellar proliposomal systems for enhanced oral delivery of progesterone. *Drug Deliv.*, 13 (3), 227-232.
- Portero, A., Remunan-Lopez, C., Vila-Jato, J.L., **1998**. Effect of chitosan and chitosan glutamate enhancing the dissolution properties of the poorly water soluble drug nifedipine. *Int. J. Pharm.*, 175 (1), 75-84.
- Pudipeddi, M., Serajuddin, A.T., **2005**. Trends in solubility of polymorphs. *J. Pharm. Sci.*, 94 (5), 929-39.
- Rao, V.M., Nerurkar, M., Pinnamaneni, S., Rinaldi, F., Raghavan, K., **2006**. Co-solubilization of poorly soluble drugs by micellization and complexation. *Int. J. Pharm.*, 319 (1-2), 98-106.
- Rasenack, N., Hartenhauer, H., Müller, B.W., **2003**. Microcrystals for dissolution rate enhancement of poorly water-soluble drugs. *Int. J. Pharm.*, 254 (2), 137-145.
- Rasenack, N., Müller, B.W., **2004**. Micron-size drug particles: common and novel micronization techniques. *Pharm. Dev. Technol.*, 9 (1), 1-13.
- Raula, J., Eerikäinen, H., Kauppinen, E.I., **2004**. Influence of the solvent composition on the aerosol synthesis of pharmaceutical polymer nanoparticles. *Int. J. Pharm.*, 284 (1-2), 13-21.
- Reitberg, D.P., Love, S.J., Quercia, G.T., Zinny, M.A., **1987**. Effect of food on nifedipine pharmacokinetics. *Clin. Pharmacol. Ther.*, 42 (1), 72-75.
- Reverchon, E., Della Porta, G., Spada, A., Antonacci, A., **2004**. Griseofulvin micronization and dissolution rate improvement by supercritical assisted atomization. *J. Pharm. Pharmacol.*, 56 (11), 1379-1387.
- Robertson, R.M., Robertson, D., **1996**. In: *Drugs used for the treatment of myocardial ischemia. The pharmacological basis of therapeutics*, ninth edition. Goodman & Gilman, International edition, 1996, 767-774.
- Rogers, T.L., Johnston, K.P., Williams III, R.O., **2001**. Solution-Based Particle Formation of Pharmaceutical Powders by Supercritical or Compressed Fluid CO<sub>2</sub> and Cryogenic Spray-Freezing Technologies. *Drug Dev. Ind. Pharm.*, 27 (10), 1003-1015.
- Rogers, T.L., Hu, J., Yu, Z., Johnston, K.P., Williams III, R.O., **2002**. A novel particle engineering technology: spray-freezing into liquid. *Int. J. Pharm.*, 242 (1-2), 93-100.
- Rogers, T.L., Gillespie, I.B., Hitt, J.E., Fransen, K.L., Cowl, C.A., Tucker, C.J., Kupperblatt, G.B., Becker, J.N., Wilson, D.L., Todd, C., Broomall, C.F., Evans, J.C., Elder, E.J., **2004**. Development and Characterization of a Scalable Controlled Precipitation Process to Enhance the Dissolution of Poorly Water-Soluble Drugs. *Pharm. Res.*, 21 (11), 2048-2057.

- Qiu, Y., Zhang, G., **2000**. In: Research and development aspects of oral controlled-release dosage forms. *Drugs and the Pharmaceutical Sciences: Handbook of Pharmaceutical Controlled Release Technology*; Ed. D.L. Wise; Marcel Dekker, New York, 465-504.
- Sangalli, M.E., Maroni, A., Zema, L., Buseti, C., Giordano, F., Gazzaniga, A., **2001**. In vitro and in vivo evaluation of an oral system for time and/or site-specific drug delivery. *J. Control. Release*, 73 (1), 103-110.
- Sangalli, M.E., Maroni, A., Foppoli, A., Zema, L., Giordano, F., Gazzaniga, A., **2004**. Different HPMC viscosity grades as coating agents for an oral time and/or site-controlled delivery system: a study on process parameters and in vitro performances. *Eur. J. Pharm. Sci.*, 22 (5), 469-476.
- Sansdrap, P., **1996**. Préparation, caractérisation et évaluation in vitro et in vivo de microsphères biodégradables en poly(DL-lactide-co-glycolide) renfermant de la nifedipine; Thèse de doctorat en Sciences Pharmaceutique, Institut de Pharmacie, Laboratoire de Pharmacie Galénique et Biopharmacie. Université Libre de Bruxelles.
- Sarkari, M., Brown, J., Chen, X., Swinnea, S., Williams III, R.O., Johnston, K.P., **2002**. Enhanced drug dissolution using evaporative precipitation into aqueous solution. *Int. J. Pharm.*, 243 (1-2), 17-31.
- Schmiedlin-Ren, P., Thummel, K.E., Fisher, J.M., Paine, M.F., Lown, K.S., Watkins, P.B., **1997**. Expression of enzymatically active CYP3A4 by Caco-2 cells grown on extracellular matrix-coated permeable supports in the presence of 1  $\alpha$ , 25-dihydroxyvitamin D3. *Mol. Pharmacol.*, 51 (5), 741-754.
- Schneider, Y.J., **1989**. Optimisation of hybridoma cell growth and monoclonal antibody secretion in a chemically defined, serum- and protein-free culture medium. *J. Immunol. Methods*, 116, 65-77.
- Scholz, A., Abrahamsson, B., Diebold, S.M., Kostewicz, E., Polentarutti, B.I., Ungell, A.L., Dressman, J.B., **2002**. Influence of hydrodynamics and particle size on the absorption of felodipine in labradors. *Pharm. Res.*, 19 (1), 42-46.
- Seedher, N., Bhatia, S., **2003**. Solubility enhancement of Cox-2 inhibitors using various solvent systems. *AAPS PharmSciTech.*, 4 (3), E33.
- Sencar-Bozic, P., Srcic, S., Knez, Z., Kerc, J., **1997**. Improvement of nifedipine dissolution characteristics using supercritical CO<sub>2</sub>. *Int. J. Pharm.*, 148 (2), 123-130.
- Serajuddin, A.T., **1999**. Solid dispersion of poorly water-soluble drugs: early promises, subsequent problems, and recent breakthroughs. *J. Pharm. Sci.*, 88 (10), 1058-1066.
- Shah, V.P., Tsong, Y., Sathe, P., Liu, J-P., **1998**. In vitro dissolution profile comparison - Statistics and analysis of the similarity factor f<sub>2</sub>. *Pharm. Res.*, 15 (6), 889-896.
- Shefter, E., **1981**. In: Solubilization by solid state manipulation. *Drugs and the Pharmaceutical Sciences: Techniques of solubilization of drugs*; Volume 12; Marcel Dekker, New York, 159-182.
- Shekunov, B.Y., Chattopadhyay, P., Seitzinger, J., Huff, R., **2006**. Nanoparticles of Poorly Water-Soluble Drugs Prepared by Supercritical Fluid Extraction of Emulsions. *Pharm. Res.*, Vol. 23 (1), 196-204.
- Singhal, D., Curatolo, W., **2004**. Drug polymorphism and dosage form design: a practical perspective. *Adv. Drug Deliv. Rev.*, 56 (3), 335-347.
- Sinswat, P., Gaob, X., Yacaman, M.J., Williams III, R.O., Johnston, K.P., **2005**. Stabilizer choice for rapid dissolving high potency itraconazole particles formed by evaporative precipitation into aqueous solution. *Int. J. Pharm.*, 302 (1-2), 113-124.
- Smart, J.D., **2005**. The basics and underlying mechanisms of mucoadhesion. *Adv. Drug Deliv. Rev.*, 57 (11), 1556-1568.
- Stella, V.J., Rao, V.M., Zannou, E.A., Zia, V.V., **1999**. Mechanisms of drug release from cyclodextrin complexes. *Adv. Drug Deliv. Rev.*, 36 (1), 3-16.

- Strickley, R.G., **2004**. Solubilizing Excipients in Oral and Injectable Formulations. *Pharm. Res.*, 21 (2), 201-230.
- Sugimoto, M., Okagaki, T., Narisawa, S., Koida, Y., Nakajima, K., **1998**. Improvement of dissolution characteristics and bioavailability of poorly water-soluble drugs by novel cogrinding method using water-soluble polymer. *Int. J. Pharm.*, 160 (1), 11-19.
- Suryanarayanan, R., Rastogi, S., **2002**. In: X-ray powder diffractometry. *Encyclopaedia of Pharmaceutical Technology*, 2<sup>nd</sup> Edition, Vol.3, Marcel Dekker, New York, USA, 3005-3019.
- Suzuki, H., Ogawa, M., Hironaka, K., Ito, K., Sunada, H., **2001**. A nifedipine coground mixture with sodium deoxycholate. II. Dissolution characteristics and stability. *Drug. Dev. Ind. Pharm.*, 27 (9), 951-958.
- Tabibi, S.E., Gupta, S.L., **2000**. In: Soft gelatin capsules development. *Water-insoluble drug formulation*. Ed. R. Liu; Interpharm Press, Denver, CO, USA; 609-633.
- Teraoka, R., Otsuka, M., Matsuda, Y., **1999**. Evaluation of photostability of solid-state dimethyl 1,4-dihydro-2,6-dimethyl-4-(2-nitro-phenyl)-3,5-pyridinedicarboxylate by using Fourier transformed reflection-absorption infrared spectroscopy. *Int. J. Pharm.*, 184 (1), 35-43.
- Thakur, R., Gupta, R.B., **2006**. Formation of phenytoin nanoparticles using rapid expansion of supercritical solution with solid cosolvent (RESS-SC) process. *Int. J. Pharm.*, 308 (1-2), 190–199.
- Thanou, M., Verhoef, J.C., Junginger, H.E., **2001**. Oral drug absorption enhancement by chitosan and its derivatives. *Adv. Drug Deliv. Rev.*, 52 (2), 117-126.
- Thummel, K.E., Brimer, C., Yasuda, K., Thottassery, J., Senn, T., Lin, Y., Ishizuka, H., Kharasch, E., Schuetz, J., Schuetz, E., **2001**. Transcriptional control of intestinal cytochrome P-4503A by 1 $\alpha$ ,25-dihydroxy vitamin D3. *Mol. Pharmacol.*, 60(6), 1399-1406.
- Tolls, J., van Dijk, J., Verbruggen, E.J.M., Hermens, J.L.M., Loeprecht, B., Schüürmann, G., **2002**. Aqueous Solubility-Molecular Size Relationships: A Mechanistic Case Study Using C<sub>10</sub>- to C<sub>19</sub>-Alkanes. *J. Phys. Chem. A*, 106 (11), 2760 -2765.
- Tong, W.-Q., **2000**. In: Preformulation aspects of insoluble compounds. *Water-insoluble drug formulation*. Ed. R. Liu; Interpharm Press, Denver, CO, USA; 65-96.
- Tong, W.-Q., **2000b**. In: Applications of complexation in the formulation of insoluble compounds. *Water-insoluble drug formulation*. Ed. R. Liu; Interpharm Press, Denver, CO, USA; 111-140.
- Trivedi, J.S., Wells, M.L., **2000**. In: Solubilization using cosolvent approach. *Water-insoluble drug formulation*. Ed. R. Liu; Interpharm Press, Denver, CO, USA; 141-168.
- Trotta, M., Gallarate, M., Pattarino, F., Morel, S., **2001**. Emulsions containing partially water-miscible solvents for the preparation of drug nanosuspensions. *J. Control. Release*, 76 (1-2), 119-128.
- Van Nijlen, T., Brennan, K., Van den Mooter, G., Blaton, N., Kinget, R., Augustijns, P., **2003**. Improvement of the dissolution rate of artemisinin by means of supercritical fluid technology and solid dispersions. *Int. J. Pharm.*, 254 (2), 173-181.
- Varma, M.M., Pandi, J.K., **2005**. Dissolution, solubility, XRD, and DSC studies on flurbiprofen-nicotinamide solid dispersions. *Drug Dev. Ind. Pharm.*, 31 (4-5), 417-423.
- Vatsaraj, N.B., Gao, D., Kowalski, D.L., **2003**. Optimization of the operating conditions of a lab scale Aljet mill using lactose and sucrose: a technical note. *AAPS Pharm. Sci. Tech.*, 4 (2), E27.
- Vergote, G.J., Vervaet, C., Van Driessche, I., Hoste, S., De Smedt, S., Demeester, J., Jain, R.A., Ruddy, S., Remon J.P., **2001**. An oral controlled release matrix pellet formulation containing nanocrystalline ketoprofen. *Int. J. Pharm.*, 219 (1-2), 81-87.
- Vipparagunta, S.R., Brittain, H.G., Grant, D.J., **2001**. Crystalline solids. *Adv. Drug Deliv. Rev.*, 48 (1), 3-26.

- Vippagunta, S.R., Maul, K.A., Tallavajhala, S., Grant, D.J.W., **2002**. Solid-state characterization of nifedipine solid dispersions. *Int. J. Pharm.*, 236 (1-2), 111-123.
- Walter, E., Janich, S., Roessler, B.J., Hilfinger, J.M., Amidon G.L., **1996**. HT29-MTX/Caco-2 cocultures as an in vitro model for the intestinal epithelium: in vitro-in vivo correlation with permeability data from rats and humans. *J. Pharm. Sci.*, 85 (10), 1070-1076.
- Wang, L., Cui, F.D., Hayase, T., Sunada, H., **2005**. Preparation and evaluation of solid dispersion for nitrendipine-carbopol and nitrendipine-HPMCP systems using a twin screw extruder. *Chem. Pharm. Bull.*, 53 (10), 1240-1245.
- Wei, L., Sun, P., Nie, S., Pan, W., **2005**. Preparation and evaluation of SEDDS and SMEDDS containing carvedilol. *Drug Dev. Ind. Pharm.*, 31 (8), 785-794.
- Wilding, I.R., **2000**. Site-Specific drug delivery in the gastrointestinal tract. *Crit. Rev. Ther. Drug Carr. Syst.*, 17, 557-620.
- Wilson, C.G., **2000**. In: *Gastrointestinal transit and drug absorption. Drugs and the Pharmaceutical Sciences: Oral Drug Absorption: Prediction and assessment; Volume 106*; Ed. J.B. Dressman, H. Lennernäs; Marcel Dekker, New York, 1-9.
- Wong, S.M., Kellaway, I.W., Murdan, S., **2006**. Enhancement of the dissolution rate and oral absorption of a poorly water soluble drug by formation of surfactant-containing microparticles. *Int. J. Pharm.*, 317 (1), 61-68.
- Wu, Y., Loper, A., Landis, E., Hettrick, L., Novak, L., Lynn, K., Chen, C., Thompson, K., Higgins, R., Batra, U., Shelukar, S., Kwei, G., Storey, D., **2004**. The role of biopharmaceutics in the development of a clinical nanoparticle formulation of MK-0869: a Beagle dog model predicts improved bioavailability and diminished food effect on absorption in human. *Int. J. Pharm.*, 285 (1-2), 135-146.
- Yamamura, S., Rogers, J.A., **1996**. Characterization and dissolution behavior of nifedipine and phosphatidylcholine binary systems. *Int. J. Pharm.*, 130 (1), 65-73.
- Yang, L., Chu, J.S., Fix, J.A., **2002**. Colon-specific drug delivery: new approaches and in vitro/in vivo evaluation. *Int. J. Pharm.*, 235 (1-2), 1-15.
- Yang, G., Jain, N., Yalkowsky, S.H., **2004**. Combined effect of SLS and (SBE)(7M)-beta-CD on the solubilization of NSC-639829. *Int. J. Pharm.*, 269 (1), 141-148.
- Yang, W., de Villiers, M.M., **2004**. The solubilization of the poorly water soluble drug nifedipine by water soluble 4-sulphonic calix[n]arenes. *Eur. J. Pharm. Biopharm.*, 58 (3), 629-636.
- Yang, W., de Villiers, M.M., **2004b**. Aqueous solubilization of furosemide by supramolecular complexation with 4-sulphonic calix[n]arenes. *J. Pharm. Pharmacol.*, 56 (6), 703-708.
- Yan-Yu, X., Yun-Mei, S., Zhi-Peng, C., Qi-Neng, P., **2006**. Preparation of silymarin proliposome: A new way to increase oral bioavailability of silymarin in beagle dogs. *Int. J. Pharm.*, 319 (1-2), 162-168.
- Yoshioka, M., Ohnishi, N., Sone, N., Egami, S., Takara, K., Yokoyama, T., Kuroda, K., **2004**. Studies on interactions between functional foods or dietary supplements and medicines. III. Effects of *Ginkgo biloba* leaf extract on the pharmacokinetics of nifedipine in rats - *Biol. Pharm. Bull.*, 27 (12), 2042-2045.
- Yu, H., Cook, T.J., Sinko, P.J., **1997**. Evidence for diminished functional expression of intestinal transporters in Caco-2 cell monolayers at high passages. *Pharm. Res.*, 14 (6), 757-762.
- Zajc, N., Obreza, A., Bele, M., Srcic, S., **2005**. Physical properties and dissolution behaviour of nifedipine/mannitol solid dispersions prepared by hot melt method. *Int. J. Pharm.*, 291 (1-2), 51-58.
- Zana, R., **1997**. Micellization of amphiphiles: selected aspects. *Colloids Surf. A*, 123-124, 27-35.
- Zerrouk, N., Chemtob, C., Arnaud, P., Toscani, S., Dugue, J., **2001**. In vitro and in vivo evaluation of carbamazepine-PEG 6000 solid dispersions. *Int. J. Pharm.*, 225 (1-2), 49-62.

- Zhang, J.Y., Shen, Z.G., Zhong, J., Hu, T.T., Chen, J.F., Ma, Z.Q., Yun, J., **2006**. Preparation of amorphous cefuroxime axetil nanoparticles by controlled nanoprecipitation method without surfactants. *Int. J. Pharm.*, In press.
- U.S. Department of Health and Human Services, Food and Drug Administration, Center for Drug Evaluation and Research (CDER). Guidance for Industry: Dissolution Testing of Immediate Release Solid Oral Dosage Forms, August **1997a**.
- U.S. Department of Health and Human Services, Food and Drug Administration, Center for Drug Evaluation and Research (CDER). Guidance for Industry: Development, Evaluation and Application of In vitro/In vivo correlations, September **1997b**.
- U.S. Department of Health and Human Services, Food and Drug Administration, Center for Drug Evaluation and Research (CDER). Guidance for Industry: SUPAC-SS: Nonsterile Semisolid Dosage Forms - Manufacturing Equipment Addendum, December **1998**.
- U.S. Department of Health and Human Services, Food and Drug Administration, Center for Drug Evaluation and Research (CDER). Guidance for industry: Waiver of in vivo bioavailability and bioequivalence studies for immediate-release solid oral dosage forms based on a biopharmaceutical classification system. August **2000**.
- U.S. Department of Health and Human Services, Food and Drug Administration, Center for Drug Evaluation and Research (CDER). Guidance for Industry: ANDAs: Pharmaceutical Solid Polymorphism Chemistry, Manufacturing, and Controls Information, December **2004**.
- Genesis Health, **2006**; [http://www.genesishealth.com/services/digestive\\_system.aspx](http://www.genesishealth.com/services/digestive_system.aspx). (consulted 22/05/2006)
- LSBU, London South Bank University, **2006**. <http://www.lsbu.ac.uk/water/cyclodextrin.html>. (consulted 20/06/2006).
- US NIH- NCI SEER, **2005**. [http://training.seer.cancer.gov/ss\\_module07\\_ugi/unit02\\_sec02\\_anatomy.html](http://training.seer.cancer.gov/ss_module07_ugi/unit02_sec02_anatomy.html) (consulted 22/05/2006).
- ICH - Q1A (R2), **2003**. ICH harmonised tripartite guideline - Stability testing of new drug substances and products - Q1A (R2), <http://www.ich.org/LOB/media/MEDIA419.pdf>. (consulted 09/08/2006).



## **ANNEXES**





## VII. Annexes

## Annex 1

**Table A1.** Data for Figure IV 2 6 (size in  $\mu\text{m}$ ).

	<b>d (0.1) <math>\pm</math> SD</b>	<b>d (0.5) <math>\pm</math> SD</b>	<b>d (0.9) <math>\pm</math> SD</b>	<b>D[4,3] <math>\pm</math> SD</b>	<b>span <math>\pm</math> SD</b>
<b>SDS 100%</b>	<b>0.783 <math>\pm</math> 0.019</b>	<b>1.26 <math>\pm</math> 0.09</b>	<b>1.98 <math>\pm</math> 0.07</b>	<b>1.33 <math>\pm</math> 0.04</b>	<b>2.50 <math>\pm</math> 0.82</b>
<b>Polysorbate 80 100%</b>	<b>0.126 <math>\pm</math> 0.008</b>	<b>0.705 <math>\pm</math> 0.068</b>	<b>1.80 <math>\pm</math> 0.05</b>	<b>0.838 <math>\pm</math> 0.029</b>	<b>2.38 <math>\pm</math> 0.53</b>
<b>Poloxamer 407 200%</b>					
<b>HPMC 100%</b>	<b>0.094 <math>\pm</math> 0.005</b>	<b>0.521 <math>\pm</math> 0.081</b>	<b>2.373 <math>\pm</math> 0.053</b>	<b>0.932 <math>\pm</math> 0.032</b>	<b>4.47 <math>\pm</math> 0.70</b>

**Table A2.** Data for Figure IV 2 7 (size in  $\mu\text{m}$ ).

	<b>d (0.1) <math>\pm</math> SD</b>	<b>d (0.5) <math>\pm</math> SD</b>	<b>d (0.9) <math>\pm</math> SD</b>	<b>D[4,3] <math>\pm</math> SD</b>	<b>span <math>\pm</math> SD</b>
<b>2%</b>	<b>1.61 <math>\pm</math> 0.19</b>	<b>2.98 <math>\pm</math> 0.42</b>	<b>5.39 <math>\pm</math> 0.96</b>	<b>3.27 <math>\pm</math> 0.51</b>	<b>1.26 <math>\pm</math> 0.06</b>
<b>6%</b>	<b>0.230 <math>\pm</math> 0.151</b>	<b>1.18 <math>\pm</math> 0.32</b>	<b>3.49 <math>\pm</math> 0.22</b>	<b>1.57 <math>\pm</math> 0.24</b>	<b>2.92 <math>\pm</math> 0.76</b>
<b>8%</b>	<b>0.137 <math>\pm</math> 0.023</b>	<b>1.04 <math>\pm</math> 0.16</b>	<b>3.36 <math>\pm</math> 0.09</b>	<b>1.43 <math>\pm</math> 0.10</b>	<b>3.11 <math>\pm</math> 0.41</b>
<b>10%</b>	<b>0.097 <math>\pm</math> 0.004</b>	<b>0.356 <math>\pm</math> 0.008</b>	<b>2.06 <math>\pm</math> 0.10</b>	<b>0.788 <math>\pm</math> 0.051</b>	<b>5.52 <math>\pm</math> 0.01</b>
<b>50%</b>	<b>0.094 <math>\pm</math> 0.001</b>	<b>0.460 <math>\pm</math> 0.034</b>	<b>2.04 <math>\pm</math> 0.03</b>	<b>0.812 <math>\pm</math> 0.018</b>	<b>4.26 <math>\pm</math> 0.30</b>
<b>75%</b>	<b>0.093 <math>\pm</math> 0.002</b>	<b>0.518 <math>\pm</math> 0.048</b>	<b>2.53 <math>\pm</math> 0.02</b>	<b>0.980 <math>\pm</math> 0.024</b>	<b>4.74 <math>\pm</math> 0.43</b>
<b>100%</b>	<b>0.094 <math>\pm</math> 0.005</b>	<b>0.521 <math>\pm</math> 0.081</b>	<b>2.37 <math>\pm</math> 0.05</b>	<b>0.932 <math>\pm</math> 0.032</b>	<b>4.47 <math>\pm</math> 0.70</b>
<b>200%</b>	<b>0.101 <math>\pm</math> 0.009</b>	<b>0.710 <math>\pm</math> 0.123</b>	<b>2.70 <math>\pm</math> 0.04</b>	<b>1.10 <math>\pm</math> 0.06</b>	<b>3.77 <math>\pm</math> 0.66</b>

**Table A3.** Data for Figure IV 2 8 (size in  $\mu\text{m}$ ).

	<b>d (0.1) <math>\pm</math> SD</b>	<b>d (0.5) <math>\pm</math> SD</b>	<b>d (0.9) <math>\pm</math> SD</b>	<b>D[4,3] <math>\pm</math> SD</b>	<b>span <math>\pm</math> SD</b>
<b>SDS</b>	<b>5.42 <math>\pm</math> 1.02</b>	<b>10.7 <math>\pm</math> 1.9</b>	<b>20.3 <math>\pm</math> 3.7</b>	<b>11.9 <math>\pm</math> 2.1</b>	<b>1.39 <math>\pm</math> 0.04</b>
<b>HPMC - methocel E15</b>	<b>0.083 <math>\pm</math> 0.001</b>	<b>0.182 <math>\pm</math> 0.007</b>	<b>1.46 <math>\pm</math> 0.05</b>	<b>0.563 <math>\pm</math> 0.023</b>	<b>7.57 <math>\pm</math> 0.17</b>
<b>HPMC - methocel E5</b>	<b>0.085 <math>\pm</math> 0.002</b>	<b>0.607 <math>\pm</math> 0.032</b>	<b>2.05 <math>\pm</math> 0.04</b>	<b>0.843 <math>\pm</math> 0.021</b>	<b>3.24 <math>\pm</math> 0.15</b>
<b>PVA</b>	<b>0.082 <math>\pm</math> 0.002</b>	<b>0.262 <math>\pm</math> 0.054</b>	<b>1.50 <math>\pm</math> 0.10</b>	<b>0.603 <math>\pm</math> 0.038</b>	<b>5.57 <math>\pm</math> 0.89</b>
<b>acaciae gum</b>	<b>0.090 <math>\pm</math> 0.001</b>	<b>0.407 <math>\pm</math> 0.006</b>	<b>1.18 <math>\pm</math> 0.05</b>	<b>0.542 <math>\pm</math> 0.016</b>	<b>2.68 <math>\pm</math> 0.12</b>
<b>poloxamer</b>	<b>0.079 <math>\pm</math> 0.001</b>	<b>0.183 <math>\pm</math> 0.003</b>	<b>1.20 <math>\pm</math> 0.05</b>	<b>0.483 <math>\pm</math> 0.011</b>	<b>6.14 <math>\pm</math> 0.28</b>

**Table A4.** Data for Figure IV 2 9 (size in  $\mu\text{m}$ ).

	<b>d (0.1) <math>\pm</math> SD</b>	<b>d (0.5) <math>\pm</math> SD</b>	<b>d (0.9) <math>\pm</math> SD</b>	<b>D[4,3] <math>\pm</math> SD</b>	<b>span <math>\pm</math> SD</b>
<b>1</b>	<b>0.092 <math>\pm</math> 0.001</b>	<b>0.480 <math>\pm</math> 0.007</b>	<b>1.84 <math>\pm</math> 0.01</b>	<b>0.762 <math>\pm</math> 0.004</b>	<b>3.64 <math>\pm</math> 0.06</b>
<b>2</b>	<b>0.095 <math>\pm</math> 0.000</b>	<b>0.404 <math>\pm</math> 0.002</b>	<b>1.86 <math>\pm</math> 0.00</b>	<b>0.755 <math>\pm</math> 0.001</b>	<b>4.38 <math>\pm</math> 0.03</b>
<b>3</b>	<b>0.085 <math>\pm</math> 0.001</b>	<b>0.325 <math>\pm</math> 0.021</b>	<b>1.02 <math>\pm</math> 0.01</b>	<b>0.456 <math>\pm</math> 0.010</b>	<b>2.89 <math>\pm</math> 0.16</b>

**Table A5.** Data for Figure IV 2 11 (size in  $\mu\text{m}$ ).

	<b>d (0.1) <math>\pm</math> SD</b>	<b>d (0.5) <math>\pm</math> SD</b>	<b>d (0.9) <math>\pm</math> SD</b>	<b>D[4,3] <math>\pm</math> SD</b>	<b>span <math>\pm</math> SD</b>
<b>NIF</b>					
no milling	<b>21.9 <math>\pm</math> 0.2</b>	<b>98.7 <math>\pm</math> 0.4</b>	<b>267.2 <math>\pm</math> 0.5</b>	<b>126.2 <math>\pm</math> 0.6</b>	<b>2.48 <math>\pm</math> 0.08</b>
Turrax milling	<b>3.07 <math>\pm</math> 0.17</b>	<b>15.7 <math>\pm</math> 0.3</b>	<b>51.6 <math>\pm</math> 0.4</b>	<b>22.3 <math>\pm</math> 0.3</b>	<b>3.07 <math>\pm</math> 0.04</b>
PMC	<b>0.509 <math>\pm</math> 0.017</b>	<b>2.43 <math>\pm</math> 0.09</b>	<b>5.20 <math>\pm</math> 0.25</b>	<b>2.71 <math>\pm</math> 0.16</b>	<b>1.93 <math>\pm</math> 0.83</b>
<b>ucb-35440-3</b>					
no milling	<b>8.78 <math>\pm</math> 2.10</b>	<b>140.5 <math>\pm</math> 11.3</b>	<b>340.6 <math>\pm</math> 15.1</b>	<b>160.4 <math>\pm</math> 9.4</b>	<b>2.37 <math>\pm</math> 0.11</b>
PMC	<b>0.082 <math>\pm</math> 0.004</b>	<b>0.623 <math>\pm</math> 0.282</b>	<b>2.75 <math>\pm</math> 0.12</b>	<b>1.07 <math>\pm</math> 0.11</b>	<b>5.6 <math>\pm</math> 3.29</b>
<b>UCB-A</b>					
no milling	<b>1.47 <math>\pm</math> 0.03</b>	<b>3.00 <math>\pm</math> 0.02</b>	<b>6.52 <math>\pm</math> 0.21</b>	<b>3.59 <math>\pm</math> 0.06</b>	<b>1.68 <math>\pm</math> 0.07</b>
Turrax milling	<b>1.43 <math>\pm</math> 0.03</b>	<b>2.92 <math>\pm</math> 0.02</b>	<b>6.29 <math>\pm</math> 0.22</b>	<b>3.47 <math>\pm</math> 0.06</b>	<b>1.66 <math>\pm</math> 0.07</b>
PMC	<b>0.105 <math>\pm</math> 0.001</b>	<b>1.14 <math>\pm</math> 0.02</b>	<b>3.47 <math>\pm</math> 0.01</b>	<b>1.46 <math>\pm</math> 0.01</b>	<b>2.96 <math>\pm</math> 0.06</b>
<b>UCB-B</b>					
no milling	<b>2.75 <math>\pm</math> 0.04</b>	<b>6.97 <math>\pm</math> 0.03</b>	<b>18.3 <math>\pm</math> 0.5</b>	<b>9.24 <math>\pm</math> 0.23</b>	<b>2.23 <math>\pm</math> 0.07</b>
Turrax milling	<b>2.66 <math>\pm</math> 0.00</b>	<b>6.67 <math>\pm</math> 0.03</b>	<b>17.19 <math>\pm</math> 0.31</b>	<b>8.75 <math>\pm</math> 0.20</b>	<b>2.18 <math>\pm</math> 0.04</b>
PMC	<b>1.26 <math>\pm</math> 0.03</b>	<b>2.38 <math>\pm</math> 0.05</b>	<b>4.64 <math>\pm</math> 0.13</b>	<b>2.71 <math>\pm</math> 0.05</b>	<b>1.42 <math>\pm</math> 0.05</b>

**Table A6.** Data for Figure IV 2 12 (size in  $\mu\text{m}$ ).

	<b>d (0.1) <math>\pm</math> SD</b>	<b>d (0.5) <math>\pm</math> SD</b>	<b>d (0.9) <math>\pm</math> SD</b>	<b>D[4,3] <math>\pm</math> SD</b>	<b>span <math>\pm</math> SD</b>
no milling	<b>21.9 <math>\pm</math> 0.2</b>	<b>98.7 <math>\pm</math> 0.4</b>	<b>267.2 <math>\pm</math> 0.5</b>	<b>126.2 <math>\pm</math> 0.6</b>	<b>2.48 <math>\pm</math> 0.08</b>
Turrax milling	<b>3.07 <math>\pm</math> 0.17</b>	<b>15.7 <math>\pm</math> 0.3</b>	<b>51.6 <math>\pm</math> 0.4</b>	<b>22.3 <math>\pm</math> 0.3</b>	<b>3.07 <math>\pm</math> 0.04</b>
PMC	<b>0.509 <math>\pm</math> 0.017</b>	<b>2.43 <math>\pm</math> 0.09</b>	<b>5.20 <math>\pm</math> 0.25</b>	<b>2.71 <math>\pm</math> 0.16</b>	<b>1.93 <math>\pm</math> 0.83</b>
10C 23-24000PSI	<b>0.097 <math>\pm</math> 0.005</b>	<b>0.463 <math>\pm</math> 0.012</b>	<b>2.53 <math>\pm</math> 0.10</b>	<b>0.963 <math>\pm</math> 0.063</b>	<b>5.26 <math>\pm</math> 0.11</b>
20C 23-24000PSI	<b>0.097 <math>\pm</math> 0.004</b>	<b>0.356 <math>\pm</math> 0.008</b>	<b>2.06 <math>\pm</math> 0.10</b>	<b>0.788 <math>\pm</math> 0.051</b>	<b>5.52 <math>\pm</math> 0.10</b>

**Table A7.** Data for Figure IV 2 13 (size in  $\mu\text{m}$ ).

	<b>d (0.1) <math>\pm</math> SD</b>	<b>d (0.5) <math>\pm</math> SD</b>	<b>d (0.9) <math>\pm</math> SD</b>	<b>D[4,3] <math>\pm</math> SD</b>	<b>span <math>\pm</math> SD</b>
no milling	8.78 $\pm$ 2.10	140.5 $\pm$ 11.3	340.6 $\pm$ 15.1	160.4 $\pm$ 9.4	2.37 $\pm$ 0.11
PMC 7000PSI	1.26 $\pm$ 0.02	2.16 $\pm$ 0.04	3.85 $\pm$ 0.09	2.38 $\pm$ 0.04	1.20 $\pm$ 0.03
PMC 120000PSI	0.082 $\pm$ 0.004	0.623 $\pm$ 0.282	2.75 $\pm$ 0.11	1.07 $\pm$ 0.11	5.60 $\pm$ 3.29
HPH 2C 23-24000PSI	0.082 $\pm$ 0.001	0.197 $\pm$ 0.007	1.97 $\pm$ 0.02	0.721 $\pm$ 0.011	9.63 $\pm$ 0.35
HPH 4C 23-24000PSI	0.087 $\pm$ 0.010	0.189 $\pm$ 0.033	1.72 $\pm$ 0.07	0.639 $\pm$ 0.024	8.81 $\pm$ 1.25
HPH 6C 23-24000PSI	0.084 $\pm$ 0.004	0.197 $\pm$ 0.019	1.61 $\pm$ 0.05	0.609 $\pm$ 0.019	7.79 $\pm$ 0.76
HPH 8C 23-24000PSI	0.085 $\pm$ 0.004	0.187 $\pm$ 0.016	1.53 $\pm$ 0.05	0.583 $\pm$ 0.021	7.74 $\pm$ 0.59
HPH 10C 23-24000PSI	0.086 $\pm$ 0.006	0.196 $\pm$ 0.028	1.47 $\pm$ 0.05	0.576 $\pm$ 0.027	7.17 $\pm$ 0.84
HPH 12C 23-24000PSI	0.080 $\pm$ 0.001	0.198 $\pm$ 0.011	1.40 $\pm$ 0.04	0.552 $\pm$ 0.013	6.66 $\pm$ 0.37
HPH 14C 23-24000PSI	0.081 $\pm$ 0.001	0.200 $\pm$ 0.015	1.36 $\pm$ 0.04	0.544 $\pm$ 0.016	6.43 $\pm$ 0.50
HPH 16C 23-24000PSI	0.081 $\pm$ 0.001	0.203 $\pm$ 0.010	1.31 $\pm$ 0.02	0.532 $\pm$ 0.010	6.06 $\pm$ 0.29
HPH 18C 23-24000PSI	0.081 $\pm$ 0.001	0.200 $\pm$ 0.007	1.27 $\pm$ 0.05	0.525 $\pm$ 0.018	5.98 $\pm$ 0.30
HPH 20C 23-24000PSI	0.082 $\pm$ 0.004	0.202 $\pm$ 0.019	1.14 $\pm$ 0.02	0.482 $\pm$ 0.019	5.27 $\pm$ 0.48

**Table A8.** Data for Figure IV 2 14 (size in  $\mu\text{m}$ ).

	<b>d (0.1) <math>\pm</math> SD</b>	<b>d (0.5) <math>\pm</math> SD</b>	<b>d (0.9) <math>\pm</math> SD</b>	<b>D[4,3] <math>\pm</math> SD</b>	<b>span <math>\pm</math> SD</b>
<b>no milling</b>	1.47 $\pm$ 0.03	3.00 $\pm$ 0.02	6.52 $\pm$ 0.21	3.59 $\pm$ 0.06	1.68 $\pm$ 0.07
<b>Turrax milling</b>	1.43 $\pm$ 0.03	2.92 $\pm$ 0.02	6.29 $\pm$ 0.22	3.47 $\pm$ 0.06	1.66 $\pm$ 0.07
<b>PMC 7000PSI</b>	0.129 $\pm$ 0.002	1.68 $\pm$ 0.02	4.55 $\pm$ 0.02	2.04 $\pm$ 0.02	2.63 $\pm$ 0.02
<b>PMC 120000PSI</b>	0.105 $\pm$ 0.001	1.14 $\pm$ 0.02	3.47 $\pm$ 0.01	1.46 $\pm$ 0.01	2.96 $\pm$ 0.06
<b>10C 23-24000PSI</b>	0.095 $\pm$ 0.003	0.465 $\pm$ 0.057	2.17 $\pm$ 0.07	0.867 $\pm$ 0.039	4.50 $\pm$ 0.43
<b>20C 23-24000PSI</b>	0.095 $\pm$ 0.000	0.404 $\pm$ 0.002	1.86 $\pm$ 0.00	0.755 $\pm$ 0.001	4.38 $\pm$ 0.03

**Table A9.** Data for Figure IV 2 15 (size in  $\mu\text{m}$ ).

	<b>d (0.1) <math>\pm</math> SD</b>	<b>d (0.5) <math>\pm</math> SD</b>	<b>d (0.9) <math>\pm</math> SD</b>	<b>D[4,3] <math>\pm</math> SD</b>	<b>span <math>\pm</math> SD</b>
<b>no milling</b>	2.75 $\pm$ 0.04	6.97 $\pm$ 0.03	18.26 $\pm$ 0.48	9.24 $\pm$ 0.23	2.23 $\pm$ 0.07
<b>Turrax milling</b>	2.66 $\pm$ 0.00	6.67 $\pm$ 0.03	17.19 $\pm$ 0.31	8.75 $\pm$ 0.20	2.18 $\pm$ 0.04
<b>PMC 7000PSI</b>	1.708 $\pm$ 0.037	3.17 $\pm$ 0.01	5.99 $\pm$ 0.14	3.57 $\pm$ 0.03	1.35 $\pm$ 0.06
<b>PMC 120000PSI</b>	1.264 $\pm$ 0.034	2.38 $\pm$ 0.05	4.64 $\pm$ 0.13	2.71 $\pm$ 0.05	1.42 $\pm$ 0.05
<b>10C 23-24000PSI</b>	0.094 $\pm$ 0.002	0.525 $\pm$ 0.028	1.60 $\pm$ 0.04	0.729 $\pm$ 0.021	2.87 $\pm$ 0.09
<b>20C 23-24000PSI</b>	0.085 $\pm$ 0.001	0.325 $\pm$ 0.021	1.02 $\pm$ 0.01	0.456 $\pm$ 0.010	2.89 $\pm$ 0.16

**Table A10.** Data for Figure IV 2 17 (size in  $\mu\text{m}$ ).

	<b>d (0.1) <math>\pm</math> SD</b>	<b>d (0.5) <math>\pm</math> SD</b>	<b>d (0.9) <math>\pm</math> SD</b>	<b>D[4,3] <math>\pm</math> SD</b>	<b>span <math>\pm</math> SD</b>
<b>20C 23-24000PSI</b>	0.095 $\pm$ 0.000	0.404 $\pm$ 0.002	1.86 $\pm$ 0.00	0.755 $\pm$ 0.001	4.38 $\pm$ 0.03
<b>5C 30000PSI</b>	0.098 $\pm$ 0.001	0.331 $\pm$ 0.010	1.40 $\pm$ 0.01	0.584 $\pm$ 0.005	3.94 $\pm$ 0.10
<b>10C 30000PSI</b>	0.095 $\pm$ 0.001	0.322 $\pm$ 0.007	1.29 $\pm$ 0.00	0.540 $\pm$ 0.004	3.70 $\pm$ 0.07

**Table A11.** Data for Figure IV 2 18 (size in  $\mu\text{m}$ ).

	<b>d (0.1) <math>\pm</math> SD</b>	<b>d (0.5) <math>\pm</math> SD</b>	<b>d (0.9) <math>\pm</math> SD</b>	<b>D[4,3] <math>\pm</math> SD</b>	<b>span <math>\pm</math> SD</b>
<b>20C 23-24000PSI</b>	0.085 $\pm$ 0.001	0.325 $\pm$ 0.021	1.02 $\pm$ 0.01	0.456 $\pm$ 0.010	2.89 $\pm$ 0.16
<b>5C 30000PSI</b>	0.085 $\pm$ 0.002	0.273 $\pm$ 0.005	0.907 $\pm$ 0.014	0.405 $\pm$ 0.005	3.01 $\pm$ 0.06
<b>10C 30000PSI</b>	0.086 $\pm$ 0.003	0.256 $\pm$ 0.013	0.840 $\pm$ 0.011	0.377 $\pm$ 0.007	2.96 $\pm$ 0.14

**Table A12.** Data for Figure IV 2 19 (size in  $\mu\text{m}$ ).

	<b>d (0.1) <math>\pm</math> SD</b>	<b>d (0.5) <math>\pm</math> SD</b>	<b>d (0.9) <math>\pm</math> SD</b>	<b>D[4,3] <math>\pm</math> SD</b>	<b>span <math>\pm</math> SD</b>
<b>10°C</b>	<b>0.089 <math>\pm</math> 0.003</b>	<b>0.291 <math>\pm</math> 0.006</b>	<b>1.29 <math>\pm</math> 0.07</b>	<b>0.526 <math>\pm</math> 0.022</b>	<b>4.11 <math>\pm</math> 0.03</b>
<b>45°C</b>	<b>0.097 <math>\pm</math> 0.004</b>	<b>0.356 <math>\pm</math> 0.008</b>	<b>2.06 <math>\pm</math> 0.10</b>	<b>0.788 <math>\pm</math> 0.051</b>	<b>5.52 <math>\pm</math> 0.10</b>

**Table A13.** Data for Figure IV 2 20 A/B (size in  $\mu\text{m}$ ).

<b>10°C</b>	<b>d (0.1) <math>\pm</math> SD</b>	<b>d (0.5) <math>\pm</math> SD</b>	<b>d (0.9) <math>\pm</math> SD</b>	<b>D[4,3] <math>\pm</math> SD</b>	<b>span <math>\pm</math> SD</b>
no milling	1.51 $\pm$ 0.00	3.12 $\pm$ 0.00	6.97 $\pm$ 0.02	3.79 $\pm$ 0.01	1.75 $\pm$ 0.01
turrax milling	1.33 $\pm$ 0.00	2.75 $\pm$ 0.00	6.21 $\pm$ 0.02	3.36 $\pm$ 0.01	1.77 $\pm$ 0.01
PMC 7000PSI	0.137 $\pm$ 0.002	1.84 $\pm$ 0.01	4.42 $\pm$ 0.15	2.11 $\pm$ 0.04	2.33 $\pm$ 0.09
PMC 120000PSI	0.111 $\pm$ 0.006	1.27 $\pm$ 0.09	3.40 $\pm$ 0.10	1.50 $\pm$ 0.07	2.60 $\pm$ 0.12
HPH 10C 23-24000PSI	0.093 $\pm$ 0.001	0.566 $\pm$ 0.005	2.14 $\pm$ 0.01	0.880 $\pm$ 0.005	3.61 $\pm$ 0.02
HPH 20C 23-24000PSI	0.092 $\pm$ 0.001	0.480 $\pm$ 0.007	1.84 $\pm$ 0.01	0.762 $\pm$ 0.004	3.64 $\pm$ 0.06
HPH 5C 30000PSI	0.097 $\pm$ 0.002	0.403 $\pm$ 0.021	1.43 $\pm$ 0.02	0.615 $\pm$ 0.014	3.30 $\pm$ 0.12
HPH 10C 30000PSI	0.101 $\pm$ 0.002	0.413 $\pm$ 0.008	1.33 $\pm$ 0.02	0.587 $\pm$ 0.007	2.98 $\pm$ 0.08

<b>23°C</b>	<b>d (0.1) <math>\pm</math> SD</b>	<b>d (0.5) <math>\pm</math> SD</b>	<b>d (0.9) <math>\pm</math> SD</b>	<b>D[4,3] <math>\pm</math> SD</b>	<b>span <math>\pm</math> SD</b>
no milling	1.51 $\pm$ 0.00	3.12 $\pm$ 0.00	6.97 $\pm$ 0.02	3.79 $\pm$ 0.01	1.75 $\pm$ 0.01
turrax milling	1.33 $\pm$ 0.00	2.75 $\pm$ 0.00	6.21 $\pm$ 0.02	3.36 $\pm$ 0.01	1.77 $\pm$ 0.01
PMC 7000PSI	0.138 $\pm$ 0.002	1.75 $\pm$ 0.01	4.49 $\pm$ 0.01	2.07 $\pm$ 0.01	2.49 $\pm$ 0.01
PMC 120000PSI	0.098 $\pm$ 0.006	0.787 $\pm$ 0.094	2.64 $\pm$ 0.07	1.10 $\pm$ 0.05	3.26 $\pm$ 0.30
HPH 5C 23-24000PSI	0.092 $\pm$ 0.000	0.437 $\pm$ 0.022	1.75 $\pm$ 0.03	0.721 $\pm$ 0.016	3.79 $\pm$ 0.14
HPH 10C 23-24000PSI	0.094 $\pm$ 0.002	0.357 $\pm$ 0.037	1.39 $\pm$ 0.05	0.586 $\pm$ 0.028	3.66 $\pm$ 0.25
HPH 15C 23-24000PSI	0.098 $\pm$ 0.002	0.336 $\pm$ 0.029	1.20 $\pm$ 0.03	0.523 $\pm$ 0.021	3.30 $\pm$ 0.20
HPH 20C 23-24000PSI	0.106 $\pm$ 0.002	0.357 $\pm$ 0.024	1.08 $\pm$ 0.02	0.495 $\pm$ 0.017	2.74 $\pm$ 0.12
HPH 5C 30000PSI	0.112 $\pm$ 0.004	0.367 $\pm$ 0.009	0.995 $\pm$ 0.012	0.474 $\pm$ 0.002	2.41 $\pm$ 0.11
HPH 10C 30000PSI	0.113 $\pm$ 0.003	0.354 $\pm$ 0.005	0.934 $\pm$ 0.009	0.450 $\pm$ 0.001	2.32 $\pm$ 0.07

<b>45°C</b>	<b>d (0.1) <math>\pm</math> SD</b>	<b>d (0.5) <math>\pm</math> SD</b>	<b>d (0.9) <math>\pm</math> SD</b>	<b>D[4,3] <math>\pm</math> SD</b>	<b>span <math>\pm</math> SD</b>
no milling	1.51 $\pm$ 0.00	3.12 $\pm$ 0.00	6.97 $\pm$ 0.02	3.79 $\pm$ 0.01	1.75 $\pm$ 0.01
turrax milling	1.33 $\pm$ 0.00	2.75 $\pm$ 0.00	6.21 $\pm$ 0.02	3.36 $\pm$ 0.01	1.77 $\pm$ 0.01
PMC 7000PSI	0.149 $\pm$ 0.002	1.91 $\pm$ 0.01	5.01 $\pm$ 0.01	2.31 $\pm$ 0.01	2.55 $\pm$ 0.01
PMC 120000PSI	0.113 $\pm$ 0.005	1.27 $\pm$ 0.06	3.56 $\pm$ 0.07	1.56 $\pm$ 0.05	2.72 $\pm$ 0.07
HPH 5C 23-24000PSI	0.095 $\pm$ 0.001	0.597 $\pm$ 0.010	2.17 $\pm$ 0.00	0.898 $\pm$ 0.003	3.47 $\pm$ 0.06
HPH 10C 23-24000PSI	0.093 $\pm$ 0.001	0.468 $\pm$ 0.008	1.75 $\pm$ 0.01	0.731 $\pm$ 0.001	3.54 $\pm$ 0.07
HPH 15C 23-24000PSI	0.102 $\pm$ 0.000	0.447 $\pm$ 0.002	1.39 $\pm$ 0.01	0.619 $\pm$ 0.002	2.89 $\pm$ 0.03
HPH 20C 23-24000PSI	0.104 $\pm$ 0.001	0.422 $\pm$ 0.002	1.26 $\pm$ 0.01	0.572 $\pm$ 0.003	2.75 $\pm$ 0.02
HPH 5C 30000PSI	0.107 $\pm$ 0.002	0.407 $\pm$ 0.006	1.13 $\pm$ 0.01	0.526 $\pm$ 0.004	2.52 $\pm$ 0.05
HPH 10C 30000PSI	0.109 $\pm$ 0.001	0.399 $\pm$ 0.002	1.07 $\pm$ 0.01	0.505 $\pm$ 0.004	2.40 $\pm$ 0.01

**Table A14.** Data for Figure IV 2 30 (size in  $\mu\text{m}$ ) (SD: Spray-drying, BSD: before spray-drying, F: formulation, NM: no mannitol, M: mannitol).

	<b>d (0.1) <math>\pm</math> SD</b>	<b>d (0.5) <math>\pm</math> SD</b>	<b>d (0.9) <math>\pm</math> SD</b>	<b>D[4,3] <math>\pm</math> SD</b>	<b>span <math>\pm</math> SD</b>
<b>F1 BSD</b>	<b>0.090 <math>\pm</math> 0.000</b>	<b>0.293 <math>\pm</math> 0.001</b>	<b>1.20 <math>\pm</math> 0.00</b>	<b>0.501 <math>\pm</math> 0.001</b>	<b>3.78 <math>\pm</math> 0.01</b>
<b>SD F1 NM</b>	<b>0.101 <math>\pm</math> 0.001</b>	<b>0.746 <math>\pm</math> 0.024</b>	<b>3.07 <math>\pm</math> 0.08</b>	<b>1.260 <math>\pm</math> 0.09</b>	<b>3.99 <math>\pm</math> 0.20</b>
<b>SD F1 M</b>	<b>0.103 <math>\pm</math> 0.000</b>	<b>1.10 <math>\pm</math> 0.01</b>	<b>4.21 <math>\pm</math> 0.02</b>	<b>1.67 <math>\pm</math> 0.01</b>	<b>3.73 <math>\pm</math> 0.02</b>
<b>F2 BSD</b>	<b>0.090 <math>\pm</math> 0.000</b>	<b>0.360 <math>\pm</math> 0.005</b>	<b>1.55 <math>\pm</math> 0.00</b>	<b>0.640 <math>\pm</math> 0.002</b>	<b>4.07 <math>\pm</math> 0.06</b>
<b>SD F2 NM</b>	<b>0.092 <math>\pm</math> 0.001</b>	<b>0.518 <math>\pm</math> 0.004</b>	<b>1.89 <math>\pm</math> 0.03</b>	<b>0.790 <math>\pm</math> 0.007</b>	<b>3.48 <math>\pm</math> 0.08</b>
<b>SD F2 M</b>	<b>0.091 <math>\pm</math> 0.001</b>	<b>0.458 <math>\pm</math> 0.011</b>	<b>1.72 <math>\pm</math> 0.02</b>	<b>0.719 <math>\pm</math> 0.009</b>	<b>3.57 <math>\pm</math> 0.05</b>
<b>F3 BSD</b>	<b>0.096 <math>\pm</math> 0.002</b>	<b>0.436 <math>\pm</math> 0.025</b>	<b>1.43 <math>\pm</math> 0.02</b>	<b>0.624 <math>\pm</math> 0.014</b>	<b>3.07 <math>\pm</math> 0.16</b>
<b>SD F3 NM</b>	<b>0.097 <math>\pm</math> 0.000</b>	<b>0.952 <math>\pm</math> 0.023</b>	<b>2.85 <math>\pm</math> 0.05</b>	<b>1.21 <math>\pm</math> 0.02</b>	<b>2.90 <math>\pm</math> 0.03</b>
<b>SD F3 M</b>	<b>0.092 <math>\pm</math> 0.001</b>	<b>0.594 <math>\pm</math> 0.035</b>	<b>2.11 <math>\pm</math> 0.08</b>	<b>0.879 <math>\pm</math> 0.035</b>	<b>3.40 <math>\pm</math> 0.08</b>
<b>F4 BSD</b>	<b>0.101 <math>\pm</math> 0.002</b>	<b>0.413 <math>\pm</math> 0.008</b>	<b>1.33 <math>\pm</math> 0.02</b>	<b>0.587 <math>\pm</math> 0.01</b>	<b>2.98 <math>\pm</math> 0.08</b>
<b>SD F4 NM</b>	<b>0.100 <math>\pm</math> 0.003</b>	<b>0.481 <math>\pm</math> 0.047</b>	<b>2.07 <math>\pm</math> 0.13</b>	<b>0.841 <math>\pm</math> 0.036</b>	<b>4.15 <math>\pm</math> 0.61</b>
<b>SD F4 M</b>	<b>not tested</b>				
<b>SD F5 NM</b>	<b>0.096 <math>\pm</math> 0.001</b>	<b>0.464 <math>\pm</math> 0.009</b>	<b>2.27 <math>\pm</math> 0.01</b>	<b>0.923 <math>\pm</math> 0.007</b>	<b>4.68 <math>\pm</math> 0.07</b>
<b>SD F5 M</b>	<b>not tested</b>				

**Table A15.** Data for Figure IV 2 32 (size in  $\mu\text{m}$ ).

	<b>d (0.1) <math>\pm</math> SD</b>	<b>d (0.5) <math>\pm</math> SD</b>	<b>d (0.9) <math>\pm</math> SD</b>	<b>D[4,3] <math>\pm</math> SD</b>	<b>span <math>\pm</math> SD</b>
<b>Before spray-drying</b>	<b>0.086 <math>\pm</math> 0.003</b>	<b>0.256 <math>\pm</math> 0.013</b>	<b>0.840 <math>\pm</math> 0.011</b>	<b>0.377 <math>\pm</math> 0.007</b>	<b>2.96 <math>\pm</math> 0.14</b>
<b>no mannitol</b>	<b>2.43 <math>\pm</math> 0.08</b>	<b>4.38 <math>\pm</math> 0.04</b>	<b>7.86 <math>\pm</math> 0.23</b>	<b>4.84 <math>\pm</math> 0.06</b>	<b>1.24 <math>\pm</math> 0.07</b>
<b>mannitol</b>	<b>not tested</b>				

**Table A16.** Data for Figure IV 5 7 (size in  $\mu\text{m}$ ) (% expressed w/v).

	<b>d (0.1) <math>\pm</math> SD</b>	<b>d (0.5) <math>\pm</math> SD</b>	<b>d (0.9) <math>\pm</math> SD</b>	<b>D[4,3] <math>\pm</math> SD</b>	<b>span <math>\pm</math> SD</b>
<b>NIF 5% HPMC 0.5% BSD</b>	<b>0.089 <math>\pm</math> 0.003</b>	<b>0.291 <math>\pm</math> 0.006</b>	<b>1.29 <math>\pm</math> 0.07</b>	<b>0.526 <math>\pm</math> 0.022</b>	<b>4.11 <math>\pm</math> 0.03</b>
<b>NIF 5% HPMC 0.5% chitosan 0.5% BSD</b>	<b>0.093 <math>\pm</math> 0.002</b>	<b>0.417 <math>\pm</math> 0.031</b>	<b>3.01 <math>\pm</math> 0.07</b>	<b>1.09 <math>\pm</math> 0.03</b>	<b>7.029 <math>\pm</math> 0.37</b>
<b>Flw SD (no mannitol)</b>	<b>5.79 <math>\pm</math> 0.12</b>	<b>12.1 <math>\pm</math> 0.1</b>	<b>22.1 <math>\pm</math> 0.5</b>	<b>13.0 <math>\pm</math> 0.1</b>	<b>1.35 <math>\pm</math> 0.05</b>
<b>Flw SD (mannitol)</b>	<b>0.233 <math>\pm</math> 0.043</b>	<b>10.00 <math>\pm</math> 4.80</b>	<b>32.4 <math>\pm</math> 3.3</b>	<b>13.3 <math>\pm</math> 2.6</b>	<b>3.99 <math>\pm</math> 1.90</b>

**Table A17.** Data for Figure IV 5 8 (size in  $\mu\text{m}$ ).

	<b>d (0.1) <math>\pm</math> SD</b>	<b>d (0.5) <math>\pm</math> SD</b>	<b>d (0.9) <math>\pm</math> SD</b>	<b>D[4,3] <math>\pm</math> SD</b>	<b>span <math>\pm</math> SD</b>
<b>redispersion in H2O</b>	<b>0.233 <math>\pm</math> 0.043</b>	<b>10.00 <math>\pm</math> 4.80</b>	<b>32.4 <math>\pm</math> 3.3</b>	<b>13.3 <math>\pm</math> 2.6</b>	<b>3.99 <math>\pm</math> 1.90</b>
<b>redispersion in Hac 1%</b>	<b>0.227 <math>\pm</math> 0.034</b>	<b>5.66 <math>\pm</math> 4.17</b>	<b>30.4 <math>\pm</math> 2.7</b>	<b>13.8 <math>\pm</math> 6.1</b>	<b>7.89 <math>\pm</math> 3.92</b>

**Table A18.** Results from stability studies (drug content - chemical stability) for data shown in Figures IV 8 1, IV 8 2 and IV 8 3.

NIF nanoparticles			Un-milled NIF		
25°C / 60% RH					
Time (month)	% NIF	SD	Time (month)	% NIF	SD
0	100.0	0.0	0	100.0	0.0
1	100.7	7.7	1	100.3	6.4
3	99.8	6.4	3	103.9	2.1
6	99.1	1.1	6	101.9	3.4
12	98.9	3.1	12	101.8	3.2
30°C / 65% RH					
Time (month)	% NIF	SD	Time (month)	% NIF	SD
0	100.0	0.0	0	100.0	0.0
1	105.5	2.9	1	102.0	3.6
3	101.4	3.8	3	102.6	2.5
6	97.8	1.3	6	102.5	2.0
12	97.5	2.3	12	99.3	2.3
40°C / 75% RH					
Time (month)	% NIF	SD	Time (month)	% NIF	SD
0	100.0	0.0	0	100.0	0.0
1	103.1	0.7	1	99.9	6.4
3	103.8	5.2	3	103.7	3.4
6	98.1	3.7	6	103.4	2.6
12	96.7	0.7	12	103.8	0.8

**Table A19.** Similarity factor  $f_2$  between dissolution curves of **Figures III 8 4, III 8 5 and III 8 6**. Similarity between curves verified if  $f_2$  is  $> 50$ . Comparison for U3M40 and N1M25 was not made as time points 15 and 30 min and 30 and 45 min were missing, respectively (these curves being although similar than the others if other time points are used for similarity assessment).

	U0	U1M 25	U3M 25	U6M 25	U12M 25	U1M 30	U3M 30	U6M 30	U12M 30	U1M 40	U3M 40	U6M 40	U12M 40
U0		99,02	91,04	97,96	88,52	81,48	94,01	97,62	94,16	97,23	-	97,20	79,68
U1M 25	99,02		88,95	96,23	86,09	78,76	91,72	95,54	92,38	94,47	-	94,96	77,29
U3M 25	91,04	88,95		95,42	78,94	92,56	97,18	87,26	86,45	90,20	-	87,25	72,53
U6M 25	97,96	96,23	95,42		85,10	85,21	98,29	94,94	93,37	96,43	-	94,88	77,19
U12M 25	88,52	86,09	78,94	85,10		72,48	82,47	93,05	92,00	94,66	-	92,96	92,74
U1M 30	81,48	78,76	92,56	85,21	72,48		88,03	78,77	78,70	84,13	-	78,83	67,50
U3M 30	94,01	91,72	97,18	98,29	82,47	88,03		91,68	91,75	95,37	-	91,88	75,40
U6M 30	97,62	95,54	87,26	94,94	93,05	78,77	91,68		98,05	99,06	-	99,93	88,33
U12M 30	94,16	92,38	86,45	93,37	92,00	78,70	91,75	98,05		98,11	-	98,61	83,33
U1M 40	97,23	94,47	90,20	96,43	94,66	84,13	95,37	99,06	98,11		-	98,64	88,69
U3M 40	-	-	-	-	-	-	-	-	-	-		-	-
U6M 40	97,20	94,96	87,25	94,88	92,96	78,83	91,88	99,93	98,61	98,64	-		83,35
U12M 40	79,68	77,29	72,53	77,19	92,74	67,50	75,40	88,33	83,33	88,69	-	83,35	

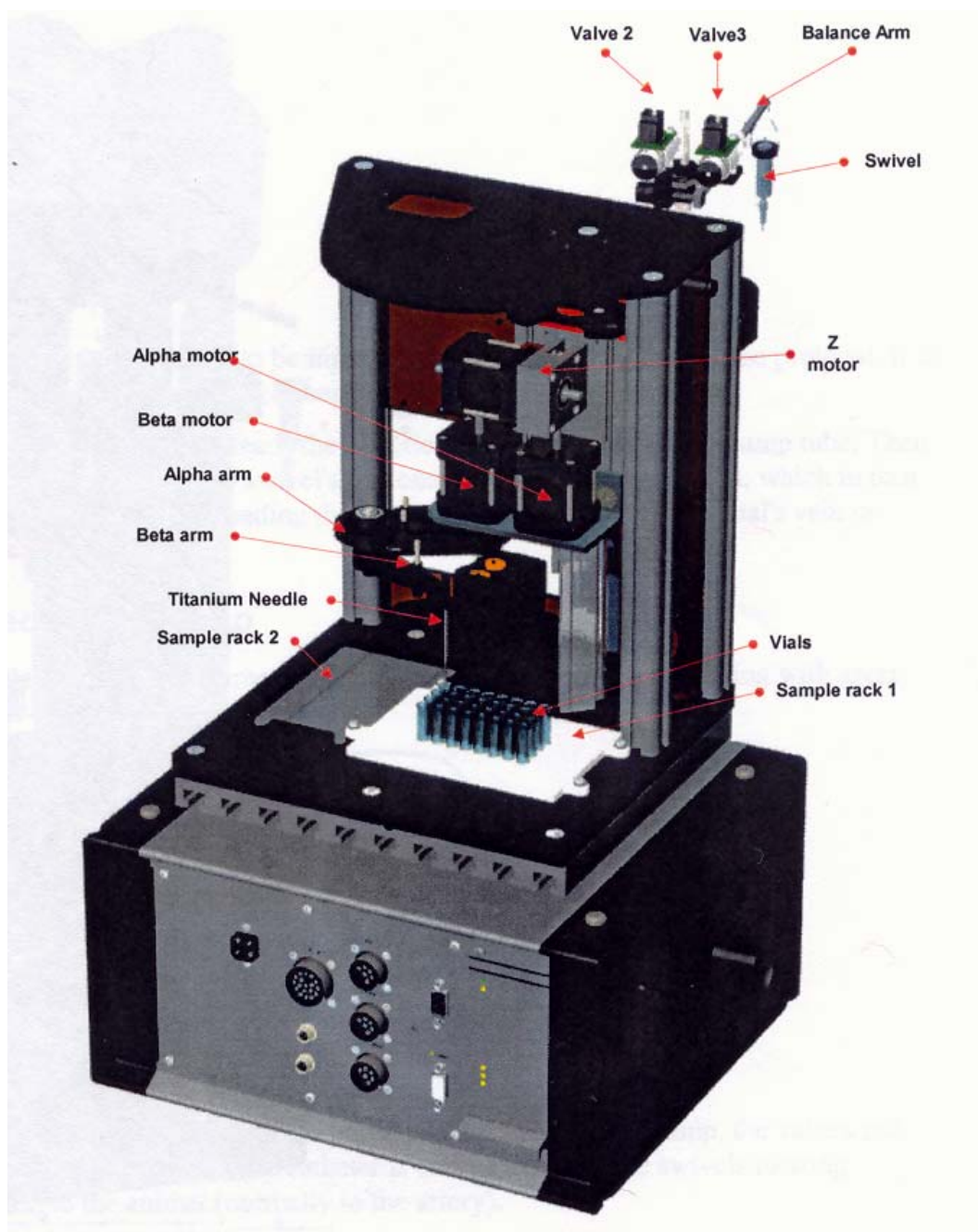
  

	NT0	N1M 25	N3M 25	N6M 25	N12M 25	N1M 30	N3M 30	N6M 30	N12M 30	N1M 40	N3M 40	N6M 40	N12M 40
NT0		-	97,50	92,30	78,89	88,72	96,79	93,59	91,79	92,72	87,14	94,70	94,21
N1M 25	-		-	-	-	-	-	-	-	-	-	-	-
N3M 25	97,50	-		93,23	77,33	86,91	96,12	94,49	89,51	92,48	90,88	95,72	91,82
N6M 25	92,30	-	93,23		73,03	80,29	97,11	99,75	83,08	83,89	83,20	99,18	85,27
N12M 25	78,89	-	77,33	73,03		90,67	76,58	73,87	88,18	82,94	75,00	74,64	85,81
N1M 30	88,72	-	86,91	80,29	90,67		84,87	81,45	98,58	94,51	83,26	82,47	96,78
N3M 30	96,79	-	96,12	97,11	76,58	84,87		98,20	88,24	87,95	84,36	98,93	90,73
N6M 30	93,59	-	94,49	99,75	73,87	81,45	98,20		84,34	85,18	83,95	99,67	86,63
N12M 30	91,79	-	89,51	83,08	88,18	98,58	88,24	84,34		94,66	83,61	85,46	99,38
N1M 40	92,72	-	92,48	83,89	82,94	94,51	87,95	85,18	94,66		90,33	86,11	95,33
N3M 40	87,14	-	90,88	83,20	75,00	83,26	84,36	83,95	83,61	90,33		84,69	84,65
N6M 40	94,70	-	95,72	99,18	74,64	82,47	98,93	99,67	85,46	86,11	84,69		87,80
N12M 40	94,21	-	91,82	85,27	85,81	96,78	90,73	86,63	99,38	95,33	84,65	87,80	

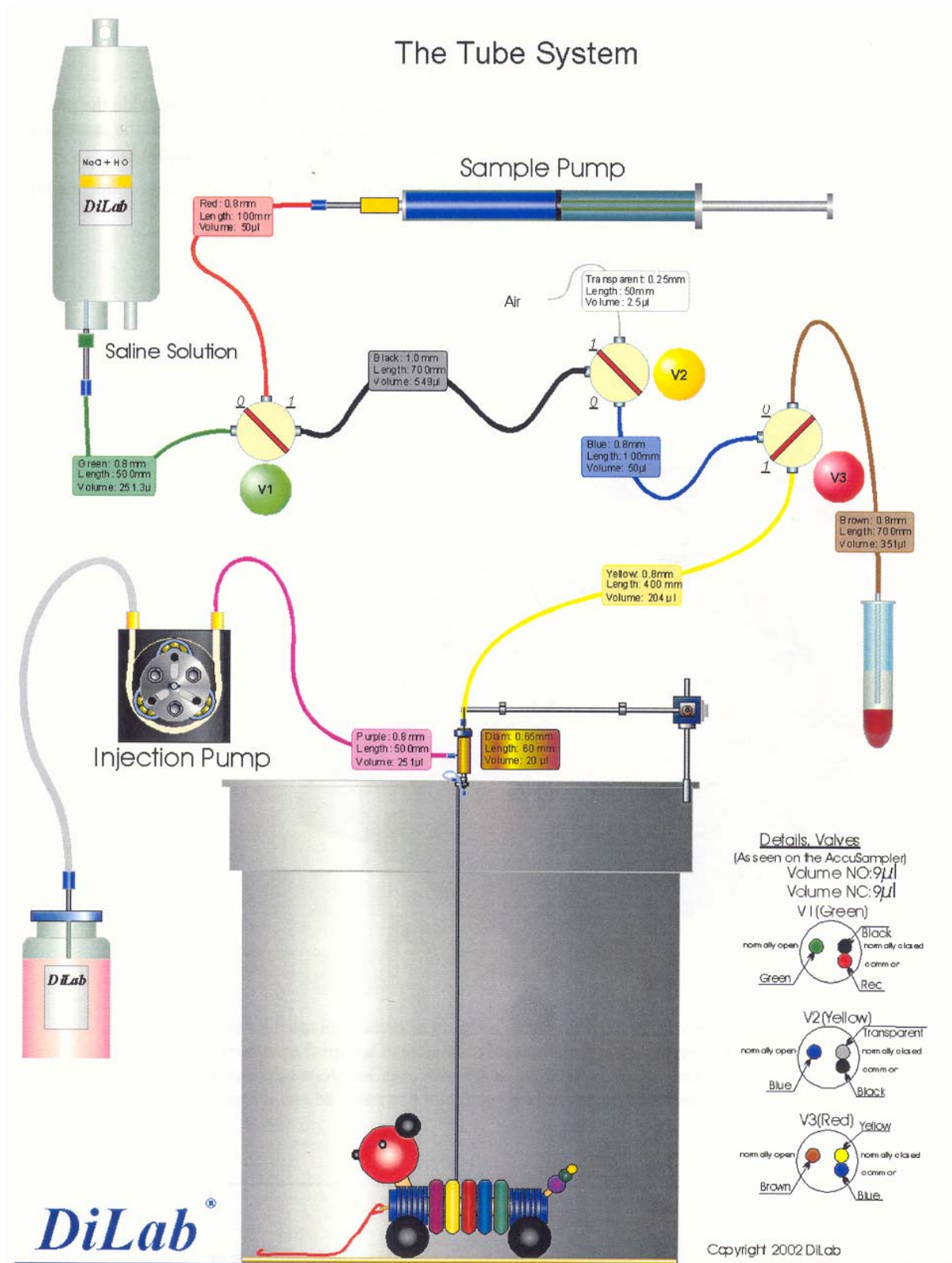
**Table A20.** Data for **Figures IV 8 7, IV 8 8 and IV 8 9** (size in  $\mu\text{m}$ ).

	$d(0.1) \pm \text{SD}$	$d(0.5) \pm \text{SD}$	$d(0.9) \pm \text{SD}$	$D[4,3] \pm \text{SD}$	$\text{span} \pm \text{SD}$
BSD	$0.093 \pm 0.003$	$0.397 \pm 0.046$	$1.82 \pm 0.07$	$0.731 \pm 0.034$	$4.40 \pm 0.47$
NT0	$0.098 \pm 0.001$	$0.581 \pm 0.016$	$2.12 \pm 0.03$	$0.879 \pm 0.008$	$3.49 \pm 0.13$
N1M 25°C	$0.098 \pm 0.003$	$0.375 \pm 0.015$	$1.92 \pm 0.05$	$0.754 \pm 0.010$	$4.87 \pm 0.29$
N3M 25°C	$0.096 \pm 0.001$	$0.389 \pm 0.020$	$1.98 \pm 0.03$	$0.774 \pm 0.006$	$4.86 \pm 0.30$
N6M 25°C	$0.099 \pm 0.002$	$0.388 \pm 0.004$	$1.90 \pm 0.03$	$0.753 \pm 0.006$	$4.64 \pm 0.05$
N12M 25°C	$0.097 \pm 0.002$	$0.411 \pm 0.031$	$1.96 \pm 0.03$	$0.776 \pm 0.008$	$4.57 \pm 0.42$
N1M 30°C	$0.096 \pm 0.002$	$0.370 \pm 0.015$	$1.90 \pm 0.04$	$0.744 \pm 0.010$	$4.89 \pm 0.25$
N3M 30°C	$0.096 \pm 0.001$	$0.386 \pm 0.015$	$1.99 \pm 0.03$	$0.777 \pm 0.006$	$4.93 \pm 0.28$
N6M 30°C	$0.097 \pm 0.002$	$0.369 \pm 0.009$	$1.94 \pm 0.05$	$0.757 \pm 0.013$	$4.99 \pm 0.19$
N12M 30°C	$0.096 \pm 0.002$	$0.421 \pm 0.034$	$2.00 \pm 0.05$	$0.792 \pm 0.015$	$4.55 \pm 0.45$
N1M 40°C	$0.098 \pm 0.002$	$0.382 \pm 0.016$	$1.90 \pm 0.05$	$0.751 \pm 0.013$	$4.72 \pm 0.30$
N3M 40°C	$0.094 \pm 0.002$	$0.408 \pm 0.011$	$2.09 \pm 0.06$	$0.812 \pm 0.015$	$4.90 \pm 0.21$
N6M 40°C	$0.095 \pm 0.002$	$0.378 \pm 0.009$	$1.98 \pm 0.07$	$0.771 \pm 0.020$	$4.99 \pm 0.21$
N12M 40°C	$0.094 \pm 0.003$	$0.418 \pm 0.025$	$2.09 \pm 0.12$	$0.815 \pm 0.033$	$4.79 \pm 0.50$

## Annex 2

**Schematic representation of the AccuSampler® (DiLab, Lund, Sweden)**





## Annex 3

**Cathétérisation de l'artère fémorale chez le rat, modèle adapté au prélèvement automatisé.****Matériel et protocole chirurgical****Matériel et produits****Matériel**

- Cathéters :
  - Artère fémorale : ReCathCo, polyuréthane, diamètre interne : 0,61 mm, diamètre externe : 1,02 mm, longueur= 60 cm. Arrêt situé à 4 cm de l'extrémité distale qui est arrondie.
- Suture : Vicryl 3-0 ou 4-0
- Colle chirurgicale : Histoacryl (Braun, Aesculap, Germany)
- Dacron button (Instech)
- Pompe : Becton Dickinson, Vial médical, Program 2, Version S, option RS 232
- Téter métallique (longueur=30 cm)
- Double cage
- Système de perfusion Instech (Swivel 2 voies 20G, bras balancier)

**Produits**

Les différentes solutions doivent être préparées stérilement.

- Iso-Bétadine savon germicide : polyvidon. Iod. 7.5% (ASTA Medica n.v.)
- Isobétadine dermique à diluer 10 fois
- Rimadyl® (carprofen, 50mg/ml), flacon de 20 ml
- Clamoxyl® RTU (amoxycilline, 150 mg/ml), flacon de 100 ml
- Natrii Chloridum 0.9% (Plurule®, Baxter, pochette de 250 ml)
- Heparinum natricum (Liquemine\*, Roche, flask 5 mL 25.000 IU/5 mL, formula: heparin.(natricum) 25.000 IU, chlorocresol. 4 mg, Natr. Sulfis, Natr. Chlorid., Natr. Hydroxid./Acid. Hydrochlorid. Ad pH 7, Aqua ad inj. Pro amp.una 5 mL).
- Solution de rinçage/ de perfusion : héparine à 25 IU/mL dans Natrii Chloridum 0.9%
- Isoflurane (Forene\*, Abbott, flask 100 ou 250 mL, formula: 1-chloro-2,2,2-trifluoroéthyl difluorométhyl ether 100 mL).

**Protocole opératoire****Anesthésie**

Le rat est placé dans la boîte à induction (isoflurane 3,5 %, débit d'O<sub>2</sub> = 2 L/min) pendant une durée moyenne de 2 minutes, après quoi il est transféré sur un plan ou un coussin chauffant (T°= environ 37°C) sur lequel il est maintenu anesthésié à l'aide d'un masque.

Le pourcentage d'isoflurane est alors réduit à 2.5 ou 2 % en fonction des besoins de l'animal.

L'anesthésie est contrôlée durant toute la chirurgie et est adaptée en fonction du stade de la chirurgie et de la réponse individuelle de chaque rat (voir la procédure opératoire : « Anesthésie générale des rongeurs »).

Généralement, le pourcentage d'isoflurane est progressivement diminué au cours de l'intervention : en fin de cathétérisation (1.5-2 %), après la fermeture de la cavité abdominale (1 %) et finalement lorsque la tunnelisation est achevée (0.5 %).

## Technique chirurgicale

Les animaux ne sont pas mis à jeun la veille de la chirurgie. Celle-ci se déroule dans des conditions d'asepsie chirurgicale.

### a) Prémédication

La prémédication se compose d'un analgésique et d'un antibiotique qui sont injectés par voie sous-cutanée à des sites différents avant de procéder à l'asepsie de la zone à inciser. L'analgésique utilisé est le Rimadyl® (carprofen) à 50mg/ml. La solution est diluée 10 fois dans une solution stérile de NaCl 0,9%. La dose à administrer est de 5 mg/kg.

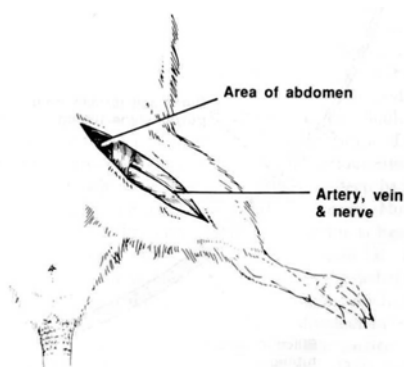
L'antibiotique utilisé est le clamoxyl® RTU. La dose à administrer est de 150 mg/kg.

### b) Désinfection des sites opératoires

- Le rat est rasé au niveau de la nuque ainsi que sur la face ventrale de l'abdomen depuis l'appendice xiphoïde du sternum, jusqu'à la hauteur des dernières mamelles, 1 à 1,5 cm de part et d'autre de la ligne médiane. On rase également la face latérale droite de l'abdomen et la face médiale de la cuisse gauche.
- La désinfection du site chirurgical se fait en faisant 2 applications alternées d'isobétadine savon et d'alcool (Isobétadine savon puis alcool, Isobétadine savon puis alcool), suivie d'une application d'isobétadine dermique. L'application des différentes solutions se fait toujours en partant du centre de la région et en allant vers la périphérie, en prenant garde de ne pas revenir vers le centre de la région à désinfecter.
- La première région à désinfecter est la région de la nuque. Quand cette étape a été réalisée, une petite incision (0,5 à 1 cm de long) est pratiquée à l'aide d'un ciseau pointu et le tissu sous cutané est légèrement dégage. Ensuite, on place une compresse stérile et légèrement humide sur la zone désinfectée et on place l'animal sur le dos pour procéder à la désinfection des face ventrale et latérale droite de l'abdomen.

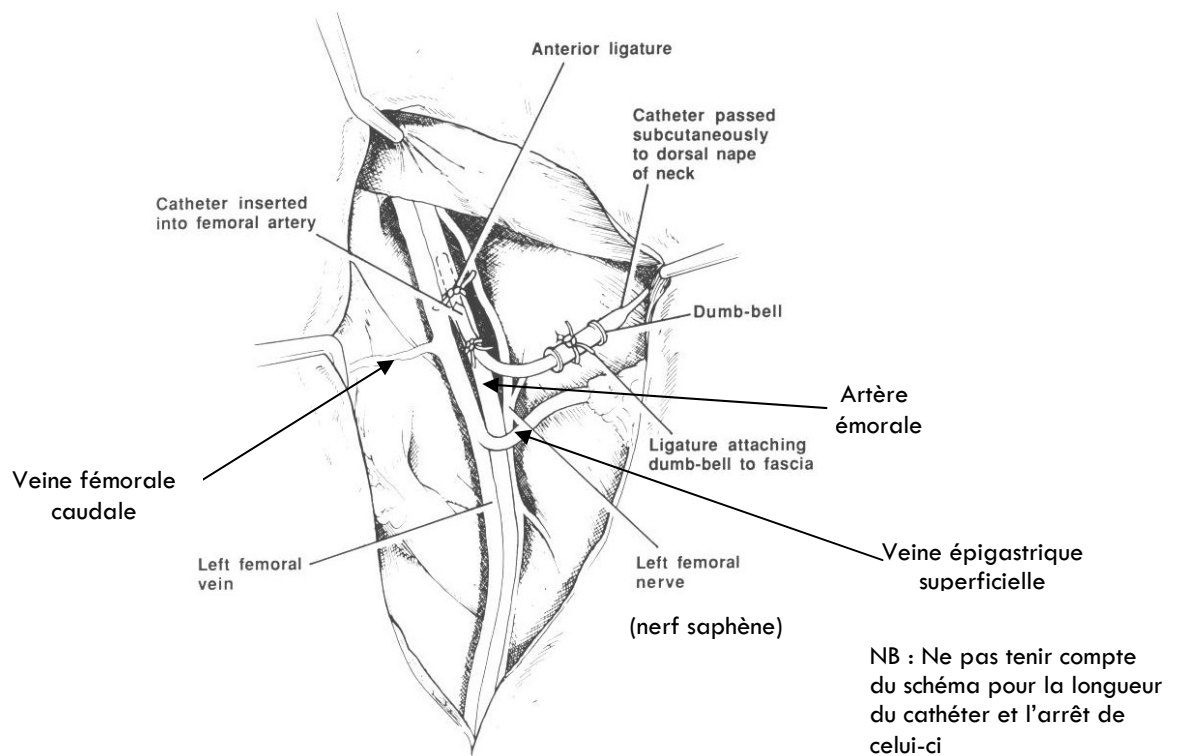
### c) Cathétérisation de l'artère fémorale

- Un champ opératoire stérile, dans lequel une incision a été pratiquée, est appliqué sur le site chirurgical à la face interne de la cuisse.
- Une incision d'environ 2 cm est pratiquée. Un guide chirurgical est introduit par l'incision située au niveau de la nuque et rejoint l'incision qui vient d'être pratiquée.

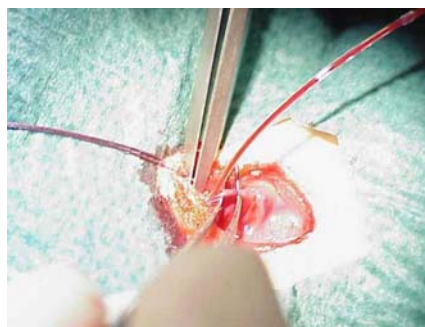


- Le cathéter est introduit à travers ce guide jusqu'à ce qu'environ 10 cm de cathéter soit accessible au niveau fémoral ; le guide est alors retiré.

- Après une dissection mousse, l'artère fémorale, située entre la veine fémorale (plus grosse) et le nerf fémoral, est localisée.
- L'artère fémorale est ligaturée un peu au-dessus de la veine épigastrique superficielle. Ensuite, elle est percée à l'aide d'une aiguille 23G recourbée.



- Le cathéter est introduit dans cette incision jusqu'à l'arrêt.



- Une ligature englobant le vaisseau et le cathéter est réalisée. Les 2 chefs de la ligature doivent revenir se lier derrière l'arrêt du cathéter pour le solidariser au vaisseau.
- Vérifier le fonctionnement du cathéter (voir plus haut)
- Une troisième ligature fixe le cathéter dans le muscle de la face médiale de la cuisse
- Le tissu sous-cutané est refermé à l'aide d'un surjet et la peau à l'aide d'un surjet intradermique.

## Soins post-opératoires

Les animaux sont hébergés individuellement et sont nourris 2 heures après la fin de la chirurgie.

On administre de la buprénorphine le lendemain et le surlendemain de la cathétérisation.

Les rats sont contrôlés deux fois par jour, excepté lors des week-end ou jours fériés (contrôle journalier, sauf avis contraire du vétérinaire ou du directeur d'étude).

1-Préliminaires: Prendre les précautions et observations "classiques" (T° / HR de la pièce, porte fermée, etc.)  
Particularités: les animaux sont plus sensibles aux bruits et aux manipulations ==> éviter de trop les manipuler

## 2-Appareillage et vue d'ensemble:

### Par convention:

**Canal 1: Veine porte (VP)**, débit de **0,1 ml/h**, position horizontale sur le swivel  
**Canal 2: Artère fémorale (AF)**, débit de **0,4 ml/h**, position verticale sur le swivel

Vérifier l'absence d'alarme sonore, de sang dans les cathéters, de fuites au niveau des raccords, le niveau des seringues, la position du cathéter.

### Flush:

Canal 1-VP

- Clamper le prolongateur et déconnecter la seringue
- Connecter une seringue de 1 ml remplie de liquide physiologique (NaCl 0,9 % avec 20 UI/ml d'héparine)
- Déclamper et administrer lentement 0,1 ml pour s'assurer du passage du liquide
- Aspirer lentement
- **Si retour du sang OK**, réadministrer 0,3 ml de liquide physiologique, camper, reconnecter, déclamper
- **En absence de sang**, réadministrer 0,2 ml de liquide physiologique, aspirer lentement et répéter jusqu'à obtention d'un retour sanguin

Avertir le technicien responsable

Canal 2-AF

- Clamper le prolongateur et déconnecter la seringue
- Connecter une seringue de 1 ml remplie de liquide physiologique (NaCl 0,9 % avec 20 UI/ml d'héparine)
- Déclamper et administrer lentement 0,1 ml pour s'assurer du passage du liquide
- Aspirer lentement
- **Si retour du sang OK**, réadministrer 0,3 ml de liquide physiologique, camper, reconnecter, déclamper
- **En absence de sang**, réadministrer 0,2 ml de liquide physiologique, aspirer lentement et répéter jusqu'à obtention d'un retour sanguin

Avertir le technicien responsable

### Recharge seringue

Clamper le prolongateur et déconnecter la seringue  
 Recharger la seringue avec du liquide physiologique (NaCl 0,9 % avec 20 UI/ml d'héparine)  
 Reconnecter et déclamper

3-Soins:

Vérifier l'identité de l'animal par rapport à la feuille de suivi (nature de la chirurgie)

**JOUR 1**

- a) Changer le bac et mettre sur sciure
- b) Contrôler l'état général de l'animal et l'état des sutures
- c) Administrer les médicaments. Réaliser l'administration **en sous cutanée**, à **deux**, en tenant compte du **trajet des cathéters**

<b>CLAMOXYL<sup>®</sup></b> (antibiotique)	<b>RIMADYL<sup>®</sup></b> (anti-inflammatoire)
Dose : <b>1 ml/kg de rat</b>	<b>Diluer 10 fois</b> le produit avec du liquide physiologique et injecter <b>1 ml de ce mélange/kg de rat</b>
Agiter et administrer en SC avec une aiguille 23 G	Retourner le mélange plusieurs fois et administrer en SC avec une aiguille 23 G

- d) Flusher les cathéters (cfr 3-Appareillage)
- e) Donner boisson et nourriture si nécessaire
- f) Remplir la feuille de suivi (et noter les remarques éventuelles)

**JOUR 2** Répéter les étapes b, c, d, e et f**JOUR 3** Répéter les étapes b, c, d, e et f**JOUR 4 et suivants:** Répéter les étapes b, e, et f

## Annex 4

**Articles :**

- Hecq, J., Deleers, M., Fanara, D., Vranckx, H., Amighi, K., **2005**. Preparation and characterization of nanocrystals for solubility and dissolution rate enhancement of nifedipine. Int. J. Pharm., 299 (1-2), 167-177.
- Hecq, J., Deleers, M., Fanara, D., Vranckx, H., Boulanger P., Le Lamer, S., Amighi, K., **2006**. Preparation and in vitro/in vivo evaluation of nano-sized crystals for dissolution rate enhancement of ucb-35440-3, a highly-dosed poorly water-soluble weak base. Eur. J. Pharm. Biopharm. 64 (3), 360-368.

## Pharmaceutical Nanotechnology

# Preparation and characterization of nanocrystals for solubility and dissolution rate enhancement of nifedipine

J. Hecq<sup>a</sup>, M. Deleers<sup>b</sup>, D. Fanara<sup>b</sup>, H. Vranckx<sup>b</sup>, K. Amighi<sup>a,\*</sup><sup>a</sup> *Laboratory of Pharmaceutics and Biopharmaceutics, Université Libre de Bruxelles, Campus Plaine, CP 207, Boulevard du Triomphe, Brussels 1050, Belgium*<sup>b</sup> *UCB S.A., Department of Product Process and Analytical Developments, Chemin du Foriest, Braine-l'Alleud 1420, Belgium*

Received 28 February 2005; received in revised form 10 May 2005; accepted 18 May 2005

## Abstract

Poorly water-soluble drugs such as nifedipine (NIF) ( $\sim 20 \mu\text{g/ml}$ ) offer challenging problems in drug formulation as poor solubility is generally associated to poor dissolution characteristics and thus to poor oral bioavailability. In order to enhance these characteristics, preparation of nifedipine nanoparticles has been achieved using high pressure homogenization. The homogenization procedure has first been optimized in regard to particle size and size distribution. Nanoparticles were characterized in terms of size, morphology and redispersion characteristics following water-removal. Saturation solubility and dissolution characteristics were investigated and compared to the un-milled commercial NIF to verify the theoretical hypothesis on the benefit of increased surface area. Crystalline state evaluation before and following particle size reduction was also conducted through differential scanning calorimetry (DSC) and powder X-ray diffraction (PXRD) to denote eventual transformation to amorphous state during the homogenization process. Through this study, it has been shown that initial crystalline state is maintained following particle size reduction and that the dissolution characteristics of nifedipine nanoparticles were significantly increased in regards to the commercial product. The method being simple and easily scaled up, this approach should have a general applicability to many poorly water-soluble drug entities.

© 2005 Elsevier B.V. All rights reserved.

**Keywords:** Nanoparticles; Drugs; High pressure homogenization; Dissolution; Crystalline state; Nifedipine

## 1. Introduction

Together with membrane permeability, the solubility/dissolution behaviour of a drug is a key determi-

nant to its oral bioavailability, the latest frequently being the rate-limiting step to absorption of drugs from the gastrointestinal tract. Since an increasing number of newly developed drug candidates present poor water-solubility, approaches to overcome this factor are of great importance in drug formulation. Nifedipine (NIF) (Fig. 1), a highly potent calcium-channel blocker

\* Corresponding author. Tel.: +32 2 650 5254; fax: +32 2 650 5269.  
E-mail address: [kamighi@ulb.ac.be](mailto:kamighi@ulb.ac.be) (K. Amighi).

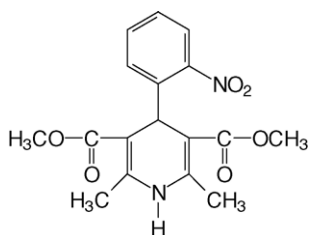


Fig. 1. Chemical structure of nifedipine (1,4-dihydro-2,6-dimethyl-4-(2-nitrophenyl)-3,5-pyridine-dicarboxylic acid dimethyl ester).

belonging to the group of 1,4-dihydropyridines widely used in the treatment of vascular diseases such as hypertension and angina pectoris, was used as a model drug.

Formulations approaches that have been reported, with mixed results, for dissolution rate enhancement of NIF include compaction with hydroxy-propylmethylcellulose (HPMC) (Mitchell et al., 2003), cogrinding with HPMC (Sugimoto et al., 1998) or bile salts (Suzuki et al., 2001), formation of solid dispersions as coprecipitates or coevaporates with mannitol (Zajc et al., 2005), phosphatidylcholine esters (Yamamura and Rogers, 1996), HPMC (Cilurzo et al., 2002), chitosan derivatives (Portero et al., 1998), polyethylene glycols (Lin and Cham, 1996; Sencar-Bozic et al., 1997) and polyoxyethylene–polyoxypropylene copolymers (Vippagunta et al., 2002), and inclusion complexes with beta-cyclodextrins (Hirayama et al., 1994; Bayomi et al., 2002).

In addition to the general solubility enhancement techniques described above, drug particle size reduction has often been used, in regards to the Noyes–Whitney and Ostwald–Freundlich equations, to enhance dissolution and solubility characteristics of poorly water-soluble compounds (Hintz and Johnson, 1989; Lu et al., 1993; Kondo et al., 1993a,b; Mosharraf and Nyström, 1995). Although micronization of drugs to micrometer-range sizes has been shown insufficient in this purpose (Müller et al., 2001), formation of drug nanoparticles is actually a very promising approach. Particle size reduction to the nanometer-range can be achieved through high pressure homogenization (HPH). This technique has been extensively described relative to particle size reduction efficiency by Müller et al. in respect with reproducibility (Grau et al., 2000) and processing of highly concentrated suspensions (Krause and Müller, 2001). It presents various

advantages over other milling techniques as it is very simple, time-saving and is a solvent-free process.

In this study, HPH was evaluated for NIF nanoparticle preparation. NIF nanoparticles were assayed for their dissolution and solubility behaviour to confirm theoretical enhancement predictions. NIF crystalline state was also evaluated before and following particle size reduction as another advantage of nanoparticulate systems relative to other dissolution rate-enhancing methods, such as solid dispersions, is that initial crystalline state shall be maintained; the method thus not relying on the presence of the amorphous form of the drug, which is characterized by long-term time instability, for the solubility/dissolution rate increase. Optimization of formulations has also been achieved through dispersion of nanoparticles in highly hydrophilic carriers such as mannitol to prevent particle agglomeration in powdered state and further increase dissolution characteristics. This agglomeration phenomenon, inherent to nanoparticulate systems, was thought in various *in vivo* studies, to limit the dissolution rate enhancement advantage procured by particle size reduction (Liversidge and Cundy, 1995).

## 2. Materials and methods

### 2.1. Materials

NIF was purchased from Indis (Aarteseelaar, Belgium). Methocel E15 (hydroxy-propylmethylcellulose) was purchased from Colorcon (West Point, PA, USA). Mannitol was purchased from Roquette (Roquette Frères, Lestrem, France). Water used was obtained through a CFOF 01205 Milli-Q Water Purification System (Millipore Corporation, Bedford, MA, USA). The other materials were of analytical reagent grade.

Nifedipine being a highly photolabile compound, all experiments were performed under subdued light; the photodegradation rate constant being indeed found to increase with decreasing particle size when NIF is in powder state (Teraoka et al., 1999).

### 2.2. Preparation of samples

The steps in the preparation of drug nanoparticles were as follows.



### 2.2.1. Formation of drug nanosuspensions

Nifedipine powder was poured in an aqueous surfactant solution (5% NIF, w/v, suspensions) under magnetic stirring (500 rpm). After dispersion, a first size-reduction step using an Ultra-Turrax T25 Basic homogenizer (IKA-Werke, Staufen, Germany) at 24,000 rpm (10 min for a 50 ml sample) was conducted on the suspension (in an ice bath to prevent sample temperature increase). Nanosuspensions were then prepared using an EmulsiFlex-C5 high pressure homogenizer (Avestin Inc., Ottawa, Canada). Pre-milling low pressure homogenization cycles (C) were first conducted on the NIF suspension to further decrease particle size (15C 7000 PSI–10C 12,000 PSI). High pressure homogenization was then finally applied for 20 cycles at 24,000 PSI. Since HPH causes sample temperature increase (increase of 30 °C following 20C at 24,000 PSI), all operations were carried out using an heat exchanger, placed ahead of the homogenizing valve, with sample temperature maintained at  $10 \pm 1$  °C. Samples were withdrawn after the different size reduction steps for size distribution analysis.

### 2.2.2. Water-removal

Spray-drying using a Büchi B191a Mini Spray-Dryer (Büchi, Flawil, Switzerland) was applied in order to retrieve nanoparticles in dried-powder state from the nanosuspensions described above. Suspensions were passed at a spray rate of 3.5 ml/min. The drying temperature was set at 115 °C. Spray airflow was set at 800 l/h and drying airflow was set at 35 m<sup>3</sup>/h.

### 2.3. Particle size and shape characterization

Size and size distribution of the particles in suspension following the different homogenization steps and in dried state following water redispersion were determined through laser diffraction (LD), with a wet sampling system (MasterSizer 2000, Malvern Instruments, Worcestershire, UK) and the diameters reported were calculated using volume distribution (three sets of five measurements). The median volume particle size,  $d(v; 0.5)$  (size of the particles for which 50% of the sample volume contains particles smaller than “ $d$  0.5”, the other particles being larger than “ $d$  0.5”),  $d(v; 0.1)$  and  $d(v; 0.9)$  were used as characterization parameters. Estimated specific surface areas of dispersed particles (m<sup>2</sup>/g) were also retrieved from LD data. A

refractive index of 1.54 was used for measurements. Morphological evaluation of nanoparticles was conducted through scanning electron microscopy (SEM) (JSM-6100, JEOL, Tokyo, Japan) following platinum coating.

### 2.4. Dissolution

A Distek 2100C USP dissolution apparatus (Distek Inc., North Brunswick, NJ, USA) Type II (paddle method) at rotation speed of 60 rpm was used for in vitro testing of drug dissolution from the various formulations. Dissolution was carried out on an equivalent of 10 mg of nifedipine (in powder state). Deionized water (0.05% polysorbate 20) was used as the dissolution medium. The volume, pH and temperature of the dissolution medium were 900 ml, 7.0 and  $37.0 \pm 0.2$  °C, respectively. Automatic withdrawals at fixed times were filtered in-line and assayed through ultraviolet absorbance determination at 235 nm using an Agilent 8453 UV/vis Dissolution Testing System (Agilent, USA). The mean results of triplicate measurements and the standard deviation were reported.

### 2.5. Solubility

Saturation solubility measurements were assayed through ultraviolet absorbance determination at 235 nm using an Agilent 8453 UV/vis Spectrophotometer (Agilent). Fifty millilitres of suspensions (water pH 7.0–0.05% polysorbate 20) (nifedipine content = 2 mg/ml) prepared from NIF in powder state, was placed at a temperature of  $37 \pm 0.1$  °C and shaken at 150 min<sup>-1</sup> using a GFL 1086 shaker—thermostatic cabinet (Labortechnik, Burgwedel, Germany). Both micro- and nanosuspensions were filtered using 0.1 µm Millex-VV PVDF filters (Millipore Corporation) prior to analysis. The mean results of triplicate measurements and the standard deviation were reported.

### 2.6. Crystalline state evaluation of dried samples

#### 2.6.1. Differential scanning calorimetry (DSC)

Thermal properties of the powder samples were investigated with a Perkin-Elmer DSC-7 differential scanning calorimeter/TAC-7 thermal analysis controller with an intracooler-2 cooling system (Perkin-Elmer Instruments, USA). The amount of product to

be analyzed shall range from 3 to 5 mg and be placed in perforated aluminium sealed 50  $\mu$ l pans. Heat runs for each sample has been set from 40 to 200 °C at 5 °C/min, using nitrogen as blanket gas. The apparatus is indium/cyclohexane calibrated.

### 2.6.2. Powder X-ray diffraction (PXRD)

PXRD diffractograms of each of the excipients, and all of the un-milled and milled nifedipine formulations were recorded using a Siemens Diffractometer D5000 (Siemens, Germany) with a Cu line as the source of radiation. Standard runs using a 40 kV voltage, a 40 mA current and a scanning rate of 0.02° min<sup>-1</sup> over a 2 $\theta$  range of 3–40° were used.

## 3. Results and discussion

Commercial nifedipine used for this study was characterized by relatively large particles ( $d(v; 0.5)$  about 100  $\mu$ m as reported in Table 1) and had to follow preliminary size reduction steps prior to high pressure homogenization operation as the homogenizing gaps of the homogenizer are too small at the homogenizing pressures used (i.e. 25  $\mu$ m at 22,000 PSI; Müller et al., 2001). Table 1 shows the results of size analysis following the different size reduction steps and indicate that the low pressure pre-milling homogenization cycles are not sufficient for adequate particle size reduction achievement as they only yield a small percentage of sub-micrometer sized particles (18% in volume below 1  $\mu$ m). High pressure homogenization cycles were found necessary in that regard; yielding a nanoparticle population with a  $d(v; 0.5)$  around 300 nm and 86% (in volume) of the particles below 1  $\mu$ m. The small fraction of microparticles left after the HPH cycles, responsible for a bimodal size distribution curve, indicate the limitations of the apparatus. These microparticles can eventually be eliminated by simple centrifugation.

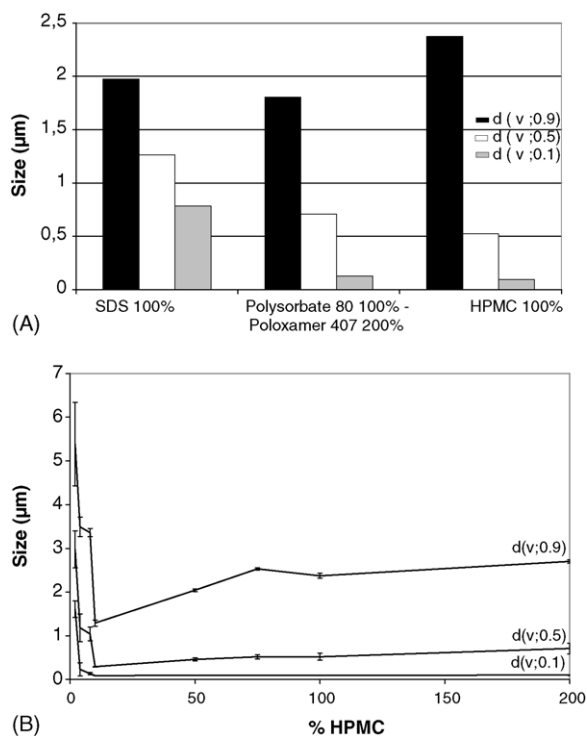


Fig. 2. (A) Influence of type of surfactant and (B) influence of HPMC % on NIF particle size reduction efficiency (all % expressed relative to NIF content, w/w).

HPMC of low viscosity grade was used for the suspension's stabilization as this water-soluble polymer offers adequate surface active properties when compared to other commonly used surfactants such as sodium dodecyl sulphate, polysorbates and poloxamers (ethylene oxide/propylene oxide copolymer). Indeed, a surfactant being necessary for nanoparticle stabilization after the homogenization operation, HPMC was found to yield the best results in regards to NIF particle size reduction efficiency (Fig. 2A). Furthermore, HPMC also has the advantage of having a high melting point when compared to polysorbates and poloxam-

Table 1

LD results following successive size reduction steps for a nifedipine 5%–HPMC 0.5% (w/w) suspension

Milling operation	$d(v; 0.5) \pm \text{S.D.} (\mu\text{m})$	$d(v; 0.1) \pm \text{S.D.} (\mu\text{m})$	$d(v; 0.9) \pm \text{S.D.} (\mu\text{m})$
No milling	98.7 $\pm$ 0.4	21.9 $\pm$ 0.2	267.2 $\pm$ 0.5
Turrax® milling	15.7 $\pm$ 0.3	3.07 $\pm$ 0.17	51.6 $\pm$ 0.4
Pre-milling HPH	2.43 $\pm$ 0.09	0.509 $\pm$ 0.017	5.20 $\pm$ 0.25
HPH 24,000 PSI	0.291 $\pm$ 0.006	0.089 $\pm$ 0.003	1.29 $\pm$ 0.07

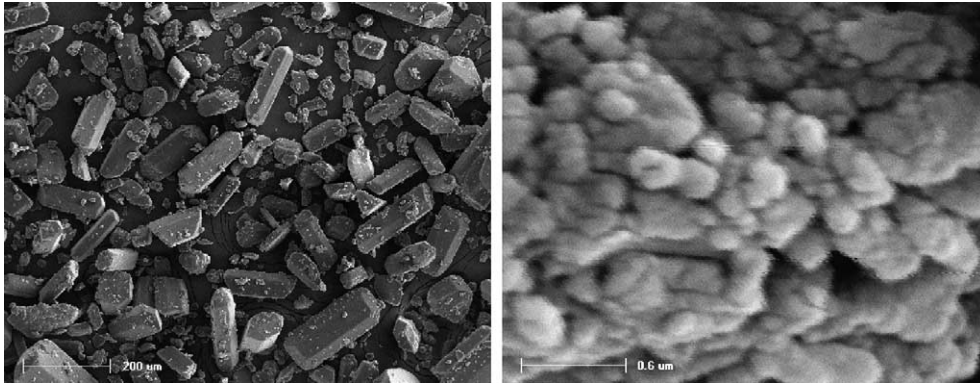


Fig. 3. SEM micrographs of un-milled commercial nifedipine (left) (magnification 100 $\times$ ; scale = 200  $\mu$ m); spray-dried nifedipine nanosuspension (right) (magnification 40,000 $\times$ ; scale = 0.6  $\mu$ m).

ers; a low melting point being problematic during the spray-drying operation (particle agglomeration) particularly if no carriers are used. An HPMC concentration of 10% (w/w) relative to nifedipine content was found optimal (Fig. 2B), over a range of 2–200%, in regards to particle size reduction and to suspension processing (i.e. increase in sample viscosity with increasing HPMC %).

NIF nanoparticles being prepared in a suspension state, water needs to be removed after the homogenization operation in order retrieve particles in a powder state for storage purpose and for the various assays conducted. As expected, nanoparticle agglomeration following the water-removal operation is clearly observed on SEM micrographs of Fig. 3 and represented through particle size analysis after redispersion (Fig. 4; Table 2) where the nanoparticle population has completely disappeared (% of particles in volume below 1  $\mu$ m < 1%) leaving a population with a  $d(v; 0.5)$  around 4  $\mu$ m. This agglomeration leading to a decrease in specific surface area (Table 2) and thus to a predicted decrease in dissolution rate, a water-soluble carrier was used to prevent this phenomenon; its role being to recrystallize around

NIF nanoparticles during the water-removal operation, thus preventing particle interaction and agglomeration. The carrier used was mannitol, added at 100% (w/w) relative to nifedipine content (Table 3) prior to the spray-drying operation. Fig. 4 and Table 2 show the results of size analysis following water-redispersion (magnetic stirring 300 rpm for 10 min) for mannitol and mannitol-less formulations. The influence of the carrier was clearly shown to be beneficial and critical regarding prevention of nanoparticle agglomeration as original particle size is restored. Mannitol, being a highly water-soluble compound, shall also procure the advantage of creating a highly hydrophilic environment around NIF nanoparticles.

Dissolution profiles for nifedipine un-milled crystals and nifedipine nanoparticles for mannitol-less and mannitol-added formulations are shown in Fig. 5. Comparison of the profiles obtained for the mannitol-less formulation and un-milled NIF clearly shows the dissolution rate enhancement obtained with nano-sized systems as 95% of the drug is dissolved following 60 min to 5% for the un-milled drug. Complete dissolution coming after about 90 min for nifedipine nanoparticles.

Table 2  
LD results following water-redispersion of spray-dried formulations A and B

Formulation	$d(v; 0.5) \pm \text{S.D.}$ ( $\mu$ m)	$d(v; 0.1) \pm \text{S.D.}$ ( $\mu$ m)	$d(v; 0.9) \pm \text{S.D.}$ ( $\mu$ m)	Below 1 $\mu$ m (%)	Estimated specific surface area ( $\text{m}^2/\text{g}$ )
Before spray-drying	$0.291 \pm 0.006$	$0.089 \pm 0.003$	$1.29 \pm 0.07$	86	29.9
Spray-dried formulation A	$3.70 \pm 0.09$	$1.73 \pm 0.04$	$8.60 \pm 0.33$	<1	1.88
Spray-dried formulation B	$0.339 \pm 0.006$	$0.093 \pm 0.002$	$1.60 \pm 0.04$	80	27.5

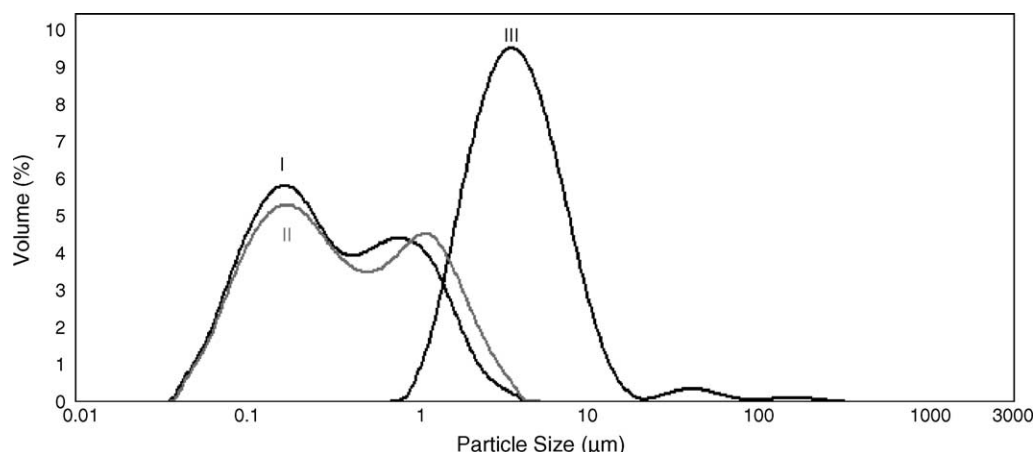


Fig. 4. LD volume size distribution curves prior to spray-drying (I) and after water-redispersion (magnetic stirring: 300 rpm for 10 min) of spray-dried formulations A (II) and B (III).

Fig. 5 also reports the influence of HPMC, a hydrophilic polymer, on un-milled drug dissolution characteristics. HPMC was shown to only slightly enhance the dissolution of un-milled nifedipine when both were physically mixed; the effect being more pronounced following hydrophylization of the drug particles (spray-dried formulation A prior to size reduction operations), as these are now homogeneously coated with the water-soluble polymer.

NIF micrometer-sized particles, obtained after Turrax<sup>®</sup> milling ( $d(v; 0.5) = 15 \mu\text{m}$ ), were also assayed for their dissolution behaviour (Fig. 5). The approximate 10-fold decrease in particle size from the un-milled commercial NIF, accompanied by a surface area increasing from  $0.134$  to  $0.758 \text{ m}^2/\text{g}$ , yielded a 19-fold increase in dissolution rate (DR) at the beginning of dissolution ( $0.019$ – $0.366 \text{ mg}/\text{min}$ ). Although the DR enhancement is clearly shown, it is still limited and

smaller than the one obtained with NIF nanoparticles ( $1.09$  and  $3.77 \text{ mg}/\text{min}$  for formulations A and B, respectively), this mainly due to higher specific surface area achievement with the latest ( $1.88$  and  $27.5 \text{ m}^2/\text{g}$  for formulations A and B, respectively; Table 2).

Dissolution profiles for mannitol-less and mannitol-added NIF formulations are also compared on Fig. 5. This water-soluble additive is shown to further increase the NIF nanoparticle DR as 75% of the drug is already dissolved after 2 min versus 20% for formulation A. Complete dissolution being reached after only 10 min versus 90 min for formulation A. The difference observed between formulations A and B shall be attributed to the fact that mannitol acts as a carrier preventing particle agglomeration during the spray-drying operation (Fig. 4; Table 2) and that it creates a highly hydrophilic environment around NIF nanoparticles beneficial for drug dissolution. No correlations can be made between surface areas and DR for both systems as surface areas have been estimated through LD data and that, for formulation A, it is not representative of the effective surface area directly in contact with the dissolution medium. Formulation A is in fact represented by agglomerates of nanoparticles thought to show high porosity and thus having an effective surface area greater than the  $1.88 \text{ m}^2/\text{g}$  value found. Direct correlations will only be found when agglomeration is limited as in the case of formulation B versus un-milled NIF, where an approximate 200-fold increase in surface results in a 200-fold increase in DR.

Table 3  
Nifedipine formulations A and B

Formulation A	
Nifedipine	5%
Methocel E15	0.5%
H <sub>2</sub> O	Ad 100%
Formulation B	
Nifedipine	5%
Methocel E15	0.5%
Mannitol	5%
H <sub>2</sub> O	Ad 100%

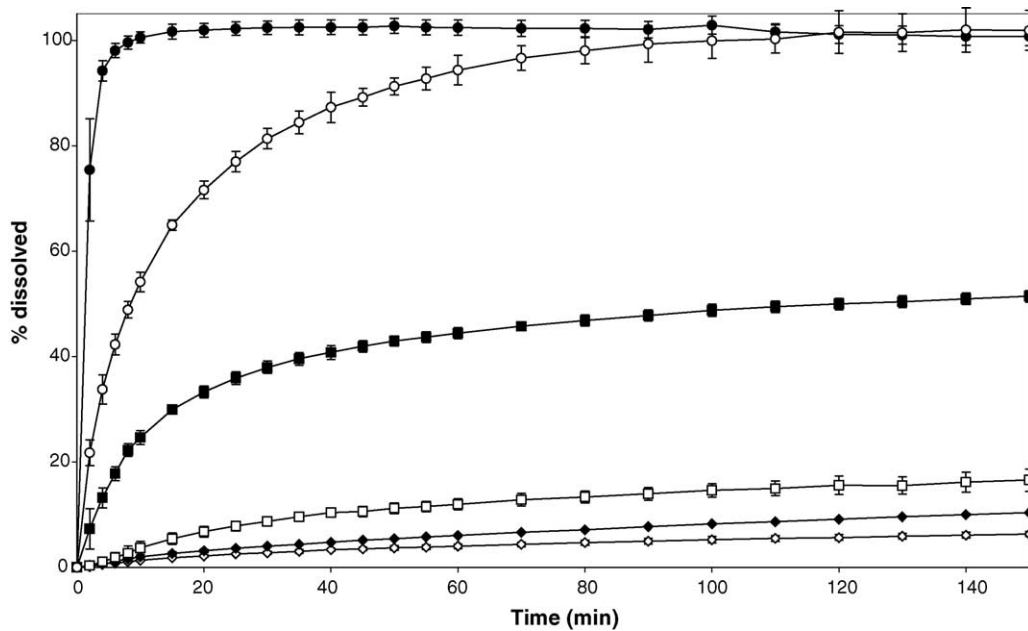


Fig. 5. Dissolution profiles for: (◇) un-milled commercial NIF; (◆) NIF/HPMC, 10:1 (w/w) physical mixture (mortar); (□) spray-dried formulation A (no milling); (■) spray-dried formulation A (Turrax<sup>®</sup> milling); (○) spray-dried formulation A (HPH milling); (●) spray-dried formulation B (HPH milling).

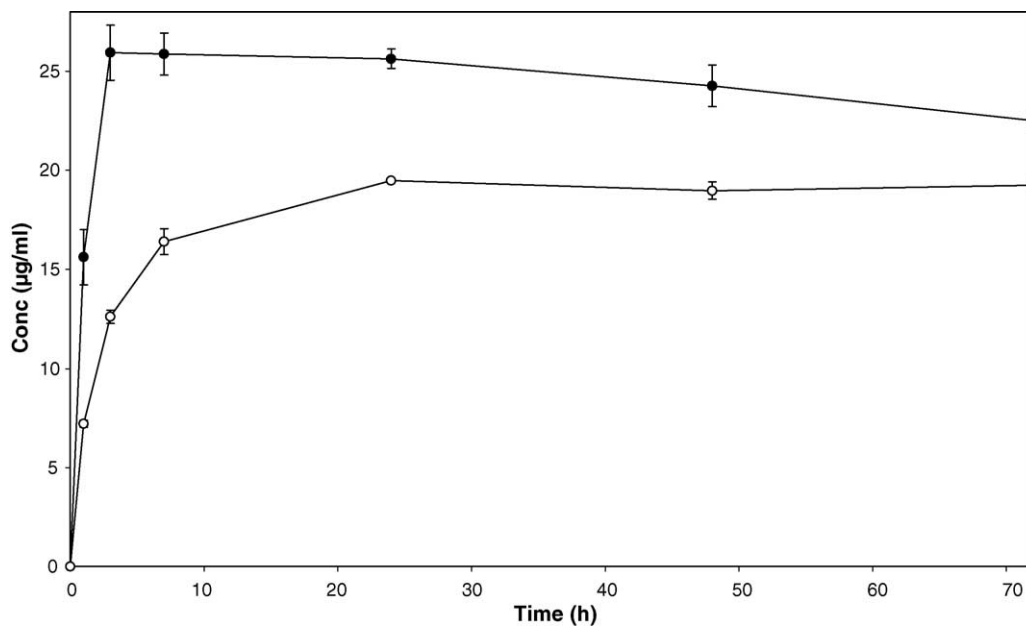


Fig. 6. Kinetics to saturation solubility achievement (37 °C) for: (○) un-milled commercial NIF and (●) and spray-dried formulation B (HPH milling).

Besides the obvious DR enhancement characteristics, NIF nanoparticles also show, to a lesser extent, increased saturation solubility when compared to the un-milled commercial drug (Fig. 6). At 37 °C, commercial NIF shows a water-solubility of  $19.5 \pm 0.1 \mu\text{g/ml}$ ; concentration reached after 24 h. For NIF nanoparti-

cles, a concentration of  $25.9 \pm 1.4 \mu\text{g/ml}$  was reached after 3 h. This concentration was, however, further shown to decrease slowly with time indicating achievement of a super-saturated NIF media.

In order to verify that this dissolution rate/solubility enhancement is not due to the presence of NIF

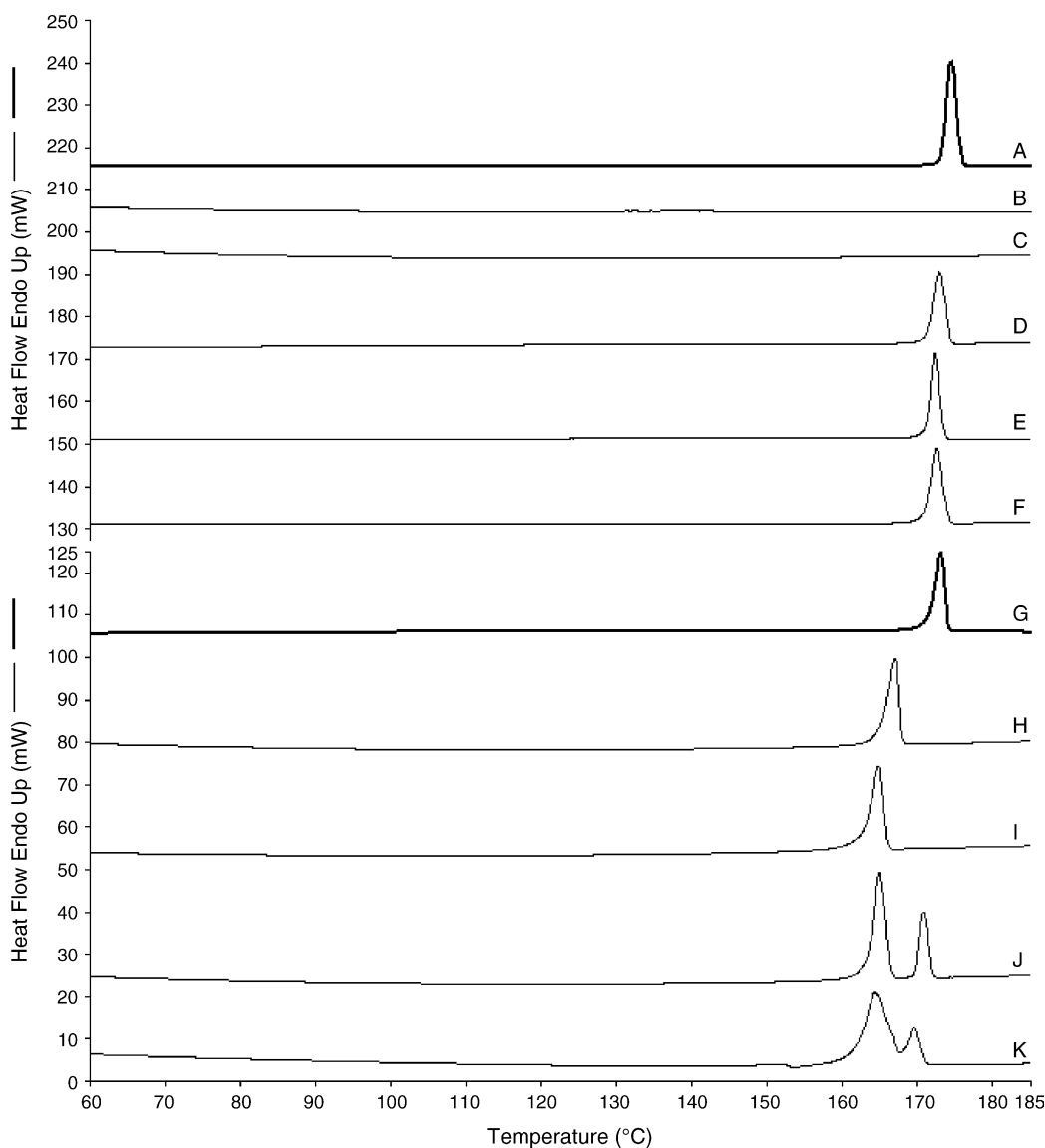


Fig. 7. DSC thermograms for: (A) un-milled commercial NIF; (B) HPMC; (C) spray-dried HPMC; (D) NIF/HPMC, 10:1 (w/w) physical mixture (mortar); (E) spray-dried formulation A (no-milling); (F) spray-dried formulation A (Turrax® milling); (G) spray-dried formulation A (nanoparticles); (H) mannitol; (I) spray-dried mannitol; (J) NIF/HPMC/mannitol, 10:1:10 (w/w) physical mixture (mortar); (K) spray-dried formulation B (nanoparticles).

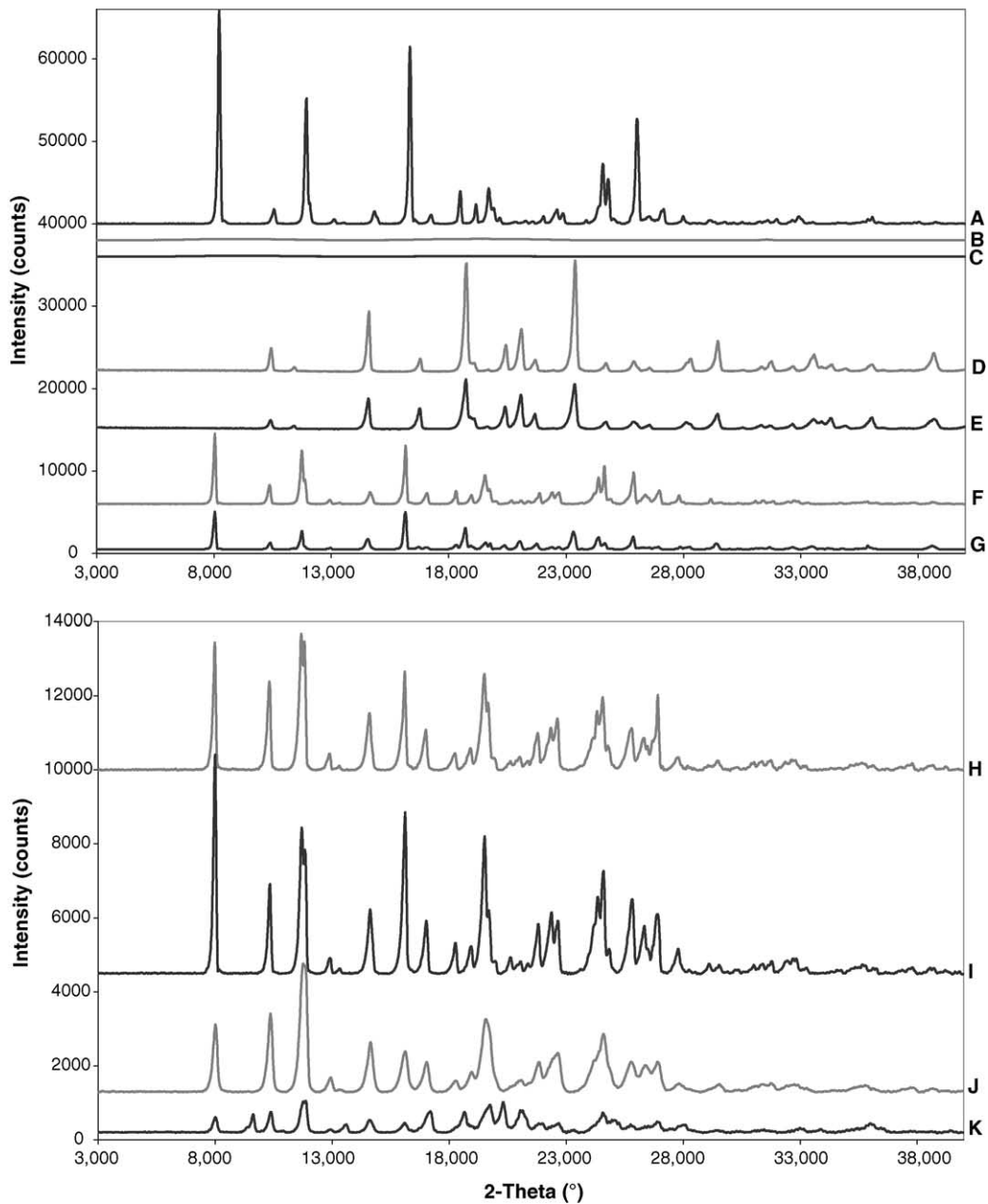


Fig. 8. PXRD diffractograms for: (A) un-milled commercial NIF; (B) HPMC; (C) spray-dried HPMC; (D) mannitol; (E) spray-dried mannitol; (F) NIF/HPMC, 10:1 (w/w) physical mixture (mortar); (G) NIF/HPMC/mannitol, 10:1:10 (w/w) physical mixture (mortar); (H) spray-dried formulation A (no-milling); (I) spray-dried formulation A (Turrax<sup>®</sup> milling); (J) spray-dried formulation A (nanoparticles); (K) spray-dried formulation B (nanoparticles).

Table 4

Influence of HPMC % (w/w, relative to NIF content) on PXRD peak intensity (counts–height) of NIF nanoparticles for given diffraction angles ( $2\theta$ )

HPMC (%)	8.00°	10.34°	11.72°	14.62°	16.04°	19.58°	22.62°	24.60°
2	3171	3581	5586	2216	1703	3301	1888	2703
10	2783	2976	4950	1873	1319	3049	1600	2354
20	2687	2963	4528	1806	1294	2600	1462	2171
40	2428	2542	4144	1586	1174	2455	1278	1957

amorphous form, crystalline state evaluation of NIF nanoparticles was carried out. Three polymorphic forms of NIF have been identified through thermal analysis (Keymolen et al., 2002) and confirmed in our laboratory. Polymorphic form I present a melting peak at 172 °C, form II at 163 °C and form III at 140 °C; form I being the most stable polymorphic form, which is generally characterized by the lowest solubility. As it is shown on the DSC thermograms of Fig. 7, both NIF un-milled commercial product and NIF nanoparticles are present as polymorphic form I. The peaks were found to be nearly identical, with a calculated  $\Delta H$  around 110 J/g for both un-milled NIF and NIF nanoparticles. The only difference observed was a slight shift in fusion temperature (174–173 °C) and a broadening of the peaks. These modifications were attributed to the presence of HPMC as we can clearly see on the other thermograms (Fig. 7D and E); decrease in particle size not showed to influence (Fig. 7F and G). These differences were further enhanced in the presence of mannitol (Fig. 7J and K), where the dilution of NIF particles is even higher.

PXRD diffractograms of Fig. 8 confirm that the high pressure homogenization operation does not interfere with NIF crystalline state as the diffraction pattern for NIF is conserved for nanoparticles. The only difference observed between un-milled NIF and NIF nanoparticles lies in peaks intensities, which was found smaller for nanoparticles. Here again, this difference was attributed to the presence of HPMC in the formulation. As we can see on Fig. 8, peaks intensities are in fact reduced for a NIF/HPMC physical mixture (Fig. 8F) and even further reduced for a spray-dried NIF/HPMC suspension prior to milling operations (Fig. 8H), where HPMC is thought to be more evenly distributed around NIF particles. The diffraction pattern and indeed the peak intensity for the latest were found similar for the spray-dried NIF nanoparticles (formulation A). Particle size, as observed for Turrax®-milled NIF, was

not shown to alter peak intensity. Table 4 shows the influence of HPMC % relative to NIF in regards to peak intensity, which is clearly shown to decrease with increasing HPMC %. As expected from the observations presented above, spray-dried NIF nanoparticles (formulation B) show further decrease in peak intensity as dilution of the particles in mannitol is even higher than with HPMC. These results confirm that the reduction in peak intensity is essentially due to dilution of the particles in the additives (i.e. surfactant, carrier) rather than from particle size reduction or any change of the polymorphic form of the active ingredient.

Another interesting feature represented by the DSC thermograms of Fig. 7H and I and PXRD diffractograms of Fig. 8D and E is that mannitol is found to be crystalline which shall be of relevant importance when considering stability of formulation B NIF nanoparticles.

#### 4. Conclusions

Through this study, it has been shown that formulation of nifedipine as nanoparticles has met great success in regards to dissolution rate and saturation solubility enhancement. High pressure homogenization was shown to be a simple and adequate operation for particle size reduction and is a technique that shall have general applicability depending on hardness of drug and adequate stabilizer utilization. Furthermore, crystalline state of NIF was shown not to be altered through particle size reduction, and shall be of great importance when considering long-term time stability of NIF formulations. Future work shall consist in permeation studies on cell lines and in the evaluation of in vivo pharmacokinetic properties of NIF nanoparticulate systems. Study of bioadhesive properties of these systems shall also be carried out.



## Acknowledgements

The authors would like to thank UCB Pharma for the sponsorship of this work and the Industrial Chemistry Department of ULB for PXRD and SEM analysis.

## References

- Bayomi, M.A., Abanumay, K.A., Al-Angary, A.A., 2002. Effect of inclusion complexation with cyclodextrins on photostability of nifedipine in solid state. *Int. J. Pharm.* 243, 107–117.
- Cilurzo, F., Minghetti, P., Casiraghi, A., Montanari, L., 2002. Characterization of nifedipine solid dispersions. *Int. J. Pharm.* 242, 313–317.
- Grau, M.J., Kayser, O., Müller, R.H., 2000. Nanosuspensions of poorly soluble drugs—reproducibility of small scale production. *Int. J. Pharm.* 196, 155–157.
- Hintz, R.J., Johnson, K.C., 1989. The effect of particle size distribution on dissolution rate and oral absorption. *Int. J. Pharm.* 51, 9–17.
- Hirayama, F., Wang, Z., Uekema, K., 1994. Effect of 2-hydroxypropyl-beta-cyclodextrin on crystallisation and polymorphic transition of nifedipine in solid state. *Pharm. Res.* 11, 1766–1770.
- Keymolén, B., Ford, J.L., Powell, M.W., Rajabi-Siahboomi, A.I., 2002. Investigation of the polymorphic transformations from glassy nifedipine. *Thermochim. Acta* 7093, 1–15.
- Kondo, N., Iwao, T., Masuda, H., Yamanouchi, K., Ishihara, Y., Yamada, N., Haga, T., Ogawa, Y., Yokoyama, K., 1993a. Improved oral absorption of a poorly water-soluble drug, HO-221, by wet-bead milling producing particles in submicron region. *Chem. Pharm. Bull.* 41, 737–740.
- Kondo, N., Iwao, T., Kikuchi, M., Shu, H., Yamanouchi, K., Yokoyama, K., Ohya, K., Ogyu, S., 1993b. Pharmacokinetics of a micronized, poorly water-soluble drug, HO-221, in experimental animals. *Biol. Pharm. Bull.* 16, 796–800.
- Krause, K.P., Müller, R.H., 2001. Production and characterisation of highly concentrated nanosuspensions by high pressure homogenization. *Int. J. Pharm.* 214, 21–24.
- Lin, C.-W., Cham, T.-M., 1996. Effect of particle size on the available surface area of nifedipine from nifedipine–polyethylene glycol 6000 solid dispersions. *Int. J. Pharm.* 127, 261–272.
- Liversidge, G.G., Cundy, K.C., 1995. Particle size reduction for improvement of oral bioavailability of hydrophobic drugs: I. Absolute oral bioavailability of nanocrystalline danazol in beagle dogs. *Int. J. Pharm.* 125, 91–97.
- Lu, A.T.K., Frisella, M.E., Johnson, K.C., 1993. Dissolution modeling: factors affecting the dissolution rates of polydisperse powders. *Pharm. Res.* 10, 1308–1314.
- Mitchell, S.A., Reynolds, T.D., Dasbach, T.P., 2003. A compaction process to enhance dissolution of poorly water-soluble drugs using hydroxypropyl methylcellulose. *Int. J. Pharm.* 250, 3–11.
- Mosharraf, M., Nyström, C., 1995. The effect of particle size and shape on the surface specific dissolution rate of micro-sized practically insoluble drugs. *Int. J. Pharm.* 122, 35–47.
- Müller, R.H., Jacobs, C., Kayser, O., 2001. Nanosuspensions as particulate drug formulations in therapy ‘Rationale’ for development and what we can expect for the future. *Adv. Drug. Del. Rev.* 47, 3–19.
- Portero, A., Remunan-Lopez, C., Vila-Jato, J.L., 1998. Effect of chitosan and chitosan glutamate enhancing the dissolution properties of the poorly water soluble drug nifedipine. *Int. J. Pharm.* 175, 75–84.
- Sencar-Bozic, P., Srcic, S., Knez, Z., Kerc, J., 1997. Improvement of nifedipine dissolution characteristics using supercritical CO<sub>2</sub>. *Int. J. Pharm.* 148, 123–130.
- Sugimoto, M., Okagaki, T., Narisawa, S., Koida, Y., Nakajima, K., 1998. Improvement of dissolution characteristics and bioavailability of poorly water-soluble drugs by novel cogrinding method using water-soluble polymer. *Int. J. Pharm.* 160, 11–19.
- Suzuki, H., Ogawa, M., Hironaka, K., Ito, K., Sunada, H., 2001. A nifedipine coground mixture with sodium deoxycholate. II. Dissolution characteristics and stability. *Drug. Dev. Ind. Pharm.* 27, 951–958.
- Teraoka, R., Otsuka, M., Matsuda, Y., 1999. Evaluation of photostability of solid-state dimethyl 1,4-dihydro-2,6-dimethyl-4-(2-nitro-phenyl)-3,5-pyridinedicarboxylate by using Fourier-transformed reflection-absorption infrared spectroscopy. *Int. J. Pharm.* 184, 35–43.
- Vippagunta, S.R., Maul, K.A., Tallavajhala, S., Grant, D.J.W., 2002. Solid-state characterization of nifedipine solid dispersions. *Int. J. Pharm.* 236, 111–123.
- Yamamura, S., Rogers, J.A., 1996. Characterization and dissolution behavior of nifedipine and phosphatidylcholine binary systems. *Int. J. Pharm.* 130, 65–73.
- Zajc, N., Obreza, A., Bele, M., Srcic, S., 2005. Physical properties and dissolution behaviour of nifedipine/mannitol solid dispersions prepared by hot melt method. *Int. J. Pharm.* 291, 51–58.



Research paper

# Preparation and in vitro/in vivo evaluation of nano-sized crystals for dissolution rate enhancement of ucb-35440-3, a highly dosed poorly water-soluble weak base

J. Hecq<sup>a</sup>, M. Deleers<sup>b</sup>, D. Fanara<sup>b</sup>, H. Vranckx<sup>b</sup>, P. Boulanger<sup>c</sup>,  
S. Le Lamer<sup>c</sup>, K. Amighi<sup>a,\*</sup>

<sup>a</sup> Laboratory of Pharmaceutics and Biopharmaceutics, Université Libre de Bruxelles, Campus Plaine, Boulevard du Triomphe, Brussels, Belgium

<sup>b</sup> UCB S.A., Department of Product Process and Analytical Developments, Chemin du Foriest, Braine-l'Alleud, Belgium

<sup>c</sup> UCB S.A., R&D, Laboratory of Drug Metabolism and Pharmacokinetics, Chemin du Foriest, Braine-l'Alleud, Belgium

Received 15 March 2006; accepted in revised form 18 May 2006

Available online 18 July 2006

## Abstract

ucb-35440-3 is a new drug entity under investigation at UCB S.A. Due to its physicochemical characteristics, the drug, a poorly water-soluble weak base, shows poor solubility and dissolution characteristics. In rat, the low oral bioavailability ( $F < 10\%$ ) is largely due to poor absorption. In order to enhance the solubility and dissolution characteristics, formulation of ucb-35440-3 as nanocrystals has been achieved in this study. Nanoparticles were prepared using high pressure homogenization and were characterized in terms of size and morphology. In vitro dissolution characteristics were investigated and compared to the un-milled drug in order to verify the theoretical hypothesis on the benefit of increased surface area. In vivo pharmacokinetic evaluation of ucb-35440-3 nanoparticles was also carried out on rats. Crystalline state evaluation before and following particle size reduction was conducted through polarized light microscopy and PXRD to denote any possible transformation to an amorphous state during the homogenization process. Drug chemical stability was also assessed following homogenization. The dissolution rate increased significantly at pH 3.0, 5.0 and 6.5 for ucb-35440-3 nanoparticles. However, the pharmacokinetic profile obtained yielded lower systemic exposure than the un-milled compound (in fed state), this although being thought to be the consequence of the drug and formulation characteristics.

© 2006 Elsevier B.V. All rights reserved.

**Keywords:** Nanoparticles; High pressure homogenization; Dissolution; Drug reprecipitation; In vivo evaluation

## 1. Introduction

Poor aqueous solubility is actually a very challenging problem in drug formulation development as it is considered, at least for BCS class II compounds, to be, in association to poor dissolution characteristics, the limiting step to drug absorption from the gastrointestinal tract [1], in

association to poor dissolution characteristics. As an increasing number of newly developed drug entities present such characteristics, approaches to overcome this factor are of great importance.

Among the various solubility/dissolution rate enhancement methodologies available for poorly water-soluble compounds (e.g. amorphous dispersions as solid dispersions/inclusion complexes, salt formation, surfactant/lipid based excipients addition, etc.), drug particle size reduction is meeting great interest in drug formulation [2,3]. Size reduction offers, in regard to the Noyes–Whitney and Ostwald–Freundlich equations, increased dissolution and solubility characteristics. Size reduction to nanometer

\* Corresponding author. Laboratory of Pharmaceutics and Biopharmaceutics, Université Libre de Bruxelles, Campus Plaine, CP 207, Boulevard du Triomphe, 1050 Brussels, Belgium. Tel.: +32 2 650 5254; fax: +32 2 650 5269.

E-mail address: [k.amighi@ulb.ac.be](mailto:k.amighi@ulb.ac.be) (K. Amighi).

range has been shown to be a very promising approach as it increases specific surface area further than micronization and thus leads to enhanced dissolution characteristics and increased systemic exposure (for BCS class II compounds). Nanoparticles have been showed in various in vivo studies to significantly enhance oral bioavailability of poorly water-soluble drugs [4,5]. ucb-35440-3 nanoparticles were obtained through high pressure homogenization. This milling technique has been extensively described by Müller and co-workers [6–9].

ucb-35440-3 (Patent No. WO 00/58295), a new drug entity under investigation at UCB S.A. for the oral treatment of asthma and allergic rhinitis, was used as a model drug. The molecule, a poorly water soluble weak base (fumarate salt), presents two ionisable ternary nitrogen placed in a piperazine cycle ( $pK_a \approx 9.6$ ; 5.7) (Fig. 1). Given the interesting results obtained in recent work with nifedipine nanoparticles [10], evaluation of the size reduction technology on ucb-35440-3 was carried out. ucb-35440-3 shows interesting features study-wise as, when compared to nifedipine, it is a highly dosed drug (anticipated human pharmacologically active dose should have been predicted at around 250–500 mg/day) and that it shows a pH-dependent solubility profile.

The object of this paper was to evaluate high pressure homogenization on the efficiency of ucb-35440-3 particle size reduction to nanometer range and to evaluate the hypothesis of enhanced dissolution properties at this size range. Correlation of the in vitro dissolution results with the pharmacokinetic profile following oral administration in rats was also evaluated. Drug crystalline state and chemical stability was also assessed to denote any possible alteration during the milling operation.

## 2. Materials and methods

### 2.1. Materials

ucb-35440-3 was supplied from UCB S.A.. Methocel E15 (hydroxy-propylmethylcellulose – HPMC) and Methocel A400 (methylcellulose – MC) were purchased from Colorcon (West Point, PA, USA). Polyvinyl alcohol ( $M_w$  13,000–23,000) was purchased from Aldrich Chemical Company Inc. (Milwaukee, WI, USA). Texapon K 12<sup>®</sup>

(sodium dodecyl sulfate) was purchased from Henkel (Düsseldorf, Germany). Acacia gum was purchased from Sigma–Aldrich (St. Louis, MO, USA). Lutrol F127<sup>®</sup> (equivalent to poloxamer 407) was purchased from BASF (Ludwigsbafen, Germany). Water was obtained using a CFOF 01205 Milli-Q Water Purification System (Millipore Corporation, Bedford, MA, USA). All other materials were of analytical reagent grade.

### 2.2. Preparation of samples

The steps in the preparation of drug nanoparticles were as follows.

#### 2.2.1. Preparation of drug nanosuspensions

ucb-35440-3 powder was poured in an aqueous surfactant solution (5% ucb-35440-3 w/v suspensions) (all surfactants tested were used at a concentration of 2% w/w relative to ucb-35440-3 content) under magnetic stirring (500 rpm). Nanosuspensions were prepared using an EmulsiFlex-C5 high pressure homogenizer (HPH) (Avestin Inc., Ottawa, Canada). Pre-milling low-pressure homogenization cycles (C) were run before the high pressure homogenizing cycles for a first significant size reduction (preventing blockage of the homogenizing gaps which present relatively low openings at the high pressure used; i.e.  $\pm 25 \mu\text{m}$  at 22,000 psi ([7])). The pre-milling low pressure cycles adopted are 15 cycles at 7000 psi and 10 cycles at 12,000 psi. High pressure homogenization was then finally applied for 10–20 cycles at 23–24,000 psi. During all pre-milling and milling cycles, agitation (Ultra-Turax<sup>®</sup> T25 Basic – 8000 rpm, IKA<sup>®</sup>-Werke GmbH & Co. KG, Staufen, Germany) was maintained in the sample reservoir to avoid sedimentation of particles. As ucb-35440-3 is heat-sensitive and the HPH causes sample temperature increase (increase of 30 °C following 20 °C at 24,000 psi), all operations were carried out using an heat exchanger, placed ahead of the homogenizing valve, with sample temperature maintained at  $10 \pm 1$  °C. Samples were withdrawn after the different size-reduction steps for size distribution analysis.

#### 2.2.2. Water-removal

In order to retrieve nanoparticles in dried-powder state from the nanosuspensions, water-removal was conducted through freeze-drying. The homogenized suspensions were frozen at  $-80$  °C overnight and freeze-dried using a Lyovac GT-2 apparatus (Leybold–Heraeus, Köln, Germany) under vacuum (pressure  $< 0.01$  mbar) for 15 h in open Petri dishes.

### 2.3. Particle size and shape characterization

Size and size distribution of the particles in suspension following the different homogenization steps and in dried-state following water redispersion were determined through laser diffraction (LD), with a wet-sampling

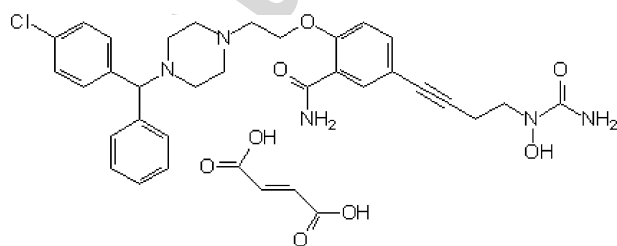


Fig. 1. Chemical structure of ucb-35440-3 (5-{4-[(aminocarbonyl)-(hydroxy)amino]but-1-ynyl}-2-(2-{4-[(R)-(4-chlorophenyl)(phenyl)methyl]-piperazin-1-yl}ethoxy)benzamide).

system (MasterSizer 2000, Malvern Instruments, Worcestershire, UK). The diameters reported were calculated using volume distribution. The median-volume particle size,  $d(v, 0.5)$  (size of the particles for which 50% of the sample volume contains particles smaller than ' $d 0.5$ ', the other particles being larger than ' $d 0.5$ '),  $d(v, 0.1)$ ,  $d(v, 0.9)$  and the volume mean diameter  $D[4,3]$  were used as characterization parameters. The refractive and absorption indexes of ucb-35440-3 were both approximated, by selection of the combination yielding the best residuals and fit data, at 1.610 and 0.001, respectively, and were used for measurements conducted. Morphological evaluation of nanoparticles was conducted through scanning electron microscopy (SEM) (JSM-6100, JEOL, Tokyo, Japan) following platinum coating.

## 2.4. Dissolution – solubility

A Distek 2100C USP dissolution apparatus (Distek Inc., North Brunswick, NJ, USA) Type II (paddle method) operating at a rotation speed of 60 rpm was used for in vitro testing of drug dissolution. All dissolution tests were carried out on an equivalent of 200 mg of ucb-35440-3 (in powder state) placed into HPMC capsules (placed into sinkers). Fifty millimoles phosphate buffers (0.05% polysorbate 20) at pH 3.0, 5.0 and 6.5 were used as dissolution media. The volume and temperature of the dissolution medium were 900 ml and  $37.0 \pm 0.2$  °C respectively. Automatic withdrawals at fixed times were filtered in-line and assayed through ultraviolet absorbance determination at 255 nm using an Agilent 8453 UV/visible Dissolution Testing System (Agilent Technologies, USA). The mean results of triplicate measurements and the standard deviation were reported. Saturation solubility evaluations were carried out at varying pHs at 25 °C following shaking of 10 mg/ml suspensions for 70 h (saturation checked). Withdrawals were filtered on 0.45 µm pore membranes. A Kontron chromatograph HPLC system type 400 (Kontron Instruments, Eching, Germany) was used for ucb-35440-3 quantification. Chromatographic separation was accomplished using a Kromasil C18, 3.5 µm,  $250 \times 4.6$  mm stainless steel column (AIT Chromato, France). The mobile phase consisted of a solvent A (ACN 10%/phosphate buffer, pH 3.0 90%)/solvent B (ACN 75%/phosphate buffer, pH 3.0 25%) mixture (50:50 v/v). The mobile phase was pumped isocratically at a flow rate of 1.0 ml/min during analysis, at 25 °C. The effluent was monitored at 210 nm.

## 2.5. Crystalline state evaluation of dried samples

### 2.5.1. Powder X-ray diffraction (PXRD)

PXRD diffractograms were recorded using a Siemens D5000 diffractometer (Siemens, Germany) with a Cu line as the source of radiation. Standard runs using a 40 kV voltage, a 40 mA current and a scanning rate of 0.02°/min over a  $2\theta$  range of 2–40° were used.

### 2.5.2. Polarized light microscopy

Optical microscopy analysis was conducted on an Olympus-BX 60 microscope (Olympus – Nihon Kodan, Japan) equipped with a JVC TK-C1381 colour video camera (JVC, Japan). A U-POT Polaroid filter is placed ahead of the sample for light polarization.

## 2.6. In vivo PK study

### 2.6.1. Animals

Male Wistar rats (6–7 weeks old) were obtained from Charles River Laboratories (Charles River, Brussels, Belgium). The rats' weights ranged from 180 to 200 g. All animals had free access to tap water and pelleted diet. Fast-ed rats were deprived of food 18 h before the experiment and food was reoffered 4 h post-dosing. ucb-35440-3 suspensions were administered orally to six male Wistar rats at a dose of 100 mg/kg. Suspensions of un-milled drug and drug nanoparticles (un-buffered suspension/0.5 M phosphate, pH 6.5, buffered suspension) were dosed at 10 ml/kg. For homogeneity reasons, un-milled ucb-35440-3 suspensions were prepared in 1% Methocel A400 solutions (i.e. particle sedimentation). Six hundred microliters blood samples were withdrawn from the caudal vein at predose, 30 min, 1, 2, 4, 8, 12 and 24 h post-dosing and placed into Li Heparin plastic tubes. Blood samples were held on ice (+4 °C) until centrifuged at 3000g, 4 °C for 5 min. Plasma was transferred to individual Eppendorfs and stored at –20 °C until analysed.

### 2.6.2. Analysis

**2.6.2.1. Sample preparation procedure.** Plasma samples were prepared by liquid–liquid extraction. Two hundred microliters of plasma sample were pipetted into an Eppendorf tube and fortified with 50 µL of the internal standard (ucb-46680) working solution (100 ng/mL). Three hundred microliters of a glycine–sodium chloride 2.0 mol/L buffer adjusted at pH 10.0 with sodium hydroxide 2.0 mol/L were added. The content of the tube was gently mixed and then extracted with 1 mL of hexane–isopropanol 1:1 (v/v). This involved thorough vortex-mixing for 10 min and subsequent centrifugation at 13,000 rpm (H 14750g) for 10 min. The upper organic phase was transferred into another Eppendorf tube and evaporated to dryness in a preheated concentrator–evaporator (pulse vent = 1, heating level = 0) (JOUAN RC 10.22; Saint-Herblain, France). The residue was reconstructed with 75 µL of acetonitrile–water 23:77 (v:v) containing 0.1% trifluoroacetic acid and adjusted to pH 3.0 with ammonium hydroxide, vortex mixed and then filtered on a Ultrafree MC 0.45 µm device at 13,000 rpm (H 14750g) for 15 min using an ALC micro-centrifuge 4214 (Milan, Italy). An aliquot (10 µL) was injected into the LC/ESI/MS/MS system described below.

**2.6.2.2. ucb-35440-3 analysis.** A HP1100 HPLC system (Hewlett–Packard, Palo Alto, USA), coupled to a Quattro Ultima mass spectrometer (Micromass, Manchester, UK)

was used to measure ucb-35440-3 in plasma samples. The analytical column (Inertsil ODS 3, 5  $\mu\text{m}$ , 50  $\times$  2.1 mm ID (Varian, Harbor City, USA)) was protected by a guard column (Inertsil ODS 3, 5  $\mu\text{m}$ , 10  $\times$  2.1 mm ID (Varian, Harbor City, USA)). The column and the pre-column were placed in an oven set to a temperature of 40  $^{\circ}\text{C}$ . Analyses were performed in a binary gradient mode. Solvents A and B consisted of acetonitrile–water 5:95 and 95:5 (v/v), respectively, both containing 0.1% trifluoroacetic acid and adjusted to pH 3.0 with ammonium hydroxide. The HPLC gradient started at 25% B and was linearly increased to 50% B over 7 min. It was then increased to 100% B over 0.1 min (0.9 min hold) before returning to 25% B over 0.1 min. The system was allowed to re-equilibrate for 1.9 min before injection of the next sample. The flow was adjusted to 0.250 mL/min and split post-column (ratio of 1:5) in order to get 0.050 mL/min into the electrospray source. Electrospray experiments used a capillary voltage set at 4.00 kV. The source temperature was kept at 100  $^{\circ}\text{C}$  and the desolvation temperature at 350  $^{\circ}\text{C}$ . The cone gas flow ( $\text{N}_2$ ) was adjusted to *ca* 90 L/h and the desolvation gas flow ( $\text{N}_2$ ) to *ca* 850 L/h. The collision gas pressure (argon) was adjusted to about  $2 \times 10^{-3}$  mbar. Spectra were acquired at *ca.* 1 mass unit resolution (10% valley definition) for parent and daughter ions. The inter-channel delay was fixed at 0.1 s. ucb-35440-3 concentrations were determined by the peak area ratio technique. The limit of quantification of the method is 0.5 ng/mL. Calibration curves were established over a range of 0.5–100 ng/mL ( $r^2 > 0.997$ ) and study samples were diluted with blank human plasma when required.

**2.6.2.3. Data processing.** Individual plasma concentrations and nominal sampling times were used to assess the pharmacokinetic parameters by non-compartmental analysis

using the Watson Lims (6.4.0.03, Innaphase, Philadelphia, PA, USA).  $C_{\text{max}}$  refers to the peak plasma level and  $t_{\text{max}}$  refers to the time at which  $C_{\text{max}}$  occurred. The area under the curve  $\text{AUC}(0 - t)$  (i.e. area under the concentration–time curve calculated from zero up to time corresponding to the last measurable concentration) was calculated using the linear trapezoidal rule using individual concentrations.

### 3. Results and discussion

#### 3.1. Nanoparticle preparation

Un-milled ucb-35440-3 used in this study was characterized by relatively large particles ( $d(v, 0.5)$  about 140  $\mu\text{m}$  as reported in Fig. 2 and particles up to 500  $\mu\text{m}$ ). These particles had to follow preliminary size-reduction steps prior to the high pressure homogenization operation in order to be small enough to pass the homogenizing gaps of the homogenizer at the homogenizing pressures used (i.e. 25  $\mu\text{m}$  at 22,000 psi [7]. Fig. 2 shows that low pressure pre-milling homogenizing cycles were found to be very effective as preliminary size reduction step when compared to previous work with another model drug where similar cycles were used [10], as a population with  $d(v, 0.5)$  of around 600 nm and comprising 59% (in volume) of sub-micron particles is obtained. The following high pressure homogenization cycles were shown to further decrease particle size; the size distribution being characterized by  $d(v, 0.5)$  of around 200 nm and comprising 83% (in volume) of sub-micron particles. Additional high pressure homogenization cycles (up to 20) were found to slightly decrease only  $d(v, 0.9)$  and  $D[4,3]$  with  $d(v, 0.5)$  and  $d(v, 0.1)$  being unaffected.

HPMC of low viscosity grade was chosen, at a concentration of 2% w/w relative to ucb-35440-3 content, for

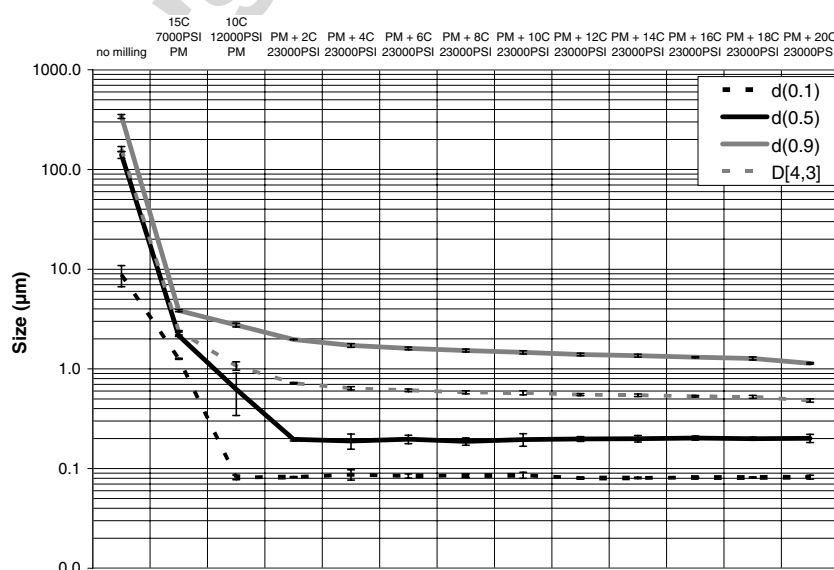


Fig. 2. Influence of pre-milling (PM) operation and number of high pressure homogenization cycles (C) on ucb-35440-3 particle size for a ucb-35440-3 5% – HPMC 0.1% w/w suspension.



Table 1

Surfactant screening (% w/w relative to ucb-35440-3 content) – particle size ( $n \geq 10$ : mean  $\pm$  SD) following PMC + 10C 23,000 psi

		$d(v, 0.5) \pm \text{SD} (\mu\text{m})$	$d(v, 0.1) \pm \text{SD} (\mu\text{m})$	$d(v, 0.9) \pm \text{SD} (\mu\text{m})$	$D[4, 3] \pm \text{SD} (\mu\text{m})$
Sodium lauryl sulfate	2%	$10.7 \pm 1.9$	$5.42 \pm 1.02$	$20.3 \pm 3.7$	$11.9 \pm 2.1$
HPMC (Methocel E15)	2%	$0.182 \pm 0.007$	$0.083 \pm 0.001$	$1.46 \pm 0.05$	$0.563 \pm 0.023$
Polyvinyl alcohol	2%	$0.262 \pm 0.054$	$0.082 \pm 0.002$	$1.50 \pm 0.10$	$0.603 \pm 0.038$
Acaciae Gum	2%	$0.407 \pm 0.006$	$0.090 \pm 0.001$	$1.18 \pm 0.05$	$0.542 \pm 0.016$
Poloxamer 407	2%	$0.183 \pm 0.003$	$0.079 \pm 0.001$	$1.20 \pm 0.05$	$0.483 \pm 0.011$

nanosuspension stabilization. This was because this water-soluble polymer offers adequate surface active properties (i.e. stabilization of nanoparticles formed during homogenization) when compared to other commonly used surfactants such as sodium dodecyl sulfate, polyvinyl alcohol and acacia gum (Table 1), and because it is a widely used pharmaceutical excipient with no known toxicity. Although poloxamers have been shown to be quite successful in regard to nanoparticle stabilization, their use is limited due to their low melting-point characteristics which are problematic for further sample processing (i.e. freeze-drying and especially spray-drying operations). As observed in previous studies when no carriers (i.e. mannitol) are used [10] and on the SEM micrograph of Fig. 3, nanoparticle agglomeration is clearly observed following water-removal from the nanosuspensions (redispersion of the freeze-dried powder, yielding a population with  $d(v, 0.5)$  around  $90 \mu\text{m}$  and no submicron particles). Although the presence of a carrier is very useful regarding optimization of nanoparticle redispersion characteristics following water-removal, none was used in this study; the projected ucb-35440-3 dose being set at 200 mg, further addition of excipients for sample processing was limited due to the low density of the powder obtained.

### 3.2. Dissolution rate evaluation

Being a weak base, ucb-35440-3 presents a pH-dependant solubility profile; solubility decreasing with increasing

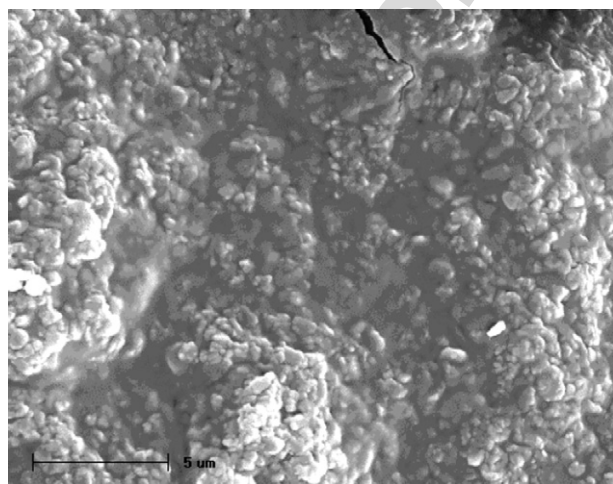


Fig. 3. SEM micrograph of a freeze-dried ucb-35440-3 nanosuspension (magnification 5000 $\times$ ; scale =  $5 \mu\text{m}$ ).

pH (Fig. 4) and being predictive of intestinal-dissolution and/or absorption limitations. According to this profile, dissolution evaluations were carried out at pH 3.0 (Aq. Sol.  $\sim 0.65 \text{ mg/ml}$ ), pH 5.0 (Aq. Sol.  $\sim 0.2 \text{ mg/ml}$ ) and pH 6.5 (Aq. Sol.  $< 0.03 \text{ mg/ml}$ ). Dissolution profiles at these pHs, with comparison of un-milled ucb-35440-3 and ucb-35440-3 nanoparticles, are respectively shown in Fig. 5A–C. The approximate 10 min lag time observed for each formulation can be attributed to capsule disintegration. Dissolution rate (DR) enhancement is clearly observed at all tested pHs. At pH 3.0, more than 95% of the drug was already dissolved after 60 min for ucb-35440-3 nanoparticles compared to dissolution of around 30% of the un-milled ucb-35440-3 after the same time period and complete dissolution being unachieved for the latest over a span of 13 h. Similar observations could be made for dissolution at pH 5.0 (which is less favorable to ucb-35440-3 dissolution) as after 60 min, 85% of the drug in nanoparticle form was already dissolved compared to 20% of un-milled ucb-35440-3, with the same observation regarding complete dissolution as for pH 3.0. Increased DR for ucb-35440-3 nanoparticles was also observed at pH 6.5 (Fig. 5C), where after 60 min approximately 20% of the drug was dissolved compared to 3% for un-milled ucb-35440-3. Due to the low saturation solubility, saturation of the dissolution media is rapidly reached for nanoparticles at this pH, and recrystallization is observed. Drug dissolution at this pH shall be evaluated under different conditions (e.g. flow-through dissolution). Standard deviations observed in the dissolution profiles were also shown to be smaller for ucb-35440-3 nanoparticles; un-milled drug received as a coarse powder with a large polydispersity.

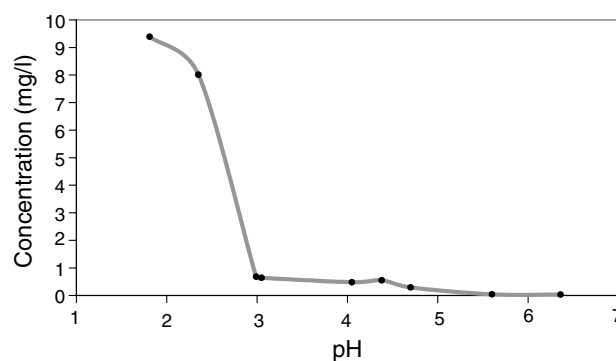


Fig. 4. Aqueous solubility profile (25 °C) of un-milled ucb-35440-3.

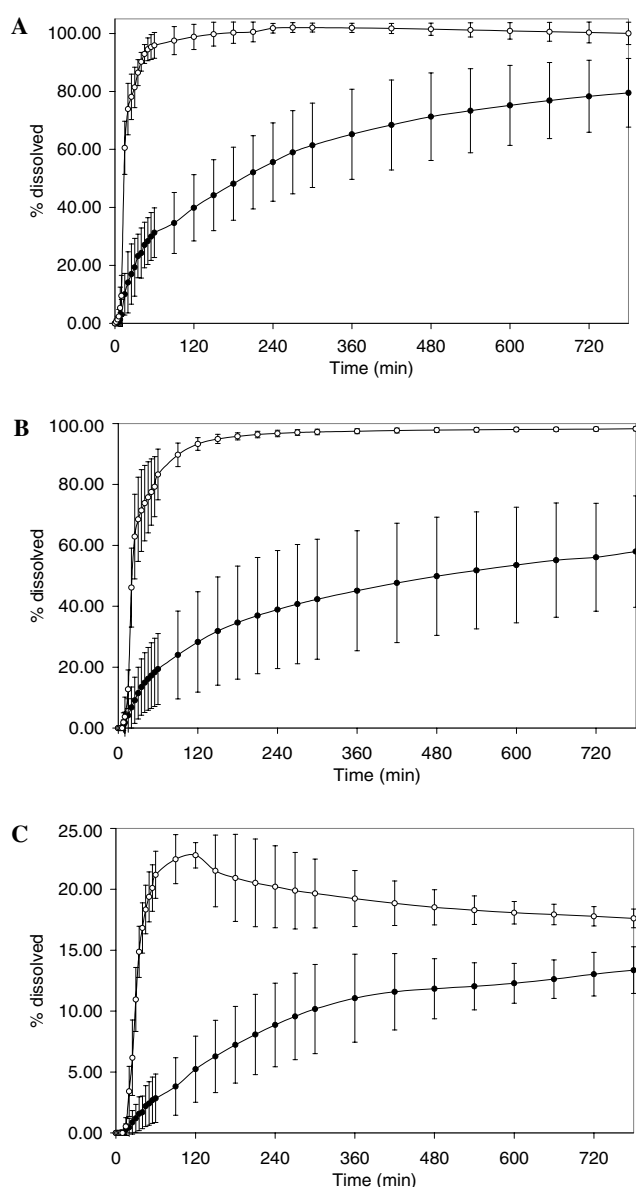


Fig. 5. Dissolution profiles [phosphate 50 mM buffer, pH 3.0 (A); 5.0 (B) and 6.5 (C)] for un-milled ucb-35440-3 (●) and for ucb-35440-3 5% - HPMC 0.1% freeze-dried nanosuspensions (○) samples (mean  $\pm$  SD -  $n \geq 3$ ).

### 3.3. Crystalline state evaluation

To verify that the DR increase observed for ucb-35440-3 nanoparticles is not the consequence of the presence of amorphous drug (the un-milled drug received in crystalline powder form), crystalline state evaluation was carried out after the homogenization operation. Polarized-light optical microscopy clearly showed the anisotropic nature of the un-milled drug (Fig. 6). The same observations can be made for ucb-35440-3 nanoparticles, indicating that crystalline state seems to be unaltered following the homogenization operation. PXRD diffractograms of Fig. 7 confirm this statement as the diffraction pattern is preserved for ucb-35440-3 nanoparticles. The decrease in

peak intensity for certain diffraction angles can be attributed to the presence of HPMC at the surface of the particles, as it has already been reported in previous studies [10]. Chemical stability was also verified following high pressure homogenization as no degradation was observed (data not shown).

### 3.4. In vivo pharmacokinetic evaluation

Pharmacokinetic evaluation following an oral dose of 100 mg/kg (suspension state) of both ucb-35440-3 un-milled drug and nanoparticles was carried out on male Wistar rats in fed and fasted states. A positive food effect on the drug absorption is reported for the drug. Based on the pH-dependent solubility profile of the drug and as it is clearly shown when mimicking GIT pH conditions through in vitro dissolution tests (Fig. 8), reprecipitation entering small intestine should be expected. Fig. 8 shows the difference between the two ucb-35440-3 systems regarding dissolution at pH 1.3. It shows that the fast dissolution behaviour at this pH for the nanoparticulate formulation should allow for rapid drug disposal in the stomach (particularly if the stomach residence time is prolonged as it is the case in fed state). The data also suggest that when drug dissolution is so important at acidic pH, reprecipitation will occur when pH increases. LD analysis of the dissolution media after passage from pH 5.0 to 6.3, where most of the reprecipitation occurs, show a population of particles with a  $d(v,0.5)$  of  $2.68 \pm 0.13 \mu\text{m}$  and no submicron particles. We can anticipate that this phenomenon might also be observed in vivo when entering small intestine. No data regarding the particles in the precipitate were retrieved, except for particle size; the physicochemical state of the drug in the precipitate being unknown.

To investigate the eventuality of drug reprecipitation following stomach exiting, as well as its consequence on drug absorption, formulation of ucb-35440-3 nanoparticles in a 0.5 M pH 6.5 phosphate buffer was assayed. This formulation was expected to limit drug dissolution in stomach and thus prevent the presumed drug reprecipitation following its exit. This limitation shall particularly be observed in fasted conditions where the stomach's pH is at its lowest (e.g. the rat stomach pH in fasted state and fed state being of 3 and 5, respectively [11]).

Fig. 9 shows the pharmacokinetic profile for un-milled ucb-35440-3 and for nanoparticle formulations in fed and fasted state. The results showed on Fig. 9 and Table 2 clearly indicate a positive food effect on ucb-35440-3 absorption. An extent of exposure of 7100 ng h/ml was found for fed animals compared to 327 ng h/ml for fasted animals (un-milled drug). The same conclusions could be drawn for ucb-35440-3 nanoparticles as an extent of exposure of 3736 and 2614 ng h/ml were found for fed animals compared to 1282 and 1366 ng h/ml for fasted animals, in un-buffered and buffered conditions, respectively.

When comparing the PK profile of the un-milled ucb-35440-3 formulation and the ucb-35440-3 nanoparticle



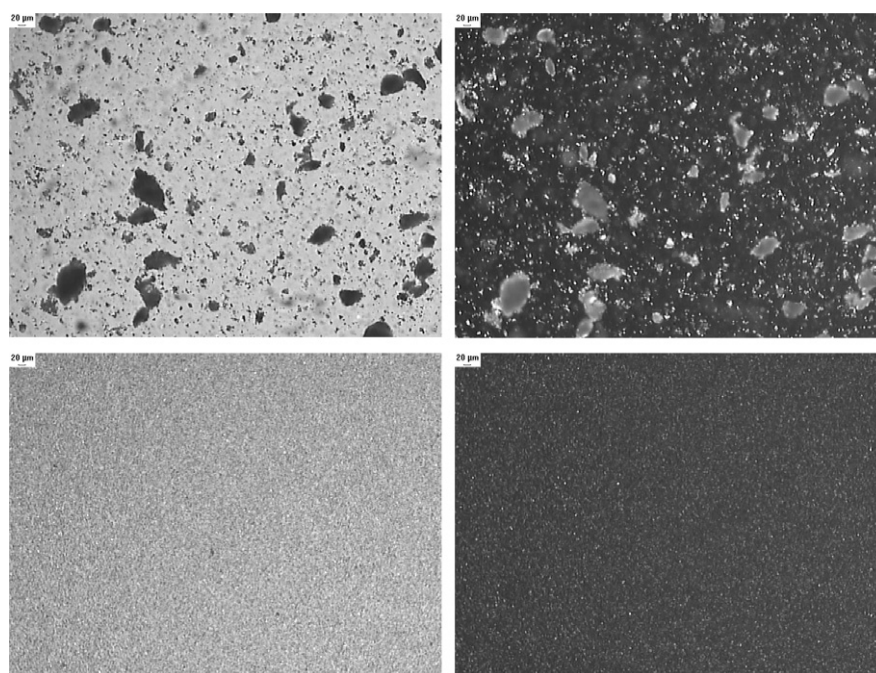


Fig. 6. Optical microscopy – polarized light (PL) analysis (magnification 50× – scale = 20 µm): un-milled ucb-35440-3 non PL (upper left) and PL (upper right); ucb-35440-3 nanosuspension non PL (lower left) and PL (lower right).

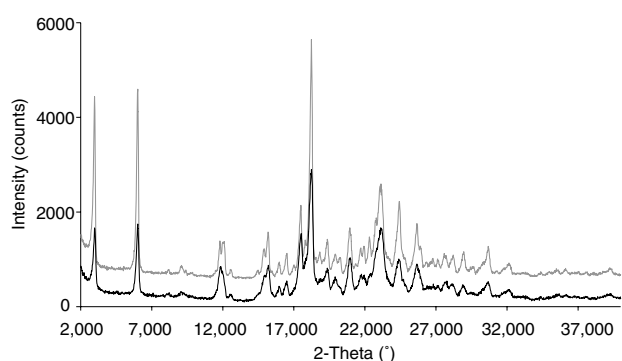


Fig. 7. PXRD diffractograms for un-milled ucb-35440-3 (gray) and ucb-35440-3 5% – HPMC 0.1% freeze-dried nanosuspension (black).

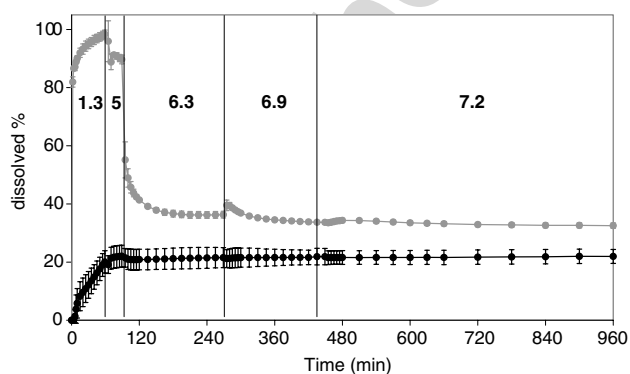


Fig. 8. Dissolution profiles (GIT pH simulation – 1.3 (1 h); 5 (0.5 h); 6.3 (3 h); 6.9 (3 h) and 7.2 (till end of test)) for un-milled ucb-35440-3 (●) and for ucb-35440-3 5% – HPMC 0.1% freeze-dried nanosuspension (●) samples (mean ± SD –  $n = 3$ ).

formulations in both fed and fasted state, we observe, respectively, a decrease and an increase of the drug extent of exposure for ucb-35440-3 nanoparticles. Keeping in

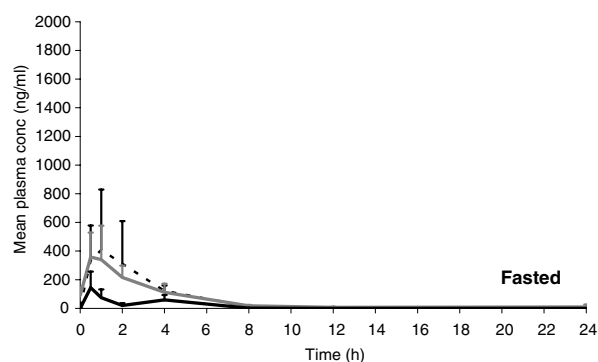
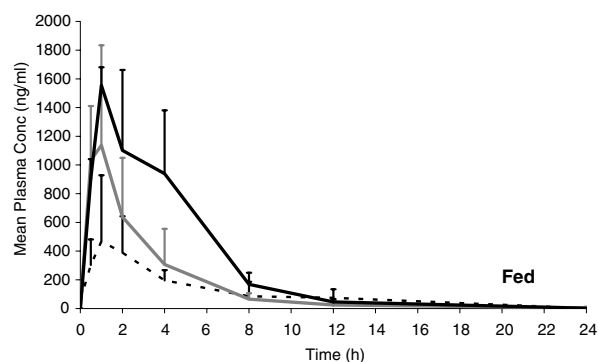


Fig. 9. Mean plasma concentrations (±SD) (fed state (top) and fasted state (bottom)) for un-milled ucb-35440-3 (Black bold line) (fed and fasted:  $n = 3$ ); ucb-35440-3 nanoparticles (un-buffered suspension) (grey thick line) (fed and fasted:  $n = 6$ ) and ucb-35440-3 nanoparticles (buffered suspension) (black dashed line) (fed:  $n = 6$  and fasted:  $n = 5$ ).

Table 2

Mean plasma pharmacokinetic parameter values for ucb-35440-3 in the Wistar rat after single oral administration (100 mg/kg) of different tested ucb-35440-3 formulations: influence of particle size and media buffering

	Fed			Fasted		
	$C_{\max}$ (ng/ml)	$T_{\max}$ (h)	Mean $AUC_{(0-t)}$ (ng h/ml)	$C_{\max}$ (ng/ml)	$T_{\max}$ (h)	Mean $AUC_{(0-t)}$ (ng h/ml)
Un-milled	1554 ± 127	1	7100	144 ± 112	0.5	327
Nano (un-buffered suspension)	1244 ± 594	0.75	3736	383 ± 202	0.75	1282
Nano (buffered suspension)	555 ± 396	1	2614	443 ± 390	0.5	1366

mind the pH dependant solubility profile of the drug, these observations can be explained by the amount of drug dissolved in the stomach and by the time given for this dissolution. The gastric residence time (GRT) being longer in fed state than in fasted state, the amount of dissolved ucb-35440-3 will be lower for the latest condition, this even though gastric pH is lower.

When comparing the three formulations in fasted state, where GRT is short and where only dissolution rate shall limit the amount of drug dissolved, we can clearly understand the increased extent of exposure for ucb-35440-3 nanosuspensions. No differences were observed between the buffered and un-buffered nanosuspension in fasted state. This could be explained by the fact that the amount of drug dissolved in the stomach for the un-buffered suspension might be higher than for the buffered suspension, but that drug reprecipitation might take place following stomach's exiting. Intestinal drug concentrations would thus be similar for the two suspensions. This observation could also find an explanation in the fact that gastric emptying is very fast in fasted state and that drug dissolution might mostly take place in intestinal media. Contrarily to stomach's conditions where the buffered suspension should play a role in limiting drug dissolution, no differences shall be observed between the two systems in this case. In fact, the lower extent of exposure observed in fed state for the buffered ucb-35440-3 nanosuspension (2614 ng.h/ml) compared to the un-buffered nanosuspension (3736 ng.h/ml) can be explained by a smaller dissolved amount due to the higher pH of the buffer compared to the nominal stomach pH in fed state. The GRT in both cases was thought to be the same.

When comparing the pharmacokinetic profile of both un-milled ucb-35440-3 and ucb-35440-3 nanoparticles in un-buffered media, we observe an approximate twofold decrease (7100 → 3736 ng.h/ml) in extent of exposure for the latest in fed state. This rather unexpected result could be explained by the fact that un-milled ucb-35440-3, unlike ucb-35440-3 nanoparticles, was administered as a viscous suspension (i.e. suspension homogeneity – sedimentation of large particles). This might increase the GRT of the drug and thus increase the time available for ucb-35440-3 dissolution. The arrival of the drug in dissolved state in the intestine being more progressive, chance for drug reprecipitation is smaller than for nanoparticulate formulations.

Through the data obtained, we can see that highly dosed, poorly water soluble weak base, as ucb-35440-3,

represents a model with great complexity when considering nanoparticulate systems as formulation approach for systemic exposure enhancement. We could see that for basic compounds, there is an interest to increase drug solubilization in the stomach and to increase GRT. Further investigations in the eventuality of drug reprecipitation, which was only posed as an hypothesis, need to be carried out in future work.

#### 4. Conclusions

Through this study, it has been shown that formulation of ucb-35440-3, a model poorly water-soluble weak base, as nanocrystals has met great success in regard to enhancement of drug dissolution characteristics. High pressure homogenization was shown to be a simple and adequate technique for drug particle size reduction and did not seem to alter the crystalline state of the drug, which should be highly relevant when considering drug time-stability. Pharmacokinetic evaluation of the systems clearly indicated the carefullness needed to be taken when considering poorly water-soluble drugs with pH-dependant solubility profile. Further evaluations in the in vivo behavior of the systems formed need to be carried out in order to understand phenomenon such as the eventuality of intestinal drug reprecipitation.

#### Acknowledgements

The authors thank UCB S.A. Pharma for the sponsorship of this work and the Industrial Chemistry Department of ULB for SEM and PXRD analysis.

#### References

- [1] R. Löbenberg, G.L. Amidon, Modern bioavailability, bioequivalence and biopharmaceutics classification system. New scientific approaches to international regulatory standards, *Eur. J. Pharm. Biopharm.* 50 (2000) 3–12.
- [2] N. Rasenack, H. Hartenhauer, B.W. Müller, Microcrystals for dissolution rate enhancement of poorly water-soluble drugs, *Int. J. Pharm.* 254 (2003) 137–145.
- [3] M. Mosharraf, C. Nyström, The effect of particle size and shape on the surface specific dissolution rate of micro-sized practically insoluble drugs, *Int. J. Pharm.* 122 (1995) 35–47.
- [4] Y. Wu, A. Loper, E. Landis, L. Hettrick, L. Novak, K. Lynn, C. Chen, K. Thompson, R. Higgins, U. Batra, S. Shelukar, G. Kwei, D. Storey, The role of Biopharmaceutics in the development of a clinical nanoparticle formulation of MK-0869: a Beagle dog model predicts

- improved bioavailability and diminished food effect on absorption in humans, *Int. J. Pharm.* 285 (2004) 135–146.
- [5] G.G. Liversidge, K.C. Cundy, Particle size reduction for improvement of oral bioavailability of hydrophobic drugs: I. Absolute oral bioavailability of nanocrystalline danazol in beagle dogs, *Int. J. Pharm.* 125 (1995) 91–97.
- [6] R.H. Müller, K. Peters, Nanosuspensions for the formulation of poorly soluble drugs: I. Preparation by a size reduction technique, *Int. J. Pharm.* 160 (1998) 229–237.
- [7] R.H. Müller, C. Jacobs, O. Kayser, Nanosuspensions as particulate drug formulations in therapy rationale for development and what we can expect for the future, *Adv. Drug. Del. Rev.* 47 (2001) 3–19.
- [8] M.J. Grau, O. Kayser, R.H. Müller, Nanosuspensions of poorly soluble drugs – reproducibility of small scale production, *Int. J. Pharm.* 196 (2000) 155–157.
- [9] K.P. Krause, R.H. Müller, Production and characterisation of highly concentrated nanosuspensions by high pressure homogenization, *Int. J. Pharm.* 214 (2001) 21–24.
- [10] J. Hecq, M. Deleers, D. Fanara, H. Vranckx, K. Amighi, Preparation and characterization of nanocrystals for solubility and dissolution rate enhancement of nifedipine, *Int. J. Pharm.* 299 (2005) 167–177.
- [11] S. Chu, S. Tanaka, J.D. Kaunitz, M.H. Montrose, Dynamic regulation of gastric surface pH by luminal pH, *J. Clin. Invest.* 103 (1999) 605–612.





